15174

NATIONAL LIBRARY
OTTAWA

CANADA

BIBLIOTHÈQUE NATIONALE
OTTAWA

NAME OF AUTHOR... Mitsunobu AKIYAMA...

TITLE OF THESIS.. Thermal Entrance Region...
..Heat Transfer and...
..Hydrodynamic Stability in...
Curved Channels

UNIVERSITY..... U. of Alberta.....

DEGREE FOR WHICH THESIS WAS PRESENTED..... Ph. D.

YEAR THIS DEGREE GRANTED..... 1973.....

Permission is hereby granted to THE NATIONAL LIBRARY OF CANADA to microfilm this thesis and to lend or sell copies of the film.

The author reserves other publication rights, and neither the thesis nor extensive extracts from it may be printed or otherwise reproduced without the author's written permission.

(Signed) M. Akiyama

PERMANENT ADDRESS:

5-21, Sakura 5,
Utsunomiya City
JAPAN

DATED 5th April 1973

NL-91 (10-68)

THE UNIVERSITY OF ALBERTA

# THERMAL ENTRANCE REGION HEAT TRANSFER AND HYDRODYNAMIC STABILITY IN CURVED CHANNELS

by

© MITSUNOBU AKIYAMA

A THESIS

SUBMITTED TO THE FACULTY OF GRADUATE STUDIES AND RESEARCH

IN PARTIAL FULFILMENT OF THE REQUIREMENTS

FOR THE DEGREE OF DOCTOR OF PHILOSOPHY

DEPARTMENT OF MECHANICAL ENGINEERING

EDMONTON, ALBERTA

Spring, 1973

UNIVERISTY OF ALBERTA

FACULTY OF GRADUATE STUDIES AND RESEARCH

The undersigned certify that they have read, and recommend to the Faculty of Graduate Studies and Research for acceptance, a thesis entitled "THERMAL ENTRANCE REGION HEAT TRANSFER AND HYDRODYNAMIC STABILITY IN CURVED CHANNELS" submitted by MITSUNOBU AKIYAMA in partial fulfilment of the requirements for the degree of Doctor of Philosophy.

K. C. Cheng
Supervisor

F. W. Seyer

C. A. Rodhiewicz

E. S. St. Lock

R. J. Goldstein
External Examiner

Date April 3, 1973

ABSTRACT

A deductive analysis is carried out for the basic general equations governing the steady flow and heat transfer in curved circular pipes and rectangular channels for an incompressible fluid with constant properties except for density variations in the buoyancy term. The effects of viscous dissipation are neglected. As a result of the order of magnitude analysis, the important physical parameters and the mathematically tractable sets of governing equations for entrance flow and heat transfer in curved channels are clearly identified.

The boundary vorticity method is applied to the numerical solution of fully developed laminar flow and forced convection heat transfer in curved pipes subjected to axially uniform wall heat flux with peripherally uniform wall temperature for Dean numbers from 0 to approximately 200, and Prandtl numbers from 0 to 500. The boundary vorticity method is compared with the conventional stream function vorticity method.

The numerical solution for Graetz problem in curved pipes is also carried out for the two basic thermal boundary conditions of uniform wall temperature and uniform wall heat flux. The Prandtl number effect on thermal entrance region heat transfer is studied and the numerical results are examined carefully against the reported results in the literature.

A direct vorticity method is developed and applied to the numerical solution of laminar flow development in the hydrodynamic

entrance region of curved parallel-plate channels with uniform, parabolic and triangular entrance velocity profiles.

The Dean's hydrodynamic instability analysis for Taylor-Gortler longitudinal vortices is extended to the hydrodynamic entrance flow in curved parallel-plate channels and the neutral stability results are obtained for fully developed condition with various curvature ratios.

## ACKNOWLEDGEMENTS

The author wishes to express his deep indebtedness to Professor K.C. Cheng, thesis adviser, who suggested the thesis topics and offered valuable suggestions and advice throughout the course of this investigation and the preparation of the manuscript.

Special gratitude is extended to Dr. G.J. Hwang, a former graduate student, for useful discussions during the early stage of the investigation and consultation regarding boundary vorticity method. Professor J.R. Pounder of Mathematics Department assisted in the derivation of basic equations in helical system. The author consulted Professors S. Cabay and K.V. Leung of Computing Science Department and Professor D. Quon of Chemical and Petroleum Engineering Department on numerical methods. Thanks are also extended to Professors G.S.H. Lock, C.M. Rodkiewicz and F.A. Seyer, members of the supervisory committee, for their interest and comments. Mr. B. Luft, a graduate student, read and commented the manuscript.

The author takes this opportunity to express his sincere appreciation to Professor N. Nishiwaki and A. Tsuchida of Seikei University and Professor M. Hirata of Tokyo University for their inspiring guidance during his earlier professional development.

The author received financial support from the Univeristy of Alberta, the National Research Council of Canada through Grant NRC A1655 during his graduate studies. The computing grant was provided by the National Research Council of Canada through special computing grant C255.

The author extends his appreciation to Miss N. Farolan and Miss H. Wozniuk for their excellent typing of the thesis.

Lastly, the author wishes to express his deep appreciation to his wife, Shigeko, for her constant encouragement and patience throughout the course of his graduate studies.

TABLE OF CONTENTS


| | | Page |
|---|---|---|
| ABSTRACT | | iii |
| ACKNOWLEDGEMENTS | | v |
| TABLE OF CONTENTS | | vii |
| LIST OF TABLES | | xiii |
| LIST OF FIGURES | | xiv |
| LIST OF SYMBOLS | | xxiii |
| CHAPTER I | INTRODUCTION | 1 |
| | 1.1 Statement of the Problem | 1 |
| | 1.2 Background Literature | 11 |
| CHAPTER II | THEORETICAL ANALYSIS FOR FLOW AND HEAT TRANSFER IN CURVED CHANNELS | 30 |
| | 2.1 Introduction | 30 |
| | 2.2 Deductive Analysis of Fundamental Equations for Flow and Heat Transfer in a Curved Circular Pipe | 32 |
| | 2.3 Deductive Analysis with the Centrifugal Force Term Considered to be of Order Unity | 35 |
| | An Order of Magnitude Analysis Based on the Assumption that the Axial Inertia Term is of Order Unity | 43 |
| | An Order of Magnitude Analysis Considering the Axial Convective Term to be of Order Unity | 55 |

Page

2.4 Deductive Analysis Considering Advective Terms Due to Secondary Flow to be of Order Unity 58

An Order of Magnitude Analysis Considering the Axial Inertia Term to be of Order Unity 63

An Order of Magnitude Analysis Considering the Axial Convective Term to be Order Unity 69

2.5 Some Further Remarks on the Axial Viscous and Conduction Terms 74

2.6 A Deductive Analysis of Fundamental Equations Governing Laminar Flow and Heat Transfer in Curved Rectangular Channels 78

2.7 Basic Equations for the Graetz Problem in Curved Pipes or Channels 79

Basic Equations for Curved Rectangular Channels with the Centrifugal Force Term Considered to be of Order Unity 82

Basic Equations for Curved Rectangular Channels with Convective Terms in the Energy Equations Due to Secondary Flow Considered to be of Order Unity 82

2.8 Some Consideration of Pitch Effects in Helical Pipes 91

CHAPTER III FULLY DEVELOPED LAMINAR FORCED CONVECTION HEAT TRANSFER IN CURVED PIPES 100

3.1 Introduction 100

3.2 Formulation of the Problem 101

3.3 Finite Difference Approximation and Boundary Vorticity Method 107

3.4 Flow and Heat Transfer Results 115

3.5 Concluding Remarks 136

| | | Page |
|---|---|---|
| CHAPTER IV | GRAETZ PROBLEM IN CURVED PIPES WITH UNIFORM WALL TEMPERATURE | 138 |
| | 4.1 Introduction | 138 |
| | 4.2 Graetz Problem in Curved Pipes | 139 |
| | 4.3 Numerical Solution Using ADI Method | 144 |
| | 4.4 Development of Temperature Field in Thermal Entrance Region | 155 |
| | 4.5 Numerical Results for Nusselt Numbers | 164 |
| | 4.6 Heat Transfer Results for Thermally Fully Developed Region | 177 |
| | Temperature Field Characteristics | 177 |
| | Nusselt Number Results | 181 |
| | Comparison with Results from Approximate Analytical Methods | 184 |
| | A Correlation Equation for Prandtl Number Effects | 187 |
| | 4.7 Concluding Remarks | 191 |
| CHAPTER V | GRAETZ PROBLEM IN CURVED PIPES WITH UNIFORM WALL HEAT FLUX | 195 |
| | 5.1 Introduction | 195 |
| | 5.2 Formulation of the Problem | 195 |
| | 5.3 A General Finite-Difference Approximation to the Convective Term | 197 |
| | 5.4 Numerical Experiments on the Effects of Different Finite-Difference Approximations for Convective Terms on Local Nusselt Number Result | 200 |
| | 5.5 Temperature Profile Development | 204 |

| | | | Page |
|---|---|---|---|
| | 5.6 | Heat Transfer Results | 212 |
| | 5.7 | Some Observations on Dravid's Work [83] | 229 |
| | 5.8 | Concluding Remarks | 233 |
| CHAPTER VI | | LAMINAR FLOW IN THE HYDRODYNAMIC ENTRANCE REGION OF CURVED PARALLEL-PLATE CHANNELS | 236 |
| | 6.1 | Introduction | 236 |
| | 6.2 | Deductive Analysis of the General Basic Equations for Entry Flows | 240 |
| | 6.3 | A Note on Pressure Drop for Fully Developed Laminar Flow in Straight and Curved Parallel-Plate Channels | 247 |
| | 6.4 | Formulation of Laminar Entry Flow in Curved Parallel-Plate Channels | 250 |
| | 6.5 | Numerical Solution Using the Direct Vorticity Method | 255 |
| | 6.6 | Laminar Entry Flow in a Parallel-Plate Channel ($\lambda = 0$) with a Uniform Inlet Velocity Profile | 260 |
| | 6.7 | Laminar Flow Development in a Curved Parallel-Plate Channel with a Uniform Inlet Velocity Profile | 268 |
| | 6.8 | Laminar Flow Development in a Curved Parallel-Plate Channel with a Parabolic Inlet Velocity Profile | 278 |
| | 6.9 | Laminar Flow Development in a Curved Parallel-Plate Channel with a Triangular Inlet Velocity Profile | 286 |
| | 6.10 | Concluding Remarks | 297 |

| | | Page |
|---|---|---|
| CHAPTER VII | HYDRODYNAMIC INSTABILITY OF LAMINAR FLOW IN CURVED PARALLEL-PLATE CHANNELS | 300 |
| | 7.1 Introduction | 300 |
| | 7.2 Formulation of the Stability Problem | 303 |
| | 7.3 Numerical Method of Solution | 315 |
| | 7.4 Stability Results and Discussion | 325 |
| | 7.5 Concluding Remarks | 336 |
| CHAPTER VIII | SCOPE OF RESULTS, CONCLUSIONS, AND SIGNIFICANCE | 339 |
| REFERENCES | | 347 |
| APPENDIX 1 | GOVERNING EQUATIONS IN GENERAL ORTHOGONAL COORDINATES | 364 |
| APPENDIX 2 | DERIVATION OF GOVERNING EQUATIONS IN TOROIDAL COORDINATES FOR FLOW IN CURVED PIPES | 369 |
| APPENDIX 3 | DERIVATION OF GOVERNING EQUATIONS IN RECTANGULAR TOROIDAL COORDINATES FOR FLOW IN CURVED RECTANGULAR CHANNELS | 374 |
| APPENDIX 4 | A DEDUCTIVE ANALYSIS OF THE GOVERNING EQUATIONS FOR CURVED RECTANGULAR CHANNELS | 378 |
| APPENDIX 5 | A NOTE ON VORTICITY METHODS IN NUMERICAL SOLUTION | 385 |
| APPENDIX 6 | NUMERICAL RESULTS FOR CHAPTER III | 400 |
| APPENDIX 7 | NUMERICAL RESULTS FOR CHAPTER IV | 405 |
| APPENDIX 8 | NUMERICAL RESULTS FOR CHAPTER V | 409 |

| | | Page |
|---|---|---|
| APPENDIX 9 | NUMERICAL RESULTS FOR CHAPTER VI | 413 |
| APPENDIX 10 | COMPUTER PROGRAMS | 417 |

LIST OF TABLES


| Table | | Page |
|---|---|---|
| 1 | A Summary of Possible Hydrodynamic and Thermal Entrance Region Problems | 54 |
| 2 | A Possible Classification of Simultaneous Hydrodynamic and Thermal Entrance Region Problems in Curved and Straight Circular Pipes Considering Advective Terms due to Secondary Flow to be of Order Unity. | 73 |
| 3 | Buoyant Force Terms with Helix Effect | 98 |
| 4 | Comparison of Pressure-drop Results, $[\Delta p - (\Delta p)_\infty]$ | 265 |
| 5 | Entrance Length for a Parallel-Plate Channel ($\lambda = 0$) with Uniform Entrance Velocity Profile | 267 |
| 6 | $[\Delta p - (\Delta p)_\infty]$ and Entrance Lengths $\omega_{98}$ and $\omega_{99}$ for Curved Parallel-Plate Channel Flow with Uniform Entrance Velocity Profile | 276 |
| 7 | $[\Delta p - (\Delta p)_\infty]$ and Entrance Lengths $\omega_{98}$ and $\omega_{99}$ for Curved Parallel-Plate Channel Flow with Triangular Entrance Velocity Profile | 296 |
| 8 | Neutral Stability Results | 326 |
| 9 | Minimum Critical Dean Number $K_c$ and Critical Wave Number $A_c$ | 329 |
| 10 | Curvature Ratio Effect on Neutral Stability Results | 330 |

LIST OF FIGURES


| Figure | | Page |
|---|---|---|
| 1 | Curved Rectangular Channel Flow | 2 |
| 2 | Curved Parallel-Plate Channel Flow | 5 |
| 3 | Instability in Curved Parallel-Plate Channel Flow | 7 |
| 4 | Coexistence of Boundary-Value and Instability Problems | 9 |
| 5 | Flow Chart for Topics Considered in Chapter II | 31 |
| 6 | Relative Importance of Axial and Radial Momentum or Thermal Diffusion for Three Entry Flow Problems | 76 |
| 7 | Helical Tube | 92 |
| 8 | A Coordinate System for Helical Tube | 92 |
| 9 | Expanded View of Helical Pipe on a Plane | 97 |
| 10 | Coordinate System and Numerical Grid | 102 |
| 11 | Comparison of Numerical Solution between Boundary Vorticity Method and Stream Function-Vorticity Method | 116 |
| 12 | Comparison of Velocity Profile along $\phi = 0$ and $\pi$, and Isolines for Velocity at K = 196 from this Work with Adler's Experimental Data at K = 205 and Streamlines at K = 196 from this Work | 118 |
| 13 | Local Angular Distribution of $(fRe)_\phi/(fRe)_0$ with Dean Number K as a Parameter | 120 |
| 14 | $(fRe)_\phi/(fRe)_0$ versus K at Outer Surface ($\phi = 0$) and Inner Surface ($\phi = \pi$) with Comparison Made against $fRe/(fRe)_0$ | 121 |

| Figure | | Page |
|---|---|---|
| 15 | Comparison of Friction Factor Results from this Work with Theoretical and Experimental Results Available in Literature | 123 |
| 16 | Temperature Profiles and Isothermals at K = 7.66 for Pr = 100 | 124 |
| 17 | Local Angular Distribution of $(Nu)_\phi/(Nu)_0$ with Dean Number K as a Parameter for Pr = 0.7 and 100 | 126 |
| 18 | $(Nu)_\phi/(Nu)_0$ versus K at Outer Surface ($\phi = 0$) and Inner Surface ($\phi = \pi$) with Comparison Made against $Nu/(Nu)_0$ for Pr = 0.7 | 127 |
| 19 | Comparison of Heat Transfer Results from this Work with Theoretical and Experimental Results Available in Literature | 129 |
| 20 | Comparison of a New Correlation Curve for Heat Transfer Results for $Pr \geq 1.0$ from this Work Using a New Parameter with Theoretical and Experimental Results Available in Literature | 132 |
| 21 | Comparison of Heat Transfer Results for Uniform Wall Heat Flux Case Available in Literature | 135 |
| 22 | Development of Temperature Profile in a Curved Pipe | 140 |
| 23 | Numerical Experiments on Asymptotic Limiting Nusselt Number | 150 |
| 24 | Temperature Profile Development along Dimesionless Downstream Distance at Pr = 0.1 and K = 123.2 | 156 |

| Figure | | Page |
|---|---|---|
| 25 | Temperature Profile Development along Dimensionless Downstream Distance at Pr = 0.7 and K = 123.2 | 157 |
| 26 | Temperature Profile Development along Dimensionless Downstream Distance at Pr = 10 and K = 37.1 | 158 |
| 27 | Temperature Profile Development along Dimensionless Downstream Distance at Pr = 500 and K = 4.45 | 159 |
| 28 | Development of Isothermals at Six Downstream Cross-Sections for Pr = 0.7 and K = 123.2 | 162 |
| 29 | Development of Isothermals at Six Downstream Cross-Sections for Pr = 10 and K = 37.1 | 163 |
| 30 | Local Nusselt Number Variation along Dimensionless Downstream Distance for Pr = 0.1 with Dean Number as Parameter | 165 |
| 31 | Local Nusselt Number Variation along Dimensionless Downstream Distance for Pr = 0.7 with Dean Number as Parameter | 166 |
| 32 | Local Nusselt Number Variation along Dimensionless Downstream Distance for Pr = 10 with Dean Number as Parameter | 167 |
| 33 | Local Nusselt Number Variation along Dimensionless Downstream Distance for Pr = 500 with Dean Number as Parameter | 168 |
| 34 | Average Nusselt Numbers along Dimensionless Downstream Distance for Pr = 0.1 with Dean Number as Parameter | 169 |

| Figure | | Page |
|---|---|---|
| 35 | Average Nusselt Numbers along Dimensionless Downstream Distance for Pr = 0.7 with Dean Number as Parameter | 170 |
| 36 | Average Nusselt Numbers along Dimensionless Downstream Distance for Pr = 10 with Dean Number as Parameter | 171 |
| 37 | Average Nusselt Numbers along Dimensionless Downstream Distance for Pr = 500 with Dean Number as Parameter | 172 |
| 38 | Temperature Distributions for Typical Dean Numbers with Pr = 0.7 | 179 |
| 39 | Comparison of Isothermals Between Uniform Wall Temperature Case and Uniform Wall Heat Flux Case from Chapter III with K = 123.2 and Pr = 0.7 | 180 |
| 40 | Local Angular Distribution of $(Nu)_\phi/(Nu)_0$ with Dean Number K as a Parameter for Pr = 0.7 | 182 |
| 41 | A Comparison Between Heat Transfer Results for Uniform Wall Temperature Case and Uniform Wall Heat Flux Case from Chapter III for Several Prandtl Numbers | 183 |
| 42 | Comparison Between Heat Transfer Results from Numerical Analysis and Perturbation Analysis | 185 |
| 43 | Comparison of Heat Transfer Results from Present Work and from Chapter III with those from Boundary Layer Approximation [65] | 188 |

| Figure | | Page |
|---|---|---|
| 44 | Proposed Correlation Curves for Prandtl Number Effects on Heat Transfer Results Valid for $Pr \geq 1$ using a Parameter $KPr^{1/2}$ | 190 |
| 45 | Effect of $\beta$ on Local Nusselt Number Fluctuation | 201 |
| 46 | Temperature Profile Development for Pr = 0.7 and K = 123.2 | 205 |
| 47 | Temperature Profile Development for Pr = 10 and K = 27.8 | 206 |
| 48 | Development of Isothermals for Pr = 0.7 and K = 123.2 | 208 |
| 49 | Development of Isothermals for Pr = 10 and K = 27.8 | 209 |
| 50 | Axial Temperature Distributions for $\bar{\theta}_w$, $\theta_b$ and $\Delta\theta = \bar{\theta}_w - \theta_b$ for K = 0 and Pr = 0.7, K = 123.2 | 211 |
| 51 | A Comparison Between Present Numerical Result and Results from Kays [108] and Hsu [109,110] | 214 |
| 52 | Local Nusselt Number Variation for Pr = 0.1 with Dean Number as Parameter | 215 |
| 53 | Local Nusselt Number Variation for Pr = 0.7 with Dean Number as Parameter | 216 |
| 54 | Local Nusselt Number Variation for Pr = 10 with Dean Number as Parameter | 217 |
| 55 | Local Nusselt Number Variation for Pr = 500 with Dean Number as Parameter | 218 |

| Figure | | Page |
|---|---|---|
| 56 | Average Nusselt Number Variation for Pr = 0.1 with Dean Number as Parameter | 222 |
| 57 | Average Nusselt Number Variation for Pr = 0.7 with Dean Number as Parameter | 223 |
| 58 | Average Nusselt Number Variation for Pr = 10 with Dean Number as Parameter | 224 |
| 59 | Average Nusselt Number Variation for Pr = 500 with Dean Number as Parameter | 225 |
| 60 | Summary of Heat Transfer Results for Thermally Fully Developed Region | 226 |
| 61 | A Proposed Model for Nusselt Number Behavior with Dean Number as Parameter | 228 |
| 62 | Dravid et al's Numerical and Experimental Results [82,83] | 230 |
| 63 | The Effect of Prandtl Number on Wavelength $\lambda_w$ at K = 7.66 | 232 |
| 64 | Dravid's Wall Temperature Measurements [83] | 234 |
| 65 | Coordinate System for Curved Channel | 238 |
| 66 | Effect of Curvature Ratio $\lambda$ on Friction Coefficient and Pressure Drop | 251 |
| 67 | Coordinate System and Numerical Grid for a Curved Parallel-Plate Channel | 255 |

| Figure | | Page |
|---|---|---|
| 68 | Developing Axial Velocity Profiles in a Parallel-Plate Channel ($\lambda = 0$) with Uniform Entrance Velocity | 262 |
| 69 | Developing Transverse Velocity Profiles in a Parallel-Plate Channel ($\lambda = 0$) with Uniform Entrance Velocity | 263 |
| 70 | Pressure Drop Result for a Parallel-Plate Channel ($\lambda = 0$) with Uniform Entrance Velocity | 266 |
| 71 | Developing Axial Velocity Profiles for $\lambda = 0.01$ with Uniform Entrance Velocity | 269 |
| 72 | Developing Transverse Velocity Profiles for $\lambda = 0.01$ with Uniform Entrance Velocity | 270 |
| 73 | Developing Axial Velocity Profiles for $\lambda = 0.1$ with Uniform Entrance Velocity | 271 |
| 74 | Developing Transverse Velocity Profiles for $\lambda = 0.1$ with Uniform Entrance Velocity | 272 |
| 75 | Developing Axial Velocity Profiles for $\lambda = 0.5$ with Uniform Entrance Velocity | 273 |
| 76 | Developing Transverse Velocity Profiles for $\lambda = 0.5$ with Uniform Entrance Velocity | 274 |
| 77 | Pressure Drop Result for $\lambda = 0$, 0.1 and 0.5 with Uniform Entrance Velocity | 277 |

| Figure | | Page |
|---|---|---|
| 78 | Friction Factor Results for $\lambda$ = 0, 0.1 and 0.5 with Uniform Entrance Velocity | 279 |
| 79 | Developing Axial Velocity Profiles for $\lambda$ = 0.1 with Parabolic Entrance Velocity | 280 |
| 80 | Developing Transverse Velocity Profiles for $\lambda$ = 0.1 with Parabolic Entrance Velocity | 281 |
| 81 | Developing Axial Velocity Profiles for $\lambda$ = 0.5 with Parabolic Entrance Velocity | 282 |
| 82 | Developing Transverse Velocity Profiles for $\lambda$ = 0.5 with Parabolic Entrance Velocity | 283 |
| 83 | Pressure Drop Result for $\lambda$ = 0.5 with Parabolic Entrance Velocity | 285 |
| 84 | Developing Axial Velocity Profiles for $\lambda$ = 0 with Triangular Entrance Velocity | 287 |
| 85 | Developing Transverse Velocity Profiles for $\lambda$ = 0 with Triangular Entrance Velocity | 288 |
| 86 | Developing Axial Velocity Profiles for $\lambda$ = 0.1 with Triangular Entrance Velocity | 289 |
| 87 | Developing Transverse Velocity Profiles for $\lambda$ = 0.1 with Triangular Entrance Velocity | 290 |
| 88 | Developing Axial Velocity Profiles for $\lambda$ = 0.5 with Triangular Entrance Velocity | 291 |

| Figure | | Page |
|---|---|---|
| 89 | Developing Transverse Velocity Profiles for $\lambda$ = 0.5 with Triangular Entrance Velocity | 292 |
| 90 | Pressure Drop Result for $\lambda$ = 0 and 0.5 with Triangular Entrance Velocity | 294 |
| 91 | Friction Factor Results for $\lambda$ = 0, 0.1 and 0.5 with Triangular Entrance Velocity | 295 |
| 92 | Coordinate System and Numerical Grid | 303 |
| 93 | Effect of Mesh Size on Critical Dean Number $K_c$ with A = 4 and $\lambda$ = 0.01 | 324 |
| 94 | Neutral Stability Curve for Small Curvature Ratio | 328 |
| 95 | Effect of Curvature Ratio $\lambda$ on Critical Dean Number $K_c$ | 331 |
| 96 | Critical Reynolds Number Results for Various Curvature Ratios $\lambda$ | 334 |
| 97 | Critical Dean Number $K_c$ and Reynolds Number $Re_c$ vs. Curvature Ratio $\lambda$ | 337 |

## LIST OF SYMBOLS

$A$ = dimensionless wave number, $2a\alpha$

$A_c$ = critical wavenumber

$a$ = radius of pipe or half width of the curved channel

$B$ = dimensionless amplification factor, $\beta R_c$

$C$ = constant, $-C_1(a^3/4\nu\mu)$

$C_1$ = axial pressure gradient, $\partial P_0/R_c\partial\Omega$

$cp$ = specific heat at constant pressure

$Fr$ = centrifugal Froude number. $W_c^2/R_c g$

$f$ = friction factors defined by equations (112) and (158)

$Gr$ = Grashof number, $\beta g\theta_c(2a)^3/\nu^2$

$Gz$ = modified Graetz number, $PrRe(2a/R_c\Omega)$

$g$ = gravitational acceleration

$h$ = dimensionless grid spacing in X-direction, $2/M$

$\bar{h}$ = average heat transfer coefficient at a given circumference

$K$ = Dean number, $Re(a/R_c)^{1/2}$, see equation (11)

$K_c$ = critical Dean number

$k$ = thermal conductivity

$M$ = number of divisions in r-direction or x-direction

$N$ = number of divisions in $\phi$-direction

$Nu$ = Nusselt numbers, $\bar{h}(2a)/k$ defined by (112), (125), and (131)

$\bar{Nu}$ = average Nusselt number

$P$ = pressure

$P_0$ = axial pressure measured along the center line and a function of $R_c\Omega$ only

$P'$ = pressure deviation which is a function of R and $\phi$ only or disturbance pressure defined by equation (179)

$P^*$ = amplitude of the disturbance pressure

Pr = Prandtl number, $\nu/\alpha$

$p$ = dimensionless pressure

$p_0$ = dimensionless pressure at the channel inlet

$p^*$ = dimensionless amplitude of the disturbance pressure

$\Delta p$ = dimensionless pressure drop, $p_0 - p$

Q = parameter, $(K^2Pr)^{1/4}$

$R, \Phi, \Omega$ = torous coordinates

$Ra_c$ = centrifugal Rayleigh number, $K^2Pr$

$R_c$ = radius of curvature of a curved pipe or channel

Re = Reynolds number, $2aW_m/\nu$ or $2aW_c/\nu$

$r$ = dimensionless radial coordinate, R/a

$r_c$ = dimensionless radius of curvature of a curved pipe, $R_c/a = 1/\lambda$

$r, \phi, \omega$ = dimensionless torous coordinates

T = temperature

$T_W$ = wall temperature

$T_0$ = uniform fluid temperature at thermal entrance

U,V,W = velocity compnents in R, $\Phi$ and $\Omega$-directions or in X, Y, and $\Omega$-directions

U',V',W' = disturbance velocity components in X,Y and $\Omega$-directions

U*,V*,W* = amplitudes of the disturbance velocities in X, Y, and $\Omega$-directions and function of X only.

$u,v,w$ = dimensionless velocity components in r, $\phi$ and $\omega$-directions or in x, y and $\omega$-directions

$u^*,v^*,w^*$ = dimensionless amplitudes of the disturbance velocities in x, y and $\omega$-directions and function of x only

$W_m$ = mean velocity in $\Omega$-direction

$X,Y,\Omega$ = rectangular torous coordinates

$x,y,\omega$ = dimensionless torous coordinates

GREEK LETTERS

$\alpha$ = thermal diffusivity or wavenumber defined by equation (186)

$\beta$ = coefficient of thermal expansion or amplification factor defined by equation (186)

$\zeta$ = dimensionless vorticity

$\theta$ = dimensionless temperature difference $(T - T_W)/(T_0 - T_W)$ or $k(T - T_0)/q_W a$

$\lambda$ = curvature ratio $a/R_c$

$\lambda_W$ = wavelength defined in Section 5.7

$\mu$ = viscosity

$\nu$ = kinematic viscosity

$\rho$ = density

$\sigma$ = entrance length geometric ratio $a/(R_c\Omega_c)$

$\sigma_\theta$ = thermal entrance length geometric ratio $a/(R_c\Omega_{c\theta})$

$\tau$ = axial temperature gradient, $\partial T/R_c\partial\Omega$

$\Psi$ = dimensionless stream functions defined by equations (71) and (147)

$\nabla^2$ = dimensionless Laplacian operator, $\frac{\partial^2}{\partial r^2} + \frac{1}{r}\frac{\partial}{\partial r} + \frac{1}{r^2}\frac{\partial^2}{\partial \phi^2}$ or $\frac{\partial}{\partial x^2} + \frac{\lambda}{(1 + \lambda x)}\frac{\partial}{\partial x}$

SUBSCRIPTS AND SUPERSCRIPTS

b = basic flow quantity or mixed mean temperature

c = value for curved parallel channel or for critical point

i,j = space subscripts of a grid point in r and $\phi$-directions, or x and $\omega$-directions

k = step level in axial direction

n = nth iteration for superscript

s = value for straight parallel channel

w = value at wall

0 = value at channel inlet

- = average value

# CHAPTER I

# INTRODUCTION

## 1.1 STATEMENT OF THE PROBLEM

Curved pipes or channels for fluid flow are used in various engineering applications notably in tubular heat exchanger for heating or cooling in the forms of helices, spirals, 90 and 180 degree or other short pipe bends. Curved flow of fluids are also found in various fluid machineries, heat engines, cryogenic systems, canals, rivers and many other natural phenomena. In contrast to fluid flows in straight channels, curved channel flows are characterized by secondary flow in the cross-section normal to the main flow as a result of centrifugal forces acting on the fluid. Also the velocity profile for fully developed laminar flow in curved pipes due to the action of the centrifugal forces exerted on the fluid particles. Besides centrifugal forces, other body forces such as buoyancy forces in gravitational field, acceleration forces due to rotation, Coriolis forces, and body forces in magnetic and electric fields may give rise to the secondary flow in a fluid passage. For the purpose of illustrating the possibility of obtaining different types of laminar flows depending on the geometrical shape, and to clarify the role of the body forces in setting up the secondary flow, a fully developed laminar flow in a curved rectangular channel with constant radius of curvature $R_c$ is shown in Fig. 1, and will be considered next. In this connection, it is noted that, in contrast to flow in straight pipes, analytical solutions for entry flow in curved pipes or channels

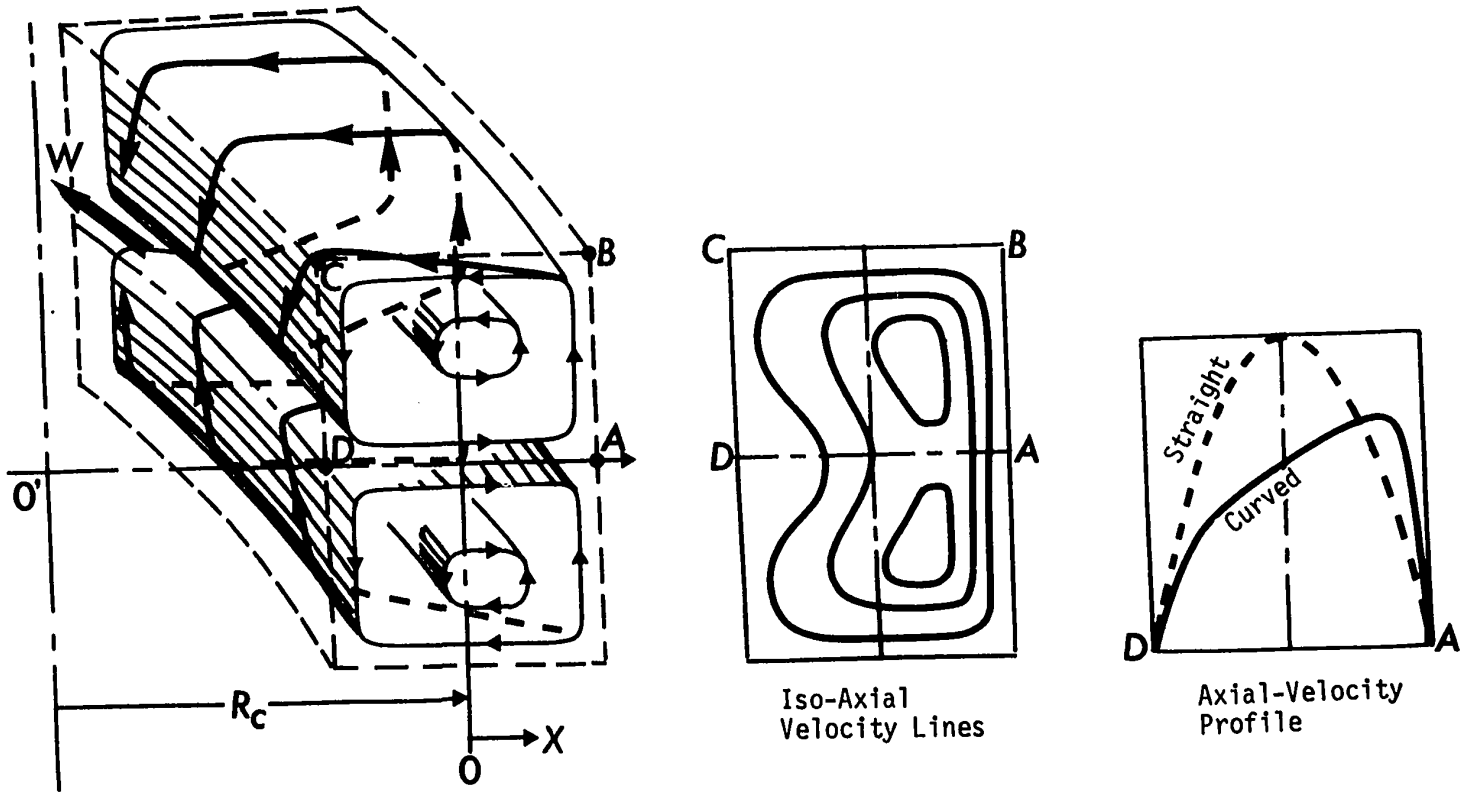


General Flow Structure

Iso-Axial Velocity Lines

Axial-Velocity Profile

Fig. 1 Curved Rectangular Channel Flow

do not seem to be available in the literature.

At a given point in the channel, the centrifugal force acting in a direction away from the center of curvature is proportional to $W^2/(R_c + X)$ and as a result a pressure gradient prevails throughout the whole cross-section. Noting the velocity distribution in the rectangular channel, the fluid in the central portion is subjected to a larger centrifugal force than the fluid near the wall. As a consequence, the fluid in the central core will be pushed toward the outer wall. It is seen that the pressure is greatest at the outer wall, and least at the inner wall for a given fluid layer parallel to the plane of curvature. At the outer wall, the pressure at A in Fig. 1 is greater than that at B, whilst at the inner wall the pressure at D is less than that at C. Because of a smaller horizontal pressure near the top and bottom walls, a secondary flow in the form of a pair of vortices is set up as indicated in the figure. With the superposition of the secondary flow on the main flow, a pair of resultant helical flows appears. With secondary flow, the region of maximum velocity is displaced from the center of the channel toward the outer wall as well as towards the upper and lower wall as shown in Fig. 1. The iso-axial velocity lines in the domain ABCD and the axial velocity profile along the centerline DA are also shown in Fig. 1. Since the secondary flow derives its kinetic energy from the main flow, the wall friction in the curved channel becomes greater than that for a straight channel for a given axial pressure gradient and geometrical shape.

It should be pointed out that the type of secondary flow which appears in curved pipes or channels mentioned above is set up immediately after the fluid is brought into motion in the passage regardless of the shape of its cross-section. However, for a curved rectangular channel, as the aspect ratio $\gamma$ (vertical height divided by horizontal width) is increased, the "eyes" of a pair of vortices will move further toward the upper or lower wall, and the intensity of the secondary flow in the central region of the channel decreases. For the limiting case of an infinite aspect ratio it is not difficult to visualize that the secondary flow disappears completely. Based on the mechanism of secondary flow explained so far, one cannot have secondary flow without the existence of the upper and lower walls shown in Fig. 1. As the aspect ratio $\gamma \to \infty$, one obtains a curved parallel-plate channel, or a flow in the annulus between two infinite coaxial cylinders as shown in Fig. 2. Apparently, a new flow situation arises now. The creation of the centrifugal forces due to the curvature, and the associated pressure gradients in the cross-section of the channel remains much the same as that of the previous case shown in Fig. 1. For the present case, the horizontal pressure gradient in the channel is independent of the height. Fig. 1 shows that with secondary flow, a much thicker layer of slowly moving fluid exists at the inner wall of a curved channel than at the outer wall. Thus there is an accumulation of retarded fluid at the inner wall. For a curved parallel-plate channel shown in Fig. 2, an exactly opposite situation occurs with an accumulation of retarded fluid at the outer wall. The reason for this can be explained from an

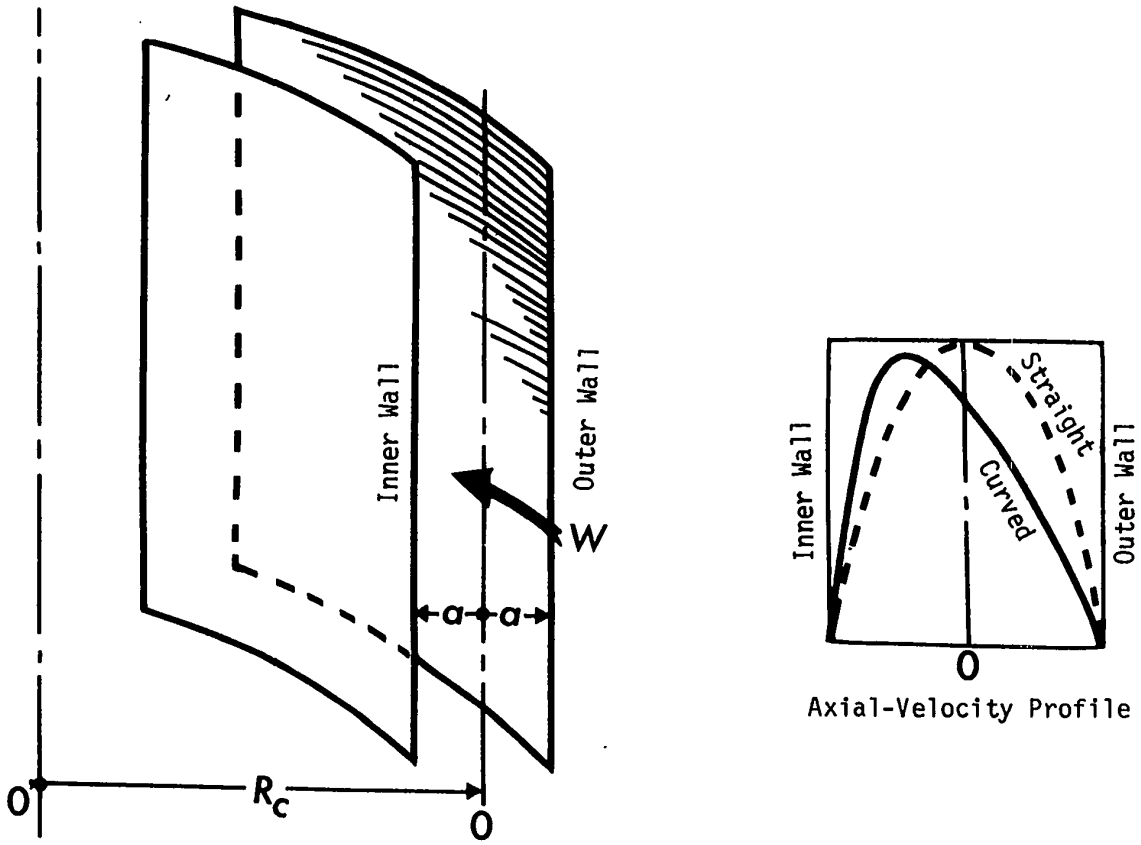


Fig. 2 Curved Parallel-Plate Channel Flow

inspection of the equation of motion in the axial direction. As a result, a distortion of the main flow toward the inner wall occurs as shown in Fig. 2. In a two-dimensional curved flow shown in Fig. 2, the centrifugal force on a fluid element must be balanced by a pressure gradient inwards. The pressure is still greatest at the outer wall, and least at the inner wall. The pressure is seen to increase monotonically from the inner wall to the outer wall. On the other hand, the centrifugal force (body force) increases from zero at the inner wall to a maximum value at a point of maximum velocity, and then decreases to zero again at the outer wall. Therefore, the region near the inner wall up to the point of maximum velocity is always stable and the outer region is potentially unstable. Thus an instability problem arises, and it may lead to another type of laminar flow. With further increase of Reynolds number for a given radius of curvature, a secondary flow pattern in the form of longitudinal vortices with axes parallel to main flow as shown in Fig. 3 may appear. After the onset of longitudinal vortices, the main flow will be further distorted. The present longitudinal vortices may be called Taylor-Goertler vortices since the physical mechanism is similar.

If now one has a curved rectangular channel with a large aspect ratio of say 10, the secondary flow is confined to the ends. Near the middle of the channel, no appreciable pressure gradient towards or away from the upper or lower wall is induced. Consequently, the longitudinal vortices due to hydrodynamic instability as shown in Fig. 3 may appear in the central portion of this curved rectangular

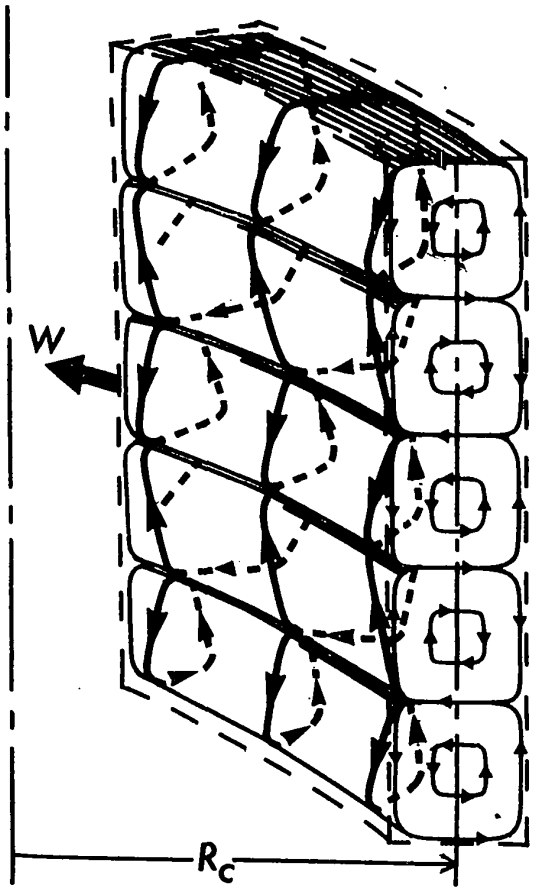


A Secondary Motion in the Form of
Longitudinal Vortices due to the Instability

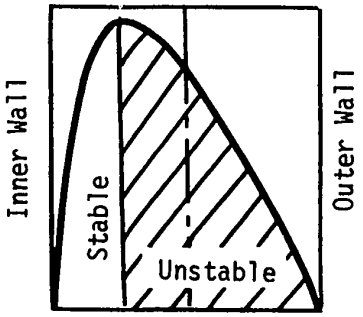


Axial-Velocity Profile
and Its Distinct Two Regions

Fig. 3 Instability in Curved Parallel-Plate Channel Flow

channel. In other words, a pair of vortices near the upper and lower walls and longitudinal vortices (Taylor-Goertler vortices) in the central portion may coexist under certain conditions. Apparently, the coexistence of boundary-value and instability problems in the same channel will lead to a formidable flow and heat transfer problem.

The above reasoning is suggested from the experimental work carried out by Akiyama, Hwang, and Cheng [1] for the onset of longitudinal vortices due to thermal instability (onset of natural convection) in laminar forced convection between horizontal parallel plates using a wide horizontal rectangular channel shown in Fig. 4. A pair of vortices due to free convection near the side walls and longitudinal vortices in the central portion of the channel due to thermal instability are depicted in Fig. 4. The central portion of the longitudinal vortices due to thermal instability shown in Fig. 4 may arise under various thermal boundary conditions [2], and experimental details including the flow visualization technique employed are described in Reference [1]. It should be noted that in the case of thermal-instability, buoyant forces are the cause of instability whereas in the case of hydrodynamic-instability under consideration, centrifugal forces are the cause. A situation similar to that shown in Fig. 4 also arises in the case where the body force is a Coriolis force instead of the centrifugal and buoyancy forces considered so far. If a rectangular straight channel with large aspect ratio is rotating about an axis normal to the main flow direction with constant angular velocity, for example, in such a way that its longer

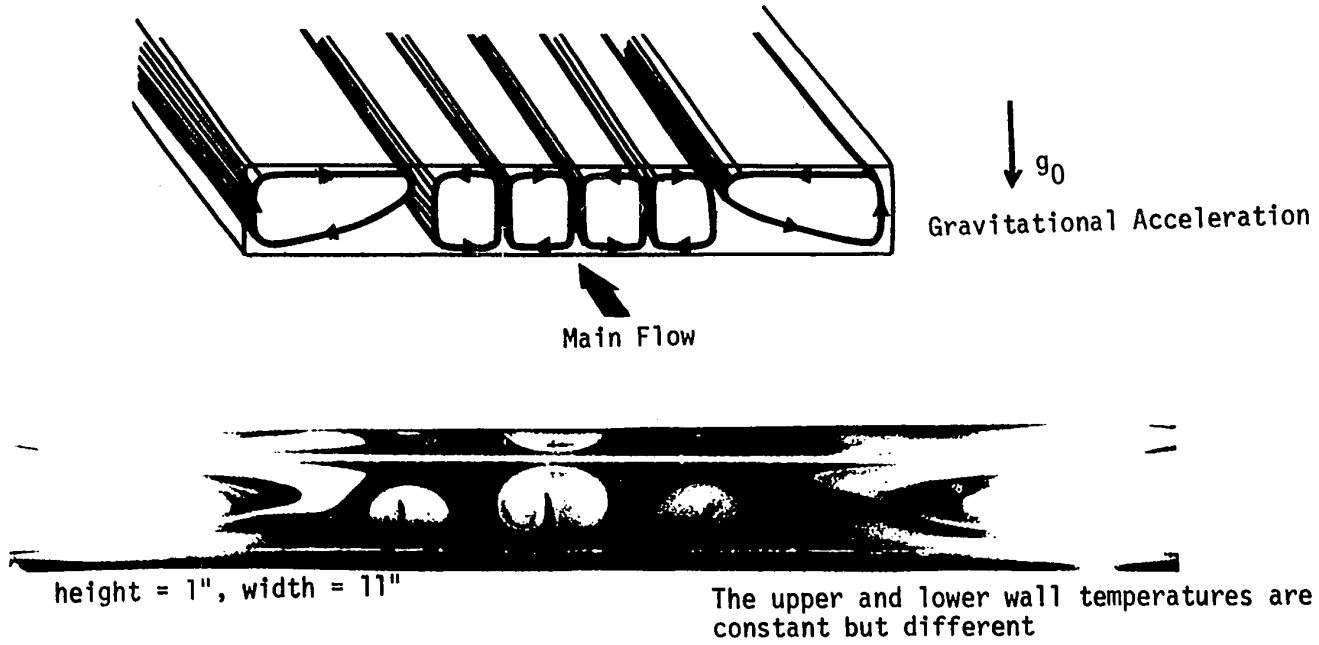


Fig. 4 Coexistence of Boundary-Value and Instability Problems

side is parallel to the axis of rotation, then a pair of vortices appear near the ends, and a series of periodic longitudinal vortices may appear in the central portion due to hydrodynamic instability caused by the Coriolis forces. Such a flow pattern may occur in various rotating fluid machineries such as centrifugal pumps and turbines.

It is clear that secondary flow in a channel will enhance heat or mass transfer in various industrial equipments utilizing various shapes of curved or straight channels such as those in heat exchangers, heat engines, nuclear reactors, chemical reactors and cryogenic devices. Recent applications of secondary flow effects include desalination processes and an artificial kidney in the bioengineering field.

Before presenting a brief historical background and review of the pertinent literature, it is appropriate at this point to state the scope of the present work. In view of the lack of theoretical solutions involving laminar forced convection in the thermal entrance region of curved pipes or channels (analogous to the Graetz problem for a straight channel) at the time of initiation of this work, an attempt was made to obtain numerical solutions for the classical Graetz problem in curved pipes for the two basic or reference thermal boundary conditions of uniform wall heat flux and uniform wall temperature. Since more than one kind of body force may appear in a given curved channel flow under certain conditions, an order of magnitude analysis is carried out to assess the importance of buoyancy and Coriolis forces in curved pipes and rectangular channels.

However, the numerical results will be presented for the cases where the secondary flow is caused solely by centrifugal forces acting on the fluid elements.

As a preliminary step toward the study of hydrodynamic stability in a curved parallel-plate channel or flow in the annular space between two coaxial infinite cylinders, a hydrodynamic entrance region problem is solved for the curved parallel-plate channel using three different entrance velocity profiles. The final portion of this thesis is concerned with the solution of the hydrodynamic stability problem for fully developed flow in a curved parallel-plate channel.

## 1.2 BACKGROUND LITERATURE

Transport processes with secondary flow can be found in many natural or artificial physical phenomena. If one dissolves a cube of sugar in a cup of tea by stirring with a teaspoon, one can observe that the tea leaves and undissolved sugar are deposited near the center at the bottom of the cup due to the secondary flow. In river bends [3,4,5] one observes that sand, gravel or other material is continually being picked up from the bottom at the outer bank and piled up on the inner bank. The effect of the secondary flow at bends is to increase the depth and curvature at the outer side, and shallowness near the inner one. This confirms the observed fact that beds of rivers are scoured near the outer bank and silted near the inner bank with the bend becoming more and more pronounced. This explanation was given by Thomson [3,4] who also presented an experimental confirmation. In meteorology, the combined thermal

and rotational effects on secondary flow are of interest in investigating the mechanisms of such atmospheric phenomena as storm systems and jet streams. In geophysics, one is interested in the secondary flows that could be induced in the earth's molten core due to the earth's rotation and magnetic field. It is seen that the transport phenomena involving secondary flow cover a wide range of physical subjects. Attention will now be focussed on secondary flow problems in fluid engineering.

In 1963, Ito [6] discussed secondary flow problems in fluid engineering quoting 100 references. Ito [7] in 1965, also reviewed recent trends in secondary flow studies listing 29 references. Since secondary flow appears in a variety of fluid mechanics problems including various fluid machineries [6,7], it is impractical to present a list of all the work that has been done in this area. Instead, an attempt will be made here to review published works on fluid flow and heat transfer in curved pipes and closely related problems. Secondary flow problems also arise in hydrodynamic stability investigations, and this class of problems will be reviewed in a separate section as an introduction to hydrodynamic entrance and stability problems in a curved parallel-plate channel treated in this thesis. A brief account on historical background in the field of curved pipes will serve to indicate the scope and limitation of the present work on the Graetz problem in curved pipes.

Fluid flow problems in curved pipes have received the attention of many investigators since the early part of the present

century. Earlier works in this field are mainly concerned with obtaining experimental or theoretical data on the increase of friction resistance due to secondary flow in a curved pipe, whose axis has a constant radius of curvature. In 1908, Grindley and Gibson [8] presented experimental data on a coil which indicate the increased resistance to air flow. Experimental investigations on fluid flow in coils were reported by Eustice [9,10,11] in 1910, 1911, and 1925. His work [10], demonstrating the skewed streamlines for helical flow in glass coils using the flow visualization technique of injecting a colored dye into the fluid, is praticularly noteworthy.

Dean [12] in 1927, presented the first theoretical analysis for fully developed laminar flow in a curved pipe. The Navier-Stokes equations were written for an incompressible fluid and it was assumed that the curvature ratio, representing the ratio of pipe radius to radius of curvature, was small compared to unity. A solution was obtained applying a perturbation method. He pointed out that the secondary flow in curved pipes is characterized by a dynamical similarity parameter, $K = Re\lambda^{1/2}$, which has since been called the Dean number in the literature. His analytical solution predicts a secondary flow field similar to that observed by Eustice in the dye injection experiments. Dean's second analytical solution [13] using a higher order approximation in the series solution is now known to be applicable only for very small Dean numbers. In this connection, it is of interest to note that the perturbation method employed by Morton [14] in solving the combined free and forced convection problem for fully developed laminar flow in uniformly

heated horizontal pipes at low Rayleigh numbers is similar to that used originally by Dean. Later Trefethen [15] pointed out that the secondary flow patterns caused by Coriolis forces in radial rotating tubes, centrifugal forces in curved pipes, or buoyancy forces in heated horizontal tubes with fully developed laminar flow are at least qualitatively analogous, and one would expect that similar mathematical methods may be used in solving physically analogous problems. Indeed, the perturbation method remains to be the only analytical method available for the solution of secondary flow problems in various channels involving rather low characteristic parameters. It can be said that Dean's pioneer work [12,13] has sparked the series of theoretical and experimental works on curved pipes which appeared since then.

The secondary flow in curved pipes has also been confirmed in a striking manner by Taylor [16] in 1929 using a colored thread. Taylor [16] provided experimental data on transition from laminar to turbulent flow and concluded that a higher speed of flow is necessary to maintain turbulence in a curved pipe than in a straight one. White [17,18] in 1929, conducted resistance measurements in curved pipes using curvature ratios of 1/8.9, 1/15.15, 1/112, and 1/2050. His empirical resistance formula based on the correlation of experimental data involving the Dean number K has subsequently been verified both experimentally and theoretically to be accurate, and is quoted widely. In 1934, Adler [19] introduced the important concept of the boundary layer for secondary flow along the pipe wall in his

analysis of laminar flow with large Reynolds number. His experimental work covers a rather wide range encompassing both laminar and turbulent flows. His accurate experimental result for local velocity measurements in curved pipes is also noteworthy. White's empirical equation for flow resistance and the experimental data of White [17] and Adler [18] are given in a book edited by Goldstein [5]. In 1932, Hawes [20] presented measured velocity distributions in the horizontal and vertical directions of a coiled pipe with curvature ratio of 1/10. Yarmell and Nagler [21] in 1934, presented the results of a series of experiments on the flow of water around bends of various shapes and various degrees of curvature in 6 in. diameter pipes. Wattendorf [22] in 1935 presented the results of an experimental study of the effect of curvature on fully developed turbulent flow. In 1937, Keulegan and Beij [23] presented the results of an experimental study of the flow of water in smooth-walled, large-radius curved pipes for the laminar and turbulent regimes over a range of Reynolds numbers from 500 to 60,000. A method of computing a first approximation for the length of curve (hydrodynamic entrance length) required for the establishment of the velocity distribution characteristic of a curved pipe was also presented. In 1948, Weske [24] pointed out that turbulent flow in curved ducts may be analyzed by methods adapted from the theory of boundary layers. Ito [25] in 1951, reported a theory on laminar flows through curved pipes of elliptic and rectangular cross-sections using a series expansion in terms of the Dean number. Using boundary layer approximations along the wall,

Ludwieg [26] in 1951, presented analytical results for friction factors for fully developed laminar flow in helically coiled square channels rotating around its axis. Extensive experimental results for both laminar and turbulent flows are presented. Comparison between theoretical and experimental results for laminar flow shows good agreement. Experimental results for friction factors are also presented for the case of stationary curved square channels for both laminar and turbulent flows. Hawthorne [27] in 1951, analyzed the flow in bent circular pipes and the theory based on inviscid fluid is compared with experiments on bent pipes and rectangular ducts. Cuming [28] in 1952, presented a theoretical analysis for flow in curved pipes of circular, elliptic and rectangular sections using the perturbation method. Eichenberger [29] in 1953, analyzed the entrance region flow problem in a curved rectangular bend with secondary flow by assuming an inviscid flow. Detra [30] in 1953, presented a study on experimental investigation of the secondary flow phenomenon, and a theoretical investigation on the initial or starting phases of the secondary flow in slightly bent pipes by assuming an incompressible inviscid fluid. He listed 17 references. Eskinazi and Yeh [31] in 1956, reported an experimental investigation on fully developed turbulent air flows in a plane curved channel between concentric circular walls. Dean and Hurst [32] in 1959, obtained some analytical results for laminar flow in a curved square channel by assuming a uniform stream for the secondary flow.

Ito [33] in 1959, proposed accurate semi-empirical formulas for friction factors in fully developed turbulent flow in curved pipes

and an empirical equation for transition from laminar to turbulent flow. Ito's data range from a Reynolds number of 1,000 to 300,000 using curvature ratios of 1/16.40, 1/40, 1/100, 1/250, and 1/648 and are quoted widely since they agree with earlier reported results.

Barua [34] in 1963, approached Dean's problem [12,13] for the high Dean number regime using a boundary layer approximation near the wall. His theoretical results agree with the experimental data of White [17] and Adler [19] for Dean numbers as low as about 200. In 1963, Truesdell [35,36] presented a numerical solution for fully developed laminar flow in helically coiled tubes of circular cross-sections for curvature ratios ranging from 0.01 to 0.1, and Dean numbers ranging from 1.0 to about 280 obtaining a good accuracy in his numerical results for Dean numbers up to approximately 200. A relaxation technique was applied for the numerical solution of a coupled fourth-order partial differential equation involving the stream function for secondary flow and a second-order partial differential equation for the axial velocity written in terms of rectangular coordinates. His formulation includes the curvature ratio as an independent parameter in addition to the Dean number. His results reveal no appreciable effect of curvature ratio on flow resistance. Also some references quoted by Truesdell [35] are worth consulting.

In 1964, Kapur, Tyagi and Srivastava [37] solved the fully developed laminar flow problem in a curved annulus of concentric cross-sections for the case when the radius of curvature of the annulus is large compared with the radius of the outer curved pipe. Kubair and

Kuloor [38] in 1964, presented data on diametrical pressure drop for water flowing through copper spirals of different geometry at various points on the spirals. The effect of curvature ratio and length to diameter ratio on diametral pressure drop and the influence of diametrical pressure drop on total pressure drop, and onset of turbulence in spiral coils are investigated. Topakoglu [39] in 1967, presented an approximate solution using a method similar to that of Dean [12] for steady laminar flows of an incompressible viscous fluid in curved pipes of circular and annular cross-sections without the assumption of small curvature ratio. For the curved pipes with concentric annular cross-section, his solution predicts the existence of four vortices for the secondary flow in contradiction with a pair of vortices predicted by Kapur et. al. [37] on the basis of a simplified analysis. In 1968, McConalgue and Srivastava [40] extended Dean's pioneering work on the steady motion of an incompressible fluid through a curved tube of circular cross-section. A method using a Fourier-series development with respect to the polar angle in the plane of a cross-section was formulated and the resulting coupled nonlinear equations solved numerically up to a Dean number of K = 77.05. In 1969, Ito [41] presented a theoretical analysis for steady laminar flow in a curved pipe of circular cross-section. He assumed that the flow consists of a frictionless central core surrounded by a boundary layer for the large Dean number flow regime. A formula for the friction factor of a curved pipe was derived by using Pohlhausen's approximate method. A comparison between his resistance formulas (theoretical and experimental) and various

experimental data shows good agreement except in the low Dean number region where some discrepancy exists. In 1970, Larrain and Bonilla [42] presented a theoretical analysis of pressure drop in the laminar flow of fluid in a coiled pipe applicable to Dean numbers below about 16. This is the normal range for viscometry with coiled capillaries. A series solution with terms depending on the curvature of the pipe is presented for the coiling effect. In 1971, Baylis [43] presented experimental results on laminar flow in curved channels of square section.

It is of interest to note that laminar flow results for non-Newtonian fluids in curved pipes are reported, for example, by Jones [44] in 1960, Clegg and Power [45] in 1963, Thomas and Walters [46,47] in 1963 and 1965, Jones [48] in 1967, and Jones and Walters [49] in 1968. Also, Barnes and Walters [50] in 1969 reported an experimental study on the flow of viscous and elastico-viscous liquids through curved pipes.

It is more convenient to mention other recent results for flow in curved pipes or channels in connection with a review of the literature on heat transfer in curved pipes or channels. Before proceeding to heat transfer prblems in curved pipes, it is useful to summarize the status up to this point in regard to flow problems in curved pipes. The mechanism of secondary flow in curved pipes is now well understood for fully developed laminar flow in curved pipes. For the very low Dean number regime, a perturbation method used by Dean [17,18] appears to be the only analytical method available for the

solution of fully developed laminar flow problems in curved pipes. On the other hand, in the high Dean number range, an analytical solution is possible only if the physical model of a frictionless central core sourrounded by a boundary layer near the wall is employed. It is seen that an analytical solution is ineffective for the intermediate Dean number-flow regime. The effect of curvature ratio on flow in a curved pipe is also well understood. It can be said that accurate design data are now available for predicting pressure drop for fully developed laminar and turbulent flows in curved pipes. An accurate empirical equation is also available for predicting the critical Reynolds number determining the transition from laminar to turbulent flow in a curved pipe. In contrast to the many analytical investigations in the area of developing laminar flows in straight pipes or channels, no theoretical work appears to have been reported so far in the literature for the hydrodynamic laminar entrance region problem involving viscous flow in curved pipes.

Turning to heat transfer problems in curved pipes, it is noted that the earlier reported works are mainly experimental. In 1925, Jeschke [51,52] presented an empirical equation for heat transfer for turbulent flow of air in helically coiled tubes. His empirical equation was modified by Merkel [53] and the result is given in McAdams' book [54]. Hawes' experimental investigation [20] in 1932 was concerned with the measurement of velocity and temperature distributions for water in a coiled pipe. His temperature profiles near the inner wall show somewhat unusual character but his isothermals on a cross-section is

now known to be qualitatively correct. Pratt's work [55] in 1947 reported heat transfer in a reaction tank cooled by means of a coil. He developed empirical equations for internal and external heat transfer coefficients for turbulent flow in a cooling coil immersed in a stirred liquid contained in a tank. In 1950, Berg and Bonilla [56] presented an experimental investigation on the thermal entrance region problem in curved pipes under the condition of uniform wall temperature. Their work is mainly concerned with the development of empirical correlation equations for heat transfer and as such the range of applicability is rather limited. In 1955, Kreith [57] investigated the influence of curvature on heat transfer to incompressible fluids for Reynolds numbers ranging from $10^4$ to $10^6$ and Prandtl numbers ranging from 0.01 to 100, and for radii of curvature ranging from 0.12 to 1.2 ft. In 1958, Eckert and Irvine [58] presented measurements of the temperature and velocity fields for a specific duct geometry (square at entrance and a rectangle with aspect ratio 2 at exit) which bends the flow by 90 degrees and simultaneously accelerates it to an average exit velocity which is twice the inlet velocity. It is found that the temperature field existing in a cross-section upstream of the bend is considerably rearranged by the action of the secondary flow. The temperature field also influences the velocity field at the exit cross-section. In 1961, Ede [59] pointed out the lack of heat transfer data on various pipe bends and reported the experimental results on local heat transfer coefficients for water in a right-angled pipe bend covering a range of Reynolds numbers from

500 to 50,000. He noted that with laminar flow the effect of the ratio of bend radius to pipe radius is large. In 1962, Tangri and Jayaraman [60] presented heat transfer studies on a spiral plate heat exchanger and showed that the heat transfer coefficient is increased by more than 60 per cent compared to a conventional heat exchanger for transfer from water to water and from moisture-laden air to water. In 1963, Seban and McLaughlin [61] presented friction and heat transfer results for the laminar flow of oil and the turbulent flow of water in tube coils with uniform heating having the ratios of coil to tube diameter of 17 and 104, for Reynolds numbers from 12 to 65,000. Correlation equations for the asymptotic heat transfer coefficient are presented for both laminar and turbulent flows. Their experimental study has clarified some aspects of the thermal entrance region heat transfer in curved pipes. They too noted the need for additional experimental data to properly define the heat transfer in curved tubes. In 1963, Kubair and Kuloor [62] presented correlation equations for pressure drop and heat transfer in spiral tube coils. Rogers and Mayhew [63] in 1964, provided additional experimental results for forced convection heat transfer and friction factors using water in steam-heated helically coiled tubes with turbulent flow.

It should be noted that no theoretical analysis on convection heat transfer in curved pipes appears to exist up to 1964. It is clear that experimental correlation of heat transfer data will have rather limited applicability if the correlation is not based on the complete theoretical understanding of the heat transfer mechanism involved.

In 1964, Maekawa [64] approached the problem of fully developed laminar forced convection in curved pipes by a perturbation method similar to that of Dean [12,13] and presented heat transfer results for the thermal boundary conditions of uniform wall temperature and uniform wall heat flux. Because of the perturbation method used, his results are valid only for extremely small Dean number region. However, his analytical results are useful in understanding the effects of Dean number and Prandtl number. Noting the need for theoretical work, Mori and Nakayama [65,66,67] presented a series of rather comprehensive studies on forced convective heat transfer in curved pipes for both laminar and turbulent flows starting in 1965. The results of theoretical analysis based on boundary layer approximation along the pipe wall for fully developed laminar flow in a curved pipe under the condition of uniform heat flux at large Dean numbers were shown to be in good agreement with experimental study using air. For fully developed turbulent flow under the condition of uniform heat flux, the results of theoretical analysis assuming a boundary layer along the pipe wall and experimental results using air were again shown to be in good agreement. The theoretical analysis under the condition of uniform wall temperature and the presentation of practical formulae for both laminar and turbulent flows rounded out this series of investigations. In 1966, Kubair and Kuloor [68] presented experimental data on pressure drop and heat transfer to aqueous solutions of glycerol flowing in different types of coiled pipes with uniform wall temperature for laminar flow in the Reynolds number range 80 to 6,000. An empirical correlation in the thermal entrance region is

given but one finds it difficult to obtain the asymptotic Nusselt number. In 1966, Kubair and Kuloor [69] also compared the performance of helical and spiral coil heat exchangers. In 1967, Mori and Uchida [70] presented analytical results using boundary layer approximation for fully developed laminar flow in a curved square channel under the thermal condition of axially uniform wall temperature gradient. Their results for flow and heat transfer are applicable for the regime where the Dean number is large. Velocity and temperature fields were obtained by dividing the cross-section into core and boundary regions and considering the balances of kinetic energy and entropy production for the boundary layers. In 1967, Mori, Nakayama and Uchida [71] presented a review paper on convection heat transfer in ducts with secondary flow considering possible combinations of body force (buoyancy, Coriolis and centrifugal forces) and geometrical shape of the channel cross-section (circular, rectangular and parallel-plate channels). Analytical methods of solution for both small and large parameter regions are outlined. Schmidt [72] in 1967, discussed heat transfer and pressure drop in curved pipes. Experimental correlation equations for Nusselt number are given for laminar and turbulent conditions. A discussion on related published works is also given. In 1967, Shchukin and Filin [73] presented an experimental investigation on the dependence of the heat transfer coefficient on the length of a short curved channel. The effect of buoyancy forces on convective heat transfer in short curved channels is also discussed. Some correlation equations are given. In 1968, Özisik and Topakoglu [74] presented heat transfer

results for hydrodynamically and thermally fully developed laminar flow in a curved pipe under the conditions of axially uniform heat flux and uniform peripheral wall temperature at any cross-section for the small Dean number region using a perturbation method. Their analysis includes curvature ratio as an independent parameter but the result shows that the curvature ratio effect is small. The various published correlation equations for pressure drop and heat transfer in coils are summarized by Srinivason, Nandapukar and Holland [75] in 1968 quoting 57 references. In 1969, Shchukin [76] reported correlation of experimental data on heat transfer in curved pipes. In 1969, Miropol'skii, Annadurdyev and Kakabaev [77] reported experiments for water flow in coiled tubes, and showed that the heat transfer coefficient and friction factor increase during heating and decrease during cooling when the tube-to-coil diameter ratio is increased.

At this point, it is noted that theoretical results on heat transfer in curved pipes are available only for hydrodynamically and thermally fully developed conditions only. Moreover, from the viewpoint of method of solution, the perturbation method is applicable only for extremely low Dean numbers which is practically not important; on the other hand, the method of boundary layer approximation is valid only for high Dean numbers. For the intermediate Dean number regime, neither the perturbation method nor the boundary layer technique proves to be effective. It is clear that a numerical solution presents another possibility.

In 1970, Cheng and Akiyama [78,79] presented numerical results for flow and heat transfer in curved rectangular channels under the thermal boundary conditions of axially uniform wall heat flux and peripherally uniform wall temperature at any axial position. The numerical method yields solutions up to a reasonably high Dean number for the aspect ratios $\gamma$ = 0.2, 0.5, 1, 2 and 5. In particular, for a square channel with Prandtl number of 0.71, the solution reaches a Dean number of 500 complementing Mori and Uchida's work [70]. Subsequently, in the course of the present thesis investigation, flow and heat transfer results for hydrodynamically and thermally fully developed laminar forced convection in curved pipes subjected to the thermal boundary condition of uniform wall heat flux per unit axial length were reported by Akiyama and Cheng [80] in 1971. The numerical solution converges for Dean numbers ranging from small to intermediate values. The Prandtl number effect on heat transfer was studied and a possible correlation for heat transfer using a new parameter ($K^2Pr$) was proposed [80,81]. In 1971, Dravid, Smith, Merrill and Brian [82,83] reported a numerical study on thermal entrance region problem (Graetz problem) in curved pipes for three wall boundary conditions of constant wall temperature, constant wall heat flux, and axially uniform wall heat flux but circumferentially uniform wall temperature with a Dean number of 225 only. For the fully developed flow field, they used Mori and Nakayama's approximate solution [65] based on a boundary layer model. Some experimental results for the case of an isothermal periphery with axially constant

wall heat flux are also reported. Dravid et al. [82] reported that the numerical solution exhibits a cyclic oscillation of local Nusselt number value before reaching an asymptotic limiting value with Dean number of 225. It may be of some interest to point out that the author became aware of Dravid et al's work [82] on the Graetz problem in curved pipes in September 1971 after part of the present thesis work dealing with the same Graetz problem was completed, and was right in the process of preparing the manuscript for publication. An abstract of one phase of the present work on the Graetz problem was presented in 1972 [84].

In 1971, Miyazaki [85] reported a numerical study on combined free and forced convective heat transfer and fluid flow in a rotating curved circular tube for the fully developed flow with the thermal boundary condition of constant heat flux per unit length of tube. In 1972, Akiyama and Cheng [86] reported asymptotic heat transfer results for fully developed laminar forced convection in curved pipes with uniform wall temperature. Also in 1972, Kalb and Seader [87] presented numerical results for fully developed velocity and temperature fields under the thermal boundary condition of axially uniform wall heat flux with peripherally uniform wall temperature by including curvature ratio as an independent parameter in the formation of the problem. The numerical solutions are presented for Dean numbers ranging from 1 to 1,200 and Prandtl number and curvature ratio varying from 0.005 to 1,600 and 1/10 to 1/100, respectively. With the exception of including the curvature ratio

effect in the analysis, the problem treated is exactly the same as that reported by Akiyama and Cheng [80]. Kalb and Seader [87] also note that the curvature ratio effect on over-all heat transfer result is negligibly small.

In contrast to the abundance of literature on convective heat transfer in straight pipes, the corresponding literature for curved pipes is rather limited except for the fully developed asymptotic cases. For example, the literature on heat transfer involving simultaneous development of flow and temperature fields in curved pipes is nonexistent. Because of the rather limited theoretical and experimental works on the Graetz problem in curved pipes reported so far, some uncertainties still exist. In this review of heat transfer literature relating to convection heat transfer in curved pipes, no attempt is made to present a complete list of all the work that has been published in this area. Rather a literature closely related to the present work is surveyed. In particular, heat transfer literature on curved bends and two-phase flow in curved pipes is not mentioned here. Since an analogy exists between heat and mass transfer problems, some mention on works relating to mass transfer in curved tubes and channels may be in order. In 1967, Erdogan and Chatwin [88] studied laminar dispersion in a curved circular pipe with no buoyancy effect. In 1968, Weissman and Mockros [89] demonstrated experimentally as well as theoretically that helical coiling of tube leads to significant improvement in gas transfer rate to blood flowing in curved tubes because of induced secondary flow. In 1970, McConalogue [90] studied

the effects of secondary flow on the laminar dispersion of an injected substance in a curved tube. Chang and Mockros [91] in 1971, studied theoretically the convective dispersion of blood gases in curved channel exchangers. Ruthven [92] in 1971, derived a theoretical residence time distribution for ideal laminar flow through a helical tube with no diffusion. Nunge, Lin and Gill [93] in 1972, presented a theoretical analysis on laminar dispersion in curved tubes and channels by using the velocity distribution of Topakoglu [39] for tubes, and that of Goldstein [5] for curved channels. It is seen that curved tubes and channels have applications also in biological systems.

# CHAPTER II

# THEORETICAL ANALYSIS FOR FLOW AND HEAT TRANSFER IN CURVED CHANNELS

## 2.1 INTRODUCTION

In order to identify or establish the possible flow and heat transfer problems which may arise in curved channels and clarify the limitations of the various mathematical formulations such as those reported in the literature, a general study of the governing equations will be made in this chapter. The present study will also serve as a basis for the work of later chapters, and bring out the dynamical similarity and other characteristic parameters. Thus the governing equations to be used in this investigation will be obtained in a somewhat formal manner instead of resorting to a purely intuitive approach. The following assumptions are made to limit the scope of the investigation:

1. Newtonian fluids
2. Steady laminar incompressible flow
3. Constant physical properties with the Boussinesq approximation for the buoyancy force
4. Negligible viscous dissipation effects and no heat sources

The flow of any fluid with temperature variations due to applied heating is described by the differential equations expressing the conservation of mass, momentum and energy. With the above assumptions, the fundamental governing equations in vector notation become:

Continuity Equation:

$$\nabla \cdot \overline{V} = 0$$

Navier-Stokes Equation:

$$\rho(\overline{V} \cdot \nabla)\overline{V} = -\nabla p + \mu\nabla^2\overline{V} + \overline{F}$$

Energy Equation:

$$\rho Cp(\overline{V} \cdot \nabla)T = k\nabla^2 T$$

The governing equations in a toroidal coordinate system will be studied specifically for the two practical configurations in the form of curved circular pipes and curved rectangular channels. Some simplifications are usually required in making the problem tractable. To provide a basis for simplification is also one of the objectives of the present general study. With free convection, the additional motion results from density variations throughout the fluid which are due to temperature differences. Then the momentum and energy equations become coupled. The topics to be discussed in this chapter are shown by the flow chart in Fig. 5.

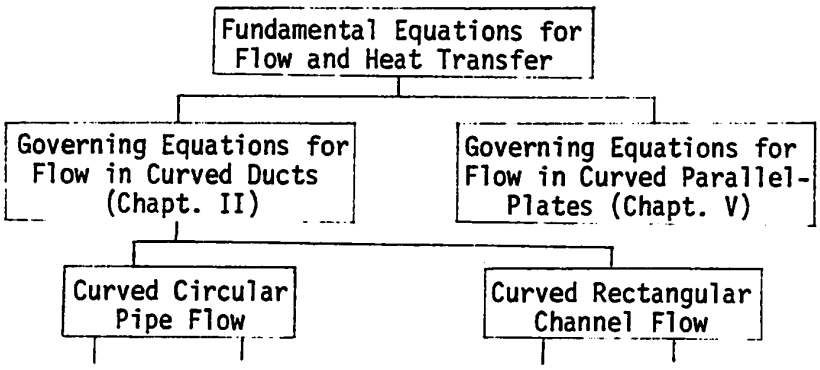

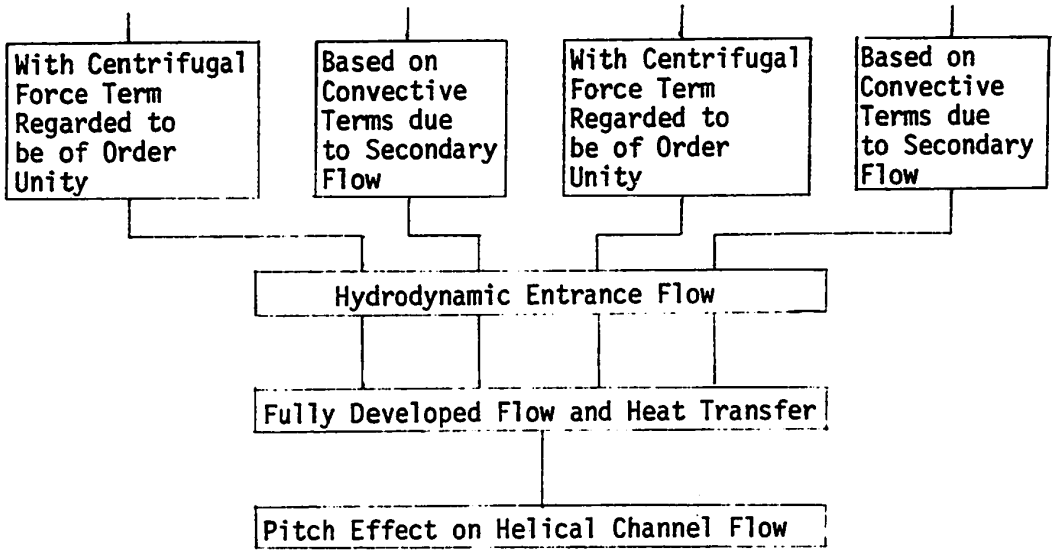


Fig. 5. Flow Chart for Topics Considered in Chapter II

Specifically, the basic equations applicable to curved circular pipes and rectangular channels, respectively, will be studied using two different physical reasonings by employing proper reference scales or quantities for the normalization procedure. Several systems of equations will be derived and categorized. The sets of governing equations appearing in the literature will be identified whenever possible. Also a detailed discussion on some important sets of equations will be made.

## 2.2 DEDUCTIVE ANALYSIS OF FUNDAMENTAL EQUATIONS FOR FLOW AND HEAT TRANSFER IN A CURVED CIRCULAR PIPE

The invariant vector forms of the continuity equation, equations of motion and energy apply for any coordinate system. In order to expand them in component form for any particular system, it is

necessary to employ the formulae for the gradient of a scalar and the divergence and curl of a vector in that system [94]. For convenience, the governing equations in a general orthogonal coordinate system are given in Appendix 1. The derivation of the governing equations applicable to flow in curved circular pipes using toroidal coordinates is given in Appendix 2. The fundamental difficulty in solving the Navier-Stokes equations either exactly or approximately is the non-linearity introduced by the convection terms in the momentum equations (A - 10) - (A - 12). For the formulation of complex physical problems, a study of the relative importance of the various terms in the fundamental equations and the dimensionless parameters pertaining to the physical phenomenon is required. The first step in the procedure of carrying out the deductive analysis [95] is to normalize the general equations by finding the proper scales or reference quantities so that the variables and their derivatives when made dimensionless will be of order unity. The appropriate characteristic or reference quantities are determined by using all the known physical information and intuition. After normalization, the important dimensionless parameters appear directly as coefficients of the unit order terms in the equations.

Although a physical understanding and justification of the governing equations applicable to the Graetz problem in curved pipes is the main goal, an attempt will be made to deal with a general flow and heat transfer problem. The following dimensionless variables are defined by using proper reference quantities:

$$r = R/a,\ \phi = \Phi/\Phi_c,\ \omega = \Omega/\Omega_c,\ u = U/U_c,\ v = V/V_c,\ w = W/W_c,$$

and $p = P/P_c$,

where a denotes the radius of the circular pipe and the subscript c signifies the characteristic quantity. For the temperature field, one may define

$$\omega_\theta = \Omega/\Omega_{c\theta} \text{ and } \theta = (T - Tw)/\Theta_c$$

All the characteristic or reference quantities employed are considered to be suitable for normalization at this point and will be identified clearly later on. Using the dimensionless variables, the continuity equation (A - 9) becomes

$$\frac{\partial u}{\partial r} + \frac{u}{r} + \left[\frac{a}{R_c}\right] \frac{u \cos\phi}{(1 + [a\Phi_c/R_c]\, r \cos\phi)}$$

$$+ \left[\frac{V_c}{a\Phi_c}\,\frac{a}{U_c}\right] \left\{ \frac{1}{r}\frac{\partial v}{\partial \phi} - \left[\frac{a}{R_c}\right] \frac{v \sin\phi}{(1 + [\, a\Phi_c/R_c\,]\, r \cos\phi)} \right\}$$

$$+ \left[\frac{W_c}{R_c\Omega_c}\,\frac{a}{U_c}\right] \frac{1}{(1 + [\, a_c/R_c\,]\, r \cos\ )} \frac{\partial w}{\partial \omega} = 0$$

Noting that the secondary velocity components in the R- and $\Phi$- directions are of equal importance, one obtains

$$\left[\frac{V_c}{a\Phi_c} \cdot \frac{a}{U_c}\right] = 1 \qquad (1)$$

If the flow problem is symmetric with respect to the horizontal plane, the value of $\Phi_c$ varies from 0 to $\Pi$. Otherwise, $\Phi_c$ may vary from 0 to $2\Pi$. For the purpose of simplicity in the argument, the reference quantity

$\Phi_c$ will be assumed to vary from 0 to 1. Since one is interested in an order of magnitude analysis, this simplification is justifiable, and will not lead to any loss of generality in the deductive analysis. In this regard, $\phi = \Phi/\Phi_c$ may be considered to be a quasi-normalization. With the above simplification, one obtains $O[U_c] = O[V_c]$.

One may now proceed to the normalization of the momentum and energy equations. In carrying out the deductive analysis, two possibilities may arise depending on the physical emphasis to be placed on the problem. The first possibility is based on the reasoning that the centrifugal force term in the momentum equations (A - 10) or (A - 11) should be of the same order of magnitude as the viscous force terms representing the highest order term in the equation. This reasoning is based on the physical fact that centrifugal forces play an important role when investigating flow inside a curved pipe or channel. Another possibility arises by considering the convective terms due to secondary flow to be of the same order as the conduction terms in the energy equation. The consequences of the two different normalization procedures will also be investigated.

## 2.3 DEDUCTIVE ANALYSIS WITH THE CENTRIFUGAL FORCE TERM CONSIDERED TO BE OF ORDER UNITY

After normalization equation (A - 10) and noting that the centrifugal force term and the viscous terms are of the same order of magnitude, one obtains

$$\frac{\omega U_c}{a^2} = \frac{W_c^2}{R_c}$$

Rewriting the above relationship, one has

$$\frac{U_c}{W_c} = \frac{W_c a^2}{\nu R_c} = \frac{1}{2} Re\lambda = \frac{1}{2} K\lambda^{1/2} \tag{2}$$

where $\lambda = a/R_c$ (3)

It is also expected that in the axial momentum equation the lateral viscous terms and the axial pressure gradient term are of the same order of magnitude. This observation leads to the following relationship:

$$\frac{P_c}{\rho R_c \Omega_c} = \frac{\nu W_c}{a^2}$$

In terms of the known characteristic parameters, one has

$$\frac{P_c}{\rho W_c^2} = \frac{2}{\sigma\, Re} \tag{4}$$

where

$$\sigma = \lambda/\Omega_c = a/R_c\Omega_c \tag{5}$$

After introducing equations (2) and (4), the normalized governing equations become:

Continuity equation

$$\frac{\partial u}{r} + \frac{u}{r} + \lambda \left( \frac{u \cos \phi}{(1 + \lambda r \cos \phi)} - \frac{v \sin \phi}{(1 + \lambda r \cos \phi)} \right) + \frac{1}{r} \frac{\partial v}{\partial \phi}$$

$$+ 2K^{-1}\sigma\lambda^{-1/2}\frac{1}{(1+\lambda r\cos\phi)}\frac{\partial w}{\partial\omega} = 0 \qquad (6)$$

R- momentum equation

$$\frac{K^2}{4}\left(u\frac{\partial u}{\partial r} + \frac{v}{r}\frac{\partial u}{\partial\phi} - \frac{v^2}{r}\right) + \frac{1}{2}K\sigma\lambda^{-1/2}\frac{1}{(1+\lambda r\cos\phi)}w\frac{\partial u}{\partial\omega}$$

$$= -\sigma^{-1}K^{-1}\lambda^{-1/2}\frac{\partial p}{\partial r} + \left(\frac{1}{r^2}\frac{\partial^2 u}{\partial\phi^2} - \frac{1}{r^2}\frac{\partial v}{\partial\phi} - \frac{1}{r}\frac{\partial^2 v}{\partial\phi\partial r}\right)$$

$$+ \lambda\frac{\sin\phi}{(1+\lambda r\cos\phi)}\left(\frac{\partial v}{\partial r} + \frac{v}{r} - \frac{1}{r}\frac{\partial u}{\partial\phi}\right)$$

$$- \sigma^2\frac{1}{(1+\lambda r\cos\phi)^2}\frac{\partial^2 u}{\partial\omega^2} + 2K^{-1}\sigma\lambda^{-1/2}\frac{1}{(1+\lambda r\cos\phi)}\frac{\partial^2 w}{\partial r\partial\omega}$$

$$+ 2K^{-1}\sigma\lambda^{1/2}\frac{\cos\phi}{(1+\lambda r\cos\phi)^2}\frac{\partial w}{\partial\omega}$$

$$+ \frac{(\cos\phi)w^2}{(1+\lambda r\cos\phi)}\left(1 - \frac{1}{2}GrK^{-2}Fr\Theta\right) + \frac{1}{2}GrK^{-2}\Theta\sin\phi \qquad (7)$$

It is noted here that the following two familiar characteristic parameters, namely the Grashof and Froude numbers, appear naturally. These are defined by

$$Gr = \beta g\Theta_c(2a)^3/\nu^2$$

$$Fr = W_c^2/R_c g$$

Here the Froude number may be interpreted as the ratio of centrifugal acceleration ($W_c^2/R_c$) to gravitational acceleration (g). In this sense, it may be called a centrifugal Froude number. The last three terms on the right-hand side of equation (7) are of special interest. The term $\cos\phi\ w^2/(1 + \lambda r \cos\phi)$ can be readily identified as that due to a centrifugal force effect. The terms involving the parameter $GrK^{-2}$ represent the buoyancy force effects in the centrifugal force field. When the product of the Froude number and the buoyancy force parameter $GrK^{-2}$ is of order unity or greater, the additional centrifugal force effect appears as a term involving the Froude number and is also seen to give a coupled effect.

$\phi$-momentum equation

$$\frac{K^2}{4}\left(u\frac{\partial v}{\partial r} + \frac{v}{r}\frac{\partial v}{\partial \phi} + \frac{uv}{r}\right) + \frac{1}{2}K\sigma\lambda^{-1/2}\frac{1}{(1 + \lambda r\cos\phi)}w\frac{\partial v}{\partial \omega}$$

$$= -\sigma^{-1}K^{-1}\lambda^{-1/2}\frac{1}{r}\frac{\partial p}{\partial \phi} + \left(\frac{\partial^2 v}{\partial r^2} + \frac{1}{r}\frac{\partial v}{\partial r} - \frac{v}{r^2} - \frac{1}{r}\frac{\partial^2 u}{\partial \phi \partial r} + \frac{1}{r^2}\frac{\partial u}{\partial \phi}\right)$$

$$+ \lambda\frac{\cos\phi}{(1 + \lambda r\cos\phi)}\left(\frac{\partial v}{\partial r} + \frac{v}{r} - \frac{1}{r}\frac{\partial u}{\partial \phi}\right)$$

$$+ \sigma^2\frac{1}{(1 + \lambda r\cos\phi)^2}\frac{\partial^2 v}{\partial \omega^2} - K^{-1}\sigma\lambda^{-1/2}\frac{2}{(1 + \lambda r\cos\phi)}\frac{\partial^2 w}{r\partial\phi\partial\omega}$$

$$+ K^{-1}\sigma\lambda^{1/2}\frac{2\sin\phi}{(1 + \lambda r\cos\phi)^2}\frac{\partial w}{\partial \omega}$$

$$- \frac{\sin\phi \; w^2}{(1 + \lambda r \cos\phi)} (1 - \frac{1}{2} GrK^{-2}Fr\theta) - \frac{1}{2} GrK^{-2}\theta\cos\phi \qquad (8)$$

It is noted that the last three terms on the right-hand side of equation (8) correspond to those in equation (7) and the physical meanings are identical.

Ω-momentum equation

$$\frac{K^2}{4} (u \frac{\partial w}{\partial r} + \frac{v}{r} \frac{\partial w}{\partial \phi}) + \frac{1}{2} K\sigma\lambda^{-1/2} \frac{1}{(1 + \lambda r \cos\phi)} w \frac{\partial w}{\partial \omega}$$

$$= - \frac{1}{(1 + \lambda r \cos\phi)} \frac{\partial P}{\partial \omega} + (\frac{\partial^2 w}{\partial r^2} + \frac{1}{r} \frac{\partial w}{\partial r} + \frac{1}{r^2} \frac{\partial^2 w}{\partial \phi^2})$$

$$+ \lambda(\frac{\cos\phi}{(1 + \lambda r \cos\phi)} \frac{\partial w}{\partial r} - \frac{\sin\phi}{(1 + \lambda r \cos\phi)} \frac{1}{r} \frac{\partial w}{\partial \phi}) - \lambda^2 \frac{1}{(1 + \lambda r \cos\phi)^2} w$$

$$+ \sigma^2 \{ \frac{1}{(1 + \lambda r \cos\phi)^2} \frac{\partial^2 w}{\partial \omega^2} + 2\lambda( \frac{\cos\phi}{(1 + \lambda r \cos\phi)^2} \frac{\partial w}{\partial \omega} - \frac{\sin\phi}{(1 + \lambda r \cos\phi)^2} \frac{\partial v}{\partial \omega})\}$$

$$+ \lambda( \frac{\sin\phi}{(1 + \lambda r \cos\phi)} vw - \frac{\cos\phi}{(1 + \lambda r \cos\phi)} uw) \qquad (9)$$

The last two terms involving the products uw and vw on the right-hand side of equation (9) are readily identified to be the Coriolis force terms. For the energy equation, one may further introduce the geometric ratio $\sigma_\theta = \lambda/\Omega_{c\theta} = a/R_e\Omega_{c\theta}$ for convenience.

Energy equation

$$\frac{K^2 Pr}{4}\left(u\frac{\partial\theta}{\partial r}+\frac{v}{r}\frac{\partial\theta}{\partial\phi}\right)+\frac{1}{2}KPr\sigma_\theta\lambda^{-1/2}\frac{w}{(1+\lambda r\cos\phi)}\frac{\partial\theta}{\partial\omega_\theta}$$

$$=\left(\frac{\partial^2\theta}{\partial r^2}+\frac{1}{r}\frac{\partial\theta}{\partial r}+\frac{1}{r^2}\frac{\partial^2\theta}{\partial r^2}\right)$$

$$+\lambda\left(\frac{\cos\phi}{(1+\lambda r\cos\phi)}\frac{\partial\theta}{\partial r}-\frac{\sin\phi}{(1+\lambda r\cos\phi)}\frac{1}{r}\frac{\partial\theta}{\partial\phi}\right)$$

$$+\sigma_\theta^2\frac{1}{(1+\lambda r\cos\phi)^2}\frac{\partial^2\theta}{\partial\omega_\theta^2} \qquad (10)$$

The viscous dissipation is neglected in the above energy equation for steady viscous flow of a constant-property fluid. The foregoing set of governing equations (6) through (10) are valid for general flow and heat transfer such as the general convection heat transfer problem involving simultaneous development of velocity and temperature fields in the entrance region. A study of the non dimensionalized equations reveals that the following dimensionless parameters are of importance for flow and heat transfer problems in a curved pipe.

Primary Parameters:

Curvature ratio $\lambda = a/R_c$

Reynolds number $Re = 2aW_c/\nu$

Grashof number $Gr = \beta g\Theta_c(2a)^3/\nu^2$

Centrifugal Froude number $Fr = W_c^2/R_c g$

Prandtl number $Pr = \nu/\alpha$

Entrance length geometric ratio $\sigma = a/(R_c \Omega_c)$

Thermal entrance length geometric ratio $\sigma_\theta = a/(R_c \Omega_{c\theta})$

Derived Parameters:

Dean number $K = Re\ \lambda^{1/2}$

A ratio of Grashof number to Dean number squared $C = Gr\ K^{-2}$

Centrifugal Rayleigh number $Ra_c = K^2\ Pr$

It is noted that the Dean number K is not essentially an independent characteristics parameter and consists of Re and $\lambda^{1/2}$. However, it becomes an independent parameter when the curvature ratio $\lambda = a/Rc$ is small. This situation will be confirmed later. In order to see the physical meaning or quantitative criterion, the Dean number K may be rewritten as

$$K = (\frac{1}{2} Re \cdot Re_c)^{1/2} = (\frac{\rho W_c^2/2a}{\mu W_c/(2a)^2})^{1/2} \cdot (\frac{\rho W_c^2/R_c}{\mu W_c/(2a)^2})^{1/2} \cdot (\frac{1}{2})^{1/2} \quad (11)$$

It is seen that the Dean number can be decomposed into a product of

Reynolds number representing the ratio of inertia force ($\rho W_c^2/(2a)$) and viscous force ($\mu W_c/(2a)^2$) and the centrifugal Reynolds number representing the ratio of centrifugal force ($\rho W_c^2/R_c$) and viscous force ($\mu W_c/(2a)^2$).

The parameter $C = Gr\ K^{-2}$ represents a measure of the buoyancy force relative to the centrifugal force. Consequently, the importance of the free convection effect in the centrifugal force field can be ascertained by the magnitude of this characteristic parameter. A striking similarity exists between the parameter $Gr\ K^{-2}$ and the familiar parameter $Gr\ Re^{-2}$ indicating the relative effect of buoyancy upon forced convection in the combined forced and natural convection problem. Furthermore, when the buoyancy and centrifugal force effects are comparable, one obtains $Gr = O[K^2]$. From this relationship, one may reason that the effect of the Grashof number in combined free and forced convection, for example, in a horizontal pipe is similar to the effect of $K^2$ on the flow in a curved pipe. As a matter of fact the roles of Gr and $K^2$ are seen to be almost identical or equivalent in the respective vorticity transport equation for secondary flow [96,80]. With the above observation, it is not difficult to see the physical meaning of the new parameter $K^2Pr$. For combined free and forced convection problems, the Rayleigh number ($Gr \cdot Pr$) arises naturally. Noting that $K^2$ corresponds to the Grashof number for the present problem, one obtains the parameter $K^2Pr$. The new parameter may be called the "centrifugal Rayleigh number" because of its physical similarity. As will be confirmed later, the parameter $K^2Pr$ becomes an independent parameter when the Prandtl number is large.

A study of the governing equations (6) - (10), reveals that the independent dimensionless parameters are $\lambda$, Re, Gr, Fr, Pr, $\sigma$ and $\sigma_\theta$. The foregoing set of governing equations is a general one and is applicable to the entrance region problem involving the simultaneous development of velocity and temperature fields. When the buoyancy force terms are retained in the momentum equations, the momentum and energy equations become coupled. At this point, the relative magnitudes of the entrance length parameters, $\sigma$ and $\sigma_\theta$, still remain to be determined. Equations (9) and (10) clearly indicate that the relative importance of the axial viscous terms such as $\partial^2 w/\partial\omega^2$ and the axial conduction term $\partial^2\theta/\partial\omega_\theta^2$ depend on the coefficients $\sigma^2$ and $\sigma_\theta^2$, respectively. Apparently, these terms cannot be neglected near the hydrodynamic or thermal entrance. It would be useful if the order of magnitude for $\sigma$ and $\sigma_\theta$ can be estimated. For this purpose, it is noted that the axial inertia terms in the momentum equations vanish when the flow becomes fully developed. Consequently, in the hydrodynamic entrance region one may regard the axial inertia terms to be of the same order as the viscous terms. This viewpoint will be pursued further next.

An Order of Magnitude Analysis Based on the Assumption that the Axial Inertia Term is of Order Unity

Noting that the axial inertia terms in the momentum equations are of order unity, one obtains

$$\frac{1}{2} K\sigma\lambda^{-1/2} = 1 \text{ or } \sigma = 2K^{-1}\lambda^{1/2} = 2Re^{-1} \qquad (12)$$

Using the above relationship, the set of governing equaiions (6) to (10) become:

Continuity equation

$$\frac{\partial u}{\partial r} + \frac{u}{r} + \frac{1}{r}\frac{\partial v}{\partial \phi} + \lambda\left(\frac{u \cos \phi}{(1 + \lambda r \cos \phi)} - \frac{v \sin \phi}{(1 + \lambda r \cos \phi)}\right)$$

$$4K^{-2} \frac{1}{(1 + \lambda r \cos \phi)}\frac{\partial w}{\partial \omega} = 0 \qquad (13)$$

R-momentum equation

$$\frac{K^2}{4}\left(u \frac{\partial u}{\partial r} + \frac{v}{r}\frac{\partial u}{\partial \phi} - \frac{v^2}{r}\right) + \frac{1}{(1 + \lambda r \cos \phi)} w \frac{\partial u}{\partial \omega}$$

$$= -\frac{1}{2} K\lambda^{-3/2} \frac{\partial p}{\partial r} + \left(\frac{1}{r^2}\frac{\partial^2 u}{\partial \phi^2} - \frac{1}{r^2}\frac{\partial v}{\partial \phi} - \frac{1}{r}\frac{\partial^2 v}{\partial \phi \partial r}\right)$$

$$+ \lambda \frac{\sin \phi}{(1 + \lambda r \cos \phi)}\left(\frac{\partial v}{\partial r} + \frac{v}{r} - \frac{1}{r}\frac{\partial u}{\partial \phi}\right)$$

$$- 4K^{-2} \lambda \frac{1}{(1 + \lambda r \cos \phi)^2}\frac{\partial^2 u}{\partial \omega^2} + 4K^{-2} \frac{1}{(1 + \lambda r \cos \phi)}\frac{\partial^2 w}{\partial r \partial \omega}$$

$$+ 4K^{-2} \lambda \frac{\cos \phi}{(1 + \lambda r \cos \phi)^2}\frac{\partial w}{\partial \omega} + \frac{\cos \phi\, w^2}{(1 + \lambda r \cos \phi)}\left(1 - \frac{1}{2} GrK^{-2} Fr\theta\right)$$

$$+ \frac{1}{2} GrK^{-2}\theta \sin \phi \qquad (14)$$

$\phi$-momentum equation

$$\frac{K^2}{4}\left(u\frac{\partial v}{\partial r}+\frac{v}{r}\frac{\partial v}{\partial \phi}+\frac{uv}{r}\right)+\frac{1}{(1+\lambda r\cos\phi)}w\frac{\partial v}{\partial \omega}$$

$$=-\frac{1}{2}K\lambda^{-3/2}\frac{1}{r}\frac{\partial p}{\partial \phi}+\left(\frac{\partial^2 v}{\partial r^2}+\frac{1}{r}\frac{\partial v}{\partial r}-\frac{v}{r^2}-\frac{1}{r}\frac{\partial u}{\partial \phi \partial r}+\frac{1}{r^2}\frac{\partial u}{\partial \phi}\right)$$

$$+\lambda\frac{\cos\phi}{(1+\lambda r\cos\phi)}\left(\frac{\partial v}{\partial r}+\frac{v}{r}-\frac{1}{r}\frac{\partial u}{\partial \phi}\right)$$

$$+4K^{-2}\lambda\frac{1}{(1+\lambda r\cos\phi)^2}\frac{\partial^2 v}{\partial \omega^2}-4K^{-2}\frac{1}{(1+\lambda r\cos\phi)}\frac{\partial^2 w}{r\partial\phi\partial\omega}$$

$$+4K^{-2}\lambda\frac{\sin\phi}{(1+\lambda r\cos\phi)^2}\frac{\partial w}{\partial \omega}-\frac{\sin\phi\, w^2}{(1+\lambda r\cos\phi)}\left(1-\frac{1}{2}GrK^{-2}Fr\theta\right)$$

$$+\frac{1}{2}GrK^{-2}\theta\cos\phi \qquad (15)$$

$\Omega$-momentum equation

$$\frac{K^2}{4}\left(u\frac{\partial w}{\partial r}+\frac{v}{r}\frac{\partial w}{\partial \phi}\right)+\frac{1}{(1+\lambda r\cos\phi)}w\frac{\partial w}{\partial \omega}$$

$$=-\frac{1}{(1+\lambda r\cos\phi)}\frac{\partial p}{\partial \omega}+\left(\frac{\partial^2 w}{\partial r^2}+\frac{1}{r}\frac{\partial w}{\partial r}+\frac{1}{r^2}\frac{\partial^2 w}{\partial \phi^2}\right)$$

$$+\lambda\left(\frac{\cos\phi}{(1+\lambda r\cos\phi)}\frac{\partial w}{\partial r}-\frac{\sin\phi}{(1+\lambda r\cos\phi)}\frac{1}{r}\frac{\partial w}{\partial \phi}\right)$$

$$-\lambda^2\left(\frac{1}{(1+\lambda r\cos\phi)}\right)^2 w$$

$$+ 4K^{-2}\lambda \left\{\frac{1}{(1 + \lambda r \cos\phi)^2} \frac{\partial^2 w}{\partial \omega^2} + 2\lambda \left(\frac{\cos\phi}{(1 + \lambda r \cos\phi)^2} \frac{\partial u}{\partial \omega}\right.\right.$$

$$\left.\left. - \frac{\sin\phi}{(1 + \lambda r \cos\phi)^2} \frac{\partial v}{\partial \omega}\right)\right\}$$

$$+ \lambda\left(\frac{-\cos\phi}{(1 + \lambda r \cos\phi)} uw + \frac{\sin\phi}{(1 + \lambda r \cos\phi)} vw\right) \qquad (16)$$

Energy equation

$$\frac{K^2 Pr}{4}\left(u \frac{\partial\theta}{\partial r} + \frac{v}{r} \frac{\partial\theta}{\partial\phi}\right) + Pr \frac{w}{(1 + \lambda r \cos\phi)} \frac{\partial\theta}{\partial\omega}$$

$$= \left(\frac{\partial^2\theta}{r^2} + \frac{1}{r} \frac{\partial\theta}{\partial r} + \frac{1}{r^2} \frac{\partial^2\theta}{\partial\theta^2}\right)$$

$$+ \lambda\left(\frac{\cos\phi}{(1 + \lambda r \cos\phi)} \frac{\partial\theta}{\partial r} - \frac{\sin\phi}{(1 + \lambda r \cos\phi)} \frac{1}{r} \frac{\partial\theta}{\partial r}\right)$$

$$+ 4K^{-2}\lambda \frac{1}{(1 + \lambda r \cos\phi)^2} \frac{\partial^2\theta}{\partial\omega^2} \qquad (17)$$

One may now proceed to the order of magnitude analysis. The dimensionless parameters will now be evaluated for the conditions of particular interest. Since the terms themselves have physical meaning, it is possible to ascertain the dominance of particular physical aspects of the general problem. A study of the parameters may suggest various possible mathematical simplifications depending on the emphasis

of physical aspects. The quantitative criteria or conditions with physical meaning will be sought to indicate the order of the approximation from the general governing equations and to identify the physical problem represented by the simplified set of equations.

As noted earlier, the relative importance of the free convection effect in the centrifugal force field is represented by the parameter $GrK^{-2}$. Thus the free convection effect may be neglected provided the following restriction is satisfied.

$$2K^2 \gg Gr \tag{18}$$

In the absence of heat transfer results for curved pipes taking both centrifugal and buoyancy force effects into consideration, the above relation provides the quantitative criterion for neglecting buoyancy effects. When the buoyancy effect is negligible, the momentum and energy equations are effectively decoupled. It is noted that the term involving $GrK^{-2}Fr$ appears in the R- and $\phi$-momentum equations for secondary flow. In the centrifugal force field, one readily obtains the condition $Fr \geq$ Order [1] for most practical problems. Consequently, the effect of the centrifugal Froude number in the form of $\frac{1}{2} GrK^{-2}Fr$ must also be considered in assessing the effect of the buoyancy force. In this respect, when the magnitude of Fr is of order unity, then the buoyancy effect can be neglected under the condition given by equation (18).

Depending on the emphasis of the physical situation or condition of interest, the following four cases arise and may be of practical interest. A study of the important special cases also leads to greater

physical understanding, and formal justification of the mathematical simplification.

Case (1)

Disregarding the buoyancy and centrifugal Froude number effects, one sees that the remaining coefficients with unit order terms in the momentum equations are $\lambda$, $K^2$ and $K^{-2}\lambda$. The terms with $K^{-2}\lambda$ represent the axial viscous terms. Consequently, one may regard the axial viscous term or viscous normal stress to be of importance under the following condition:

$$4K^{-2}\lambda \geq O[10^{-2}] \tag{19}$$

The geometrical restriction requires that $\lambda \leq O[1]$. Thus one concludes that the axial viscous terms must be retained when the Dean number satisfies the condition given by

$$K \leq O[20] \tag{20}$$

It is further noted that the lateral inertia terms (the terms with $K^2/4$) in the momentum equations may be neglected if $K^2/4 \leq O[10^{-2}]$ or $K \leq O[2 \times 10^{-1}]$. It is then concluded that when $O[2 \times 10^{-1}] \leq K \leq O[20]$, every term of the whole set of equations (13) through (17) must be retained. Apparently, it is not practical to solve the set of equations in its entirety either numerically or analytically. It is also of interest to note that even in the case of curved pipes the axial viscous terms are governed by the parameter $4K^{-2}\lambda = 4Re^{-2}$ which is seen to be

independent of the curvature ratio $\lambda$.

Case (2)

Consideration will now be given to the curvature ratio effect. When the curvature ratio $\lambda$ is small or

$$\lambda \leq O[10^{-2}]$$

one may neglect the terms involving $\lambda$ and $\lambda^2$ alone in the governing equations. However, the resulting simplified set of equations is expected to be still difficult to solve even numerically because of the existence of the second derivative terms in the axial direction (axial viscous term or viscous normal stress term).

Case (3)

It is desirable to study the condition under which the axial viscous terms (or terms involving $4K^{-2}\lambda$) may be neglected. The condition is given by

$$4K^{-2}\lambda << O[1] \tag{21}$$

Noting that $\lambda \leq O[1]$ practically, the above condition does not necessarily imply $K^2 >> O[1]$. Since $K^{-2}\lambda = Re^{-2}$, the relation (21), corresponds to large Reynolds number flow conditions in the limiting case of a straight tube. However, a stricter condition of $K^2 >> O[1]$ provides an important criterion for neglecting the term involving $\partial w/\partial\omega$ in the continuity equation (13). Considering the condition given by equation

(21), one may say that when $K \geq 20$, the axial viscous terms in the momentum equations are negligible. The condition $K \geq 20$ is nearly equivalent to that given by $K^2 >> O[1]$. Using also the latter condition the set of governing equations become:

Continuity equation

$$\frac{\partial u}{\partial r} + \frac{u}{r} + \frac{1}{r}\frac{\partial v}{\partial \phi} + \lambda\left(\frac{u\cos\phi}{1+\lambda r\cos\phi} - \frac{v\sin\phi}{(1+\lambda r\cos\phi)}\right) = 0 \qquad (22)$$

R-momentum equation

$$\frac{K^2}{4}\left(u\frac{\partial u}{\partial r} + \frac{v}{r}\frac{\partial u}{\partial \phi} - \frac{v^2}{r}\right) + \frac{1}{(1+\lambda r\cos\phi)} w\frac{\partial u}{\partial \omega}$$

$$= -\frac{1}{2}K\lambda^{-3/2}\frac{\partial p}{\partial r} + \left(\frac{1}{r^2}\frac{\partial^2 u}{\partial \phi^2} - \frac{1}{r^2}\frac{\partial v}{\partial \phi} - \frac{1}{r}\frac{\partial^2 v}{\partial \phi \partial r}\right)$$

$$+ \lambda\frac{\sin\phi}{(1+\lambda r\cos\phi)}\left(\frac{\partial v}{\partial r} + \frac{v}{r} - \frac{1}{r}\frac{\partial u}{\partial \phi}\right)$$

$$+ \frac{\cos\phi}{(1+\lambda r\cos\phi)} w^2 \qquad (23)$$

$\phi$-momentum equation

$$\frac{K^2}{4}\left(u\frac{\partial v}{\partial r} + \frac{v}{r}\frac{\partial v}{\partial \phi} + \frac{uv}{r}\right) + \frac{1}{(1+\lambda r\cos\phi)} w\frac{\partial v}{\partial \omega}$$

$$= -\frac{1}{2}K\lambda^{-3/2}\frac{1}{r}\frac{\partial p}{\partial \phi} + \left(\frac{\partial^2 v}{\partial r^2} + \frac{1}{r}\frac{\partial v}{\partial r} - \frac{v}{r^2} - \frac{1}{r}\frac{\partial^2 u}{\partial \phi \partial r} + \frac{1}{r^2}\frac{\partial u}{\partial \phi}\right)$$

$$+ \lambda \frac{\cos \phi}{(1 + \lambda r \cos \phi)} \left(\frac{\partial v}{\partial r} + \frac{v}{r} - \frac{1}{r} \frac{\partial u}{\partial \phi}\right)$$

$$- \frac{\sin \phi}{(1 + \lambda r \cos \phi)} w^2 \qquad (24)$$

Ω-momentum equation

$$\frac{K^2}{4} \left(u \frac{\partial w}{\partial r} + \frac{v}{r} \frac{\partial w}{\partial \phi}\right) + \frac{1}{(1 + \lambda r \cos \phi)} w \frac{\partial w}{\partial \omega}$$

$$= - \frac{1}{(1 + \lambda r \cos \phi)} \frac{\partial p}{\partial \omega} + \left(\frac{\partial^2 \omega}{\partial r^2} + \frac{1}{r} \frac{\partial \omega}{\partial r} + \frac{1}{r^2} \frac{\partial^2 w}{\partial \phi^2}\right)$$

$$+ \lambda \left(\frac{\cos \phi}{(1 + \lambda r \cos \phi)} \frac{\partial w}{\partial r} - \frac{\sin \phi}{(1 + \lambda r \cos \phi)} \frac{1}{r} \frac{\partial w}{\partial \phi}\right)$$

$$- \lambda^2 \frac{1}{(1 + \lambda r \cos \phi)^2} w$$

$$+ \lambda \left(\frac{- \cos \phi}{(1 + \lambda r \cos \phi)} uw + \frac{\sin \phi}{(1 + \lambda r \cos \phi)} vw\right) \qquad (25)$$

Energy equation

$$\frac{K^2 Pr}{4} \left(u \frac{\partial \theta}{\partial r} + \frac{v}{r} \frac{\partial \theta}{\partial r}\right) + Pr \frac{w}{(1 + \lambda r \cos \phi)} \frac{\partial \theta}{\partial \omega}$$

$$= \left(\frac{\partial^2 \theta}{\partial r^2} + \frac{1}{r} \frac{\partial \theta}{\partial r} + \frac{\partial^2 \theta}{\partial \phi^2}\right)$$

$$+ \lambda \left(\frac{\cos \phi}{(1 + \lambda r \cos \phi)} \frac{\partial \theta}{\partial r} - \frac{\sin \phi}{(1 + \lambda r \cos \phi)} \frac{1}{r} \frac{\partial \theta}{\partial \phi}\right) \qquad (26)$$

It is now possible to introduce a stream function which satisfies the continuity equation automatically. In the formation of the problem, the R- and $\phi$-momentum equations may be combined into a single equation by eliminating the pressure terms. In the resulting momentum equation for secondary flow, one may introduce the vorticity. The resulting vorticity transport equation is of parabolic type. At the same time, the axial momentum and the energy equations are of parabolic type. It is obvious that the analytical solution of the set of equations cannot be obtained readily and a numerical technique must be used.

Case (4)

Further simplification of the problem is possible by using the conditions $\lambda << O[1]$ (see Case (2)) and $K^2 >> O[1]$ (see Case (3)). For convenience the resulting simplified set of equations is given below.

Continuity equation

$$\frac{\partial u}{\partial r} + \frac{u}{r} + \frac{1}{r}\frac{\partial v}{\partial \phi} = 0 \tag{27}$$

R-momentum equation

$$\frac{K^2}{4}\left(u\frac{\partial u}{\partial r} + \frac{v}{r}\frac{\partial u}{\partial \phi} - \frac{v^2}{r}\right) + w\frac{\partial u}{\partial \omega}$$

$$= -\frac{1}{2}K\lambda^{-3/2}\frac{\partial p}{\partial r} + \left(\frac{1}{r^2}\frac{\partial^2 u}{\partial \phi^2} - \frac{1}{r^2}\frac{\partial v}{\partial \phi} - \frac{1}{r}\frac{\partial^2 v}{\partial \phi \partial r}\right)$$

$$- \cos\phi\, w^2 \tag{28}$$

$\phi$-momentum equation

$$\frac{K^2}{4}\left(u\frac{\partial v}{\partial r}+\frac{v}{r}\frac{\partial v}{\partial \phi}+\frac{uv}{r}\right)+w\frac{\partial v}{\partial \omega}$$

$$=-\frac{1}{2}K\lambda^{-3/2}\frac{1}{r}\frac{\partial p}{\partial \phi}+\left(\frac{\partial^2 v}{\partial r^2}+\frac{1}{r}\frac{\partial v}{\partial r}-\frac{1}{r}\frac{\partial^2 u}{\partial \phi \partial r}+\frac{1}{r^2}\frac{\partial u}{\partial \phi}\right)$$

$$-\sin\phi\, w^2 \qquad (29)$$

$\Omega$-momentum equation

$$\frac{K^2}{4}\left(u\frac{\partial w}{\partial r}+\frac{v}{r}\frac{\partial w}{\partial \phi}\right)+w\frac{\partial w}{\partial \omega}$$

$$=-\frac{\partial p}{\partial \omega}+\left(\frac{\partial^2 w}{\partial r^2}+\frac{1}{r}\frac{\partial w}{\partial r}+\frac{1}{r^2}\frac{\partial^2 w}{\partial \phi^2}\right) \qquad (30)$$

Energy equation

$$\frac{K^2 Pr}{4}\left(u\frac{\partial \theta}{\partial r}+\frac{v}{r}\frac{\partial \theta}{\partial r}\right)+Pr\, w\frac{\partial \theta}{\partial \omega}$$

$$=\left(\frac{\partial^2 \theta}{\partial r^2}+\frac{1}{r}\frac{\partial \theta}{\partial r}+\frac{1}{r^2}\frac{\partial^2 \theta}{\partial \phi^2}\right) \qquad (31)$$

Although one cannot study the effect of curvature ratio $\lambda$ using the above set of simplified equations, the equations are believed to be in a form which is suitable for a study of the hydrodynamic or simultaneous hydrodynamic and thermal entrance region problem for curved

pipes. This observation is important in view of the fact that a theoretical analysis on hydrodynamic entry flow problems for curved pipes is not available in the literature. Also the system of equations appears to be rather simple and one may include the buoyancy force effect in addition to the centrifugal force effect for the thermal entrance region problem. An experimental work given by Shchukin and Filin [73] appears to be the only work considering the coupled effects of centrifugal and buoyancy forces in curved pipes.

Finally, a summary of the four cases under consideration is given as Table 1 for convenience. It should be noted that the present order of magnitude analysis is based on the assumptions that the centrifugal force and the axial inertia terms in the momentum equations are of order unity.

Table 1

A Summary of Possible Hydrodynamic and

Thermal Entrance Region Problems

| | $K\lambda^{-1/2}$: Arbitrary Second Derivatives in Axial Direction Retained | $K^2\lambda \gg O[1]$ Second Derivatives in Axial Direction Neglected |
|---|---|---|
| $\lambda$ = Arbitrary | Case (1) | Case (3) |
| $\lambda \ll O[1]$ | Case (2) | Case (4) |

An Order of Magnitude Analysis Considering the Axial Convective Term to be of Order Unity

Consideration is now focussed to the thermal entrance region problem. In order to obtain a measure for the thermal entry problem, one may assume that the axial convection term in the energy equation is as important as the conduction terms is of order unity. This leads to

$$\frac{1}{2} K \sigma_\theta \lambda^{-1/2} Pr = 1 \tag{32}$$

Using the above relationship, the set of governing equations (6) to (10) becomes.

Continuity equation

$$\frac{\partial u}{\partial r} + \frac{u}{r} + \frac{1}{r}\frac{\partial v}{\partial \phi} + \lambda\left(\frac{u \cos \phi}{(1 + \lambda r \cos \phi)} - \frac{v \sin \phi}{(1 + \lambda r \cos \phi)}\right)$$

$$+ 4K^{-2}Pr^{-1} \frac{1}{(1 + \lambda r \cos \phi)} \frac{\partial w}{\partial \omega_\theta} = 0 \tag{33}$$

R-momentum equation

$$\frac{K^2}{4}\left(u \frac{\partial u}{\partial r} + \frac{v}{r}\frac{\partial u}{\partial \phi} - \frac{v^2}{r}\right) + Pr^{-1} \frac{1}{(1 + \lambda r \cos \phi)} w \frac{\partial u}{\partial \omega_\theta}$$

$$= -\frac{1}{2} K\lambda^{-3/2} \frac{\partial p}{\partial r} + \left(\frac{1}{r^2}\frac{\partial^2 u}{\partial \phi^2} - \frac{1}{r^2}\frac{\partial v}{\partial \phi} - \frac{1}{r}\frac{\partial^2 v}{\partial \phi \partial r}\right)$$

$$+ \lambda \frac{\sin \phi}{(1 + \lambda r \cos \phi)} \left(\frac{\partial v}{\partial r} + \frac{v}{r} - \frac{1}{r} \frac{\partial u}{\partial \phi}\right)$$

$$- 4K^{-2}Pr^{-2}\lambda \frac{1}{(1 + \lambda r \cos \phi)^2} \frac{\partial^2 u}{\partial r \partial \omega_\theta}$$

$$+ 4K^{-2}Pr^{-1} \frac{1}{(1 + \lambda r \cos \phi)} \frac{\partial^2 w}{\partial r \partial \omega_\theta}$$

$$+ 4K^{-2}Pr^{-1}\lambda \frac{\cos \phi}{(1 + \lambda r \cos \phi)^2} \frac{\partial w}{\partial \omega_\theta}$$

$$+ \frac{\cos \phi}{(1 + \lambda r \cos \phi)} w^2 \qquad (34)$$

$\phi$-momentum equation

$$\frac{K^2}{4} \left(u \frac{\partial v}{\partial r} + \frac{v}{r} \frac{\partial v}{\partial \phi} + \frac{uv}{r}\right) + Pr^{-1} \frac{1}{(1 + \lambda r \cos \phi)} w \frac{\partial u}{\partial \omega_\theta}$$

$$= - \frac{1}{2} K\lambda^{-3/2} \frac{1}{r} \frac{\partial p}{\partial \phi} + \left(\frac{\partial^2 v}{\partial r^2} + \frac{1}{r} \frac{\partial v}{\partial r} - \frac{v}{r^2} - \frac{1}{r} \frac{\partial^2 u}{\partial \phi \partial r} + \frac{1}{r^2} \frac{\partial u}{\partial \phi}\right)$$

$$+ \lambda \frac{\cos \phi}{(1 + \lambda r \cos \phi)} \left(\frac{\partial v}{\partial r} + \frac{v}{r} - \frac{1}{r} \frac{\partial u}{\partial \phi}\right)$$

$$+ 4K^{-2}Pr^{-2}\lambda \frac{1}{(1 + \lambda r \cos \phi)^2} \frac{\partial^2 v}{\partial \omega_\theta^2}$$

$$- 4K^{-2}Pr^{-1} \frac{1}{(1 + \lambda r \cos \phi)} \frac{\partial^2 \omega}{r \partial \phi \partial \omega_\theta} + 4K^{-2}Pr^{-1}\lambda \frac{\sin \phi}{(1 + \lambda r \cos \phi)^2} \frac{\partial w}{\partial \omega_\theta}$$

$$- \frac{\sin \phi}{(1 + \lambda r \cos \phi)} w^2 \qquad (35)$$

Ω-momentum equation

$$\frac{K^2}{4} \left(u \frac{\partial w}{\partial r} + \frac{v}{r} \frac{\partial w}{\partial \phi}\right) + Pr^{-1} \frac{1}{(1 + \lambda r \cos \phi)} w \frac{\partial w}{\partial \omega_\theta}$$

$$= - \frac{Pr^{-1}}{(1 + \lambda r \cos \phi)} \frac{\partial p}{\partial \omega_\theta} + \left(\frac{\partial^2 w}{\partial r^2} + \frac{1}{r} \frac{\partial w}{\partial r} + \frac{1}{r^2} \frac{\partial^2 w}{\partial \phi^2}\right)$$

$$+ \lambda \left(\frac{\cos \phi}{(1 + \lambda r \cos \phi)} \frac{\partial w}{\partial r} - \frac{\sin \phi}{(1 + \lambda r \cos \phi)} \frac{1}{r} \frac{\partial w}{\partial \phi}\right) - \lambda^2 \frac{w}{(1 + \lambda r \cos \phi)^2}$$

$$+ 4K^{-2} Pr^{-2} \lambda \left\{\frac{1}{(1 + \lambda r \cos \phi)^2} \frac{\partial^2 w}{\partial \omega^2}\right.$$

$$\left. + 2\lambda \left(\frac{\cos \phi}{(1 + \lambda r \cos \phi)^2} \frac{\partial u}{\partial \omega} - \frac{\sin \phi}{(1 + \lambda r \cos \phi)^2} \frac{\partial v}{\partial \omega}\right)\right\}$$

$$+ \lambda \left(\frac{\sin \phi}{(1 + \lambda r \cos \phi)} vw - \frac{\cos \phi}{(1 + \lambda r \cos \phi)} uw\right) \qquad (36)$$

Energy equation

$$\frac{K^2 Pr}{4} \left(u \frac{\partial \theta}{\partial r} + \frac{v}{r} \frac{\partial \theta}{\partial \phi}\right) + \frac{w}{(1 + \lambda r \cos \phi)} \frac{\partial \theta}{\partial \omega_\theta}$$

$$= \left(\frac{\partial^2 \theta}{\partial r^2} + \frac{1}{r} \frac{\partial \theta}{\partial r} + \frac{1}{r^2} \frac{\partial^2 \theta}{\partial \phi^2}\right) + \lambda \left(\frac{\cos \phi}{(1 + \lambda r \cos \phi)} \frac{\partial \theta}{\partial r} - \frac{\sin \phi}{(1 + \lambda r \cos \phi)} \frac{1}{r} \frac{\partial \theta}{\partial \phi}\right)$$

$$+ 4K^{-2}Pr^{-2}\lambda \frac{1}{(1 + \lambda r \cos \phi)^2} \frac{\partial^2 \theta}{\partial \omega_\theta^2} \qquad (37)$$

It is seen that the coefficient $4K^{-2}\lambda Pr^{-2} = 4Pe^{-2}$ appears for both axial viscous and conduction terms and this is in contrast to the coefficient $4K^{-2}\lambda = 4Re^2$ obtained for these terms in the earlier analysis. Thus the condition under which the axial viscous and conduction terms may be neglected is given by

$$4K^{-2}Pr^{-2}\lambda = 4Pe^{-2} << O[1] \qquad (38)$$

Since the main emphasis here is on the thermal field, there is some question as to the importance of the present ordering procedure in regard to the momentum equations. It is seen that the parameter $K^2/4$ appears as the coefficient of the lateral viscous terms and the paramter $Pr^{-1}$ appears as the coefficient of the axial inertia terms in the momentum equations. Thus one sees that the significance of the lateral inertia terms depends on hydrodynamic conditions and the importance of the axial inertia terms depends on the measure of thermal properties.

## 2.4 DEDUCTIVE ANALYSIS CONSIDERING ADVECTIVE TERMS DUE TO SECONDARY FLOW TO BE OF ORDER UNITY

In contrast to the earlier emphasis on the flow field, the emphasis on physical phenomena will now be directed towards the thermal field in the entrance region of a curved pipe. Noting the importance of secondary flow in distorting the temperature field, it is reasonable

to assume that the advective terms in the energy equation are of the same order of magnitude as the conduction terms. Using the reference quantities defined in Sections 2.2 and 2.3, and by equating the coefficient of the advective terms with that of the conduction terms in the normalized energy equation for equation (A - 13), the following relationship results:

$$\frac{U_c \Theta_c}{a} = \frac{\Theta_c}{a^2}$$

or

$$\left(\frac{U_c a}{\nu}\right) = 1/Pr \tag{39}$$

As noted in Section 2.3, the axial pressure gradient term and the viscous terms in the axial momentum equation may be ragarded to be equally important and one obtains

$$\frac{P_c}{W_c^2} = \frac{2}{Re} \tag{4}$$

and

$$\sigma = \lambda/\Omega_c = a/R_c\Omega_c \tag{5}$$

Using equations (4) and (39), the normalized governing equations become:

Continuity equation

$$\frac{\partial u}{\partial r} + \frac{u}{r} + \frac{1}{r}\frac{\partial v}{\partial \phi} + \lambda\left(\frac{u \cos \phi}{(1 + \lambda r \cos \phi)} - \frac{v \sin \phi}{(1 + \lambda r \cos \phi)}\right)$$

$$+ \frac{1}{2} KPr\sigma\lambda^{-1/2} \frac{1}{(1 + \lambda r \cos \phi)} \frac{\partial w}{\partial \omega} = 0 \qquad (40)$$

R-momentum equation

$$Pr^{-1}\left(u \frac{\partial u}{\partial r} + \frac{v}{r} \frac{\partial u}{\partial \phi} - \frac{v^2}{r}\right) + \frac{1}{2} K\sigma\lambda^{-1/2} \frac{1}{(1 + \lambda r \cos \phi)} w \frac{\partial u}{\partial \omega}$$

$$= - \frac{1}{2} Pr\sigma^{-1} K\lambda^{-1/2} \frac{\partial p}{\partial r} + \left(\frac{1}{r^2} \frac{\partial^2 u}{\partial \phi^2} - \frac{1}{r^2} \frac{\partial v}{\partial \phi} - \frac{1}{r} \frac{\partial^2 v}{\partial \phi \partial r}\right)$$

$$+ \lambda \frac{\sin \phi}{(1 + \lambda r \cos \phi)} \left(\frac{\partial v}{\partial r} + \frac{v}{r} - \frac{1}{r} \frac{\partial u}{\partial \phi}\right)$$

$$- \sigma^2 \frac{1}{(1 + \lambda r \cos \phi)^2} \frac{\partial^2 u}{\partial \omega^2} + \frac{1}{2} KPr\sigma\lambda^{-1/2} \frac{1}{(1 + \lambda r \cos \phi)} \frac{\partial^2 w}{\partial r \partial \omega}$$

$$+ \frac{1}{2} KPr\sigma\lambda^{1/2} \frac{\cos \phi}{(1 + \lambda r \cos \phi)^2} \frac{\partial w}{\partial \omega}$$

$$+ \frac{1}{4} K^2 Pr \frac{\cos\phi \, w^2}{(1 + \lambda r \cos \phi)} \{1 - \frac{1}{2} GrK^{-2} Pr^{-1} Fr\}$$

$$+ \frac{1}{8} GrPr\theta \sin \phi \qquad (41)$$

$\phi$-momentum equation

$$Pr^{-1}\left(u \frac{\partial v}{\partial r} + \frac{v}{r} \frac{\partial v}{\partial \phi} + \frac{uv}{r}\right) + \frac{1}{2} K\sigma\lambda^{-1/2} \frac{1}{(1 + \lambda r \cos \phi)} w \frac{\partial v}{\partial \omega}$$

$$= - \frac{1}{2} Pr\sigma^{-1} K\lambda^{-1/2} \frac{1}{r} \frac{\partial p}{\partial \phi} + \left(\frac{\partial^2 v}{\partial r^2} + \frac{1}{r} \frac{\partial v}{\partial r} - \frac{v}{r^2} - \frac{1}{r} \frac{\partial^2 u}{\partial \phi \partial r} + \frac{1}{r^2} \frac{\partial u}{\partial \phi}\right)$$

$$+ \lambda \frac{\cos\phi}{(1 + \lambda r \cos\phi)} \left(\frac{\partial v}{\partial r} + \frac{v}{r} - \frac{1}{r}\frac{\partial u}{\partial \phi}\right)$$

$$+ \sigma^2 \frac{1}{(1 + \lambda r \cos\phi)^2}\frac{\partial^2 v}{\partial \omega^2} - \frac{1}{2} KPr\sigma\lambda^{-1/2} \frac{1}{(1 + \lambda r \cos\phi)} \frac{\partial^2 w}{r\partial\phi\partial\omega}$$

$$+ \frac{1}{2} KPr\sigma\lambda^{1/2} \frac{\sin\phi}{(1 + \lambda r \cos\phi)^2} \frac{\partial w}{\partial \omega}$$

$$- \frac{1}{4} K^2 Pr \frac{\sin\phi}{(1 + \lambda r \cos\phi)} w^2 \left(1 - \frac{1}{2} GrK^{-2}Pr^{-1}Fr\right)$$

$$+ \frac{1}{8} GrPr \cos\phi\ \theta \qquad (42)$$

Ω-Momentum equation

$$Pr^{-1}\left(u\frac{\partial w}{\partial r} + \frac{v}{r}\frac{\partial w}{\partial \phi}\right) + \frac{1}{2} K\sigma\lambda^{-1/2} \frac{1}{(1 + \lambda r \cos\phi)} w \frac{\partial w}{\partial \omega}$$

$$= -\frac{1}{(1 + \lambda r \cos\phi)}\frac{\partial p}{\partial \omega} + \left(\frac{\partial^2 w}{\partial r^2} + \frac{1}{r}\frac{\partial w}{\partial r} + \frac{1}{r^2}\frac{\partial^2 w}{\partial \phi^2}\right)$$

$$+ \lambda\left(\frac{\cos\phi}{(1 + \lambda r \cos\phi)} \frac{\partial w}{\partial r} - \frac{\sin\phi}{(1 + \lambda r \cos\phi)} \frac{1}{r}\frac{\partial w}{\partial \phi}\right)$$

$$- \lambda^2 \frac{1}{(1 + \lambda r \cos\phi)^2} w$$

$$+ \sigma^2 \frac{1}{(1+\lambda r \cos\phi)^2} \frac{\partial^2 w}{\partial \omega^2} + 2K^{-1}Pr^{-1}\sigma\lambda^{3/2}\left(\frac{\cos\phi}{(1+\lambda r \cos\phi)^2} \frac{\partial u}{\partial \omega} - \frac{\sin\phi}{(1+\lambda r \cos\phi)^2} \frac{\partial v}{\partial \omega}\right)$$

$$+ Pr^{-1}\lambda \frac{1}{(1 + \lambda r \cos\phi)} (\sin\phi\ vw - \cos\phi\ uw) \qquad (43)$$

Energy equation

$$u\frac{\partial\theta}{\partial r}+\frac{v}{r}\frac{\partial\theta}{\partial r}+\frac{1}{2}KPr\sigma_\theta\lambda^{-1/2}\frac{w}{(1+\lambda r\cos\phi)}\frac{\partial\theta}{\partial\omega_\theta}$$

$$=\frac{\partial^2\theta}{\partial r^2}+\frac{1}{r}\frac{\partial\theta}{\partial r}+\frac{1}{r^2}\frac{\partial^2\theta}{\partial\phi^2}$$

$$+\lambda\left(\frac{\cos\phi}{(1+\lambda r\cos\phi)}\frac{\partial\theta}{\partial r}-\frac{\sin\phi}{(1+\lambda r\cos\phi)}\frac{1}{r}\frac{\partial\theta}{\partial\phi}\right)$$

$$+\sigma_\theta^2\frac{1}{(1+\lambda r\cos\phi)^2}\frac{\partial^2}{\partial\omega_\theta^2} \qquad (44)$$

The physical meaning of each term in the above set of equations is similar to that discussed in Section 2.3. However, some different characteristic parameter appears because of the different physical basis. It is noted that in the R and $\phi$-momentum equations the familiar Rayleigh number, Ra = PrGr, appears. It is of interest to note that by considering the relative importance of boundary force terms with respect to the centrifugal force terms in equations (41) and (42), one obtains $Gr/2K^2$. Thus the physical meaning of the parameter $Gr/2K^2$ obtained in Section 2.3 is now clear. The centrifugal Rayleigh number $PrK^2$ now appears as the coefficient of the centrifugal force term. The foregoing set of equations is apparently still very involved and further simplifications are desired for practical solutions. The ordering procedure used in Section 2.3 will be followed next.

An Order of Magnitude Analysis Considering the Axial Inertia Term to be of Order Unity

For the hydrodynamic entrance region problem, it is reasonable to expect the axial inertia term to be the same order of magnitude as the lateral viscous terms. This observation leads to equation (12) namely, $(1/2)K\sigma\lambda^{-1/2} = 1$, and the governing equations become:

Continuity equation

$$\frac{\partial u}{\partial r} + \frac{u}{r} + \frac{1}{r}\frac{\partial v}{\partial \phi} + \lambda\left(\frac{u \cos \phi}{(1 + \lambda r \cos \phi)} - \frac{v \sin \phi}{(1 + \lambda r \cos \phi)}\right)$$

$$+ Pr \frac{1}{(1 + \lambda r \cos \phi)} \frac{\partial w}{\partial \omega} = 0 \qquad (45)$$

R-momentum equation

$$Pr^{-1}\left(u \frac{\partial u}{\partial r} + \frac{v}{r}\frac{\partial u}{\partial \phi} - \frac{v^2}{r}\right) + \frac{1}{(1 + \lambda r \cos \phi)} w \frac{\partial u}{\partial \omega}$$

$$= -\frac{1}{4} K^2 \lambda^{-1} Pr \frac{\partial p}{r} + \left(\frac{1}{r^2}\frac{\partial^2 u}{\partial \phi^2} - \frac{1}{r^2}\frac{\partial v}{\partial \phi} - \frac{1}{r}\frac{\partial^2 v}{\partial \phi \partial r}\right)$$

$$+ \lambda \frac{\sin \phi}{(1 + \lambda r \cos \phi)} \left(\frac{\partial v}{\partial r} + \frac{v}{r} - \frac{1}{r}\frac{\partial u}{\partial \phi}\right)$$

$$- 4K^{-2}\lambda \frac{1}{(1 + \lambda r \cos \phi)^2}\frac{\partial^2 u}{\partial \omega^2} + Pr \frac{1}{(1 + \lambda r \cos \phi)} \frac{\partial^2 w}{\partial r \partial \omega}$$

$$+ Pr\lambda \frac{\cos \phi}{(1 + \lambda r \cos \phi)^2} \frac{\partial w}{\partial \omega}$$

$$+ \frac{1}{4} K^2 Pr \frac{\cos \phi \, w^2}{(1 + \lambda r \cos \phi)} \{1 - \frac{1}{2} Gr K^{-2} Pr Fr\}$$

$$+ \frac{1}{8} GrPr \sin \phi \, \theta \tag{46}$$

$\phi$-momentum equation

$$Pr^{-1}(u \frac{\partial v}{\partial r} + \frac{v}{r} \frac{\partial v}{\partial \phi} + \frac{uv}{r}) + \frac{1}{(1 + \lambda r \cos \phi)} w \frac{\partial v}{\partial \omega}$$

$$= \frac{1}{4} K^2 \lambda^{-1} Pr \frac{1}{r} \frac{\partial p}{\partial \phi} + (\frac{\partial^2 v}{\partial r^2} + \frac{1}{r} \frac{\partial v}{\partial r} - \frac{v}{r^2} - \frac{1}{r} \frac{\partial^2 u}{\partial \phi \partial r} + \frac{1}{r^2} \frac{\partial u}{\partial \phi})$$

$$+ \lambda \frac{\cos \phi}{(1 + \lambda r \cos \phi)} (\frac{\partial v}{\partial r} + \frac{v}{r} - \frac{1}{r} \frac{\partial u}{\partial \phi})$$

$$+ 4K^{-2} \lambda \frac{1}{(1 + \lambda r \cos \phi)^2} \frac{\partial^2 v}{\partial \omega^2} - Pr \frac{1}{(1 + \lambda r \cos \phi)} \frac{\partial^2 w}{r \partial \phi \partial \omega}$$

$$+ Pr \lambda \frac{\sin \phi}{(1 + \lambda r \cos \phi)^2} \frac{\partial w}{\partial \omega}$$

$$- \frac{1}{4} K^2 Pr \frac{\sin \phi}{(1 + \lambda r \cos \phi)} w^2 (1 - \frac{1}{2} Gr K^{-2} Fr_c)$$

$$- \frac{1}{8} Gr \, Pr \cos \phi \, \theta \tag{47}$$

$\Omega$-momentum equation

$$Pr^{-1}(u \frac{\partial w}{\partial r} + \frac{v}{r} \frac{\partial w}{\partial \phi}) + \frac{1}{(1 + \lambda r \cos \phi)} w \frac{\partial w}{\partial \omega}$$

$$= - \frac{1}{(1 + \lambda r \cos \phi)} \frac{\partial p}{\partial \omega} + \left(\frac{\partial^2 w}{\partial r^2} + \frac{1}{r} \frac{\partial w}{r} + \frac{1}{r^2} \frac{\partial^2 w}{\partial \phi^2}\right)$$

$$+ \lambda \left(\frac{\cos \phi}{(1 + \lambda r \cos \phi)} \frac{\partial w}{\partial r} - \frac{\sin \phi}{(1 + \lambda r \cos \phi)} \frac{1}{r} \frac{\partial w}{\partial \phi}\right)$$

$$- \lambda^2 \frac{1}{(1 + \lambda r \cos \phi)^2} w$$

$$+ 4K^{-2} \lambda \frac{1}{(1 + \lambda r \cos \phi)^2} \frac{\partial^2 w}{\partial \omega^2}$$

$$+ 4K^{-2} \lambda^2 \left(\frac{\cos \phi}{(1 + \lambda r \cos \phi)^2} \frac{\partial u}{\partial \omega} - \frac{\sin \phi}{(1 + \lambda r \cos \phi)^2} \frac{\partial v}{\partial \omega}\right)$$

$$+ Pr^{-1} \lambda \frac{1}{(1 + \lambda r \cos \phi)} (\sin \phi \, vw - \cos \phi \, uw) \qquad (48)$$

Energy equation

$$u \frac{\partial \theta}{\partial r} + \frac{v}{r} \frac{\partial \theta}{\partial r} + Pr \frac{w}{(1 + \lambda r \cos \phi)} \frac{\partial \theta}{\partial \omega}$$

$$= \frac{\partial^2 \theta}{\partial r^2} + \frac{1}{r} \frac{\partial \theta}{\partial r} + \frac{1}{r^2} \frac{\partial^2 \theta}{\partial \phi^2}$$

$$+ \lambda \left(\frac{\cos \phi}{(1 + \lambda r \cos \phi)} \frac{\partial \theta}{\partial r} - \frac{\sin \phi}{(1 + \lambda r \cos \phi)} \frac{1}{r} \frac{\partial \theta}{\partial r}\right)$$

$$+ 4K^{-2} \lambda \frac{1}{(1 + \lambda r \cos \phi)^2} \frac{\partial^2 \theta}{\partial \omega^2} \qquad (49)$$

In the above formulation, the role of the Prandtl number becomes clear.

When the Prandtl number is large, the lateral inertia terms in the momentum equations can be neglected since $Pr^{-1}$ appears as the coefficient. This simplification is not obvious for the set of equations (13) through (17). As a matter of fact, the assumption $Pr \gg O[1]$ does not lead to any simplification. It is seen that with $Pr \gg O[1]$, the only remaining nonlinear term is the axial inertia term in each momentum equation. The other interesting fact is that the continuity equation for secondary flow may become independent of the main flow in equation (45). When the curvature ratio $\lambda$ is extremely small or $\lambda \ll O[1]$, one obtains the limiting case of a horizontal straight tube. With $\lambda \to 0$, one sees that $K \to 0$. However, one should note that the product $K\lambda^{-1/2} \equiv Re$ does not vanish as $\lambda \to 0$. The corresponding governing equations can be obtained by neglecting the terms involving $\lambda$ and $\lambda^2$. The resulting equations are:

Continuity equation

$$\frac{\partial u}{\partial r} + \frac{u}{r} + \frac{1}{r}\frac{\partial v}{\partial \phi} + Pr\,\frac{\partial w}{\partial z} = 0 \tag{50}$$

R-momentum equation

$$Pr^{-1}\left(u\,\frac{\partial u}{\partial r} + \frac{v}{r}\,\frac{\partial u}{\partial \phi} - \frac{v^2}{r}\right) + w\,\frac{\partial u}{\partial z}$$

$$= -\frac{1}{4}K^2\lambda^{-1}Pr\,\frac{\partial p}{\partial r} + \left(\frac{1}{r^2}\frac{\partial^2 u}{\partial \phi^2} - \frac{2}{r^2}\,\frac{\partial v}{\partial \phi} + \frac{\partial^2 u}{\partial r^2} - \frac{u}{r^2} + \frac{1}{r}\,\frac{\partial u}{\partial r}\right)$$

$$+ 4Re^{-2}\,\frac{\partial^2 u}{\partial z^2} + \frac{1}{8}\,GrPr\theta \sin\phi \tag{51}$$

$\phi$-momentum equation

$$Pr^{-1}\left(u\frac{\partial v}{\partial r} + \frac{v}{r}\frac{\partial v}{\partial \phi} - \frac{uv}{r}\right) + w\frac{\partial v}{\partial z}$$

$$= -\frac{1}{4}K^2 - 1Pr\frac{1}{r}\frac{\partial p}{\partial \phi} + \left(\frac{v}{r^2} + \frac{1}{r^2}\frac{\partial^2 v}{\partial \phi^2} + \frac{2}{r^2}\frac{\partial u}{\partial \phi}\right)$$

$$+ 4Re^{-2}\frac{\partial^2 v}{\partial z^2} - \frac{1}{8}GrPr\theta\cos\phi \qquad (52)$$

$\Omega$-momentum equation

$$Pr^{-1}\left(u\frac{\partial w}{\partial r} + \frac{v}{r}\frac{\partial w}{\partial \phi}\right) + w\frac{\partial w}{\partial z}$$

$$= -\frac{\partial p}{\partial z} + \left(\frac{\partial^2 w}{\partial r^2} + \frac{1}{r}\frac{\partial w}{\partial r} + \frac{1}{r^2}\frac{\partial^2 w}{\partial \phi^2}\right)$$

$$+ 4Re^{-2}\frac{\partial^2 w}{\partial z^2} \qquad (53)$$

Energy equation

$$u\frac{\partial \theta}{\partial r} + \frac{v}{r}\frac{\partial \theta}{\partial \theta} + Pr\ w\frac{\partial \theta}{\partial z}$$

$$= \frac{\partial^2 \theta}{\partial r^2} + \frac{1}{r}\frac{\partial \theta}{\partial r} + \frac{1}{r^2}\frac{\partial^2 \theta}{\partial \phi^2} + 4Re^{-2}\frac{\partial^2 \theta}{\partial z^2} \qquad (54)$$

The problem now reduces to the combined free and forced convection problem in the hydrodynamically and thermally developing entrance region in a horizontal pipe. Some observations are of special

interest here. With buoyancy effects, the momentum and energy equations are coupled. The axial viscous terms $\partial^2 u/\partial z^2$, $\partial^2 v/\partial z^2$ and $\partial^2 w/\partial z^2$ and the axial conduction term $\partial^2\theta/\partial^2 z$ are negligible when the Reynolds number is large (say 100). The importance of the axial viscous terms is seen to depend on the magnitude of $Re^{-2}$. Of course in the neighbourhood of the hydrodynamic entrance ($R_c\Omega \simeq O[a]$), the second derivative terms mentioned cannot be neglected under any circumstance. In view of the practical importance of the entrance region problem, the case of $Pr \gg O[1]$ and $Re \gg O[1]$ is of special interest. For this case, the governing equations are seen to be of parabolic type and the lateral inertial terms involving $Pr^{-1}$ can be neglected. The Rayleigh number $Ra = GrPr$ becomes the only characteristic parameter remaining in the momentum equations. It is also seen that the axial momentum equation is independent of the momentum equations for secondary flow. Also, the continuity equation (50) can now be effectively split into two parts; one for the secondary flow, $\frac{\partial u}{\partial r} + \frac{u}{r} + \frac{1}{r}\frac{\partial v}{\partial \phi} = 0$, and another for the main flow in the integral form. Considering the importance and difficulty of solving of solving the general entrance region problem, the resulting simplified set of equations for $Pr \gg O[1]$ and $Re \gg O[1]$ is particularly noteworthy. The problem can be further simplified for the thermal entrance region problem where the flow field becomes fully developed with $\partial w/\partial z = 0$. In the energy equation, one sees that the advective terms cannot be neglected under any circumstances and must be retained.

An Order of Magnitude Analysis Considering the Axial Convective Term to be of Order Unity

The axial convective term in the energy equation is important both in the thermal entrance region and in the thermally fully developed region. Consequently the axial convective term may be considered to be of the same order of magnitude as the lateral conduction terms. This observation leads to equation (32) again and subsequently the governing equations (40) - (44) become:

Continuity equation

$$\frac{\partial u}{\partial r} + \frac{u}{r} + \frac{1}{r}\frac{\partial v}{\partial \phi} + \lambda\left(\frac{u \cos \phi}{(1 + \lambda r \cos \phi)} - \frac{v \sin \phi}{(1 + \lambda r \cos \phi)}\right)$$

$$+ \frac{1}{(1 + \lambda r \cos \phi)}\frac{\partial w}{\partial \omega_\theta} = 0 \qquad (55)$$

R-momentum equation

$$Pr^{-1}\left(u\frac{\partial u}{\partial r} + \frac{v}{r}\frac{\partial u}{\partial \phi} - \frac{v^2}{r} + \frac{1}{(1 + \lambda r \cos \phi)} w \frac{\partial u}{\partial \omega_\theta}\right)$$

$$= -\frac{\partial p}{\partial r} + \left(\frac{1}{r^2}\frac{\partial^2 u}{\partial \phi} - \frac{1}{r^2}\frac{\partial v}{\partial \phi} - \frac{1}{r}\frac{\partial^2 v}{\partial \phi \partial r}\right)$$

$$+ \lambda\frac{\sin \phi}{(1 + \lambda r \cos \phi)}\left(\frac{\partial v}{\partial r} + \frac{v}{r} - \frac{1}{r}\frac{\partial u}{\partial \phi}\right)$$

$$- 4K^{-2}Pr^{-2}\lambda \frac{1}{(1 + \lambda r \cos \phi)^2}\frac{\partial^2 u}{\partial \omega_\theta^2}$$

$$+ \frac{1}{(1 + \lambda r \cos \phi)} \frac{\partial^2 w}{\partial r \partial \omega_\theta} + \lambda \frac{\cos \phi}{(1 + \lambda r \cos \phi)^2} \frac{\partial w}{\partial \omega_\theta}$$

$$+ \frac{1}{4} K^2 Pr \frac{\cos \phi \, w^2}{(1 + \lambda r \cos \phi)} (1 - \frac{1}{2} GrFr \, \theta)$$

$$+ \frac{1}{8} GrPr \, \theta \sin \phi \qquad (56)$$

$\phi$-momentum equation

$$Pr^{-1}(u \frac{\partial v}{\partial r} + \frac{v}{r} \frac{\partial v}{\partial \phi} + \frac{uv}{r} + \frac{1}{(1 + \lambda r \cos \phi)} w \frac{\partial v}{\partial \omega_\theta})$$

$$= - \frac{1}{r} \frac{\partial p}{\partial \phi} + (\frac{\partial^2 v}{\partial r^2} + \frac{1}{r} \frac{\partial v}{\partial r} - \frac{v}{r^2} - \frac{1}{r} \frac{\partial^2 u}{\partial \phi \partial r} + \frac{1}{r^2} \frac{\partial u}{\partial \phi})$$

$$+ \lambda \frac{\cos \phi}{(1 + \lambda r \cos \phi)} (\frac{\partial v}{\partial r} + \frac{v}{r} - \frac{1}{r} \frac{\partial u}{\partial \phi})$$

$$+ 4K^{-2} Pr^{-2} \lambda \frac{1}{(1 + \lambda r \cos \phi)^2} \frac{\partial^2 v}{\partial \omega_\theta^2}$$

$$- \frac{1}{(1 + \lambda r \cos \phi) r} \frac{\partial^2 w}{\partial \phi \partial \omega_\theta} + \lambda \frac{\sin \phi}{(1 + \lambda r \cos \phi)^2} \frac{\partial w}{\partial \omega_\theta}$$

$$- \frac{1}{4} K^2 Pr \frac{\sin \phi \, w^2}{(1 + \lambda r \cos \phi)} (1 - \frac{1}{2} GrFr \, \theta)$$

$$- \frac{1}{8} GrPr \theta \cos \phi \qquad (57)$$

Ω-momentum equation

$$Pr^{-1}\left(u\frac{\partial w}{\partial r}+\frac{v}{r}\frac{\partial w}{\partial \phi}+\frac{1}{(1+\lambda r\cos\phi)}w\frac{\partial w}{\partial \omega_\theta}\right)$$

$$=-\frac{1}{(1+\lambda r\cos\phi)}\frac{\partial p}{\partial \omega_\theta}+\left(\frac{\partial^2 w}{\partial r^2}+\frac{1}{r}\frac{\partial w}{\partial r}+\frac{1}{r^2}\frac{\partial^2 w}{\partial \phi^2}\right)$$

$$+\lambda\left(\frac{\cos\phi}{(1+\lambda r\cos\phi)}\frac{\partial w}{\partial r}-\frac{\sin\phi}{(1+\lambda r\cos\phi)}\frac{1}{r}\frac{\partial w}{\partial \phi}\right)$$

$$-\lambda^2\frac{1}{(1+\lambda r\cos\phi)^2}w$$

$$-4K^{-2}Pr^{-2}\lambda\left\{\frac{1}{(1+\lambda r\cos\phi)^2}\frac{\partial^2 w}{\partial \omega_\theta^2}+2\lambda\left(\frac{\cos\phi}{(1+\lambda r\cos\phi)^2}\frac{\partial u}{\partial \omega_\theta}-\frac{\sin\phi}{(1+\lambda r\cos\phi)^2}\frac{\partial v}{\partial \omega_\theta}\right)\right\}$$

$$+\lambda\left(\frac{\sin\phi}{(1+\lambda r\cos\phi)}vw-\frac{\cos\phi}{(1+\lambda r\cos\phi)}uw\right) \qquad (58)$$

Energy equation

$$u\frac{\partial \theta}{\partial r}+\frac{v}{r}\frac{\partial \theta}{\partial \phi}+w\frac{\partial \theta}{\partial \omega_\theta}$$

$$=\frac{\partial^2\theta}{\partial r^2}+\frac{1}{r}\frac{\partial \theta}{\partial r}+\frac{1}{r^2}\frac{\partial^2\theta}{\partial \phi^2}$$

$$+\lambda\frac{1}{(1+\lambda r\cos\phi)}\left(\cos\phi\frac{\partial\theta}{\partial r}-\sin\phi\frac{1}{r}\frac{\partial\theta}{\partial r}\right)$$

$$+4K^{-2}Pr^{-2}\lambda\frac{1}{(1+\lambda r\cos\phi)^2}\frac{\partial^2\theta}{\partial \omega_\theta^2} \qquad (59)$$

It is seen again that the axial viscous and conduction terms may be neglected for the following conditions:

$$4K^{-2}Pr^{-2}\lambda << O[1] \tag{38}$$

It is useful to recall that $K^{-2}Pr^{-2} = Re^{-2}Pr^{2} = Pe^{-2}$ and that the criterion for the neglect of second derivative terms in the axial direction is identical to that for a straight tube. Generally, the present system of equations is similar to that of equations (45) - (49). It is again seen that the governing equations can be simplified considerably if $Pr >> O[1]$. However, it is worth noting that the assumption $Pr >> O[1]$ does not simplify the continuity equation (55) and the three momentum equations are coupled through the continuity equation, but have no inertia terms. The governing equations are valid for both hydrodynamically and thermally developing flow problems. Also the effect of curvature ratio $\lambda$ is clear.

For convenience, a summary of the results for the present deductive analysis is given in Table 2. The degree of difficulty involved in solving various possible systems of equations listed in Table 2 cannot be explained readily. However, considering the order of derivative in each space variable, one may say that the degree of difficulty in obtaining the solution increases in the order of the systems of equation indicated by broken lines, solid lines and finally those without markings. Generally, those systems of equations identified under the "Arbitrary" column for $K\lambda^{-1/2}$ are the most difficult to solve.

Table 2

A Possible Classification of Simultaneous Hydrodynamic and Thermal Entrance Region Problems in Curved and Straight Circular Pipes Considering Advective Terms due to Secondary Flow to be of Order Unity

| Pr | | Arbitrary Pr | | Pr >> O[1] | |
|---|---|---|---|---|---|
| | $\omega$ | 0 → $O[Re^{-2}]$ | | $O[Pr^{-1}]$ → | $O[Pr]$ |
| Axial inertia term to be unit order | $K\lambda^{-1/2}$ | Arbitrary | $K^2\lambda^{-1} = Re^2 >> O[1]$ | | |
| | Any $\lambda$ | Eqns. (45) (49) | No axial viscous and axial conduction terms | Two dimensional continuity eqn. and no lateral inertia term | |
| | $\lambda << O[1]$ | No $\lambda$ term but with centrifugal force term | | | |
| | $\lambda \to 0$ | Eqns. (50) (54) | | | |
| | $\omega_\theta$ | 0 → $O[Re^{-2}Pr^{-2}]$ → | | 0 → | $O[Pr^{-1}]$ |
| Axial convective terms to be unit order | $PrK\lambda^{-1/2}$ | Arbitrary | $Pr^2Re^2 = Pr^2K^2\lambda^{-1} >> O[1]$ | | |
| | Any $\lambda$ | Eqns. (55) (59) | No axial viscous and axial conduction terms | No equation | Three dimensional continuity eqn. and no inertia terms in momentum eqns. |
| | $\lambda << O[1]$ | No $\lambda$ term but with centrifugal force term | | | |
| | $\lambda \to 0$ | Straight pipe | | | |

## 2.5 SOME FURTHER REMARKS ON THE AXIAL VISCOUS AND CONDUCTION TERMS

As shown in the previous two sections, the axial viscous terms for the hydrodynamic entrance region problem and the axial conduction term for the thermal entrance region problem can be neglected under the conditions, $4K^{-2}\lambda = 4Re^{-2} << O[1]$ and $4K^{-2}Pr^{-2}\lambda = 4Pe^{-2} << O[1]$, respectively. These conditions are obtained by considering the axial inertia term and the axial convection term to be equally as important as the lateral viscous and conduction terms, respectively. The above two conditions reveal that the importance of axial momentum or thermal diffusion in curved pipes is exactly the same as that in straight pipes. Another analysis such as that shown in [95] for the Graetz problem reveals that near the discontinuity (thermal entrance), axial conduction dominates over the radial conduction. For the Graetz problem the role of the axial conduction term is now well understood. The role of the axial viscous term in the hydrodynamic entry flow problem is similar to that of the axial conduction term in thermal entry flow problems.

By comparing the magnitudes of the axial second derivative terms, one can obtain the additional conditions under which the axial viscous and conduction terms, respectively, can be neglected. The analysis (see equations (9) and (10) in Section 2.3) shows that the relative magnitude of the axial and lateral momentum or thermal diffusion depends only on the geometric ratio $\sigma^2 = (a/R_c\Omega_c)^2$ or the other geometric ratio $\sigma_\theta^2 = (a/R_c\Omega_{c\theta})^2$, respectively. Thus, for $(a/R_c\Omega)^2 << 1$ or equivalently $(a/R_c\Omega) < 1$, the axial momentum diffusion will be small relative to the radial momentum diffusion and can be neglected. Similarly,

for $(a/R_c\Omega_\theta) \ll 1$ or $(a/R_c\Omega_\theta) < 1$, the axial thermal diffusion terms may be neglected in comparison to the radial thermal diffusion terms. It is now clear that the relative importance of the axial momentum or thermal diffusion depends on the axial distance from the discontinuity or entrance point. For clarity, the general situation regarding the relative importance of axial momentum or thermal diffusion is illustrated in Fig. 6 for three kinds of entry flow problems. In region I, the axial momentum or thermal diffusion is more important than radial momentum or diffusion. In region II, the axial and radial momentum or thermal diffusion are comparable. In region III, the axial momentum or thermal diffusion is negligible in comparison to the radial direction. In region IV, the flow or thermal field becomes a fully developed one. For reference this region is identified and some further details will be given in Section 2.7.

Regarding the relationship between $\alpha = a/R_c\Omega$ and $\sigma_\theta = a/R_c\Omega_\theta$, a remark will be added next.

When one considers the momentum and energy equations separately (see equations (9) and (10)), both quantities $a/R_c\Omega$ and $a/R_c\Omega_\theta$ appear purely as geometric ratio. The thickness of the thermal boundary layer relative to the hydrodynamic boundary layer in the simultaneously developing flow field, depends on the magnitude of the Prandtl number. Some indication of the relationship between velocity and temperature fields may be obtained by equating $\sigma$ and $\sigma_\theta$ from equations (12) and (32), respectively. The result is $R_c\Omega_c = R_c\Omega_{c\theta}Pr^{-1}$. Attention is now given to case (3) of Fig. 6 for the simultaneous development of velocity

(1) Hydrodynamic entrance region problem

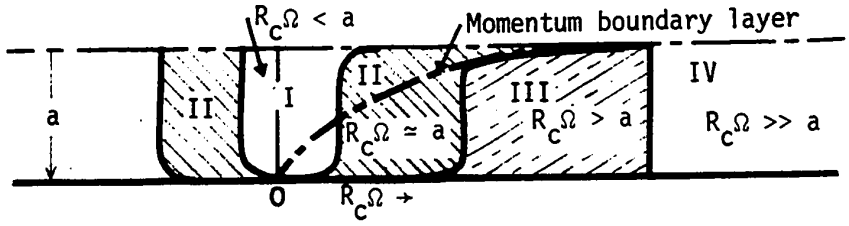


(2) Thermal entrance (Graetz) problem

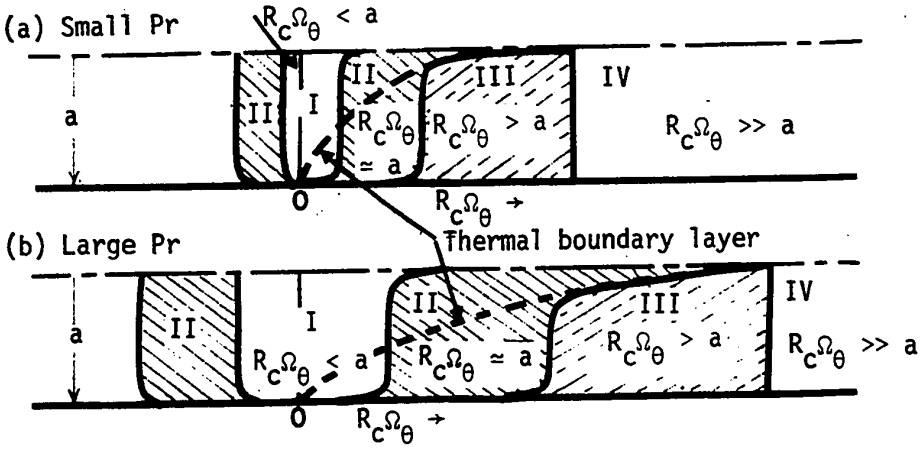


(3) Simultaneous hydrodynamic and thermal entrance problem

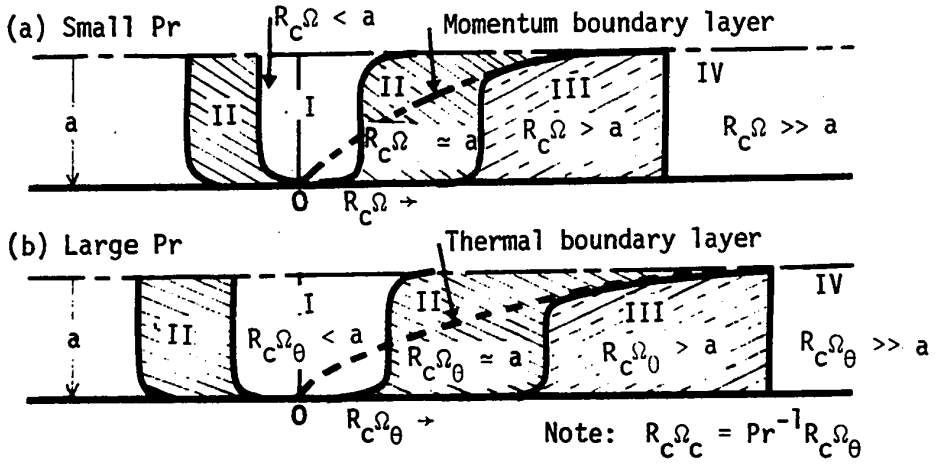


Fig. 6 Relative Importance of Axial and Radial Momentum or Thermal Diffusion for Three Entry Flow Problems.

and temperature fields. When the Prandtl number is small, the relative importance of the axial second derivative terms with respect to the lateral second derivative terms depends on the geometric ratio $a/R_c\Omega$. This observation is based on a slower development of the velocity field in comparison with the thermal field. The situation is seen to be similar to Case (1) shown in Fig. 6. On the other hand, when the Prandtl number is large, the relative significance of axial momentum or thermal diffusion with respect to the transverse one depends on the geometric ratio $a/R_c\Omega_\theta$. In view of the relationship $R_c\Omega_c = R_c\Omega_{c\theta}Pr^{-1}$, the length of the specific region I, II, or III may actually become longer than that for the hydrodynamic entrance problem shown as Case (1) in Fig. 6.

When the two criteria, $4Re << O[1]$ and $4Pe^{-2} << O[1]$, given earlier for assessing the importance of the axial momentum or thermal diffusion in comparison to the radial one contradict each other or do not agree, then one must check whether or not the length scales used are proper in carrying out the particular normalization procedure.

It is significant to note that one analysis provides the restrictions on Reynolds and Peclet numbers under which the axial momentum and thermal diffusions, respectively, can be neglected. This is in contrast with the result of another analysis where the restriction is mainly on geometric ratio $a/R_c\Omega$ or $a/R_c\Omega_\theta$ depending on whether the emphasis is on the hydrodynamic or thermal entrance problem. Apparently, the two analyses complement each other.

## 2.6 A DEDUCTIVE ANALYSIS OF FUNDAMENTAL EQUATIONS GOVERNING LAMINAR FLOW AND HEAT TRANSFER IN CURVED RECTANGULAR CHANNELS

A study of the basic equations for flow and heat transfer in curved rectangular channels similar to that reported in earlier sections for curved circular pipes is also possible. However, for the present problem the aspect ratio of the rectangular cross-section appears as an additional parameter. For reference purposes, the basic equations for curved rectangular channels are given in Appendix 3, and the results of a deductive analysis are listed in Appendix 4.

## 2.7 BASIC EQUATIONS FOR THE GRAETZ PROBLEM IN CURVED PIPES OR CHANNELS

In this investigation the Graetz problem in curved pipes and its asymptotic case of thermally fully developed conditions will be studied in detail. The basic equations for the general problem of hydrodynamically and thermally developing flow in curved pipes or channels have been studied in some detail in earlier sections. In order to gain a clearer physical understanding and for convenience in later use, the basic equations for the special case of the thermal entrance region problem will be studied in some detail. It should be pointed out that no theoretical analysis for hydrodynamic entrance flow in curved pipes or channels is available at present in literature. The basic equations for a hydrodynamically fully developed flow can be obtained by noting that the velocity components are independent of the axial coordinate. The above statement also corresponds to the case with a very small entrance length geometric ratio $\sigma <<< O[1]$. Curved rectangular channels

will be considered first. At this point, it is recalled that two sets of formulation are possible depending on whether the centrifugal force term in the normalized momentum equation is regarded to be of unit order of magnitude or whether the convective terms due to secondary flow in the normalized energy equation are considered to be of unit order of magnitude.

Basic Equations for Curved Rectangular Channels With the Centrifugal Force Term Considered to be of Order Unity

For simplicity the case of curved square channels ($\gamma = 1$) will be considered here. This effectively eliminates the aspect ratio effect. For the hydrodynamically fully developed flow with aspect ratio $\gamma = 1$, the basic equations (A - 27) to (A - 31) become

$$\frac{\partial u}{\partial x} + \lambda \frac{u}{(1 + \lambda x)} + \frac{\partial v}{\partial y} = 0 \tag{60}$$

x-momentum equation

$$K^2 \frac{1}{4} \left(u \frac{\partial u}{\partial x} + v \frac{\partial u}{\partial y}\right)$$

$$= \left[\frac{P_c}{\rho w_c^2} \lambda^{-1}\right] \frac{\partial p}{\partial x} + \left(\frac{\partial^2 u}{\partial y^2} - \frac{\partial^2 v}{\partial x \partial y}\right) + \frac{w^2}{(1 + \lambda x)} \tag{61}$$

y-momentum equation

$$K^2 \frac{1}{4} \left(u \frac{\partial v}{\partial x} + v \frac{\partial v}{\partial y}\right)$$

$$= \left[\frac{P_c}{\rho w_c^2}\lambda^{-1}\right]\frac{\partial p}{\partial y} + \left(\frac{\partial^2 v}{\partial x^2} - \frac{\partial^2 u}{\partial x \partial y} - \frac{\lambda}{(1+\lambda x)}\frac{\partial u}{\partial y}\right.$$

$$\left. + \frac{\lambda}{(1+\lambda x)}\frac{\partial v}{\partial x}\right) + \frac{1}{4}\,Gr K^{-2}\theta \qquad (62)$$

Ω-momentum equation

$$K^2\,\frac{1}{4}\left(u\frac{\partial w}{\partial x} + v\frac{\partial w}{\partial y}\right)$$

$$= \left[\frac{P_c}{\rho w_c^2}\sigma\right]\frac{\partial p}{\partial \omega} + \left(\frac{\partial^2 w}{\partial x^2} + \frac{\lambda}{(1+\lambda x)}\frac{\partial w}{\partial x}\right.$$

$$\left. - \frac{\lambda^2}{(1+\lambda x)}w + \frac{\partial^2 w}{\partial y^2}\right) - \frac{K^2}{4}\frac{\lambda}{(1+\lambda x)}uw \qquad (63)$$

Energy equation

$$K^2 Pr\,\frac{1}{4}\left(u\frac{\partial \theta}{\partial x} + v\frac{\partial \theta}{\partial y}\right) + KPr^{-1/2}\,\frac{w}{2(1+\lambda x)}\frac{\partial \theta}{\partial \omega}$$

$$= \frac{\partial^2 \theta}{\partial x^2} + \frac{\lambda}{(1+\lambda x)}\frac{\partial \theta}{\partial x} + \frac{\partial^2 \theta}{\partial y^2} + \sigma\,\frac{\lambda}{(1+\lambda x)}\,w\,\frac{\partial^2 \theta}{\partial \omega^2} \qquad (64)$$

It is of interest to note that Truesdell [35] treated the fully developed laminar flow in curved pipes by using a set of equations similar to equations (60) through (63). The above set of equations suggests that the inertia terms in the momentum equations may be neglected if $K \leq O[10^{-1}]$.

The two basic thermal boundary conditions of uniform wall

heat flux and uniform wall temperature are of interest for reference purposes. For the limiting case of a thermally fully developed flow, the energy equation for uniform wall heat flux becomes

$$K^2Pr\,\frac{1}{4}\left(u\,\frac{\partial\theta}{\partial x}+v\,\frac{\partial\theta}{\partial y}\right)+KPr\lambda^{-1/2}\,\frac{w}{2(1+\lambda x)}\,C$$

$$=\frac{\partial^2\theta}{\partial x^2}+\frac{\lambda}{(1+\lambda x)}\,\frac{\partial\theta}{\partial x}+\frac{\partial^2\theta}{\partial y^2} \qquad (65)$$

where $$\theta=\frac{k}{q_w a}\,(T-T_0) \qquad (66)$$

and $$C=\sigma\,\frac{\partial\theta}{\partial\omega}=\text{constant} \qquad (67)$$

and $q_w$ is the uniform wall heat flux. It is noted that with the uniform wall heat flux condition, the axial conduction term vanishes from the energy equation for thermally developed flow.

For a uniform wall temperature, the energy equation for thermally fully developed flow becomes

$$K^2Pr\,\frac{1}{4}\left(u\,\frac{\partial\theta}{\partial x}+v\,\frac{\partial\theta}{\partial y}\right)+KPr\lambda^{-1/2}\;\frac{w}{2}\,\frac{\theta}{\theta_b}\,\frac{\partial\theta_b}{\partial\omega}$$

$$=\frac{\partial^2\theta}{\partial x^2}+\frac{\lambda}{(1+\lambda x)}\,\frac{\partial\theta}{\partial x}+\frac{\partial^2\theta}{\partial y^2}+\lambda\sigma w\,\frac{\theta}{\theta_b}\,\frac{\partial^2\theta_b}{\partial\omega^2} \qquad (68)$$

where $$\theta=\frac{(T_w-T)}{(T_w-T_0)},\quad \theta_b=\frac{(T_w-T_b)}{(T_w-T_0)} \qquad (69)$$

$T_w$ = uniform wall temperature,

$T_b$ = bulk temperature, and

$T_0$ = uniform entrance temperature.

It is noted that the terms $\partial\theta/\partial\omega$ and $\partial^2\theta/\partial\omega^2$ vanish for fully developed thermal field and do not appear in equation (68). For the condition of uniform wall temperature, the terms with $\partial\theta_b/\partial\omega$ and $\partial^2\theta_b/\partial\omega^2$ do not vanish and are not known in advance. In this connection, Maekawa's method of solution [64] for the thermally fully developed flow with a uniform wall temperature is noteworthy. His method of solution is in contrast to the usual trial-and-error solution required for the case of uniform wall temperature. The details of the method can be found in [64]. The other possibility for normalizing the basic equations will be considered next.

Basic Equations for Curved Rectangular Channels With the Convective Terms in the Energy Equations Due to Secondary Flow Considered to be of Order Unity

For simplicity, a small curvature ratio $\lambda \ll O[1]$ and negligible free convection effects ($Gr \ll K^2$) for fully developed laminar flow in a curved square channel will be considered. Using equations (A - 32) to (A - 36) and applying the stated assumptions, the following normalized governing equations can be obtained after eliminating the pressure terms in the momentum equations for secondary flow. The momentum equation for secondary flow becomes

$$\frac{1}{Pr}\left(\frac{\partial\Psi}{\partial y}\frac{\partial\zeta}{\partial x} - \frac{\partial\Psi}{\partial x}\frac{\partial\zeta}{\partial y}\right) = \nabla_{x,y}^{2}\zeta + \frac{1}{4}K^{2}Pr\ 2w\frac{\partial w}{\partial y} \tag{70}$$

where $$u = \frac{\partial\Psi}{\partial y} \quad \text{and} \quad v = -\frac{\partial\Psi}{\partial x} \tag{71}$$

Vorticity equation

$$\zeta = \nabla_{x,y}^{2} \tag{72}$$

Axial momentum equation

$$\frac{1}{Pr}\left(\frac{\partial\Psi}{\partial y}\frac{\partial w}{x} - \frac{\partial\Psi}{x}\frac{\partial w}{y}\right) = \nabla_{x,y}^{2}\ w - \left[\frac{P_c}{\rho w_c^{2}}\frac{1}{Pr}\right]\frac{\partial p}{\partial\omega} \tag{73}$$

Energy equation

$$\left(\frac{\partial\Psi}{\partial y}\frac{\partial}{\partial x} - \frac{\partial\Psi}{\partial x}\frac{\partial\theta}{\partial y}\right) + w\frac{\partial\theta}{\partial\omega} = \nabla_{x,y}^{2}\theta \tag{74}$$

Cheng and Akiyama [78] solved numerically the above set of equations (70) to (74) for the asymptotic case of thermally fully developed flow in curved rectangular channels with various aspect ratios subjected to an axially uniform wall heat flux. The above formulation reveals that when the Prandtl number is large, say $Pr \geq O[10^2]$, the only parameter appearing in the normalized equations is $K^2Pr$ and the inertia terms (non-linear terms) in the momentum equations may be neglected. When the Prandtl number is large, considerable simplifications are possible and the resulting set of equations will be listed below for reference purposes.

Momentum equation for secondary flow

$$0 = \nabla_{x,y}^2 \zeta + \frac{1}{2} K^2 Pr \, w \frac{\partial w}{\partial y} \tag{75}$$

Vorticity equation

$$\zeta = \nabla_{x,y}^2 \tag{72}$$

Axial momentum equation

$$0 = -\left[\frac{P_c}{\rho w_c^2} \frac{1}{Pr}\right] \frac{\partial p}{\partial \omega} + \nabla_{x,y}^2 w \tag{76}$$

Energy equation

$$\left(\frac{\partial \Psi}{\partial y} \frac{\partial \theta}{\partial x} - \frac{\partial \Psi}{\partial x} \frac{\partial \theta}{\partial y}\right) + w \frac{\partial \theta}{\partial \omega} = \nabla_{x,y}^2 \tag{74}$$

It is observed that the above set of equations is valid regardless of the order of magnitude of the Dean number K. Furthermore, the secondary flow cannot be regarded as a creeping flow since the inertia term, in the form of a centrifugal force term, is included in the momentum equation for secondary flow.

Since curved circular pipes will be studied in detail in this thesis, it is convenient to list also the normalized basic equations in cylindrical toroidal coordinates. For a hydrodynamically fully developed flow, the basic equations (40) to (44) for curved pipes, where the convective terms in the energy equation are considered to be of unit order, become

Continuity equation

$$\frac{\partial u}{\partial r} + \frac{u}{r} + \frac{1}{r}\frac{\partial v}{\partial \phi} + \frac{\lambda}{(1 + \lambda r \cos \phi)}(u \cos\phi - v \sin\phi) = 0 \qquad (77)$$

R-momentum equation

$$Pr^{-1}\left(u\frac{\partial u}{\partial r} + \frac{v}{r}\frac{\partial u}{\partial \phi} - \frac{v^2}{r}\right)$$

$$= -2K^{-1}\lambda^{-1/2}\sigma^{-1}\frac{\partial p}{\partial r} + \left(\frac{1}{r^2}\frac{\partial^2 u}{\partial \phi^2} - \frac{1}{r^2}\frac{\partial v}{\partial \phi} - \frac{1}{r}\frac{\partial^2 v}{\partial \phi \partial r}\right)$$

$$+ \lambda\frac{\sin \phi}{(1 + \lambda r \cos \phi)}\left(\frac{\partial v}{\partial r} + \frac{v}{r} - \frac{1}{r}\frac{\partial u}{\partial \phi}\right)$$

$$+ \frac{1}{4}K^2 Pr \frac{\cos \phi}{(1 + \lambda r \cos \phi)}\{1 - \frac{1}{2}GrK^{-2}Pr^{-1}Fr\}$$

$$+ \frac{1}{8}GrPr\theta \sin \phi \qquad (78)$$

$\phi$-momentum equation

$$Pr^{-1}\left(u\frac{\partial v}{\partial r} + \frac{v}{r}\frac{\partial v}{\partial \phi} + \frac{uv}{r}\right)$$

$$= -2K^{-1}\lambda^{-1/2}\sigma^{-1}\frac{1}{r}\frac{\partial p}{\partial \phi} + \left(\frac{\partial^2 v}{\partial r^2} + \frac{1}{r}\frac{\partial v}{\partial r} - \frac{v}{r^2} - \frac{1}{r}\frac{\partial^2 u}{\partial \phi \partial r} + \frac{1}{r^2}\frac{\partial u}{\partial \phi}\right)$$

$$+ \frac{\lambda}{(1 + \lambda r \cos \phi)}\cos \phi\left(\frac{\partial v}{\partial r} + \frac{v}{r} - \frac{1}{r}\frac{\partial u}{\partial \phi}\right)$$

$$- \frac{1}{4} K^2 Pr \frac{\sin \phi \, w^2}{(1 + \lambda r \cos \phi)} \{1 - \frac{1}{2} GrK^{-2} Pr^{-1} Fr\}$$

$$- \frac{1}{8} GrPr \cos \phi \, \theta \tag{79}$$

Ω-momentum equation

$$Pr^{-1}(u \frac{\partial w}{\partial r} + \frac{v}{r} \frac{\partial w}{\partial \phi})$$

$$= - \frac{1}{(1 + \lambda r \cos \phi)} \frac{\partial p}{\partial \omega} + (\frac{\partial^2 w}{\partial r^2} + \frac{1}{r} \frac{\partial w}{\partial r} + \frac{1}{r^2} \frac{\partial^2 w}{\partial \phi^2})$$

$$+ \frac{\lambda}{(1 + \lambda r \cos \phi)} (\cos \phi \frac{\partial w}{\partial r} - \sin \phi \frac{1}{r} \frac{\partial w}{\partial \phi})$$

$$- \frac{\lambda^2}{(1 + \lambda r \cos \phi)^2} w$$

$$+ Pr^{-1} \frac{\lambda}{(1 + \lambda r \cos \phi)} (\sin \phi \, vw - \cos \phi \, uw) \tag{80}$$

Energy equation

$$u \frac{\partial \theta}{\partial r} + \frac{v}{r} \frac{\partial \theta}{\partial r} + \frac{1}{2} KPr\sigma_\theta \lambda^{-1/2} \frac{w}{(1 + \lambda r \cos \phi)} \frac{\partial \theta}{\partial \omega_\theta}$$

$$= \frac{\partial^2 \theta}{\partial r^2} + \frac{1}{r} \frac{\partial \theta}{\partial r} + \frac{1}{r^2} \frac{\partial^2 \theta}{\partial \phi^2} + \frac{\lambda}{(1 + \lambda r \cos \phi)} (\cos \phi \frac{\partial \theta}{\partial r} - \sin \phi \frac{1}{r} \frac{\partial \theta}{\partial \phi})$$

$$+ \sigma_\theta^2 \frac{1}{(1 + \lambda r \cos \phi)^2} \frac{\partial^2 \theta}{\partial \omega_\theta^2} \tag{81}$$

The above set of equations, which take the curvature ratio effect ($\lambda$) into consideration, was first derived by Dean [12] for the flow problem only, and recently Kalb and Seader [87] used a similar set of equations for solving the thermally fully developed convective heat transfer problem in curved circular tubes with buoyant force effects omitted. Assuming that $\lambda \ll O[1]$, the set of equations becomes:

Continuity equation

$$\frac{\partial u}{\partial r} + \frac{u}{r} + \frac{1}{r}\frac{\partial v}{\partial \phi} = 0 \tag{82}$$

R-momentum equation

$$Pr^{-1}\left(u\frac{\partial u}{\partial r} + \frac{v}{r}\frac{\partial u}{\partial \phi} - \frac{v^2}{r}\right)$$

$$= -2K^{-2}\lambda^{-1/2}\sigma^{-1}\frac{\partial p}{\partial r} + \left(\frac{1}{r^2}\frac{\partial^2 u}{\partial \phi^2} - \frac{1}{r^2}\frac{\partial v}{\partial \phi} - \frac{1}{r}\frac{\partial^2 v}{\partial \phi \partial r}\right)$$

$$+ \frac{1}{4}K^2 Pr \cos\phi\, w^2 \left\{1 - \frac{1}{2}GrK^{-2}Pr^{-1}Fr\right\}$$

$$+ \frac{1}{8}GrPr\theta \sin\phi \tag{83}$$

$\phi$-momentum equation

$$Pr^{-1}\left(u\frac{\partial v}{\partial r} + \frac{v}{r}\frac{\partial v}{\partial \phi} + \frac{uv}{r}\right)$$

$$= -2K^{-2}\lambda^{-1/2}\sigma^{-1}\frac{1}{r}\frac{\partial p}{\partial \phi} + \left(\frac{\partial^2 v}{\partial r^2} + \frac{1}{r}\frac{\partial v}{\partial r} - \frac{v}{r^2} - \frac{1}{r}\frac{\partial^2 u}{\partial \phi \partial r} + \frac{1}{r^2}\frac{\partial u}{\partial \phi}\right)$$

$$-\frac{1}{4}K^2 Pr \sin\phi\, w^2 \left\{1 + \frac{1}{2}GrK^{-2}Pr^{-1}Fr_c\right\}$$

$$-\frac{1}{8}GrPr\theta\cos\phi \qquad (84)$$

$\Omega$-momentum equation

$$Pr^{-1}\left(u\frac{\partial w}{\partial r} + \frac{v}{r}\frac{\partial w}{\partial \phi}\right)$$

$$= -\frac{\partial p}{\partial \omega} + \left(\frac{\partial^2 w}{\partial r^2} + \frac{1}{r}\frac{\partial w}{\partial r} + \frac{1}{r^2}\frac{\partial^2 w}{\partial \phi^2}\right) \qquad (85)$$

Energy equation

$$u\frac{\partial \theta}{\partial r} + \frac{v}{r}\frac{\partial \theta}{\partial r} + \frac{1}{2}KPr\sigma_\theta\lambda^{-1/2}\, w\frac{\partial \theta}{\partial \omega_\theta} = \frac{\partial^2 \theta}{\partial r^2} + \frac{1}{r}\frac{\partial \theta}{\partial r} + \frac{1}{r^2}\frac{\partial^2 \theta}{\partial \phi^2}$$

$$+ \sigma_\theta^2 \frac{\partial^2 \theta}{\partial \omega_\theta} \tag{86}$$

The above momentum equations without the terms involving Gr were first derived and solved by Dean [12,13] using a perturbation method. It is interesting to observe that the perturbation method used by Dean is similar to that used by Morton [4] in solving combined forced and free convection for laminar flow in horizontal tubes with uniform heat flux at low Rayleigh numbers. Apparently Morton [14] was not aware of the similarity between the secondary flow caused by centrifugal forces in curved pipes and the secondary flow caused by buoyancy forces in horizontal pipes. Dean's formulation for curved pipe flow is a standard one and subsequently has been employed by many investigators. The above set of equations without free convection effects will be solved by numerical methods in Chapters III, IV and V for thermally fully developed flows and for the Graetz problem in curved pipes.

As pointed out earlier, a large Prandtl number is of special interest because it is of practical importance as well as resulting in a simplified set of equations. With Pr >> O[1], one obtains

Continuity equation

$$\frac{\partial u}{\partial r} + \frac{u}{r} + \frac{1}{r} \frac{\partial v}{\partial \phi} = 0 \tag{82}$$

R-momentum equation

$$0 = - 2K^{-1}\lambda^{-1/2}\sigma^{-1} \frac{\partial p}{\partial r} + \left(\frac{1}{r^2} \frac{\partial^2 u}{\partial \phi^2} - \frac{1}{r^2} \frac{\partial v}{\partial \phi} - \frac{1}{r} \frac{\partial^2 v}{\partial \phi \partial r}\right)$$

$$+ \frac{1}{4} K^2 Pr \cos \phi \, w^2 \{1 - \frac{1}{2} GrK^{-2}Pr^{-1}Fr\}$$

$$+ \frac{1}{8} GrPr\theta \sin \phi \qquad (87)$$

$\phi$-momentum equation

$$0 = - 2K^{-2}\lambda^{-1/2}\sigma^{-1} \frac{1}{r} \frac{\partial p}{\partial \phi} + (\frac{\partial^2 v}{\partial r^2} + \frac{1}{r} \frac{\partial v}{\partial r} - \frac{v}{r^2} - \frac{1}{r} \frac{\partial^2 u}{\partial \phi \partial r} + \frac{1}{r^2} \frac{\partial u}{\partial \phi})$$

$$- \frac{1}{4} K^2 Pr \sin \phi \, w^2 \{1 - \frac{1}{2} GrK^{-2}Pr^{-1}Fr\}$$

$$- \frac{1}{8} GrPr\theta \cos \phi \qquad (88)$$

Energy equation

$$u \frac{\partial \theta}{\partial r} + \frac{v}{r} \frac{\partial \theta}{\partial r} + \frac{1}{2} KPr\sigma_\theta \lambda^{-1/2} w \frac{\partial \theta}{\partial \omega_\theta}$$

$$= \frac{\partial^2 \theta}{\partial r^2} + \frac{1}{r} \frac{\partial \theta}{\partial r} + \frac{1}{r^2} \frac{\partial^2 \theta}{\partial \phi^2} + \sigma_\theta^2 \frac{\partial^2 \theta}{\partial \omega_\theta} \qquad (86)$$

It is seen $K^2Pr$ is the only characteristic parameter in the normalized equations when (1/8)GrPr and GrFr $<<$ O[1]. The above formulation is valid regardless of the value of the Dean number K. An examination of the above set of equations reveals that the Graetz problem in curved pipes with significant free convection effects can be approached at least by a numerical method. This observation for large Prandtl number fluids in curved pipes is believed to be significant since the problem now becomes tractable.

## 2.8 SOME CONSIDERATIONS OF PITCH EFFECTS IN HELICAL PIPES

Curved pipes are usually used in the form of helices and flat spirals and for simplicity only helical coils will be considered here. Consideration is now given to a helical tube with its center line in the form of a circular helix obtained by winding a tube around a circular cylinder with a constant pitch as shown in Fig. 7. For this configuration the perpendicular distance from the cylinder axis to the tube center line is a constant $R_c$. Geometrical restrictions require that the pitch h must be at least equal or greater than the outside diameter of the tube. Due to the pitch effect, one sees clearly that the tube center line is inclined to the horizontal plane and the radius of curvature at any point on the helical center line will deviate from $R_c$ and becomes $R_c + (1/R_c)\,(h/2\pi)^2$. The latter aspect of the pitch effects was discussed briefly by Truesdell and Adler [35] and in some detail by Truesdell [35].

Geometrically, a helical pipe is generated by translating a circle along and normal to a circular helix. Thus, a point in the tube cross-section at a distance $R_c + X$ from the helical axis has a radius of curvature $(R_c + X) + (1/R_c + X)\,(h/2\pi)^2$. Under the conditions that h is small in comparison to the helical circumference $(2\pi R_c)$ and $R_c >> X$ or equivalently $R_c >> a$, the radius of curvature at any point in the cross-section of the tube may be approximated very closely by $R_c + X + (1/R_c)\,(h/2\pi)^2$. The basic equations for flow and heat transfer discussed in this chapter can be modified to take the above effect into consideration. However, one should note that for helical pipes

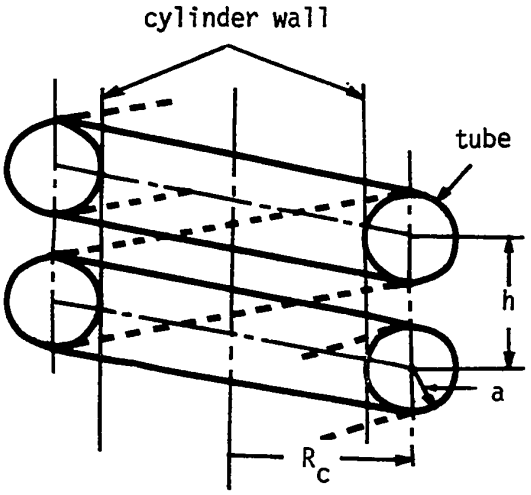


Fig. 7 Helical Tube

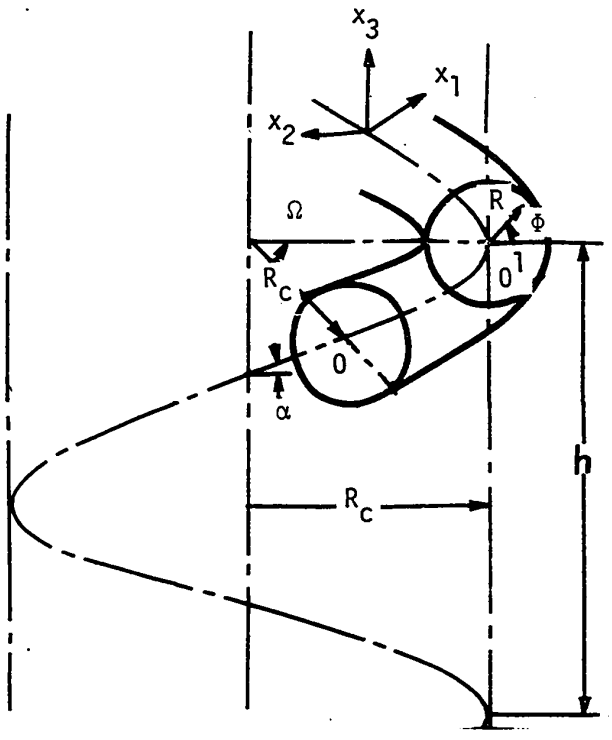


Fig. 8 A Coordinate System for Helical Tubes

the centrifugal forces cease to act solely in the plane of the cross-section normal to the circular helix or pipe center line. This fact will be elaborated further.

Every point in the cross-sectional plane of the helical pipe circumscribes a helix with the same central axis. The radii of curvature of all the points in the cross-section intersect the common helical axis and are perpendicular to the helical axis. One also observes that the tangents to a helix make a fixed angle with the axis of the helix and the pricipal normal is perpendicular to the axis of the helix. Furthermore, the inclination of the pipe cross-section with respect to the helical axis leads to the radii of curvature forming a set of skewlines intersecting and perpendicular to the helical axis. It is noted that only points on the diameter containing the radius of curvature of the pipe center line have radii of curvature solely in the plane of the cross-section. It is now obvious that the centrifugal forces will not act solely in the plane of the pipe cross-section. Excluding the points on the diameter containing the radius of curvature of the pipe center line, the centrifugal forces acting at any point on the cross-sectional plane will have components also in the direction of main flow. As pointed out by Truesdell [35], these centrifugal forces generally tend to enhance the downstream velocity in one half of the cross-section and hinder the velocities in the other half, thus completely destroying the symmetry with respect to the center line diameter. Truesdell [35] further explains this effect in some detail by using experimental information obtained by dye injection

into helical systems. This aspect of the pitch effects is now clear but is expected to introduce the additional complexity in the theoretical analysis.

To pursue this subject further, some geometrical relationships for helically couled pipes considered in this section will be given next. Referring to the Cartesian coordinates $(X_1, X_2, X_3)$ and the helical coordinate system $(R, \Phi, \Omega)$, one obtains the following relationships (see Fig. 8),

$$X_1 = \sigma \cos \alpha \cos \Phi + R_c(\cos \Omega \cos \Phi + \sin \Omega \sin \theta \sin \alpha)$$

$$X_2 = \sigma \cos \alpha \sin \Phi + R_c(\cos \Omega \sin \Phi - \sin \Omega \cos \theta \sin \alpha)$$

$$X_3 = \sigma \sin \alpha \cdot \Phi + R_c \sin \Phi \cos \alpha$$

where $2\pi R_c = \sigma \cos \alpha$, $2\pi C = h = \sigma \sin \alpha$, $\sigma = (R_c^2 + C^2)^{1/2}$, $\alpha$ = pitch angle and $h$ = pitch. Using the above relations, the metric coefficients $h_1, h_2, h_3$ can be obtained and are given below for future reference.

$$h_1 = \{[\frac{\partial}{\partial R}(\sigma \cos \alpha \cos \Phi + R_c(\cos \Omega \cos \Phi + \sin \Omega \sin \theta \sin \alpha))]^2 + [\frac{\partial}{R}(\sigma \cos \alpha \sin \Phi + R_c(\cos \Omega \sin \Phi - \sin \Omega \cos \theta \sin \alpha))]^2 + [\frac{\partial}{\partial R}(\sigma \sin \alpha \cdot \Phi + R_c \sin \Phi \cos \alpha)]^2\}^{1/2}$$

$$h_2 = \left[\frac{\partial}{\partial \Phi}\left(\sigma \cos\alpha \cos\Phi + R_c(\cos\Omega \cos\Phi + \sin\Omega \sin\theta \sin\alpha)\right)\right]^2$$
$$+ \left[\frac{\partial}{\partial \Phi}\left(\sigma \cos\alpha \sin\Phi + R_c(\cos\Omega \sin\Phi - \sin\Omega \cos\theta \sin\alpha)\right)\right]^2$$
$$+ \left[\frac{\partial}{\partial \Phi}\left(\sigma \sin\alpha \cdot \Phi + R_c \sin\Phi \cos\alpha\right)\right]^2\Big\}^{1/2} \qquad (89)$$

$$h_3 = \left[\frac{\partial}{\partial \Omega}\left(\sigma \cos\alpha \cos\Phi + R_c(\cos\Omega \cos\Phi + \sin\Omega \sin\theta \sin\alpha)\right)\right]^2$$
$$+ \left[\frac{\partial}{\partial \Omega}\left(\sigma \cos\alpha \sin\Phi + R_c(\cos\Omega \sin\Phi - \sin\Omega \cos\theta \sin\alpha)\right)\right]^2$$
$$+ \left[\frac{\partial}{\partial \Omega}\left(\sigma \sin\alpha \cdot \Phi + R_c \sin\Phi \cos\alpha\right)\right]^2\Big\}^{1/2}$$

The resulting rather lengthy expressions for $h_1$, $h_2$, $h_3$ discourage one to obtain a set of general governing equations for flow and heat transfer in helical pipes taking pitch effects into account. However, it is worth noting that the additional geometrical parameters $\sigma$ and $\alpha$ appear. In view of the fact that in most practical applications the helices would be closely wound and fabrication and experimental errors may arise, the additional effort required in considering the pitch effects may not be warranted under certain circumstances.

Disregarding the unsymmetric effect due to the components of the centrifugal forces in the main flow direction, one may consider two additional factors resulting from the pitch effects of helically coiled pipes. It has already been shown that the radius of curvature of any point on the helical center line becomes $R_c + (1/R_c)\ (h/2\pi)^2$ where the increment from $R_c$ is caused by the angle of inclination. This increase of the radius of curvature is one factor. Another factor is the inclination angle itself and it becomes important when the effects

due to other body forces such as buoyancy forces become significant. An attempt will be made first to assess the effect due to the increase of radius of curvature on the helical center line. Referring to Fig. 9, one readily obtains the following relationship:

$$L = [(2\pi R_c)^2 + h^2]^{1/2} \tag{90}$$

One may now define the effective radius of curvature as

$$R_L = \frac{L}{2\pi} = R_c\left[1 + \left(\frac{h}{2\pi R_c}\right)^2\right]^{1/2} \tag{91}$$

It is useful to consider the ratio $R_L/R_c$ in evaluating the effective increase of the radius of curvature of the helical center line. The result is

$$\frac{R_L}{R_c} = \left[1 + \left(\frac{h}{2\pi R_c}\right)^2\right]^{1/2} \tag{92}$$

In most practical cases one has $R_c > h$. However, we must also consider the case $R_c = h$ in order to gain some idea about the ratio $R_L/R_c$. With $R_c = h$, one has $R_L/R_c = 1.0126$. It is now seen that the difference between $R_L$ and $R_c$ is less than 1.3 per cent and one may conclude that as far as this aspect of the pitch effect is concerned the formulation based on the torus coordinates should provide reasonable accuracy. However, one may wish to use the following expression for the effective radius of curvature, $R_L$, instead of $R_c$ in evaluating the flow and heat transfer characteristics in helically coiled pipes.

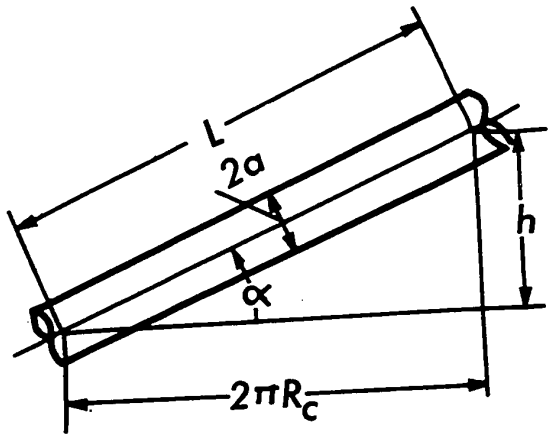


Fig. 9 Expanded view of Helical Pipe on a Plane

$$R_L = R_c \left[1 + \left(\frac{h}{2\pi R_c}\right)^2\right]^{1/2} \doteq R_c \left[1 + \frac{1}{8\pi^2}\left(\frac{h}{R_c}\right)^2\right] \qquad (93)$$

The above expression is reasonably accurate when the pitch h is small in comparison to $R_c$ and when $R_c >> a$. It should be pointed out that the above suggested correction is based purely on effective radius of curvature and does not take other factors into consideration.

Referring to Fig. 9, the inclination angle is found to be $\alpha = \tan^{-1}(h/2\pi R_c)$. When the buoyancy force effects become significant, the inclination angle effect must be assessed. In the formulation, the buoyancy force effects can be readily included by adding the terms listed in Table 3 to the respective momentum equation as noted.

Table 3

Buoyant Force Terms with Helix Effect

| | Equation No. | Plane Torus | With Helix Effect |
|---|---|---|---|
| Circular Pipe | R-Mom. (A-10) | $-\beta g(T-T_w)\sin\Phi$ | $-\beta g(T-T_w)\sin\Phi\cos\alpha$ |
| | $\Phi$-Mom. (A-11) | $\beta g(T-T_w)\cos\Phi$ | $\beta g(T-T_w)\cos\Phi\cos\alpha$ |
| | $\Omega$-Mom. (A-12) | 0 | $-\beta g(T-T_w)\sin\alpha$ |
| Rectangular Channel | X-Mom. (A-17) | 0 | |
| | Y-Mom. (A-18) | $\beta g(T-T_w)$ | $\beta g(T-T_w)\cos\alpha$ |
| | $\Omega$-Mom. (A-19) | 0 | $\beta g(T-T_w)\sin\alpha$ |

With the limiting case $h = R_c$, the angle of inclination $\alpha$ is found to be approximately $9^o$. According to a recent analysis by Cheng and Hong [97], for a range of inclination angle $\alpha = 0 \simeq 9^o$, the inclination angle effect depends on the Rayleigh number and becomes particularly important for high Rayleigh numbers. In general, the concept of effective radius of curvature may be applied to plane spiral tubes. When the central plane of the spiral tubes is not horizontal, the inclination angle effect caused by the orientation of buoyancy forces may become significant under certain circumstances such as for high Rayleigh numbers.

# CHAPTER III

# FULLY DEVELOPED LAMINAR FORCED CONVECTION HEAT TRANSFER IN CURVED PIPES*

## 3.1 INTRODUCTION

A review of the literature shows that accurate fluid flow and heat transfer results are not available for the intermediate Dean number flow regime under hydrodynamically and thermally fully developed conditions. The perturbation method [12,39] is known to be applicable only when the Dean number is very small. On the other hand, the approximate method [34,65] based on boundary layer concept near the pipe wall is valid only for high Dean numbers. For the intermediate Dean number flow regime, neither the perturbation method nor the boundary layer technique is effective. It is obvious that solution by numerical methods provide the only practical approach for the intermediate Dean number region.

Recently studies by McConalogue and Srivastava [40] and Truesdell and Adler [35,36] have also carried out the numerical solutions for fully developed laminar flow in curved pipes. The work by Truesdell [35] completed in 1963 remained unpublished until 1970.

The purpose of this study is to present an accurate numerical solution, using boundary vorticity method [96] for a steady fully developed laminar forced convection in axially uniformly heated curved

---

*Reference [80] is based on this part of the thesis work.

pipes, valid up to a reasonably high value of the Dean number in order to bridge the gap between perturbation method and boundary layer approximation. This work was carried out as a first step toward the numerical solution of Graetz problem for curved pipes. In addition to presenting accurate flow and heat transfer results, the Prandtl number effect on laminar forced convection heat transfer in curved pipes is clarified for the first time. The numerical results for flow and heat transfer from this study will be compared with the data available in the literature, and the discrepancy will be clearly pointed out.

## 3.2 FORMULATION OF THE PROBLEM

Consideration is given to a steady hydrodynamically and thermally fully developed laminar flow of viscous incompressible fluid in a curved pipe under the thermal boundary conditions of axially uniform wall heat flux and peripherally uniform wall temperature at any axial position. In order to facilitate the analysis, the following assumptions are made:

1. The radius of curvature of the pipe axis is large in comparison to the radius of the pipe.
2. Physical properties are constant and buoyancy effect is neglected.
3. Viscous dissipation is negligible and heat sources do not exist.

Referring to the cylindrical coordinates $(R,\phi,R_c\Omega)$ shown in Fig. 10, the governing equations for the present problem can be shown to be:

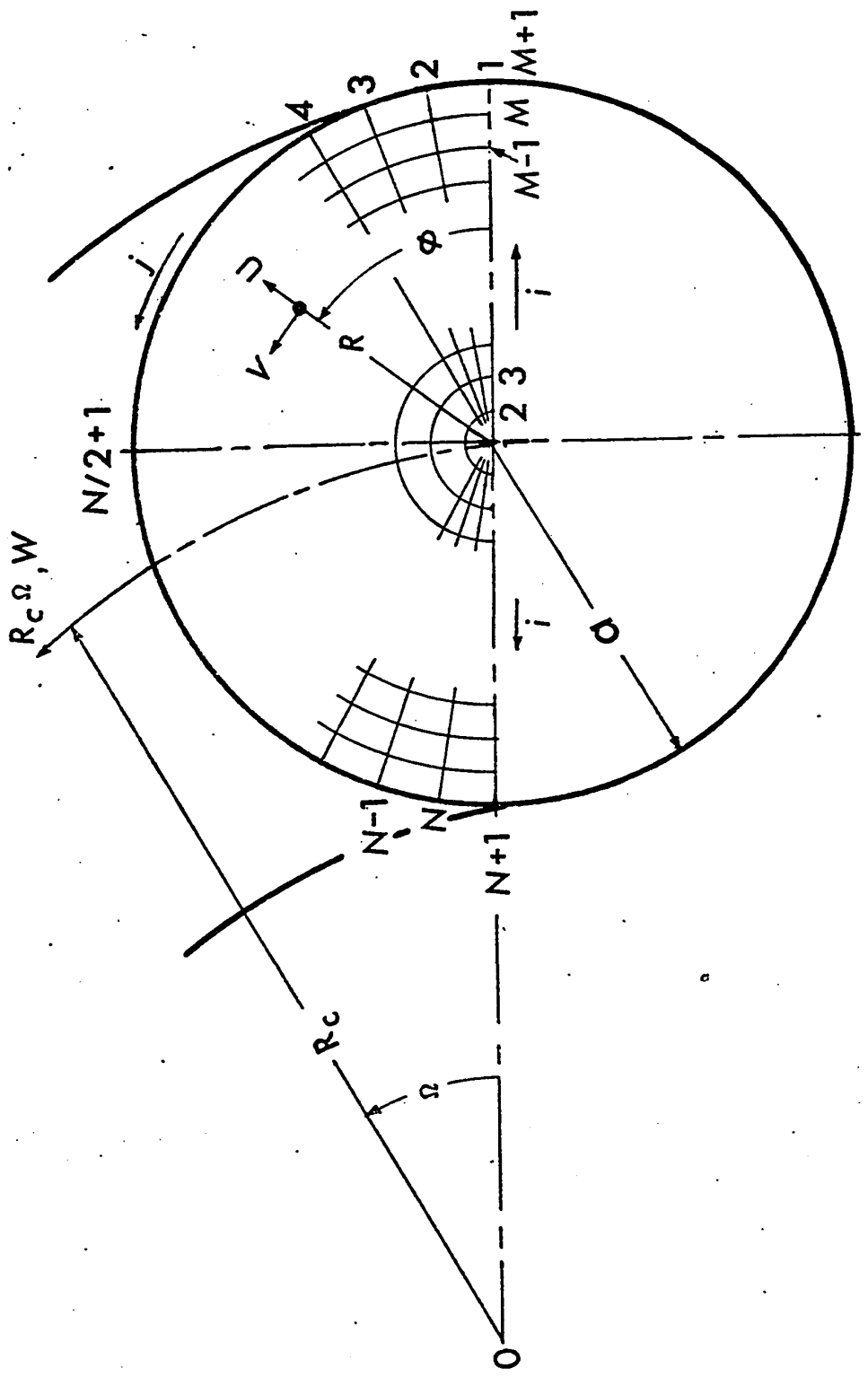


Fig. 10 Coordinate system and numerical grid

Continuity equation

$$\frac{\partial}{\partial R}(RU) + \frac{\partial V}{\partial \phi} = 0 \ . \tag{94}$$

Momentum equations in R, $\phi$ and $R_c\Omega$ directions

$$U\frac{\partial U}{\partial R} + \frac{V}{R}\frac{\partial U}{\partial \phi} - \frac{V^2}{R} = -\frac{1}{\rho}\frac{\partial P'}{\partial R} - \frac{\nu}{R}\frac{\partial}{\partial \phi}$$

$$\left(\frac{\partial V}{\partial R} + \frac{V}{R} - \frac{1}{R}\frac{\partial U}{\partial \phi}\right) + \frac{W^2}{R_c}\cos\phi \tag{95}$$

$$U\frac{\partial V}{\partial R} + \frac{V}{R}\frac{\partial V}{\partial \phi} + \frac{UV}{R} = -\frac{1}{\rho R}\frac{\partial P'}{\partial \phi} + \nu\frac{\partial}{\partial R}$$

$$\left(\frac{\partial V}{\partial R} + \frac{V}{R} - \frac{1}{R}\frac{\partial U}{\partial \phi}\right) - \frac{W^2}{R_c}\sin\phi \tag{96}$$

$$U\frac{\partial W}{\partial R} + \frac{V}{R}\frac{\partial W}{\partial \phi} = -\frac{1}{\rho R_c}\frac{\partial P_o}{\partial \Omega}$$

$$+ \nu\left[\left(\frac{\partial}{\partial R} + \frac{1}{R}\right)\frac{\partial W}{\partial R} + \frac{1}{R}\frac{\partial}{\partial \phi}\left(\frac{1}{R}\frac{\partial W}{\partial \phi}\right)\right] \tag{97}$$

where the pressure at any point consists of two parts and is expressed as,

$$P = P_o(R_c\Omega) + P'(R,\phi) \ .$$

Energy equation

$$U \frac{\partial T}{\partial R} + \frac{V}{R} \frac{\partial T}{\partial \phi} + \frac{W}{R_c} \frac{\partial T}{\partial \Omega}$$

$$= \alpha\left(\frac{\partial^2 T}{\partial R^2} + \frac{1}{R^2} \frac{\partial^2 T}{\partial \phi^2} + \frac{1}{R} \frac{\partial T}{\partial R}\right) . \qquad (98)$$

The boundary conditions are:

$$U = V = W = T - T_w = 0 \quad \text{at pipe wall.} \qquad (99)$$

The circumstances under which the above set of equations applies are well discussed in Section 2.7 and need not be repeated here. It is mentioned that the above governing equations (95) through (98) correspond to equations (82) through (86) obtained in Section 2.7.

In the present formulation, however, the free convection effects are neglected. The simplified Navier-Stokes equations (95) through (97) and the energy equation (98) are quasi-linear, second-order partial differential equations of elliptic type. Introducing the following transformations,

$$R = [a]r, \quad R_c = [a]r_c, \quad U = [\nu/a]u,$$

$$V = [\nu/a]v, \quad W = [C\nu/a]w,$$

$$T_w - T = [C\tau Pr\ a]\theta, \quad \partial P_o/R_c\partial\Omega = C_1,$$

$$- C_1 a^3/4\nu\mu = C, \quad \partial T/R_c\partial\Omega = \tau$$

and a dimensionless stream function $\psi$,

$$u = \frac{1}{r}\frac{\partial\psi}{\partial\phi}, \quad v = -\frac{\partial\psi}{\partial r} \tag{100}$$

the momentum and energy equations can be restated in the following dimensionless forms after eliminating pressure terms between equations (95) and (96).

Momentum equation for secondary flow

$$u\frac{\partial\zeta}{\partial r} + \frac{v}{r}\frac{\partial\zeta}{\partial\phi}$$

$$= \nabla^2\zeta + 2\left(\frac{C^2}{r_c}\right) w\left(\frac{1}{r}\cos\phi\frac{\partial w}{\partial\phi} + \sin\phi\frac{\partial w}{\partial r}\right) \tag{101}$$

where $$\nabla^2 = \frac{\partial^2}{\partial r^2} + \frac{1}{r}\frac{\partial}{\partial r} + \frac{1}{r^2}\frac{\partial^2}{\partial\phi^2}.$$

Vorticity equation

$$\zeta = \nabla^2\psi \tag{102}$$

Axial momentum equation

$$u \frac{\partial w}{\partial r} + \frac{v}{r} \frac{\partial w}{\partial \phi} = \nabla^2 w + 4 \tag{103}$$

Energy equation

$$Pr(u \frac{\partial \theta}{\partial r} + \frac{v}{r} \frac{\partial \theta}{\partial \phi}) = \nabla^2 \theta + w \tag{104}$$

It is noted that the vorticity function $\zeta$ is introduced here to avoid using biharmonic function $\nabla^4 \psi$ in the momentum equation for secondary flow. Because of symmetry it is only required to consider, for example, the upper half of the circular region (see Fig. 10). The boundary conditions are now restated as follows:

$$\psi = \frac{\partial \psi}{\partial r} = w = \theta = 0 \quad \text{at pipe wall } (r = 1)$$

$$\psi = \zeta = \frac{\partial w}{\partial \phi} = \frac{\partial \theta}{\partial \phi} = 0 \quad \text{along horizontal center line } (\phi = 0 \text{ and } \pi) \tag{105}$$

In contrast to the forced convection with secondary flow caused by buoyancy forces, a set of momentum equations (101)—(103) is seen to be uncoupled with the energy equation (104) and the flow problem can be solved independently. Since a perturbation method [12,39] is known to diverge quickly with the increase of Dean number, a numerical solution appears to be the only practical approach for the

accurate solution of the present problem. By substituting the vorticity function into the momentum equation (101) for secondary flow, the vorticity function can be eliminated, but the numerical solution of the resulting set of equations in cylindrical coordinates by the conventional method [98] is known to converge extremely slowly and is not practical from the viewpoint of computing time. Because of recent development of the boundary vorticity method [96], the above difficulty can be overcome readily. The vorticity at the wall is computed numerically by use of the "boundary vorticity" method. In addition the usual method "stream function-vorticity" is discussed in Appendix 5. The proposed new method called the "direct vorticity" method is also explained in the Appendix.

## 3.3 FINITE DIFFERENCE APPROXIMATIONS AND BOUNDARY VORTICITY METHOD

By using a three-point central-difference approximation and a dummy variable f for the dependent variables w, $\zeta$, $\psi$ and $\theta$, a general finite-difference equation can be written for equations (101) through (104) as follows:

$$\left[1 - \frac{\Delta r}{2r_i} + \beta\right] f_{i-1,j} + \left[-2 - 2\frac{\Delta r^2}{r_i \Delta\phi}\right] f_{i,j} + \left[1 + \frac{\Delta r}{2r_i} - \beta\right] f_{i+1,j}$$

$$= -\left[\left(\frac{\Delta r}{r_i \Delta\phi}\right)^2 + \gamma\right] f_{i,j-1} + \left[-\left(\frac{\Delta r}{r_i \Delta\phi}\right)^2 + \gamma\right] f_{i,j+1} + \sigma \qquad (106)$$

where

$$\beta = \begin{cases} \frac{\Delta r}{2} u_{i,j} \\ 0 \\ \frac{\Delta r}{2} Pr\, u_{i,j} \end{cases}, \quad \gamma = \begin{cases} \frac{(\Delta r)^2}{2r_i \Delta\phi} v_{i,j} & \text{for } f_{i,j} = \zeta_{i,j} \text{ and } w_{i,j} \\ 0 & \text{for } f_{i,j} = \psi_{i,j} \\ \frac{(\Delta r)^2}{2r_i \Delta\phi} Pr\, v_{i,j} & \text{for } f_{i,j} = \theta_{i,j} \end{cases}$$

$$\sigma = \begin{cases} \left(\frac{c^2}{r_c}\right) w_{i,j} \left[\frac{(\Delta r)^2}{r_i \Delta\phi} (w_{i,j-1} - w_{i,j+1}) \cos\phi_j + \Delta r (w_{i-1,j} - w_{i+1,j}) \sin\phi_j\right] & \text{for } f_{i,j} = \zeta_{i,j} \\ -(\Delta r)^2 \zeta_{i,j} & \text{for } f_{i,j} = \psi_{i,j} \\ -(\Delta r)^2 4 & \text{for } f_{i,j} = w_{i,j} \\ -(\Delta r)^2 w_{i,j} & \text{for } f_{i,j} = \theta_{i,j} \end{cases}$$

In order to circumvent the singularity at the origin of the cylindrical coordinates, finite difference equation in Cartesian coordinates is employed at the origin instead of the usual approximate or extrapolation method.

For the purpose of illustrating the computational procedure using boundary vorticity method, a set of finite-difference equations for secondary flow obtained by applying equation (106) to the grid points along the radial line j = 1 will be written in a matrix form as follows:

$$\begin{bmatrix} B_2 & C_2 & & & & & \\ A_3 & B_3 & C_3 & & 0 & & \\ & A_4 & B_4 & C_4 & & & \\ & & . & . & . & & \\ & & & . & . & . & \\ & 0 & & & A_{M-1} & B_{M-1} & C_{M-1} \\ & & & & & A_M & B_M \end{bmatrix} \begin{bmatrix} \zeta_{2,1} \\ \zeta_{3,1} \\ \zeta_{4,1} \\ . \\ . \\ \zeta_{M-1,1} \\ \zeta_{M,1} \end{bmatrix} = \begin{bmatrix} G_{2,1} \\ G_{3,1} \\ G_{4,1} \\ . \\ . \\ G_{M-1,1} \\ G_{M,1}-C_M\zeta_{M+1,1} \end{bmatrix} \tag{107}$$

Here the symbols $A_i$, $B_i$ and $C_i$ represent the coefficient for the dependent variables $\zeta_{i-1,1}$, $\zeta_{i,1}$ and $\zeta_{i+1,1}$ respectively, in equation (106) at the grid point (i,1) and the symbol $G_{i,1}$ represents all the terms on the right hand side of the same equation for $f_{i,1} = \zeta_{i,1}$. Similarly, by considering the radial line j = 1, a set of linear algebraic equations for the stream function $\psi_{i,1}$ can be written in a matrix form as

$$\begin{bmatrix} E_2 & F_2 & & & & & \\ D_3 & E_3 & F_3 & & 0 & & \\ & D_4 & E_4 & F_4 & F_4 & & \\ & & . & . & . & & \\ & & & . & . & . & \\ & 0 & & & D_M & E_M & F_M \\ & & & & & (D_{M+1}+F_{M+1}) & E_{M+1} \end{bmatrix} \begin{bmatrix} \psi_{2,1} \\ \psi_{3,1} \\ \psi_{4,1} \\ . \\ . \\ \psi_{M,1} \\ \psi_{M+1,1} \end{bmatrix} = \begin{bmatrix} H_{2,1} \\ H_{3,1} \\ H_{4,1} \\ . \\ . \\ H_{M,1} \\ H_{M+1,1} \end{bmatrix} \tag{108}$$

where $D_i$, $E_i$ and $F_i$ stand for the coefficient of the stream functions $\psi_{i-1,1}$, $\psi_{i,1}$ and $\psi_{i+1,1}$ respectively, in equation (106) at the grid point (i,1), and $H_{i,1}$ denotes all the terms on the right hand side of

the same equation when $f_{i,1} = \psi_{i,1}$.

It is noted that equations (107) and (108) are obtained after applying the boundary conditions $\zeta_{i,1} = \zeta_{i,N+1} = \zeta_{i,j} = 0$ for equation (101) and the boundary conditions $\psi_{i,1} = \psi_{i,N+1} = \psi_{1,j} = 0$ and $\partial\psi_{M+1,j}/\partial r = 0$ (or $\psi_{M,j} = \psi_{M+2,j}$) for equation (102). The success of the boundary vorticity method is based on the observation that a linear relationship exists between the vorticity function $\zeta_{M+1,1}$ and the stream function $\psi_{M+1,1}$ at the boundary. For example, given three sets of values at a boundary point for the vorticity function and the stream function, namely, $\zeta_b^{(1)}$ and $\zeta_b^{(1)}$, $\zeta_b^{(2)}$ and $\zeta_b^{(2)}$, and $\zeta_b^{(3)}$ and $\psi_b^{(3)}$, the following linear relationship exists.

$$\zeta_b^{(3)} = \frac{\zeta_b^{(2)} - \zeta_b^{(1)}}{\psi_b^{(2)} - \psi_b^{(1)}} (\psi_b^{(3)} - \psi_b^{(2)}) + \zeta_b^{(2)} \tag{109}$$

At the beginning one assumes that $\zeta_{M+1,1} = \zeta_b^{(1)}$ in equations (107) and (108). Then equation (107) can be solved simultaneously for $\zeta_{i,1}$, $i = 2,3,\ldots M$, by using the Gaussian elimination method. Using the obtained vorticity functions, the right hand column of the matrix equation (108) can be evaluated. Applying the Gaussian elimination method to equation (108), the values for the stream function $\psi_{i,1}$ can be found, and the boundary value $\psi_{M+1,1} = \psi_b^{(1)}$ will be stored. By assuming again $\zeta_{M+1,1} = \zeta_b^{(2)}$ and following exactly the same procedure, the secondary boundary value $\psi_{M+1,1} = \psi_b^{(2)}$ will also be stored. Using the linear relation (109) and noting that $\psi_b^{(3)} = 0$, $\zeta_b^{(3)}$ can be obtained. Substituting the newly obtained boundary vorticity $\zeta_b^{(2)}$ into equations

(107) and (108) and solving these equations, one obtains $\zeta_{i,1}$ and $\psi_{i,1}$, $i = 2,3,\ldots M$, which represent the numerical solutions along the radial line $j = 1$. The same computational procedure will be repeated for the succeeding radial lines $j = 1 + 1, 1 + 2, \ldots$ etc. with $j = 2$ at the beginning. Numerical experiments show that using $\zeta_b^{(3)}$ the values of the stream function on the boundary, $\psi_{M+1,1}$, range from $10^{-7}$ to 0 as compared with the largest value at interior point. Theoretically, of course, the stream function must vanish at the boundary. It is noted that an error of the above magnitude may be caused by a round-off error using a single precision.

With a computational procedure for the numerical determination of the boundary vorticity established, it suffices to mention that the usual line iterative relaxation method for the numerical solution of a set of finite-difference equations with the associated boundary conditions may be employed.

In the numerical computation, the prescribed error for all the dependent variables and the secondary velocity components is

$$\varepsilon = \sum_{i,j}^{\substack{M+1 \\ N+1}} \left| f_{i,j}^{(n+1)} - f_{i,j}^{(n)} \right| \Big/ \sum_{i,j}^{\substack{M+1 \\ N+1}} \left| f_{i,j}^{(n+1)} \right| < 10^{-5} \qquad (110)$$

Since the momentum equations (101) and (103) are coupled, the number of inner iterations involving the boundary vorticity method is of some interest. The following result is found to be satisfactory from the viewpoint of computing time after some numerical experiments:

| Number of inner iterations relating to boundary vorticity method | $(f\ Re)/(f\ Re)_0$ |
|---|---|
| 20 ~ 50 | 1.0 ~ 1.1 |
| 20 ~ 5 | 1.1 ~ 1.35 |
| 1 | 1.35 or higher |

The parameter f Re will be defined later. The number of inner iterations for $w_{i,j}$ is always one. It is noted that further increase of the number of inner iterations may destabilize the convergence of the iteration process.

In order to accelerate the convergence, an overrelaxation factor is used. Since nonlinear terms are involved in the elliptic type partial differential equations for the present problem, no general method is available for the evaluation of an optimum relaxation factor. However, with a mesh size of M, N = 28, a relaxation factor ranging from 1.7 for small Dean number to 1.0 for large Dean number is found to be satisfactory for all the equations except the momentum equation (101) for secondary flow where a factor of 1.0 is used always in the numerical computation. In order to stabilize the convergence in the high Dean number region, underrelaxation factors of 0.7, 0.5, 0.1 and 0.02 are also tried. However, no appreciable difference is observed in extending the parametric value as compared with the relaxation factor of 1.0, confirming that the boundary vorticity method is computationally very stable.

The convergence of the iteration process depends on whether

or not the coefficient matrix is diagonally dominant. Consider, for example, an off-diagonal element

$$A_i = 1 - \frac{\Delta r}{2r_i} + \frac{\Delta r}{2} u_{i,1}$$

in equation (107). To ensure diagonal dominance, one expects a restriction on the magnitude of the secondary flow velocity component to be $|u_{i,1}| < (2/\Delta r - 1/r_i)$. If the limit is exceeded, the coefficient may no longer be diagonally dominant, and the numerical solution starts oscillation and finally diverges. At this point it is useful to recall the convergence conditions for solving a linear system $B\zeta = G$. The convergence conditions for the coefficient matrix B are [98].

(1) $b_{i,i} > 0 \ , \quad i = 1,2,\ldots,M+1$

(2) $b_{i,i} \geq \sum_{\substack{j=1 \\ j=i}}^{M+1} |b_{i,j}|$ and for at least one i the strict inequality holds (111)

(3) The matrix B is irreducible.

Here $b_{i,j}$ denotes an element of the matrix B. In the present problem, violation of the above conditions occurs when the velocity component $u_{i,1}$ becomes large in high Dean number flow regime. This difficulty can be overcome by using finer mesh sizes, but the computing time and the round-off errors increase correspondingly. In order to extend the numerical solution into high parameter region, the

mesh sizes of M, N = 56 and M = 74, N = 42 are also tried in some cases in addition to the mesh size of M, N = 28 for most computations.

Another way of stabilizing the numerical computation is to introduce an under-relaxation factor $\omega < 1$. Numerical solution may be extended further to higher parameter values by use of the under-relaxation factor but only at the expense of considerable computing time. It is worth noting that a close analogy exists between the numerical methods of solutions for parabolic and elliptic partial differential equations. One observes that the stability criteria for parabolic equations correspond to the convergence criteria for elliptic equations [99,100]. As a matter of fact, if one consider convergence and stability in the sense of Lax and Richtmyer [101], then it can be proved equivalent for a difference equation approximating a differential equation in the formal sense [100]. In this connection it is noted that the stability condition suitable for parabolic equations with inertia or convective terms for explicit finite-difference method is given by Barakat and Clark [102]. This stability criterion was pointed out by Nunchal, Spalding and Wolfshtein [103] to be the convergence criterion for elliptic equations.

At this point a comparison between the boundary vorticity method and the conventional methods of determining the boundary vorticity is of practical interest. One may determine the boundary vorticity by writing the central finite difference equation for equation (102) at the boundary leading to the following expression:

$$\zeta_{M+1,j} = 2\psi_{M,j}/(\Delta r)^2 .$$

The approximation of the boundary vorticity is known to have a significant effect on the stability of numerical solution. Using the above expression for boundary vorticity, a set of the governing equations can be solved by the conventional line iterative method. This method of solution will be referred to as stream function-vorticity method in this paper. Figure 11 illustrates the results of numerical experiments for the boundary vorticity method and the stream function-vorticity method at the values of Dean number K = 0.32, 54 and 90, respectively. For this comparison, the number of inner iterations is fixed. At K = 0.32 and 54, the stream function-vorticity method fails to yield convergent solution with the restriction of equation (110) for relaxation factor $\omega \geq 1$. In particular, the stream function-vorticity method fails to yield convergent solution for K = 90 even with an underrelaxation factor as small as $\omega = 0.05$. In contrast, the boundary vorticity method converges quickly with $\omega = 0.8 \sim 1.0$. In high Dean number range, the boundary vorticity method has definite advantage in regard to convergence.

## 3.4 FLOW AND HEAT TRANSFER RESULTS

It is possible to obtain the expressions for the product of friction factor and Reynolds number (f Re) and Nusselt number (Nu) by considering either the velocity and temperature gradients, respectively, along the pipe wall, or the overall force and energy balances, respectively, for the axial length $R_c d\Omega$. The results are

$$(f\ Re)_1 = 4|\overline{\partial w}/\partial r|_w/\overline{w}$$

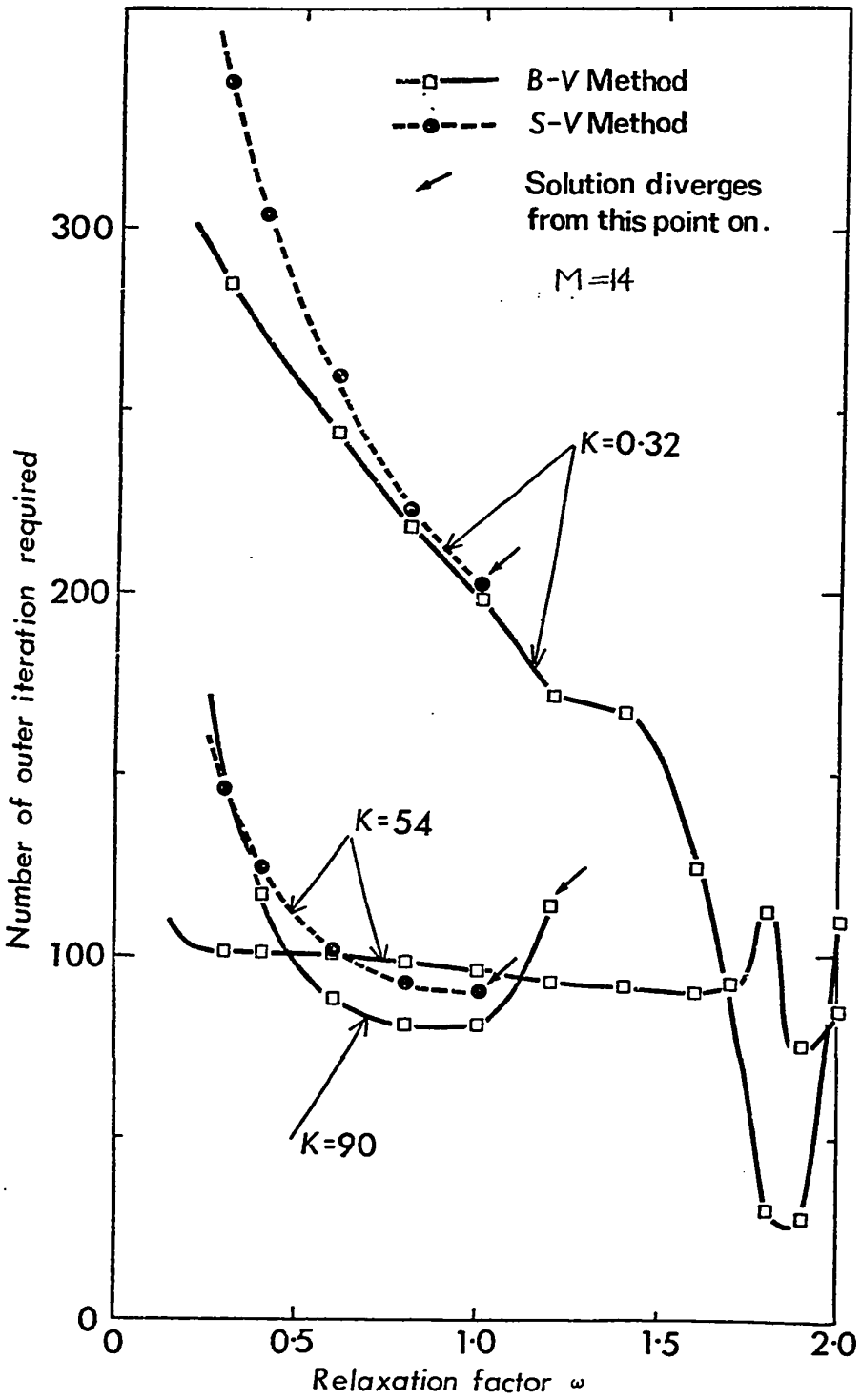


Fig. 11 Comparison of numerical solution between boundary vorticity method and stream function - vorticity

$$(Nu)_1 = 2\overline{w}\left|\overline{\partial\theta}/\partial r\right|_w / \left|\overline{w\theta}\right| \tag{112}$$

$$(f\ Re)_2 = 8/\overline{w}$$

$$(Nu)_2 = \overline{w}^2/\left|\overline{w\theta}\right| \ .$$

Evaluation of the mean values indicated above are carried out by using Simpson's rule. The above two expressions for the overall characteristics, f Re and Nu, afford checking the convergence of the numerical results.

In order to assess the accuracy of the numerical solution, the axial velocity profile along the central horizontal axis and isolines for velocity from this analysis at K = 196 are compared against Adler's experimental data [19] at K = 205 in Fig. 12. A good agreement is observed between the present numerical solution and the experimental data. The numerical solution can be extended to K = 205 with relaxation of the prescribed error but the numerical results at K = 196 are based on equation (110). The streamlines are also illustrated in Fig. 12, and one sees that at K = 196 the center of circulation is situated near the inner wall. The loci of the centers of circulation are of interest. As Dean number increases, the centers of circulation move toward the wall radially, but horizontally they move away first from the central vertical axis toward the outer wall. With further increase of Dean number they then move back toward the inner wall. The distribution of the secondary flow velocity is unsymmetric with respect to the central vertical axis. Furthermore,

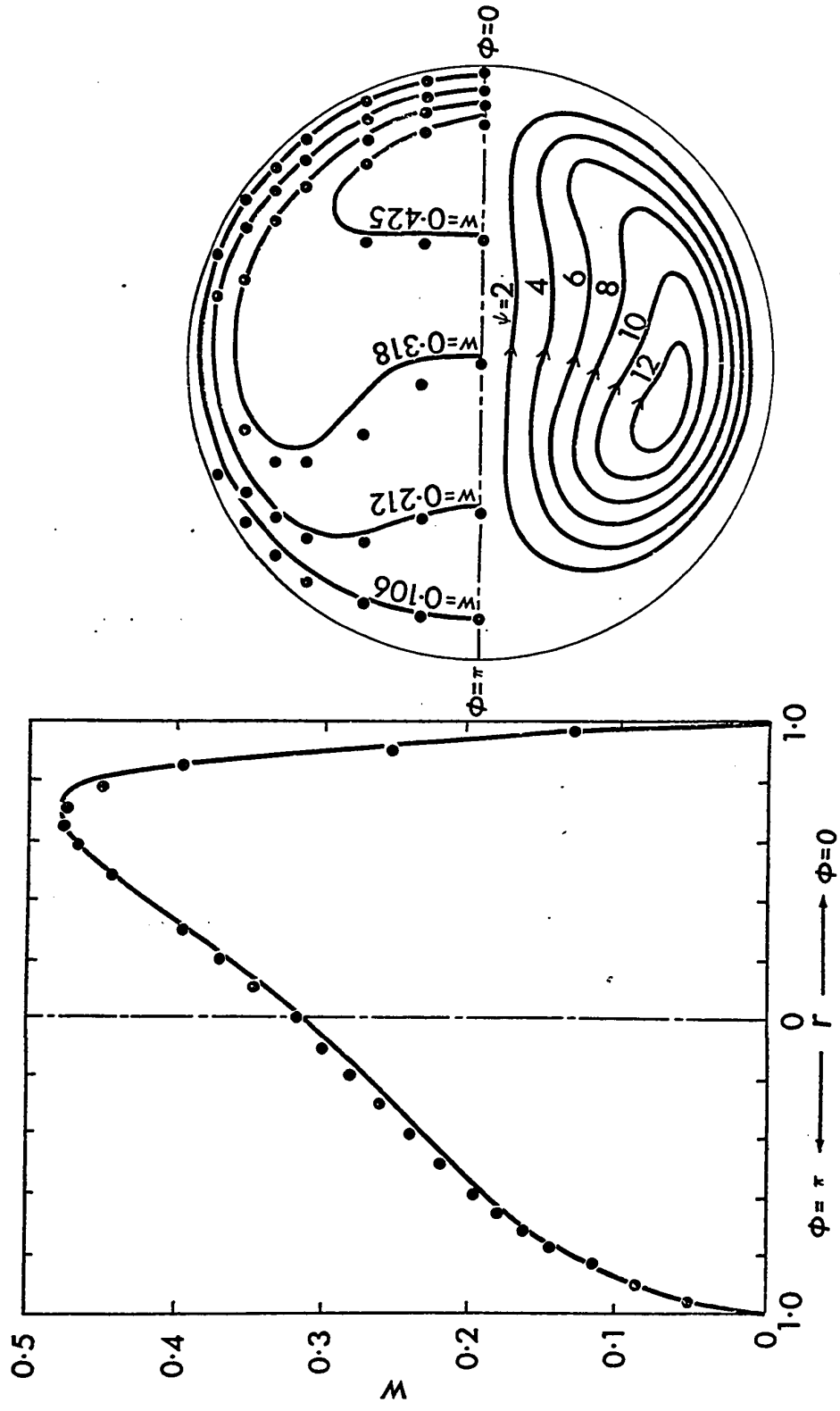


Fig. 12 Comparison of velocity profile along $\phi = 0$ and $\pi$ and isolines for velocity at K = 196 from this work with Adler's experimental data at K = 205 and streamlines at K = 196 from this work.

the distribution of the streamlines suggests that at K = 196, the boundary layer approximation cannot be applied.

The effect of Dean number on average friction factor is well understood. The effect of Dean number on the local distribution of friction factor is of theoretical interest but appears to have not been reported in the literature. Figure 13 shows the local angular distribution of $(f\ Re)_\phi/(f\ Re)_0$ as K varies from 0 to 186.8. At K = 13.8 the value of $(f\ Re)_\phi/(f\ Re)_0$ is seen to be larger than one along the outer wall ($-\pi/2 < \phi < \pi/2$) and less than one along the inner wall such that the average value is slightly larger than one. At K = 94.7, the region with $(f\ Re)_\phi > f\ Re)_0$ occupies nearly three-quarters of the whole region including the outer wall. With further increase of Dean number, the value of $(f\ Re)_\phi/(f\ Re)_0$ is always seen to be less than one in the neighbourhood of $\phi = \pi$.

In order to bring out the effect of Dean number on local friction factor more clearly, the value of $(f\ Re)_\phi/(f\ Re)_0$ is plotted against K in Fig. 14 for $\phi = 0$ and $\phi = \pi$, together with the average value $(f\ Re)/(f\ Re)_0$ indicated for comparison. In very low Dean number region, say up to K = 10, the centrifugal force effect on the average value of f Re is negligible, but one can clearly see the difference between the local value at $\phi = 0$ (or $\phi = \pi$) and the average value. Within the range of present investigation one notes that both the local value of $(f\ Re)_\phi$ at $\phi = 0$ and the average value increase continuously with K, but the local value of $(f\ Re)_\phi/(f\ Re)_0$ at $\phi = \pi$ remains at around 0.84 after reaching say K = 40.

Fully developed laminar flow in curved pipes has been

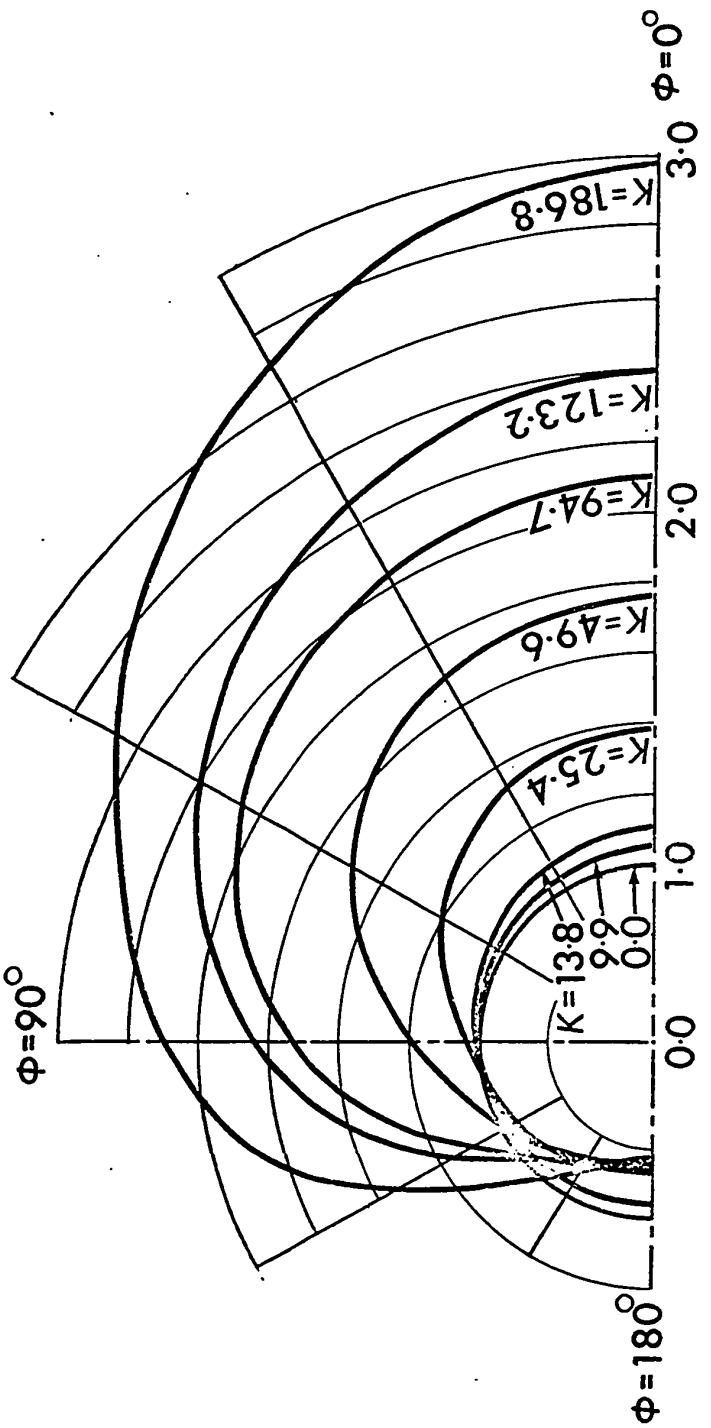


Fig. 13 Local angular distribution of $(fRe)_\phi/(fRe)_0$ with Dean number K as a parameter.

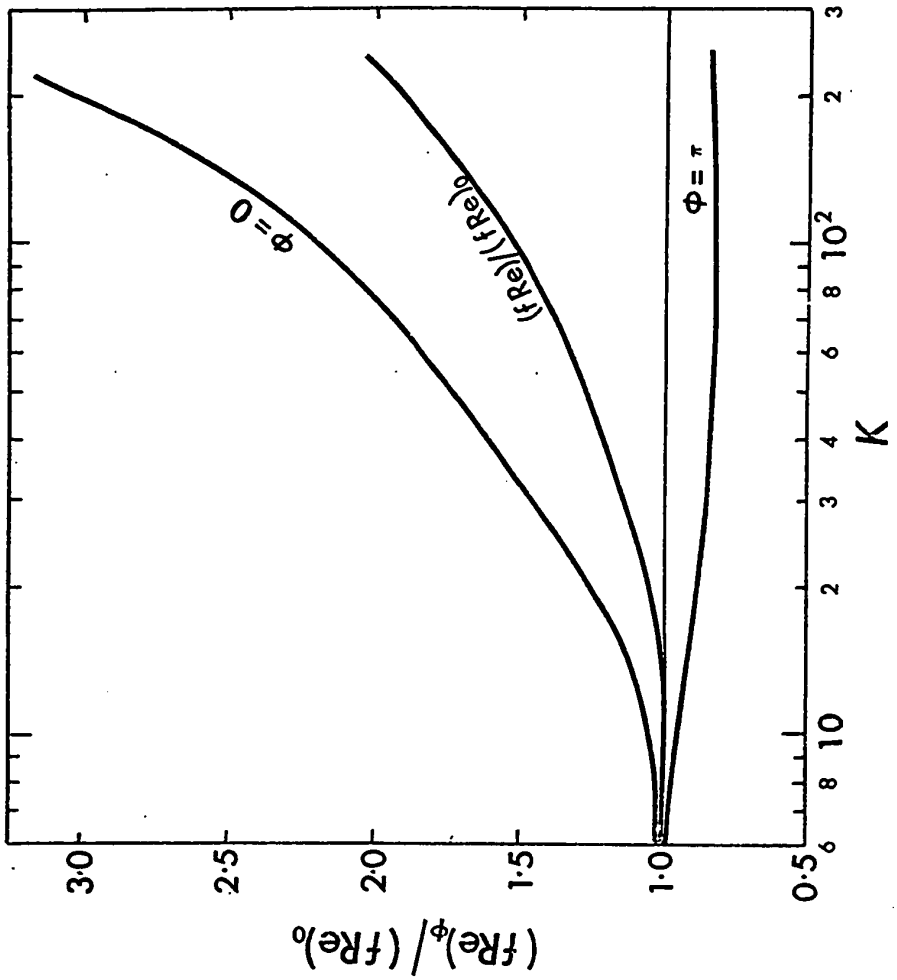


Fig. 14 $(fRe)_\phi/(fRe)_0$ versus K at outer surface ($\phi = 0$) and inner surface ($\phi = \pi$) with comparison made against $fRe/(fRe)_0$.

studied very extensively in the past because of its technical importance. Figure 15 shows the comparison between the result of present numerical analysis and the experimental and theoretical data available in the literature for $f\,Re/(f\,Re)_0$ vs. Dean number K. It is seen clearly that the present result agrees with the experimental data of White [17] and Ito [41] from relatively small to high Dean number region, while the predictions based on boundary layer approximation [19,23,65] lead to completely wrong trend in the low Dean number region. Ito's prediction is generally good for the range of Dean numbers under consideration, but has some error in the low parameter range. The above comparison serves to illustrate the relative merits of the various theoretical methods. For the high Dean number region, Ito's prediction is recommended for use in design. Ito's empirical equation is given below for reference.

$$f\,Re/(f\,Re)_0 = 0.1008K^{1/2}(1 + 3.945K^{-1/2} + 7.782K^{-2}) + 9.097K^{-3/2} + 5.608K^{-2})$$

for $K > 30$

Typical temperature profiles along the central horizontal and vertical axes and isothermals from the present analysis for $Pr = 100$ and $K = 7.66$ are shown in Fig. 16. At $K = 7.66$ it is expected that the secondary flow due to centrifugal force is rather weak. An examination of the energy equation (104) reveals that the

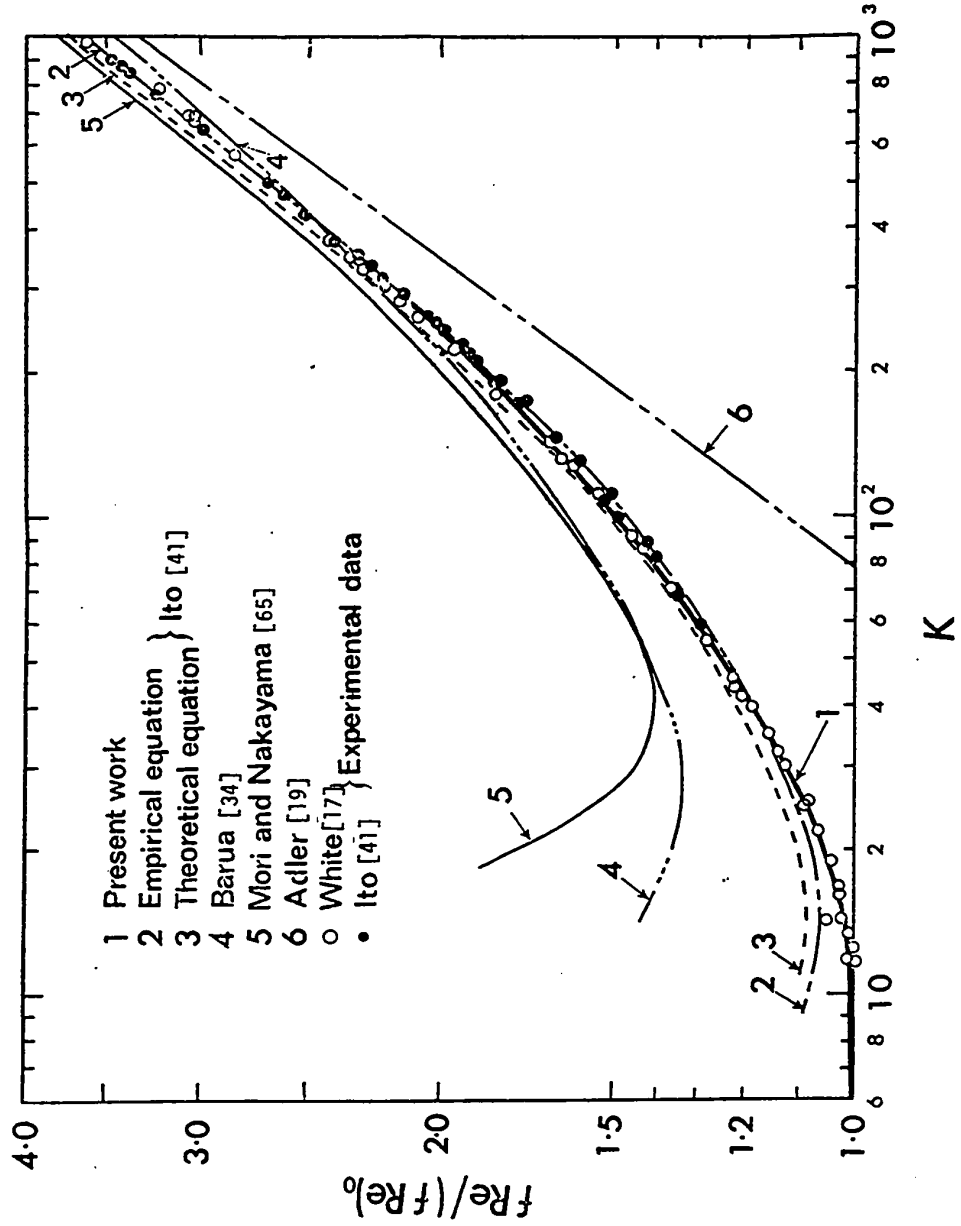


Fig. 15 Comparison of friction factor results from this work with theoretical and experimental results available in literature.

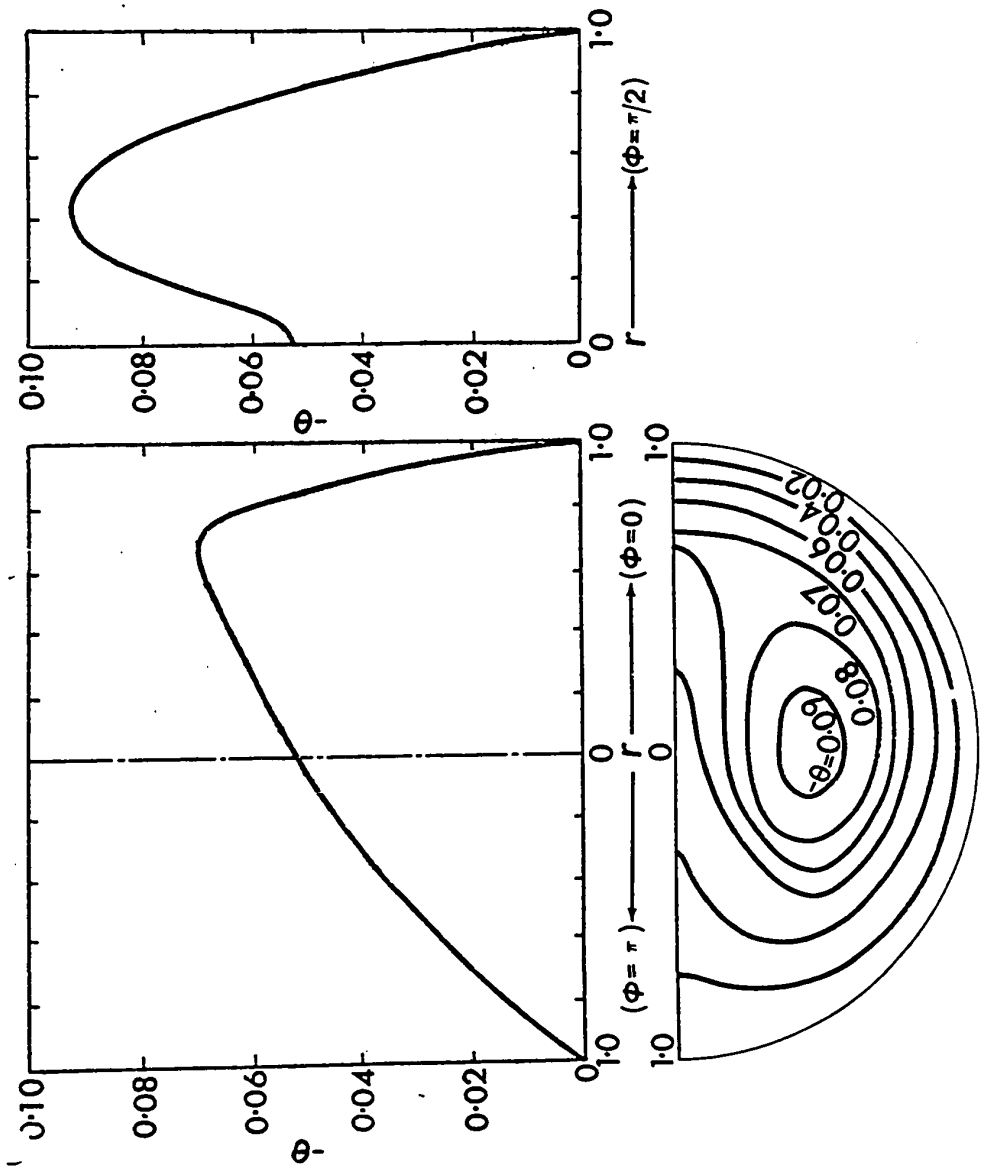


Fig. 16 Temperature profiles and isothermals at K = 7.66 for Pr = 100

role of Prandtl number in convective terms is similar to that of Dean number, and this observation is confirmed by the temperature profiles shown in Fig. 16. The temperature profile along the central vertical axis exhibits saddle shape in the central region, indicating a rather dominant convective motion therein. One should point out that the characteristics noted above for the temperature field are further magnified with the increase of the parameters K and Pr within the range of the present investigation. Unfortunately the present numerical solution cannot reach the value of K = 632 to enable one to make direct comparison with the experimental temperature profiles for air reported by Mori and Nakayama [65]. However, one notes a significant difference for temperature profile along central horizontal axis in the neighborhood of inner wall ($\phi = \pi$), with the present numerical result and the experimental data lying on opposite sides of the temperature profile for a straight pipe.

In order to consider the above discrepancy further, the angular distribution of the local Nusselt number along the pipe wall with Dean number as a parameter is shown in Fig. 17 for Pr = 0.7 and 100. The variations of the local Nusselt numbers at $\phi = 0$ (outer wall) and $\phi = \pi$ (inner wall) with Dean number K, are shown in Fig. 18 for Pr = 0.7, with the average Nusselt number included for comparison. As expected, the situation is similar to that shown in Fig. 14 for friction factor.

The overall heat transfer resutls in terms of the Nusselt

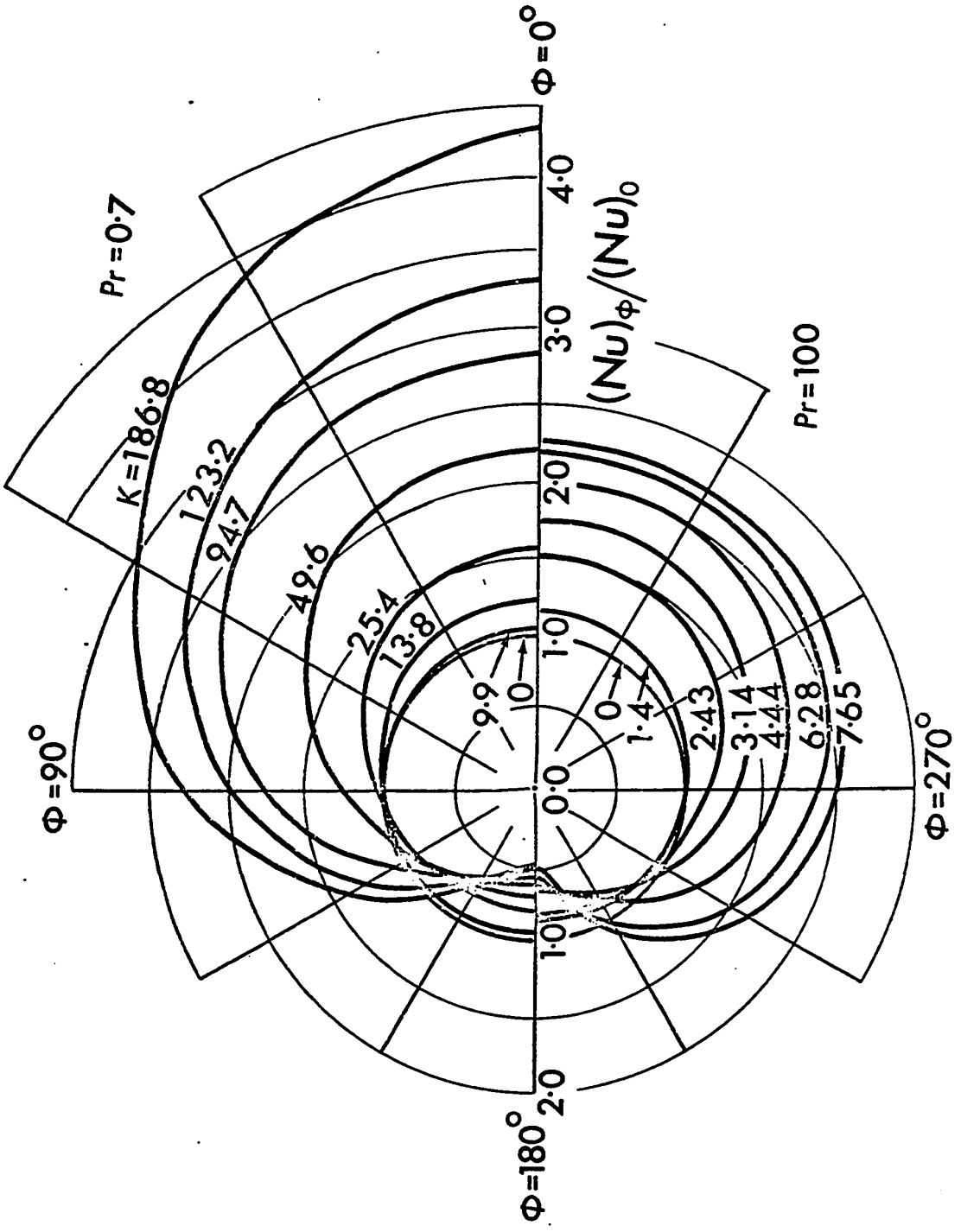


Fig. 17 Local angular distribution of $(Nu)_\phi/(Nu)_0$ with Dean number K as a parameter for Pr = 0.7 and 100.

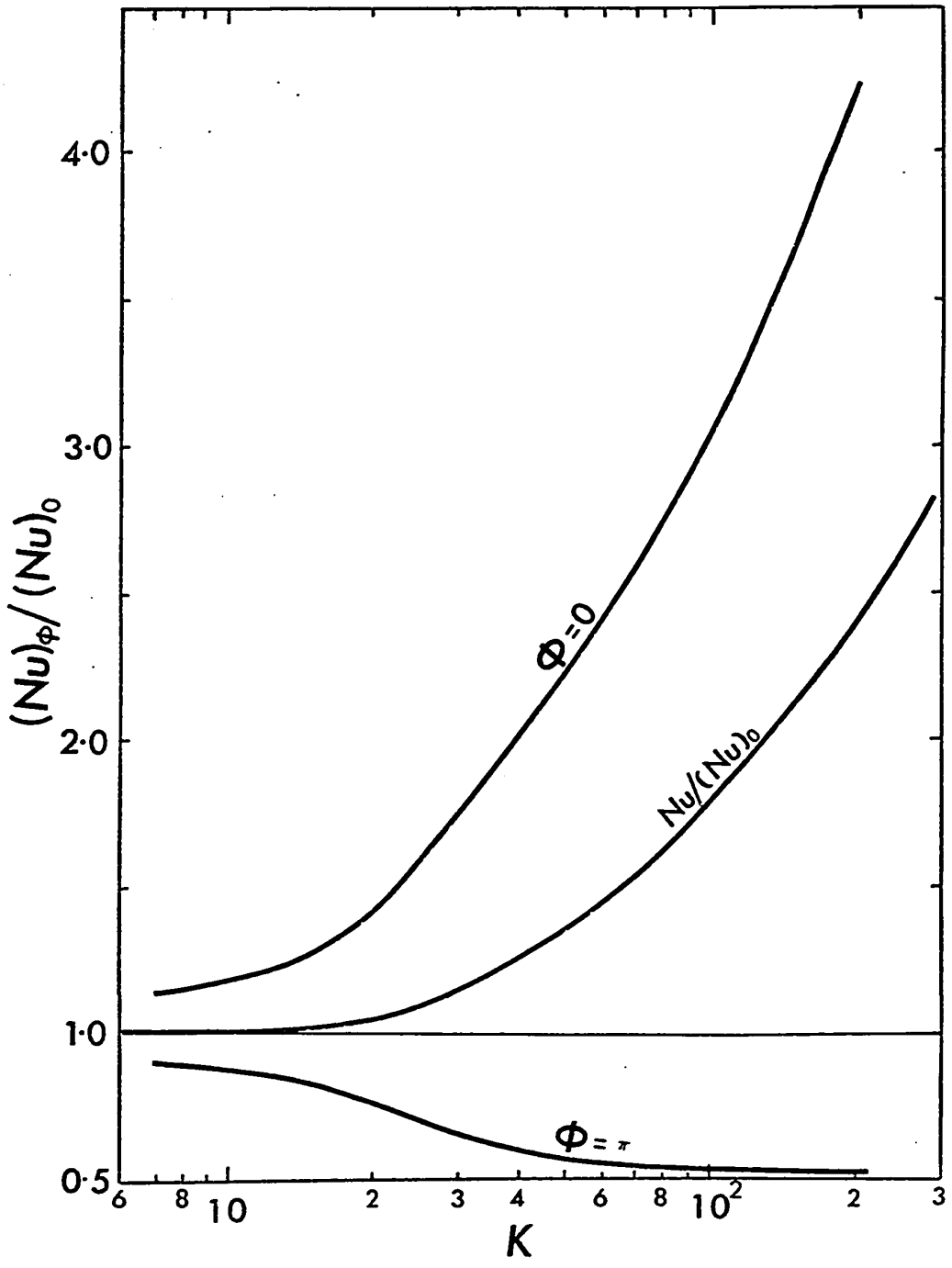


Fig. 18 $(Nu)_\phi/(Nu)_0$ versus K at outer surface ($\phi = 0$) and inner surface ($\phi = \pi$) with comparison made against $Nu/(Nu)_0$ for Pr = 0.7.

number ratio $Nu/(Nu)_0$ vs. Dean number K from this analysis are shown in Fig. 19 for various Prandtl numbers with comparison made against Özisik and Topakoglu's results [74] using perturbation method, Mori and Nakayama's theoretical results using boundary layer approximation and their experimental data [65], and also Seban and McLaughlin's experimental data [61]. It is noted that the data obtained by Seban and McLaughlin [61] are reproduced here by using the same transformation as that used by Özisik and Topakoglu [74]. It can be seen that the average Nusselt number from this analysis is closer to the experimental data at outer surface than those at inner surface given by Seban and McLaughlin [61]. For Pr = 0.7 (air) the result from the present analysis agrees with Mori and Nakayama's data [65] for air. As can be clearly seen, Özisik and Topakoglu's results from perturbation method diverge quickly with the increase of Dean number. It is now evident that the perturbation method cannot be applied to the forced convective heat transfer with secondary flow except in a very low parameter region which is practically not important. Based on the results from this analysis, it appears that Mori and Nakayama's theoretical result from boundary layer approximation is valid near Pr = 1.0 only, and the result for $Pr = \infty$ shown in [65] is believed to be invalid. The existence of asymptotic value for $Pr \to \infty$ is doubtful; but the asymptotic value does indeed exist for $Pr \to 0$, as shown in Fig. 19.

The effect of Prandtl number on forced convective heat transfer in curved pipes is of considerable theoretical and practical

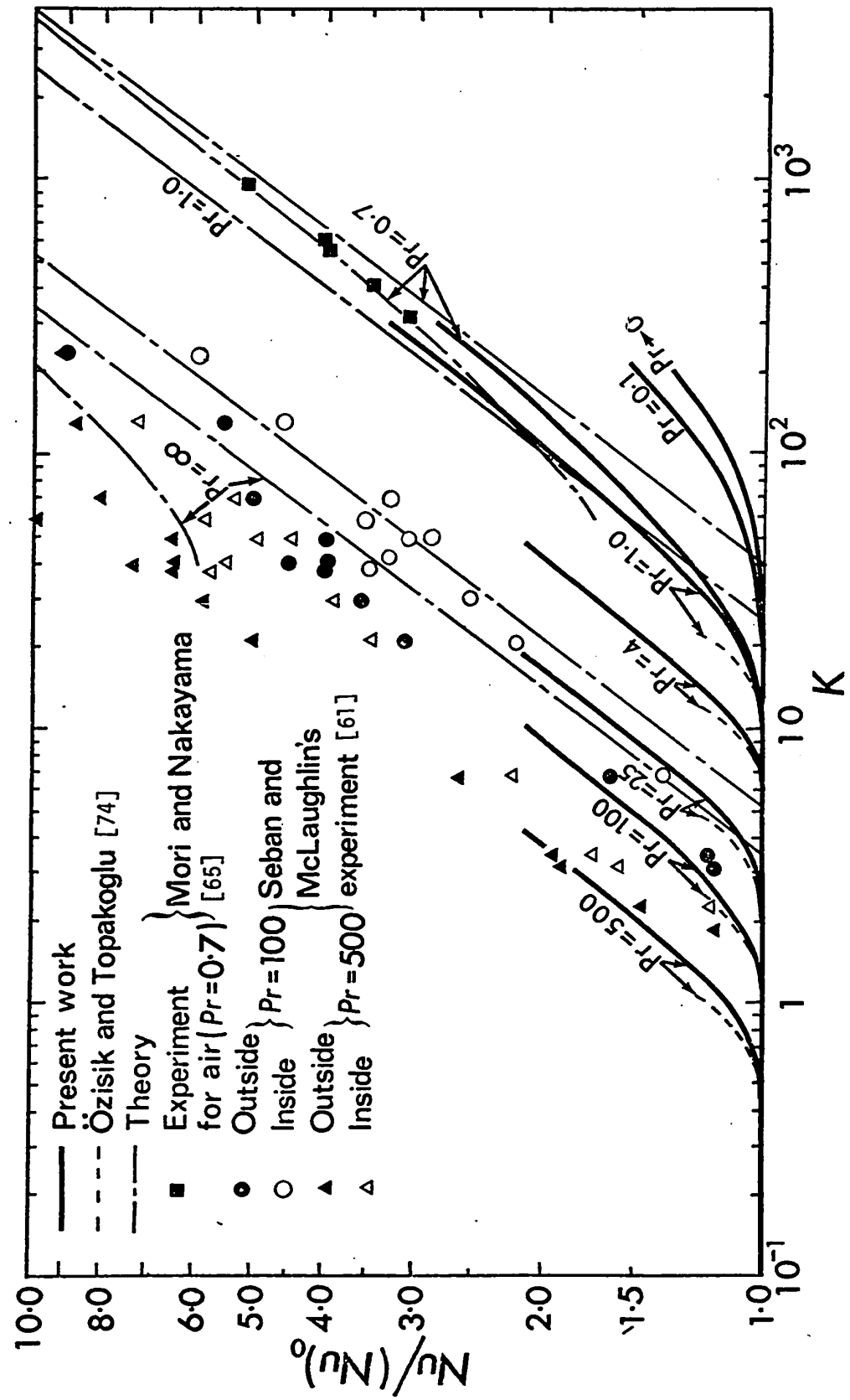


Fig. 19 Comparison of heat transfer results from this work with theoretical and experimental results available in literature.

interest. A careful study of the heat transfer results for Pr > 1 shown in Fig. 19 reveals that after reaching a certain Dean number or $Nu/(Nu)_0 \approx 1.35$, all the curves become straight lines and more or less parallel to each other. For a given value of $Nu/(Nu)_0$, the Prandtl number effect can also be seen from the decrease of K with the corresponding increase of Pr. The above observation for Prandtl number effect on heat transfer result also confirms the role of Prandtl number in the convective terms of the energy equation (104) noted earlier. A study of the basic equations shows that when the Prandtl number is large, the inertia terms in the momentum equations (101) and (103) can be neglected. This fact is also verified by the numerical results. In other words, while the secondary flow is rather weak, the convective terms in the energy equation (104) are important because of large Prandtl number. With large Prandtl number it can be shown that a new parameter $K^2Pr$ results.

For example, by introducing the secondary flow characteristic axial velocity $\overline{W}$ and other suitable characteristic quantities for $T - T_w$, $P'$ and $\Omega$, the radial momentum equation (95) and the energy equation (98) may be normalized. Noting that the centrifugal force term and the viscous terms in the momentum equation must be of the same order of magnitude, one obtains $U_c/\overline{W} = Re(a/2R_c)$. Using this relation, the new parameter $K^2Pr$ can be shown to appear as a coefficient of the convective terms in the normalized energy equation. Alternatively, by normalizing the dimensional momentum equation for secondary flow corresponding to equation (101) and the energy equation

(98), the parameter $K^2Pr$ can also be shown to arise.

It is now possible to obtain a new correlation of heat transfer results for high Prandtl number fluids as shown in Fig. 20 where all the results presented in Fig. 19 are replotted on the basis of $Nu/(Nu)_0$ vs. $(K^2Pr)^{1/2}$ for illustration. Since Seban and McLaughlin's experimental data [61] are for fluids with Prandtl number ranging from 100 to 657, the arithmetic mean value of 379 is taken as a value of Prandtl number for simplicity in replotting. It is significant to note that with the new correlation all the theoretical curves for $Pr \geq 1$ from the present analysis nearly coincide. This suggests the practical implication of "large" Pr. Furthermore, all the experimental data for Pr = 379 and 0.7 (air) are seen to scatter within a narrow band around a new correlation curve with a higher Dean number portion obtained by a linear extrapolation of the present theoretical results. The agreement between a new correlation curve and the available experimental data is considered to be remarkable in view of the fact that the new correlation is based on the assumption that the Dean number is small and the Prandtl number is large. Furthermore, one should note the inherent difficulties in the experimental measurements and the experimental simulation of the thermal boundary condition such as the uniform peripheral wall temeprature at any cross section. The following approximate equation is deduced using the new parameter $K^2Pr$ as the curve to best fit all the numerical results.

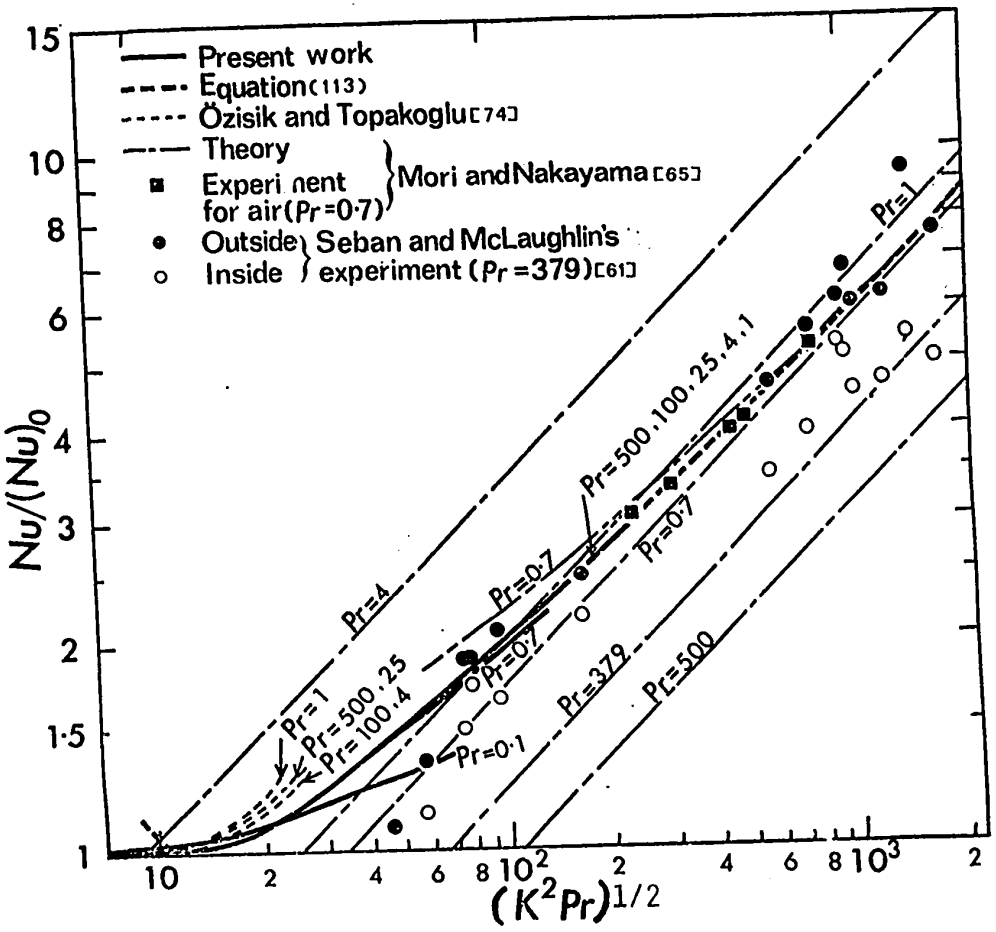


Fig. 20 Comparison of a new correlation curve for heat transfer results for Pr ≥ 1.0 from this work using a new parameter with theoretical and experimental results available in literature.

$$Nu/(Nu)_o = 0.181Q(1-0.839Q^{-1}+35.4Q^{-2}-207Q^{-3}+419Q^{-4}) \qquad (113)$$

where $Q = (K^2Pr)^{1/4} \geq 3.5$ for $Pr \geq 1$.

For $Q \leq 3.5$, the secondary flow effect is estimated to be less than 1.5 per cent in terms of the Nusselt number ratio $Nu/(Nu)_o$. In view of the possible experimental errors in the region $Q \leq 3.5$, the secondary flow effect is not considered to be important in that region. The correlation equation (113) can now be considered to be valid for all the practically important laminar regimes with sufficient accuracy. In the application of the correlation equation (113) to the flow regime where the Dean number K is greater than say 200, it is well to note that secondary flow stabilizes laminar flow with the transition Reynolds numbers of 6000-8000 being characteristic of helically coiled tubes [35] and also the present analysis is valid up to $a/R_c = O[10^{-1}]$. Recent experiments by Baylis [43] for laminar flow in curved channels of square section confirm that the present formulation is valid up to $a/R_c = 1/3.5$ in practice. Baylis [43] observes a good agreement between his experimental data [43] and the numerical results given by Cheng and Akiyama [78].

The inconsistent behavior of the boundary layer approximation [65] for the Prandtl number effect is evident from Fig. 20. For example, the heat transfer results for Pr = 1, 4, and Pr = 379, 500, are clearly on the opposite sides of the new correlation curve. This leads to the conclusion that the boundary layer approximation

[65] is valid only near Pr = 1.0.

In view of the recent experimental data for the asymptotic Nusselt numbers presented by Dravid et al [82] for the case of uniform wall heat flux, a comparison among all the existing theoretical and experimental results is believed to be pertinent and is shown in Fig. 22. The new experimental data for Pr = 5, 55 and 125, and the predictions based on empirical equation for the asymptotic Nusselt numbers presented by Dravid et al [82] and valid for K = 50 ~ 2000 and Pr = 5 ~ 175 are seen to lie below the numerical result for the corresponding Prandtl number. However, the slopes of the curves are seen to agree with each other. It is also seen that Seban and McLaughlin's experimental data do not check with either the experimental data for Pr = 175 or the empirical correlation equation suggested by Dravid et al [82].

A comment on the computing time required to obtain a complete numerical result for flow and heat transfer at each value of the parameter $C^2/r_c$ may be of interest. It takes about 2 min for $C^2/r_c = 10^3$ and 8 min for $C^2/r_c = 4 \times 10^4$ with M, N = 28 and Pr = 1.0 on IBM 360/67. On the other hand, a computing time of approximately 40 min is required to obtain a complete result up to $C^2/r_c = 4 \times 10^4$ with M, N = 28 and Pr = 1.0. One notes that the computing time depends to a large extent on the selection of a relaxation factor.

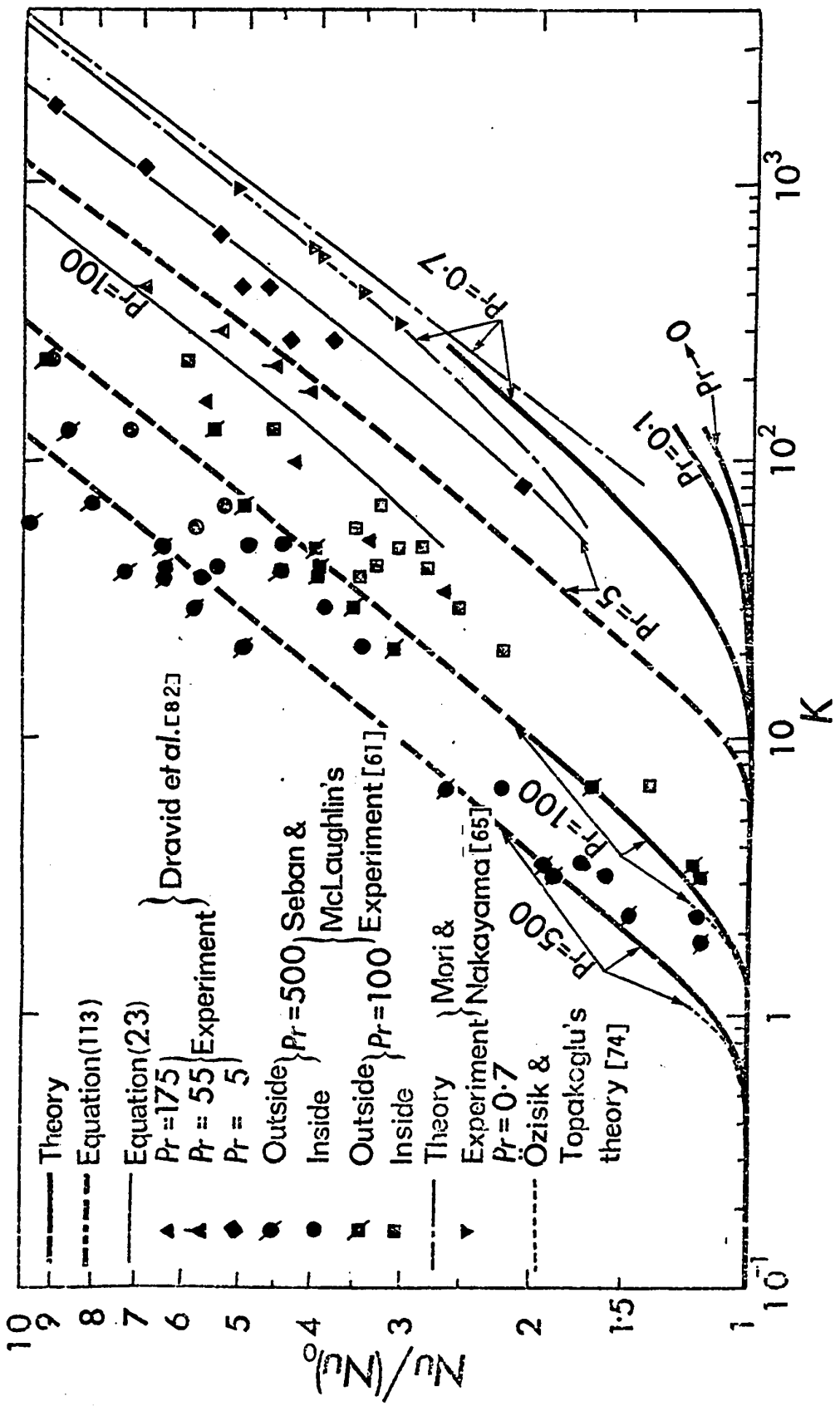


Fig. 21 Comparison of heat transfer results for uniform wall heat flux case available in literature.

## 3.5 CONCLUDING REMARKS

1. The numerical solution using a combination of the line iterative method and boundary vorticity method is shown to be very effective up to a reasonably high value of the Dean number where an asymptotic behavior already appears for flow and heat transfer results, and further result for high Dean number range can be obtained by a linear extrapolation. The distinctive features of the new method are its simplificity, computational stability, and a significant saving in computing time as compared with the conventional methods.

2. The Prandtl number effect for fully developed laminar forced convection in curved pipe is clarified for the first time. It is shown that all the heat transfer data for the present problem can be correlated by a single curve using a new parameter $Q = (K^2Pr)^{1/4}$ for $Pr \geq 1$. This observation of the asymptotic behavior in heat transfer results for Prandtl number effect is noteworthy and significant. The final validity of the proposed correlation equation using the new parameter Q should be checked critically by future theoretical and experimental data.

3. According to the order of magnitude analysis, the present formulation is considered to be valid for $a/R_c \leq O[10^{-2}]$. However, it is of practical interest to note that the assumption 1 in the formulation of the problem may be considered to be valid up to $a/R_c = 1/10$ in practice. This observation is based on the theoretical and experimental flow results available in the literature [17,41,35].

4. The correlation equation (113) clearly indicates the existence of the asymptotic behavior for large Prandtl number or large Dean number, and only the first term on the right hand side of equation (113) is significant. This finding is similar to that observed in earlier work [78] and is considered to be of practical importance.

5. Based on the present numerical results it is now evident that the perturbation method as used in the literature diverges quickly with the increase of the Dean number. This remark applies to a class of broadly similar forced laminar convection problems with secondary flow. Furthermore, it is shown that the boundary layer approximation predicts inconsistent Prandtl number effect and is valid only near Pr = 1.0.

6. The numerical results resulting from the present study are listed as Appendix 6 for future reference.

# CHAPTER IV

# GRAETZ PROBLEM IN CURVED PIPES WITH UNIFORM WALL TEMPERATURE*

## 4.1 INTRODUCTION

The thermal entrance region problem for fully developed laminar flow in curved pipes is of practical and theoretical interest but no theoretical analysis is available in the literature until recently. Dravid, Smith, Merrill and Brian [82] reported a numerical study on thermal entrance region problems in curved pipes for three basic thermal boundary conditions including those for a uniform wall temperature. Their numerical study for laminar flow is limited to the case with Dean number 225 only and with a fully developed velocity field obtained from Mori and Nakayama's theoretical solution [65] based on boundary layer approximations. The author became aware of the numerical analysis of Dravid et al [82] after the present work was completed. In view of the rather limited work reported so far on the Graetz problem in curved pipes, it is obvious that further theoretical and experimental work is required before the design data comparable to the classical Graetz problem in straight pipes is complete.

The purpose of this part of the thesis work is to present a complete numerical solution for the Graetz problem in a curved pipe

---

*The abstract for this work was presented in reference [84].

with a uniform wall temperature valid up to Dean numbers of order 100. The present numerical result and its implications will be critically examined against the main conclusions of Dravid et al [82,83] based on numerical and experimental investigations for high Dean numbers. It should be pointed out that the numerical results obtained in this investigation are directly applicable to the corresponding mass transfer problem by noting the analogy.

## 4.2 GRAETZ PROBLEM IN CURVED PIPES

The classical Graetz problem is to determine the development of the temperature profile along the heated (or cooled) section of flow passages for a steady fully developed laminar flow of an incompressible viscous fluid with constant physical properties (see Fig. 22). Since the publication of Graetz's classical work [100], the problem of thermal entrance region heat transfer has been extended in many ways to include various real effects which were not considered originally by Graetz. The Graetz problem in curved pipes is characterized by the inclusion of the convection terms due to secondary flow in the energy equation which is additional to the case of steady Poiseuille flow in straight tubes where the axial convection term represents the sole convection effect. The following assumptions are made in order to limit the scope of the present analysis:

1. The curvature ratio $a/R_c$ is small ($a/R_c << 1$).
2. The physical properties are constant and free convection effect is negligible.
3. Viscous dissipation is negligible and heat sources do not exist.

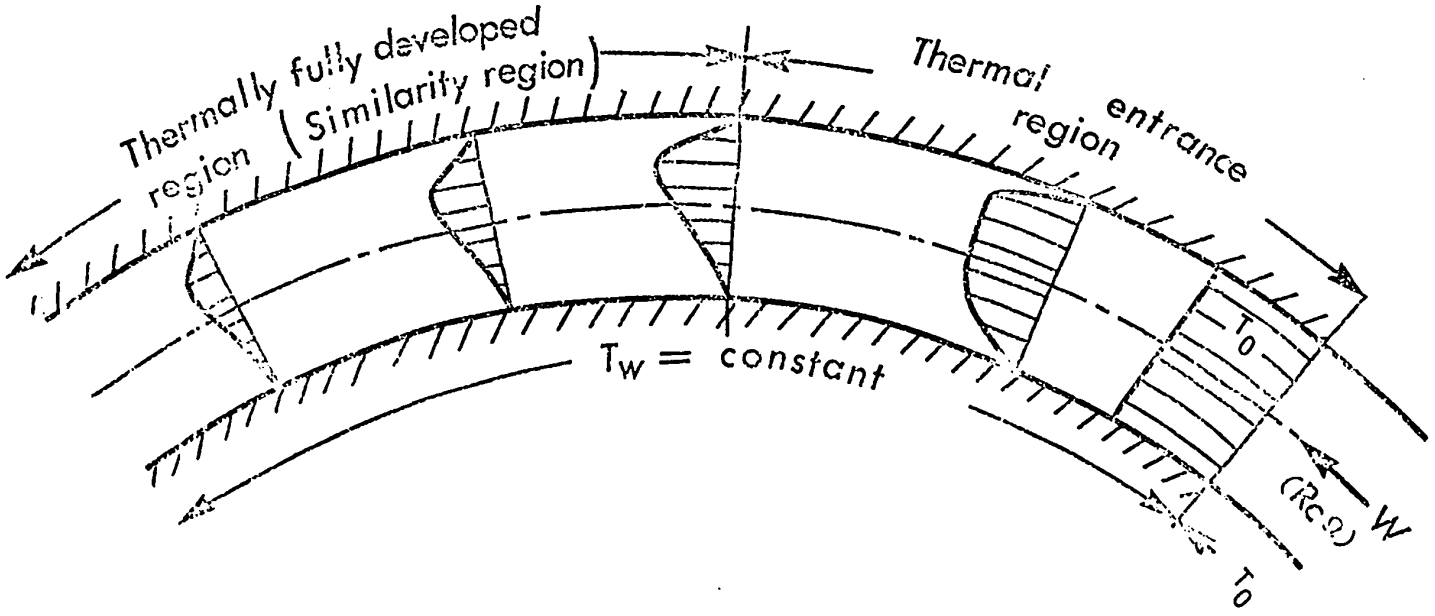


Fig. 22 Development of temperature profile in a curved pipe.

4. The axial conduction term is negligible compared with the radial conduction term in the energy equation (Pe $\gtrsim$ 50).

The practical implications of these assumptions are known. For example, according to recent work [96] the Graetz solution is found to be applicable only when the Rayleigh number [96] is less than about $10^3$. With assumption 2, the energy equation is seen to be uncoupled with the momentum equations, and the flow problem solved in Chapter III can be applied to the present problem as well. The energy equation without the axial conduction term becomes parabolic. A variety of thermal boundary conditions may be possible in practice, but the conditions most frequently studied as reference cases are uniform wall temperature and uniform heat flux at the wall. In this analysis, the fluid temperature is assumed to be constant ($T_0$) and equal to the wall temperature up to some axial position $R_c\Omega = 0$ where a step change in the wall temperature to a higher (or lower) value ($T_w$) is imposed (see Fig. 22). Referring to the coordinate system defined in Fig. 10 of Chapter III, the energy equation can be written as,

$$U \frac{\partial T}{\partial R} + \frac{V}{R} \frac{\partial T}{\partial \phi} + \frac{W}{R_c} \frac{\partial T}{\partial \Omega} = \alpha\left(\frac{\partial^2 T}{\partial R^2} + \frac{1}{R} \frac{\partial T}{\partial R} + \frac{1}{R^2} \frac{\partial^2 T}{\partial \phi^2}\right) \qquad (114)$$

It is noted that the above equation corresponds to equation (86) with the axial conduction term $\alpha\ \partial^2 T/R_c^2 \partial\Omega^2$ neglected. The circumstances under which the axial conduction term may be neglected are well discussed in Chapter II. In general, one may state that the axial conduction term is negligible except very near the thermal entrance of

a pipe and for a low Peclet number flow regime. The boundary condition is simply,

$$T = T_0 = \text{constant} \quad \text{at } \Omega = 0$$

and $$T = T_w = \text{constant} \quad \text{at } R = a \tag{115}$$

Introducing the following non-dimensional variables and the characteristic parameters,

$$R = [a]r,\ R_c = [a]r_c,\ U = [\nu/a]u,\ V = [\nu/a]v,\ W = [C\nu/a]w,$$

$$(T-T_w) = [T_0-T_w]\theta,\ (a^3/4\nu\mu)(\partial P_0/R_c\partial\Omega) = C,\ \text{and } \nu/\alpha = Pr,$$

equations (114) and (115) become

$$u\frac{\partial\theta}{\partial r} + \frac{v}{r}\frac{\partial\theta}{\partial\phi} + \left(\frac{C^2}{r_c}\right)^{1/2}\left(\frac{1}{r_c}\right)^{1/2} w\frac{\partial\theta}{\partial\Omega} = \frac{1}{Pr}\left(\frac{\partial^2\theta}{\partial r^2} + \frac{1}{r}\frac{\partial\theta}{\partial r} + \frac{1}{r^2}\frac{\partial^2\theta}{\partial\phi^2}\right) \tag{116}$$

$$\theta = 1 \quad \text{at} \quad \Omega = 0$$

$$\theta = 0 \quad \text{at} \quad r = 1 \tag{117}$$

The parabolic equation (116) is seen to be of second-order in r and $\phi$ and first-order in $\Omega$. Therefore, only one boundary condition in $\Omega$ can be satisfied with the asymptotic condition $\theta = 0$ at $\Omega = \infty$,

required for the elliptic problem abandoned. Due to symmetry of the problem, one has $\partial\theta/\partial\phi = 0$ along the horizontal center line ($\phi = 0$ and $\pi$) and a solution is required only for the upper half of the circular region (see Fig. 10). The difficulty of the analytical solution for the present Graetz problem in curved pipes is manifested by the rather limited applicability of the perturbation method [64] even for the asymptotic case involving the fully developed region. In view of the difficulty with the analytical solution and the availability of the numerical solutions for the momentum equation in Chapter III, the parabolic energy equation (116) will be solved numerically by using an alternating direction implicit method.

The limiting case of $Pr \to 0$ is of considerable practical interest. For this purpose, the energy equation (114) can be normalized by introducing additionally $\Omega = \Omega_c \omega$ with $\Omega_c$ denoting a characteristic value indicating an axial angle $\Omega$ required for the thermal entrance length. By noting that the axial convection term must be of order one in the normalized equation, one obtains

$$Pr\left(u\frac{\partial\theta}{\partial r} + \frac{v}{r}\frac{\partial\theta}{\partial\phi}\right) + w\frac{\partial\theta}{\partial\omega} = \frac{\partial^2\theta}{\partial r^2} + \frac{1}{r}\frac{\partial\theta}{\partial r} + \frac{1}{r^2}\frac{\partial^2\theta}{\partial\phi^2}$$

$$\Omega_c = Pr(C/r_c) = Pr(a/R_c)^{1/2}(K/2\bar{w}) \tag{118}$$

It is seen that when $Pr \to 0$, the convective terms involving Pr can be neglected and the secondary flow effect appears indirectly through w in the axial convection term. It is significant to note that $\Omega_c$ provides a measure of the thermal entrance length. The energy equation also

suggests that the Nusselt number is a function of the Prandtl and Dean numbers and the curvature ratio $a/R_c$ does not appear explicitly.

## 4.3 NUMERICAL SOLUTION USING THE ADI METHOD

The numerical solution of the momentum equations given in Chapter III is accomplished by a combination of the boundary vorticity method and a line iterative relaxation technique. The numerical solution of the general Graetz equation is of considerable interest, and an ADI method is employed for the integration of the parabolic equation. Since the numerical experiments concerning the stability and convergence in connection with the ADI method for the problem under consideration seem to be rather limited, and furthermore the numerical solution of the Graetz problem with secondary flow apparently has been reported only once in the past [82], a brief account of the ADI method used will be given here.

For the purpose of illustrating the computational procedure, a set of finite-difference equations in the radial and tangential directions, respectively, for equation (116) will be written in matrix form as follows using a three-point central-difference formula:

r-direction

$$\begin{bmatrix} B_{2,j} & C_{2,j} & & & 0 & \\ A_{3,j} & B_{3,j} & C_{3,j} & & & \\ & \cdot & \cdot & \cdot & & \\ & & A_{i,j} & B_{i,j} & C_{i,j} & \\ & 0 & & \cdot & \cdot & \cdot \\ & & & & A_{M,j} & C_{M,j} \end{bmatrix} \begin{bmatrix} \theta_{2,j}^{(k+1/2)} \\ \theta_{3,j} \\ \cdot \\ \theta_{i,j} \\ \cdot \\ \theta_{M,j} \end{bmatrix} = \begin{bmatrix} G_{2,j}^{(k+1/2)} \\ G_{3,j} \\ \cdot \\ G_{i,j} \\ \cdot \\ G_{M,j} \end{bmatrix}^{(k)} \qquad (119)$$

where $j = 1,2,\ldots,N+1$.

$\phi$-direction

$$\begin{bmatrix} E_{i,1} & F_{i,1} & & & 0 & \\ D_{i,2} & E_{i,2} & F_{i,2} & & & \\ & \cdot & \cdot & \cdot & & \\ & & D_{i,j} & E_{i,j} & F_{i,j} & \\ & 0 & & \cdot & \cdot & \cdot \\ & & & & D_{i,N+1} & E_{i,N+1} \end{bmatrix} \begin{bmatrix} \theta_{i,1}^{(k+1)} \\ \theta_{i,2} \\ \cdot \\ \theta_{i,j} \\ \cdot \\ \theta_{i,N+1} \end{bmatrix} = \begin{bmatrix} H_{i,1}^{(k+1/2)} \\ H_{i,2} \\ \cdot \\ H_{i,j} \\ \cdot \\ H_{i,N+1} \end{bmatrix} \qquad (120)$$

where $i = 2,2,\ldots,M$.

The elements of the coefficient matrices are:

$$A_{i,j} = -(Pr\Delta r/2)\, u_{i,j} - 1 + \Delta r/2r_i$$

$$[B_{i,j}]^{(k+1/2)}=[Pr(C^2/r_c)^{1/2}(1/r_c)^{1/2} \cdot 2(\Delta r)^2/\Delta\Omega \cdot w_{i,j}+2]^{(k+1/2)}$$

$$C_{i,j} = (Pr\Delta r/2)\, u_{i,j} - 1 - (\Delta r/2r_i)$$

$$D_{i,j} = Pr(\Delta r)^2/2\Delta\phi r_i \cdot v_{i,j} + (\Delta r)^2/r_i^2(\Delta\phi)^2$$

$$[E_{i,j}]^{(k+1)} = [-Pr(C^2/r_c)^{1/2}(1/r_c)^{1/2} \cdot 2(\Delta r)^2/\Delta\Omega \cdot w_{i,j}$$

$$- 2(\Delta r)^2/r_i^2(\Delta\phi)^2]^{(k+1)}$$

$$F_{i,j} = - Pr(\Delta r)^2/2r_i\Delta\phi \cdot v_{i,j} + (\Delta r)^2/r_i^2(\Delta\phi)^2$$

$$[G_{i,j}]^{(k)} = D_{i,j}[\theta_{i,j-1}]^{(k)} + [\{Pr(C^2/r_c)^{1/2}(1/r_c)^{1/2}\, 2(\Delta r)^2/\Delta\Omega.$$

$$w_{i,j} - 2(\Delta r)^2/r_i^2\,(\Delta\phi)^2\} \cdot \theta_{i,j}]^{(k)} + F_i,[\theta_{i,j+1}]^{(k)}$$

$$[H_{i,j}]^{(k+1/2)}=A_{i,j}[\theta_{i-1,j}]^{(k+1/2)} + [\{-Pr(C^2/r_c)^{1/2}(1/r_c)^{1/2}2(\Delta r)^2$$

$$/\Delta\Omega \cdot w_{i,j} + 2\}\, \theta_{i,j}]^{(k+1/2)} + C_{i,j}[\theta_{i+1,j}]^{(k+1/2)}$$

It is noted that the finite-difference equations along the horizontal center line, i=1,2,...M+1 for j=1 and N+1, take a special form after satisfying the symmetry condition $\partial\theta/\partial\phi = 0$ and the wall boundary condition also modifies the elements of the coefficient matrix. One also notes that the singularity inherent at the origin of the cylindrical

coordinates can be avoided by employing a finite-difference equation in Cartesian coordinates there.

Before presenting the main steps for the ADI method, the calculation procedure at the center point will be outlined. The usual procedure is to compute the value at (1,1) for the intermediate step (k+1/2) using the forward difference method based on the known values for (1,1), (2,1) and (2,N+1) from the previous step k. Using the new value for the center, the computation then proceeds to the intermediate step (k+1/2). The modified procedure used in this study consists of replacing the point (2,N/2+1) at the intermediate step (k+1/2) by the corresponding points for steps k and (k+1). The modified procedure now involves a forward difference explicit and a backward difference scheme and thus eliminates the need of using the grid point (2,N/2+1) at the intermediate step (k+1/2) in applying the ADI method.

With the procedure for the center point established, the solution of equation (116) can be accomplished by performing the following main steps:

1. The values for $u_{i,j}$, $v_{i,j}$ and $w_{i,j}$ are obtained from the solutions of the related momentum equations in Chapter III. The initial values for $\theta_{i,j}$ are set to be one, or any other reasonable values, since the fully developed condition is of primary interest here. Then the boundary condition $\theta_{M+1,j} = 0$ is applied.
2. The value of $\theta_{1,1}$ for the intermediate step (k+1/2) is computed, using the values at (1,1), (2,1), (2,N/2+1) and (2,N+1) from the previous step k.

3. After knowing $\theta_{1,1}$ for the intermediate step (k+1/2) and all the values for $\theta_{i,j}$ at the previous step (k), equation (6) can now be solved for $\theta_{i,j}$ at step (k+1/2) using Thomas' method.
4. With all the values for $\theta_{i,j}$ known at the intermediate step (k+1/2), equation (120) can be solved for $\theta_{i,j}$ at step (k+1).
5. Since the values for the center point and the adjacent three points at the intermediate step (k+1/2) are known, the value for $\theta_{1,1}$ at step (k+1) can be computed.
6. The above procedure can now be repeated until a fully developed temperature field is reached.

Since the computation of the Nusselt number is of primary interest in this study, the thermally fully developed situation is ascertained by the relative variation of the Nusselt number along the axial direction using the following relationship:

$$\varepsilon = (Nu^{(n+c)} - Nu^{(n)})/Nu^{(n)} < 5 \times 10^{-3} \qquad (121)$$

where n is an axial step number and c is a reasonably large integer such as 20 or 50.

The mesh sizes of M=N=14, M=14 and N=28, M=28 and N=14, and M=N=56 are examined to establish the accuracy for the numerical results and the mesh size of M=N=28 is found to be satisfactory from the viewpoint of accuracy and computing time. The angular coordinate $\Omega$

is transformed into $\eta$ by using the equation $\eta = 1 - e^{-\Omega}$ and the axial step sizes $\Delta\Omega = 0.1 \times 10^{-4} \sim 0.2 \times 10^{-1}$ corresponding to $\Delta\eta = 0.1 \times 10^{-4} \sim 0.1 \times 10^{-2}$ are used.

When the Dean number or Prandtl number is large, the local Nusselt number starts fluctuations after reaching a minimum Nusselt number and a subsequent maximum value at some distance from the thermal entrance as shown in Fig. 23 if the numerical solution starts with $\theta_{i,j} = 1$ at the entrance. This phenomenon is similar to that reported by Dravid et al [82,83] for the high Dean number regime. The question arises as to whether or not this is a true physical solution or merely a manifestation of numerical instability. In order to clarify this point, the limiting Nusselt number for the fully developed temperature field is computed using three different initial values for the case of Pr = 500 and K = 6.26. It is found that if the numerical solution starts at some distances from the entrance with the initial values obtained from the completely converged cases of K = 2.44 and 3.14, respectively, the limiting Nusselt number of 12.1 is obtained for both cases, (see Fig. 23). On the other hand, with $\theta_{i,j} = 1$ at the entrance, the fluctuation phenomenon as pointed out earlier appears. Eventually the oscillation of the Nusselt number is damped out and a stable lower limiting Nusselt number of 8.0 is obtained. The oscillation of the local Nusselt number remains even with a further decrease of the mesh size. It should be pointed out that the local maximum value of the Nusselt number at the start of fluctuation corresponds closely to a limiting value of 12.1. If the fluctuation of the local

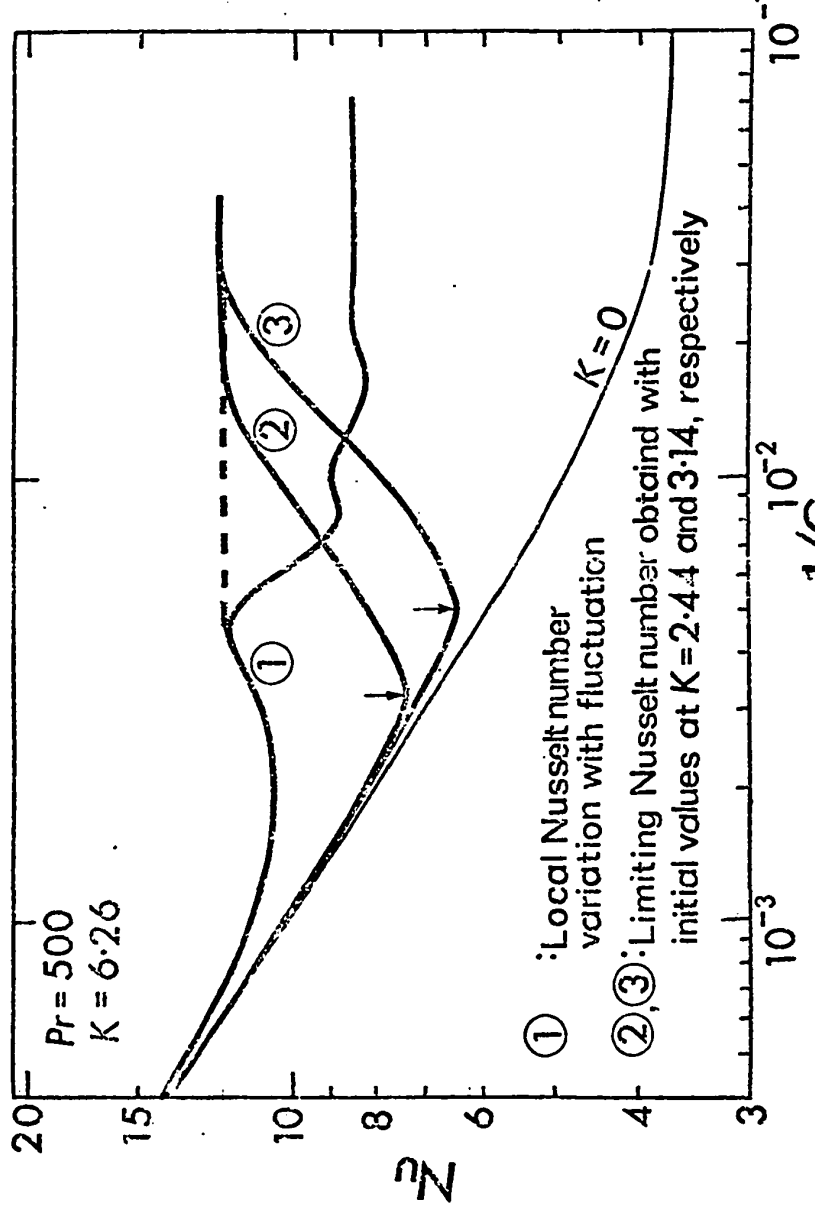


Fig. 23 Numerical experiments on asymptotic limiting Nusselt number.

Nusselt number is regarded as a true physical solution [82], then it seems to contradict the known fact that the effect of the secondary flow is to decrease the thermal entrance length. In this connection, the numerical data for local Nusselt number variation with axial distance from entrance for the case of a constant uniform wall temperature reported in [82] show that the thermal entrance length for the case Pr = 5 and K = 225 is nearly identical to that of a straight tube. In addition, if the damped limiting value of the Nusselt number is taken as a true physical solution, the plot for limiting Nusselt number versus Dean number will have a lower slope after reaching a certain high Dean number depending on the Prandtl number.

In view of the above fluctuating phenomenon for local Nusselt number observed at Pr = 500 and K = 6.26 in the thermal entrance region, it is desirable to study the possibility of a fluctuating phenomenon arising from a numerical instability of the method used. As noted in Chapter III, the stability of the numerical method for parabolic equations is somewhat similar to the convergence of the iteration method for elliptic equations and the axial steps K, K + 1/2 and K + 1 in equations (119) and (120) for the ADI method corresponds to the iteration steps in the iteration method. The repeated use of either equation (119) or (120) in the ADI method is much the same as that of the corresponding finite-difference equation in the line successive-overrelaxation method discussed in Chapter III, and the convergence criteria given by equation (111) may be applied to the

present case. However, in the present ADI method, a complete computation cycle consists of the first sweep in the r-direction using equation (119) and the second sweep in $\phi$-direction using equation (120). In general, the alternating use of the r- and $\phi$-directions, computation processes would give favorable effects on stability. As a matter of fact, the numerical solution [104] of Poisson's equation for the unsteady heat conduction problem involving a rectangular region using an ADI method is known to be stable for any combination of the time increment $\Delta t$ and spacial mesh size $\Delta h$. In contrast, the repeated use of the single direction computation process may be unstable for some combination of $\Delta t$ and $\Delta h$ [99].

One may now study the stability of the ADI method by using the convergence criteria given by equation (111). It is noted that the diagonal dominance of the coefficient matrix may be an important factor for the stability of ADI methods. An inspection of the off-diagonal elements in the coefficient matrices in equations (119) and (120) reveals that the following restriction will ensure the diagonal dominance.

$$\left|\frac{\Delta r}{2}\right| \cdot \left|\frac{1}{r_i} - \text{Pr}\, u_{i,j}\right| \leq 1$$

for equation (119)

$$\left|\frac{\Delta \phi}{2}\right| \cdot \left|r_i\, \text{Pr}\, v_{i,j}\right| \leq 1 \qquad (122)$$

for equation (120)

The above relations show that the magnitude of Pr $u_{i,j}$ and Pr $v_{i,j}$ are of primary importance for convergence criteria. The violation of the above restrictions may lead to stability problems and the solution may not be convergent. Rewriting equation (119) as $B^{(k+1/2)}\ \theta^{(k+1/2)} = G^{(k)}$, one notes that the present discussion is concerned only with the characteristics of the coefficient matrix $B^{(k+1/2)}$. A source of computational error may also arise from the column vector $G^{(k)}$ and this possibility will be considered next.

One may define the residual $R^{(k)}$ for the system involving equation (119) as

$$R^{(k)} = G^{(k)} - B^{(k+1/2)}\ \theta^{(k+1/2)} \tag{123}$$

One notes that the accumulation of the round-off errors can reasonably be represented by the above residual [105]. One may write $G^{(k)}$ as

$$G^{(k)} = [\frac{(\Delta r)^2}{2\Delta\phi\ r_i} \text{Pr}\ v_{i,j} + (\frac{\Delta r}{\Delta\phi\ r_i})^2]\ \theta_{i,j-1}^{(k)}$$

$$+ [\text{Pr}\ (\frac{c^2}{r_c})^{1/2} (\frac{1}{r_c})^{1/2} 2\ \frac{(\Delta r)^2}{\Delta\Omega}\ w_{i,j}$$

$$- 2(\frac{\Delta r}{\Delta\phi\ r_i})^2]^{(k)}\ \theta_{i,j}^{(k)}$$

$$+ [-\frac{(\Delta r)^2}{2\Delta\phi\ r_i} \text{Pr}\ v_{i,j} + (\frac{\Delta r}{\Delta\phi\ r_i})^2]\ \theta_{i,j+1}^{(k)} \tag{124}$$

Consideration will now be given to the evaluation of the coefficients for $\theta_{i,j-1}^{(k)}$, $\theta_{i,j}^{(k)}$, and $\theta_{i,j+1}^{(k)}$. Taking the

coefficient of $\theta^{(k)}_{i,j-1}$ as an example, one notes that the computational accuracy of a point velocity $v_{i,j}$ is much less than that of $(\Delta r/\Delta\phi\ r_i)^2$. The multiplication of $v_{i,j}$ by a large Prandtl number, for example may magnify the computational error for the term involving $Pr\ v_{i,j}$ in comparison to that of the term $(\Delta r/r_i\ \Delta\phi)^2$. Specifically, the difficulty may arise when $Pr\ v_{i,j}/2$ becomes more important than $1/r_i\ \Delta\phi$. This possibility may arise when either the Prandtl number is large or the secondary velocity is large for large Dean numbers. The above observation suggests that the numerical difficulty may arise when either the Prandtl number or the Dean number is large. At present this is generally the observed fact for the numerical solution involving secondary flow problems. In the computation of the coefficient for $\theta^{(k)}_{i,j-1}$, the inaccurate term involving $Pr\ v_{i,j}$ may dominate. If this happens, the numerical evaluation of the column vector $G^{(k)}$ may be quite off from its true value and the resulting error may be directly responsible for the numerical instability. This in turn may lead to the fluctuating phenomenon for the local Nusselt number. This observation cannot be regarded as conclusive, but the possibilty cannot be ruled out completely. Of course, the round-off error involving the coefficient matrix $B^{(k+1/2)}$ is also related to the residual $R^{(k)}$. The situation for the coefficient matrix and the right-hand column vector in equation (120) is similar to that discussed so far. It is now clear that the numerical instability is a possibility when either the Prandtl number or Dean number is large. Further reasoning against the oscillation phenomenon as the true physical solution can best be

achieved with a detailed study of the temperature development in the thermal entrance region.

## 4.4 DEVELOPMENT OF THE TEMPERATURE FIELD IN THE THERMAL ENTRANCE REGION

The interaction between the fully established secondary flow and the developing temperature field in curved pipes represents a departure from the classical Graetz problem in straight tubes. A study of the developing temperature field may shed some light on the physical mechanism of convective heat transfer in the thermal entrance region of a curved pipe and provide a means for the fundamental understanding of overall heat transfer characteristics. For this purpose the temperature profile developments along the central horizontal and vertical axes are illustrated in Figs. 24, to 27 for Pr = 0.1, 0.7, 10 and 500, respectively, with a typical Dean number. The characteristics of developing temperature profiles are distinctively different from those of the classical Graetz problem in straight tubes or channels in that the thermal boundary layer development along the wall around the circumference. Here the thermal boundary layer is defined as the region near the wall where the fluid temperature is different from the uniform entrance fluid temperature. It is clearly seen that the thermal boundary layer develops much more rapidly at the inner wall ($\phi = \pi$) than at the outer wall ($\phi = 0$) and eventually the thermal boundary layer at all angular positions ($\phi = 0 \sim \pi$) merges at some distance from thermal entrance depending

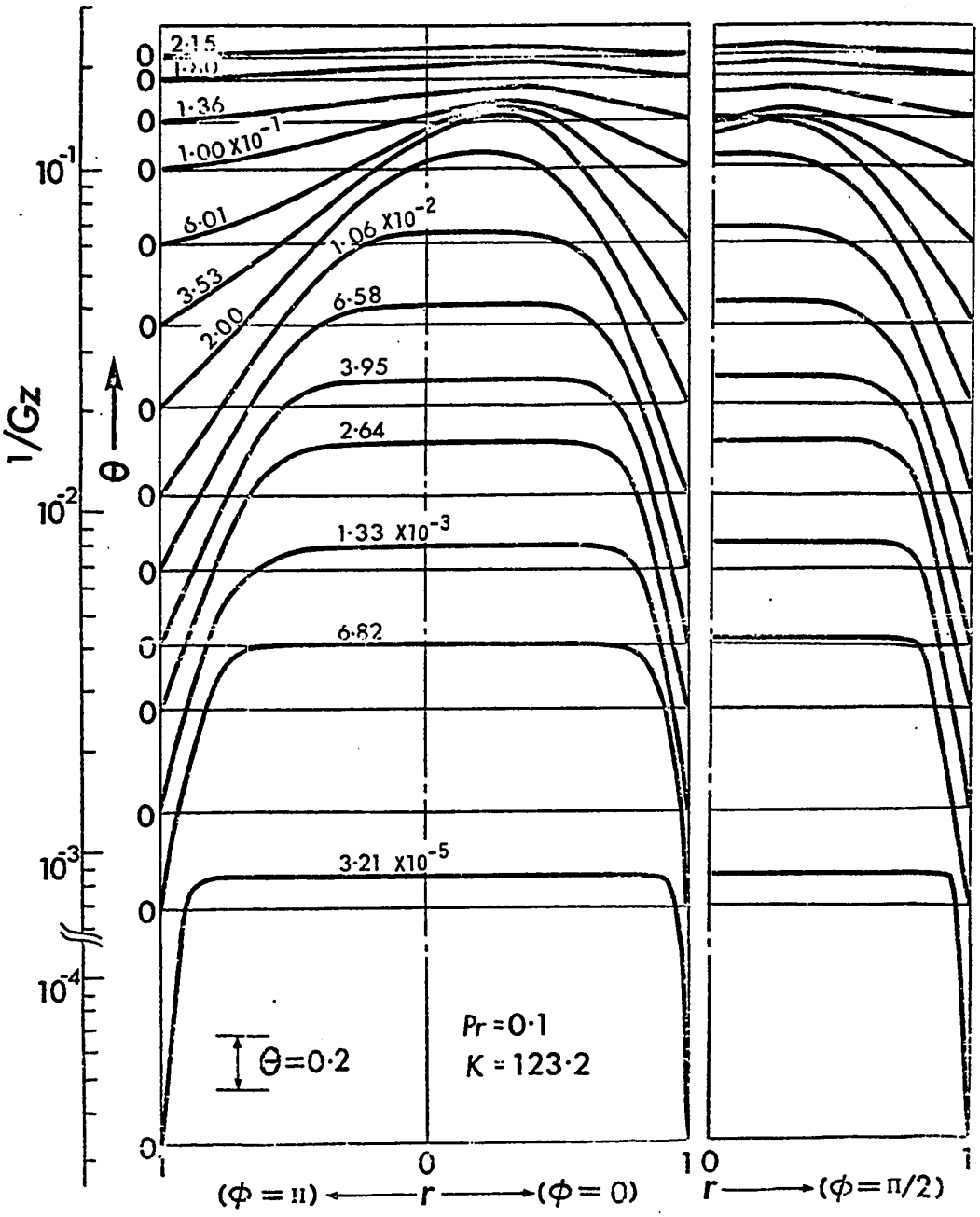


Fig. 24 Temperature profile development along dimensionless downstream distance at Pr = 0.1 and K = 123.2.

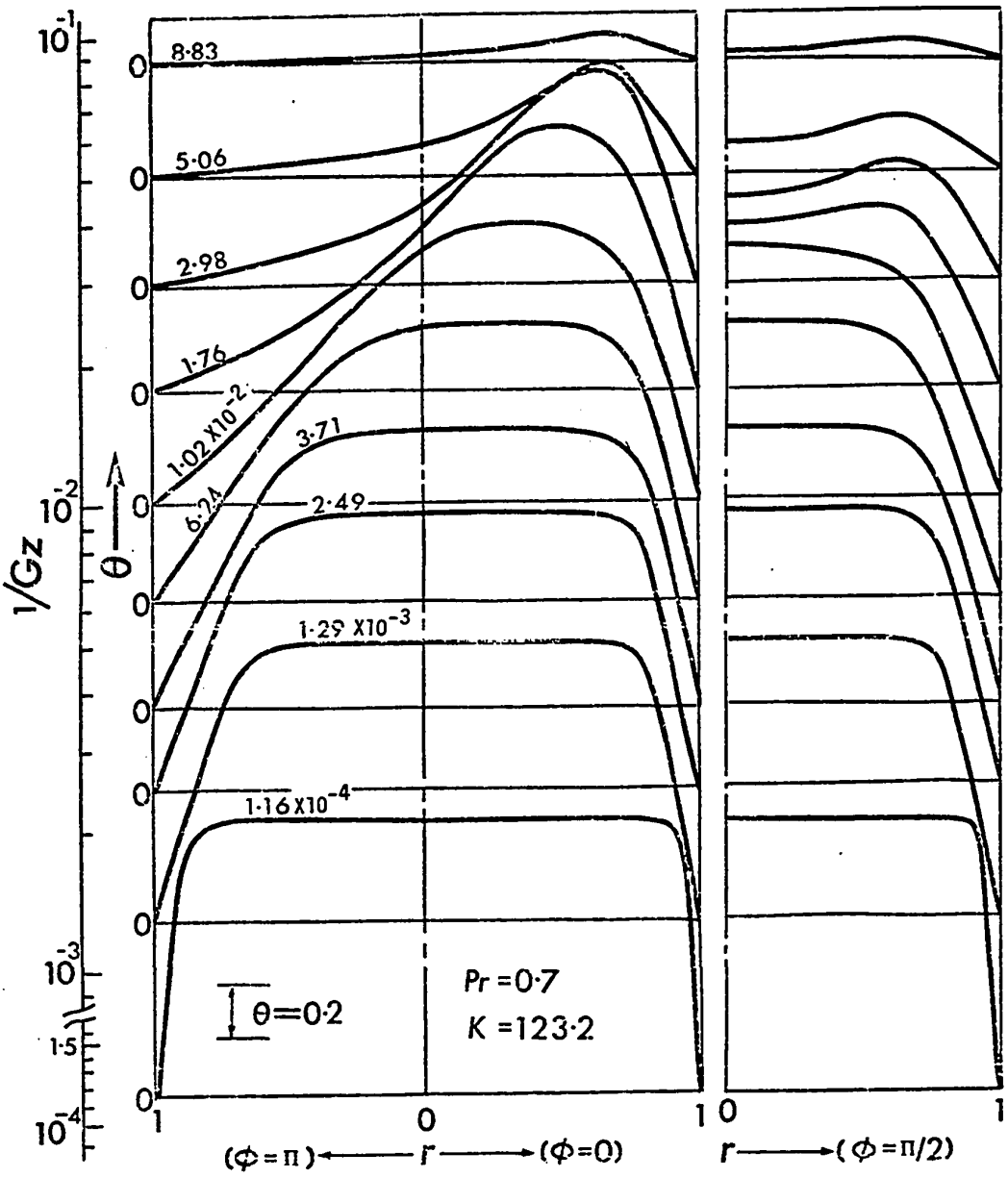


Fig. 25 Temperature profile development along dimensionless downstream distance at Pr = 0.7 and K = 123.2.

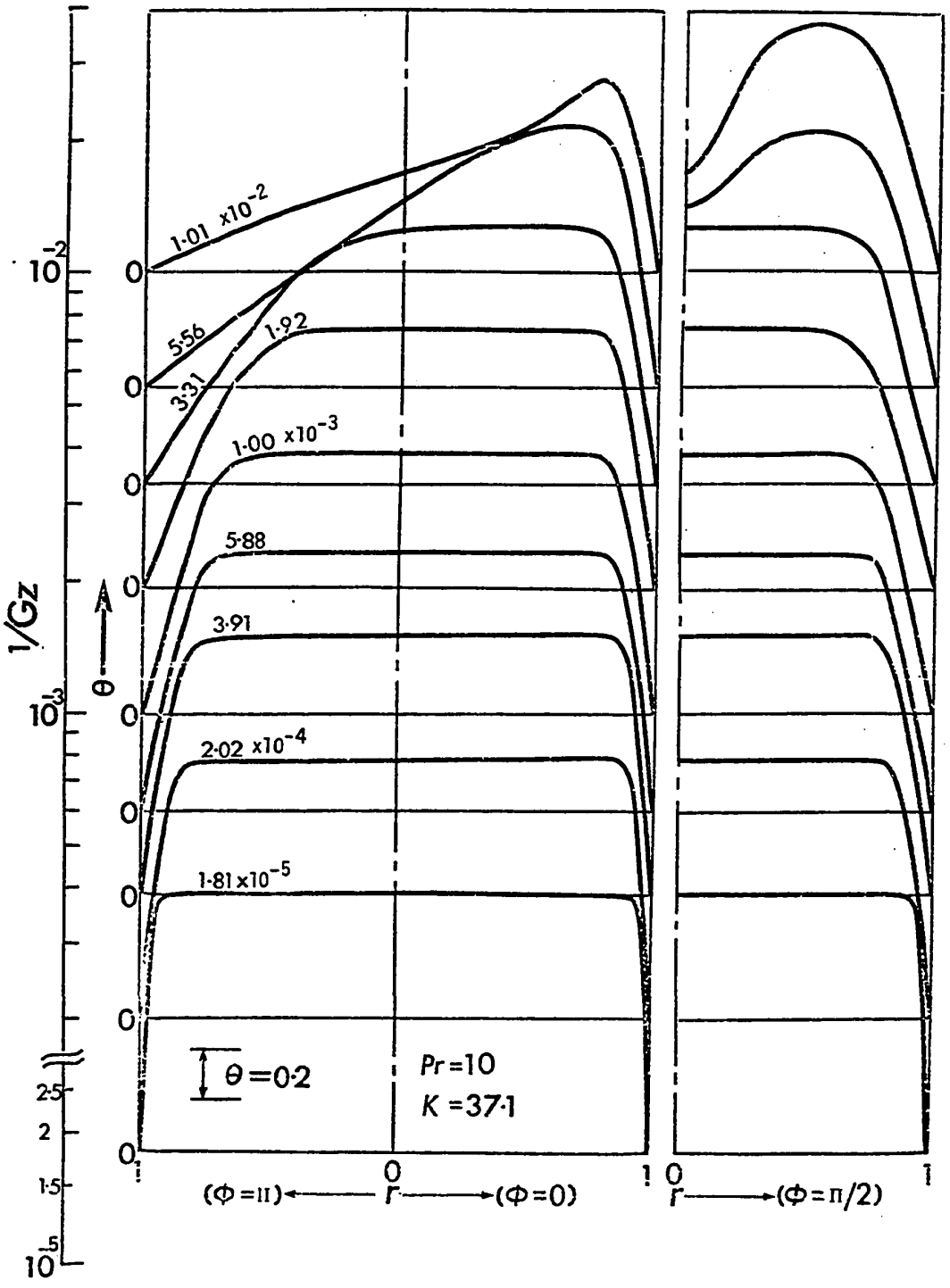


Fig. 26 Temperature profile development along dimensionless downstream distance at Pr = 10 and K = 37.1.

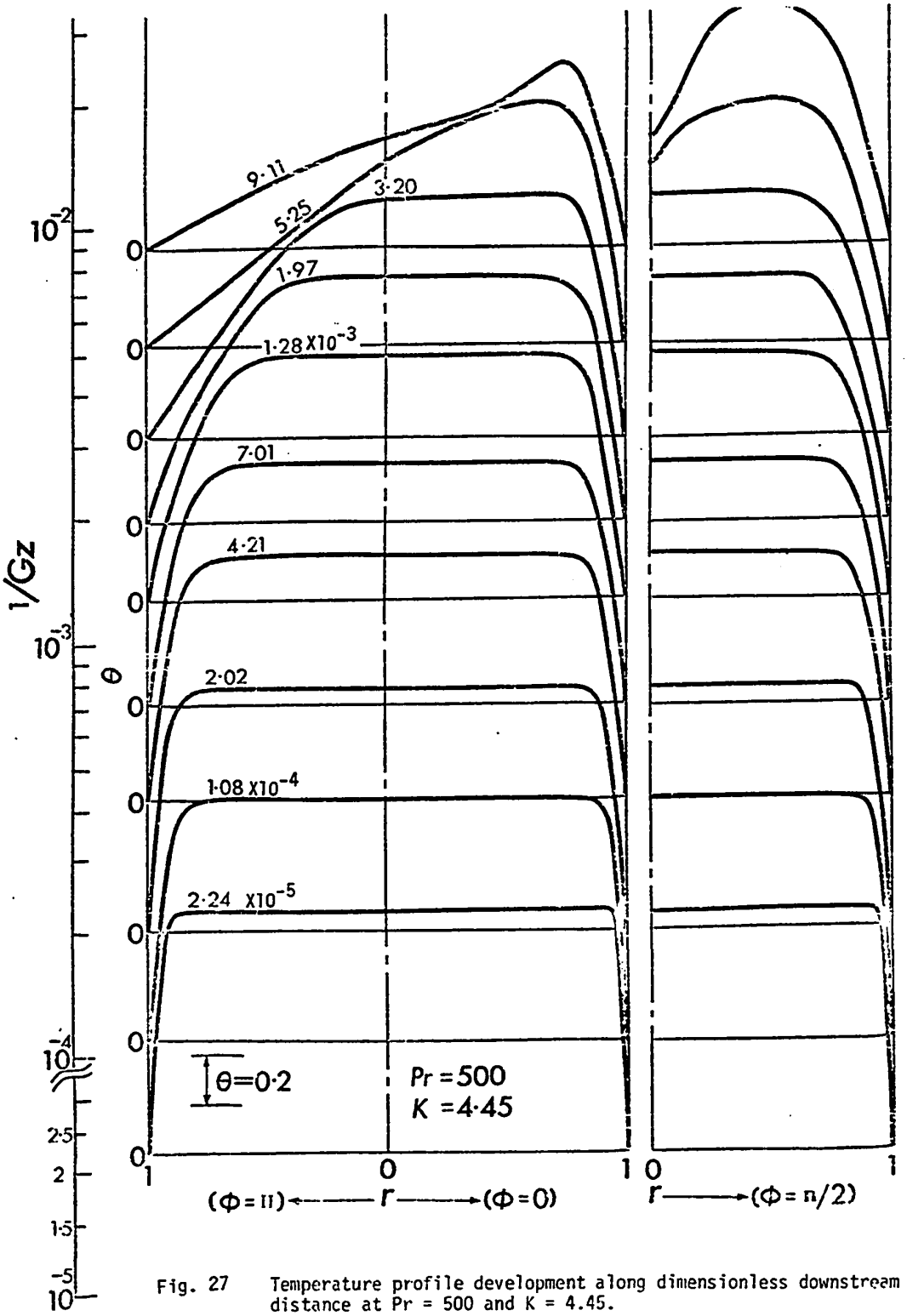


Fig. 27 Temperature profile development along dimensionless downstream distance at Pr = 500 and K = 4.45.

on the Prandtl and Dean numbers. After the merging of the thermal boundary layer at all angular positions, the temperature profile may further adjust itself and finally the fully developed temperature field is attained. The above observation is significant and a crucial one in arguing against the physical realization of the Nusselt number oscillation phenomenon observed numerically by Dravid et al [82] just before reaching the asymptotic value. This point will be critically examined when numerical results for Nusselt number are presented later. Note also the complete disappearance of the initial uniform temperature profile at the entrance does not signal the completion of the developing temperature field.

Since the Dean numbers are identical (K = 123.2) for Figs. 24 and 25, the effect of increase in Prandtl number from Pr = 0.1 in Fig. 24 to Pr = 0.7 in Fig. 25 is seen to decrease the thermal entrance length for a given value of Dean number. On the other hand, the general characteristics for developing temperature fields shown in Fig. 26 for Pr = 10 and K = 37.1 and Fig. 27 for Pr = 500 and K = 4.45 are qualitatively similar and from this, one may conclude that the effect of the Dean number on temperature profile development is similar to that of the Prandtl number for a given Peclet number. Of course, when one considers the effect of one independent parameter such as the Dean number, the other independent parameter, namely the Prandtl number, must be kept constant. In Figs. 24 to 27 the last temperature profile may be regarded as a fully developed one.

Further insight regarding developing temperature fields

may be obtained by a study on the distributions of isothermals and the cases of Pr = 0.7, K = 123.2 and Pr = 10 and K = 37.1 corresponding to the cases of Figs. 25 and 26, respectively, are shown in Figs. 28 and 29. In observing the distributions shown in Figs. 28 and 29, one should note that without secondary flow, the isothermals are concentric circles, and the gradual distortion from near circles close to the entrance represents the secondary flow effect. The effect is seen to increase with the axial distance. The patterns of isothermals at various axial distances are closely related to the Nusselt number variation which will be discussed later. At this point, it suffices to note that at $1/Gz = (1/Pe)(R_c\Omega/2a) = 2.98 \times 10^{-2}$ shown in Fig. 28, kidney-shaped isothermals with concave part appears and the isothermals for $1/Gz = 5.06 \times 10^{-2}$ and $8.83 \times 10^{-2}$ are remarkable similar since both represent thermally fully developed situations. In Fig. 29, at $1/Gz = 1.01 \times 10^{-2}$ eventually the concave portion of isothermals merges with the convex portion of isothermals near the outer wall, and the eyes of isothermals appear. As a result, the minimum temperature location is shifted toward $\phi = \pi/2$ in contrast to those along $\phi = 0$ for all axial positions shown in Fig. 28. The location of the minimum temperature point or the existence of one or two such points apparently depends on Prandtl and Dean numbers and axial position. It is interesting to note that the plume-like behavior in the form of a warm current penetrating into the cold fluid core region becomes apparent after reaching some axial position.

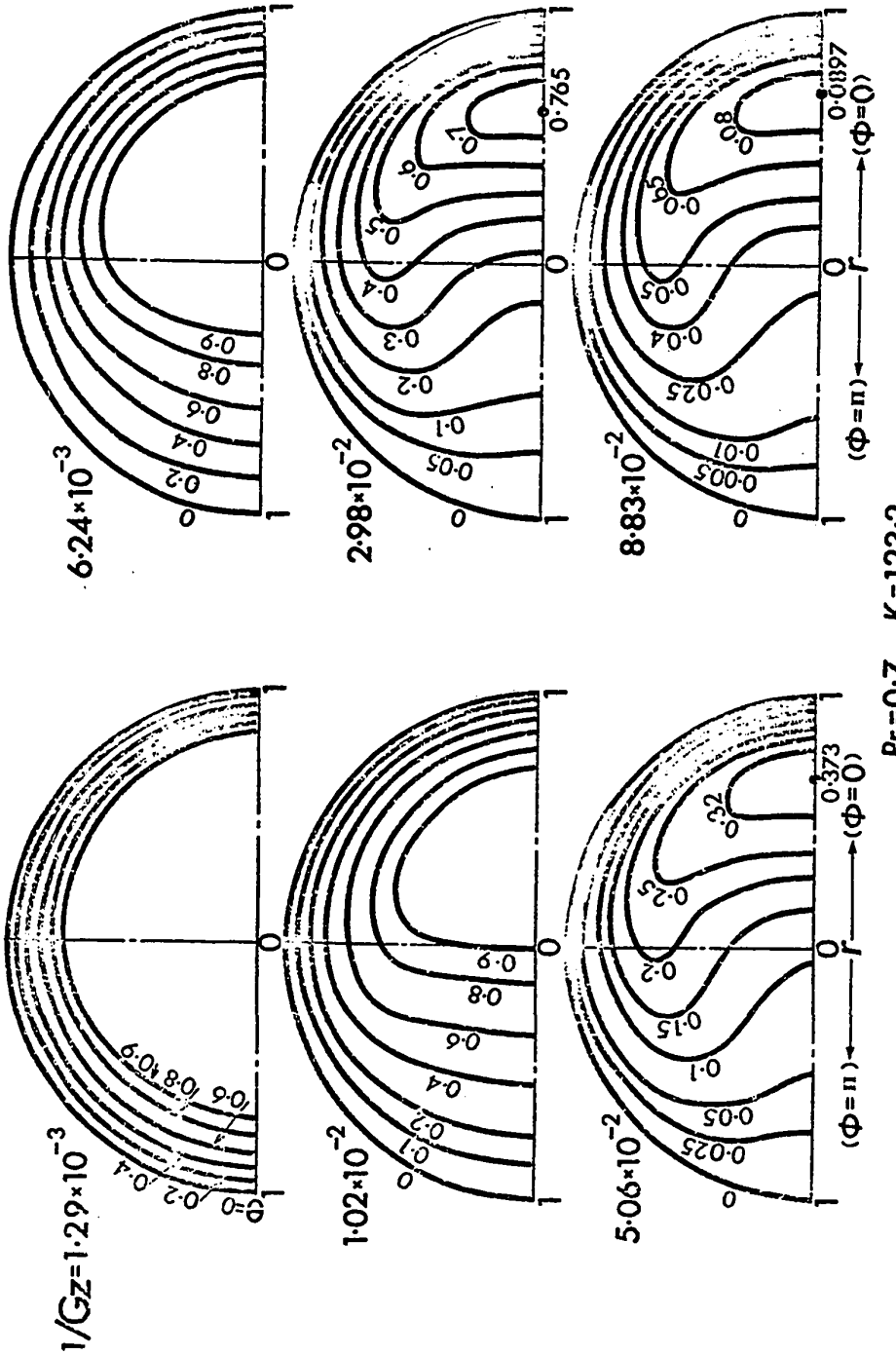


Fig. 28 Development of isothermals at six downstream cross sections for Pr = 0.7 and K = 123.2.

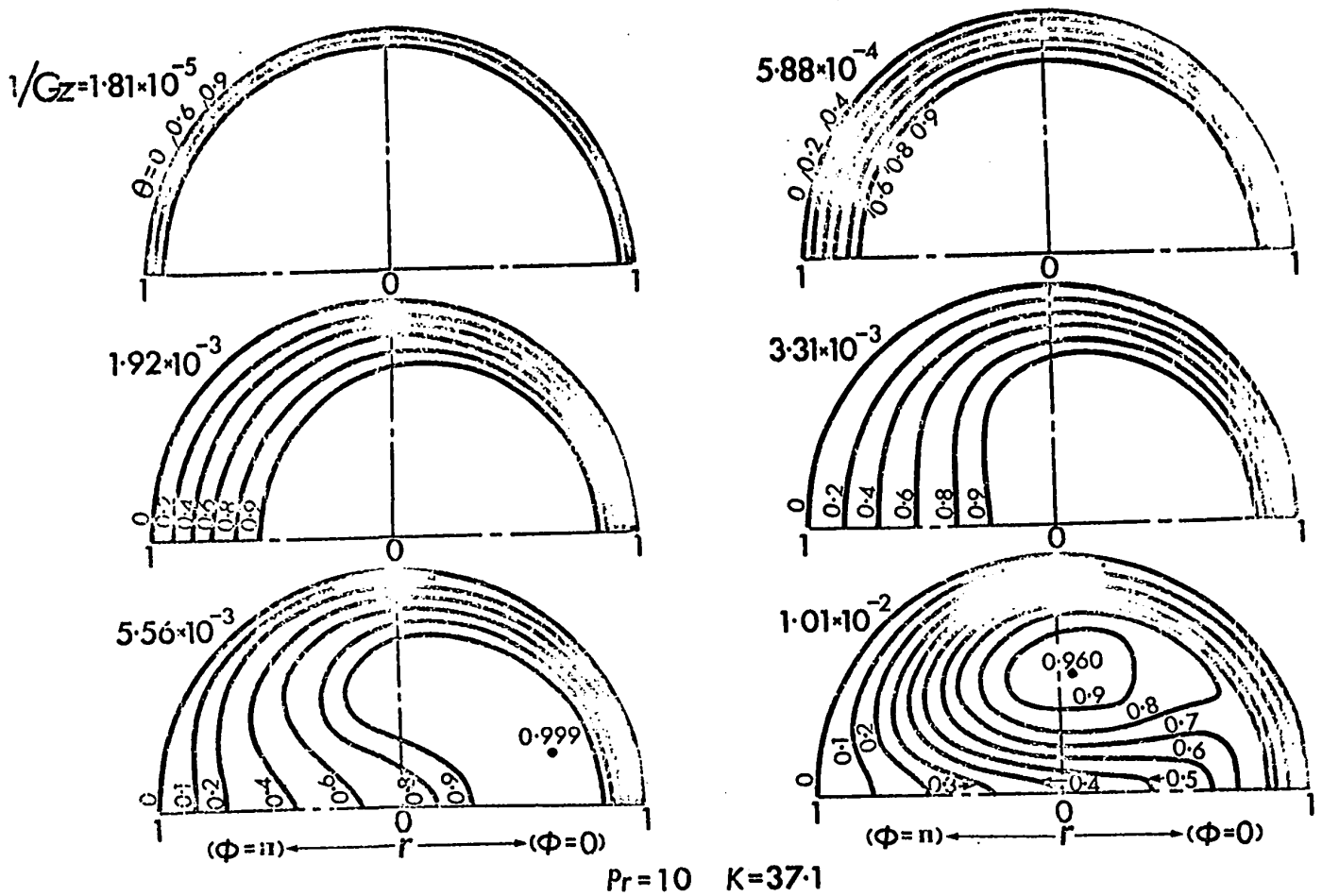


Fig. 29 Development of isothermals at six downstream cross sections for Pr = 10 and K = 37.1.

## 4.5 NUMERICAL RESULTS FOR NUSSELT NUMBERS

For the case of constant wall temperature, the average Nusselt number is of practical interest in design. However, the local Nusselt number variation in the thermal entrance region is of considerable importance for a basic understanding and might clarify the reasons behind the practical difficulty in correlating the limited experimental data as experienced by several investigators. The use of two alternative expressions in evaluating the local Nusselt number is particularly useful in checking the accuracy of the numerical results. The Nusselt number, $Nu = \bar{h}(2a)/k$, can be obtained in two ways by considering either the average wall temperature gradient or the local energy balance in the axial direction as:

$$(Nu)_1 = 2\bar{w}\ |\overline{\partial\theta/\partial r}|_w\ /\ |\overline{w\theta}|$$

$$(Nu)_2 = Pr\ (c^2/r_c)^{1/2}\ (1/r_c)^{1/2}\ \bar{w}|\overline{w\partial\theta/\partial\Omega}|\ /\ |\overline{w\theta}| \qquad (125)$$

Simpson's rule is used in evaluating the mean values appearing in equation (125) except for $|\overline{w\partial\theta/\partial\Omega}|$ where the trapezoidal rule is employed. The local Nusselt numbers versus $1/Gz = (1/Pe)(R_c\Omega/2a)$ with Dean number as a parameter for Pr = 0.1, 0.7, 10 and 500 are shown in Figs. 30 to 33, and the corresponding plots for the average Nusselt numbers over the length are included as Figs. 34 to 37. In plotting the numerical results, the average value of the two Nusselt number expressions is used and each definition is found to deviate from 0 to 1.5 per cent from the average value indicating good

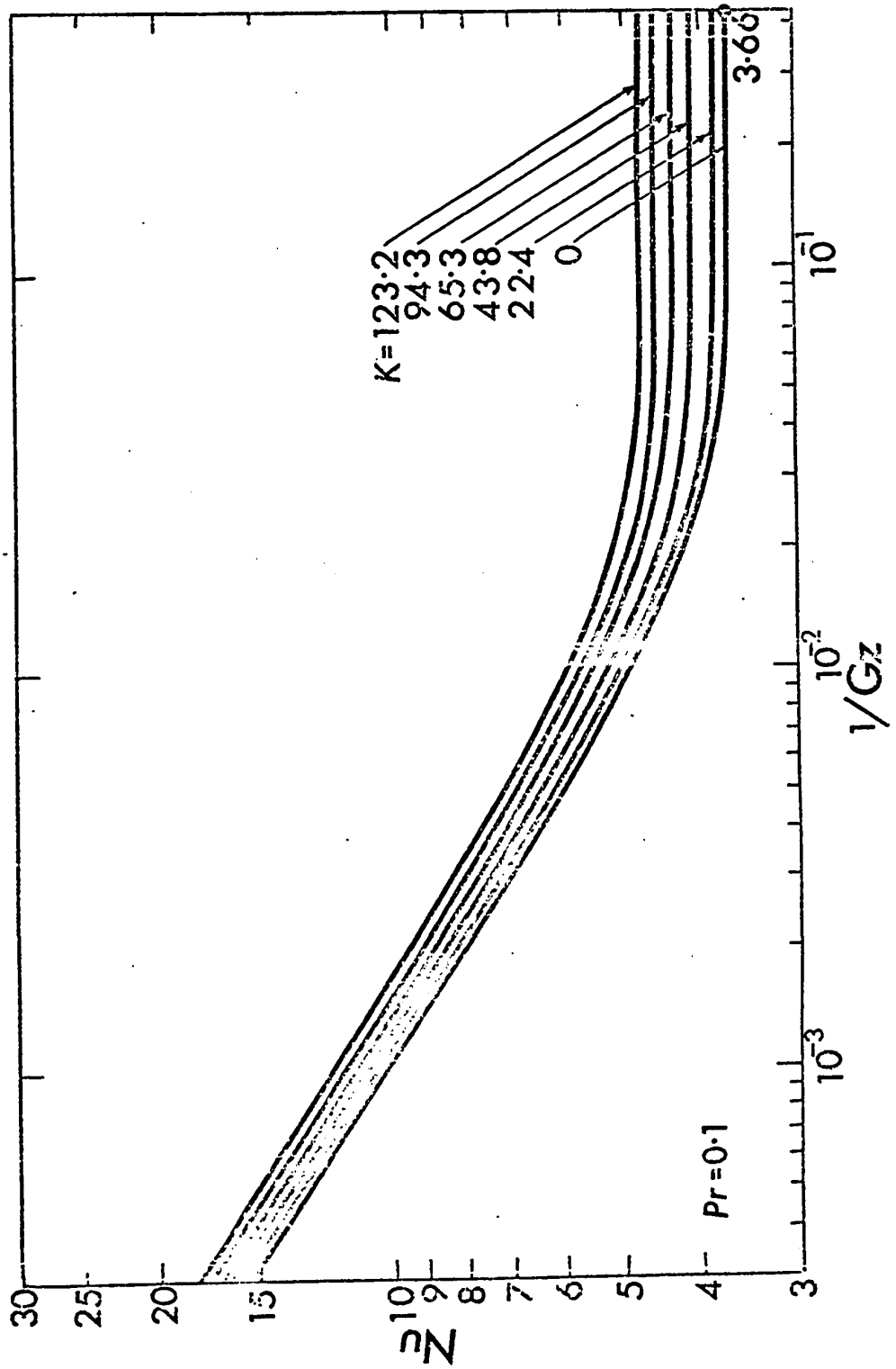


Fig. 30 Local Nusselt number variation along dimensionless downstream distance for Pr = 0.1 with Dean number as parameter.

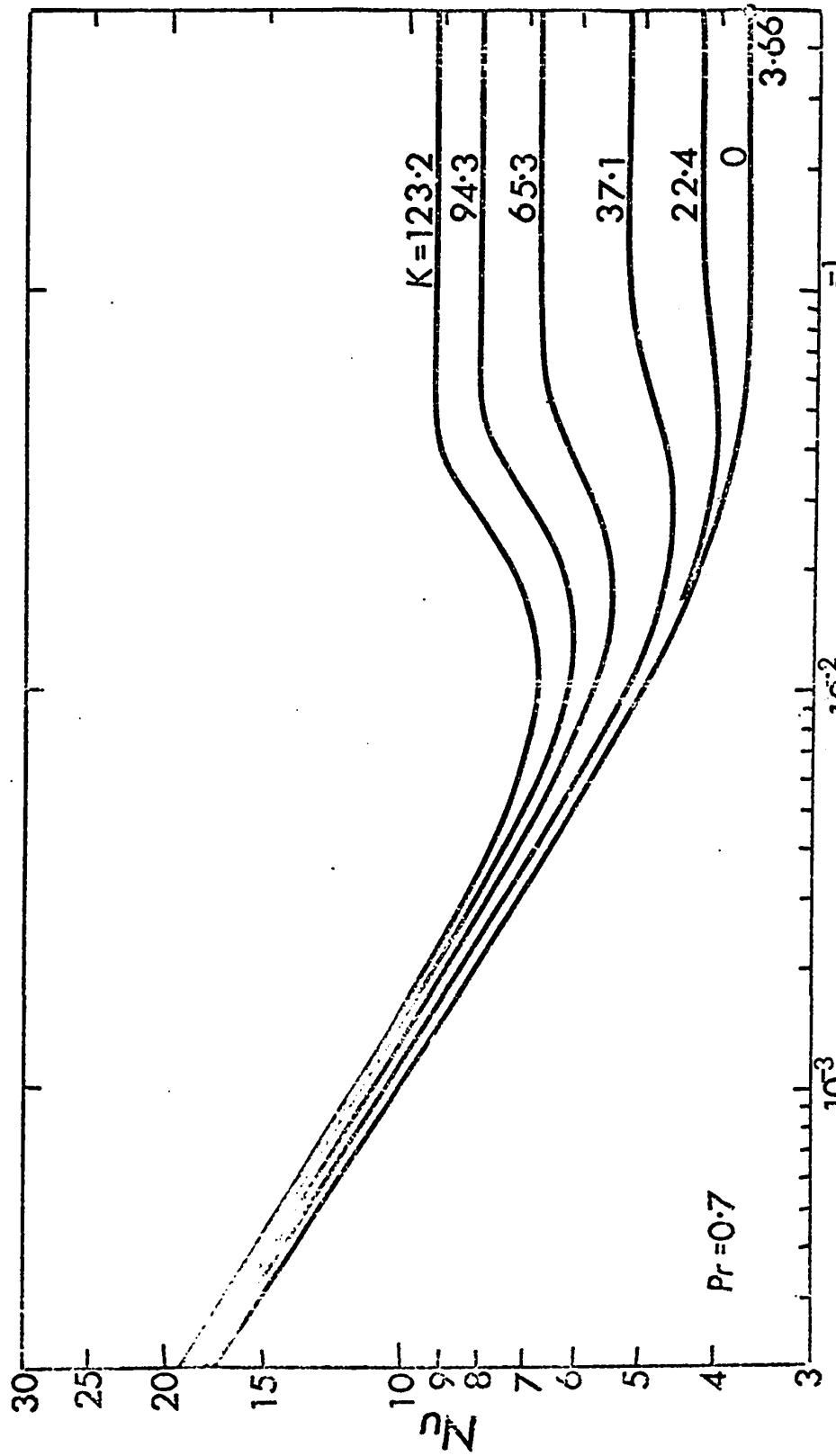


Fig. 31 Local Nusselt number variation along dimensionless downstream distance for Pr = 0.7 with Dean number as parameter.

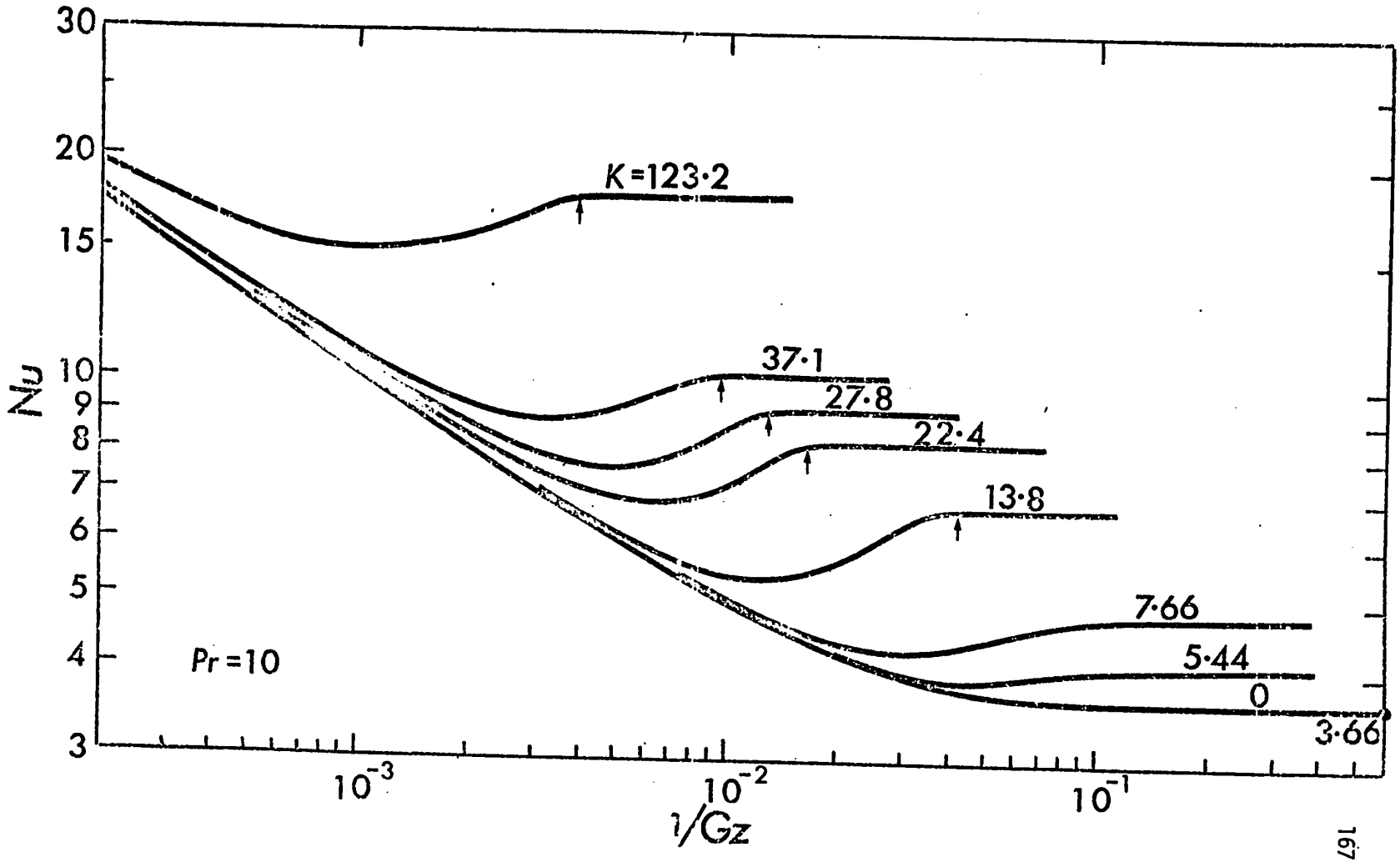


Fig. 32 Local Nusselt number variation along dimensionless downstream distance for Pr = 10 with Dean number as parameter.

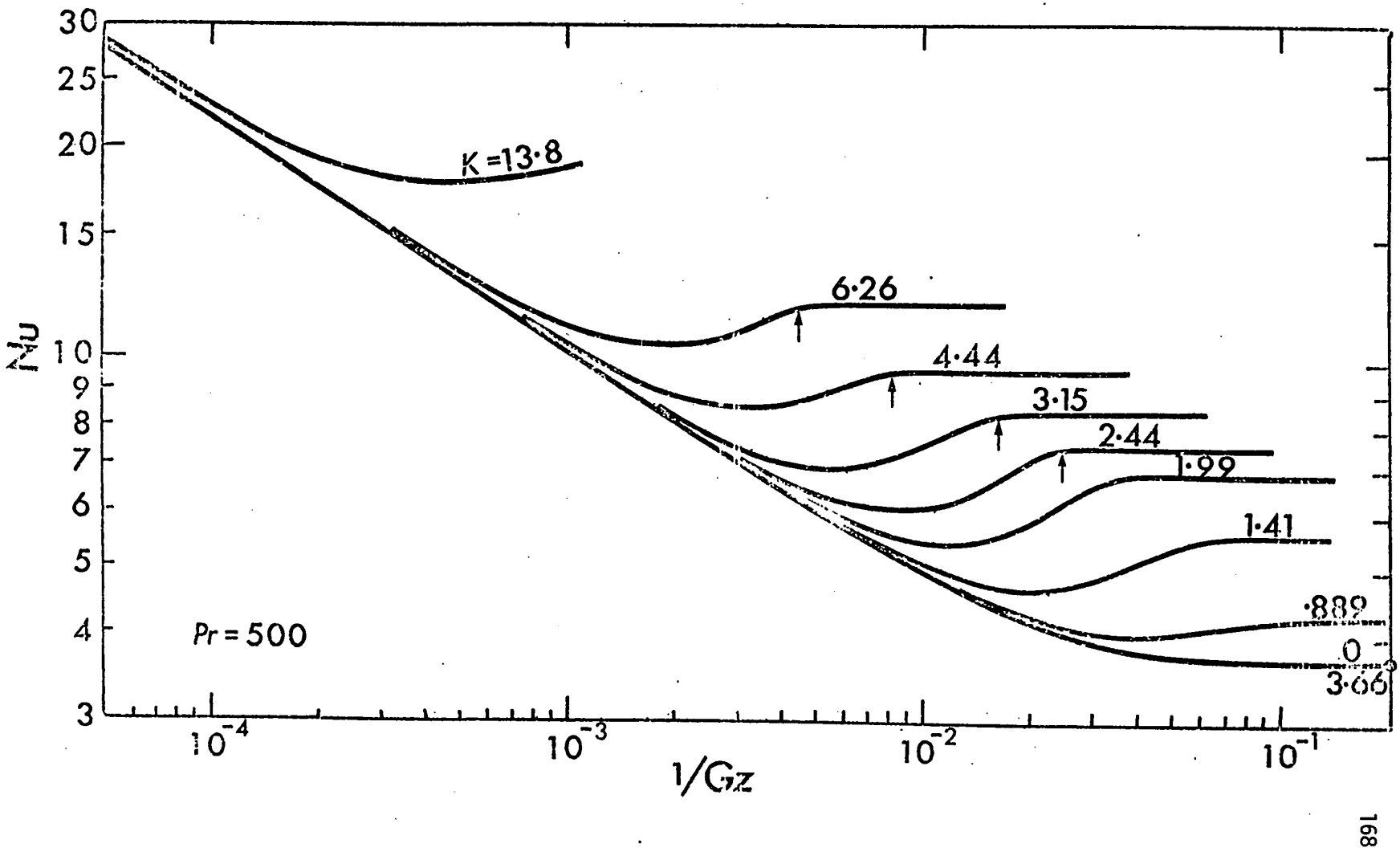


168

Fig. 33 Local Nusselt number variation along dimensionless downstream distance for Pr = 500 with Dean number as parameter.

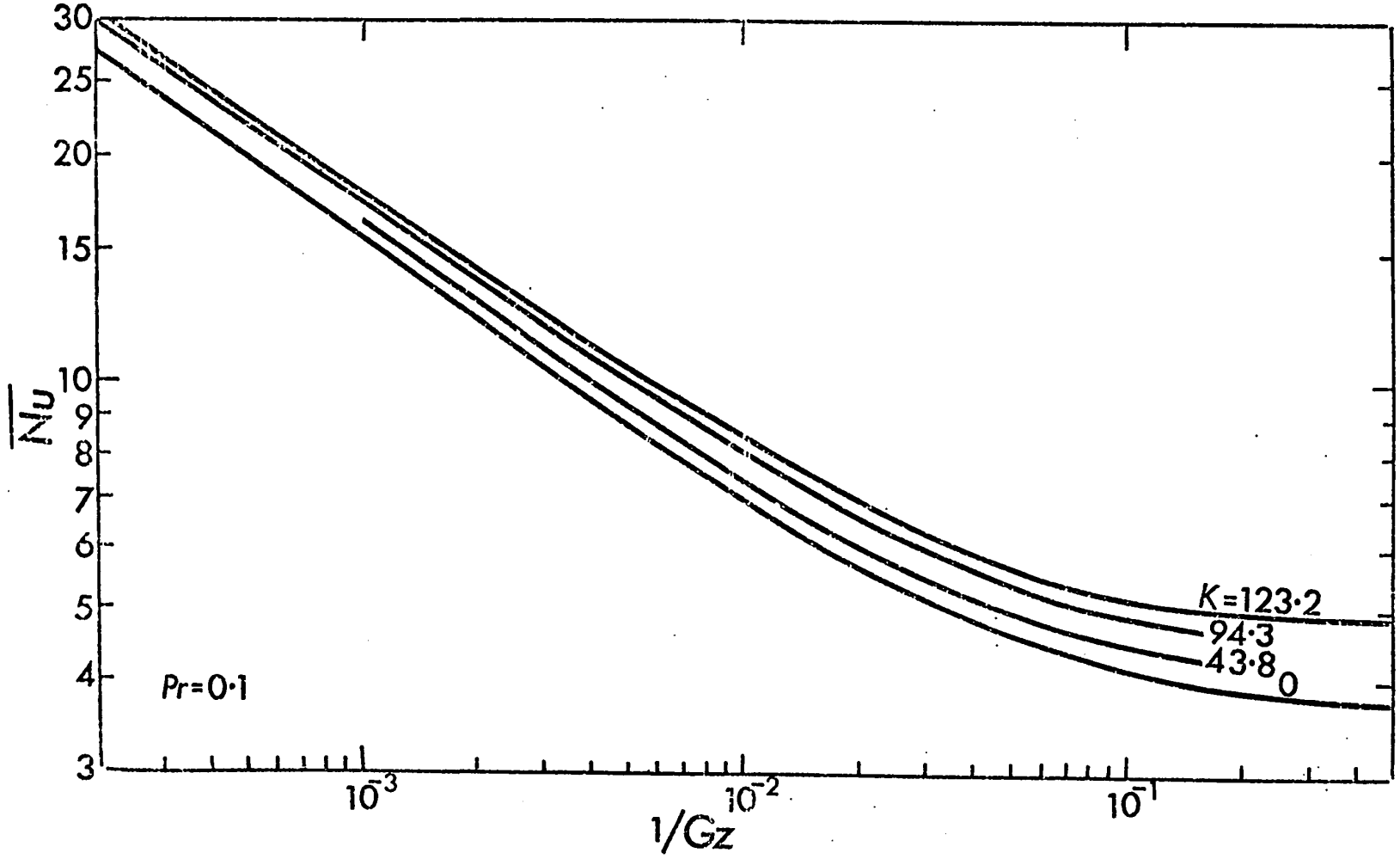




Fig. 34 Average Nusselt numbers along dimensionless downstream distance for Pr = 0.1 with Dean number as parameter.

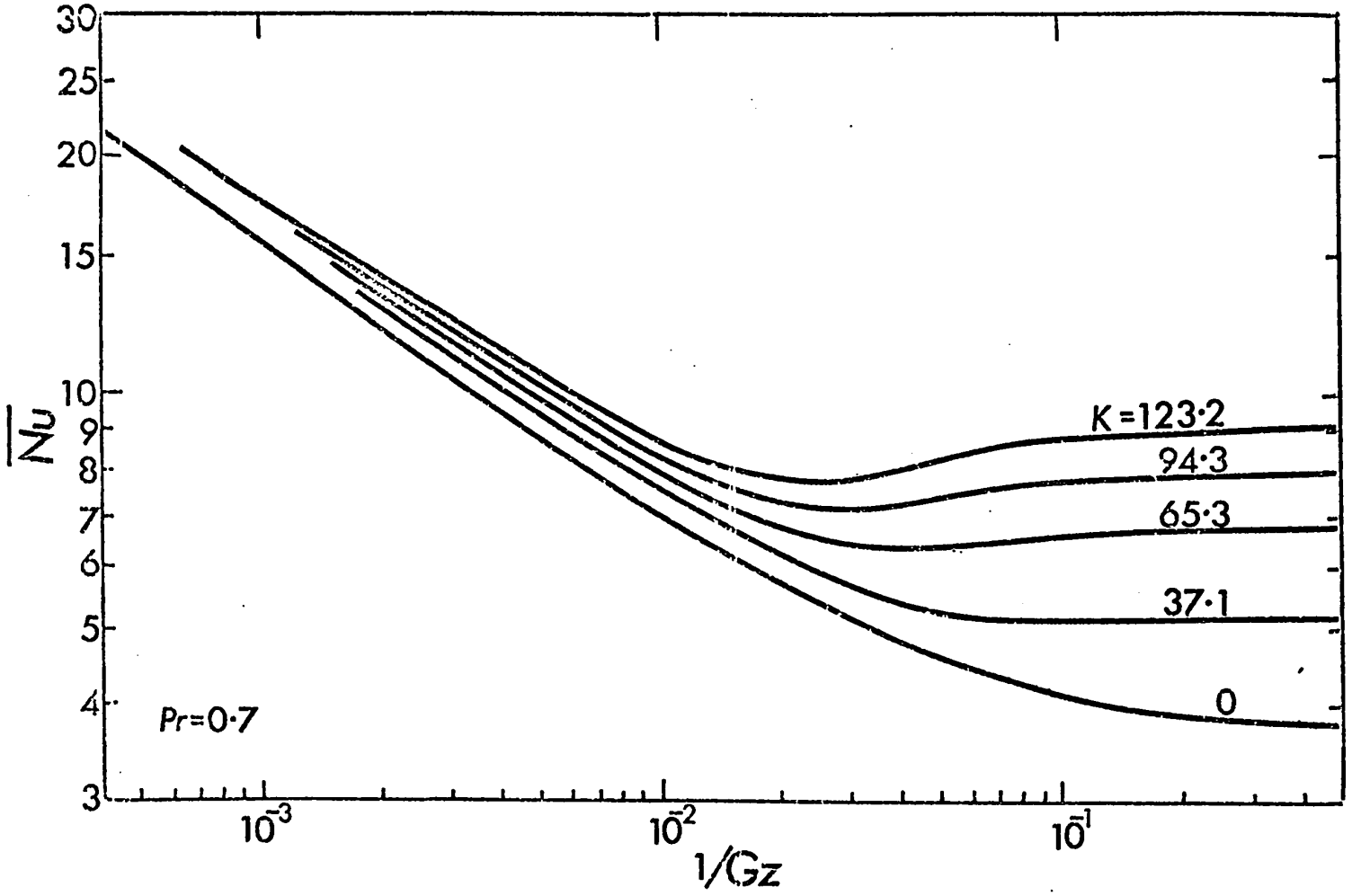


Fig. 35 Average Nusselt numbers along dimensionless downstream distance for Pr = 0.7 with Dean number as parameter.

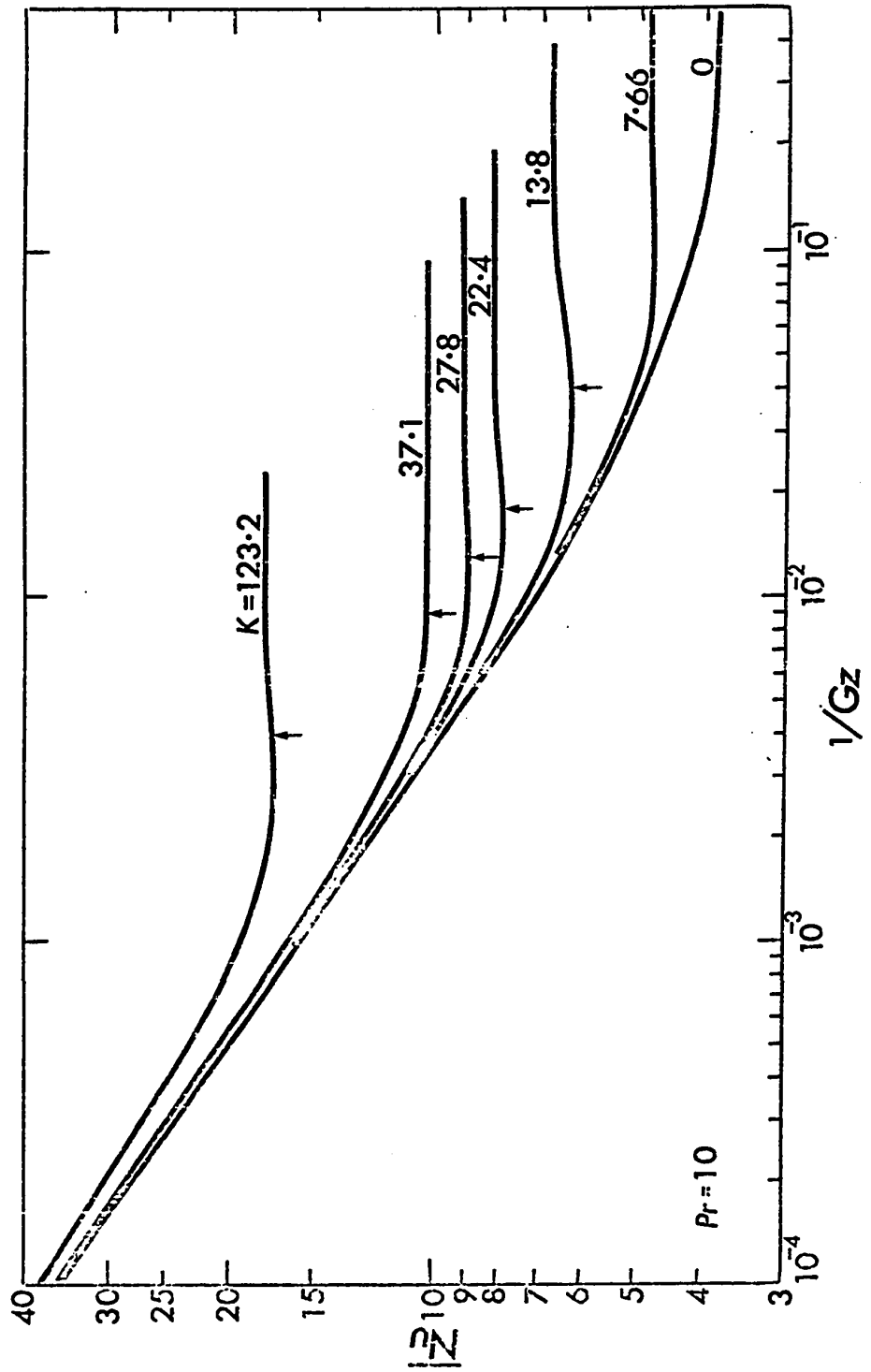


Fig. 36 Average Nusselt numbers along dimensionless downstream distance for Pr = 10 with Dean number as parameter.

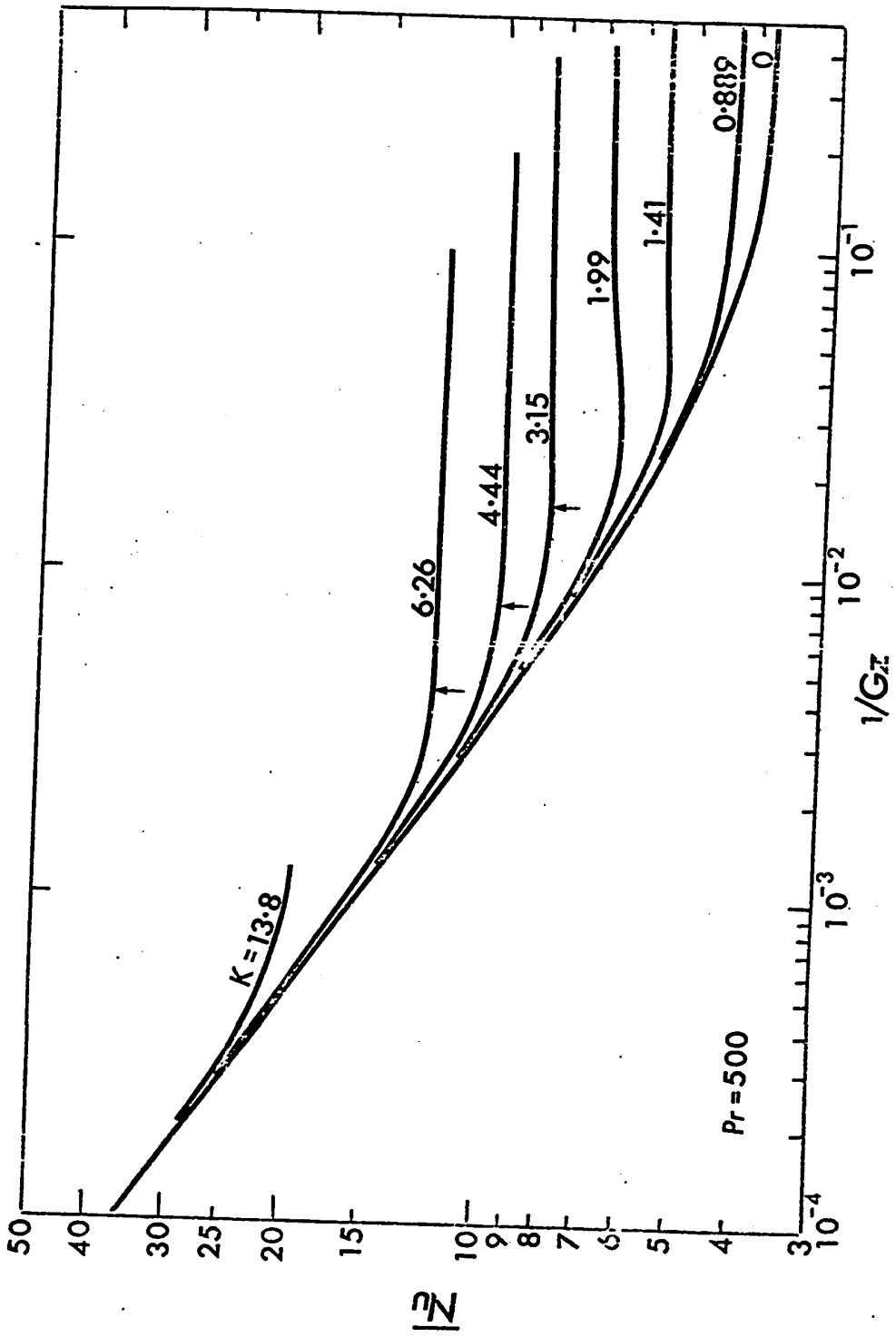


Fig. 37 Average Nusselt numbers along dimensionless downstream distance for Pr = 500 with Dean number as parameter.

convergence and accuracy. The deviation of 1.5 per cent occurs only between the minimum Nusselt number point and the fully developed point.

At Pr = 0.1, shown in Fig. 30, the general feature of the local Nusselt number variation is similar to that of the classical Graetz problem without secondary flow and one can identify easily the Leveque solution region [106] as the straight line part near the entrance. The effect of the Dean number is seen to increase the Nusselt number and shorten the thermal entrance length. At Pr = 0.7 shown in Fig. 31, the behavior of the local Nusselt number variation is considerably different from that of the classical one in that after reaching a minimum Nusselt number value depending on Dean number at some downstream axial position, the effect of secondary flow predominates over the entrance effect and the Nusselt number increases until a fully developed temperature field is reached. Once the temperature field is fully established, no further variation in Nusselt number is physically possible as shown in Fig. 31. It is instructive to contrast the local Nusselt number variation with the temperature field development in the forms of temperature profiles along $\phi = 0$, $\pi$ and $\pi/2$ and isothermals explained in Section 4.4. For example, the isothermals at $1/Gz = 1.02 \times 10^{-2}$ shown in Fig. 28 correspond to a minimum Nusselt number point shown in Fig. 31 for K = 123.2. At this axial position the isothermals are still convex everywhere, but from this position on, the concave portion appears, and the secondary effect is felt throughout the whole region of

the cross-section.

By noting the curves for K = 123.3 shown in Figs. 30 to 32, one can see clearly that the effect of Prandtl number is to increase the Nusselt number at any axial position and shorten the thermal entrance length. With Pr = 10 and 500 shown in Figs. 32 and 33, the fluctuation of Nusselt number value similar to that shown in Fig. 23 appears from the points indicated by arrows onward, and is eventually damped out. A study of the temperature development reveals that at these points the temperature field is already developed and the fluctuations observed may be attributed to numerical instability since once the temperature field is established, the Nusselt number cannot change. One possible cause for the numerical difficulty is suspected to arise from the fact that when the Prandtl or Dean number is large, two points of inflection for $\partial^2\theta/\partial r^2$ appear after the temperature field becomes established as shown in Figs. 26 and 27. This is in contrast to only one point of inflection for $\partial^2\theta/\partial r^2$ shown in Figs. 24 and 25 for Pr = 0.1 and 0.7, respectively. The change in sign of curvature for the temperature profile with large Prandtl or Dean numbers is due to the dominance of the convective terms involving $u\partial\theta/\partial r$ and $v\partial\theta/r\partial\phi$ representing the secondary flow effect over the axial convection term involving $w\partial\theta/\partial\Omega$ with the conduction terms becoming negligible in the core region, and as a result, the character of the coefficient matrix for equation (119) or (120) may change drastically leading to the off-diagonal dominant matrix.

In interpreting the graphical results shown in Figs. 30

to 37, the effect of the Peclet number appearing in the abscissa must be taken into account. For example, with Pr = 500 and the inverse of Graetz number $(1/Gz) = (1/Pe)(R_c\Omega/2a) = 10^{-4}$, the dimensionless axial distance $(R_c\Omega/2a)$ becomes 10, 100 and 500 for Re = 200, 2000, and 10,000, respectively.

At this point it is desirable to compare the present numerical result and its implications with the main conclusions of Dravid et al [82]. According to the present numerical study, the fluctuations in the values of Nusselt numbers appear only after the growth of the thermal boundary layer along the axial direction is fully arrested by the complete development of the temperature field, and furthermore the growth of the thermal boundary layer is continuous. The above observation is in complete disagreement with the interaction mechanism between secondary flow and propagating thermal boundary layer as proposed in Fig. 8 of Refernce [82]. According to Dravid et al [82], the fluctuations in the values of Nusselt numbers occur while the colder fluid core region still occupies most of the region of the tube cross-section. This is in direct contradiction with the present result, and the proposed explanation and subsequent computed prediction for the first wavelength are believed to be invalid. It should be noted that for the numerical results shown in Figs. 30 and 31 for Pr = 0.1 and 0.7, respectively, no fluctuations of the Nusselt number values are encountered. At present no satisfactory explanation can be found for the true cause of the fluctuation phenomenon after a fully developed temperature field is approached.

In contrast to the complete numerical solution presented in this work, Dravid et al [82] carried out a numerical solution for the energy equation only with the velocity field obtained directly from Mori and Nakayama's approximate analytical solution [65] based on a hydrodynamic boundary layer near the wall and a potential inner core for the secondary flow. The numerical study in Chapter III indicates that this model is inaccurate since even at K = 196 (see Fig. 12) the secondary flow streamlines are distorted considerably from the idealized model shown in [65] and the eyes are shifted toward the inner wall instead of remaining at $\phi = \pi/2$ regardless of the Dean number. Because of the idealized model, some uncertainty also exists for the convective terms due to secondary flow in the energy equation, and the situation becomes progressively worse as the Prandtl number increases. Furthermore, Dravid [83] assumes that there is no heat flow in the radial direction at the tube center in his numerical solution which is clearly incorrect. Dravid et al [82] obtained a numerical solution with a Dean number of 225 only. It should be pointed out that numerical difficulty arises when the Dean number exceeds the highest values indicated in the figures for Pr = 10 and 500 only. Generally, it can be said that the convergent solution cannot be obtained when the value for the parameter $KPr^{1/2}$ exceeds about 350. The gradual divergence is manifested by the increasing difference between the values for $(Nu)_1$ and $(Nu)_2$. Reference [82] notes that the convergence becomes progressively poorer when Re • Pr increases beyond 5,000. However, it is believed

that $KPr^{1/2}$ is a more reasonable convergence criterion.

A correlation equation for the average Nusselt number similar to that of Hausen [107] for the Graetz problem in straight tubes (K = 0) is highly desirable for the present Graetz problem in curved tubes. It is clear that the increment of Nusselt number over that of straight tubes (K = 0) is a function of the Graetz number for given Prandtl and Dean numbers. The difference in behaviour for the increment of the average Nusselt number between the Leveque type solution region very near the entrance and the limiting asymptotic region coupled with the existence of a minimum value for Nusselt number makes the development of the correlation equation rather difficult. This indirectly suggests the great difficulty in correlating the experimental data.

## 4.6 HEAT TRANSFER RESULTS FOR THE THERMALLY FULLY DEVELOPED REGION*

Heat transfer results for thermally fully developed regions in curved pipes with uniform wall temperature are of practical interset in design. As shown in Fig. 22, temperature profiles in fully developed regions are similar and only the relative magnitude of the profile varies in the axial direction. The region of interest under consideration may be termed the similarity region [65].

### Temperature Field Characteristics

In order to see the effect of the Dean number on the temperature field, temperature profiles along the central horizontal

---

* Reference [86] is based on this part of the work.

and vertical axes are illustrated in Fig. 38 for several representative Dean numbers with Pr = 0.7. Since the fully developed temperature field in the region of similarity is of interest, the temperature profile is normalized using the maximum dimensionless temperature. It is seen that the effect of centrifugal forces represented by the Dean number is to shift the location of the maximum value toward the outer wall. The change of sign of the curvature for the temperature profile in the central region from a negative value for K = 0 (straight tube) to a positive value for K = finite is caused by the fact that the terms $u\partial\theta/\partial r$ and $v\partial\theta/r\partial\phi$ are dominant over the axial convection term $w\partial\theta/r_c\partial\Omega$ which is always negative for heating. It is expected that the gradual increase of the radial temperature gradient at the outer wall ($\pi/2 \geq \phi \geq -\pi/2$) with the increase of Dean number will contribute to the gradual increase of the Nusselt number.

The distributions of isothermals will provide some insight into the heat transfer mechanism, and are shown in Fig. 39 together with the isothermals from the uniform wall heat flux case from Chapter III for Pr = 0.7 and K = 123.2. By examining the distribution for $\theta = 0.2$, one finds that the wall temperature gradient for the uniform wall heat flux case is larger than that for the uniform wall temperature case. Focussing one's attention on the distribution along the central horizontal direction ($\phi = 0$ and $\pi$), one notes that the rate of temperature drop for the uniform wall temperature case is larger than that of the uniform wall heat flux case. The relative rate of increase of the Nusselt number ratio, $Nu/(Nu)_0$, for the two

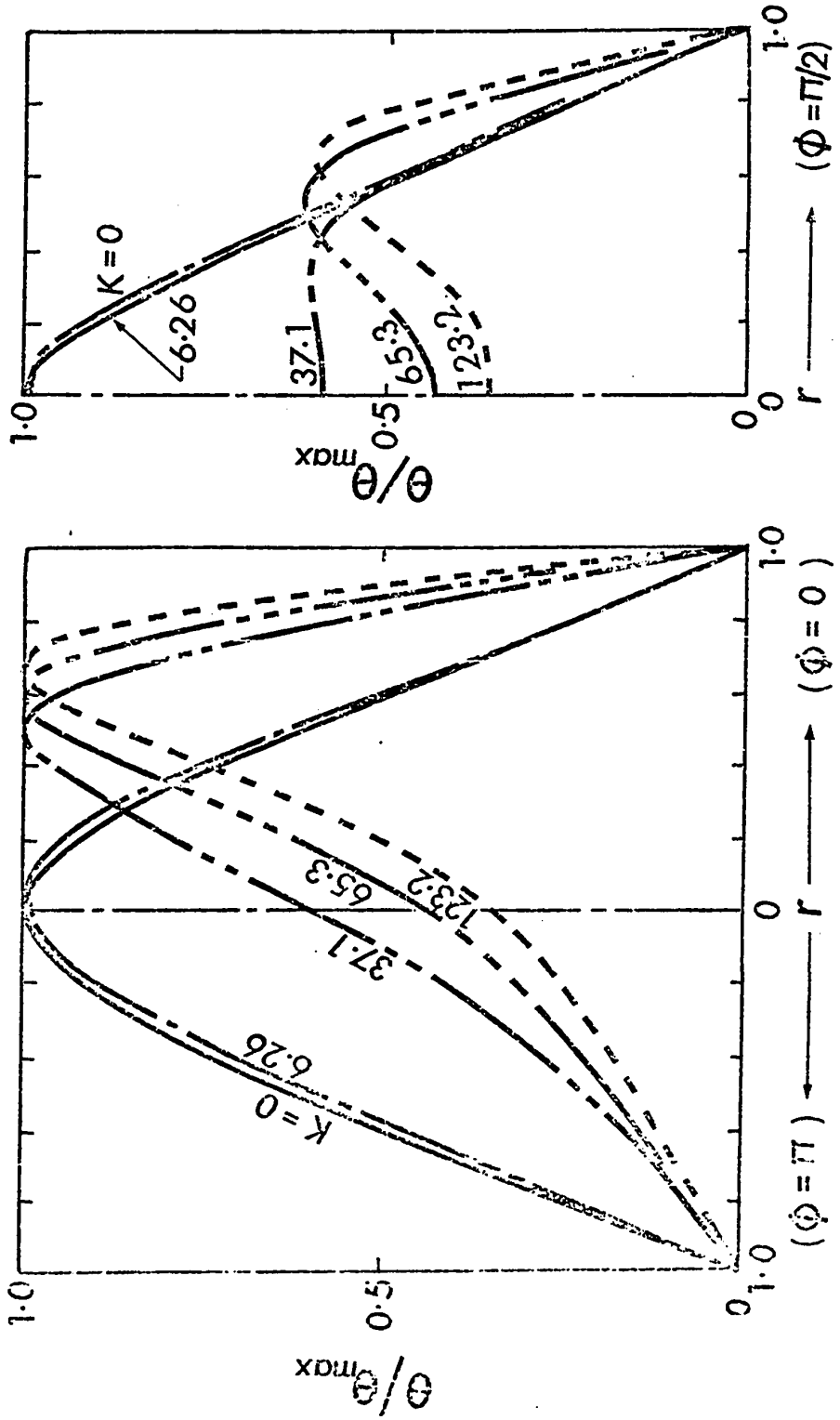


Fig. 38 Temperature distributions for typical Dean numbers with Pr = 0.7.

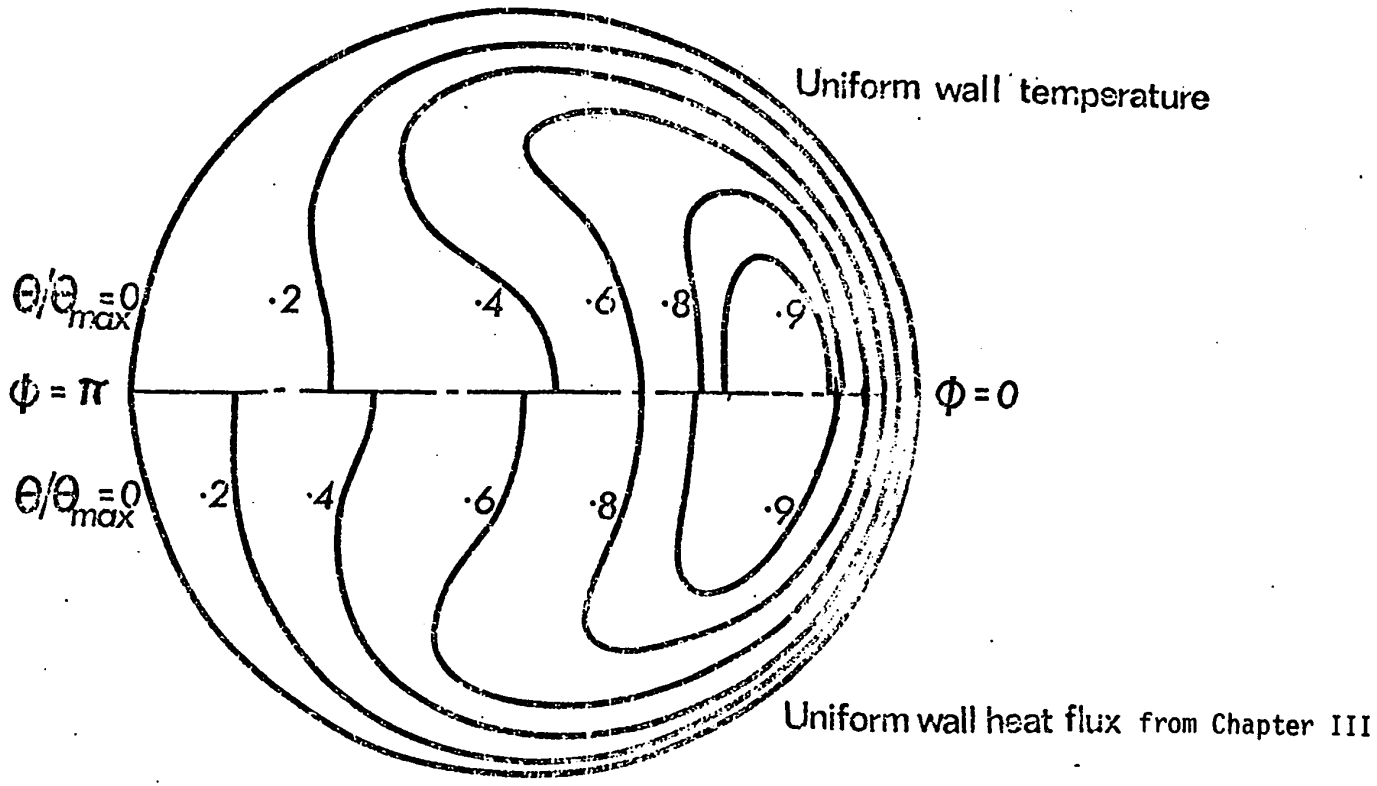


Fig. 39 Comparison of isothermals between uniform wall temperature case and uniform wall heat flux case from Chapter III with K = 123.2 and Pr = 0.7

basic thermal boundary conditions is of considerable interest. In this respect, one should note that the Nusselt number depends on the average wall temperature gradient as well as the bulk temperature of the fluid. Indeed, it will be shown later that the value of the Nusselt number ratio for the uniform wall temperature case is higher than that for a uniform wall heat flux for a given value of Dean number.

Local Nusselt Number

The effect of the Dean number on the angular distribution of local Nusselt number along the pipe wall is shown in Fig. 40 for Pr = 0.7. At K = 65.3, the region with $Nu/(Nu)_0 > 1$ occupies nearly two-thirds of the wall, including the outer wall. It is of interest to note that with further increase of Dean number, the value for $Nu/(Nu)_0$ near the inner wall $\phi = \pi$ remains to be less than one. A comparison between Fig. 40 and the corresponding plot shown in Fig. 17 of Chapter III for the case of uniform wall heat flux reveals that the local Nusselt number ratio for a uniform wall temperature is consistently higher than that for a uniform wall heat flux with the same Dean number, such as K = 123.2 shown in both figures, but the general trend is similar. For example, at $\phi = 0$ and with K = 123.2, the Nusselt number ratio is 4.75 for the uniform wall temperature case, whereas the corresponding value is 3.3 for the uniform wall heat flux case.

The overall heat transfer results in terms of the Nusselt number ratio versus Dean number are shown in Fig. 41 for several

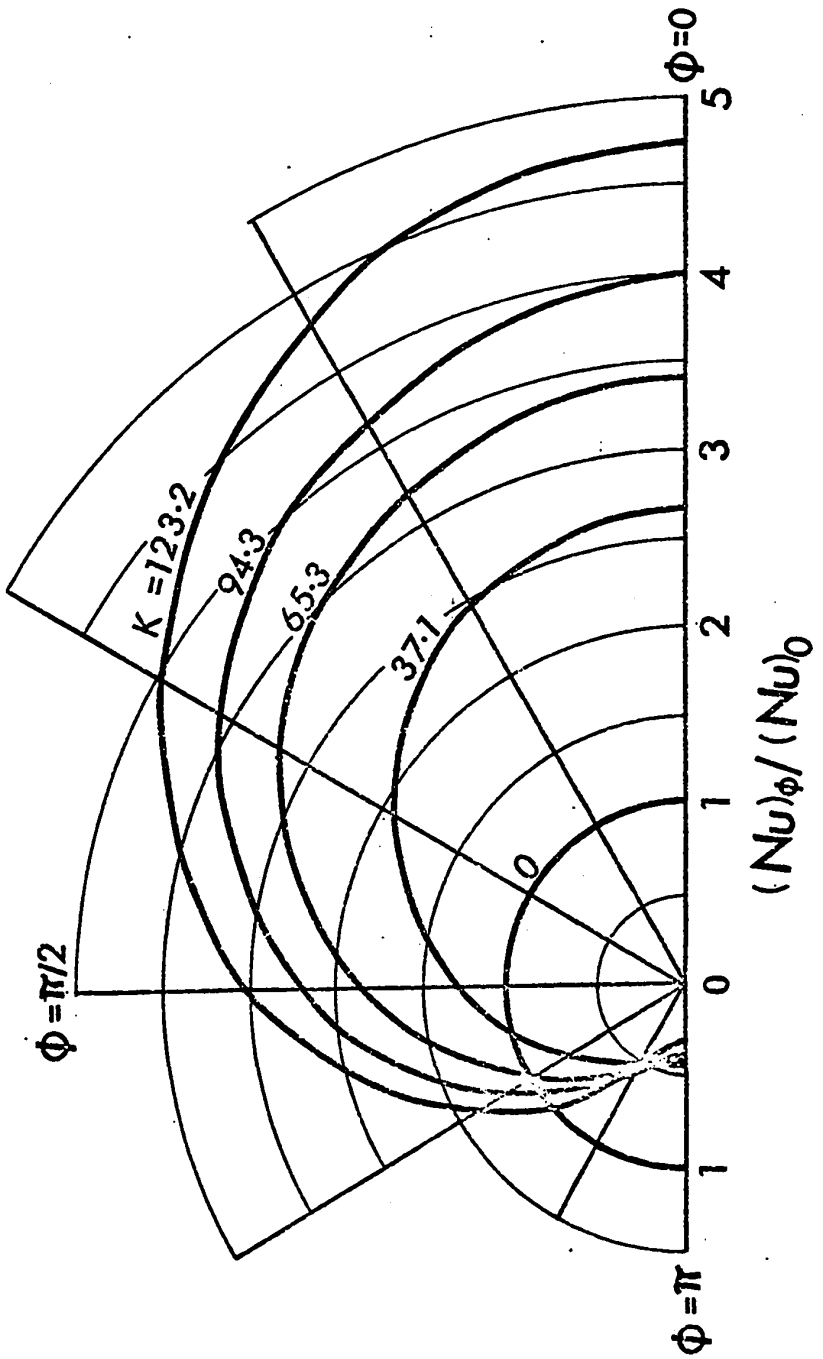


Fig. 40 Local angular distribution of $(Nu)_\phi/(Nu)_0$ with Dean number K as a parameter for Pr = 0.7.

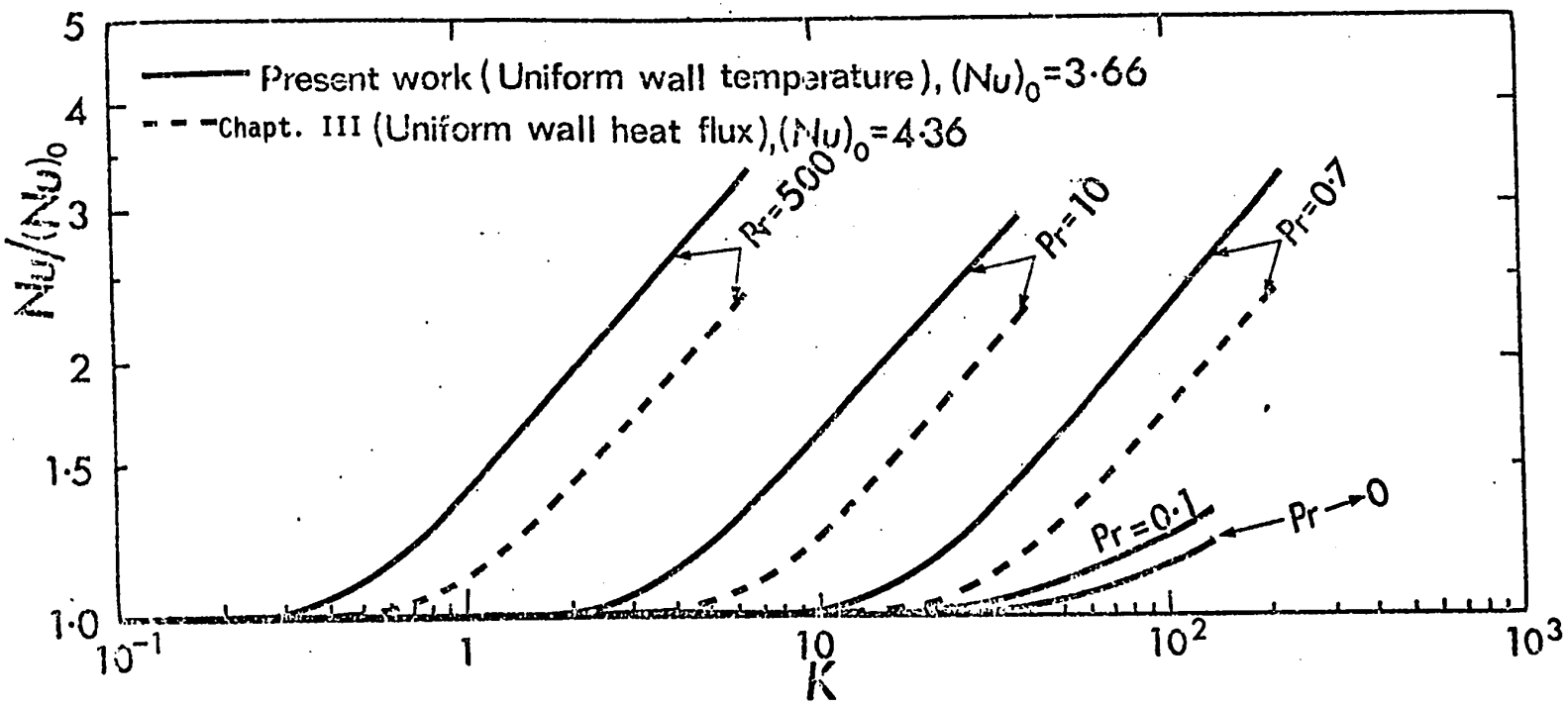


Fig. 41 A comparison between heat transfer results for uniform wall temperature case and uniform wall heat flux case from Chapter III for several Prandtl numbers.

Prandtl numbers with the results from the uniform wall heat flux case from Chapter III inclu ed for comparison. The trends of heat transfer results for both cases are seen to be quite similar except for the fact that with a given value of Dean number the value of $Nu/(Nu)_0$ for a uniform wall temperature is always higher than that for a uniform wall heat flux. This situation is in contrast to the limiting Nusselt number of 4.36 and 3.66, respectively, for fully developed laminar flow in straight tubes with uniform wall heat flux and uniform wall temperature.

Comparison with Results from Approximate Analytical Methods

In the absence of experimental data for the present problem, it is desirable to compare the present numerical results with the available results from a perturbation method [64] and a boundary-layer approximation method [65]. This comparison will also serve to ascertain the adequacy of the two currently known approximate analytical methods.

Maekawa [64] approached the problem of fully developed laminar forced convection in curved pipes with the thermal boundary conditions of both uniform wall heat flux and uniform wall temperature using a perturbation method. Maekawa used Dean's solution [13] for the momentum equations based on a second-order perturbation and carried out the solution of the energy equation up to a fourth-order perturbation. Maekawa's results are reproduced in Fig. 42 with comparison made against the numerical results from Chapter III and Özisik and

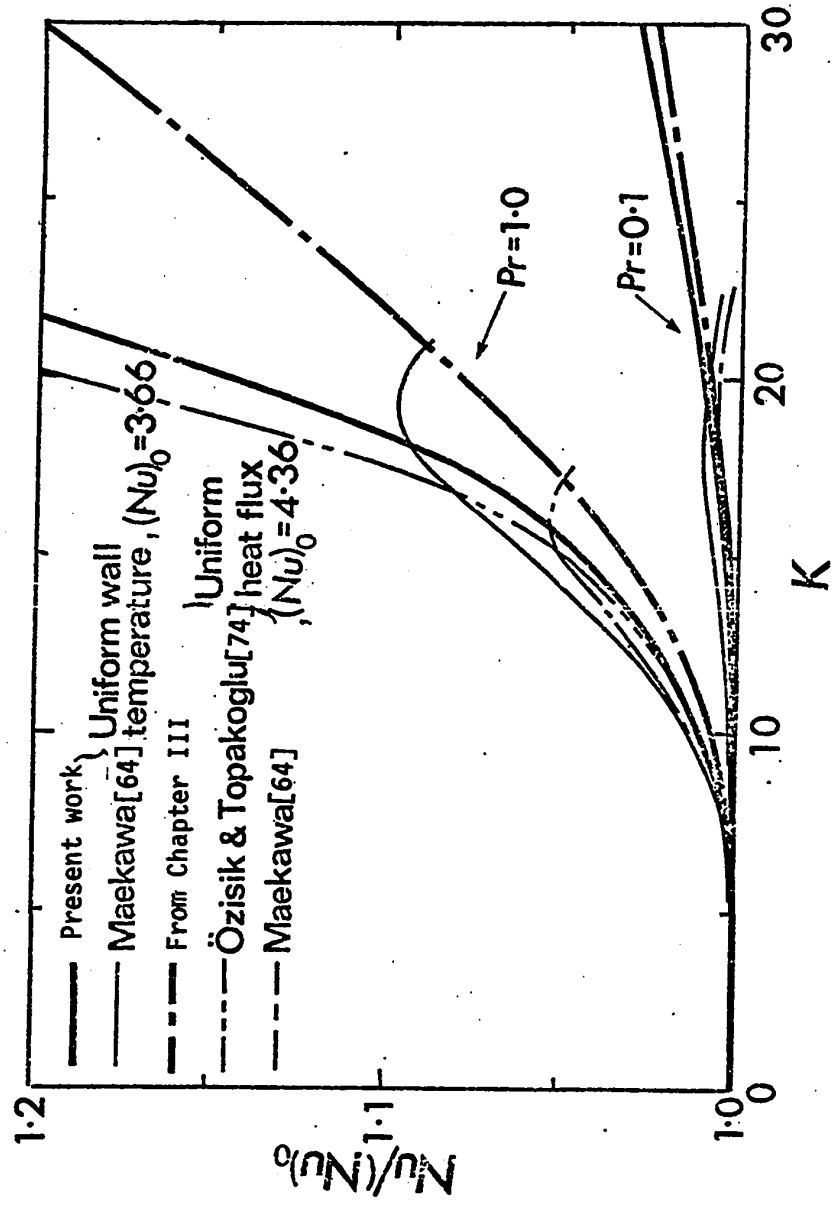


Fig. 42 Comparison between heat transfer results from numerical analysis and perturbation analysis.

Topakoglu's results [74] based on a second-order perturbation for the uniform wall heat flux case using a perturbation method. In recent years, Morton's perturbation method [14] has been applied by several investigators to the solution of fully developed convective heat transfer problems with secondary flow. It is now known that the perturbation mathod has a rather limited range of applicability. Maekawa [64] presented results up to $Nu/(Nu)_0 = 1.05$ and further results shown in Fig. 42 are based on computations from the equations for $Nu/(Nu)_0$ given in [64]. Apparently Maekawa's results are incoreect with further increase of Dean number. In contrast to Maekawa's results Özisik and Topakoglu's results show a blow-up trend as the Dean number increases. It is noted that Maekawa's results do show that at a given value of Dean number, the value of $Nu/(Nu)_0$ for a uniform wall temperature is higher than the corresponding value for the uniform wall heat flux case, and this trend is consistent with the numerical results shown in Fig. 42. Fig. 42 clearly shows that the perturbation method leads to doubtful results as the Dean number increases. It should be noted that a low Dean number range such as $K \leq 20$ for $Pr \leq 1$ is not of practical importance because of possible experimental error.

Mori and Nakayama's boundary-layer approximation [65] is valid only for high Dean numbers. Mori and Nakayama conclude that the formula for the Nusselt number for a uniform wall temperature is the same as that for a uniform wall heat flux. A comparison between the present numerical results and those of Mori and Nakayama

from their recommended correlation equation [65] is shown in Fig. 43. An asymptotic Nusselt number of 16 obtained by Dravid et al [82] for the case of Pr = 5, K = 225 and $a/R_c$ = 0.05 is also shown in Fig. 43 for comparison. As explained earlier, the asymptotic value obtained after the cyclic variation of local Nusselt number damps out is lower than the value obtained by the present numerical solution. It is evident that the correlation equation given by Mori and Nakayama does not lead to the limiting Nusselt number of 3.66, and furthermore, appears to be valid only near Pr = 1.0. This remark is similar to that reported in Chapter III for the uniform wall heat flux case. The discrepancy in predictions based on the two different methods for $Pr \geq 2$ is believed to be significant, and Mori and Nakayama's Prandtl number effect is now known to be incorrect [82]. For given Prandtl and Dean numbers, the difference in Nusselt numbers between the uniform wall temperature and uniform wall heat flux is so small that experimental confirmation would be extremely difficult. Consequently, Mori and Nakayama's conclusion [65] that the Nusselt number in curved pipes is hardly affected by the wall temperature condition at high Dean numbers, which is similar to that of turbulent flow in a straight pipe, is qualitatively correct from a practical viewpoint.

A Correlation Equation for Prandtl Number Effects

The possibility for correlating the Prandtl number effect on heat transfer results for fully developed laminar forced convection with secondary flow was pointed out in Section 2.7. The correlation

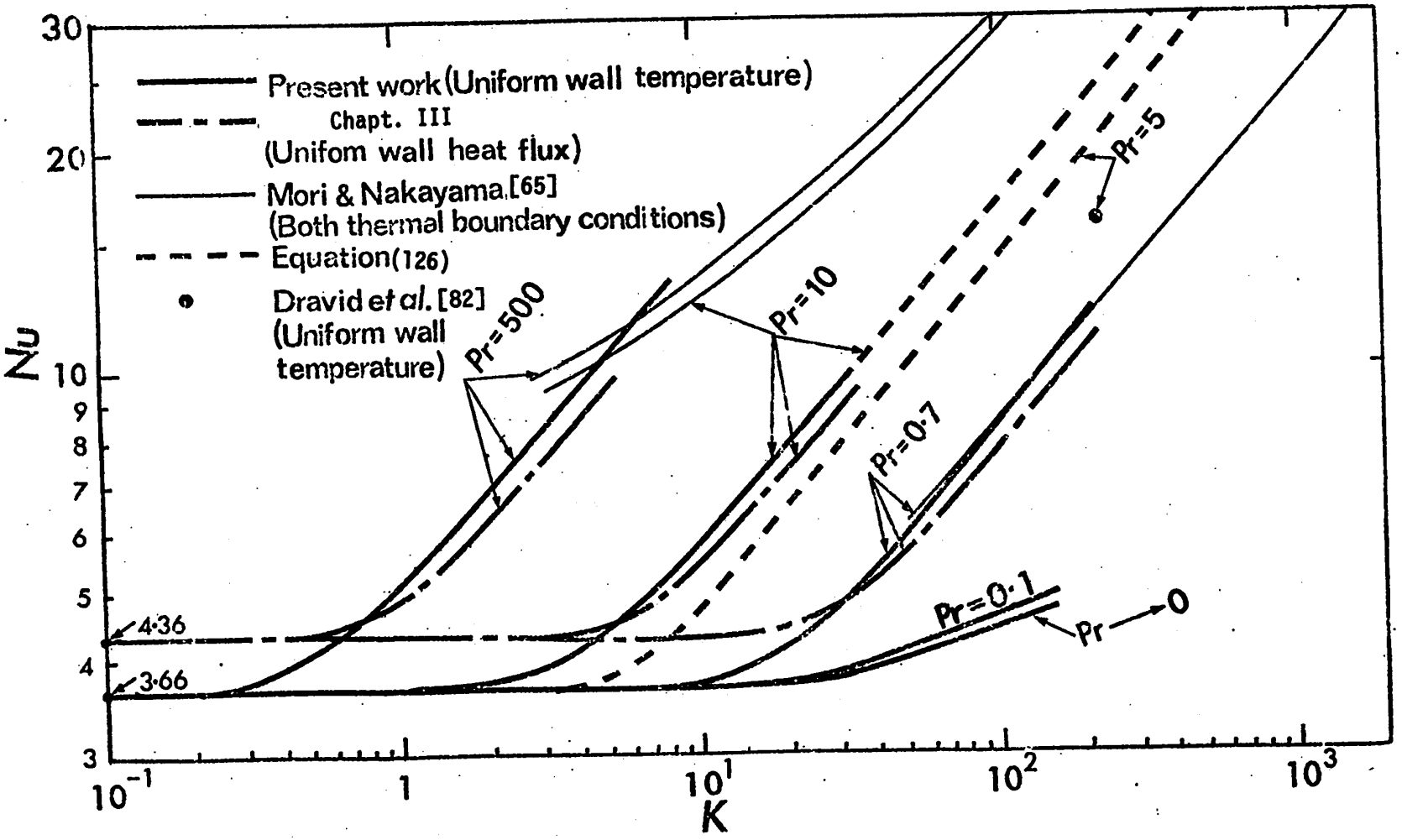


Fig. 43 Comparison of heat transfer results from present work and from Chapter III with those from boundary-layer approximation [65]

equation for Prandtl number effects on the Nusselt number in Chapter III is based on a study of the governing equations and verified by the numerical results. As pointed out earlier, and shown in Fig. 41, the heat transfer results for the two thermal boundary conditions of uniform wall temperature and uniform wall heat flux are quite similar. Consequently, one can expect that a correlation equation for the Nusselt number similar to that reported in Chapter III, using a parameter $K^2Pr$, is also possible for the present problem.

The heat transfer results from this study using the parameter $KPr^{1/2}$ instead of K are shown in Fig. 44 together with Mori and Nakayama's results [65] and the results for a uniform wall heat flux are included for comparison. The new correlation is seen to be very effective since all the numerical results for $Pr \geq 1$ nearly coincide. The correlation equation for the Nusselt number similar to the one deduced in Chapter III is

$$Nu/(Nu)_0 = 0.270\ Q(1 - 1.48Q^{-1} + 23.2Q^{-2} - 120Q^{-3} + 212Q^{-4}) \quad (126)$$

where

$$Q = (KPr^{1/2})^{1/2} \geq 3.0 \quad \text{for } Pr \gtrsim 1$$

As indicated in Chapter III, the range with $Q \leq 3.0$ is of little practical importance because of a rather weak secondary flow, and the correlation equation (126) can now be regarded as valid, with sufficient accuracy for all the practically important laminar flow regimes. In interpreting the results presented in Fig. 44, one

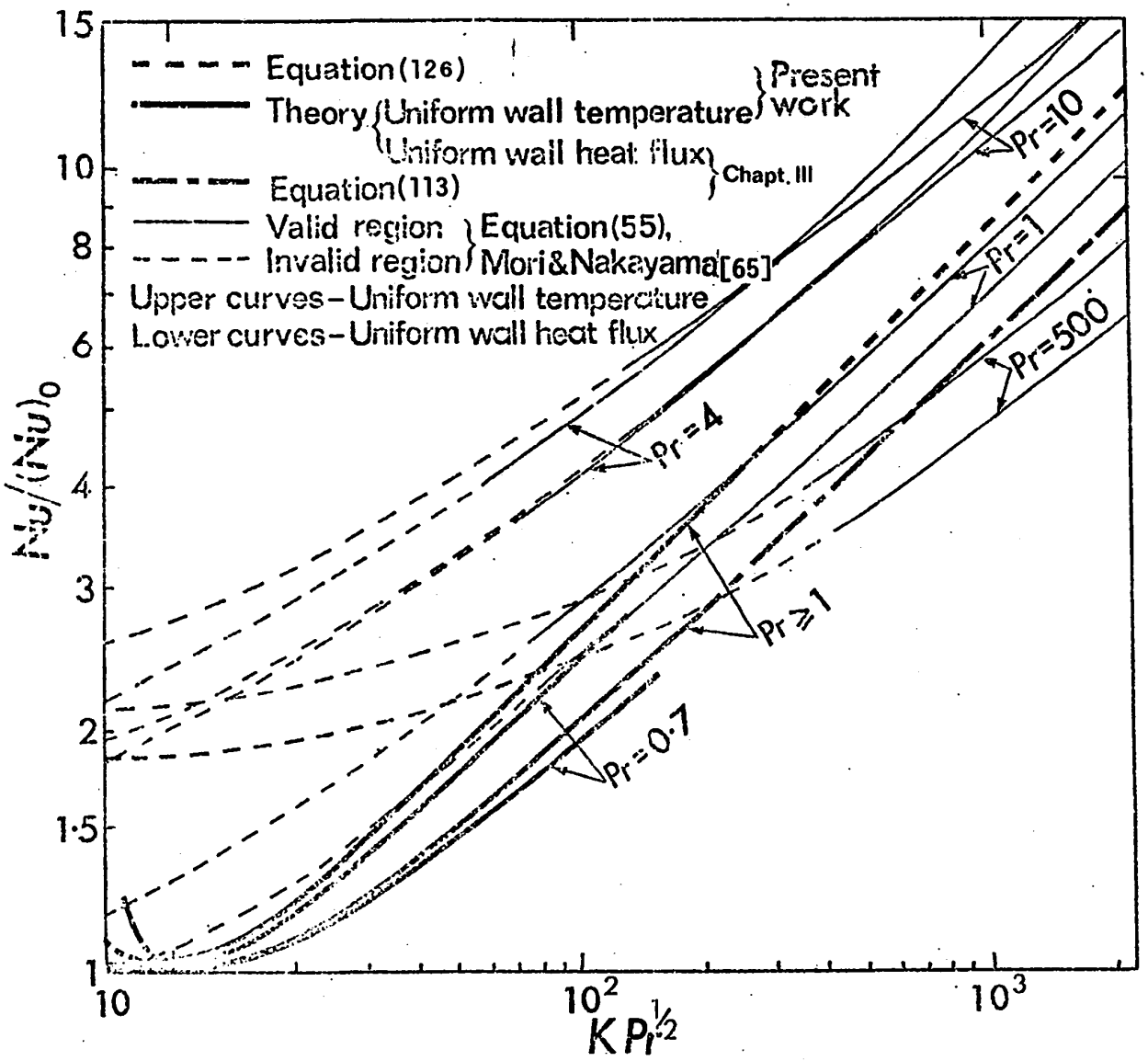


Fig. 44 Proposed correlation curves for Prandtl number effects on heat transfer results valid for Pr ≥ 1 using a parameter K $Pr^{1/2}$.

should note that $(Nu)_0 = 3.66$ for a uniform wall temperature and $(Nu)_0 = 4.36$ for a uniform wall heat flux. Fig. 44 clearly indicates that Mori and Nakayama's Prandtl number effect is in orrect except $Pr \simeq 1$.

## 4.7 CONCLUDING REMARKS

1. The Graetz problem in curved pipes is characterized by the secondary flow effect superimposed upon the usual entry effect. For given Prandtl and Dean numbers, the local Nusselt number first decreases continuously from the entrance due to the entry effect, but the gradual increase of the secondary flow effect eventually takes over the entry effect with the Nusselt number reaching a minimum value from which point on the Nusselt number increases until a fully developed temperature field is reached. Up to the point where the Nusselt number is a minimum, the isothermals are of covex shape, but from there on a kidney shape appears. The parallel straight lines for different Dean numbers such as those shown in Fig. 30 and 31 for the Leveque solution region are caused by the different degree of deviation of the axial velocity profile from the parabolic Poiseuille profile since very near the entrance only the axial convection term $(w\partial\theta/\partial\Omega)$ is significant as compared with the secondary flow convective terms. For a given Dean number, the effect of the Prandtl number is to shorten the thermal entrance length (1/Gz). For large Prandtl numbers the temperature field develops rather rapidly. The effect of the Dean number is similar to that of the Prandtl number. However,

the Dean number effect becomes much more appreciable at high Prandtl numbers than at low Prandtl numbers.

2. In this study, the development of the temperature field is contrasted clearly to the local Nusselt number variation in order to see the secondary flow effect. In particular, the fully developed temperature field is shown to be attained when the thermal boundary layer at all points around the tube circumference merges completely. It is reasoned that once the temperature field is fully established, the temperature profiles remain constant, and only the relative magnitude varies along the axial distance in the so-called similarity region, (see Fig. 22). This observation is a crucial one since Dravid et al [82] assert that the cyclic oscillation of the local Nusselt number encountered after reaching a local maximum value is a real physical effect whereas the above reasoning suggests that the oscillation phenomenon is a result of numerical instability. Other reasons for this argument are already given in Section 4.3. It is suspected that the numerical instability is caused by a deviation from the diagonal dominance for the coefficient matrix when either the Prandtl or Dean number is large. It should be noted that a convergence study based on the reduction of mesh sizes by a factor of, say 2, will not guarantee that the convergence to the physical solution is achieved. The convergence of the numerical solution at high Prandtl or Dean numbers apparently needs further study. In proposing a model for the interaction between secondary flow and the propagating thermal boundary layer to explain the first wavelength and the oscillation phenomenon,

Dravid et al [82] apparently are not aware of the fact that the temperature field is already fully established at the initiation of the fluctuation.

3. The limitation of this analysis imposed by the assumptions 1 and 2 in Section 4.2 must be emphasized. Recently, the Graetz solution is shown to be a limiting case applicable only when the Rayleigh number is less than $10^3$ [96]. Obviously in many practical applications, the free convection and variable property effects must also be taken into consideration.

4. The heat transfer results for fully developed laminar flow in curved pipes with the two basic thermal boundary conditions of uniform wall temperature and uniform wall heat flux are quite similar, but distinct. For given Prandtl and Dean numbers, the limiting Nusselt number for the uniform wall temperature case becomes higher than that for the uniform wall heat flux case after reaching a certain Dean number. This situation is opposite to that of a pure forced convection in a straight tube. This finding is consistent with the results from perturbation methods [64] for extremely low parameters but contradicts the results from the boundary-layer approximation [65] which suggests that at high Dean numbers the same formula for Nusselt number can be applied for both thermal boundary conditions.

5. A comparison between the numerical results and the approximate analytical results indicates that the perturbation method is not a practical method, and the boundary-layer approximation for high Dean numbers appears to valid only near Pr = 1.

6. The Prandtl number effect on heat transfer result for a uniform wall temperature is found to be similar to the case of uniform wall heat flux. It is significant that the new correlation equation for the Nusselt number is valid for $Pr \geq 1$.

7. It should be pointed out that the fluctuating phenomenon for the local Nusselt number observed in this study is similar to that of Dravid et al [82]. However, the physical interpretation presented in this study is completely different from that of Dravid et al [82]. The present study presents another viewpoint regarding the fluctuating phenomenon. It is not suggested that the present interpretation is a conclusive one and it is felt that much more work is required to clarify the present uncertainty.

8. The numerical results for this chapter are tabulated in Appendix 7 for future reference.

# CHAPTER V

# GRAETZ PROBLEM IN CURVED PIPES WITH UNIFROM WALL HEAT FLUX

## 5.1 INTRODUCTION

The reported theoretical and experimental works on thermal entrance region heat transfer in curved pipes with various thermal boundary conditions are rather limited and some uncertainties still exist. As pointed out in Chapter IV, the numerical solution for a large Prandtl number fluid or for a large Dean number leads to a fluctuating phenomenon for the local Nusselt number before approaching the fully developed condition. The possibility that the fluctuating phenomenon is caused by a numerical instability cannot be ruled out completely and further work in this regard is required.

The purpose of this chapter is to present results for thermal entrance region heat transfer (Graetz problem) in curved pipes with a uniform wall heat flux and report the results of some numerical experiments in an attempt to ascertain the possibility of numerical instability causing the fluctuating phenomenon.

## 5.2 FORMULATION OF THE PROBLEM

Consideration is given to a steady fully-developed laminar flow of an incompressible viscous fluid with constant properties. The present analogous Graetz problem is to find the development of the temperature profile along the heated (or cooled ) section of the curved pipe. The fluid temperature is constant and equal to the

wall temperature up to the thermal entrance where there is a discontinuous step change in wall heat flux from zero to a finite higher (or lower) value. The assumptions employed in Chapter IV for the case of a uniform wall temperature will be used for the formulation of the present problem. Using the dimensionless variables defined in Chapter IV, except for the temperature, and referring to the coordinate system defined in Fig. 10, the energy equation and the boundary conditions become:

$$u \frac{\partial \theta}{\partial r} + \frac{v}{r} \frac{\partial \theta}{\partial \phi} + \left(\frac{c}{r_c}\right)^{2^{1/2}} w \frac{\partial \theta}{\partial \omega}$$

$$= \frac{1}{P_r} \left(\frac{\partial^2 \theta}{\partial r^2} + \frac{1}{r} \frac{\partial \theta}{\partial r} + \frac{1}{r^2} \frac{\partial^2 \theta}{\partial \phi^2}\right) \qquad (127)$$

$$\theta = 0 \quad \text{at} \quad 0 \leq r < 1, \quad \omega = 0 \qquad (128)$$

$$\frac{\partial \theta}{\partial r} = 1 \quad \text{at} \quad r = 1, \quad \omega > 0$$

where

$$\theta = \frac{k}{q_w a} (T - T_0)$$

and $q_w$ = uniform wall heat flux.

It is noted that the velocity field obtained in Chapter III can be used for the present problem. Equation (127) is of parabolic type and an analytical solution is apparently not practical. The numerical method used in Chapter IV will be applied again to the present problem. At present, the numerical solution of the secondary

flow problem invariably leads to a numerical difficulty when the Dean number or the Prandtl number is large. Physically, when the Dean number is large, the convective terms due to secondary flow and the axial convection term in the energy equation dominates over the conduction terms in the core region. On the other hand, for large Prandtl numbers, the conduction terms may be negligible compared with the convection terms. Consequently, a large Dean number or a large Prandtl number leads to the same effect as far as the relative importance of the convection and conduction terms are concerned. The effects of a large Dean number and large Prandtl number are now seen to be equivalent. One may now conclude that the role of the convective terms due to secondary flow in the numerical solution is significant and presents the major source of numerical difficulty. Thus, it is believed that the key to the question of fluctuating local Nusselt number before approaching an asymptotic Nusselt number when either the Prandtl or Dean number is large lies in the behavior of the convective terms $(u\partial\theta/\partial r + v\partial\theta/r\partial\phi)$. For this reason, the effect of several different finite-difference representations for the convective terms on the Nusselt number calculations will be examined.

## 5.3 A GENERAL FINITE-DIFFERENCE APPROXIMATION TO THE CONVECTIVE TERM

In carrying out the numerical solution of the present problem using the ADI method and central difference approximations for the convective terms, difficulty is encountered when the secondary flow convective

terms are large compared with the conduction terms. This observation was also noted in the previous chapter. Thus, the problem is closely related to the question of stability and convergence of numerical solutions of parabolic equations. The stability and convergence of the numerical solution depend on the mesh size. However, a reduction of the mesh size by a factor of, say 2 or 3, will not guarantee the convergence of the numerical solution to the physical solution. Since the damped fluctuating Nusselt number phenomenon observed in the numerical solution has not been confirmed experimentally, it is desirable to ascertain whether or not a particular finite-difference representation yields a true solution to the original partial differential equation. Thus, the convergence study must be supplemented by using different finite-difference approximations.

When the Dean number or Prandtl number is large, a central difference approximation for the convective terms does not lead to a coefficient matrix with diagonal dominance. The situation can be corrected by using a non-central difference approximation, but the increased numerical stability may be accompanied by a decrease in numerical accuracy. It is possible to devise a general finite-difference approximation for the convective transport terms which represents a compromise between numerical stability and accuracy and yet recovers either a central or non-central approximation as a limiting case. In order to see this more clearly, the central and non-central approximations for the term $u\partial\theta/\partial r$ are given as,

$$u_{i,j}\left(\frac{\partial\theta}{\partial r}\right)_{i,j} = \frac{1}{2\Delta r}\left(u_{i,j}\cdot\theta_{i+1,j} - u_{i,j}\cdot\theta_{i+1,j}\right)$$

$$u_{i,j}\left(\frac{\partial\theta}{\partial r}\right)_{i,j} = \frac{1}{2\Delta r}\left[u_{i,j} - |u_{i,j}|\right]\theta_{i+1,j}$$

$$+\frac{1}{\Delta r}|u_{i,j}|\,\theta_{i,j}$$

$$-\frac{1}{2\Delta r}\left[u_{i,j} + |u_{i,j}|\right]\theta_{i-1,j} \qquad (129)$$

It is noted that the second equation becomes a backward difference when $u_{i,j}$ is positive and a forward difference is obtained when $u_{i,j}$ is negative. By introducing a coefficient $\beta$ which may vary from 0 to 1, a general finite-difference approximation for $u\partial\theta/\partial r$ can be obtained as,

$$u_{i,j}\left(\frac{\partial\theta}{\partial r}\right)_{i,j} = -\frac{1}{2\Delta r}\left(u_{i,j} + \beta|u_{i,j}|\right)\theta_{i-1,j}$$

$$+\frac{1}{\Delta r}\beta|u_{i,j}|\,\theta_{i,j}$$

$$+\frac{1}{2\Delta r}\left(u_{i,j} - \beta|u_{i,j}|\right)\theta_{i+1,j} \qquad (130)$$

where $\beta$ may vary from 0 to 1. It is seen that $\beta = 0$ represents the central difference approximation and that $\beta = 1$ recovers the non-central difference approximation. The expression similar to equation (130) can be applied to other convection terms. The numerical solution of equation (130) can now be made by specifying a value for the coefficient

such as $\beta = 0.5$ for example.

With the above modification for the finite-difference approximations of the convective terms, the ADI procedure outlined in Section 4.3 can now be applied to the present problem.

## 5.4 NUMERICAL EXPERIMENTS ON THE EFFECTS OF DIFFERENT FINITE-DIFFERENCE APPROXIMATIONS FOR CONVECTIVE TERMS ON LOCAL NUSSELT NUMBER RESULTS

Before proceeding to present numerical results such as the temperature profile development and evaluation of the Nusselt number, it is appropriate to present the results of some numerical experiments regarding the effect of using $\beta = 0$, 0.5 and 1.0 in equation (130) for the convective terms due to secondary flow.

It is noted that all the numerical results in this study are obtained by using the mesh size of M, N = 28. Other details given in Section 4.3 also apply to the present numerical solution. The computing time required to obtain a complete solution for given values of Prandtl and Dean numbers ranges from 3 to 10 minutes using the IBM 360/67 system.

The results of local Nusselt number variations using $\beta = 0$, 0.5 and 1.0 together with the Graetz solution (K = 0) for Pr = 10 and K = 43.8 are shown in Fig. 45 for comparison. By using $\beta = 0$ (central difference approximation), the fluctuation of the local Nusselt number (see Section 5.6) is seen to disappear after passing through two local maximum values of Nu and eventually a

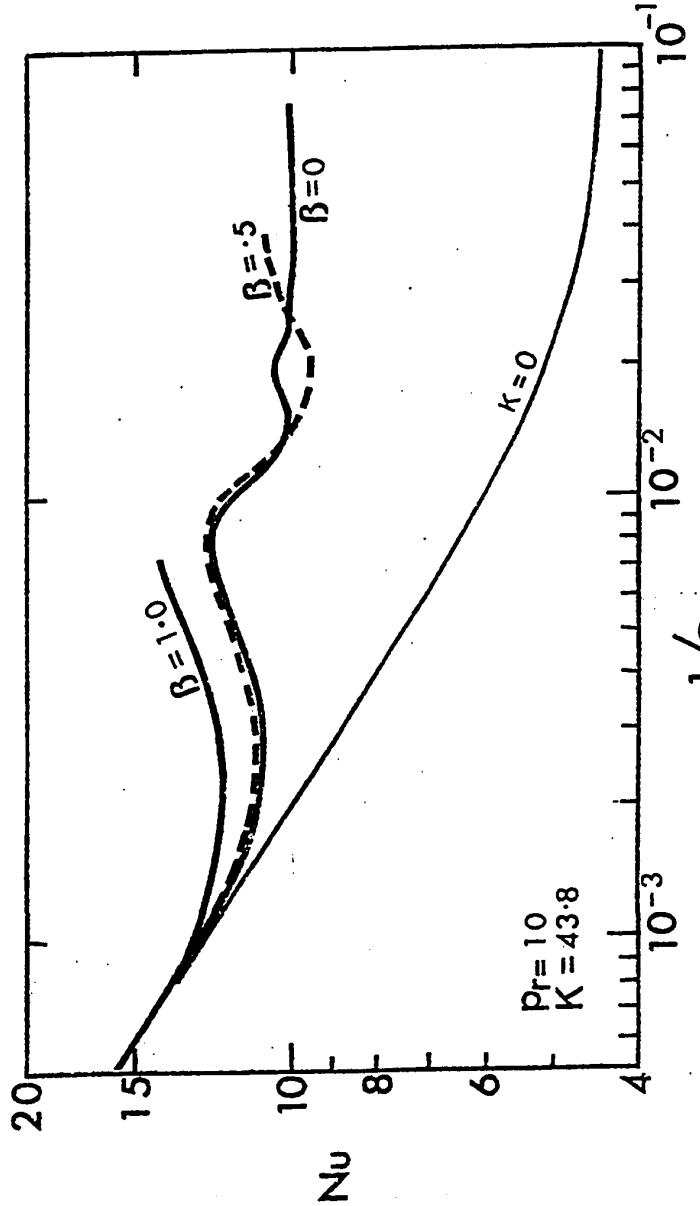


Fig. 45 Effect of β on Local Nusselt Number Fluctuation

fairly stationary value is approached. It is noted that the fluctuating phenomenon remains identical even with a change of mesh size by a factor of three. At first glance, one may think that the numerical solution with $\beta = 0$ is a reasonable one. With $\beta = 0.5$, one sees that the numerical solution agrees closely with that of $\beta = 0$ up to $1/Gz \simeq 1{\cdot}3 \times 10^{-2}$ and thereafter a different trend appears. With $\beta = 1$ (non-central difference approximation), the trend of the numerical solution follows those of $\beta = 0$ and 0.5 up to $1/Gz \simeq 10^{-2}$, but apparently the truncation error due to the non-central difference approximation is too large.

The deviation of the numerical solution from the Graetz solution ($K = 0$) at $1/Gz \simeq 10^{-3}$ represents the onset of the secondary flow effect and the first local minimum value of Nu may be considered as the balance between entrance and secondary flow effects. After passing through this local minimum Nusselt number, the secondary flow effect is seen to take over the entrance effect and the Nusselt number increases until a local maximum value is reached at $1/Gz = 8 \times 10^{-3}$. The behavior of the local Nusselt number can be explained physically up to this point but the physical mechanism for the subsequent decrease-increase cycle cannot be understood readily. It is clear that the role of secondary flow is to increase the Nusselt number over that from the Graetz solution and yet after reaching a local maximum value, the Nusselt number is seen to decrease at a rate which is greater than that of the Graetz solution further downstream. This phenomenon cannot be understood readily and at this point one hesitates to accept

the numerical solution after reaching a local maximum value as a physical meaningful solution. The role of the convective terms $(u\partial\theta/\partial r + v\partial\theta/r\partial\phi)$ is clearly seen in the energy equation (127) and it is not understood why the effects of lateral convective terms are similar to that of the axial convective terms after reaching a local maximum for Nu and thus contribute to a decrease of Nu over that of the Graetz solution. It may be concluded that even with $\beta = 0.5$ the result of the numerical solution after reaching a local maximum value of Nu is still uncertain. Apparently the possibility of numerical instability cannot be ruled out entirely and this viewpoint is completely different from that of Dravid et al [82,83] where the damped fluctuating Nusselt number phenomenon is considered to be a real physical phenomenon.

The present numerical difficulty is, to some extent, similar to that encountered in the elliptic problem treated in Chapter III with large Prandtl or Dean numbers. Physically, the present parabolic problem approached the elliptic problem asymptotically when the temperature field becomes fully established. Consequently, the deviation from diagonal dominance for the coefficient matrix (see equation (122) in Section 4.3) and the difficulty in evaluating the associated right-hand column vector accurately for the case of a large Prandtl number or strong secondary flow may contribute to the numerical difficulty for the present parabolic problem. The non-central difference approximation with $\beta = 1.0$ ensures diagonal dominance for

the coefficient matrix but apparently the resulting truncation error leads to large numerical errors.

At present it is not possible to find the best value of the parameter $\beta$ to be used. In view of the fact that different values of $\beta$ such as 0 and 0.5 lead to different fluctuating phenomenon for Nu after reaching a local maximum one may conclude that the fluctuating phenomenon is due to numerical instability and does not represent a true physical solution. Further discussion on this point will be made in connection with the presentation of temperature profile development and Nusselt number result.

## 5.5 TEMPERATURE PROFILE DEVELOPMENT

Temperature profile developments along the horizontal and vertical central axes for the cases Pr = 0.7, K = 123.2 and Pr = 10, K = 27.8 are shown in Figs. 46 and 47, respectively. The distortion of the temperature profiles from those of the Graetz solution for a straight pipe (K = 0) is obvious. It is seen that after reaching a certain downstream location, the temperature at the inner wall ($\phi = \pi$) becomes progressively greater than that at the outer wall ($\phi = 0$). The thermal boundary layer at the inner wall develops much more rapidly along the downstream than at the outer wall and eventually the thermal boundary layer at all angular positions merges. For example, with Pr = 0.7 and K = 123.2, the region with $\theta = 0$ disappears completely at a downstream distance of 1/Gz = 0.0130 and after reaching 1/Gz = 0.0504 the profiles are seen to be similar and only vary in relative

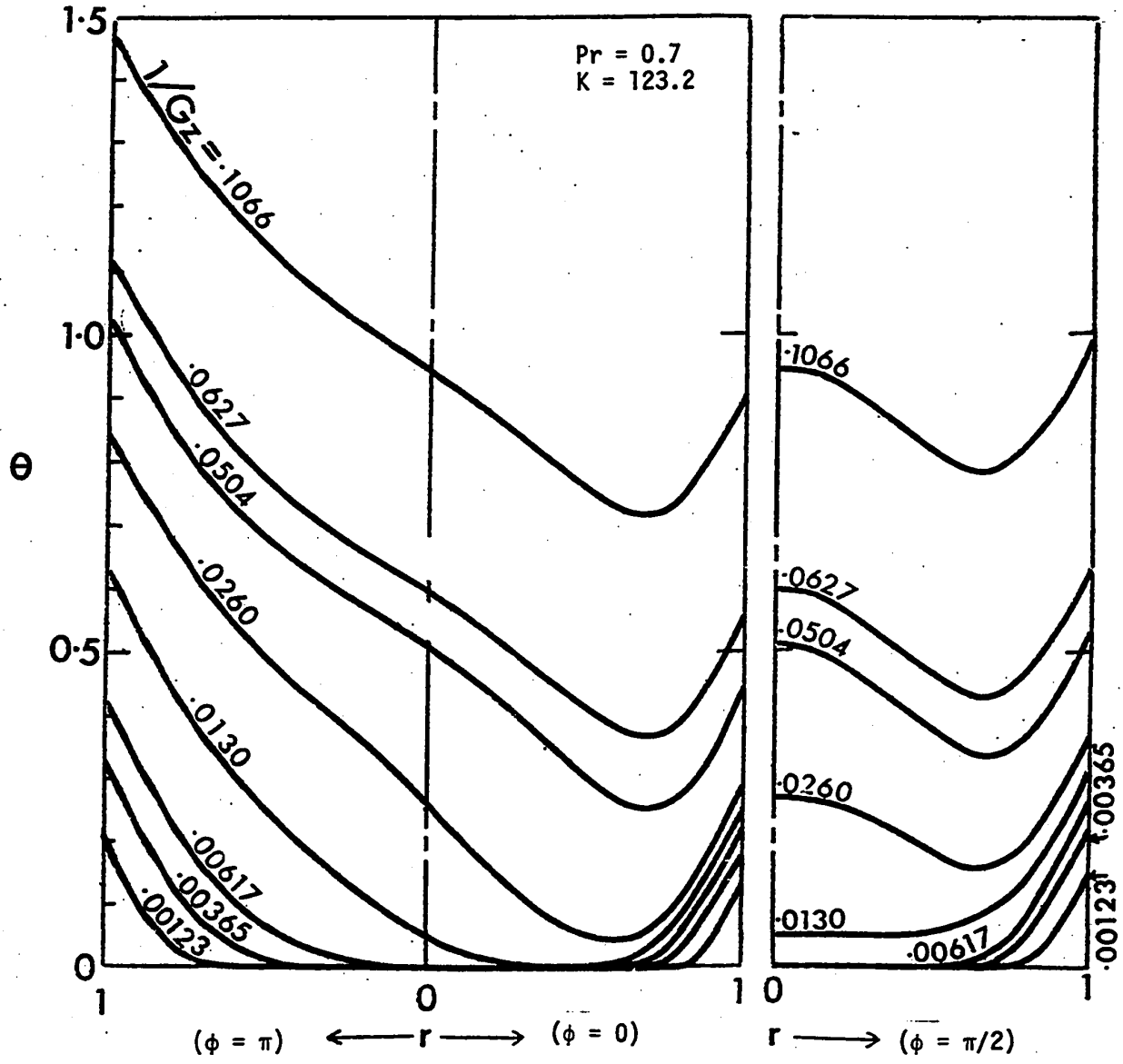


Fig. 46 Temperature Profile Development for Pr = 0.7 and K = 123.2

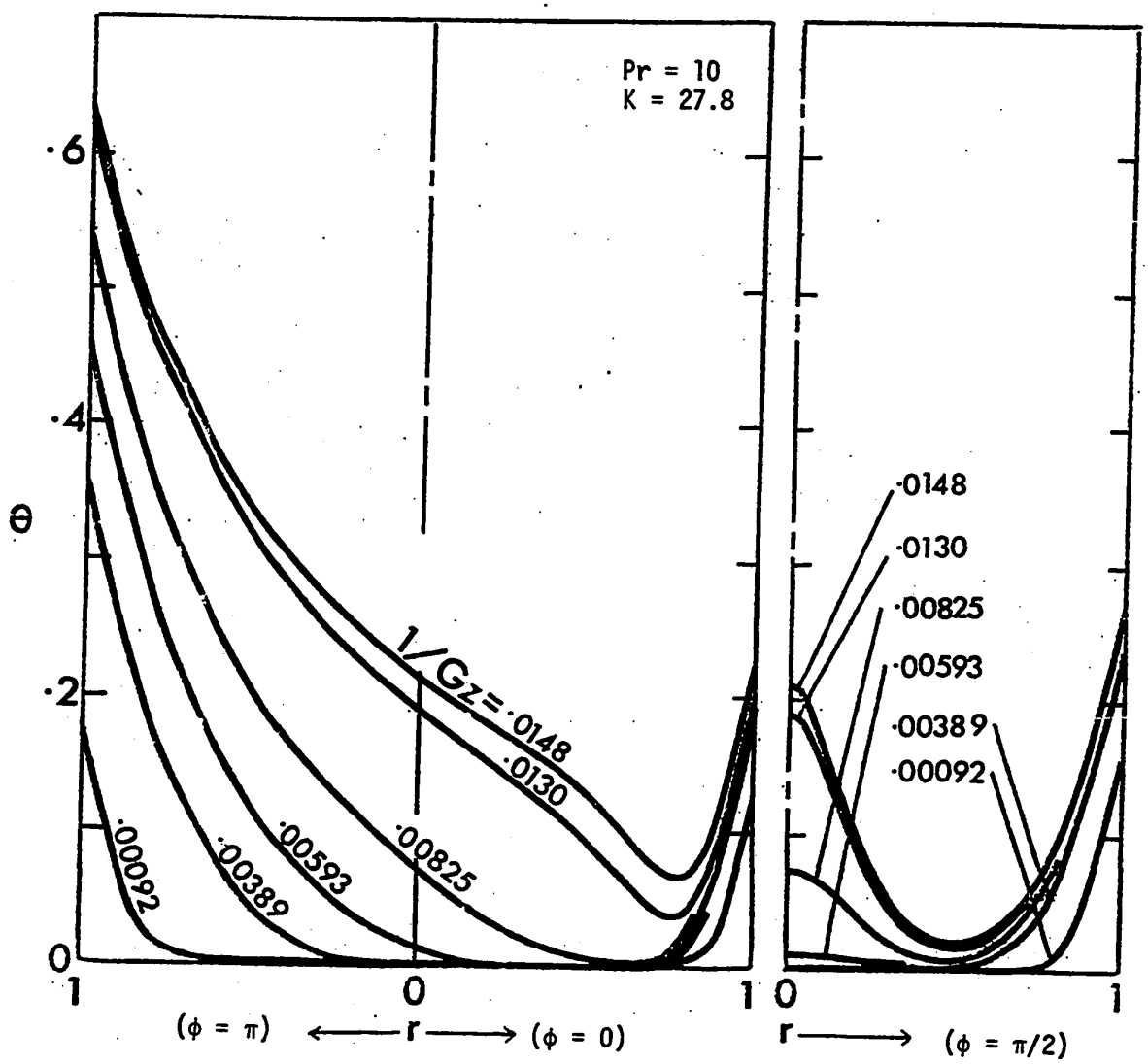


Fig. 47 Temperature Profile Development for Pr = 10 and K = 27.8

magnitude. Consequently, the temperature profile may be considered fully developed at 1/Gz = 0.0504. This fact will be confirmed further when the axial distributions of average wall temperature, bulk temperature and mixed mean temperature difference are discussed. By noting that the fully developed temperature field may be obtained at $1/GZ \doteqdot 10^{-1}$ for a straight pipe (K = 0), one sees that the thermal entrance length is shortened considerably with the existence of secondary flow.

One gains better physical insight into the development of the temperature field by studying the development of isothermals along the downstream direction. A series of isothermals corresponding to the axial locations shown in Fig. 46 and 47 are shown in Figs. 48 and 49, respectively. It is useful to contrast the profile developments shown in Figs. 46 and 47, directly with the corresponding isothermal fields illustrated in Figs. 48 and 49, respectively. For example, Fig. 48 shows that at 1/Gz = 0.0130 the region with $\theta = 0$ indeed disappears completely as indicated by the fact that the minimum temperature is $\theta = 0.00196$. As noted earlier, downstream of 1/Gz = 0.0504 the temperature field becomes fully developed as confirmed by similar isothermal fields at 1/Gz = 0.0504 and 0.1066. It is clearly seen that between 1/Gz = 0.0130 and 0.0504 the temperature field is still undergoing some change. Generally one sees from Fig. 48 that the effect of secondary flow on temperature field increases with downstream distance. Of course the pattern of isothermals at various axial distances are closely related to the Nusselt number variation.

An examination of the isothermal patterns illustrated in

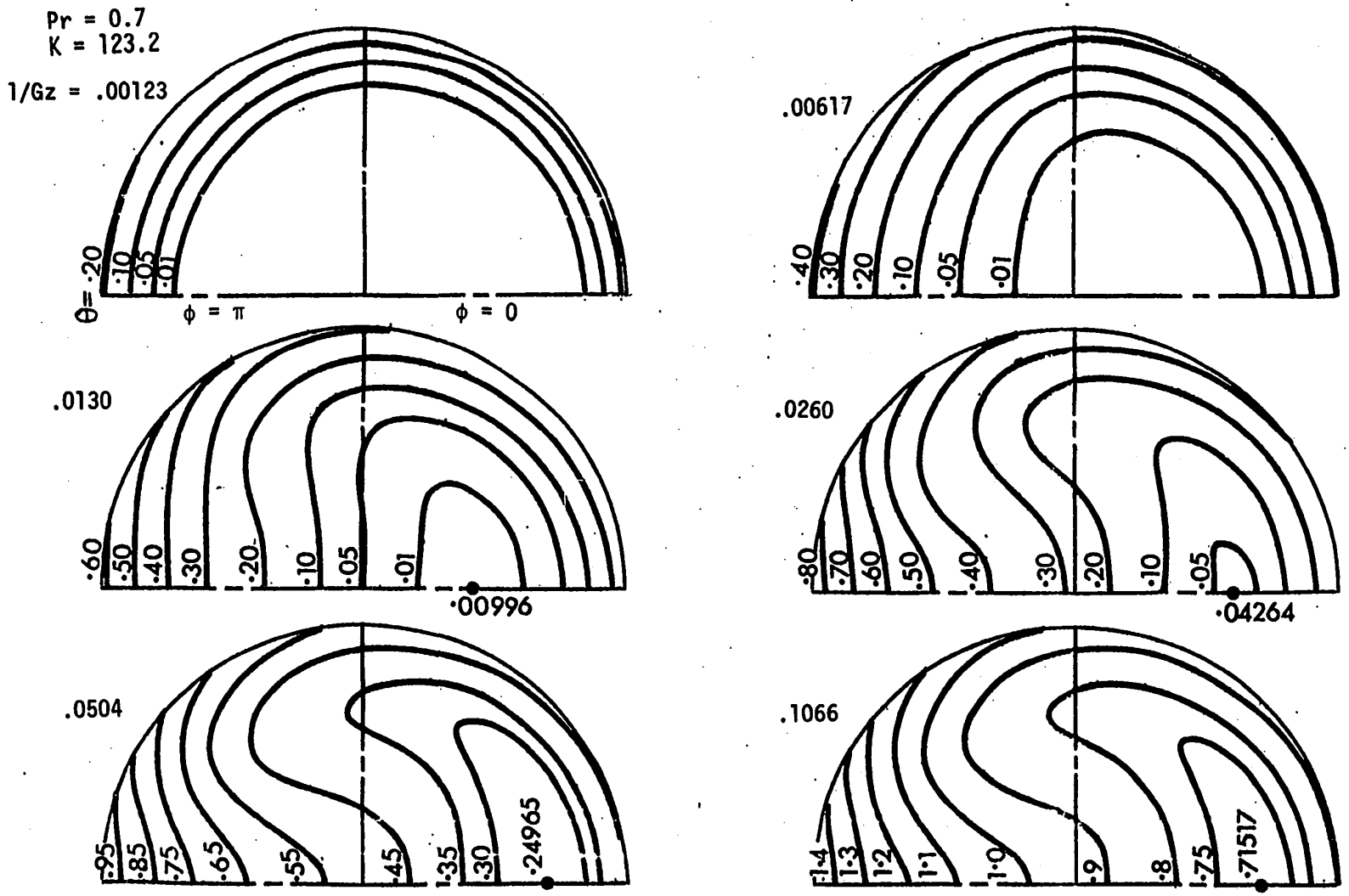


Fig. 48 Development of Isothermals for Pr = 0.7 and K = 123.2

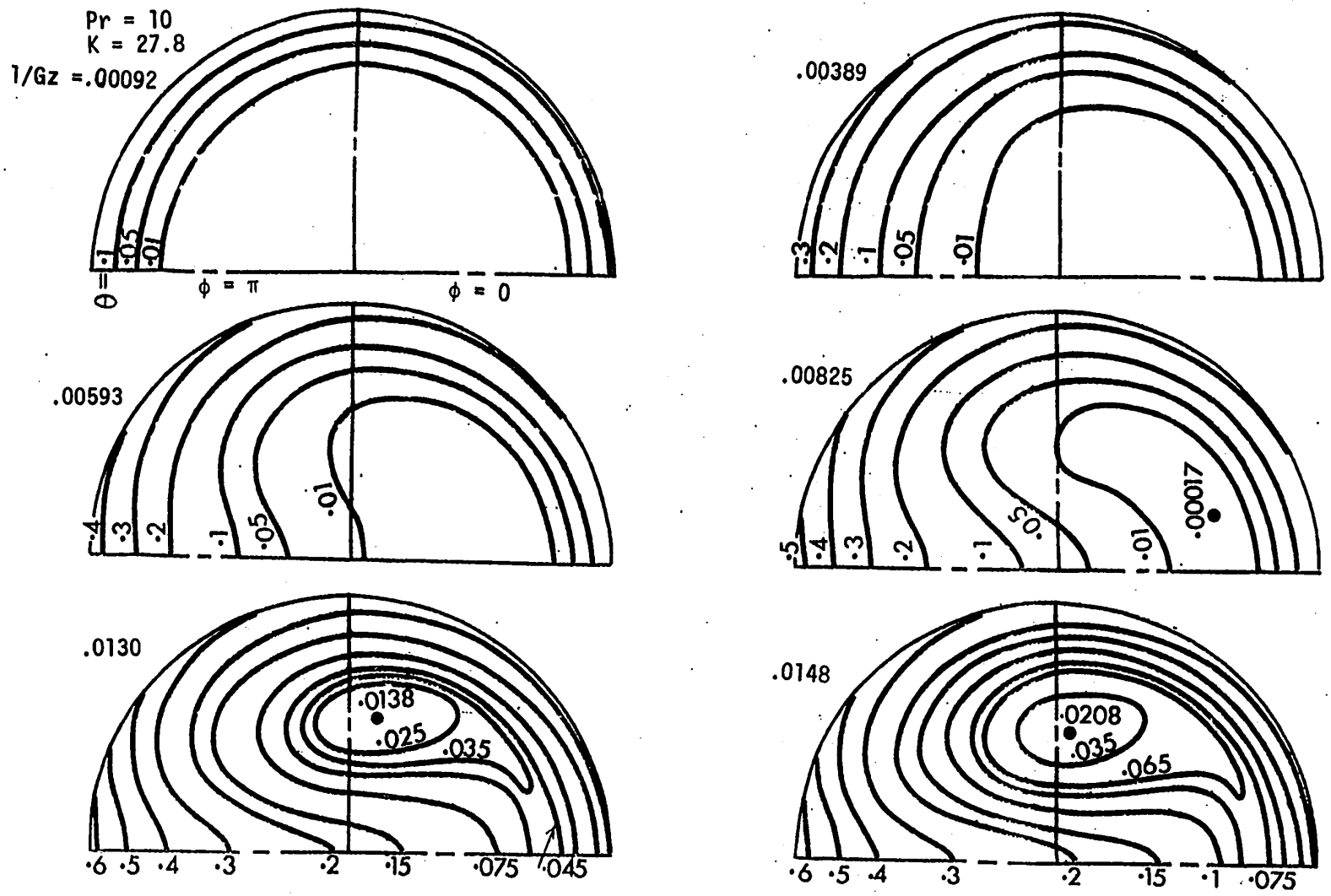


Fig. 49 Development of Isothermals for Pr = 10 and K = 27.8

Fig. 49 shows that with Pr = 10 and K = 27.8 two eyes for the isothermals appear at 1/Gz = 0.0130 and the minimum temperature point is not located along the horizontal central axis. For Pr = 10 and K = 27.8, the temperature field becomes fully established at 1/Gz = 0.0148 and the thermal entrance length is shortened considerably in comparison to $1/Gz \doteqdot 10^{-1}$ for a straight pipe (K = 0).

The temperature field development in the form of such overall quantities as bulk temperature $\theta_b$, average wall temperature $\overline{\theta}_w$ and mixed mean temperature difference $\Delta\theta$ are of considerable practical as well as theoretical interest and the results are shown in Fig. 50 for the case of Pr = 0.7 and K = 123.2 together with the limiting case of K = 0 shown for comparison. Because of the nature of a uniform wall heat flux boundary condition, the bulk temperature $\theta_b$ is known to vary linearly along the downstream distance regardless of the value of Dean number K. As a matter of fact the bulk temperature distribution $\theta_b$ is known in advance without solving the problem. It is readily understood that the average wall temperature along the axial direction for K = 123.2, for example, is lower than that of K = 0 due to the secondary flow effect. As a result, the mixed mean temperature difference $\Delta\theta$ for K = 123.2 is seen to be lower than that of K = 0 along the axial distance. This in turn will increase the local Nusselt number since the temperature gradient at the wall is constant for the present problem. It is noted that the mixed mean temperature difference $\Delta\theta$ for K = 0 and 123.2 becomes constant at approximately 1/Gz = 0.09 and 0.045, respectively, indicating the establishment of the temperature

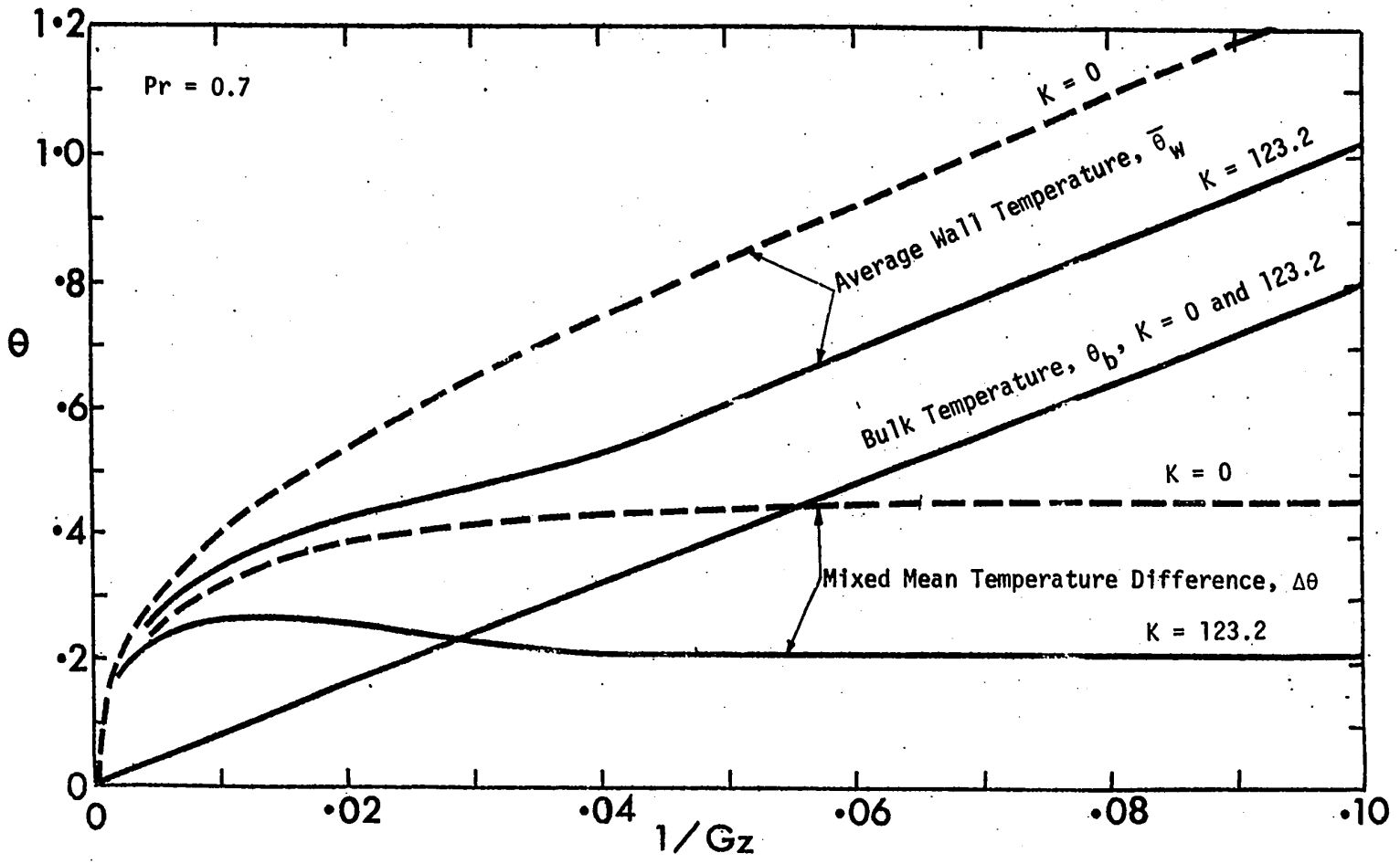


Fig. 50 Axial Temperature Distributions for $\bar{\theta}_w$, $\theta_b$ and $\Delta\theta = \theta_w - \theta_b$ for K = 0 and Pr = 0.7, K = 123.2

field. It is observed that with K = 123.2 the difference between $\bar{\theta}_w$ and $\theta_b$ or $\Delta\theta$ undergoes one undulation before reaching a fully developed condition. Once the temperature field is established, the average wall temperature $\bar{\theta}_w$ changes linearly with the axial distance and becomes parallel to the bulk temperature distribution $\theta_b$.

From Fig. 50, one can recognize generally three regions of interest. Near the thermal entrance the effect of secondary flow may be small or negligible and the region is identical with the Leveque solution region for a straight pipe (K = 0). In this region the isothermals are expected to be fairly concentric. On the other hand, far downstream, the temperature field becomes fully established as indicated by the region with constant $\Delta\theta$. In the remaining intermediate region, the secondary flow effect gradually increases along the downstream until no further increase of the effect is possible. The temperature distributions shown in Fig. 50 may be contrasted with the temperature profiles and isothermals shown in Figs. 46 and 48, respectively.

## 5.6 HEAT TRANSFER RESULTS

As noted in Section 4.5, the Nusselt number, $Nu = \bar{h}\,(2a)/k$, may be obtained in two ways as

$$Nu_1 = 2\left(\frac{\overline{\partial\theta}}{\partial r}\right)_w \frac{\bar{w}}{w(\bar{\theta}_w - \theta)}$$

$$Nu_2 = Pr\left(\frac{c^2}{r_c}\right)^{1/2}\left(\frac{1}{r_c}\right)^{1/2}\frac{\overline{\left(w\,\frac{\partial\theta}{\partial\omega}\right)}}{w(\bar{\theta}_w - \theta)} \qquad (131)$$

The numerical results show that the values for $Nu_1$ and $Nu_2$ deviate generally from 0 to 1.3 per cent from the average value of $Nu_1$ and $Nu_2$. The deviation increases to about 3 per cent in the higher parameter region when $Pr \geq 10$. The agreement between the two values $Nu_1$ and $Nu_2$ serves to confirm the accuracy and convergence of the numerical solution. It is possible to ascertain the accuracy of the numerical solution for the limiting case of a straight pipe ($K = 0$) by comparing the present numerical evaluation of the local Nusselt number with that of the numerical solution of Reference [108] and the analytical solutions of References [109,110]. The numerical result for the case of a uniform wall temperature (see Chapter IV) is also included in Fig. 51 for reference. It is seen that the present work agrees with that of Hsu [109,110]. Thus the accuracy and convergence of the numerical solution are confirmed for the limiting case with $K = 0$. The local Nusselt number variations for $Pr = 0.1$, 0.7, 10 and 500 are shown in Figs. 52 to 55 with the Dean number as a parameter. For the cases $Pr = 0.7$, $K = 123.2$ and $Pr = 10$, $K = 27.8$ shown in Figs. 53 and 54, respeectively, the Nusselt number variation can be contrasted directly with the development of the temperature profile and isothermals shown in Figs. 46, 47 and 48, 49, respectively. A close relationship exists between the temperature field development and the local Nusselt number variation and some observations will be noted next.

For the purpose of understanding the physical mechanism

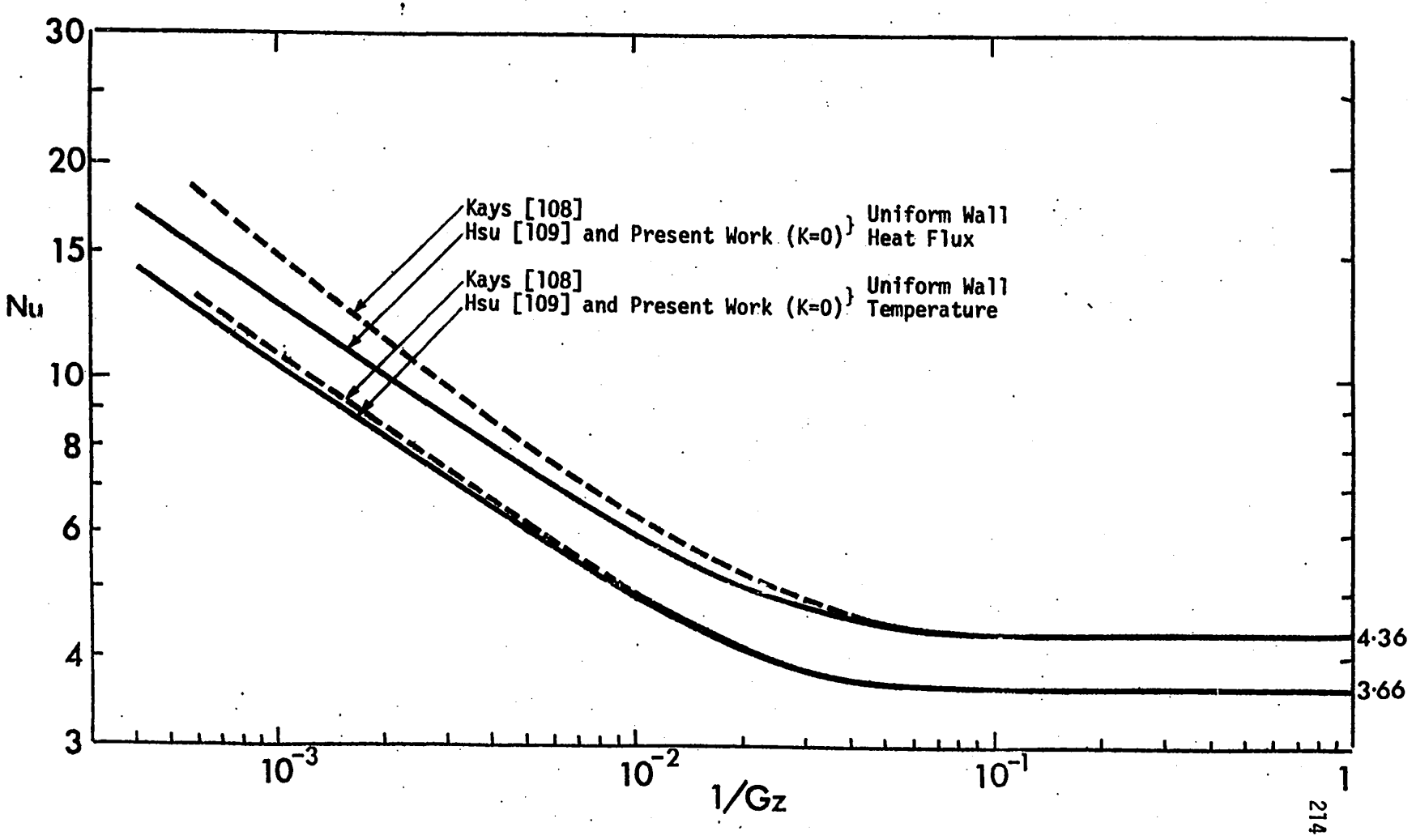


Fig. 51 A Comparison Between Present Numerical Results and Results from Kays [108] and Hsu [109,110]

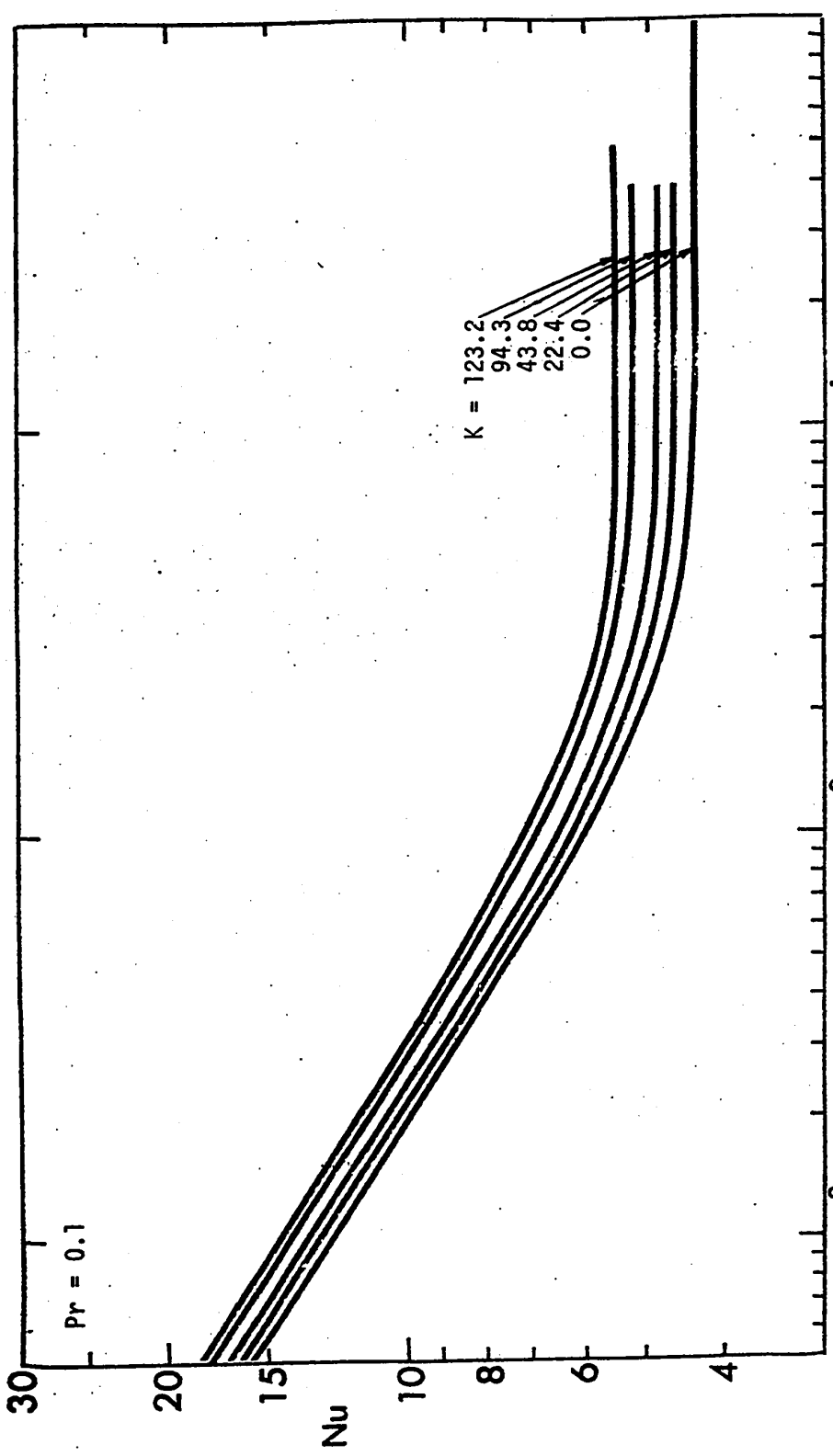


Fig. 52 Local Nusselt Number Variation for Pr = 0.1 with Dean Number as Parameter

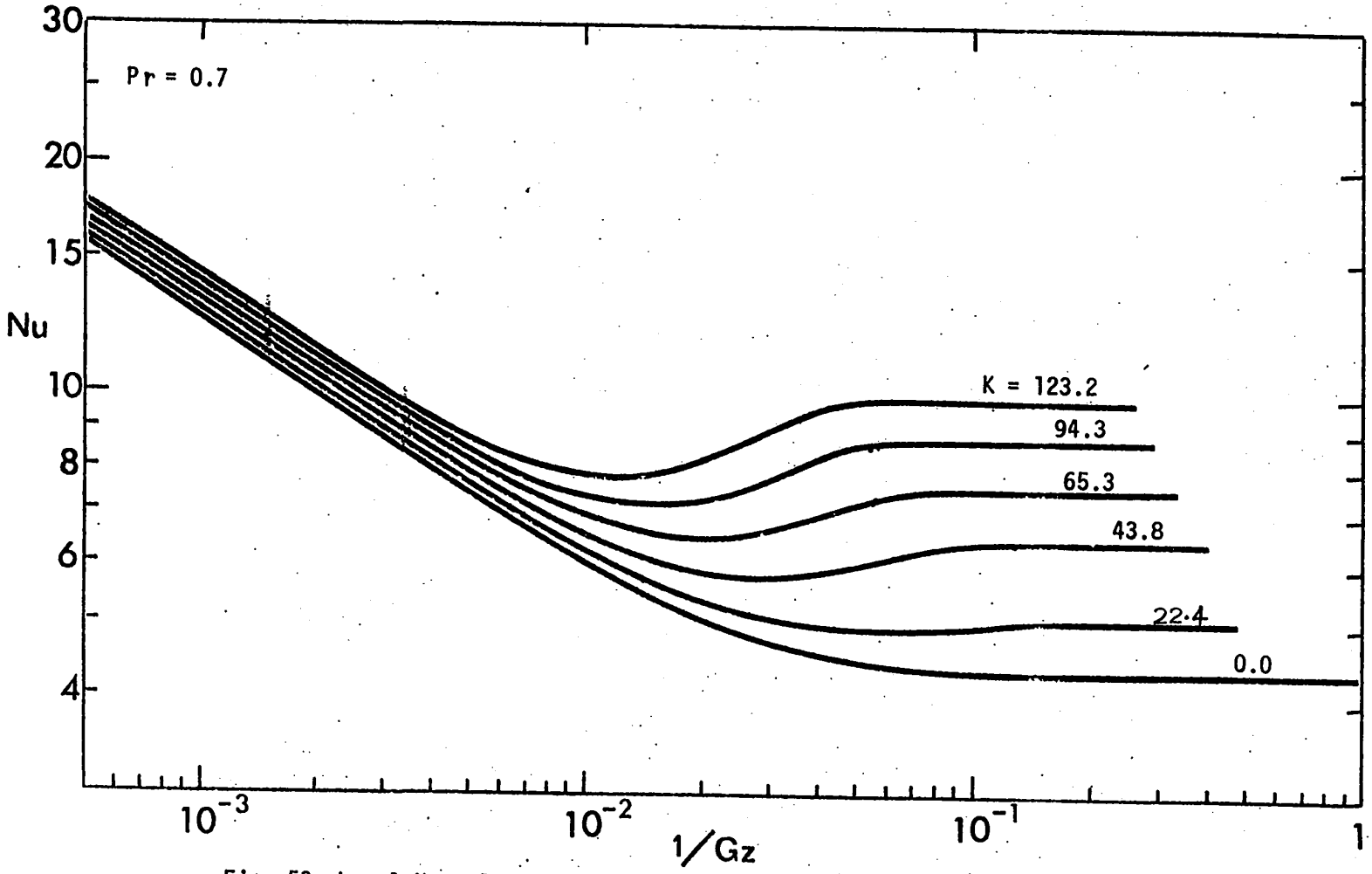


Fig. 53 Local Nusselt Number Variation for Pr = 0.7 with Dean Number as Parameter

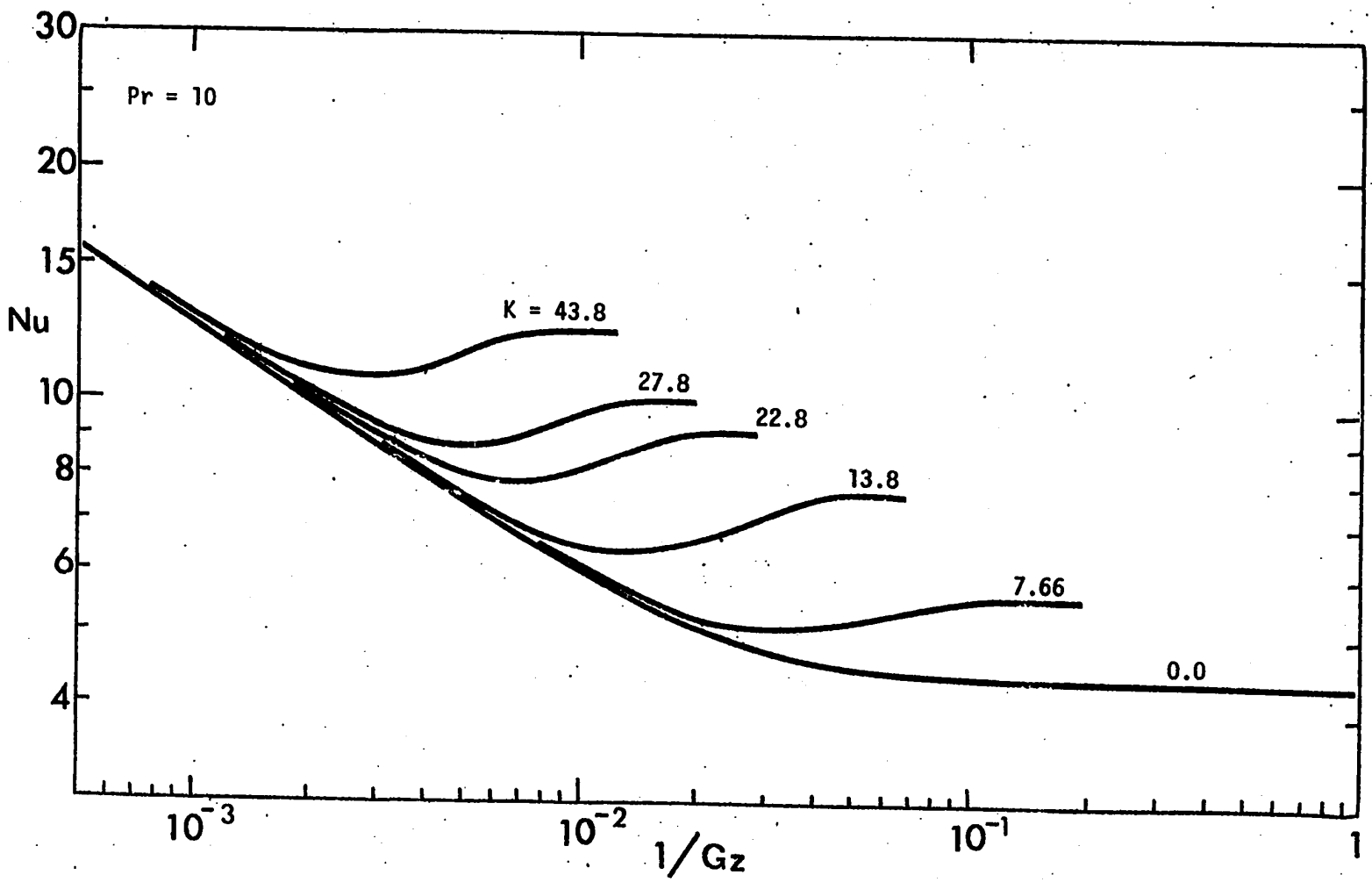


Fig. 54 Local Nusselt Number Variation for Pr = 10 with Dean Number as Parameter

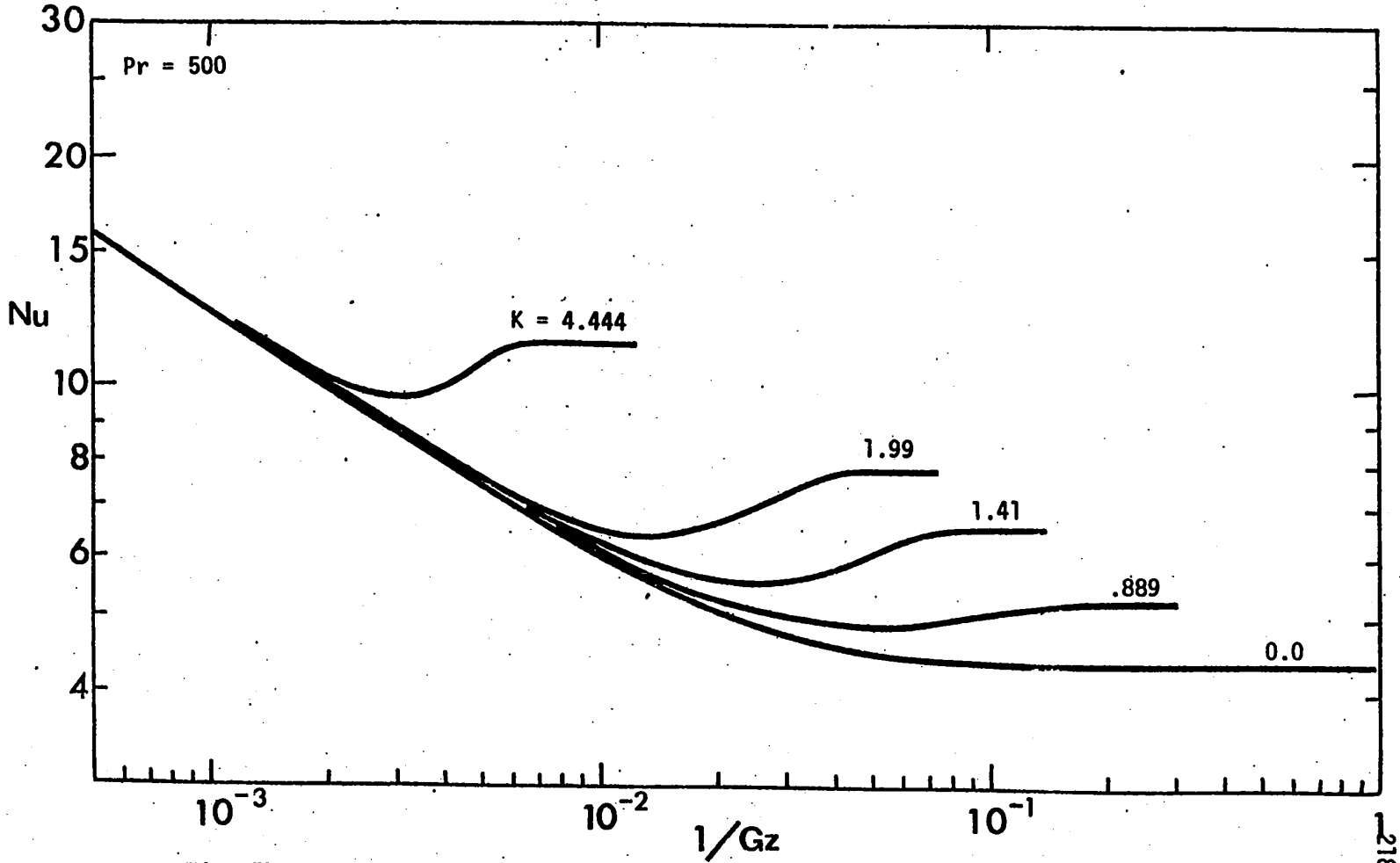


Fig. 55 Local Nusselt Number Variation for Pr = 500 with Dean Number as Parameter

behind the Nusselt number behavior, one may consider the three regions consisting of the Leveque solution region, the intermediate region where the secondary flow effect is important and finally the asymptotic region as noted in Section 5.5. In the Leveque region corresponding approximately to the straight line portion shown in Figs. 52 to 55, the behavior of the local Nusselt number depends on the Prandtl number. For example, with Pr = 0.1 and 0.7, the Nusselt number variations for different Dean numbers are seen to be parallel to each other while for Pr = 10 and 500, the Nusselt number variation for a given Dean number is seen to coincide with the Graetz solution for a straight pipe (K = 0). The parallel behavior of the local Nusselt number for Pr = 0.1 and 0.7 is caused by the distortion of the axial velocity profile w from the parabolic profile and the axial convection term involving $w\ \partial\theta/\partial\omega$ is seen to be dominant as compared with the transverse convection terms due to secondary flow, $u\ \partial\theta/\partial r + v\ \partial\theta/r\partial\phi$, in the Leveque solution region. In contrast, for the cases Pr = 10 and 500 shown in Figs, 54 and 55, respectively, the secondary flow is generally weak and the Nusselt number variation is seen to follow closely the Graetz solution (K = 0) for a straight pipe. Thus, for Pr = 10 and 500, the secondary flow effect is seen to be negligible in the Leveque region for the range of Dean numbers under investigation.

For the intermediate region noted above, the behavior of Nusselt number variation with Pr = 0.1 is similar to that of the Graetz solution (K = 0) for several Dean numbers shown in Fig. 52.

Of course, the increase of Nusselt number at any axial location is due to the secondary flow effect. For Pr = 0.7, the local Nusselt number behavior exhibits a local minimum value and finally the asymptotic value is approached and remains constant. It should be noted that for Pr = 0.7, no fluctuating Nusselt number behavior is observed up to K = 123.2 shown in Fig. 53. It is of interest to note that the minimum Nusselt number point for Pr = 0.7 and K = 123.2 shown in Fig. 53 corresponds approximately to the axial position 1/Gz = 0.013 in Figs. 40 and 48 where the heat transfer from the wall already penetrates the whole region. Similarly, the minimum Nusselt number point for Pr = 10 and K = 27.8 shown in Fig. 54 corresponds to the axial position 1/Gz = 0.00593 shown in Figs. 47 and 49. After reaching the point of mimimum Nusselt number, the temperature field will continue to develop until the fully developed condition is approached at which point the asymptotic Nusselt number appears. For Pr = 10 and 500 shown in Figs. 54 and 55, the numerical solution exhibits a fluctuating Nusselt number phenomenon at higher values of Dean number and the local maximum Nusselt number is considered to be the asymptotic value in view of the discussion given in Section 5.4. This assumption regarding the asymptotic Nusselt number is consistent with the result shown in Fig. 53 where no fluctuating phenomenon is observed and the Nusselt number remains constant in the asymptotic region. In Fig. 48, the isothermals at 1/Gz = 0.0504 and 0.1066 are seen to be remarkably similar and a check with the corresponding axial locations in Fig. 53 shows clearly

that the fully developed condition is reached. Similarly, for Pr = 10 and K = 27.8, the temperature field becomes fully developed at 1/Gz = 0.0130.

The average Nusselt numbers over the axial distance from the thermal entrance are shown in Figs. 56 to 59 for Pr = 0.1, 0.7, 10 and 500, respectively.

The asymptotic Nusselt number results are of special interest in many design problems, and the results from the present study are summarized in Fig. 60 together with the results for an axially uniform wall heat flux (circumferentially uniform wall temperature at any axial position, Chapter III), and for the uniform wall temperature case (Chapter IV) for comparison. It is to be noted that for a given Prandtl number, the uniform wall heat flux case gives the highest asymptotic Nusselt number for a given Dean number after reaching a certain Dean number depending on the Prandtl number. As $K \to 0$, all the curves are seen to approach either 4.36 for a uniform heat flux or 3.66 for a uniform wall temperature. It is also noted that the Prandtl number effect on the asymptotic Nusselt number is quite similar regardless of the kind of thermal boundary condition.

Based on the known fact and the present results, it is now possible to propose a model in order to explain the observed behavior of the local Nusselt number. It is known that for a given Prandtl number the effect of secondary flow as indicated by the Dean number is to decrease the thermal entrance length. The behavior of the asymptotic Nusselt number as a function of Dean number is also

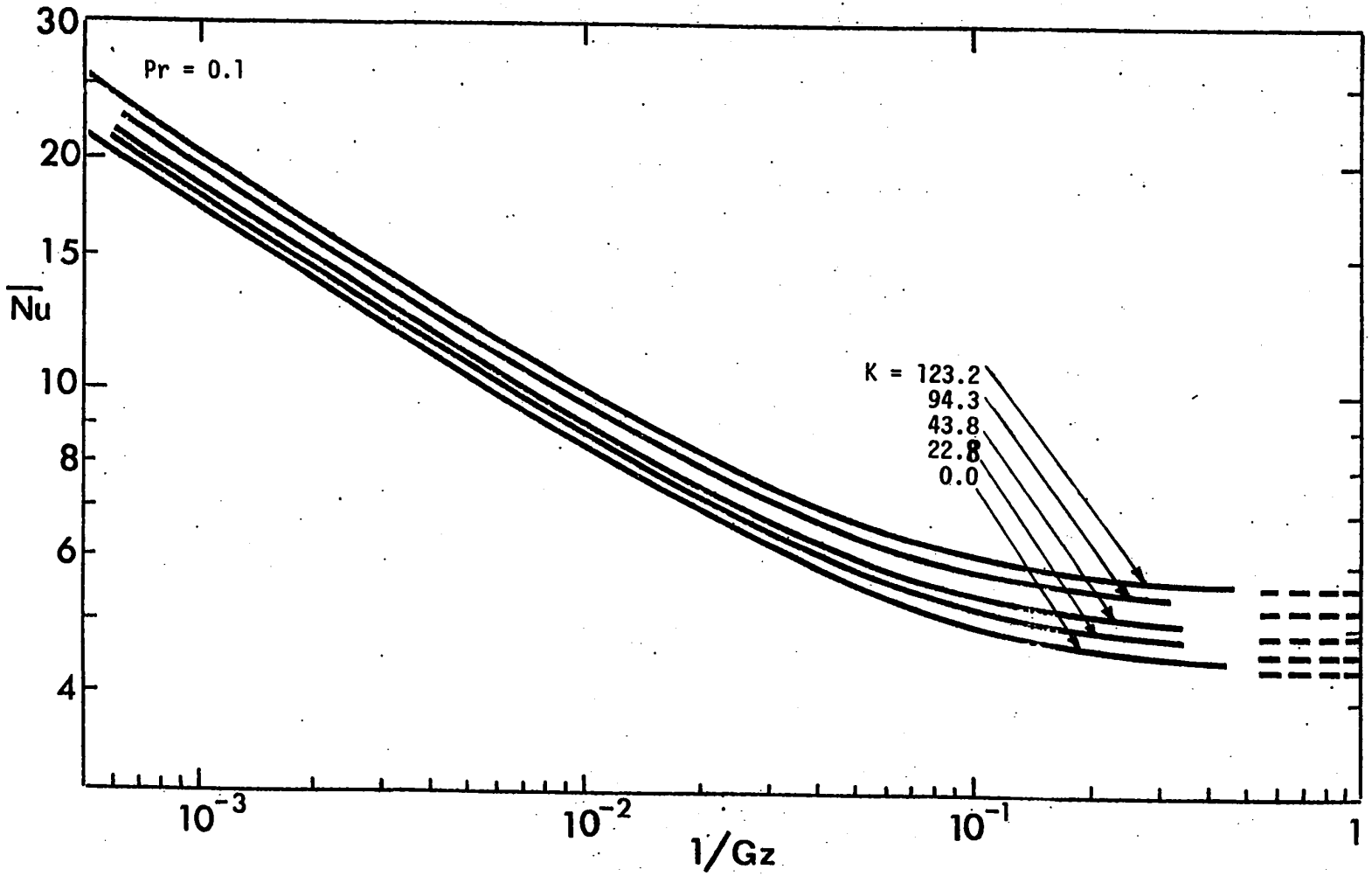


Fig. 56 Average Nusselt Number Variation for Pr = 0.1 with Dean Number as Parameter

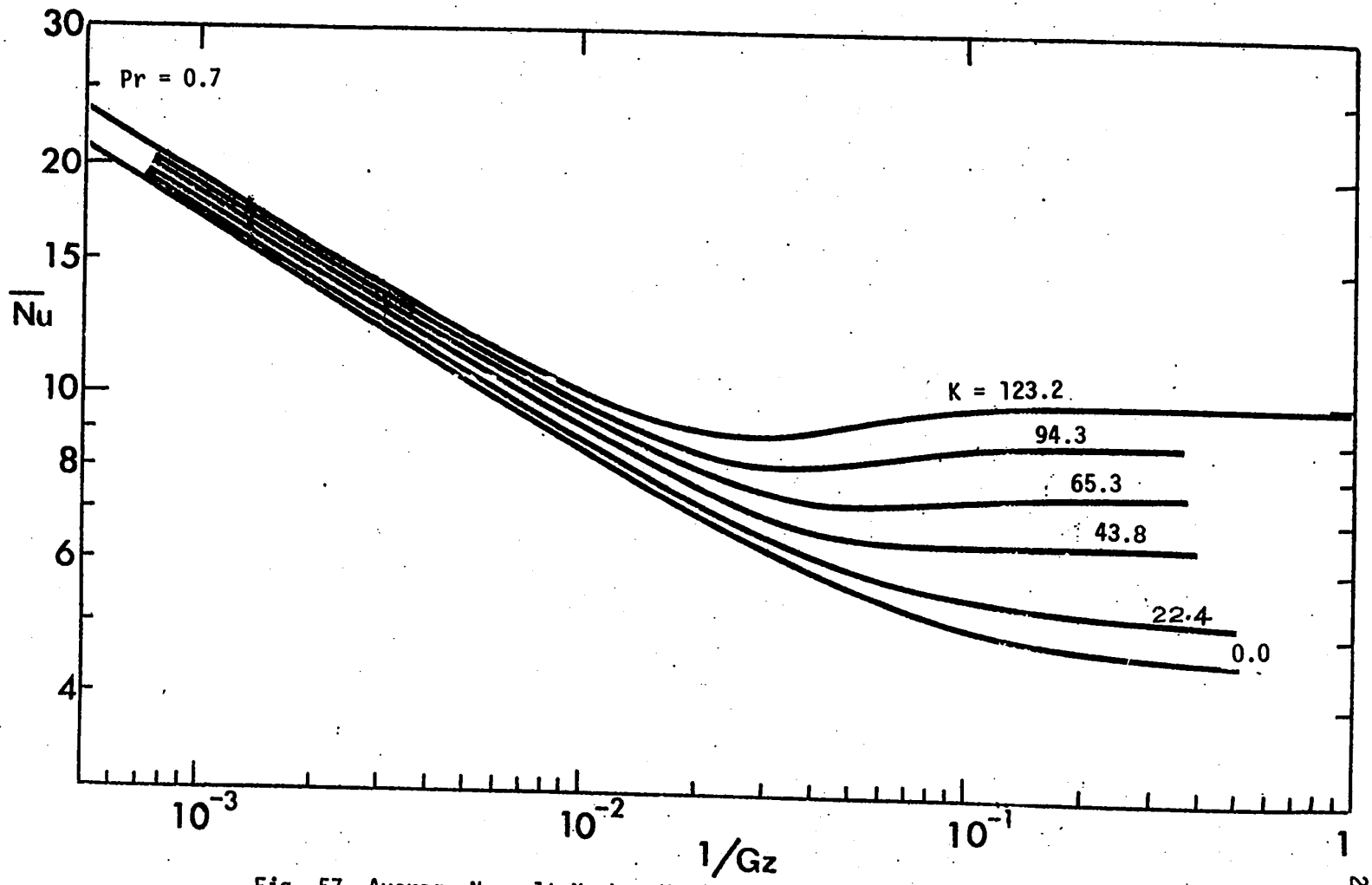


Fig. 57 Average Nusselt Number Variation for Pr = 0.7 with Dean Number as Parameter

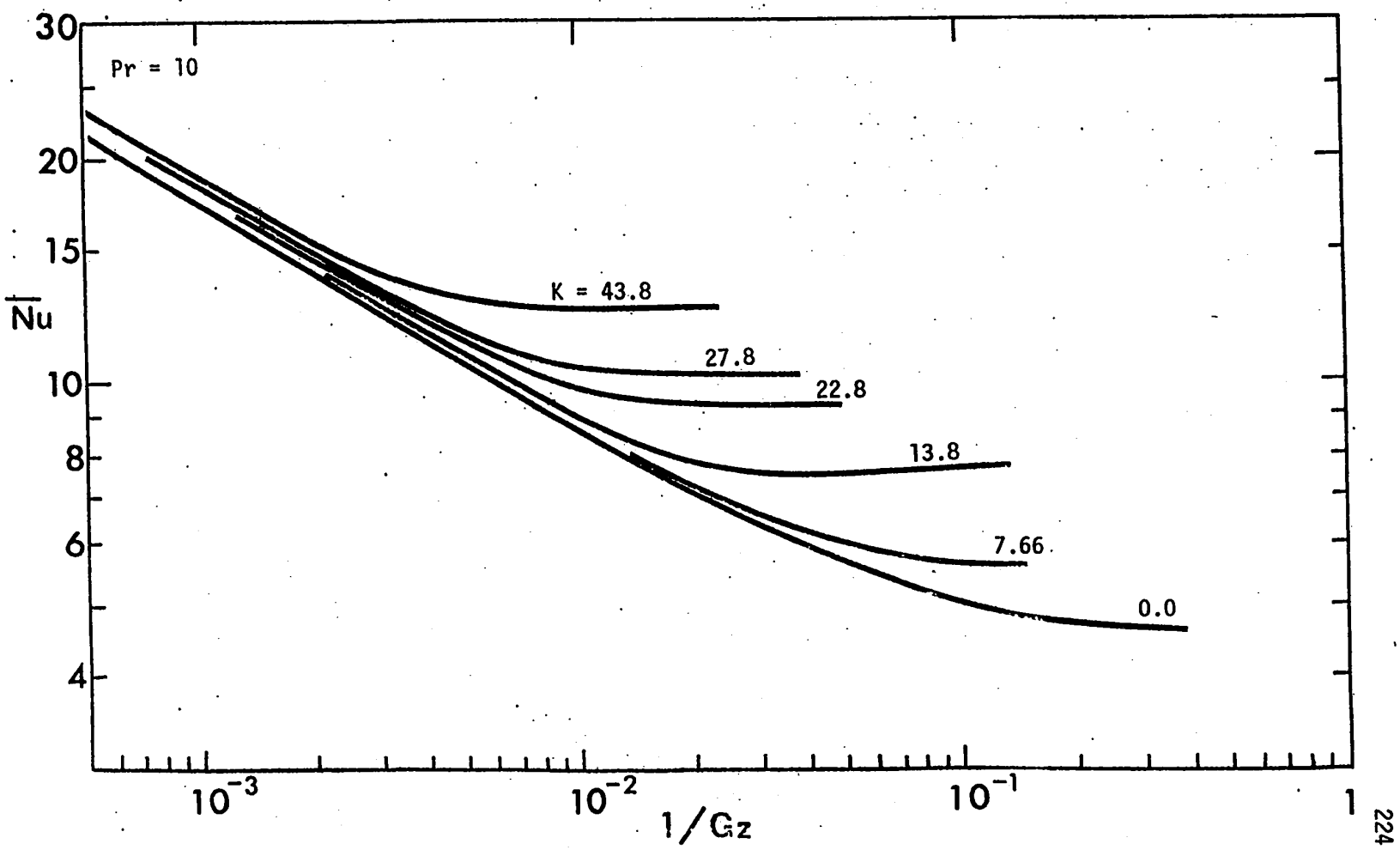


Fig. 58 Average Nusselt Number Variation for Pr = 10 with Dean Number as Parameter

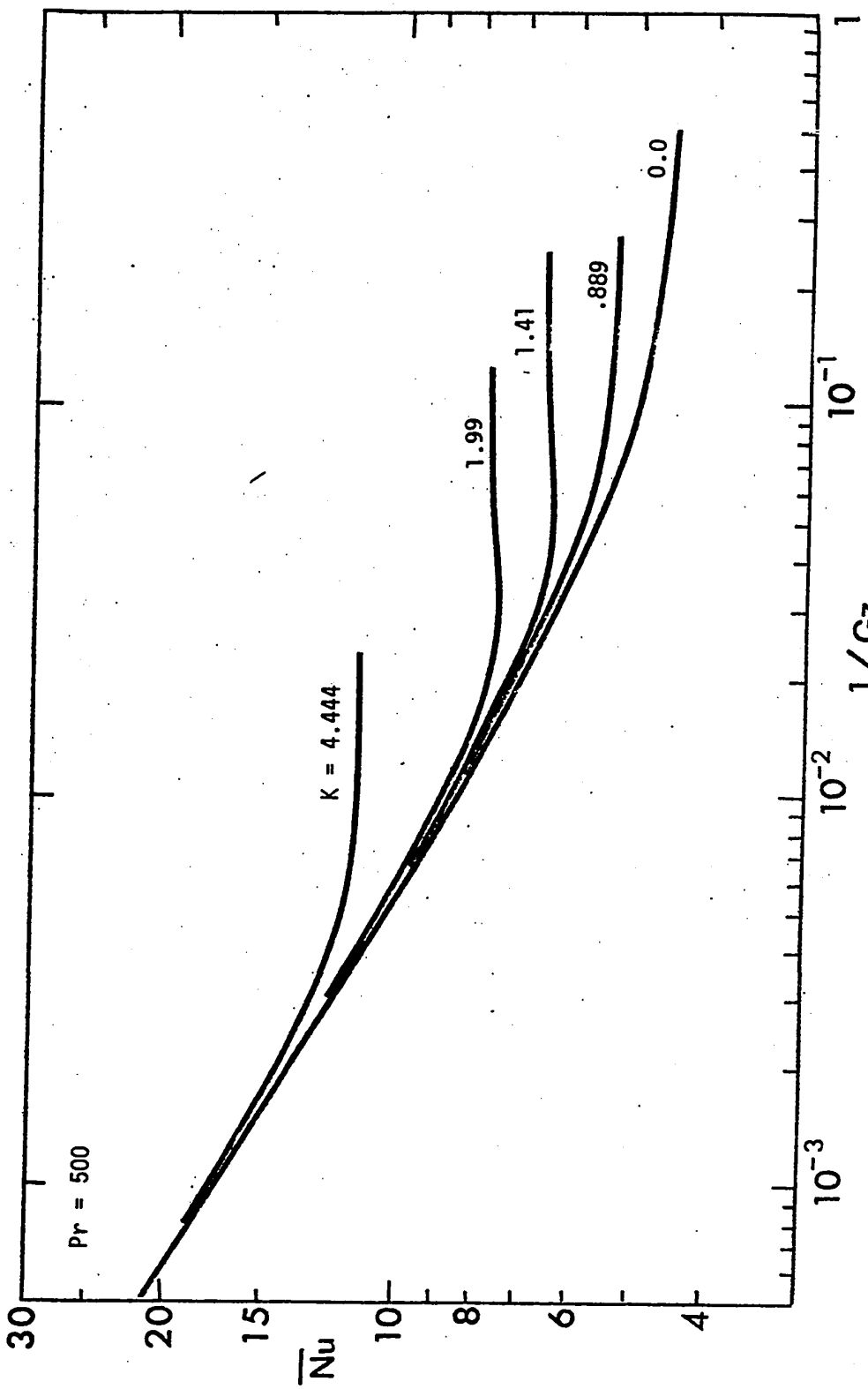


Fig. 59 Average Nusselt Number Variation for Pr = 500 with Dean Number as Parameter

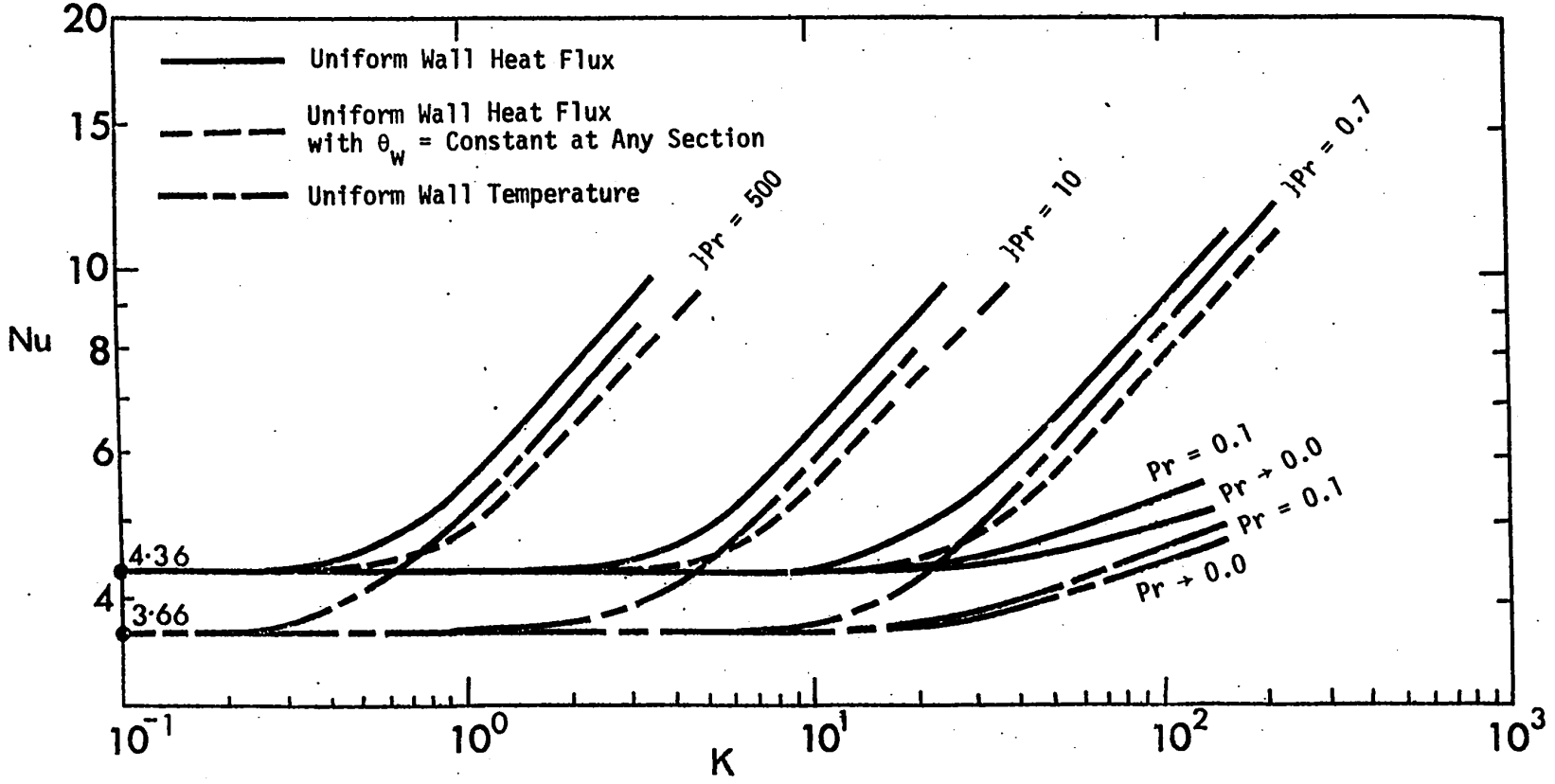


Fig. 60 A Summary of Heat Transfer Results for the Thermally Fully Developed Region

generally known. The decrease of local Nusselt number with axial distance for the Graetz problem (K = 0) is known to be caused solely by the axial convection term and the behavior is generally known to be an entrance effect. For the case of large Prandtl number fluids, say Pr $\geq$ 10, and considering only the Leveque solution region, the secondary flow effect as represented by the transverse convection term ($u\,\partial\theta/\partial r + v\,\partial\theta/r\partial\phi$) are still negligible as compared with the axial convection term in the energy equation and the local Nusselt number will coincide with the Graetz solution. This fact together with the extent of the Leveque solution region as indicated by the axial distance 1/Gz is clearly shown in Fig. 54 for Pr = 10. By regarding the local Nusselt number as consisting of a part due to the Graetz solution and an incremental part due to the secondary flow effect, one may obtain the sketch shown in Fig. 61(a). In the sketch a point indicated by the circle denotes the fully developed condition. It is now assumed that the incremental part of the Nusselt number, namely $\Delta$Nu, may increase monotonically along the axial distance 1/Gz. By superimposing the incremental part $\Delta$Nu onto the Graetz solution, one obtains the Nusselt number variation shown in Fig. 61(b). The point represented by the triangle corresponds to the local maximum value of Nu. Admittedly, the proposed model shown in Fig. 61 is a crude one but it does explain the behavior of local Nusselt number at least qualitatively in the thermal entrance region as a function of Dean number. At a certain higher Dean number the local minimum Nusselt number is seen to disappear. Because of the nonlinear effect

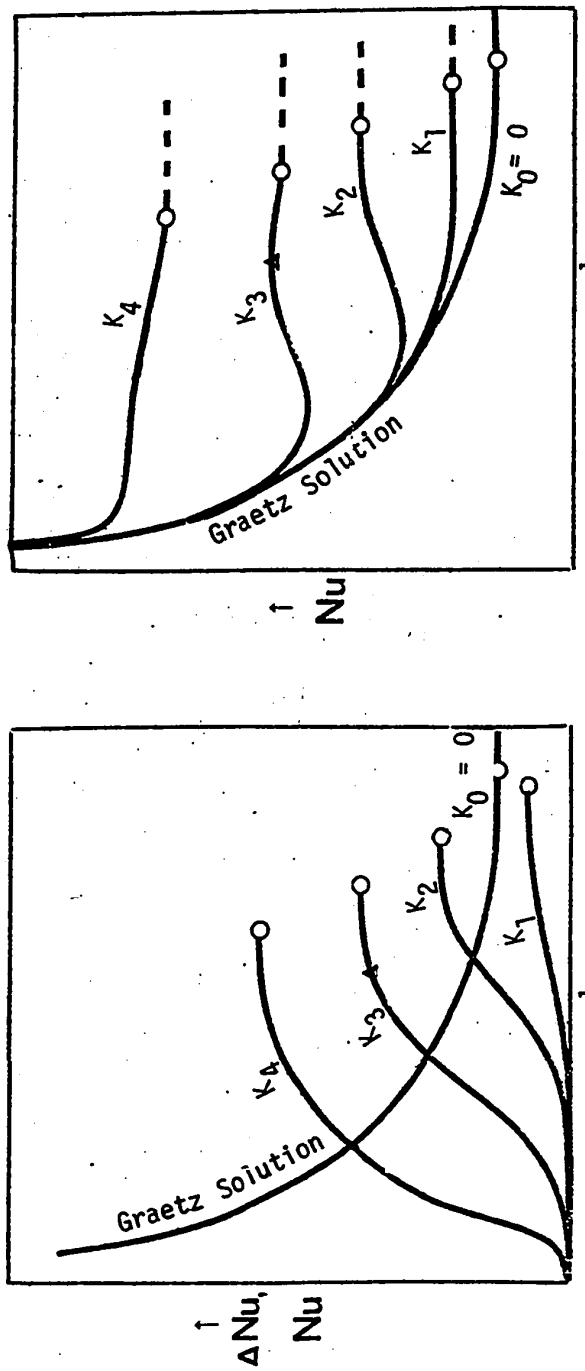


Fig. 61 A Proposed Model for Nusselt Number Behavior with Dean Number as Parameter

due to the convective terms and the distortion of the axial velocity profile from the parabolic one due to secondary flow, the superficial superposition of the two parts as represented by the Graetz solution and the incremental part $\Delta Nu$ in the intermediate region preceeding the asymptotic region may not have any physical basis. Nevertheless, the above model may serve to demonstrate the general behavior of local Nusselt number. Even with the rather simple model for large Prandtl number fluids presented here, the development of the empirical correlation equation is expected to be extremely difficult for the present problem. According to the proposed model, the asymptotic Nusselt number is approached once the temperature field becomes fully established and the asymptotic region is indicated by the dotted lines. The present model applies only to high Prandtl number fluids and it suffices to mention here that a different model is required for low Prandtl number fluids.

## 5.7 SOME OBSERVATIONS ON DRAVID'S WORK [83]

As pointed out earlier, theoretical and experimental works on the Graetz problem in curved pipes are rather limited. Recently, Dravid et al [82] conclude that the fluctuating local Nusselt number before reaching the asymptotic value is a true physical phenomenon whereas the author interprets the fluctuating phenomenon as a manifestation of numerical instability. It is useful to discuss here some of Dravid's work [83]. Dravid's numerical and experimental results are reproduced in Fig. 62. The numerical results for Pr = 5

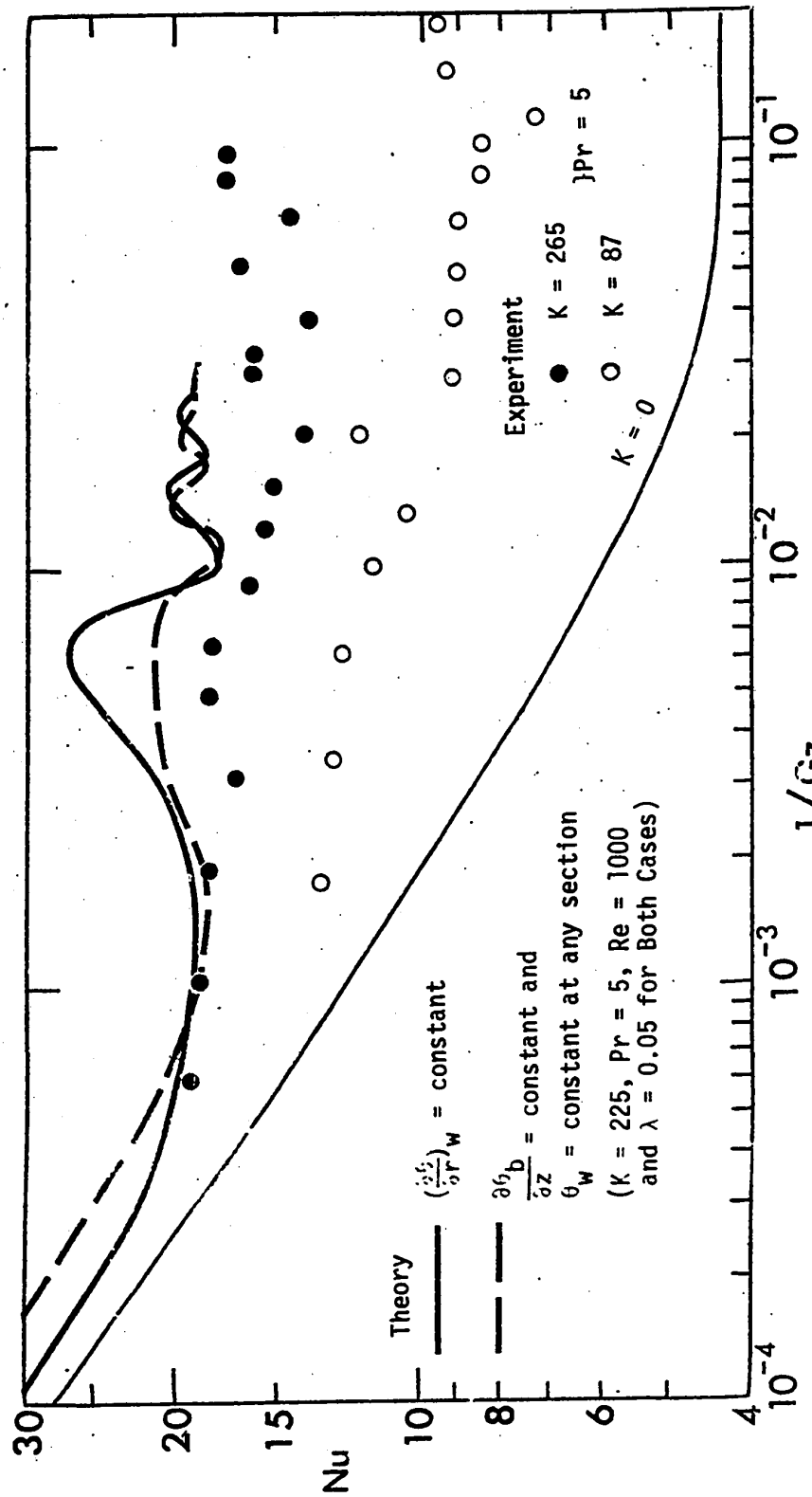


Fig. 62 Dravid et al's Numerical and Experimental Results [82,83]

and K = 225 with a uniform wall heat flux ($\partial\theta/\partial r$ = constant) and an axially uniform wall heat flux ($\partial\theta_b/\partial z$ = constant, $\theta_w$ = constant at any axial position) clearly show the fluctuating phenomenon. Because of experimental difficulty in simulating the theoretical boundary condition and the associated experimental uncertainties as indicated by the somewhat random nature of the experimental data, the results can be subjected to various interpretations and the fluctuating phenomenon is by no means obvious. In this respect many questions regarding the behavior of the results can be raised. In particular, the decrease of local Nusselt number after reaching a local maximum value cannot be explained physically. If the fluctuating phenomenon is not a true physical phenomenon, than the question of determining the asymptotic value also arises.

Dravid et al [82] define the wave length of the first oscillation $\lambda_w$ and give the following equation for $\lambda_w$;

$$\lambda_w = 1.75 \left[\frac{0.5\ Re}{1.6500 + 0.9656\ Re^{1/2}\lambda^{1/4}}\right] \qquad (132)$$

where $$\lambda = a/R_c$$

They note that the wavelength predicted seems to be insensitive to the Prandtl number in the limited range of Pr = 0.5 ~ 15. Following their definition of wavelength, the results from the present study for Pr = 0.7, 10 and 500 are shown in Fig. 63 with K = 7.66. It is seen that the wavelength $\lambda_w$ is a strong function of Prandtl number at K = 7.66. The behavior of the local Nusselt number between the

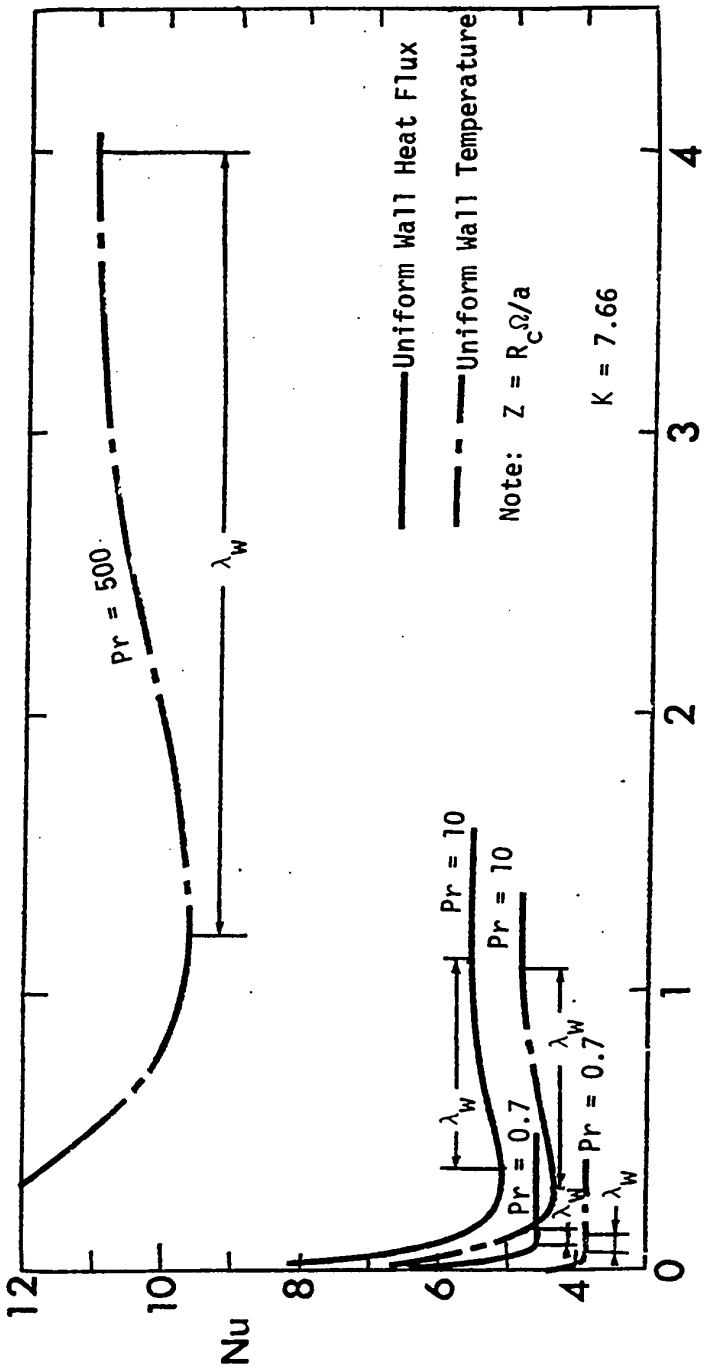


Fig. 63 The Effect of Prandtl Number on Wavelength $\lambda_w$ at K = 7.66

local minimum value and the subsequent local maximum value is known to be caused by a secondary flow effect and it is hard to regard this part as an oscillating phenomenon.

Dravid's experimental data [83] on wall temperature measurements for the case of a uniform wall heat flux are reproduced in Fig. 64. In the figure, a smooth line is drawn through the experimental data points for each set of Prandtl and Dean numbers. If the fluctuations as shown in the figure are considered to be an oscillatory phenomenon, then it appears that the wavelength, $\lambda_w$, is a function of the physical coordinate, $z = R_c\Omega/a$, instead of a function of Re and $\lambda$ as shown in equation (132).

## 5.8 CONCLUDING REMARKS

1. The numerical experiments using different finite-difference approximations ($\beta$ = 0, 0.5, 1.0) for the convective terms due to secondary flow in the energy equation seem to suggest that the fluctuating phenomenon exhibited by the Nusselt number is a manifestation of numerical instability instead of a physical phenomenon. In this study, the fluctuating phenomenon appears at high Dean numbers for Pr = 10 and 500. The numerical results for Pr = 0.1 and 0.7 are free of such fluctuations.

2. The behavior of the Nusselt number in the Leveque solution region is characteristically different for large and small Prandtl number fluids. The behavior can be explained from the roles of the convective terms due to secondary flow and the axial convective term in the energy equation.

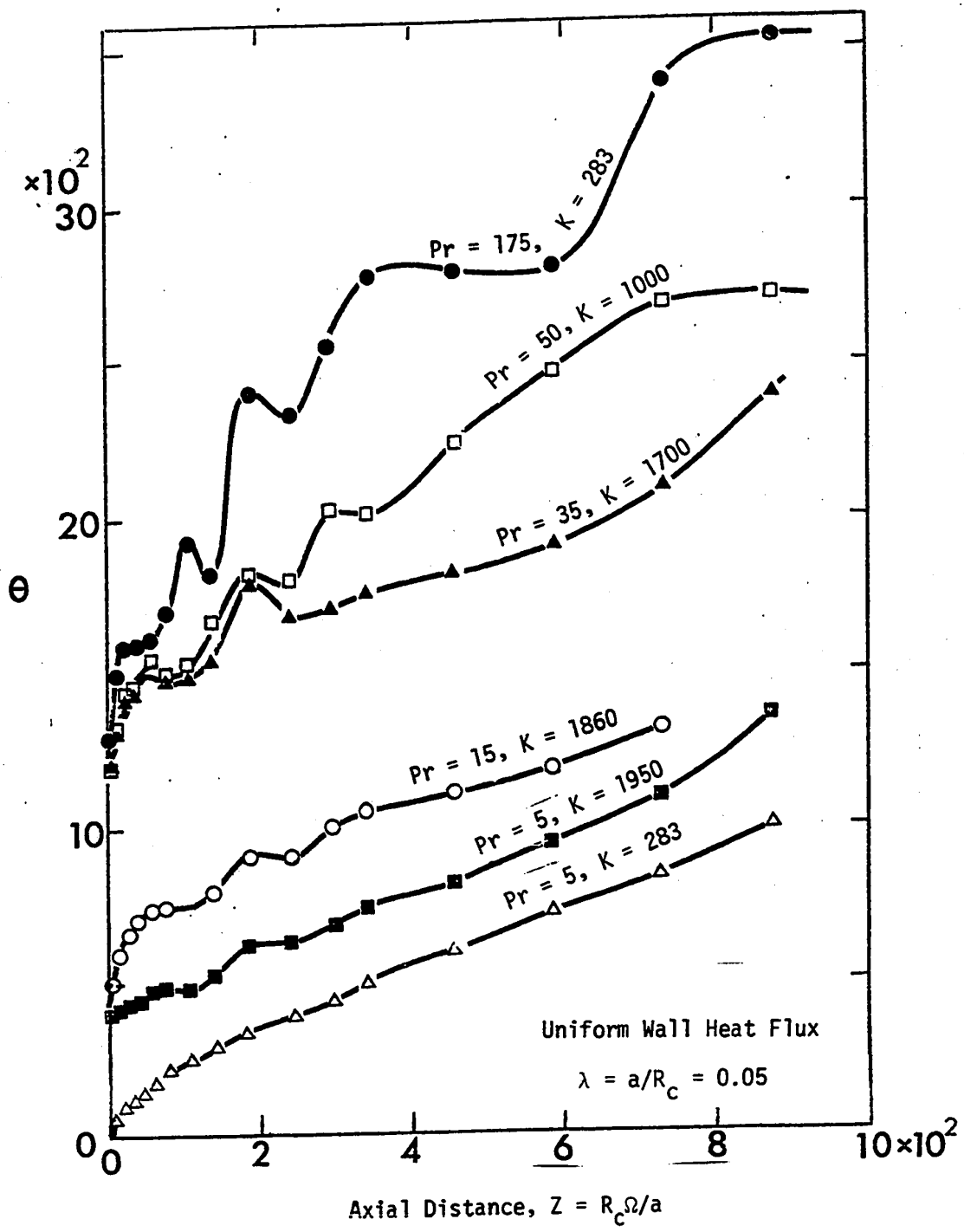


Fig. 64 Dravid's Wall Temperature Measurements [83]

3. It should be emphasized that the fluctuating phenomenon for the Nusselt number observed in the present numerical study is exactly the same as that observed in Dravid's work [82,83]. However, the present interpretation is completely different from that of Dravid. Further work is clearly required to clarify the present uncertain situation. In this study, the development of temperature fields for Pr = 0.7, K = 123.2 and Pr = 10, K = 27.8 are studied in detail and are compared with the respective Nusselt number behavior. The determination of the fully developed condition is based on a study of the temperature field development in the form of temperature profiles, isothermals, axial distributions of average wall temperature $\overline{\theta}_w$, bulk temperature $\theta_b$ and mixed mean temperature difference $\Delta\theta = \overline{\theta}_w - \theta_b$.

4. The asymptotic Nusselt number results obtained in Chapters III, IV and V are summarized in Fig. 60 for comparison. The convergence and accuracy of the numerical solution are confirmed also by the good agreement between the values for the two alternative expressions $Nu_1$ and $Nu_2$ for the Nusselt number. The numerical results for Nusselt number are listed in Appendix 8.

# CHAPTER VI

# LAMINAR FLOW IN THE HYDRODYNAMIC ENTRANCE REGION OF CURVED PARALLEL-PLATE CHANNELS

## 6.1 INTRODUCTION

The predictions of axial pressure drop, developing velocity profiles and hydrodynamic entrance length for laminar flow in the inlet section of tubes and various other non-circular ducts are of practical interest in design. For the circular straight tube, for example, both theoretical and experimental investigations have been carried out rather extensively in the past. A fluid enters the tube or channel with a velocity profile which is determined by the upstream conditions. At some distance downstream of the entrance the fluid velocity in the central portion of the cross-section increases whereas the velocity near the wall decreases. Sufficiently far downstream, the fluid velocity eventually becomes fully developed. The hydrodynamic entrance length is characterized by the developing velocity profiles. In the developing flow region, the axial pressure drop is caused by the wall shear stress and the change of momentum.

The literature on analytical solutions for entrance flows in straight circular tubes and parallel-plate channels is rather extensive. In contrast, the corresponding analytical solutions for entrance flows in curved circular tubes and parallel-plate channels do not seem to be available in the literature. An excellent review of the literature on hydrodynamic entrance region problems in straight

tubes and ducts was given by Sparrow, Lin and Lundgren [111] and Lundgren, Sparrow and Starr [112] in 1964. It is noted that many theoretical results on pressure drop in the hydrodynamic entrance region of various ducts have been reported in recent years. Recent works on flow in pipe bends by Kawaguti [113] and Hurd and Peters [114] can also be cited here.

Consideration is now given to the development of steady laminar flow of an incompressible Newtonian fluid in the entrance region of a curved parallel-plate channel. An example is shown in Fig. 65 where the channel width is uniform and constant but the radius of curvature may be variable along the flow direction. In this connection, many possibilities arise such as $90^{o}$ and $180^{o}$ channel bends and spiral or corrugated channels. In addition, one may have converging or diverging curved parallel-plate channels with the Jeffery-Hamel type flow in the converging plane-walled channels as the limiting case. Furthermore, Couette type flow in curved parallel-plate channels is also possible. In practice, the curved parallel-plate channel may be preceded by a plane parallel-plate channel or other various inlet configurations. In this respect, if the flow field upstream of the entrance must be considered, then a great variety of possible situations may arise. This brings out the question of the specification of upstream conditions. In the formulation of the entrance flow problem, if the disturbance effects upstream of the channel entrance are allowed to propagate within the channel, then certainly the disturbance propagation in the fluid upstream of the

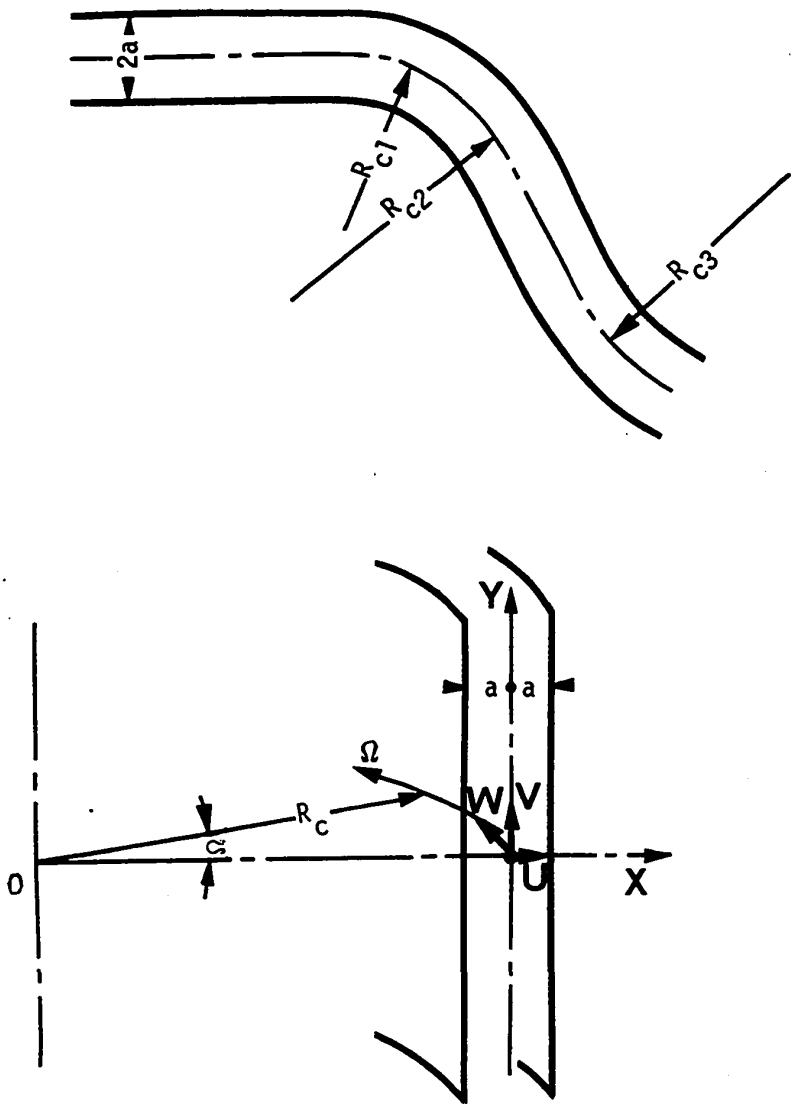


Fig. 65 Coordinate System for Curved Channel

tube entrance must be considered. From this viewpoint, the usual specification of a uniform entrance velocity must be regarded as an approximate boundary condition. The difficulty of formulating a well posed problem in terms of proper entrance conditions apparently has not been overcome so far. In the case of a plane parallel-plate channel preceding a curved parallel-plate channel, it is known that at a sufficiently large upstream distance from the entrance the fully developed parabolic velocity profile prevails and may be used as a possible boundary condition. One may summarize that a variety of entrance conditions can exist in practical problems. In this work, the conventional approach regarding the entrance boundary conditions will be employed and the case of uniform, parabolic and triangular entrance velocity profiles will be studied in detail. The solution of these three cases serves to demonstrate the applicability of the numerical method in solving entrance flow problems in a curved parallel-plate channel with an arbitrary entrance velocity profile. Besides presenting flow results such as pressure drop and hydrodynamic entrance length, the present study can provide a basis for an investigation of hydrodynamic instability of entrance flow in a curved parallel-plate channel. It is useful to recall that the present geometrical configuration in the form of a curved parallel-plate channel may be approached when the aspect ratio of the curved rectangular channel exceeds a value of say 10. To the author's knowledge, a theoretical solution for entry flow in curved pipes or channels is not available in the literature.

## 6.2 DEDUCTIVE ANALYSIS OF THE GENERAL BASIC EQUATIONS FOR ENTRY FLOWS

Referring to the coordinate system shown in Fig. 65, and noting that the present problem represents the limiting case of entry flow in a curved rectangular channel with an infinite aspect ratio, one obtains the following governing equations expressing conservation of mass, momentum and energy for a steady laminar incompressible fluid (see Appendix 3).

Continuity equation

$$\frac{\partial U}{\partial X} + \frac{U}{(R_c + X)} + \frac{1}{(R_c + X)} \frac{\partial W}{\partial \Omega} = 0 \tag{133}$$

X-momentum equation

$$U \frac{\partial U}{\partial X} + \frac{W}{(R_c + X)} \frac{\partial U}{\partial \Omega} - \frac{W^2}{(R_c + X)}$$

$$= - \frac{1}{\rho} \frac{\partial P}{\partial X} + \nu \left[ \frac{1}{(R_c + X)^2} \frac{\partial^2 U}{\partial \Omega^2} - \frac{1}{(R_c + X)} \frac{\partial^2 W}{\partial X \partial \Omega} \right.$$

$$\left. - \frac{1}{(R_c + X)^2} \frac{\partial W}{\partial \Omega} \right] \tag{134}$$

Ω-momentum equation

$$U \frac{\partial W}{\partial X} + \frac{W}{(R_c + X)} \frac{\partial W}{\partial \Omega} + \frac{UW}{(R_c \quad X)}$$

$$= - \frac{1}{\rho} \frac{1}{(R_c + X)} \frac{\partial P}{\partial \Omega} + \nu \left[ - \frac{1}{(R_c + X)} \frac{\partial^2 U}{\partial X \partial \Omega} + \frac{1}{(R_c + X)^2} \frac{\partial U}{\partial \Omega} \right.$$

$$+ \frac{\partial^2 W}{\partial X^2} + \frac{1}{(R_c + X)} \frac{\partial W}{\partial X} - \frac{W}{(R_c + X)^2}] \qquad (135)$$

Energy equation

$$U \frac{\partial T}{\partial X} + \frac{W}{(R_c + X)} \frac{\partial T}{\partial \Omega} = \alpha[\frac{\partial^2 T}{\partial X^2} + \frac{1}{(R_c + X)} \frac{\partial T}{\partial X} + \frac{1}{(R_c + X)^2} \frac{\partial^2 T}{\partial \Omega^2}] \qquad (136)$$

The channel under consideration may also be viewed as being formed by two coaxial cylinders with a two-dimensional flow between the cylinder walls due to a circumferential pressure gradient. As shown in Fig. 65, the central horizontal axis of the channel has a redius of curvature $R_c$ and the origin of the cylindrical coordinates $(R, \Omega, Y)$ is located at the center of curvature with $(R,\Omega)$ in the horizontal plane.

It is desirable to study the basic equations using the deductive procedure of Reference [95] and formulate the problem in a somewhat formal manner. Following this deductive procedure all variables must now be normalized. Considering the physics and geometry of the problem, the following dimensionless variables will be introduced.

$$x = X/a, \quad \omega = \Omega/\Omega_c, \quad u = U/U_c,$$

$$w = W/W_c, \quad p = P/P_0 \quad \text{and} \quad \theta = (T - T_W)/\Theta_c$$

where a is the half width of the channel, $T_W$ is the wall temperature and the quantity with subscript c indicates a reference quantity.

The above relationships are substituted into equations (133) to (136) to obtain the non-dimensional equations. In order to determine the order of magnitude for the characteristic or reference quantities, physical information regarding the problem must be used. For entry flow in a curved parallel-plate channel, it is reasonable to assume that the velocity components in Ω- and X-directions are equally important. Then from the continuity equation (133), it is found that

$$\Omega_c = \frac{W_c}{U_c} \lambda \tag{137}$$

where $\lambda = a/R_c$

Also for the entry flow, the axial inertia terms can be considered to be as important as the viscous terms in Ω-momentum equation. Using this information, one obtains

$$W_c/U_c = \frac{1}{2} Re_c \tag{138}$$

where $Re_c = \frac{2a\, W_c}{\nu}$

From equations (137) and (138), it can be shown that

$$\Omega_c = \frac{1}{2} Re_c \lambda = \frac{1}{2} K\lambda^{1/2} \tag{139}$$

In Ω-momentum equation, it is obvious that the pressure term must be

important because it is the driving force. Consequently, the pressure term can be equated to the viscous terms to yield the following characteristic quantity Po for pressure.

$$Po/\rho U_c^2 = \frac{1}{4} Re_c^2 \tag{140}$$

Using the above relationships (137) to (140), equations (133) to (136) in terms of the new variables become:

Continuity equation

$$\frac{\partial u}{\partial x} + \frac{\lambda}{(1 + \lambda x)} u + \frac{1}{(1 + \lambda x)} \frac{w}{\partial \omega} = 0 \tag{141}$$

X-momentum equation

$$4Re_c^{-2}\left(u \frac{\partial u}{\partial x} + \frac{w}{(1 + \lambda x)} \frac{\partial u}{\partial \omega}\right) - \frac{\lambda}{(1 + \lambda x)} w^2$$

$$= - \frac{\partial p}{\partial x} + 16Re_c^{-4} \frac{1}{(1 + \lambda x)^2} \frac{\partial^2 u}{\partial w^2} - 4Re_c^{-2} \frac{1}{(1 + \lambda x)} \frac{\partial^2 w}{\partial x \partial \omega}$$

$$- 4Re_c^{-2} \frac{\lambda}{(1 + \lambda x)^2} \frac{\partial w}{\partial \omega} \tag{142}$$

In the above equation, the centrifugal force and pressure terms are of primary importance. For entry flow problems the inertia terms must be retained, however, the viscous term involving $Re_c^{-4}$ may be neglected when the magnitude of the Reynolds number is about $10^{1/2}$ or more.

Ω-momentum equation

$$u\frac{\partial w}{\partial x} + \frac{w}{(1+\lambda x)}\frac{\partial w}{(1+\lambda x)} + \frac{\lambda}{(1+\lambda x)}uw$$

$$= -\frac{1}{(1+\lambda x)}\frac{\partial p}{\partial \omega}$$

$$+ \left(\frac{\partial^2 w}{\partial x^2} + \frac{\lambda}{(1+\lambda x)}\frac{\partial w}{\partial x} - \frac{\lambda^2}{(1+\lambda x)^2}w\right)$$

$$- 4Re_c^{-2}\left(\frac{1}{(1+\lambda x)}\frac{\partial^2 u}{\partial x \partial \omega} + \frac{\lambda}{(1+\lambda x)^2}\frac{\partial u}{\partial \omega}\right) \qquad (143)$$

Energy equation

$$Pr\left(u\frac{\partial \theta}{\partial x} + \frac{w}{(1+\lambda x)}\frac{\partial \theta}{\partial x}\right) = \frac{\partial^2 \theta}{\partial x^2} + \frac{\lambda}{(1+\lambda x)}\frac{\partial \theta}{\partial x}$$

$$+ 4Re_c^{-2}\frac{1}{(1+\lambda x)^2}\frac{\partial^2 \theta}{\partial \omega^2} \qquad (144)$$

The pressure term may be eliminated by carrying out cross-differentiation between equations (142) and (143). The following single momentum equation results after introducing the stream function $\Psi$ and the vorticity $\zeta$.

$$\frac{1}{(1+\lambda x)}\left(\frac{\partial \Psi}{\partial x}\frac{\partial}{\partial x} - \frac{\partial \Psi}{\partial \omega}\frac{\partial}{\partial x}\right)\zeta$$

$$+ 4K^{-2} \frac{\lambda}{(1+\lambda x)^3} \left( \frac{\partial \Psi}{\partial x} \frac{\partial}{\partial \omega} - \frac{\partial \Psi}{\partial \omega} \frac{\partial}{\partial x} + 2 \frac{\lambda}{(1+\lambda x)} \frac{\partial}{\partial \omega} \right) \frac{\partial^2 \Psi}{\partial \omega^2}$$

$$= \nabla^2 \zeta + 8K^{-2} \frac{\lambda}{(1+\lambda x)^2} \left( \frac{\partial^2}{\partial x^2} - \frac{\lambda}{(1+\lambda x)} \frac{\partial}{\partial x} + 2 \frac{\lambda^2}{(1+\lambda x)^2} \right.$$

$$\left. + 2K^{-2} \frac{\lambda}{(1+\lambda x)} \frac{\partial^2}{\partial \omega^2} \right) \frac{\partial^2 \Psi}{\partial \omega^2} \qquad (145)$$

$$\nabla^2 \Psi \equiv \zeta \qquad (146)$$

$$u = - \frac{1}{(1+\lambda x)} \frac{\partial \Psi}{\partial \omega} \quad \text{and} \quad w = \frac{\partial \Psi}{\partial x} \qquad (147)$$

In equation (145) one sees the primary inertia terms and the secondary inertia terms involving $K^{-2}$. It is also seen that there is a viscous term involving $K^{-4}$. The energy equation becomes

$$\frac{Pr}{(1+\lambda x)} \left( \frac{\partial \Psi}{\partial x} \frac{\partial}{\partial \omega} - \frac{\partial \Psi}{\partial \omega} \frac{\partial}{\partial x} \right) \theta$$

$$= \nabla^2 \theta + 4K^{-2} \frac{\lambda^2}{(1+\lambda x)^2} \frac{\partial^2 \theta}{\partial \omega^2} \qquad (148)$$

where the Laplacian operator is

$$\nabla^2 = \frac{\partial}{\partial x^2} + \frac{\lambda}{(1+\lambda x)} \frac{\partial}{\partial x} \qquad (149)$$

It is noted that the curvature ratio $\lambda$, the dimensionless

parameter K and Prandtl number Pr appear in the governing equations (145), (146) and (148).

Attention will now be focussed only to the hydrodynamic entrance flow problem and the energy equation will not be considered further. The values of $\lambda$ and K are now evaluated for the conditions of practical interest. Considering the practical limit of a in comparison to $R_c$ one obtains $\lambda \lesssim O[1]$. It is reasonable to assume that $Re_c \geq O[10]$. It is now found that $K \geq O[10]$ for most practical situations. On this basis the terms involving $K^{-2}$ and $K^{-4}$ in equation (145) can be neglected in comparison with other terms to give,

$$\frac{1}{(1 + \lambda x)} \left(\frac{\partial \Psi}{\partial x} \frac{\partial}{\partial \omega} - \frac{\partial \Psi}{\partial \omega} \frac{\partial}{\partial x}\right)\zeta = \nabla^2 \zeta \qquad (150)$$

It is significant to note that with the above simplification, the flow problem is independent of the parameter K and depends only on the curvature ratio $\lambda$.

A remark regarding the importance of the axial viscous term from another viewpoint for the general entry flow problem may be in order. It is noted that the normalized equation (143) results by using relationships (137) and (138). On the other hand, if relationship (137) resulting from the continuity equation alone is used, the characteristic coefficient of the terms, $[1/(1 + \lambda x)]\ \partial^2 u/\partial x \partial \omega + [\lambda/(1 + \lambda x)^2]\ \partial u/\partial \omega$, in the $\Omega$-momentum equation becomes $[a/R_c \Omega_c]^2$. Thus, it may be reasoned that the axial viscous terms may be neglected

under the restriction

$$\frac{a}{R_c \Omega_c} \leq O[10^{-1}] \tag{151}$$

The above relationship suggests that the axial viscous terms cannot be neglected for the entrance region up to a downstream distance of about 5 x (2a). The present restriction complements the earlier restriction for the flow regime, $Re_c \geq O[10]$, under which the axial viscous terms may be neglected. It is of interest to note that when the axial viscous terms and the secondary inertia terms in equation (145) are retained, then the Dean number K appears explicitly in the curved entry flow problem. This situation is analogous to the formulation used by Wang and Longwell [115] where the axial viscous terms in the momentum equations are retained for laminar entry flow in a parallel-plate channel. For the present study, the solution of equation (150), valid for most practically important cases, will be sought subjected to the restrictions mentioned earlier.

## 6.3 A NOTE ON PRESSURE DROP FOR FULLY DEVELOPED LAMINAR FLOW IN STRAIGHT AND CURVED PARALLEL-PLATE CHANNELS

Before considering further the effect of curvature ratio $\lambda$ on flow development in the hydrodynamic entrance region of a curved parallel-plate channel, it is useful to summarize the known flow results for the fully developed flow condition.

It is noted that for a fully developed flow in a curved

parallel-plate channel, the derivatives of the velocity components in the $\omega$-direction vanish and from the continuity equation (141), one obtains $\partial[(1+\lambda x)\, u]/\partial x = 0$ implying $u = 0$. For the limiting case of fully developed flow, the following governing equation results from equation (143).

$$\frac{\partial^2 w}{\partial x^2} + \frac{\lambda}{(1+\lambda x)} \frac{\partial w}{\partial x} - \frac{\lambda^2}{(1+\lambda x)^2} w = \frac{1}{(1+\lambda x)} \frac{\partial p}{\partial \omega} \tag{152}$$

The fully developed velocity w satisfying the boundary condition, $w = 0$ at walls, is given by

$$w = \frac{1}{2} \left(\frac{\partial p}{\partial \omega}\right)_{c,\infty} \left[\frac{(1+\lambda x)}{\lambda^2} \left\{ \ln \frac{(1+\lambda x)}{(1-\lambda)} - \frac{(1+\lambda)^2}{4\lambda} \left(1 - \frac{(1-\lambda)^2}{(1+\lambda x)^2}\right) \ln \frac{(1+\lambda)}{(1-\lambda)} \right\}\right] \tag{153}$$

where the subscript $\infty$ denotes the fully developed flow and c stands for a curved parallel plate channel.

The fully developed solution for two-dimensional flow through curved parallel-plate channels can also be found in a book edited by Goldstein [5]. For the limiting case of $\lambda = 0$ representing plane Poiseuille flow, the velocity profile w becomes

$$w = \frac{1}{2} \left(\frac{\partial p}{\partial \omega}\right)_{s,\infty} [x^2 - 1] \tag{154}$$

where the subscript s denotes the flow in a straight parallel-plate channel.

After integrating equation (153) with respect to x from x = -1 to x = +1 and setting the mean velocity equal to one, the following expression for the axial pressure gradient is obtained.

$$\left(\frac{\partial p}{\partial \omega}\right)_{c,\infty} = -3\left[\frac{16}{3}\frac{\lambda^4}{\{4\lambda^2 - (1-\lambda^2)^2 \ln^2\left(\frac{1+\lambda}{1-\lambda}\right)\}}\right] \qquad (155)$$

It can be shown that the quantity inside the square brackets in equation (155) approaches one when $\lambda \to 0$. Consequently, for a fully developed plane Poiseuille flow, one obtains

$$\left(\frac{\partial p}{\partial \omega}\right)_{s,\infty} = -3, \quad \text{for} \quad \lambda \to 0 \qquad (156)$$

For the limiting case $\lambda = 1$, the quantity inside the square brackets becomes 4/3 and one obtains,

$$\left(\frac{\partial p}{\partial \omega}\right)_{c,\infty} = -4, \quad \text{for } \lambda \to 1 \qquad (157)$$

For fully developed laminar flow in curved parallel-plate channels, the above value represents the maximum value attainable for the pressure gradient $(\partial p/\partial \omega)_{c,\infty}$. This fact does not appear to be pointed out clearly in the literature. By substituting equation (155) into equation (153), one obtains the expression w for fully developed velocity profile.

Following the definition for friction factor f, namely,

$$f = -\frac{2a}{\rho w_m^2 R_c}\frac{\partial P}{\partial \Omega} = \left[\frac{4}{Re}\right]\left(-\frac{\partial p}{\partial \omega}\right) \qquad (158)$$

one obtains,

$$(f)_{c,\infty} = \frac{12}{Re}\left[\frac{16}{3}\frac{\lambda^4}{\{4\lambda^2 - (1-\lambda^2)^2 \ln^2\left(\frac{1+\lambda}{1-\lambda}\right)\}}\right] \qquad (159)$$

The corresponding expression $(f)_{s,\infty}$ for straight parallel-plate channel is

$$(f)_{s,\infty} = \frac{12}{Re} \qquad (160)$$

Here the following expression for the ratio of friction factors $(f)_{c,\infty}/(f)_{s,\infty}$ is of special interest in design

$$\frac{(f)_{c,\infty}}{(f)_{s,\infty}} = \left[\frac{16}{3}\frac{\lambda^4}{\{4\lambda^2 - (1-\lambda^2)^2 \ln^2\left(\frac{1+\lambda}{1-\lambda}\right)\}}\right] \qquad (161)$$

The numerical results for equation (161) are tabulated in Appendix 9 and the graphical results for equations (155), (159) and (161) are shown in Fig. 66. It is clearly seen in Fig. 66 that the pressure loss for fully developed laminar flow in curved parallel-plate channels increases with the curvature ratio $\lambda$ and the maximum value is reached at the limiting case $\lambda = 1$. The asymptotic results presented here are useful for the present study on flow development in curved parallel-plate channels.

## 6.4 FORMULATION OF LAMINAR ENTRY FLOW IN CURVED PARALLEL-PLATE CHANNELS

Consideration is given to the development of isothermal laminar

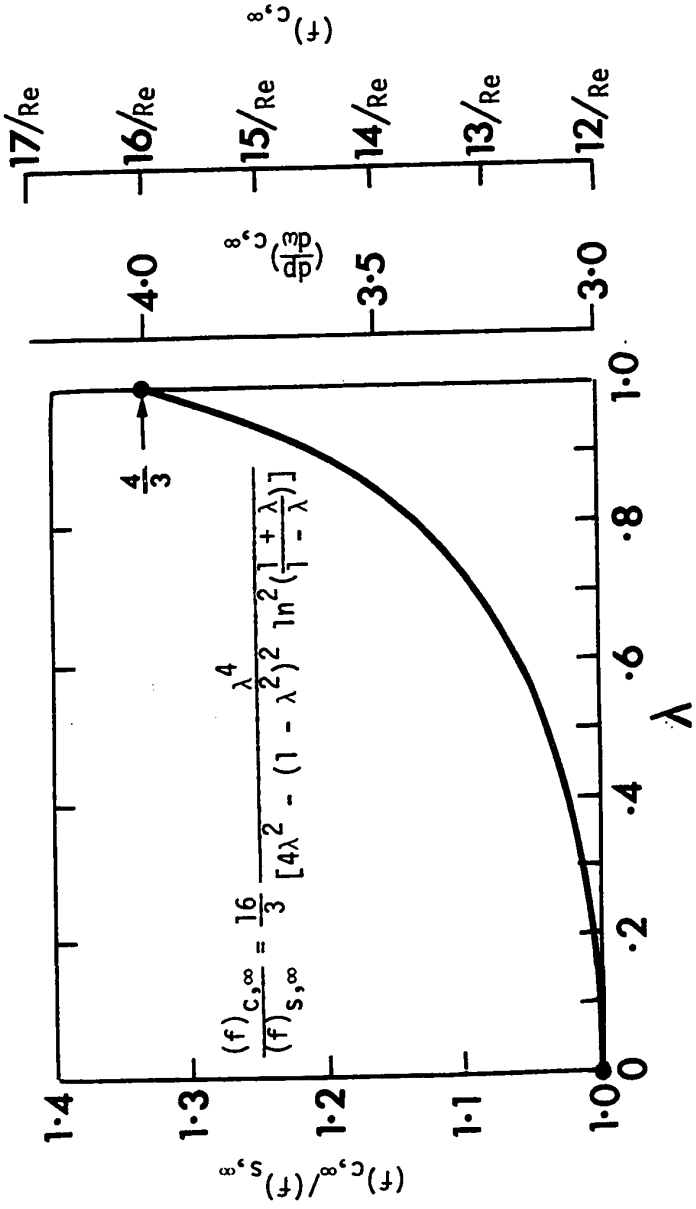


Fig. 66 Effect of Curvature Ratio λ on Friction Coefficient and Pressure Drop

flow of an imcompressible Newtonian fluid under steady state condition in a curved parallel-plate channel of semi-infinite length. Referring to the coordinate system shown in Fig. 65, the flow between the two curved plates is independent of Y, and the governing equations in dimensionless form are:

Momentum equation (Vorticity transport equation)

$$\frac{1}{(1 + \lambda x)} \left(\frac{\partial \Psi}{\partial x} \frac{\partial}{\partial \omega} - \frac{\partial \Psi}{\partial \omega} \frac{\partial}{\partial x}\right)\zeta = \nabla^2 \zeta \qquad (150)$$

Vorticity equation

$$\zeta = \nabla^2 \Psi \qquad (146)$$

where

$$\nabla^2 = \frac{\partial}{\partial x^2} + \frac{\lambda}{(1 + \lambda x)} \frac{\partial}{\partial x} \qquad (149)$$

The velocity components in terms of the stream function $\Psi$ are given by

$$u = - \frac{1}{(1 + \lambda x)} \frac{\partial \Psi}{\partial \omega} \quad \text{and} \quad w = \frac{\partial \Psi}{\partial x} \qquad (147)$$

For convenience the dimensionless variable used are given as $x = Xa$, $w = 2K^{-1}\lambda^{-1/2}\Omega$, $u = a/\nu \cdot U$, $\omega = 2a/\nu \cdot Re^{-1}W$, and $p = P/(\rho W_m^2)$. The dimensionless variables are identical to those used in Section 6.2 except that the characteristic velocity $W_c$ is now replaced by the average velocity $W_m$ for convenience. It is useful to recall that the foregoing governing equations are valid for flows with Dean number

$K \geq O[10]$. In other words, noting that $\lambda \lesssim 1$, the restriction on the Reynolds number becomes $Re \gtrsim O[10]$. Furthermore, the above formulation is not valid within the entrance region when $R_c\Omega$ is of order 0 to 10a because of the neglect of the axial viscous terms. The limitations of the present formulation are now clear. The boundary conditions are now considered next.

For the entrance channel flow problem, in general, a difficulty of specifying the proper entrance boundary conditions arises. However, in the present study, the entrance velocity will be assumed to be known and the following three entrance velocities of uniform, parabolic and triangular profiles are employed.

(a) Uniform entrance velocity

The velocity distribution at the entrance is taken to be uniform.

$$\Psi = x \quad \text{at} \quad \omega = 0, \quad x = x$$
$$\zeta = \frac{\lambda}{(1 + \lambda x)} \quad \text{at} \quad \omega = 0, \quad x = x \tag{162}$$

It can be verified readily that the secondary velocity $u = 0$ and the axial velocity $w = 1$ at the entrance.

(b) Parabolic entrance velocity

$$\Psi = -\frac{x}{2}(x^2 - 3) \quad \text{at} \quad \omega = 0, \quad x = x$$
$$\zeta = -3\left(x + \frac{(x^2 - 1)}{2(1 + \lambda x)}\right) \quad \text{at} \quad \omega = 0 \quad x = x \tag{163}$$

The above conditions correspond to $u = 0$ for the secondary velocity and $w = -3(x^2 - 1)/2$ for the axial velocity at the entrance.

(c) Triangular entrance velocity

$$\Psi = \frac{1}{2}(x^2 + 2x - 1) \quad \text{at} \quad \omega = 0, \quad x = x$$

$$\zeta = \frac{\lambda}{(1 + \lambda x)}(x + 1) + 1 \quad \text{at} \quad \omega = 0, \quad x = x \tag{164}$$

In terms of velocity components, the above conditions signify $u = 0$ and $w = x + 1$ at the entrance.

The following no-slip conditions at the wall complete the specification of boundary conditions for the present parabolic-type momentum equation.

$$\Psi = -1 \quad \text{at} \quad \omega = \omega, \quad x = -1$$

$$\Psi = +1 \quad \text{at} \quad \omega = \omega, \quad x = +1 \tag{165}$$

$$\frac{\partial \Psi}{\partial x} = 0 \quad \text{at} \quad \omega > 0, \quad x = \pm 1$$

In the above formulation, the vorticity $\zeta$ is not known explicitly at the walls ($\omega > 0$).

It is known that the laminar flow development in the entrance region does not permit an exact solution even for a straight tube. The difficulties in obtaining an analytical solution can be traced to the

nonlinear nature of the inertia terms in the momentum equation. The various approximate methods of solution which have been devised to provide needed information relating to the flow development and the pressure drop in straight ducts or channels are well summarized by Lundgren, Sparrow and Starr [112]. In the present work, a finite-difference method of solution will be employed. The detailed information on point velocities for flow development is also required, for example, for further study on forced convection problems as well as hydrodynamic stability problems in the entrance region.

## 6.5 NUMERICAL SOLUTION USING THE DIRECT VORTICITY METHOD

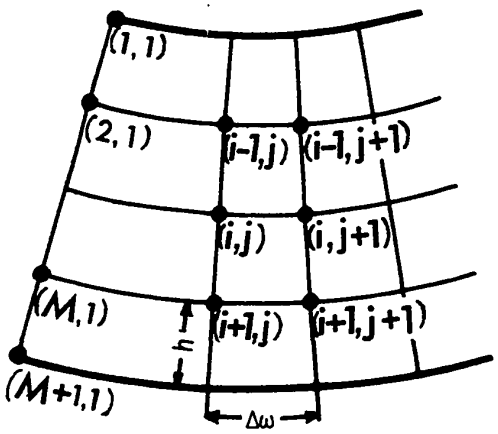


Fig. 67 Coordinate System and Numerical Grid for a Curved Parallel-Plate Channel

The vorticity transport equation (150) is a quasi-linear

second order partial differential equation of parabolic type and the vorticity equation (146) is a linear second order ordinary differential equation. Because of the nature of equation (150), the Crank-Nicolson scheme [116] of finite-difference approximations for the parabolic equation is used. Referring to the coordinate system shown in Fig. 67, and using a three-point central-difference approximation for X-derivatives, one obtains the following second-order-correct Crank-Nicolson equation and a finite-difference equation for equations (150) and (146), respectively.

$$\left[\frac{1}{2h^2} - \frac{\lambda}{4h(1+\lambda x)} - \frac{1}{4h\Delta\omega(1+\lambda x)}(\Psi_{i,j+1} - \Psi_{i,j})\right]\zeta_{i-1,j+1}$$

$$+ \left[-\frac{1}{h^2} - \frac{1}{4h\Delta\omega(1+\lambda x)}(\Psi_{i+1,j} - \Psi_{i-1,j} + \Psi_{i+1,j+1} - \Psi_{i-1,j+1})\right]\zeta_{i,j+1}$$

$$+ \left[\frac{1}{2h^2} + \frac{\lambda}{4h(1+\lambda x)} + \frac{1}{4h\Delta\omega(1+\lambda x)}(\Psi_{i,j+1} - \Psi_{i,j})\right]\zeta_{i+1,j+1}$$

$$= \left[-\frac{1}{2h^2} + \frac{\lambda}{4h(1+\lambda x)} + \frac{1}{4h\Delta\omega(1+\lambda x)}(\Psi_{i,j+1} - \Psi_{i,j})\right]\zeta_{i-1,j}$$

$$+ \left[\frac{1}{h^2} - \frac{1}{4h\Delta\omega(1+\lambda x)}(\Psi_{i+1,j} - \Psi_{i-1,j} + \Psi_{i+1,j+1} - \Psi_{i-1,j+1})\right]\zeta_{i,j}$$

$$+ \left[-\frac{1}{2h^2} - \frac{\lambda}{4h(1+\lambda x)} - \frac{1}{4h\Delta\omega(1+\lambda x)}(\Psi_{i,j+1} - \Psi_{i,j})\right]\zeta_{i+1,j} \qquad (166)$$

and

$$\left[-\frac{1}{h^2} + \frac{\lambda}{2h(1+\lambda x)}\right]\Psi_{i-1,j+1}$$

$$+ \left[\frac{2}{h^2}\right]\Psi_{i,j+1}$$

$$+ \left[-\frac{1}{h^2} - \frac{\lambda}{2h(1+\lambda x)}\right]\Psi_{i+1,j+1}$$

$$= -\zeta_{i,j+1} \qquad (167)$$

It is noted that equations (166) and (167) take special forms at the points adjacent to the wall boundary after applying the boundary conditions $\Psi_{1,j+1} = -1$, $\Psi_{M+1,j+1} = 1$, and $(\partial\Psi/\partial x)_{1,j+1} = (\partial\Psi/\partial x)_{M+1,j+1} = 0$.

In solving equation (166), the vorticity at the boundary is not known in advance. For the determination of the boundary vorticity, the direct vorticity method discussed in Appendix 5 is applied. The method is based on the observation that a linear relationship exists between vorticity and stream function at all points, including boundary points, through finite-difference equations. Following the procedure described in Appendix 5, the following expressions for the vorticities at the boundary grid point (1,j+1) and its neighbouring grid point (2,j+1) can be obtained.

$$\zeta^{(4)}_{1,j+1} = \left[\left(\Delta\Psi^{(1)}_{M+1,j+1} - \Delta\Psi^{(2)}_{M+1,j+1}\right)\left(1 - \Psi^{(1)}_{M+1,j+1}\right)\right.$$

$$\left. + \left(\Psi^{(1)}_{M+1,j+1} - \Psi^{(2)}_{M+1,j+1}\right)\Delta\Psi^{(1)}_{M+1,j+1}\right]/\alpha_{i,j+1}$$

$$\zeta^{(4)}_{2,j+1} = \left[\left(\Delta\Psi^{(3)}_{M+1,j+1} - \Delta\Psi^{(1)}_{M+1,j+1}\right)\left(1 - \Psi^{(1)}_{M+1,j+1}\right)\right.$$

$$+ (\Psi^{(3)}_{M+1,j+1} - \Psi^{(1)}_{M+1,j+1})\Delta\Psi^{(1)}_{M+1,j+1}]/\alpha_{i,j+1}$$

and

$$\alpha_{i,j+1} = [(\Psi^{(3)}_{M+1,j+1} - \Psi^{(1)}_{M+1,j+1})(\Delta\Psi^{(1)}_{M+1,j+1} - \Delta\Psi^{(2)}_{M+1,j+1})$$

$$- (\Psi^{(2)}_{M+1,j+1} - \Psi^{(1)}_{M+1,j+1})(\Delta\Psi^{(1)}_{M+1,j+1} - \Delta\Psi^{(3)}_{M+1,j+1})] \qquad (168)$$

where $\Delta\Psi_{i,j+1} = h(\partial\Psi/\partial x)_{i,j+1}$ and the superscript (n), n = 1, 2, 3, 4 represents the value obtained at the consecutive step. One notes that the boundary conditions, $\Psi_{M+1,j+1} = 1$ and $\Delta\Psi_{M+1,j+1} = 0$ given by equation (165) are used in deriving the expressions for $\zeta^{(4)}_{1,j+1}$ and $\zeta^{(4)}_{2,j+1}$. For a given curvature ratio $\lambda$, the numerical solution is effected as follows:

1. Assign two values $\zeta^{(1)}_{1,j+1} = \zeta^{(1)}_{2,j+1} = 0$ and solve equation (166) explicitly for $\zeta^{(1)}_{i,j+1}$, (i = 3, 4 .... M+1) by using direct successive substitution. With $\zeta^{(1)}_{i,j+1}$, (i = 1, 2, ...., M+1) known, the stream function $\Psi_{i,j+1}$ can be found using equation (167) and the values for $\Delta\Psi^{(1)}_{M+1,j+1}$ and $\zeta^{(1)}_{M+1,j+1}$ will be stored.

2. By setting $\zeta^{(2)}_{1,j+1} = 0$ and $\zeta^{(2)}_{2,j+1} = 1$, the procedure described in step 1 can be repeated to obtain $\Delta\Psi^{(2)}_{M+1,j+1}$ and $\Psi^{(2)}_{M+1,j+1}$ and the values will be stored.

3. By setting $\zeta^{(3)}_{1,j+1} = 1$ and $\zeta^{(3)}_{2,j+1} = 0$, and following the

procedure described in step 1 again, one obtains the values for $\Delta\Psi^{(3)}_{M+L,j+1}$ and $\Psi^{(3)}_{M+1,j+1}$.

4. Using equation (168), the values for $\zeta^{(4)}_{1,j+1}$ and $\zeta^{(4)}_{2,j+1}$ can be computed. Using the newly obtained values for $\zeta^{(4)}_{1,j+1}$ and $\zeta^{(4)}_{2,j+1}$, the procedure described in step 1 can be followed to obtain the value for $\zeta_{i,j+1}$, (i = 3, 4, .... M+1) and $\Psi_{i,j}$, (i = 2, 3, .... M+1) which represent the numerical solution at the axial position j+1.

5. With a computational procedure for the numerical determination of the vorticity established, it suffices to mention that the usual iterative relaxation method for the numerical solution of a set of finite-difference equations with the associated boundary conditions may be employed. The prescribed error for the dependent variables is

$$\sum_{i=1}^{M+1} \left| f^{(m+1)}_{i,j+1} - f^{(m)}_{i,j} \right| \Big/ \sum_{i=1}^{M+1} \left| f^{(m+1)}_{i,j+1} \right| = \varepsilon < 10^{-4}$$

where $f_{i,j}$ represents $\zeta_{i,j}$ or $\Psi_{i,j}$ and the superscript m denotes the number of iterations. It is noted that even close to the inlet section, the number of iterations required to satisfy the above convergence condition is found to be only 3 to 8 for all cases.

6. Advance the axial step to j+2 and repeat steps 1 to 5.

The numerical solution of equation (168) presents no difficulty. The marching procedure starting with j = 1 is used for the numerical solution of equation (166).

Numerical experiments are made using the mesh sizes of M = 10, 16, 20, 40 and 80 in the transverse direction. Along the main flow direction, the axial step size $\Delta\omega = 10^{-4}$ is used for the range $\omega = 0 \sim 0.01$ and $\Delta\omega = 10^{-3}$ is used for the range $\omega = 0.01 \sim 0.5$ as a rule. The mesh size of M = 40 is found to be satisfactory after examining the numerical results for the velocity field and pressure drop and is used in obtaining all the numerical results. By using the present direct vorticity method, the value of the stream function at the boundary is found to deviate by an amount ranging from 0 to $1 \times 10^{-5}$ from the known exact magnitude of one. The computing time required for a complete numerical solution for a given curvature ratio $\lambda$ and entrance velocity profile is about 4 minutes. The computations are generally continued up to $\omega = 0.4$ or 0.5 where the fully developed condition is confirmed.

## 6.6 LAMINAR ENTRY FLOW IN A PARALLEL-PLATE CHANNEL ($\lambda = 0$) WITH A UNIFORM INLET VELOCITY PROFILE

Flow development in the hydrodynamic entrance region of a parallel-plate channel with a uniform entrance velocity has been studied very extensively in the past. The parallel-plate channel ($\lambda = 0$) represents a limiting case of curved parallel-plate channels with various curvature ratios. The main purpose here is to compare the numerical results for flow development in a parallel-plate channel with those reported in the literature. This will serve to confirm the accuracy of the numerical solution.

The major effect of the entrance region is to give rise to a pressure drop which is larger than that experienced by a fully developed flow. The greater pressure drop in the entrance region can be attributed to both the change in momentum and the larger wall friction of the developing flow. For many practical applications, the predictions of the pressure drop and of the hydrodynamic entrance length are of primary importance.

The major effect of the entrance region on the developments of the axial and transverse velocity distribution are portrayed in Figs. 68 and 69, respectively, by a sequence of velocity profiles at various axial positions along the channel. It is noted that the development of the axial velocity profile agrees with the published results of Schlichting [117], Bodoia and Osterle [118] and Collins and Schowalter [119]. It is seen that the axial profiles near the entrance have a distinct flat portion in the central region indicating an iviscid core flow. With increasing distance from the entrance, the flat position eventurally disappears due to the action of viscosity at the wall. The transverse velocity profiles shown in Fig. 69 are also of interest. It is seen that the transverse velocities are directed towards the center line of the channel and the magnitudes decrease gradually along the axial direction. The locations of the maximum transverse velocities are seen to shift gradually away from the upper and lower walls along the axial direction. The transverse velocities disappear completely when the flow becomes fully developed.

According to an order of magnitude analysis shown in Section 6.2,

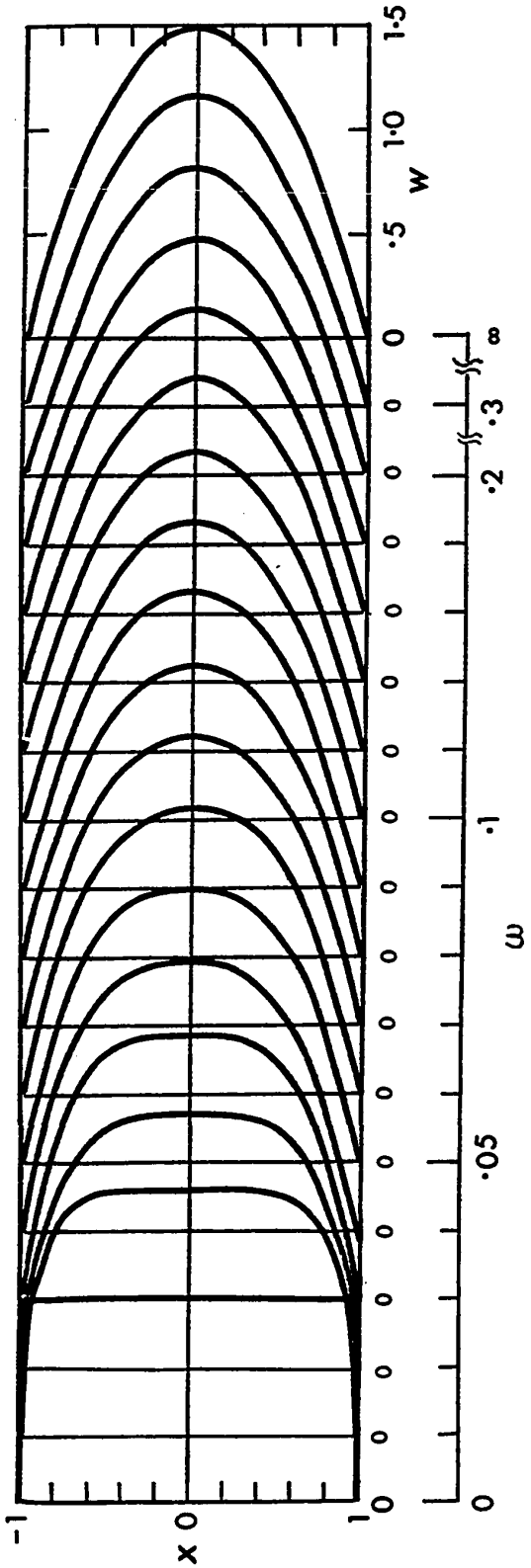
-1
0
1
x
0
0
0

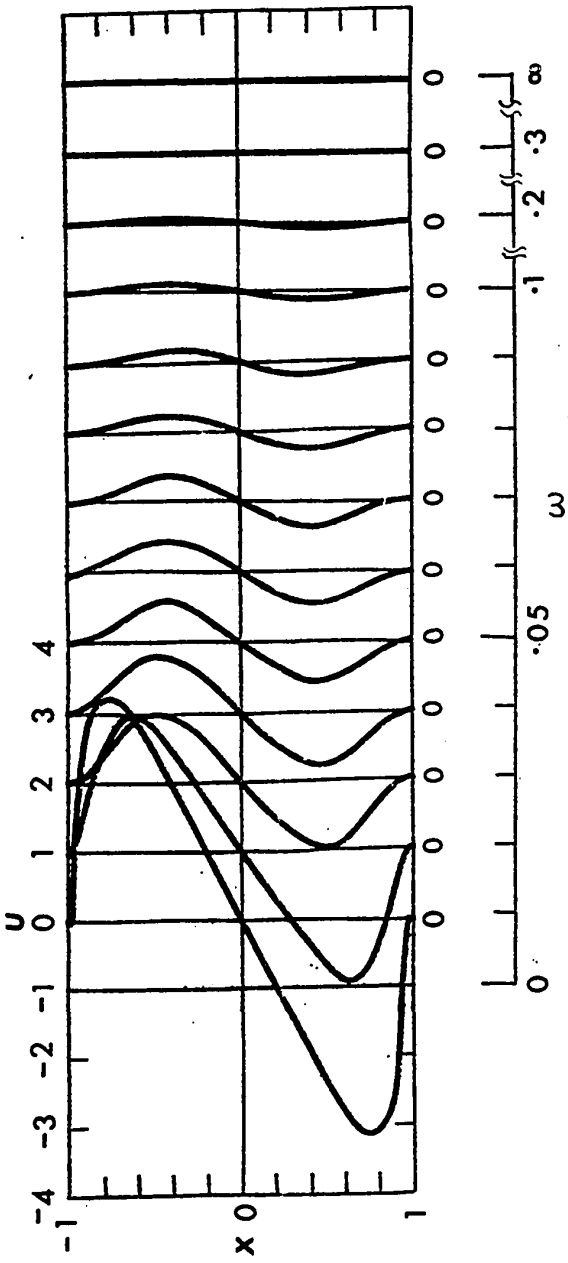


Fig. 69 Developing Transverse Velocity Profiles in a Parallel-Plate Channel ($\lambda = 0$) with Uniform Entrance Velocity

the axial viscous terms may be neglected when $K \geq O[10]$ or equivalently $Re \geq O[10]$ by noting that $\lambda \leq 1$. In this respect, according to Wang and Longwell's results [115] for a Reynolds number of 300, the axial viscous terms have influence up to an entrance distance $\omega = 0.016$ for the present problem. In terms of the physical coordinate, the corresponding entrance distance is $Z = 0.625 \times$ (Channel width). Further theoretical results regarding the effect of Reynolds number on axial viscous terms are not available. It is obvious that further work is required to bring out more clearly the limitations of the formulation based on a uniform entrance velocity and neglect of axial viscous terms. Depending on the Reynolds number, the present formulation is not valid in the immediate neighbourhood of the entrance. However, as seen from the example of Re = 300, the numerical solution is expected to be valid throughout most of the entrance region of the channel. The present numerical method of solution is applicable to any arbitrary entrance velocity profile and the simplified governing equations (146) and (150) may have definite advantages in some respects. After discussing the developing profiles, the pressure drop in the entrance region will be considered next.

The pressure drop between the channel inlet ($\omega = 0$, $p = p_0$) and any axial location ($\omega = \omega$, $p = p$) can be determined by integrating equation (143) neglecting the terms with $Re_c^{-2}$ over the cross-section and along the length of the channel. Introducing the dimensionless pressure $p = P/(\rho W_m^2)$, one obtains the pressure drop $\Delta p$ as

$$\Delta p = p_0 - p \tag{169}$$

On the other hand, the pressure drop which would be sustained by a flow if it were fully developed right from the channel inlet can be found from equation (157) as

$$(\Delta p)_\infty = 3\omega \tag{170}$$

The pressure drops $\Delta p$ and $(\Delta p)_\infty$ defined above along the dimesionless axial coordinate $\omega$ are plotted in Fig. 70 together with other theoretical results [115,117,118,119] for comparison. It is noted that the difference $\Delta p - (\Delta p)_\infty$ represent the increment in pressure drop due to the development of the flow (see Table 4). The present result is seen to agree very well with that of Bodia and Osterle [118]. Wang and Longwell's prediction [115] is seen to be somewhat higher than the present result.

Table 4

Comparison of Pressure-drop Results, $[\Delta p - (\Delta p)_\infty]$

| Work | $[\Delta p - (\Delta p)_\infty]$ |
|---|---|
| Schlichting [117] | 0.301 |
| Bodoia and Osterle [118] | 0.338 |
| Collins and Schowalter [119] | 0.370 |
| Wang and Longwell [115] | 0.394* |
| Sparrow, et al [111] | 0.325 |
| Present Work | 0.352 |

* at $x = \pm 0.1$

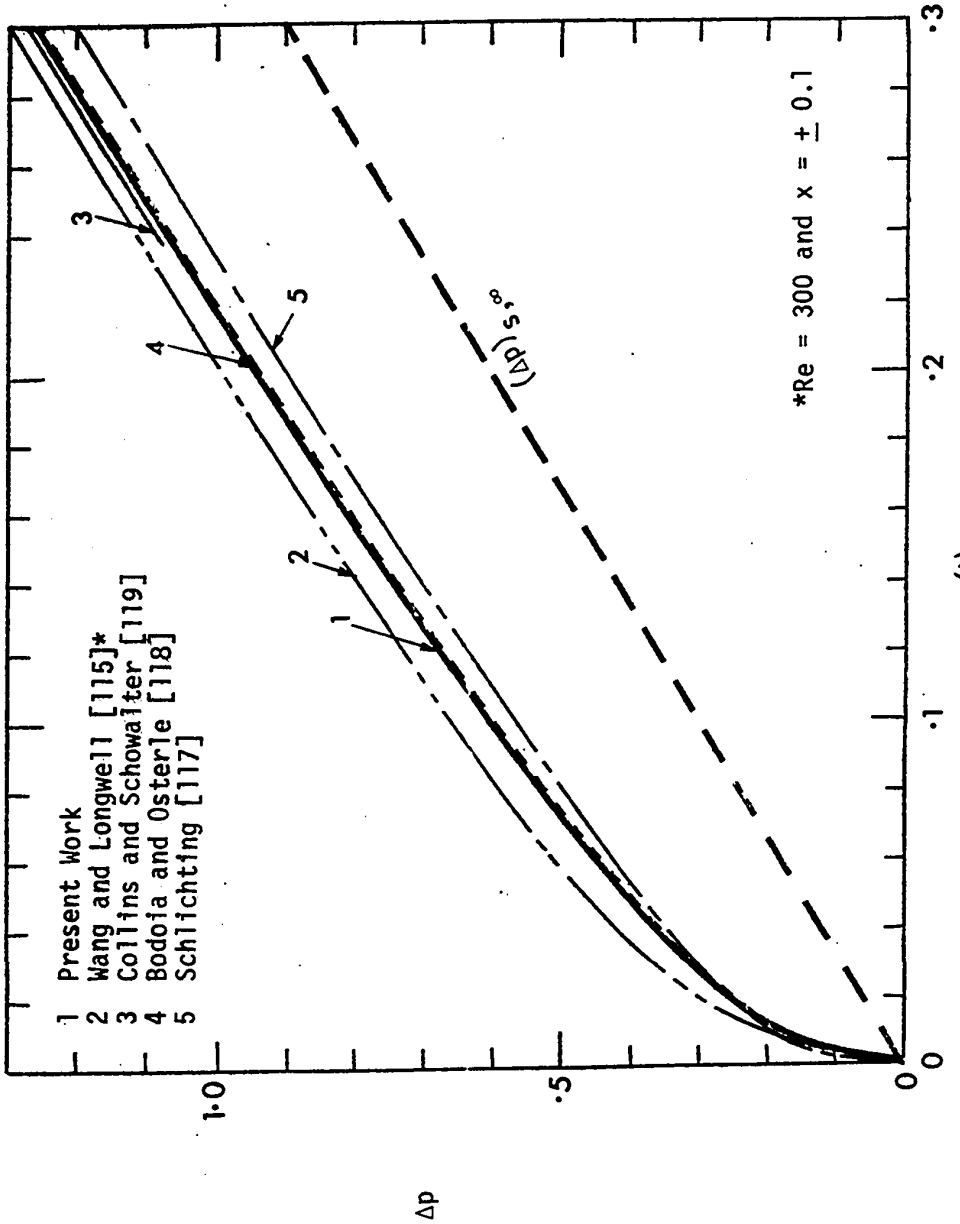


Fig. 70 Pressure Drop Result for a Parallel-Plate Channel ($\lambda = 0$) with Uniform Entrance Velocity

On the other hand, Schlichting's prediction [117] is somewhat lower than the present one. In Fig. 4C of reference [120], the results of Han [121], Bodoia and Osterle [118], and Sparrow, Lin and Lundgren [111] are compared against the experimental data of Beavers, Sparrow and Magnuson [120] for a rectangular channel with aspect ratio (width/height) 51 with generally satisfactory agreement. The above comparison in turn confirms that the present result is a reasonable one.

The prediction of hydrodynamic entrance length is also of interest in design. The hydrodynamic entrance lengths based on the attainment of 98 and 99 per cent of the center-line velocity for the fully developed value from this work are compared against other results in Table 5.

Table 5

Entrance Length for a Parallel-plate Channel ($\lambda = 0$)
With Uniform Entrance Velocity Profile

| | $\omega_{98}$ | $\omega_{99}$ |
|---|---|---|
| Schlichting [117] | | 0.160 |
| Bodoia-Osterle [118] | 0.136 | 0.176 |
| Collins-Schowalter [119] | 0.136 | |
| Present Work | 0.138 | 0.173 |

It may be useful to define the friction factor for the entrance region as

$$f = \frac{P_0 - P}{\rho W_m^2} \frac{2a}{R_c \Omega} \tag{171}$$

In dimensionless form, one obtains

$$f = \frac{4}{Re} \frac{p_0 - p}{\omega} \tag{172}$$

where $p = P/(\rho W_m^2)$, $\omega = 2Re^{-1}\lambda^{-1}\Omega$ and $Re = W_m 2a/\nu$. For fully developed laminar flow in a parallel-plate channel, one has $(f)_{s,\infty} = 12/Re$ from equation (160). Thus, the friction factor ratio $(f)_{\infty,s}$ becomes

$$\frac{f}{(f)_{s,\infty}} = \frac{1}{3} \frac{p_0 - p}{\omega} \tag{173}$$

It is noted here that the pressure drop $\Delta p = p_0 - p$ can be obtained from Fig. 70.

## 6.7 LAMINAR FLOW DEVELOPMENT IN A CURVED PARALLEL-PLATE CHANNEL WITH A UNIFORM INLET VELOCITY PROFILE

The initial and boundary conditions for the present problem are exactly the same as those for plane Poiseuille flow considered in Section 6.6. Consequently, a study of the curvature effect on flow development is of major interest here. The developments of the axial and transverse velocity profiles along the channel axis are shown in Figs. 71 to 76 for the curvature ratios $\lambda = 0.01$, 0.1 and 0.5. A comparison between the velocity profiles for $\lambda = 0$ (straight channel) and $\lambda = 0.01$ reveals that the curvature effect on velocity profile

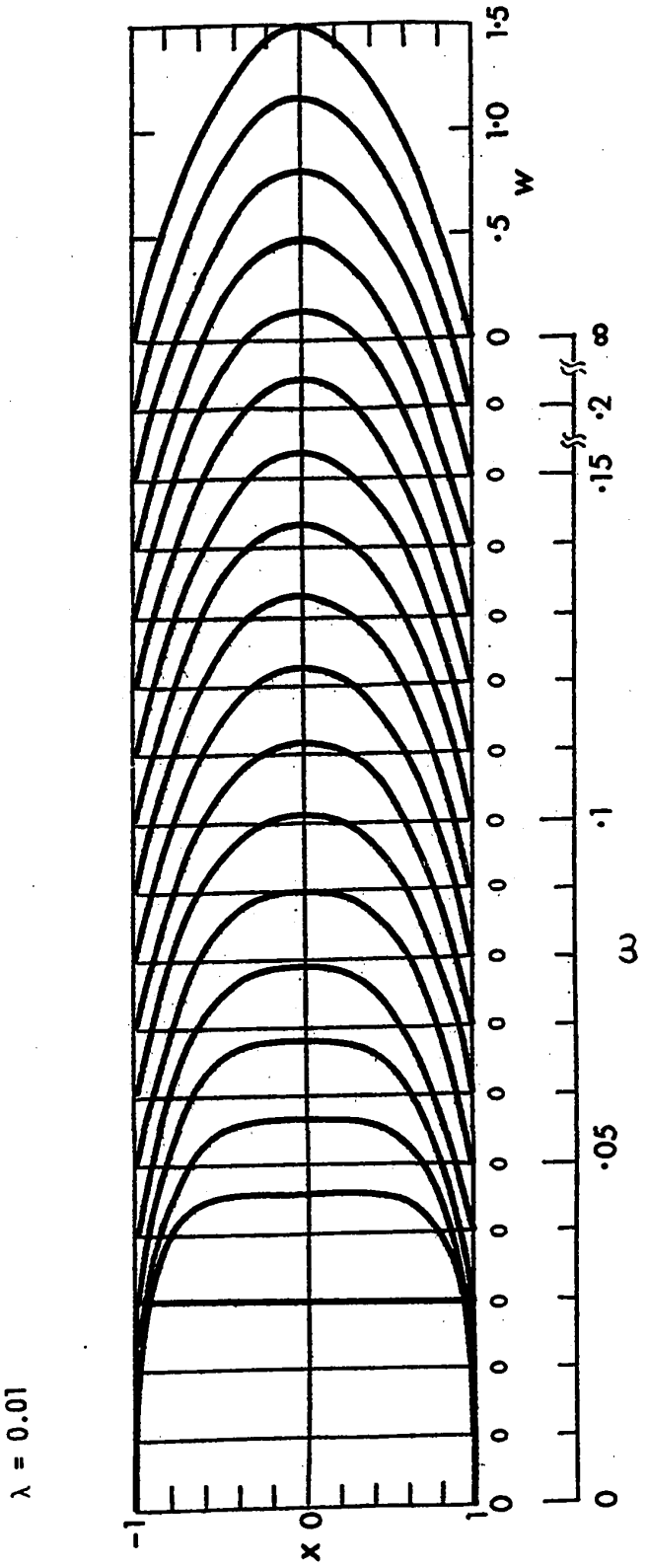


Fig. 71 Developing Axial Velocity Profiles for $\lambda = 0.01$ with Uniform Entrance Velocity

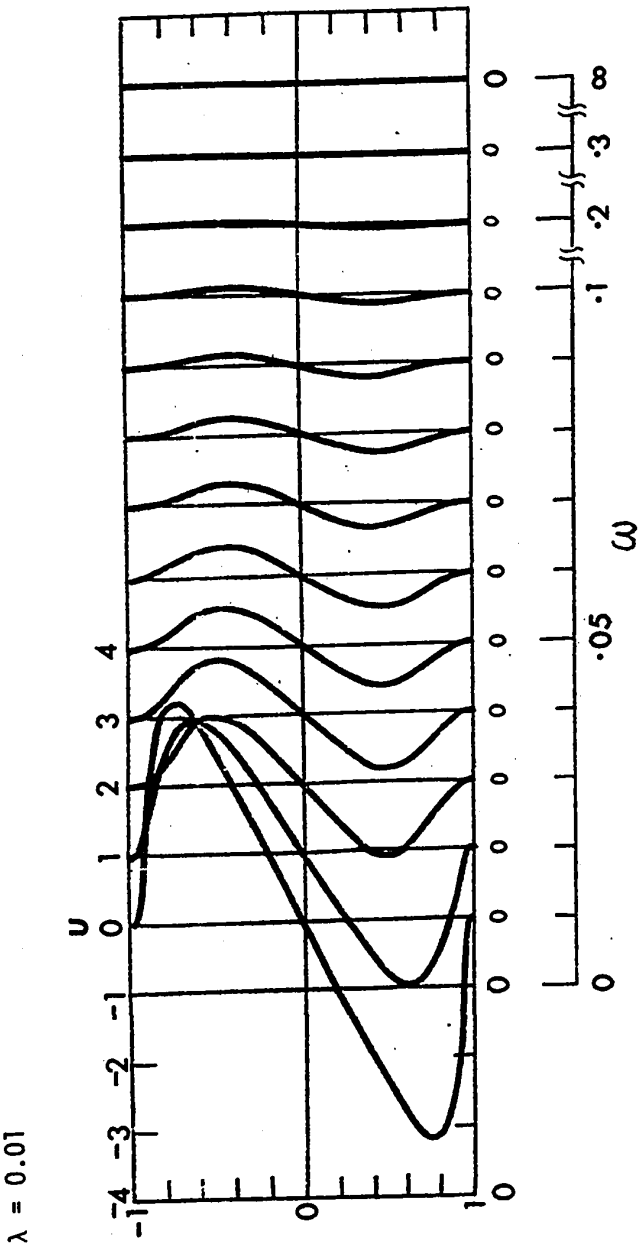
λ = 0.01
U
-4
-3
-2
-1
0
1
2
3
4
-1
0
1
0
0
0

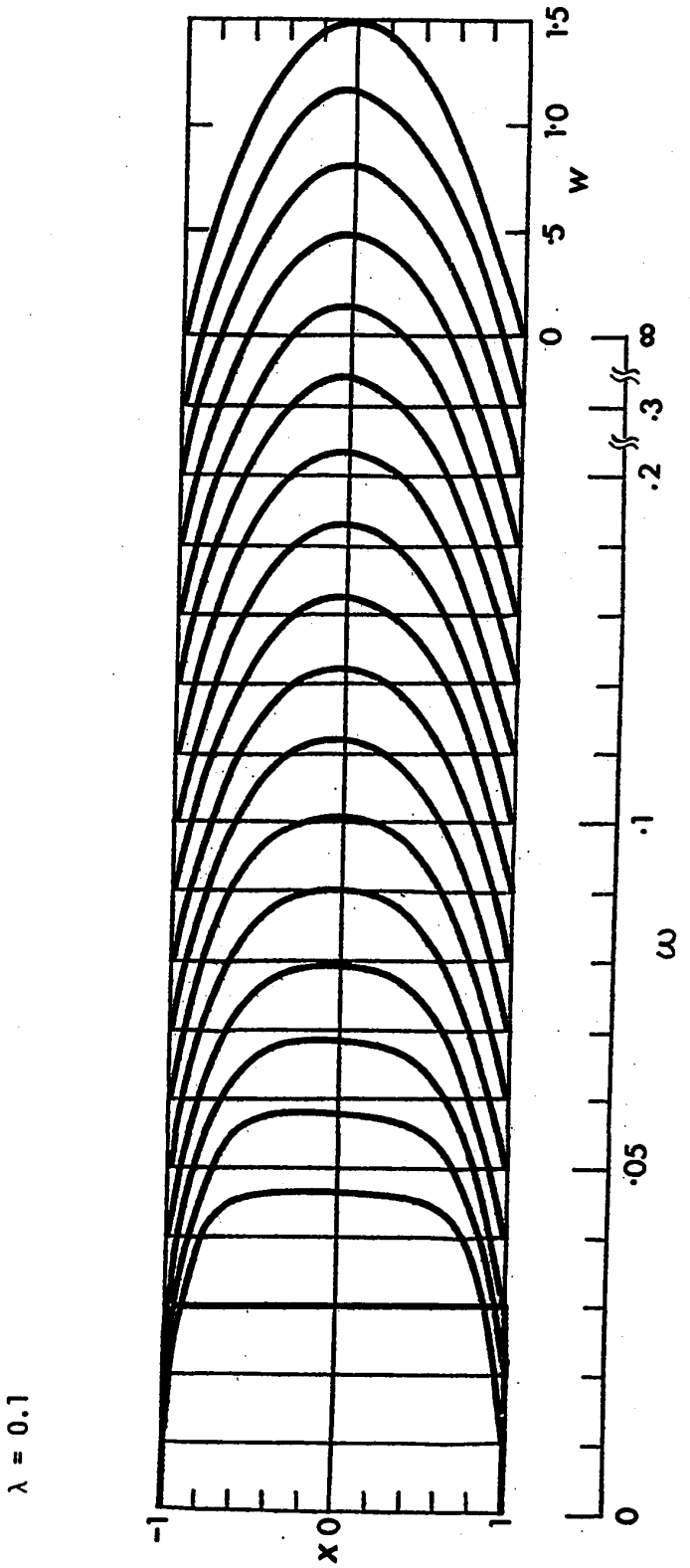


Fig. 73 Developing Axial Velocity Profiles for $\lambda = 0.1$ with Uniform Velocity

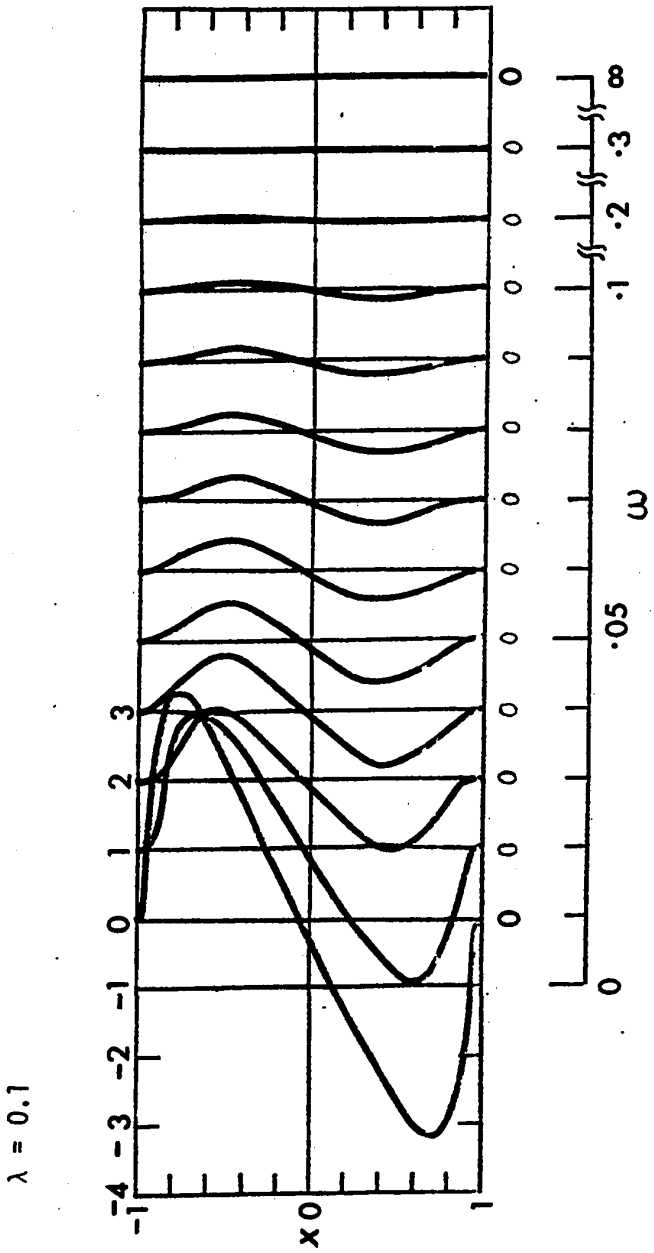


Fig. 74 Developing Transverse Velocity Profiles for $\lambda = 0.1$ with Uniform Entrance Velocity

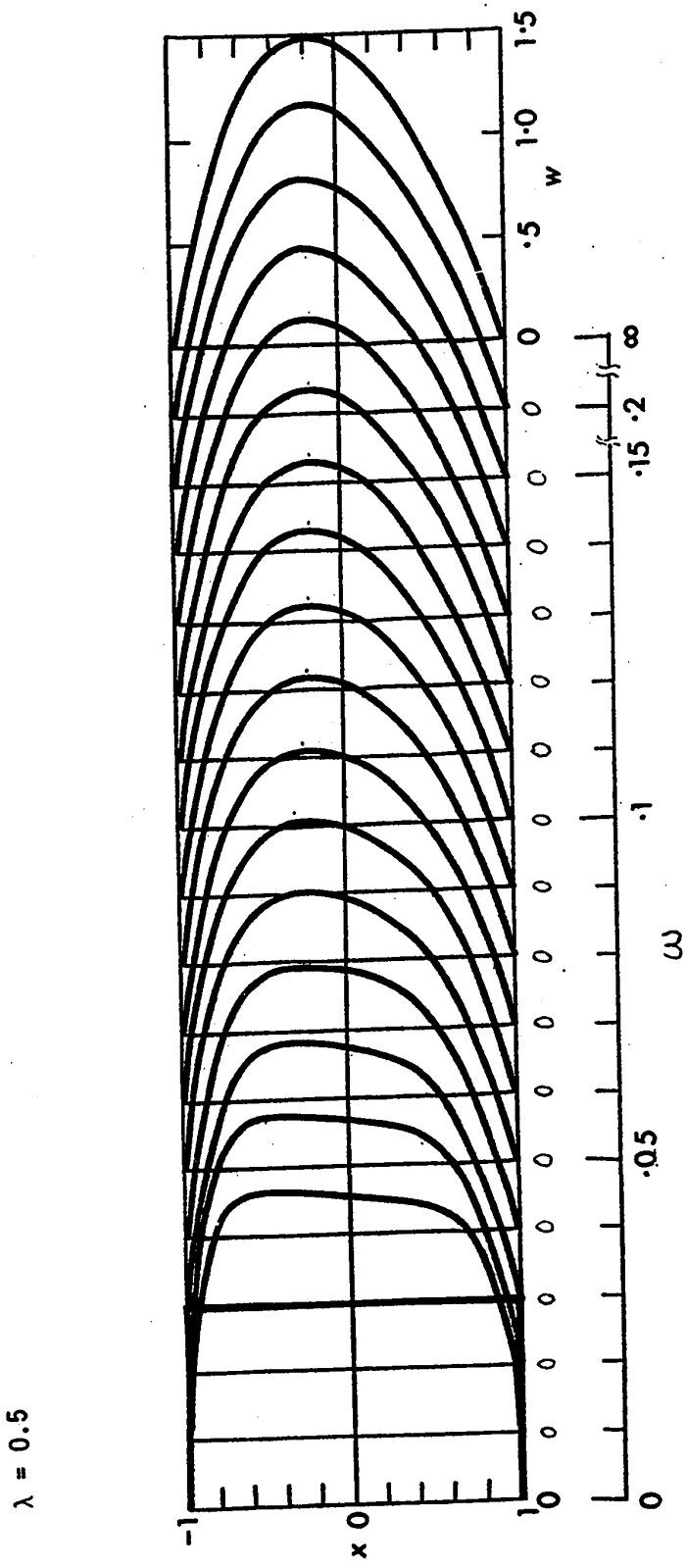


Fig. 75 Developing Axial Velocity Profiles for $\lambda = 0.5$ with Uniform Entrance Velocity

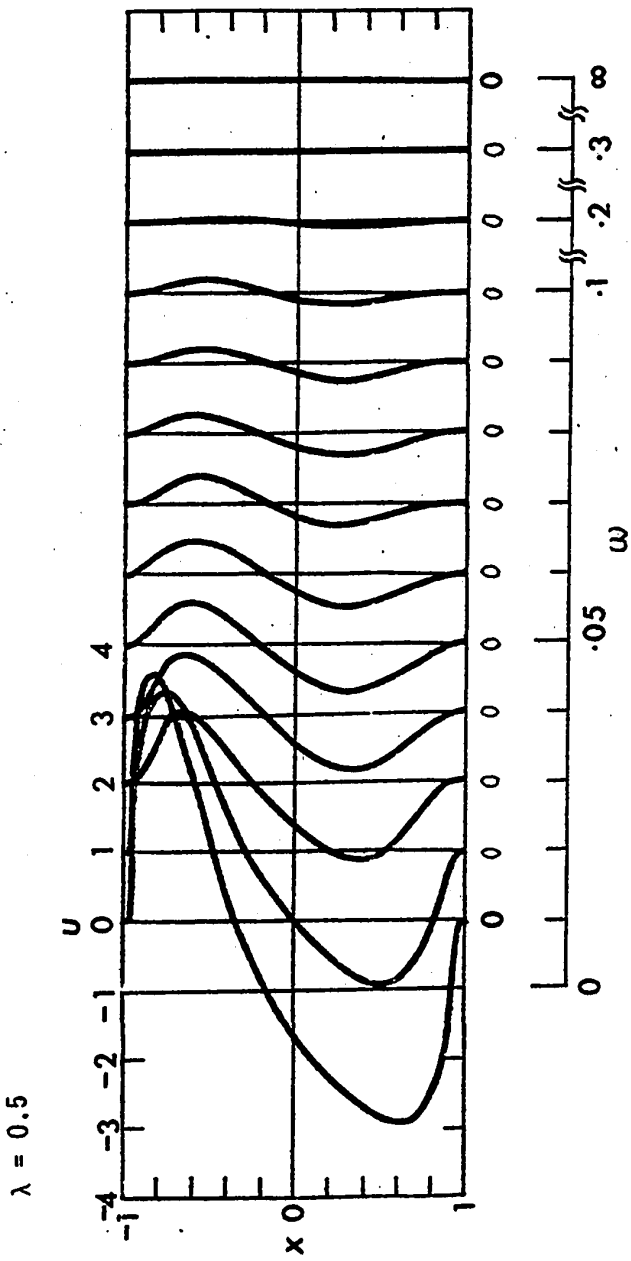


Fig. 76 Developing Transverse Velocity Profiles for $\lambda = 0.5$ with Uniform Entrance Velocity

development is almost negligible for practical purpose at $\lambda = 0.01$ since the velocity profiles for both cases ($\lambda = 0$ and 0.01) are practically identical. With $\lambda = 0.1$, the curvature effect is noticeable by observing the deviation of axial velocity profiles from axial symmetry in the immediate neighbourhood of the entrance and the non-venishing of the transverse velocity at the center line throughout the entrance region. The curvature effect is pronounced at $\lambda = 0.5$. Fig. 73 clearly shows the thickening of the boundary layer at the outer wall and the maximum axial velocity is located nearer to the inner wall. The latter fact is well-known for the fully developed condition [122] and the maximum velocity is seen to be located at approximately $x \simeq -0.2$ with its magnitude decreasing from a value of 1.5 for plane Poiseuille flow to a value of 1.495. At $\lambda = 0.5$ the distortion of the transverse velocity profile (see Fig. 76) from that of $\lambda = 0$ or 0.01 is quite appreciable and the viscosity effect is seen to be important in the entrance region. A boundary along the channel where the transverse velocity becomes zero is of special interest and the region with inward transverse velocity is seen to be greater than that with outward transverse velocity. In the entrance region, the boundary layer and centrifugal force effects coexist and at any cross-section the pressure is highest at outer wall. In the fully developed region the transverse velocity vanishes completely and the centrifugal force on a fluid element is balanced by a pressure gradient inwards.

The pressure drop between the channel inlet ($\omega = 0$, $p = p_0$)

and any axial location ($\omega = 0$, $p = p$), $\Delta p = p_0 - p$, as determined by the method discussed in Section 6.6 using Simpson's rule for integration is shown in Fig. 77 for the curvature ratio, $\omega = 0$, 0.1 and 0.5. The pressure drop $(\Delta p)_{c,\infty}$ which would be sustained by a flow if it were fully developed right from the channel inlet ($\omega = 0$) is also included in Fig. 77 for comparison. It is seen that the pressure drop $\Delta p$ at any axial position increases with the curvature ratio $\lambda$ but for the range $\lambda = 0 \simeq 0.1$ the increase of the pressure drop due to curvature effect is not significant and may be negligible for practical purposes. It is noted that the difference $[\Delta p - (\Delta p)_{c,\infty}]$ represents the incremental pressure drop due to flow development in the channel and the numerical results for the fully developed condition are listed in Table 6 together with the numerical results for the hydrodynamic entrance length based on the attainment of the center line velocity corresponding to 98 and 99 per cent, respectively, of the fully developed value. The hydrodynamic entrance length is seen to decrease with the increase of the curvature ratio .

Table 6

$[\Delta p_\infty - p_\infty]$ and Entrance Lengths $\omega_{98}$ and $\omega_{99}$ for Curved Parallel-plate Channel Flow with Uniform Entrance Velocity Profile

| $\lambda$ | $[\Delta p - \Delta p_\infty]$ | $\omega_{98}$ | $\omega_{99}$ |
|---|---|---|---|
| 0.0 | 0.352 | 0.138 | 0.173 |
| 0.01 | 0.352 | 0.137 | 0.173 |
| 0.1 | 0.356 | 0.134 | 0.172 |
| 0.5 | 0.442 | 0.123 | 0.158 |

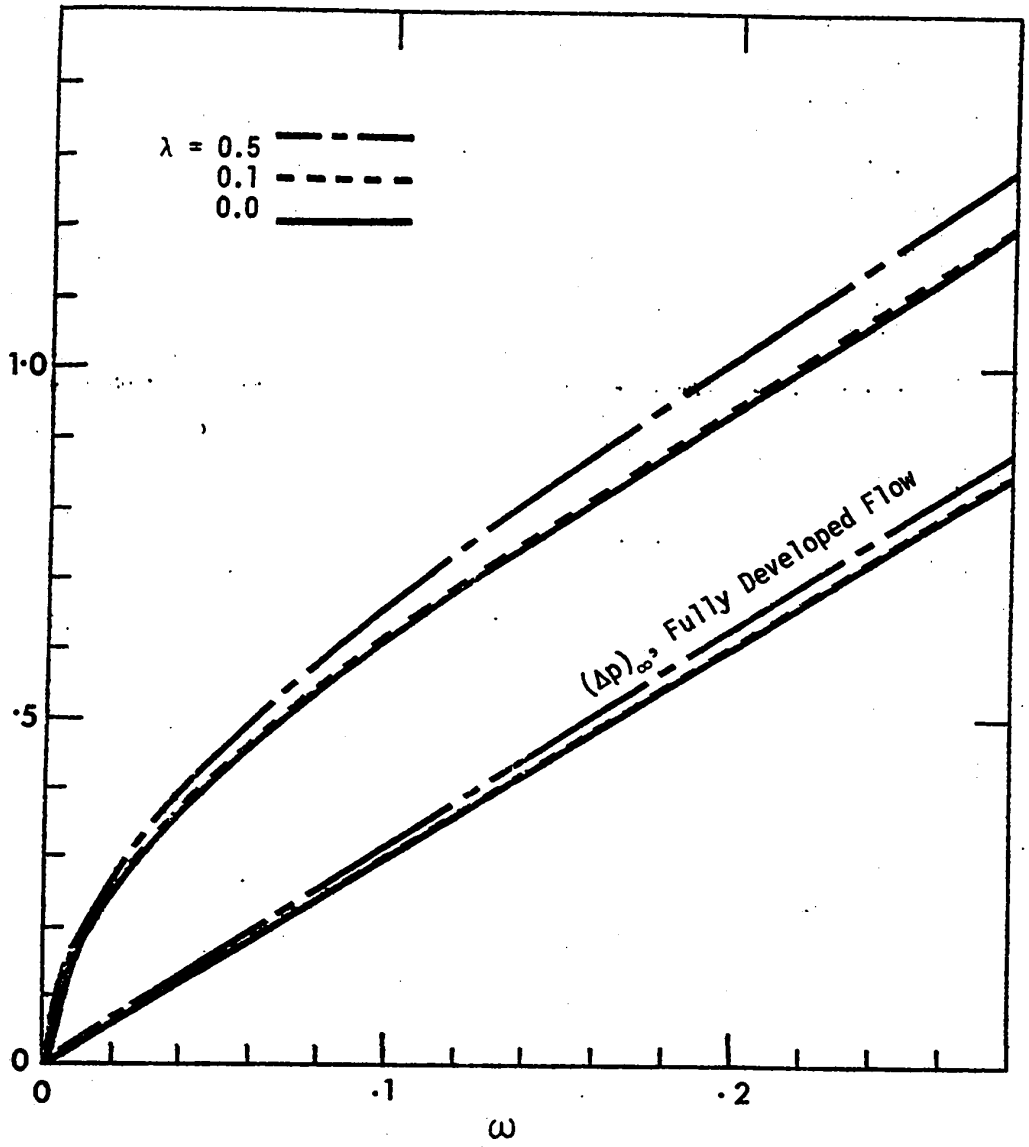


Fig. 77 Pressure Drop Result for $\lambda$ = 0, 0.1 and 0.5 with Uniform Entrance Velocity

With the pressure drop $\Delta p = p_0 - p$ known, the ratio of the friction coefficients, $f/(f)_{s,\infty}$ can be readily computed using equation (173) and the results are shown in Fig. 78.

## 6.8 LAMINAR FLOW DEVELOPMENT IN A CURVED PARALLEL-PLATE CHANNEL WITH A PARABOLIC INLET VELOCITY PROFILE

The entry flow in a straight parallel-plate channel with a parabolic inlet velocity profile becomes a trivial problem. However, with the curvature effect the situation is different. The numerical results are shown in Figs. 79 to 82 in the forms of axial and transverse velocity profile developments for $\lambda = 0.1$ and 0.5. In contrast to the case of a uniform entrance velocity, the boundary layer effect disappears in the present problem and the flow development is due solely to centrifugal force effects. Apparently the secondary flow is caused by an unbalanced transverse pressure gradient across the channel induced by the centrifugal force effect. The transverse pressure gradients $\partial p/\partial x$ at the inner and outer walls vanish and the pressure is highest at the outer wall, and least at the inner wall. Consequently, the secondary flow is toward the inner wall throughout the whole entrance region.

At $\lambda = 0.1$, the curvature effect can be detected from the gradual shift of the maximum axial velocity away from the center line toward the inner wall. The effect is more obvious from the development of the transverse velocity profiles shown in Fig. 80. The curvature effect becomes more pronounced at $\lambda = 0.5$ (see Figs. 81 and 82). Note the gradual development of the axial velocity from the initial

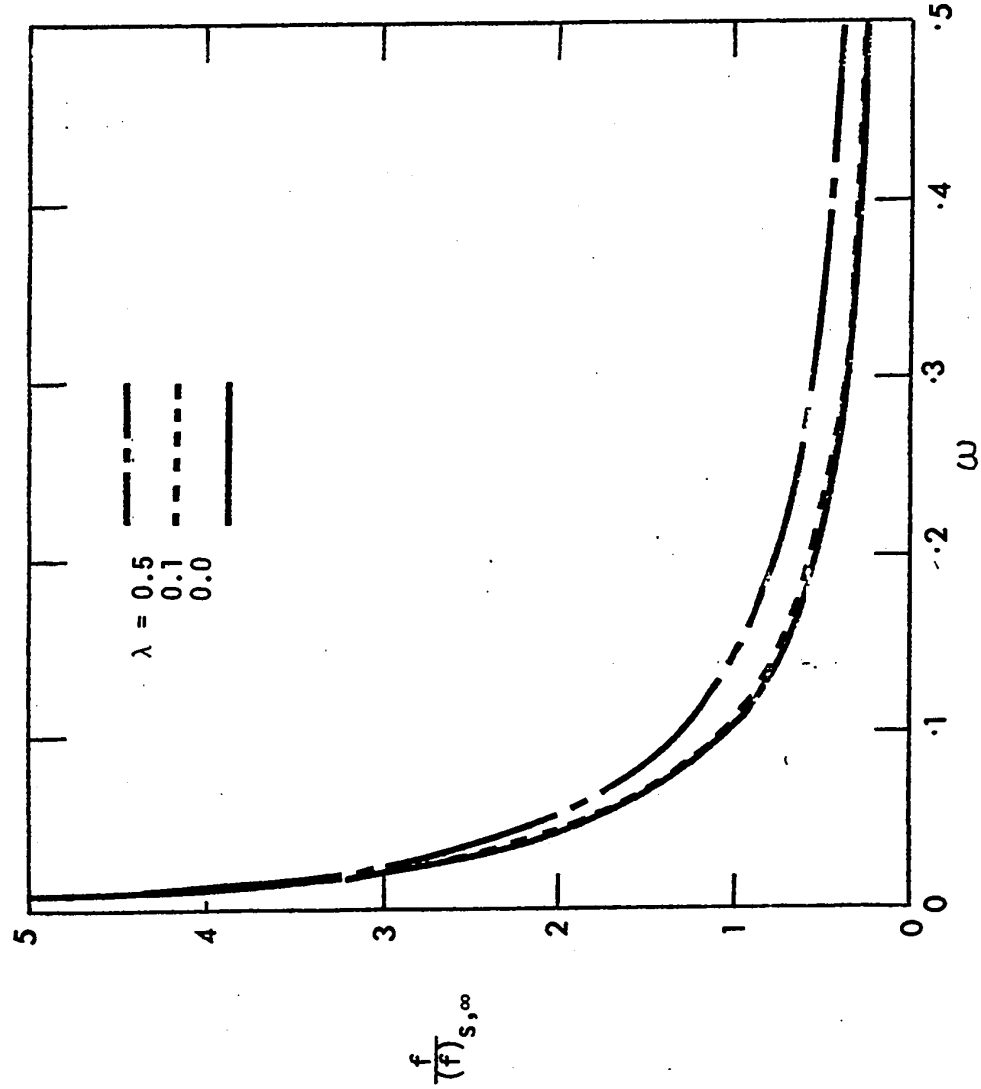


Fig. 78 Friction Factor Results for λ = 0, 0.1 and 0.5 with Uniform Entrance Velocity

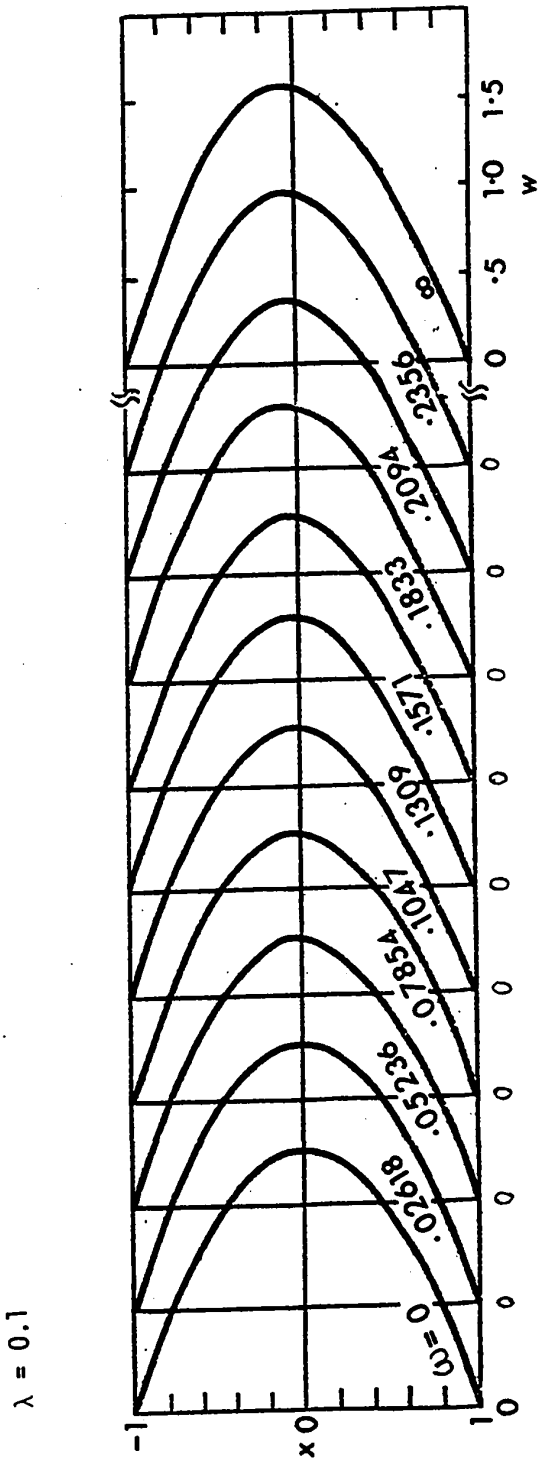


Fig. 79 Developing Axial Velocity Profiles for $\lambda = 0.1$ with Parabolic Entrance Velocity

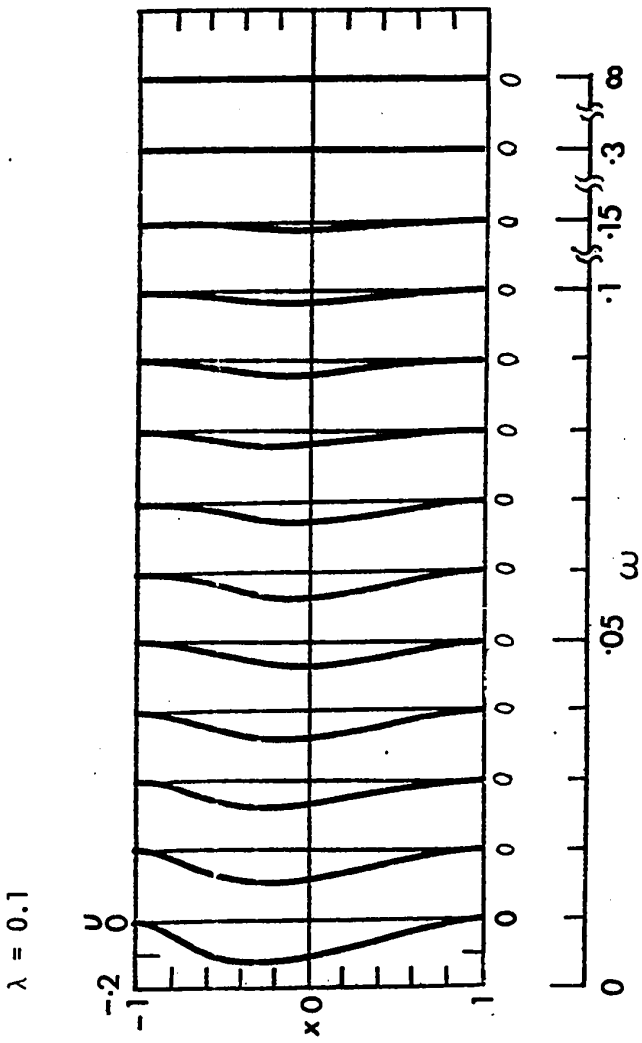


Fig. 80 Developing Transverse Velocity Profiles for $\lambda = 0.1$ with Parabolic Entrance Velocity

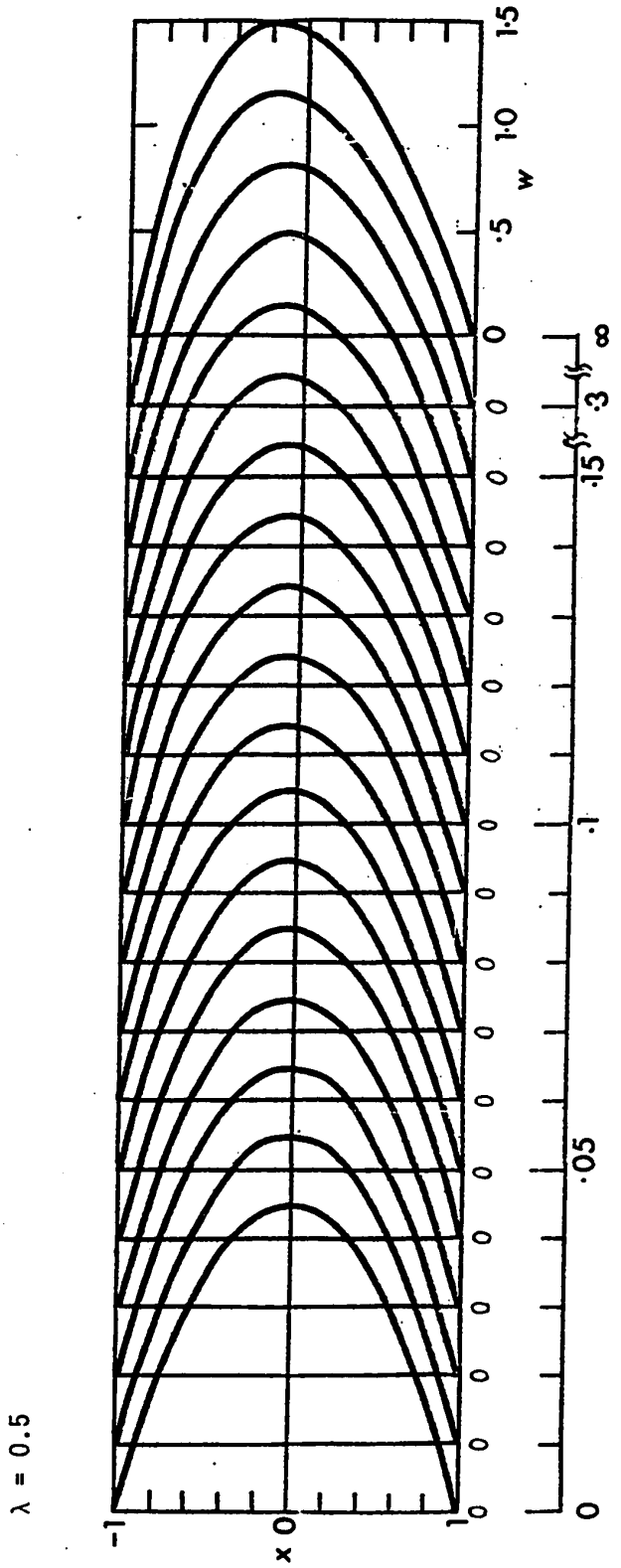


Fig. 81 Developing Axial Velocity Profiles for $\lambda = 0.5$ with Parabolic Entrance Velocity

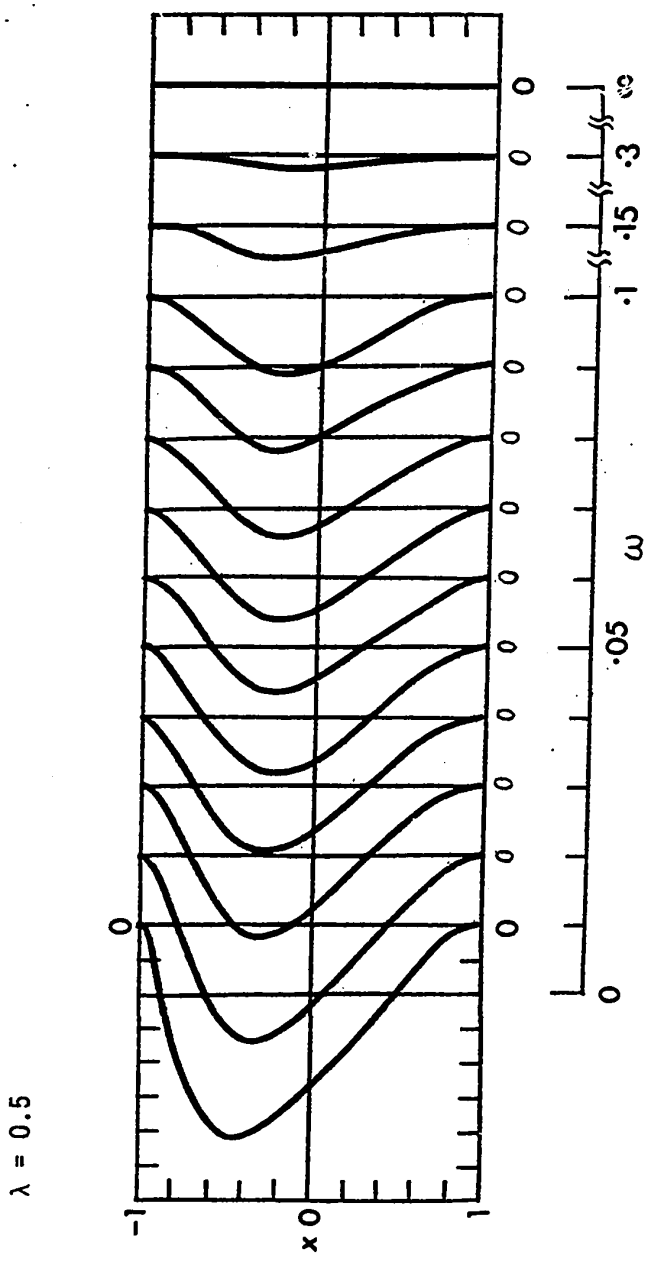
λ = 0.5
-1
x 0
1
0
0
0

parabolic profile to the fully developed unsymmetric one.

Pressure drop results in the entrance region with parabolic entrance velocity are shown in Fig. 83 for $\lambda = 0.5$ together with the pressure drop for $\lambda = 0$ and 0.5, which would result if the flow were fully developed right from the duct inlet is included for comparison. It is interesting to note that in spite of the relatively strong flow near the entrance at $\lambda = 0.5$, the pressure drop $\Delta p$ seems to follow closely the line for $\lambda = 0$ with fully developed flow in the immediate neighbourhood of the entrance and then gradually depart from it. In the fully developed region the pressure drop curve for $\lambda = 0.5$ becomes parallel to that of 0.5 for the fully developed condition. It is seen that in the developing region, the curve for $\lambda = 0.5$ lies between the two curves $\lambda = 0$ and 0.5 with fully developed conditions right from the entrance. It is noted that the pressure drop $\Delta p$ for $\lambda = 0.5$ in the entrance region is always less than that of $\lambda = 0.5$ with fully developed conditions right at the entrance. The difference between $\Delta p$ and $(\Delta p)_\infty$ for $\lambda = 0.5$ is seen to be very small and a constant value, $[\Delta p - (\Delta p)_\infty] = -0.007$ is approached at the fully developed condition.

The ratio of the friction factors, $f/(f)_{s,\infty}$ can be computed readily using equation (173), namely $f/(f)_{s,\infty} = \Delta p/(3\omega)$, since $\Delta p$ is known. It can be verified that the ratio $f/(f)_{s,\infty}$ is close to unity. Lastly, one notes that the entrance lengths are found to be $\omega_{98} = 0.046$ and $\omega_{99} = 0.099$, respectively, for $\lambda = 0.5$.

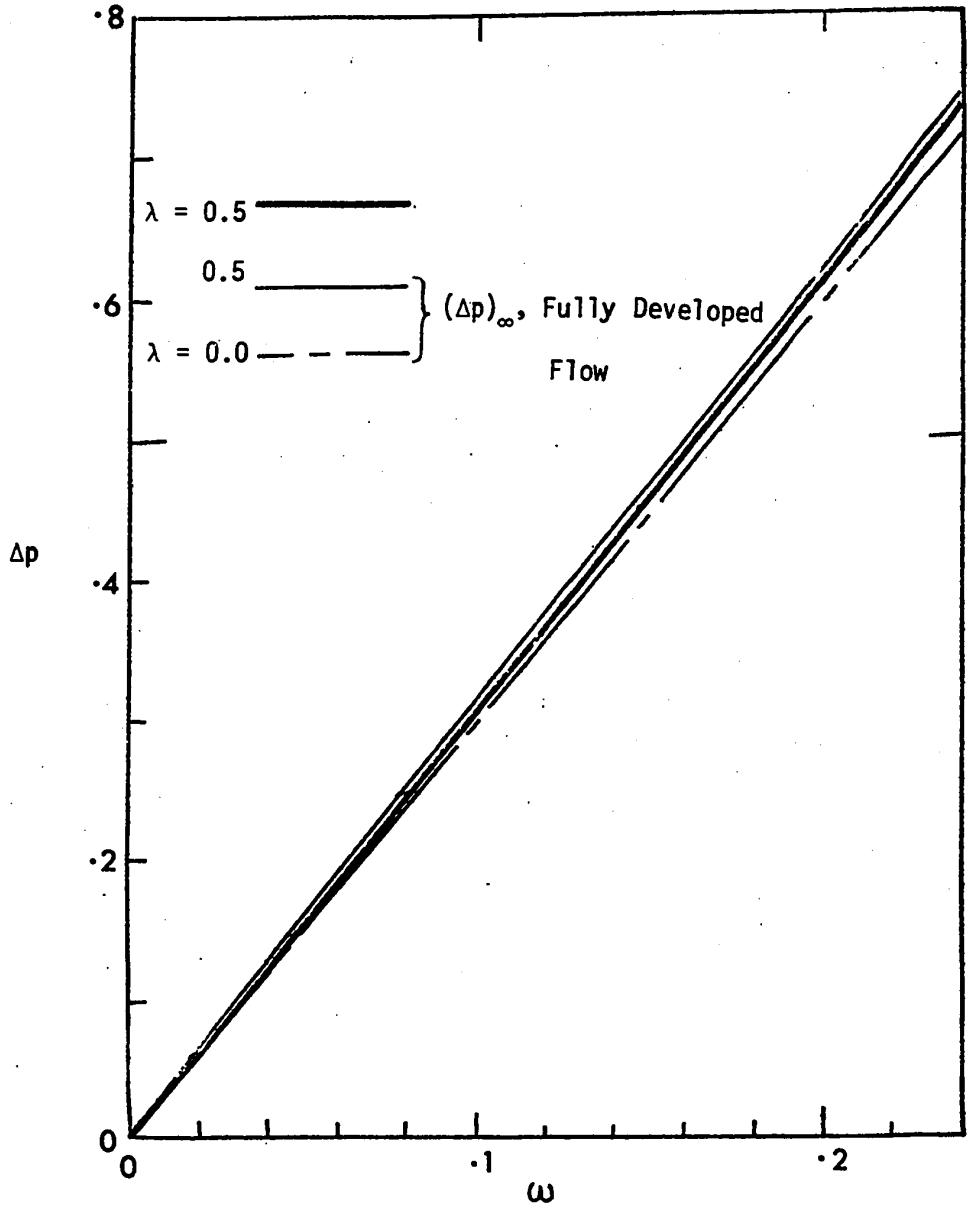


Fig. 83 Pressure Drop Result for $\lambda = 0.5$ with Parabolic Entrance Velocity

## 6.9 LAMINAR FLOW DEVELOPMENT IN A CURVED PARALLEL-PLATE CHANNEL WITH A TRIANGULAR INLET VELOCITY PROFILE

The present inlet velocity profile is characterized by an asymmetrical distribution with respect to the center line x = 0. The mean inlet velocity for this case is identical with that of uniform entrance velocity. The developing profiles for axial and transverse velocities are shown in Figs. 84 to 89 for the curvature ratios $\lambda$ = 0, 0 1 and 0.5. The case with $\lambda$ = 0 represents a parallel-plate channel and Fig. 84 shows that the location of the maximum secondary velocity occurs first near the outer wall, and then gradually shifts towards the center line along the downstream direction. Because of the inward transverse velocity throughout the entrance region, the symmetric parabolic velocity profile representing the fully developed condition is eventually approached. The secondary flow is strongest at the entrance and vanishes entirely when the flow becomes fully developed. The curvature effect can be seen by comparing the developing profiles for $\lambda$ = 0.1 and 0.5 with those for $\lambda$ = 0 (straight channel). At $\lambda$ = 0.1 the curvature effect is already detectable but the effect is rather small. Near the entrance the intensity of the secondary flow increases with the curvature effect. At = 0.5, the increase of the secondary flow intensity over that of = 0 is seen to be quite appreciable near the entrance. The development of the axial velocity profile from the initial triangular one to the final asymmetric one with its maximum located near x = -0.2 is shown in Fig. 88. As pointed out in Section 6.7,

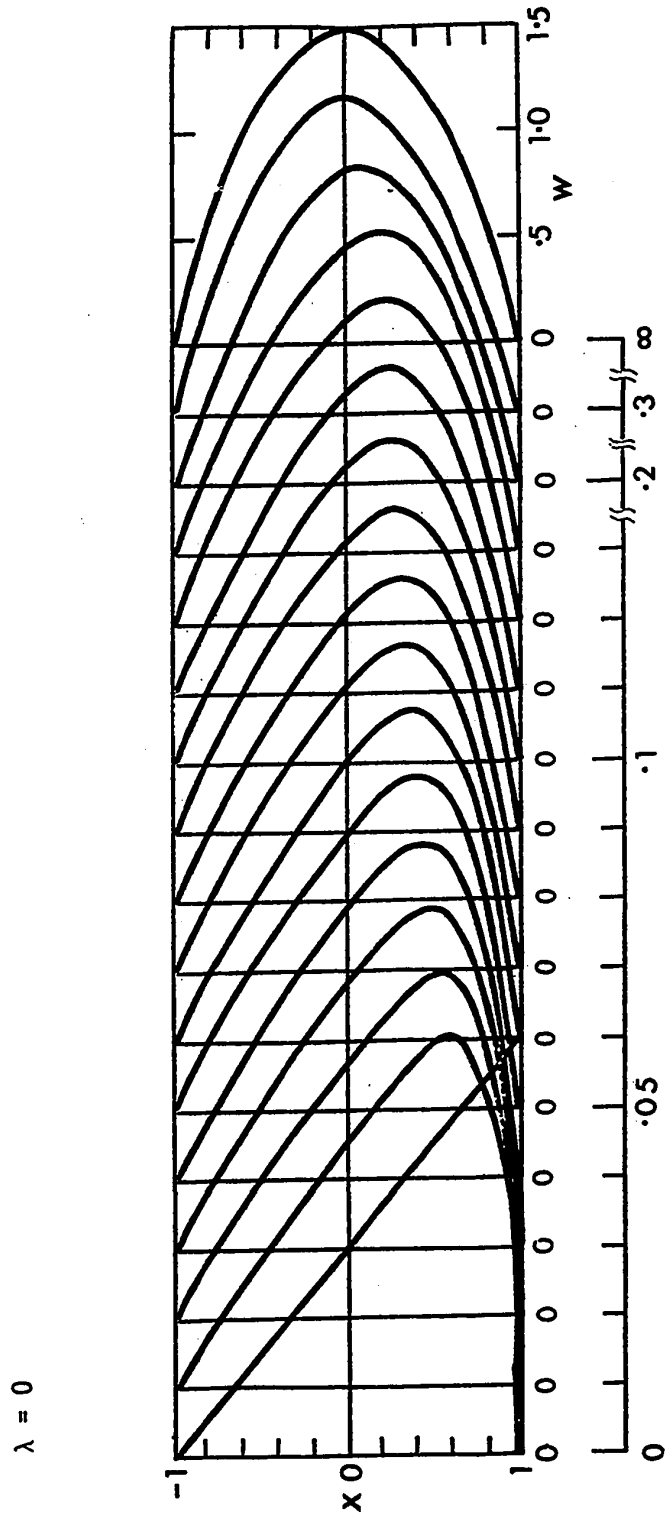


Fig. 84 Developing Axial Velocity Profiles for $\lambda = 0$ with Triangular Entrance Velocity

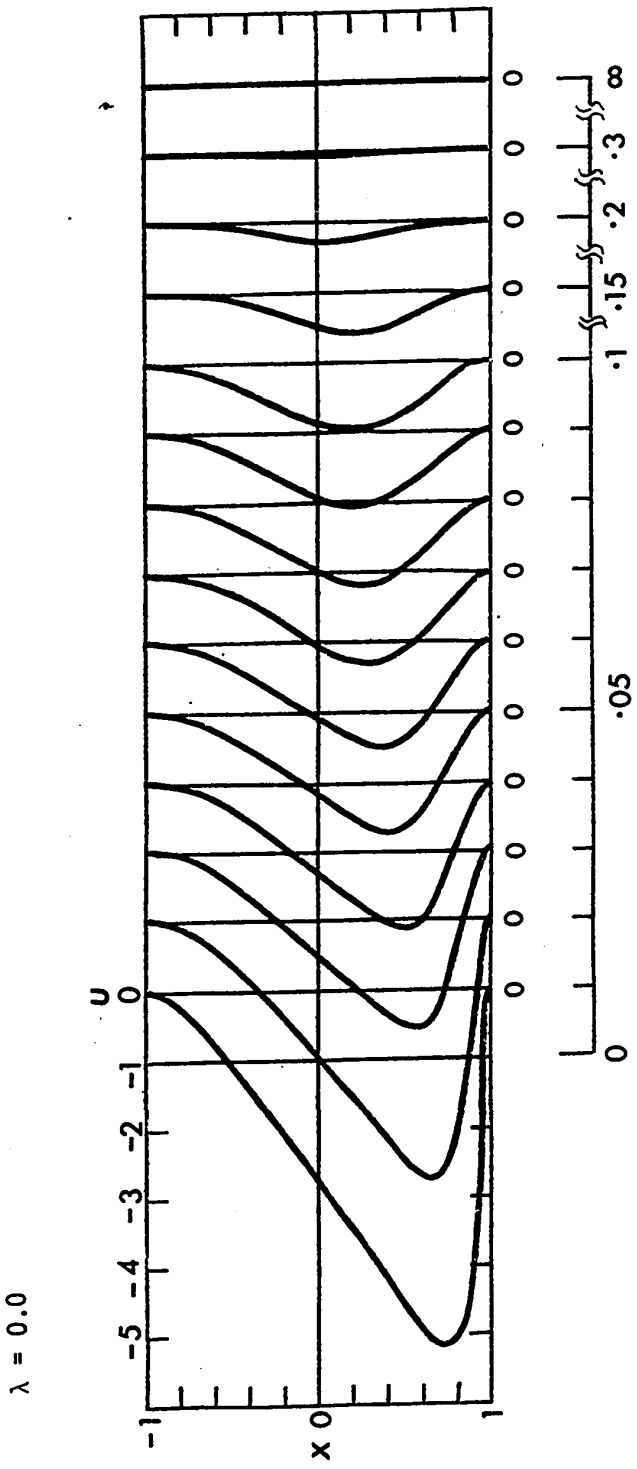


Fig. 85 Developing Transverse Velocity Profiles for $\lambda = 0$ with Triangular Entrance Velocity

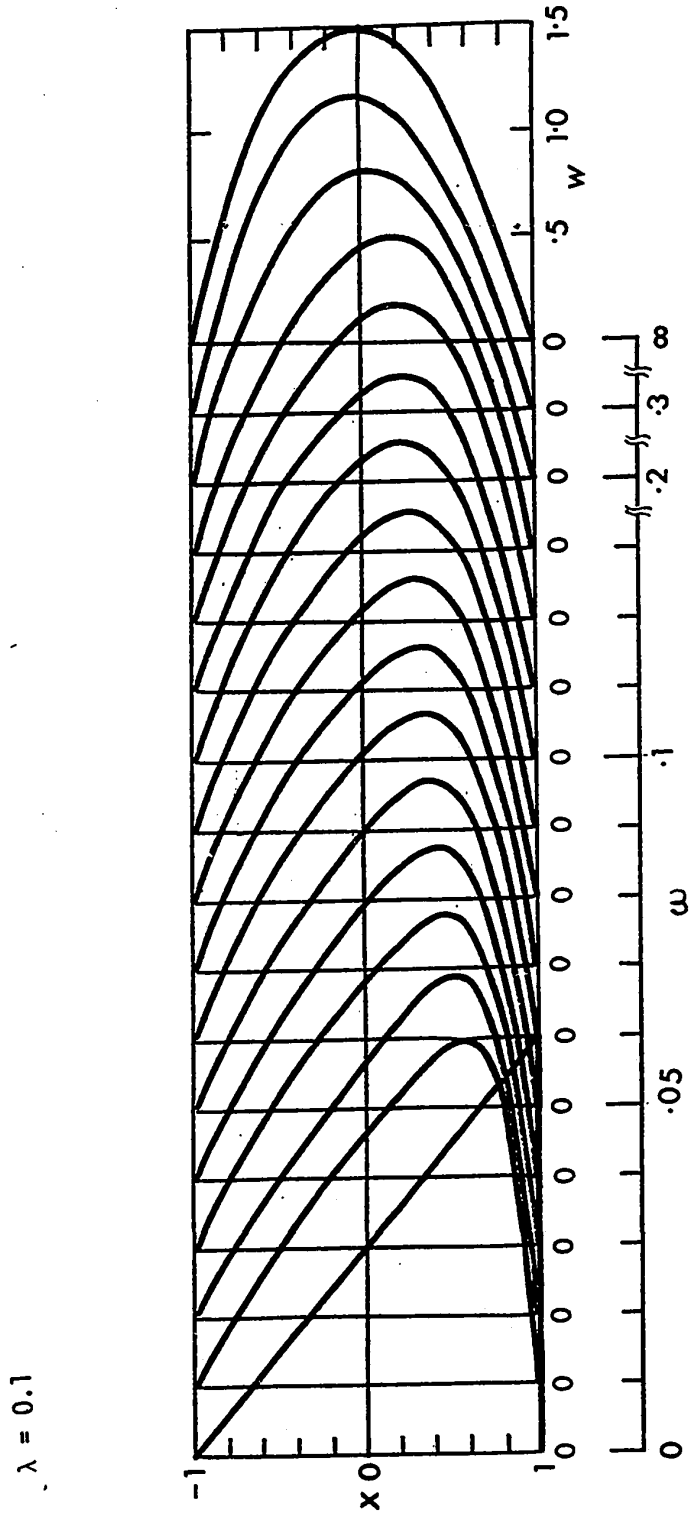


Fig. 86 Developing Axial Velocity Profiles for $\lambda = 0.1$ with Triangular Entrance Velocity

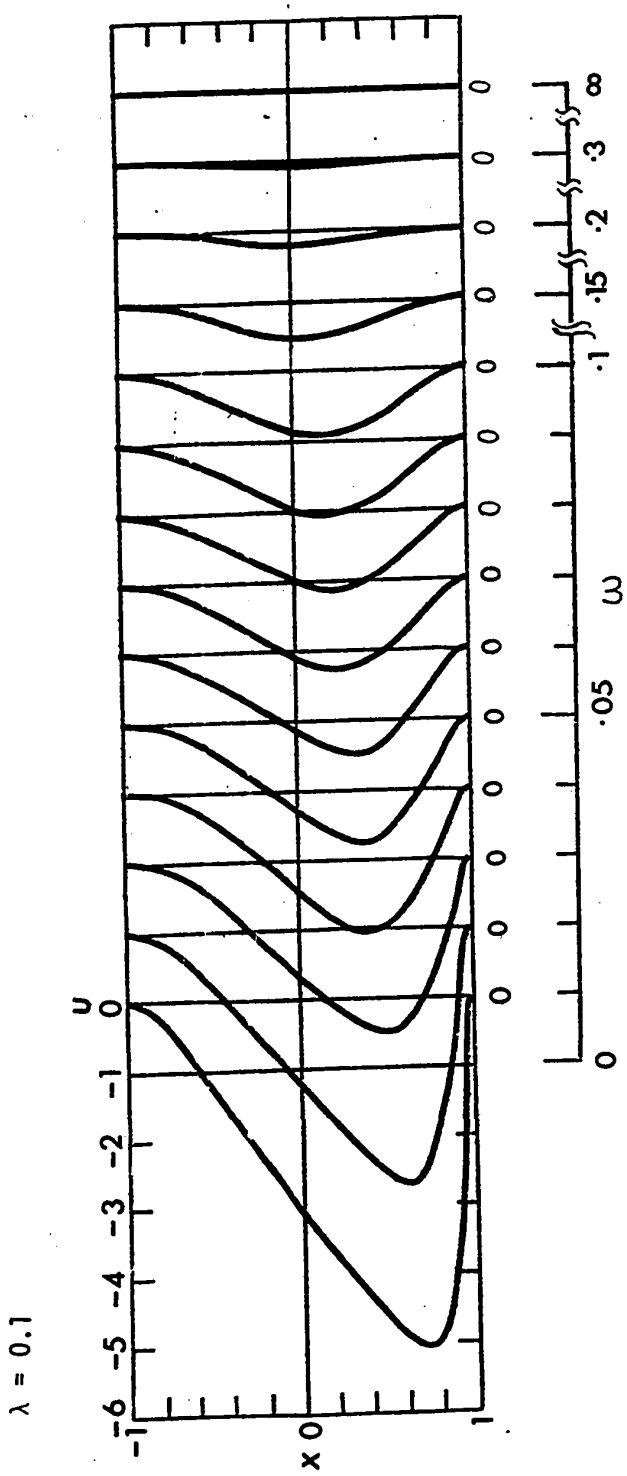


Fig. 87 Developing Transverse Velocity Profiles for $\lambda = 0.1$ with Triangular Entrance Velocity

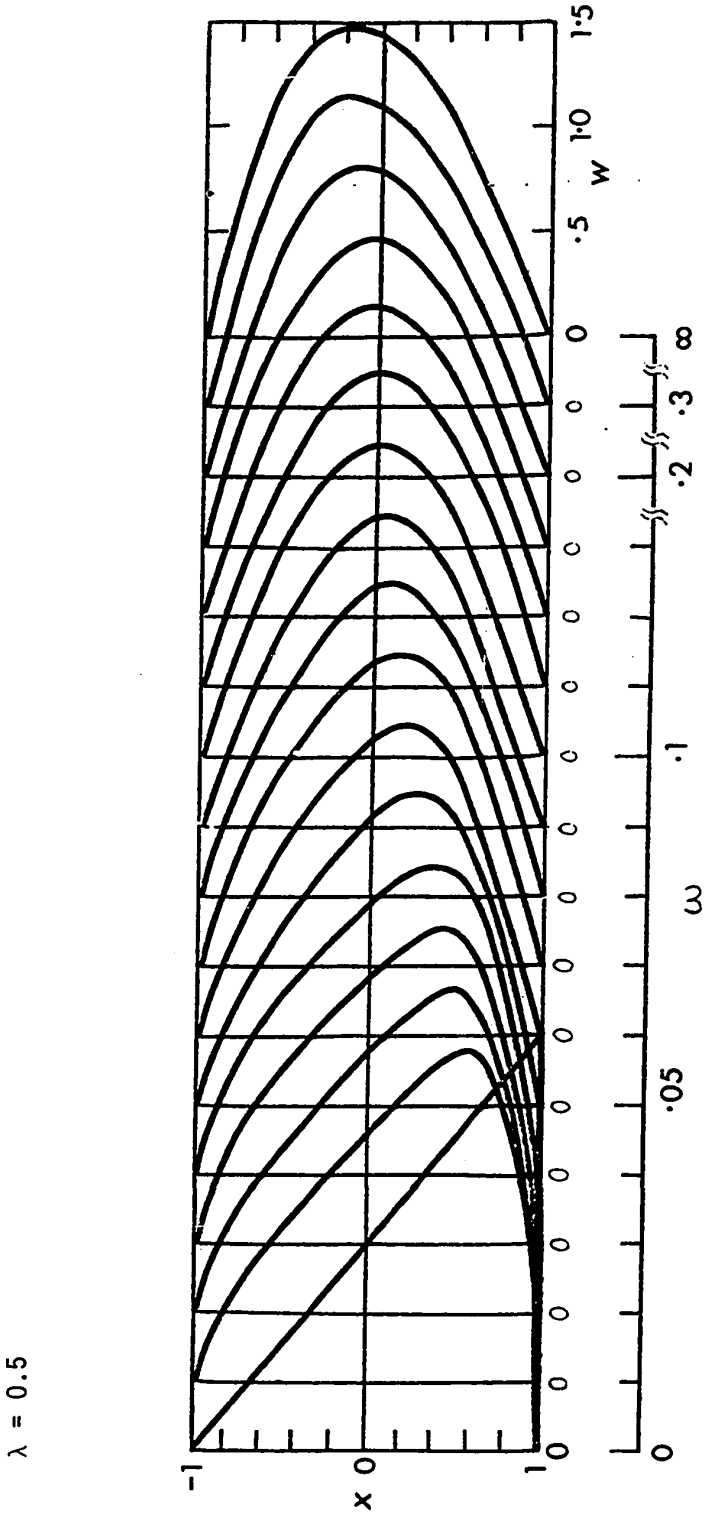


Fig. 88 Developing Axial Velocity Profiles for $\lambda = 0.5$ with Triangular Entrance Velocity

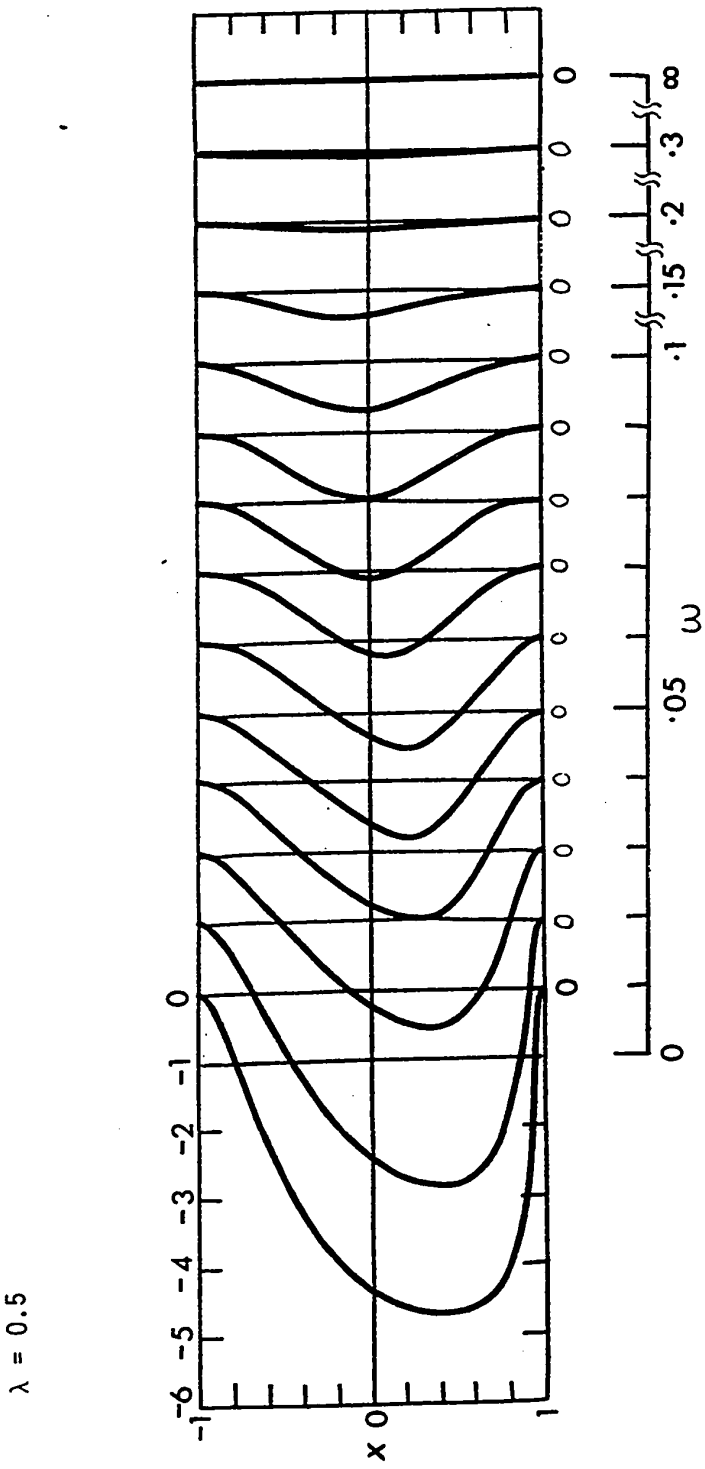


Fig. 89 Developing Transverse Velocity Profiles for $\lambda = 0.5$ with Triangular Entrance Velocity

the fully developed velocity profile in curved channels is well-known [122].

The pressure drop results, in terms of $\Delta p$ and $f/(f)_{s,\infty}$, are shown in Figs. 90 and 91, respectively. It is noted that the pressure drop in the entrance region of a curved or plane parallel-plate channel with triangular entrance velocity is smaller than the corresponding one with a uniform entrance velocity. This fact is obvious by comparing the present pressure drop and friction factor results shown in Figs. 90 and 91 with those of Figs. 77 and 78, respectively, for uniform entry flow. Fig. 90 shows that at $\lambda = 0$, the incremental pressure drop $[\Delta p - (\Delta p)_{c,\infty}]$ becomes negative. The fully developed values for the incremental pressure drop and the hydrodynamic entrance lengths are listed in Table 7 for $\lambda = 0$, 0.01, 0.1 and 0.5. It is noted that with $\lambda = 0$, the fully developed incremental pressure drop is -0.017 and even with $\lambda = 0.5$, the value is 0.104 which is smaller than the value of 0.442 for the uniform entrance velocity case. For the range of curvature ratio $\lambda = 0 \simeq 0.1$, the hydrodynamic entrance length $\omega$ with a triangular entry flow decreases by about 25 per cent from that with a uniform entry flow. On the other hand, with $\lambda = 0.5$, the corresponding value is about 28 per cent.

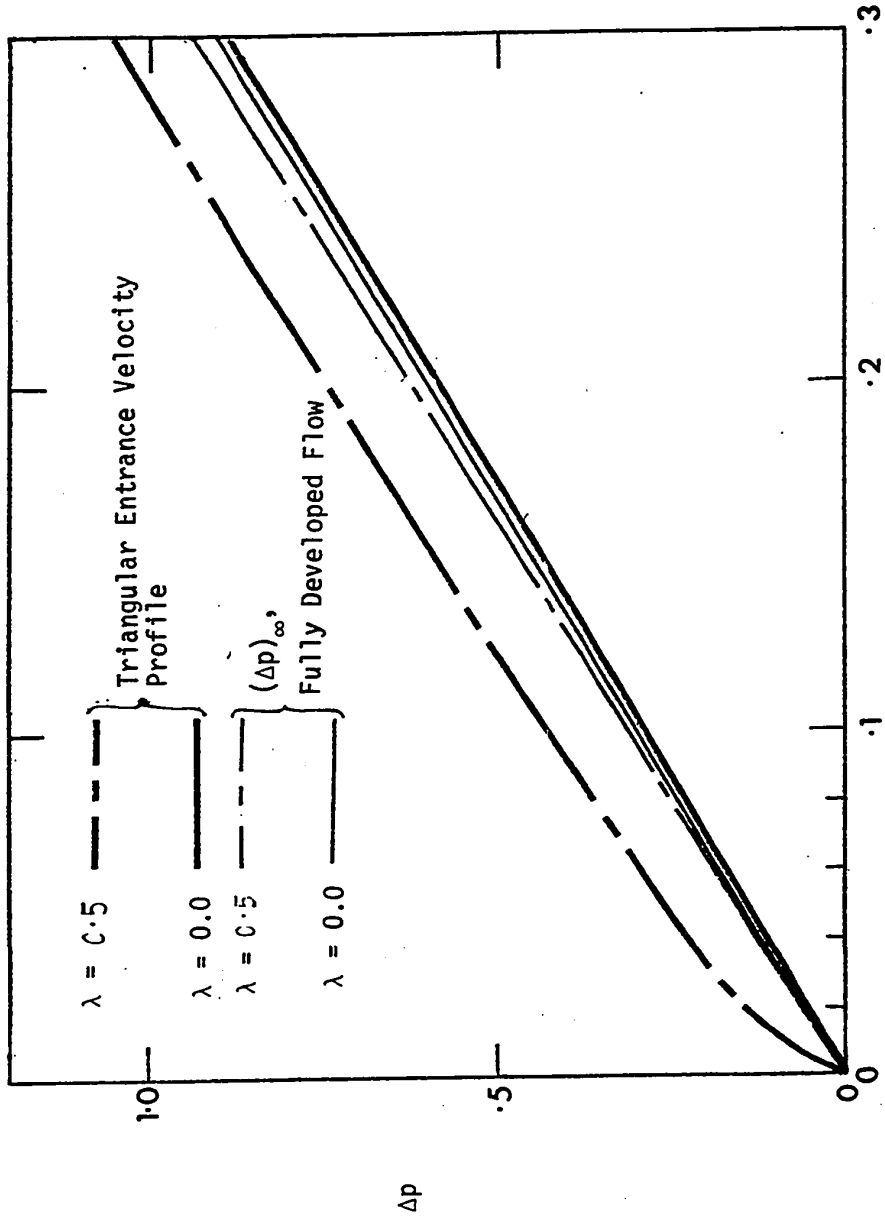


Fig. 90 Pressure Drop Result for λ = 0 and 0.5 with Triangular Entrance Velocity

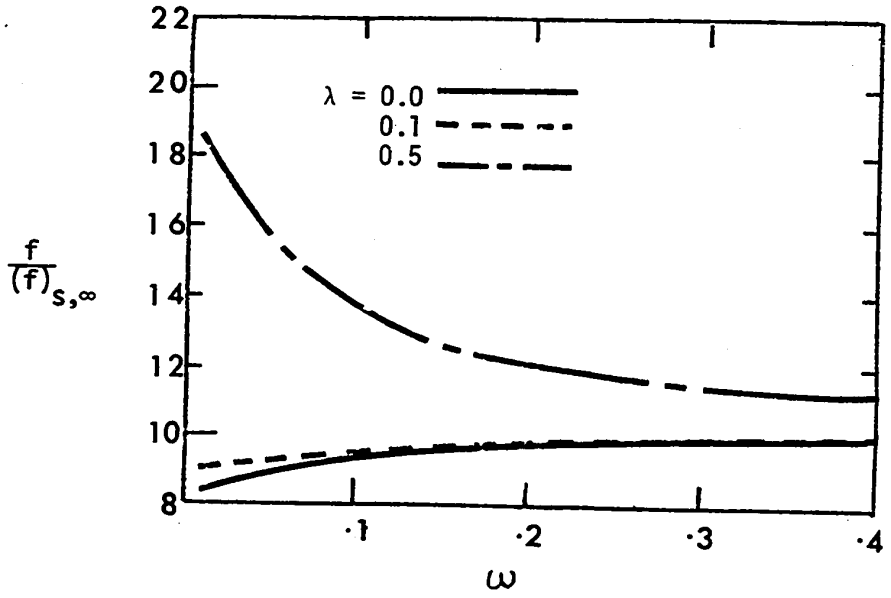


Fig. 91 Friction Factor Results for $\lambda = 0$, 0.1 and 0.5 with Triangular Entrance Velocity

Table 7

$[\Delta p - \Delta p_\infty]$ and Entrance Lengths $\omega_{98}$ and $\omega_{99}$ for Curved Parallel-plate Channel Flow with Triangular Entrance Velocity Profile

| $\lambda$ | $[\Delta p - \Delta p_\infty]$ | $\omega_{98}$ | $\omega_{99}$ |
|---|---|---|---|
| 0.0 | -0.017 | 0.103 | 0.122 |
| 0.01 | -0.017 | 0.103 | 0.122 |
| 0.1 | -0.013 | 0.101 | 0.118 |
| 0.5 | 0.104 | 0.089 | 0.109 |

In the analysis of flow development in tubes or channels, it has been standard to evaluate the static pressure difference $\Delta p$ as used in the present study. However, it may be useful to compute the total pressure drop from the viewpoint of total energy loss. The informationoon total pressure drop may be particularly useful with a non-uniform entrance velocity such as the present triangular one. For the triangular entry flow in a straight parallel-plate channel, the dynamic inlet pressure $p_{d,0}$ is found to be

$$p_{d,0} = \frac{1}{2}\overline{w}^2 \int_{-1}^{1} (1 + x)^2 dx \Big/ \int_{-1}^{1} dx = 2/3 \qquad (174)$$

On the other hand, the dynamic pressure $p_{d,\infty}$ at fully developed condition is

$$p_{d,\infty} = \frac{1}{2} \int_{-1}^{1} \frac{3}{2} (1 - x^2)^2 dx \Big/ \int_{-1}^{1} dx = 3/5 \qquad (175)$$

Thus, the dynamic pressure drop is

$$\Delta P_d = P_{d,0} - P_{d,\infty} = 2/3 - 3/5 = 1/15 \qquad (176)$$

The above dynamic pressure drop $\Delta P_d$ may now be added to the incremental static pressure drop $[\Delta p - (\Delta p)_{s,\infty}]$ at fully developed conditions to obtain an incremental total pressure drop as

$$\Delta p_d + [\Delta p - (\Delta p)_{s,\infty}] = 1/15 - 0.017 = 0.50 \qquad (179)$$

similarly, the incremental total pressure drop in a parallel-plate channel ($\lambda = 0$) with a uniform entrance velocity becomes

$$\Delta p_d + [\Delta p - (\Delta p)_{s,\infty}] = (1/2 - 3/5) + 0.352 = 0.252 \qquad (178)$$

By comparing the above two results, it is found that the incremental total pressure drop at fully developed condition in a parallel-plate channel ($\lambda = 0$) with uniform entrance velocity is about five times greater than that with a triangular entrance velocity. In general one may conclude that the situation is similar with curvature effects included.

## 6.10 CONCLUDING REMARKS

1. Laminar flow development in the entrance region of a curved parallel-plate channel is studied theoretically for entrance velocities which are uniform, parabolic and triangular with a curvature ratio ranging from $\lambda = 0$ to 0.5. For the limiting case of a plane parallel-plate channel ($\lambda = 0$) with uniform entrance velocity, the flow results

are compared with available results reported in the literature. The remaining results for the curved parallel-plate channel are believed to be new.

2. For fully developed laminar flow in curved parallel-plate channels, useful relationships for pressure drop and friction factor are derived using the known analytical solution for velocity profile. At the limiting curvature ratio $\lambda = 1$, the pressure drop and friction factor increase by a factor of 4/3 over those of a straight parallel-plate channel ($\lambda = 0$).

3, For a given entrance velocity profile, the curvature effect on pressure drop is generally small up to $\lambda = 0.1$ and may be negligible for practical purposes. However, the curvature effect gradually increases from $\lambda = 0.1$ onwards and the effect is found to be significant at $\lambda = 0.5$.

4. With a parabolic entrance velocity profile, the pressure drop is less than that which would result if the flow were fully developed right from the channel entrance for a given curvature ratio $\lambda$.

5. With a triangular entrance velocity profile, the pressure drop is less than that which would result if the flow were fully developed right from the channel inlet for a range of curvature ratios $\lambda = 0 \simeq 0.1$. For $\lambda = 0.5$, the pressure drop is much less than that for a uniform entrance velocity.

6. For a given entrance velocity profile, the hydrodynamic entrance length decreases with an increase of the curvature ratio $\lambda$.

For a given curvature ratio $\lambda$, the entrance length for the uniform entrance velocity case is longer than that for a parabolic entrance velocity is seen to be the least.

7. In the formulation of the present problem, the axial viscous terms are neglected. The results presented in this study must be understood under this light. The effects of axial viscous terms should be investigated in future work.

8. The present numerical method is applicable to entry flow problems in a curved parallel-plate channel with any arbitrary entrance velocity profile.

9. The numerical results obtained are listed in Appendix 9 for future reference.

# CHAPTER VII

# HYDRODYNAMIC INSTABILITY OF LAMINAR FLOW IN CURVED PARALLEL-PLATE CHANNELS

## 7.1 INTRODUCTION

For a laminar flow between two curved parallel plates or two coaxial cylinders, the flow in the boundary layer is known to be unstable at the concave outer wall and stable at the convex inner wall. Due to the centrifugal forces acting on a fluid element the pressure is highest at the outer wall and least at the inner wall for any cross-section. In contrast to the monotonous increase of pressure from the inner wall to the outer wall along the transverse direction, the centrifugal force increases from zero at the inner wall and then becomes zero again at the outer wall after reaching a maximum value at the point of maximum axial velocity. The outer region with decreasing centrifugal force is clearly seen to be unstable. The situation is completely analogous to Taylor's problem [123] for the stability of Couette-type flow of a viscous liquid between concentric, rotating cylinders and Görtler's problem [124] for the instability of boundary-layer flows over concave walls. The resulting secondary flow is commonly referred to as Taylor-Görtler vortices. The instability of curve flows due to centrifugal forces (centrifugal instability) is analogous to thermal instability such as that due to buoyancy forces acting on horizontal fluid layers heated from below.

Several examples of instability due to centrifugal forces

are well reviewed by Stuart [125]. Consideration is now given to a curved parallel-plate channel along which fluid is flowing under the action of a pressure gradient. A theoretical investigation of the stability of flow under pressure in a curved channel or between concentric cylinders was first made by Dean [126] in 1928. His analysis is based on the assumptions that the distance between the two cylinders is small in comparison with the inner radius and the fully developed main flow is parabolic. He shows that the motion can become unstable for a small disturbance of exactly the type found by Taylor [123] for fluid motion between two rotating cylinders. Dean [126] gives the following ciritical value for the characteristic parameter K which is now known as the Dean number.

$$K = Re\left(\frac{a}{R_c}\right)^{1/2} = 25.4$$

where $Re = W_m(2a)/\nu$, a = a half channel width and $R_c$ = the radius of curvature of the channel. Using the result of this analysis, Dean offered an explanation for the known absence of a marked critical velocity of flow in a curved pipe.

Apparently unaware of Dean's earlier work [126], Yih and Sangster [127] studied Dean's problem again in 1957. Subsequently, Reid [128] also studied Dean's instability problem in 1958 using two methods of approximate analytical solution. Reid's numerical results for the critical Dean number using two different methods agree closely with Dean's earlier result [126]. Reid also presents the radial and tengential velocity perturbations and the cell pattern

at the onset of instability. In 1958, Hämmerlin [129] also presented theoretical results for Dean's instability problem using Green's function. Hämmerlin shows the distributions for the eigenfunctions, cellular pattern and axial disturbance at the onset of instability. In 1967, Mori and Uchida [130] presented theoretical and experimental results for forced convective heat transfer in a curved channel in the post-critical flow regime.

It is noted that the reported theoretical results for hy rodynamic instability in curved parallel-plate channels are for the case of fully developed laminar flow with a plane Poiseuille velocity profile only where the curvature effect is completely neglected for the main flow, The experimental confirmation for Dean's instability problem does not seem to be available at present.

The purpose of this investigation is to present the formulation of the general perturbation equations applicable to the hydrodynamic entrance flow in curved parallel-plate channels and present numerical results for hydrodynamic instability for the limiting case of fully developed laminar flow with curvature effect. Thus the present problem can be considered to be the extension of the Dean's instability problem [126]. The numerical method of solution is developed for a study of hydrodynamic instability in the entrance region of curved parallel-plate channels with curvature effect but the numerical results are obtained only for the asymptotic case of fully developed flow in order to limit the scope of the present investigation.

## 7.2 FORMULATION OF THE STABILITY PROBLEM

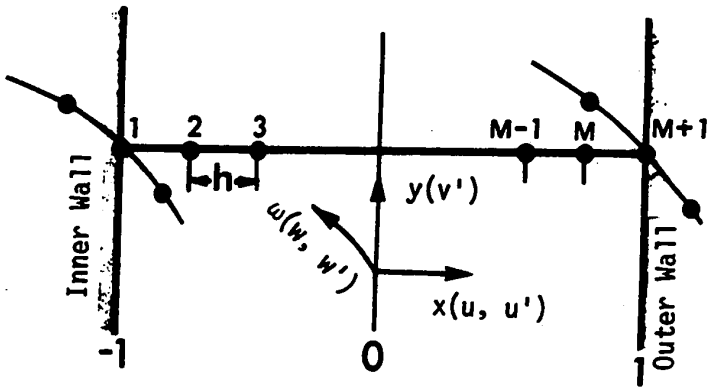


Fig. 92 Coordinate System and Numerical Grid

Consideration is given to a steady incompressible flow in the entrance region of a curved parallel-plate channel with a given entrance velocity. The coordinate system is shown in Fig. 92. It is assumed that the velocity distributions for the primary flow are available. It is known that the present two-dimensional curved flow is unstable under the three-dimensional disturbances of Taylor-Görtler type near the concave outer wall. To investigate the stability of the steady primary flow, one may superimpose the perturbations on the basic flow as,

$$U = U_b(R_c\Omega,X) + U', \quad V = V',$$

$$W = W_b(R_c\Omega,X) + W', \quad P = P_b(R_c\Omega,X) + P'$$

in which $U_b$ and $W_b$ are basic velocity components corresponding to

transverse and axial directions, respectively, and $P_b$ is the static pressure. The perturbation quantities $U'$, $V'$, $W'$ are taken to be sufficiently small for their squares and products to be neglected. The continuity and the Navier-Stokes equations expressing the conservation of mass and momentum may now be written (see equations (A-16) to (A-19)) and the foregoing perturbations introduced. Noting that the basic flow is such that the equation of continuity and Navier-Stokes equations are satisfied and that the terms of higher order than the first in the perturbation quantities may be neglected, one obtains the following set of perturbation equations.

Continuity equation

$$\frac{\partial U'}{\partial X} + \frac{U'}{(R_c + X)} + \frac{\partial V'}{\partial Y} + \frac{1}{(R_c + X)} \frac{\partial W'}{\partial \Omega} = 0 \qquad (180)$$

X-momentum equation

$$U_b \frac{\partial U'}{\partial X} + U' \frac{\partial U_b}{\partial X} + \frac{W'}{(R_c + X)} \frac{\partial U_b}{\partial \Omega} + \frac{W_b}{(R_c + X)} \frac{\partial U'}{\partial \Omega} - \frac{2W'W_b}{(R_c + X)}$$

$$= - \frac{1}{\rho} \frac{\partial P'}{\partial X}$$

$$+ \nu\left(\frac{\partial^2 U'}{\partial Y^2} + \frac{1}{(R_c + X)^2} \frac{\partial^2 U'}{\partial \Omega^2} - \frac{\partial^2 V'}{\partial X \partial Y}\right.$$

$$\left. - \frac{1}{(R_c + X)} \frac{\partial^2 W'}{X\, Y} - \frac{1}{(R_c + X)^2} \frac{\partial W'}{\partial \Omega}\right) \qquad (181)$$

Y-momentum equation

$$U_b \frac{\partial V'}{\partial X} + \frac{W_b}{(R_c + X)} \frac{\partial V'}{\partial \Omega} = - \frac{1}{\rho} \frac{\partial P'}{\partial Y}$$

$$+ \nu\left( - \frac{\partial^2 U'}{\partial X \partial Y} - \frac{1}{(R_c + X)} \frac{\partial U'}{\partial Y} + \frac{\partial^2 V'}{\partial X^2}\right.$$

$$\left. + \frac{1}{(R_c + X)} \frac{\partial V'}{\partial X} + \frac{1}{(R_c + X)^2} \frac{\partial^2 V'}{\partial \Omega^2} - \frac{1}{(R_c + X)} \frac{\partial^2 W'}{\partial Y \partial \Omega}\right) \qquad (182)$$

Ω-momentum equation

$$U_b \frac{\partial W'}{\partial X} + U' \frac{\partial W_b}{\partial X} + \frac{W_b}{(R_c + X)} \frac{\partial W'}{\partial \Omega} + W' \frac{\partial U_b}{\partial X} + \frac{U' W_b}{(R_c + X)}$$

$$= - \frac{1}{\rho} \frac{1}{(R_c + X)} \frac{\partial P'}{\partial \Omega}$$

$$+ \nu\left(- \frac{1}{(R_c + X)} \frac{\partial^2 U'}{\partial X \partial \Omega} + \frac{1}{(R_c + X)^2} \frac{\partial U'}{\partial \Omega} - \frac{1}{(R_c + X)} \frac{\partial^2 V'}{\partial Y \partial \Omega}\right.$$

$$\left. + \frac{\partial^2 W'}{\partial X^2} + \frac{1}{(R_c + X)} \frac{\partial W'}{\partial X} - \frac{W'}{(R_c + X)^2} + \frac{\partial^2 W'}{\partial Y^2}\right) \qquad (183)$$

Noting that all the velocity components vanish identically (no slip) on walls, the boundary conditions to be imposed become:

$$U_b = W_b = 0 \quad \text{and} \quad U' = V' = W' = \partial U'/\partial X = 0$$

at $$X = \pm a \qquad (184)$$

At the hydrodynamic entrance, one may impose the following initial conditions for this study,

$$U_b \text{ and } W_b \text{ are given and}$$

$$U' = V' = W' = 0 \quad \text{at} \quad \Omega = 0 \tag{185}$$

For the three-dimensisnal disturbances of the Taylor-Görtler type, one may assume the stationary normal modes of the following form following Smith's work [131]

$$\begin{aligned} U' &= U^*(X) \cos \alpha Y \exp \int \beta(R_c\Omega)d(R_c\Omega) \\ V' &= V^*(X) \sin \alpha Y \exp \int \beta(R_c\Omega)d(R_c\Omega) \\ W' &= W^*(X) \cos \alpha Y \exp \int \beta(R_c\Omega)d(R_c\Omega) \\ P' &= P^*(X) \cos \alpha Y \exp \int \beta(R_c\Omega)d(R_c\Omega) \end{aligned} \tag{186}$$

where the amplitudes of U*, V*, P* are small quantities whose squares and products can be disregarded. The quantities $\alpha$ and $\beta$ are the wave number and the amplification factor, respectively. The above disturbance modes were first introduced by Smith [131] in his study on the growth of Taylor-Görtler vortices along highly concave walls. The vortex is assumed to grow in strength by the factor exp $\int \beta d(R_c\Omega)$, that is, to grow with distance, not time [131]. Further details regarding this growth factor are given by Smith [131].

Introducing equation (186) into disturbance equations (180) to (183), one obtains the following set of ordinary differential

equations for the disturbances after linearization as noted above.

Continuity equation

$$\frac{dU^*}{dX} + \frac{1}{(R_c + X)} U^* + \alpha V^* + \frac{1}{(R_c + X)} (\beta R_c) W^* = 0 \qquad (187)$$

X-momentum equation

$$\nu \frac{d^2U^*}{dX^2} + \left[- U_b + \frac{\nu}{(R_c + X)}\right] \frac{dU^*}{dX}$$

$$+ \left[- \nu\alpha^2 - \frac{\partial U_b}{\partial X} - \frac{(\beta R_c) W}{(R_c + X)} + \frac{(\beta R_c)^2}{(R_c + X)^2}\right.$$

$$\left. + \frac{\nu R_c}{(R_c + X)^2} \frac{d\beta}{d\Omega} - \frac{\nu}{(R_c + X)^2}\right] U^*$$

$$+ \left[\frac{2W}{(R_c + X)} - \frac{1}{(R_c + X)} \frac{\partial U_b}{\partial \Omega} - \frac{2\nu(\beta R_c)}{(R_c + X)^2}\right] W^*$$

$$- \frac{1}{\rho} \frac{dP^*}{dX} = 0 \qquad (188)$$

Y-momentum equation

$$\nu \frac{d^2V^*}{dX^2} + \left[- U_b + \frac{\nu}{(R_c + X)}\right] \frac{dV^*}{dX}$$

$$+ \left[- \nu\alpha^2 - \frac{(\beta R_c)}{(R_c + X)} W + \frac{\nu(\beta R_c)^2}{(R_c + X)^2} + \frac{\nu R_c}{(R_c + X)^2} \frac{d\beta}{d\Omega}\right] V^*$$

$$+ \frac{\alpha}{\rho} P^* = 0 \qquad (189)$$

Ω-momentum equation

$$\nu \frac{d^2W^*}{dX^2} + \left[ - U_b + \frac{\nu}{(R_c + X)} \right] \frac{dW^*}{dX}$$

$$+ \left[ - \nu\alpha^2 - \frac{\partial U_b}{\partial X} - \frac{(\beta R_c)}{(R_c + X)^2} W_b + \frac{\nu(\beta R_c)^2}{(R_c + X)^2} - \frac{\nu}{(R_c + X)^2} \right] W^*$$

$$+ \left[ - \frac{dW_b}{dX} - \frac{W_b}{(R_c + X)^2} + \frac{2\nu(\beta R_c)}{(R_c + X)^2} \right] U^*$$

$$- \frac{1}{\rho} \frac{(\beta R_c)}{(R_c + X)} P^* = 0 \qquad (190)$$

Introducing the following non-dimensional variables

$$U_b = U_m u, \quad W_b = W_m w,$$

$$U^* = [\nu/a]u^*, \quad V^* = [\nu/a]v^*, \quad W^* = [\nu/a]w^*,$$

$$P^* = P_c{}^* p^*, \quad \lambda = a/R_c, \quad X = ax,$$

$$R_c\Omega = R_c\Omega_c\omega, \quad \beta = B/R_c, \quad \alpha = A/(2a),$$

and Reynolds number $Re = W_m(2a)/\nu$, the perturbation equations (187) to (190) become

Continuity equation

$$\frac{du^*}{dx} + \frac{\lambda}{(1 + \lambda x)} u^* + \frac{A}{2} v^* + B \frac{\lambda}{(1 + \lambda x)} w^* = 0 \qquad (191)$$

X-momentum equation

$$\frac{d^2u^*}{dx^2} + \left(- u + \frac{\lambda}{(1 + \lambda x)}\right) \frac{du^*}{dx}$$

$$+ \left(B^2 \frac{\lambda^2}{(1 + \lambda x)^2} - \frac{A^2}{4} - \frac{\lambda^2}{(1 + \lambda x)^2} - \frac{BRe}{2} \frac{\lambda}{(1 + \lambda x)} w\right.$$

$$\left. - \frac{\partial u}{\partial x} + \frac{\lambda^2}{(1 + \lambda x)^2} \frac{dB}{d\omega}\right) u^*$$

$$+ \left(- 2Re^{-1}\lambda^{-1} \frac{\lambda}{(1 + \lambda x)} \frac{\partial u}{\partial \omega} + Re \frac{\lambda}{(1 + \lambda x)} w - 2B\lambda \frac{\lambda}{(1 + \lambda x)}\right)w^*$$

$$- \left[\frac{P_c^*}{\rho} \frac{a^2}{\nu^2}\right] \frac{dp^*}{dx} = 0 \qquad (192)$$

Y-momentum equation

$$\frac{d^2v^*}{dx^2} + \left(- u + \frac{\lambda}{(1 + \lambda x)}\right) \frac{dv^*}{dx}$$

$$+ \left(B^2 \frac{\lambda^2}{(1 + \lambda x)^2} - \frac{A^2}{4} - \frac{BRe}{2} \frac{\lambda}{(1 + \lambda x)} w\right.$$

$$\left. + \frac{\lambda^2}{(1 + \lambda x)^2} \frac{dB}{d\omega}\right)v^*$$

$$+ \left[\frac{P_c^* a^2}{\rho \nu^2}\right] \frac{Ap^*}{2} = 0 \qquad (193)$$

Ω-momentum equation

$$\frac{d^2w^*}{dx^2} + \left(-u + \frac{\lambda}{(1+\lambda x)}\right)\frac{dw^*}{dx}$$

$$+ \left(B^2\frac{\lambda^2}{(1+\lambda x)^2} - \frac{A^2}{4} - \frac{\lambda^2}{(1+\lambda x)^2} - \frac{BRe}{2}\frac{\lambda}{(1+\lambda x)}w - \frac{\partial u}{\partial x}\right)w^*$$

$$+ \left(2B\frac{\lambda^2}{(1+\lambda x)^2} - \frac{Re}{2}\frac{\partial w}{\partial x} - \frac{Re}{2}\frac{\lambda}{(1+\lambda x)}w\right)u^*$$

$$- \left[\frac{P_c^* a^2}{\rho\nu^2}\right] B\frac{\lambda}{(1+\lambda x)}p^* = 0 \qquad (194)$$

For neutral stability, one may set B = 0 and the perturbation equations reduce to

Continuity equation

$$\frac{du^*}{dx} + \frac{\lambda}{(1+\lambda x)}u^* + \frac{A}{2}v^* = 0 \qquad (195)$$

X-momentum equation

$$\frac{d^2u^*}{dx^2} + \left(-u + \frac{\lambda}{(1+\lambda x)}\right)\frac{du^*}{dx}$$

$$+ \left(-\frac{A^2}{4} - \frac{\partial u}{\partial x} - \frac{\lambda^2}{(1+\lambda x)^2}\right)u^*$$

$$+ \left(-2Re^{-1}\lambda^{-1}\frac{\lambda}{(1+\lambda x)}\frac{\partial u}{\partial \omega} + Re\frac{\lambda}{(1+\lambda x)}w\right)w^*$$

$$+ \left[\frac{P_c^* a^2}{\rho \nu^2}\right] \frac{dp^*}{dx} = 0 \qquad (196)$$

Y-momentum equation

$$\frac{d^2 v^*}{dx^2} + \left(- u + \frac{\lambda}{(1 + \lambda x)}\right) \frac{dv^*}{dx} - \frac{A^2}{4} v^*$$

$$+ \frac{A}{2} \left[\frac{P_c^* a^2}{\rho \nu^2}\right] p^* = 0 \qquad (197)$$

Ω-momentum equation

$$\frac{d^2 w^*}{dx^2} + \left(- u + \frac{\lambda}{(1 + \lambda x)}\right) \frac{dw^*}{dx}$$

$$+ \left(- \frac{A^2}{4} - \frac{\partial u}{\partial x} - \frac{\lambda^2}{(1 + \lambda x)^2}\right) w^*$$

$$+ \left(- \frac{Re}{2} \frac{\partial w}{\partial x} - \frac{Re}{2} \frac{\lambda}{(1 + \lambda x)} w\right) u^* = 0 \qquad (198)$$

It is seen that the independent parameters are A, Re, and $\lambda$. However, for convenience, the wave number A, Dean number $K \equiv Re(a/R_c)^{1/2}$ and the curvature ratio $\lambda = a/R_c$ will be used. For the purpose of carrying out the numerical solution, the above set of four perturbation equations will next be reduced to a pair of simultaneous equations. This can be achieved by eliminating v* from the momentum equation (197) by using the continuity equation (195). Eliminating further the pressure terms betweem the X- and Y-momentum equations (196) and (197), one obtains a pair of simultaneous equations for the neutral stability as,

$$\frac{d^4u^*}{dx^4} + \left[-u + 2\frac{\lambda}{(1+\lambda x)}\right]\frac{d^3u^*}{dx^3}$$

$$+ \left[-\frac{A^2}{2} - \frac{\partial u}{\partial x} - u\frac{\lambda}{(1+\lambda x)} - 3\frac{\lambda^2}{(1+\lambda x)^2}\right]\frac{d^2u^*}{dx^2}$$

$$+ \left[\frac{A^2}{4}u + \left(-\frac{A^2}{2} - \frac{\partial u}{\partial x}\right)\frac{\lambda}{(1+\lambda x)} + 2u\frac{\lambda^2}{(1+\lambda x)^2} + 3\frac{\lambda^3}{(1+\lambda x)^3}\right]\frac{du^*}{dx}$$

$$+ \left[\frac{A^4}{16} + \frac{A^2}{4}\frac{\partial u}{\partial x} + \left(\frac{A^2}{2} + \frac{\partial u}{\partial x}\right)\frac{\lambda^2}{(1+\lambda x)^2}\right.$$

$$\left. - 2u\frac{\lambda^3}{(1+\lambda x)^3} - 3\frac{\lambda^4}{(1+\lambda x)^4}\right]u^*$$

$$= \left[-\frac{A^2}{2}K^{-1}\lambda^{-1/2}\frac{\lambda}{(1+\lambda x)}\frac{\partial u}{\partial \omega}\right.$$

$$\left. + \frac{A^2}{4}K\lambda^{-1/2}\frac{\lambda}{(1+\lambda x)}w\right]w^* \qquad (199)$$

$$\frac{d^2w^*}{dx^2} + \left[-u + \frac{\lambda}{(1+\lambda x)}\right]\frac{dw^*}{dx}$$

$$+ \left[-\frac{A^2}{4} - \frac{\partial u}{\partial x} - \frac{\lambda^2}{(1+\lambda x)^2}\right]w^*$$

$$= \left[\frac{1}{2}K\lambda^{-1/2}\frac{\lambda}{(1+\lambda x)}w + \frac{1}{2}K\lambda^{-1/2}\frac{\partial w}{\partial x}\right]u^* \qquad (200)$$

The boundary conditions at the wall are

$$u^* = w^* = du^*/dx = 0$$

and $$u = w = 0 \quad \text{at} \quad x = \pm 1 \tag{201}$$

The initial conditions are

$$u^* = w^* = 0 \tag{202}$$

The above differential system represents an eigenvalue problem and the solution of which will result in a fundamental relationship between the Dean number K and the wave number A for a given curvature ratio $\lambda$. Equation (199) shows that the transverse disturbance $u^*$ is caused by the centrifugal effect as represented by the term involving $ww^*$ and the axial velocity grandient effect of the basic transverse velocity u through the product $(\partial u/\partial \omega)\cdot w^*$. On the other hand, the axial disturbance $w^*$ is caused by the velocity gradient $(\partial w/\partial x)$ in the transverse direction through the product $(\partial w/\partial x)\cdot u^*$ and the Coriolis effect through the product $wu^*$. The latter effect is seen to be of secondary importance. Of course, the two equations for perturbation velocities $u^*$ and $w^*$ are coupled.

The neutral stability for the case of a fully developed basic flow is of particular interest here since the numerical result will be sought for this limiting case only in this investigation. It is noted that for the fully developed basic flow, the secondary velocity u vanishes and consequently, the terms $\partial u/\partial x$, $\partial u/\partial \omega$ also vanish. The neutral stability equations for the fully developed basic flow then become

$$\frac{d^4u^*}{dx^4} + \frac{2\lambda}{(1 + \lambda x)} \frac{d^3u^*}{dx^3}$$

$$+ \left[- \frac{A^2}{2} - 3 \frac{\lambda^2}{(1 + \lambda x)^2}\right] \frac{d^2u^*}{dx^2}$$

$$+ \left[- \frac{A^2}{2} \frac{\lambda}{(1 + \lambda x)} + 3 \frac{\lambda^3}{(1 + \lambda x)^3}\right] \frac{du^*}{dx}$$

$$+ \left[\frac{A^4}{16} + \frac{A^2}{2} \frac{\lambda^2}{(1 + \lambda x)^2} - 3 \frac{\lambda^4}{(1 + \lambda x)^4}\right] u^*$$

$$= \frac{A^2}{4} K\lambda^{-1/2} \frac{\lambda}{(1 + \lambda x)} ww^* \tag{203}$$

$$\frac{d^2w^*}{dx^2} + \frac{\lambda}{(1 + \lambda x)} \frac{dw^*}{dx} + \left[- \frac{A^2}{4} - \frac{\lambda^2}{(1 + \lambda x)^2}\right] w^*$$

$$= \left[\frac{1}{2} K\lambda^{-1/2} \frac{\lambda}{(1 + \lambda x)} w + \frac{1}{2} K\lambda^{-1/2} \frac{\partial w}{\partial x}\right] u^* \tag{204}$$

It is recalled that Dean's instability problem [126] assumes a small curvature ratio $\lambda << 1$ and a plane Poiseuille profile for the basic flow neglecting altogether the curvature effect. For reference purposes, the simplified set of perturbation equations negelecting the curvature effect is given below as,

$$(D^2 - \frac{A^2}{4})^2 u^+ = \frac{A^2}{4} K^2 \frac{3}{2} (1 - x^2) w^* \tag{205}$$

$$(D^2 - \frac{A^2}{4})^2 w^* = - \frac{3}{2} x u^+ \tag{206}$$

The boundary conditions are reduced to

$$u^+ = w^* = du^+/dx = u = w = 0 \quad \text{at } x = \pm 1 \tag{207}$$

where $D^2 = d^2/dx^2$, $u^+ = K\lambda^{-1/2}u^*$

and the fully developed parabolic velocity profile is $w = (3/2)(1 - x^2)$. In the above formulation following Dean's earlier work [126], the only parameters are seen to be Dean number K and the wave number A. It is noted that the above linearized disturbance equations correspond to the equations (7) and (8) given by Reid [128]. It is instructive to note that the term on the right-hand side of equation (205) represents the centrifugal force effect and is balanced by the viscous terms. In equation (206), the right-hand side term represents the inertia force effect $u^+(\partial w/\partial x)$ which is caused by the coupled effect of transverse disturbance velocity $u^+$ and the transverse gradient of basic velocity and is seen to be balanced by the viscous terms.

## 7.3 NUMERICAL METHOD OF SOLUTION

It is apparently not practical to seek an analytical solution for the pair of disturbance differential equations (199) and (200) since an analytical solution for the entry flow problem in a curved parallel-plate channel is not available. In the present investigation, a finite-difference technique will be employed. By applying the five-point central-difference approximations (see Fig. 92) and using the dummy variables f and g for the disturbances u* and w* or w* and u*, respectively, one obtains the following set of algebraic equations applicable to both equations (199) and (200).

$$\begin{bmatrix} B_2 & C_2 & D_2 & E_2 & F_2 & & & & \\ A_3 & B_3 & C_3 & D_3 & E_3 & & & 0 & \\ & A_4 & B_4 & C_4 & D_4 & E_4 & & & \\ & & \cdots & \cdots & & & & & \\ & & & A_i & B_i & C_i & D_i & E_i & \\ & & & & \cdots & \cdots & & & \\ 0 & & & & A_{M-2} & B_{M-2} & C_{M-2} & D_{M-2} & E_{M-2} \\ & & & & & A_{M-1} & B_{M-1} & C_{M-1} & D_{M-1} & E_{M-1} \\ & & & & & F_M & A_M & B_M & C_M & D_M \end{bmatrix} \begin{bmatrix} f_2 \\ f_3 \\ f_4 \\ \cdot \\ f_i \\ \cdot \\ f_{M-2} \\ f_{M-1} \\ f_M \end{bmatrix} = \begin{bmatrix} g_2 \\ g_3 \\ g_4 \\ \cdot \\ g_i \\ \cdot \\ g_{M-2} \\ g_{M-1} \\ g_M \end{bmatrix} \quad (208)$$

It is noted that in the case of equation (199), one has $f_i = u_i^*$ and $g_i = w_i^*$ with the elements of the coefficient matrix given as

$$A_i = [\frac{1}{h^4} - \frac{1}{2h^3}(u_i + \frac{2\lambda}{(1+\lambda x)})$$

$$- \frac{1}{12h^2}(\frac{A^2}{2} + (\frac{\partial u}{\partial x})_i - \frac{\lambda}{(1+\lambda x)} u_i - 3\frac{\lambda^2}{(1+\lambda x)^2})$$

$$+ \frac{1}{12h^2}(-(\frac{\partial u}{\partial x})_i \frac{\lambda}{(1+\lambda x)} + \frac{A^2}{2}\frac{\lambda}{(1+\lambda x)} + \frac{2\lambda^2}{(1+\lambda x)^2} u_i$$

$$+ \frac{3\lambda^3}{(1+\lambda x)^3} - \frac{A^2}{4} u_i)]/\alpha_i$$

$$B_i = [-\frac{4}{h^4} + \frac{1}{h^3}(-u_i + \frac{2\lambda}{(1+\lambda x)})$$

$$+ \frac{4}{3h^2}\left(\frac{A^2}{2} + \left(\frac{\partial u}{\partial x}\right)_i - \frac{\lambda}{(1+\lambda x)} u_i - \frac{3\lambda^2}{(1+\lambda x)^2}\right)$$

$$- \frac{2}{3h}\left(-\left(\frac{\partial u}{\partial x}\right)_i \frac{\lambda}{(1+\lambda x)} + \frac{A^2}{2}\frac{\lambda}{(1+\lambda x)} + \frac{2\lambda^2}{(1+\lambda x)^2} u_i\right.$$

$$\left. + \frac{3\lambda^3}{(1+\lambda x)^3} - \frac{A^2}{4} u_i\right)]/\alpha_i$$

$$C_i = \left[\frac{6}{h^4} - \frac{1}{4h^2}\left(\frac{A^2}{2} + \left(\frac{\partial u}{\partial x}\right)_i - \frac{\lambda}{(1+\lambda x)} u_i - \frac{3\lambda^2}{(1+\lambda x)^2}\right)\right.$$

$$+ \left(-\frac{3\lambda^4}{(1+\lambda x)^4} - \frac{2\lambda^3}{(1+\lambda x)^3} u_i - \frac{A^2}{2}\frac{\lambda^2}{(1+\lambda x)^2}\right.$$

$$\left. + \frac{\lambda^2}{(1+x)^2}\left(\frac{\partial u}{\partial x}\right)_i - \frac{A^2}{4}\left(\frac{\partial u}{\partial x}\right)_i + \frac{A^4}{16}\right)]/\alpha_i$$

$$D_i = \left[-\frac{4}{h^4} - \frac{1}{h^3}\left(-u_i + \frac{2\lambda}{(1+\lambda x)}\right)\right.$$

$$+ \frac{4}{3h^2}\left(\frac{A^2}{2} + \left(\frac{\partial u}{\partial x}\right)_i - \frac{\lambda}{(1+\lambda x)} u_i - \frac{3\lambda^2}{(1+\lambda x)^2}\right)$$

$$+ \frac{2}{3h}\left(-\left(\frac{\partial u}{\partial x}\right)_i \frac{\lambda}{(1+\lambda x)} + \frac{A^2}{2}\frac{\lambda}{(1+\lambda x)} + \frac{2\lambda^2}{(1+\lambda x)}\right] u_i$$

$$\left. + \frac{3\lambda^3}{(1+\lambda x)^3} - \frac{A^2}{4} u_i\right)]/\alpha_i$$

$$E_i = [\frac{1}{h^4} + \frac{1}{2h^3}(- u_i + \frac{2\lambda}{(1+\lambda x)})$$

$$- \frac{1}{12h^2}(\frac{A^2}{2} + (\frac{\partial u}{\partial x})_i - \frac{\lambda}{(1+\lambda x)} u_i - \frac{3\lambda^2}{(1+\lambda x)^2})$$

$$- \frac{1}{12h}(- (\frac{\partial u}{\partial x})_1 \frac{\lambda}{(1+\lambda x)} + \frac{A^2}{2}\frac{\lambda}{(1+\lambda x)} + \frac{2\lambda^2}{(1+\lambda x)^2} u_i$$

$$+ \frac{3\lambda^3}{(1+\lambda x)^3} - \frac{A^2}{4} u_i)]/\alpha_i \qquad (209)$$

where $\alpha_i = \frac{A^2}{2}\frac{\lambda}{(1+\lambda x)} \lambda^{-1/2} (- K^{-1}(\frac{\partial u}{\partial \omega})_i + \frac{1}{2} K w_i)$

On the other hand, for equation (200), one has $f_i = w_i^*$ and $g_i = u_i^*$ with the elements of the coefficient matrix given by,

$$A_i = [- \frac{1}{12h^2} + \frac{1}{12h}(\frac{\lambda}{(1+\lambda x)} - u_i]/\beta_i$$

$$B_i = [\frac{4}{3h^2} - \frac{2}{2h}(\frac{\lambda}{(1+\lambda x)} - u_i]/\beta_i$$

$$C_i = [- \frac{1}{4h^2} + (- \frac{\lambda^2}{(1+\lambda x)^2} + A^2 + (\frac{\partial u}{\partial x})_i]/\beta_i$$

$$D_i = [\frac{4}{3h^2} + \frac{2}{3h}(\frac{\lambda}{(1+\lambda x)} - u_i)]/\beta_i$$

$$E_i = [- \frac{1}{12h^2} - \frac{1}{12h}(\frac{\lambda}{(1+\lambda x)} - u_i)]/\beta_i \qquad (210)$$

where $$\beta_i = \frac{1}{2} K\lambda^{-1/2}\left(\left(\frac{\partial w}{\partial x}\right)_i + \frac{\lambda}{(1+\lambda x)} w_i\right)$$

It is noted that the elements along the first and the last rows of the coefficent matrix in equation (208) are obtained after applying the boundary conditions given by equation (201). The numerical values for $u_i$, $w_i$, $(\partial u/\partial x)_i$, $(\partial u/\partial \omega)_i$ and $(\partial w/\partial x)_i$ are available, for example, from the numerical solution obtained in Chapter VI for the developing main flow.

In order to illustrate the numerical method of solution for the present eigenvalue problem, the two systems of algebraic equations arising after applying finite-difference approximations for a pair of simultaneous differential equations (199) and (200) will be cast into the following forms by introducing the coefficient matrices L and N.

$$L\,\bar{u}^* = \bar{w}^*$$

$$N\,\bar{w}^* = \bar{u}^*$$

where $\bar{u}^*$ and $\bar{w}^*$ denote the column vectors consisting of $u_i^*$ and $w_i^*$, respectively, When one eliminates $\bar{u}^*$ from the above equations, one obtains

$$(LN - I)\bar{w}^* \equiv D\bar{w}^* = 0 \qquad (211)$$

where I is a $(M-1) \times (M-1)$ unit matrix. It is seen that equation (211) represents $(M-1)$ linear, homogeneous algebraic equations for

(M - 1) unknowns $\overline{w}_i^*$ (i = 2, 3 ... M). Solution of such an algebraic system is possible only if the determinant |D| for the coefficient matrix D vanishes.

$$|D| = 0$$

The elements of the determinant |D| are denoted by $d_{i,j}$ (i = 2, 3 ... M, j = 2, 3 ... M). The value of the determinant depends upon three parameters--the Dean number K, the wave number A, and the curvature ratio $\lambda$. When the curvature ratio is held fixed, then for each and every value of A which one might select, a Dean number that causes the determinant of the coefficient matrix to be zero can be found. In particular one is interested in finding a minimum Dean number which permits a solution of the disturbance equations. Below this Dean number, a solution cannot be found and this implies that the primary (or basic) flow is stable. It is then clear that the aforementioned minimum Dean number corresponds to the onset of instability. This is generally called the critical Dean number. The numerical computations which are required to find the critical Dean number are effected by the following computational procedure:

1. For a given value of curvature ratio $\lambda$, assign a value for the wave number A. The main flow field quantities such as $u_i$, $w_i$, $(\partial u/\partial x)_i$, $(\partial u/\partial \omega)_i$ and $(\partial w/\partial x)_i$ are assumed to be already known.

2. Two initial values for the Dean number $K_1$ and $K_2$ are assigned and the value for the determinant $|D(K_1)|$ and $|D(K_2)|$ are evaluated

by using Gaussian elimination [132].

3. Compute a successive improved approxiamtion for the eigenvalue $K_{n+1}$ using the following iteration formula for the secant method [133].

$$K_{n+1} = K_n - \frac{(K_n - K_{n-1})}{[|D(K_n)| - |D(K_{n+1})|]} \cdot |D(K_n)| \qquad (212)$$

4. The above process will be repeated until the following convergence condition is satisfied.

$$\frac{|K_{n+1} - K_n|}{|K_n|} \leq \varepsilon = 10^{-5} \qquad (213)$$

It is noted that the process of finding the critical eigenvalue $K_c$ can be facilitated by starting with a pair of initial values $K_1$, $K_2$ which are higher than the sought critical value $K_c$ and another pair of initial values $K_1'$, and $K_2'$ which are lower than the critical value. In order to obtain a result with high accuracy, the individual elements of the determinant $|D|$ may be divided by a constant $\gamma$ in the initial scaling such that

$$\max [d_{i,j}/\gamma] = c$$

where the constant c can be taken to be unity. However, for the present problem, the value c is chosen arbitrarily but a fixed constant value is used throughout the computational steps 1 to 4. It is found that the values of the determinant consisting of the

elements ($d_{i,j}/\gamma$) are bounded with $\pm 10^{+3}$. In carrying out the Gussian elimination, pivotal condensation [134] is applied. According to Wilkinson [135], and Forsythe and Moler [136], the computational procedure involving the initial scaling of the elements of the determinant and partial pivoting [137] during Gaussian elimination tends to suppress the growth of round-off errors.

It is noted that the present computational procedure and the developed computer program are applicable to the hydrodynamic instability problem in a curved parallel-plate channel. However, the numerical results are obtained only for the fully developed flow regime. It is also noted that the disturbance components can be obtained by using an iteration procedure [137] but no attempt was made to obtain the disturbance profiles in this study. The present study is concerned with the onset of the primary mode of disturbances but the second and higher modes may be of theoretical interest.

Since the accuracy of the numerical results depends on the mesh size, the effect of the mesh size on the accuracy of the eigenvalue $K_c$ will be examined in some detail. Disregarding the round-off error, the exact value of the eigenvalue corresponding to given values of the curvature ratio $\lambda$ and wavenumber A can be approached only when the mesh size h approaches zero. However, in practice the mesh size can be chosen small enough to achieve a reasonable accuracy for practical purposes.

For a given finite-difference approximation, the truncation error is known. For example, for the present finite-difference

approximation, the truncation error is of order $h^2$. If it is assumed that the numerical error is mainly due to the truncation error, then the effect of truncation error $h^2$ on the computation of the eigenvalue $K_c$ may be of interest. The results of numerical experiment are plotted in Fig. 93 where the effects of the mesh size M, the square of the grid size $h^2_M$ and $(h_M/h_{20})^2$ on the numerical values of the eigenvalue $K_c$ and the relative errors $[(K_{c,M} - K_{c,20})/K_{c,20}] \times 100$ are clearly shown for $\lambda = 0.01$. The relationship for $M \geq 20$ is seen to be linear. It is noted that when a mesh size $M = 10$ is used, the eigenvalue $K_c$ is found to be well below the value obtained by a linear extrapolation of the result shown in Fig. 93. On the other hand, when the mesh size h is extrapolated to zero, the critical Dean number $K_c$ is found to be 25.03 as compared to the value of 24.983 for $h = 0.025$ (or $M = 40$). Thus if one may allow for an error of 0.1 per cent, the mesh size $M = 40$ is seen to be satisfactory.

Although one may obtain the critical Dean number $K_c$ by the aforementioned extrapolation method, the corresponding wave-number A is clearly no longer the pre-assigned value. The above observation is confirmed by examining the numerical results for the critical Dean number $K_c$ and the corresponding critical wavenumber $A_c$ for various mesh sizes with a given curvature ratio. For example, with $\lambda = 0.01$, the critical values are $K_c = 24.909$, $A_c = 3.96$ for $M = 20$ and $K_c = 24.974$, $A_c = 3.90$ for $M = 40$. The difference between the two values for wavenumber $A_c$ is found to be 1.5 per cent based

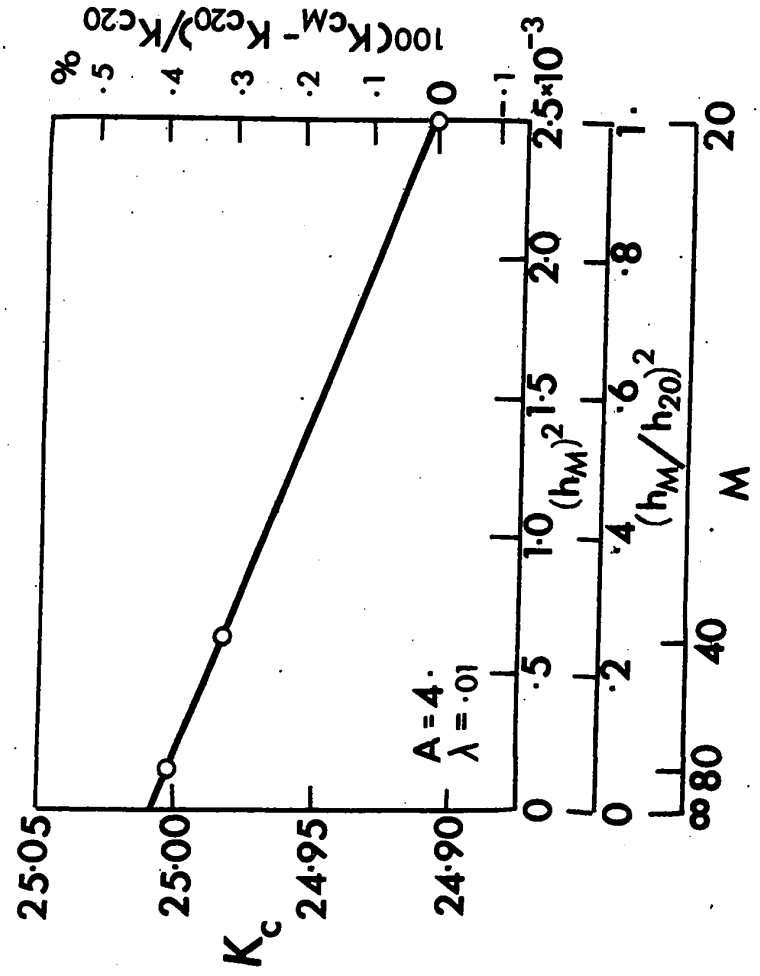


Fig. 93 Effect of Mesh Size on Critical Dean Number $K_c$ with $A = 4$ and $\lambda = 0.01$

on the value for M = 40. On the other hand, with M = 80 the difference is found to be 0.2 per cent based on the value for M = 40. From the viewpoint of computing time, the mesh size M = 40 is clearly a proper choice. For this reason, most of the numerical results are obtained using M = 40 but the mesh size M = 80 is also used in assessing the curvature effect.

The computing time required in obtaining a critical value for the Dean number $K_c$ with given $\lambda$ and A is usually 15 to 20 minutes for M = 40. The required time depends on the initial guess for $K_c$.

## 7.4 STABILITY RESULTS AND DISCUSSION

The onset of the hydrodynamic instability in the form of Taylor-Görtler vortices is studied for the fully developed laminar flow in curved parallel-plate channels with the curvature ratios $\lambda = 10^{-10}$, $10^{-2}$, $10^{-1}$, and 0.5. The curvature effect is included in the formulation for both basic and perturbed flows. The numerical results for critical Dean number $K_c$ and wavenumber $A_c$ marking the onset of instability are presented in Table 8 with $\lambda = 10^{-10}$ for the perturbation equations and using a parabolic basic flow profile ($\lambda = 0$).

TABLE 8

NEUTRAL STABILITY RESULTS

| Wavenumber A | Critical Dean Number $K_c$ Present Work[1] | Reid [128] Orthogonal Functions | Fourier Series | Hämmerlin [129] |
|---|---|---|---|---|
| 0 | - | ∞ | | |
| 0.5 | 110.78 | 110.31 | | |
| 1.0 | 57.198 | 57.21 | | |
| 1.5 | 40.953 | 40.57 | | |
| 2.0 | 32.090 | 32.82 | | |
| 2.5 | 28.276 | 28.87 | | |
| 3.0 | 26.010 | 26.81 | | 26.541 |
| 3.5 | 25.395 | 25.87 | | |
| 3.9 | 25.319 | 25.684 | 25.234[2] | |
| 3.96 | 25.313 | - | 25.410 | |
| 4.0 | 25.351 | 25.698 | 25.413 | 25.254 |
| 4.1 | 25.386 | 25.734 | 25.247[2] | |
| 4.5 | - | 26.09 | | |
| 5.0 | 26.307 | 26.88 | | 26.226 |
| 5.5 | - | 28.04 | | |
| 6.0 | 28.858 | 29.52 | | |
| 7.0 | - | 33.21 | | |
| 8.0 | 33.714 | 37.83 | | |
| 9.0 | - | 43.31 | | |
| 10.0 | 39.951 | | | |
| 16.0 | 70.569 | | | |
| 32.0 | 239.240 | | | |
| ∞ | - | ∞ | | |

Note: 1. $\lambda = 10^{-10}$ for perturbation equations and $\lambda = 0$ for main flow.

2. 1st approximation [128]

Reid's numerical results [128] based on two approximate methods of solution using an expansion in orthogonal functions and a Fourier expansion are also listed for comparison. In addition, Hämmerlin's results [129] are also included. With $\lambda = 10^{-10}$ for the perturbation equations (203) and (204)and using the parabolic basic velocity profile, the Dean number K and wavenumber A become the only parameters and the curvature effect disappears. This situation corresponds to the case governed by perturbation equations (205) and (206) and the problem reduces to the instability problem solved by Dean [126], Reid [128] and Hämmerlin [129]. The values for critical Dean number $K_c$ and vavenumber $A_c$ from this work ($\lambda = 10^{-10}$ for the perturbation equations and using a parabolic basic velocity profile) agrees very well with Reid's results which in turn are known to agree excellently with Dean's results. The agreement may serve to confirm the accuracy of the present numerical results.

The neutral stability curves from this work and Reid's results are shown in Fig. 94 for comparison. The agreement is seen to be excellent except for the region with larger values of A where Reid's appro imate solution is believed to be the source of the discrepancy. The main interest here is the minimum critical Dean number and the corresponding wavenumber. The numerical results are compared against those of Dean [126], Reid [128] and Hämmerlin [129] in Table 9. The agreement is again seen to be very good.

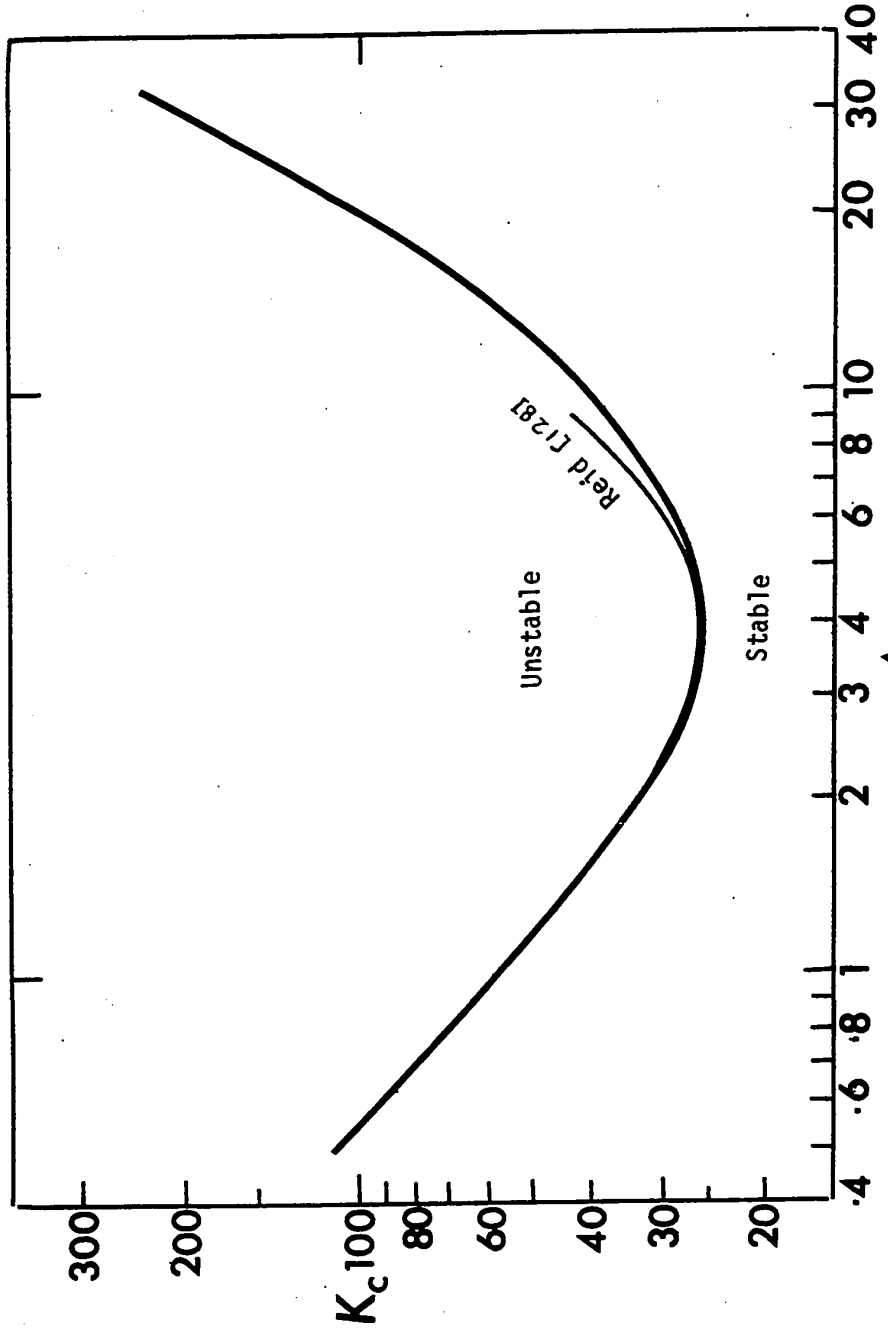


Fig. 94 Neutral Stability Curve for Small Curvature Ratio

TABLE 9

Minimum Critical Dean Number $K_c$
and Critical Wave Number $A_c$

| | Critical Dean Number $K_c$ | Critical Wavenumber $A_c$ |
|---|---|---|
| Present Work* | 25.313 | 3.960 |
| Dean [126] | 25.42 | 3.954 |
| Reid [128] | | |
| Orthogonal Functions | 25.683 | 3.889 |
| Fourier Series | 25.291 | 3.963 |
| Hämmerlin [129] | 25.254 | 4.00 |

*$\lambda = 10^{-10}$ for perturbation equations and $\lambda = 0$ for main flow.

The effects of curvature ratio $\lambda$ on neutral stability results are of considerable theoretical and practical interest. The numerical results for $\lambda = 0.01$, and 0.5 are listed in Table 10 and are presented graphically in Fig. 95. It is noted here that the neutral stability results with $\lambda = 10^{-10}$ for the perturbation equation and $\lambda = 0$ for the basic flow almost coincide with those of $\lambda = 10^{-2}$.

TABLE 10

Curvature Ratio Effect

On Neutral Stability Results

| Wavenumber A | Critical Dean Number $K_c$ Curvature Ratio $\lambda$ | | |
|---|---|---|---|
| | 0.01 | 0.1 | 0.5 |
| 2.0 | 31.907 | - | 18.400 |
| 3.0 | 26.083 | 22.801 | 17.000 |
| 3.5 | - | 22.316 | 16.646 |
| 3.8 | 24.987 | 22.249 | 16.650 |
| 3.9 | 24.974 | 22.250 | 16.682 |
| 3.96 | 24.977 | 22.251 | 16.731 |
| 4.0 | 24.983 | 22.252 | 16.743* |
| 4.1 | 25.013 | 22.253 | 16.751 |
| 4.5 | - | 22.321 | 16.824 |
| 5.0 | 26.051 | 22.653 | 16.901 |
| 6.0 | 28.448 | 24.001 | 17.602 |
| 8.0 | 33.302 | 26.756 | 20.073 |
| 10.0 | 39.214 | 29.767 | 23.204 |

* The critical value based on a parabolic velocity profile for main flow is 18.50.

It is useful to recall again that the curvature effects in the basic and disturbance equations and the effects show up in two

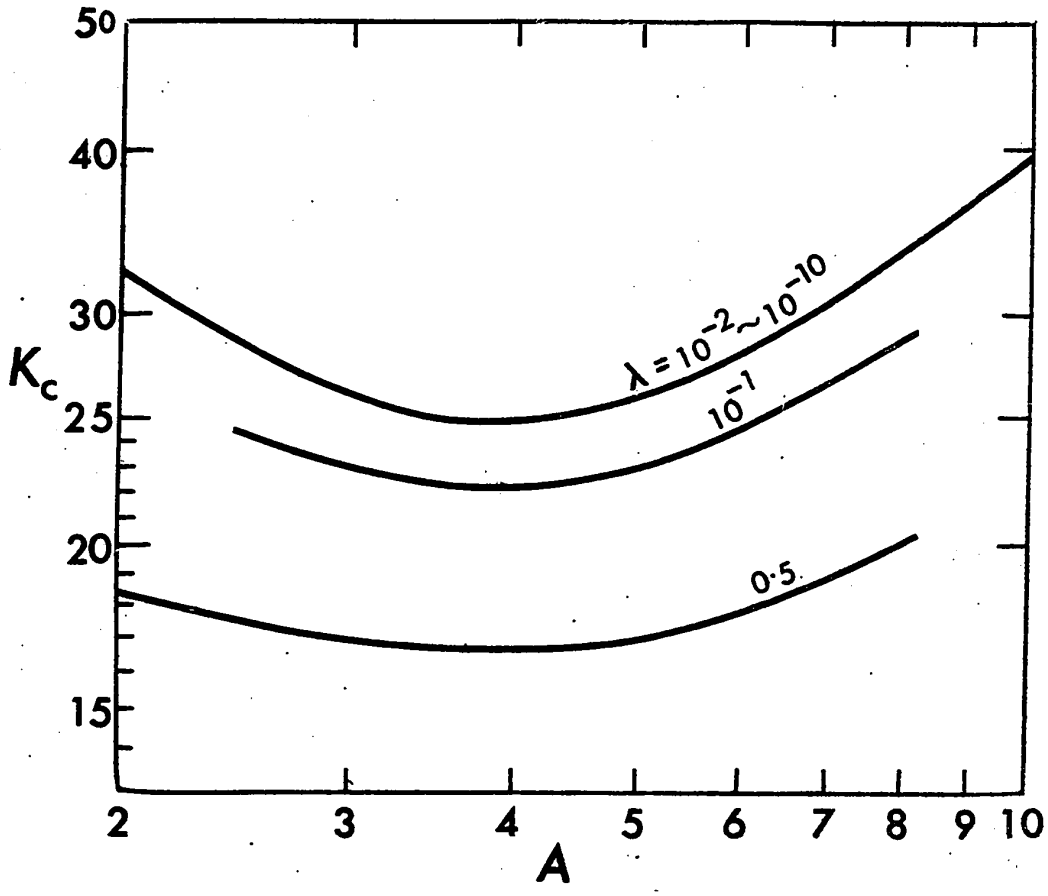


Fig. 95 Effect of Curvature Ratio $\lambda$ on Critical Dean Number $K_c$

different ways. As shown in Chapter VI, the curvature effect tends to distort the fully developed main flow profile from the plane Poiseuille one and shift the location of maximum velocity away from the centerline towards the inner wall. Considering the transverse distributions of centrifugal forces and pressure gradient $\partial P_b/\partial X$, one can readily understand that the curvature effect contributes to the increase of the unstable region near the concave outer wall. Another effect of curvature ratio $\lambda$ on the present neutral stability problem appears in the perturbation equations as can be seen from equations (203) and (204).

With $\lambda = 0.01$, the deviation of the numerical results for the neutral stability from those with $\lambda = 10^{-10}$ is found to be within 1.5 per cent for $K_c$. Considering a possible numerical error due to the method used, one may conclude that the curvature effect may be practically neglected when $\lambda \leq 0.01$.

At $\lambda = 0.1$, the curvature effect becomes significant as shown in Fig. 95. The neutral stability curve for $\lambda = 0.1$ is seen to be generally about 10 per cent lower than that of $\lambda = 0.01$. With the curvature ratio $\lambda = 0.5$, the neutral stability curve is seen to be markedly lower than that of $\lambda = 0.01$. In Table 10, the critical value of Dean number K for $\lambda = 0.5$ and $A = 4.0$ based on a parabolic basic velocity profile is given as 18.50 which is about 10 per cent higher than the value of 16.743 obtained considering the curvature effects for both the basic and perturbed flow. From an inspection of Table 10, it is seen that as the curvature ratio $\lambda$ increases, the

value of the wavenumber corresponding to the minimum critical Dean number decreases.

Finally the question regarding the priority for the onset of Taylor - Görtler longitudinal vortices over that of Tollmien-Schlicting waves in a curved parallel-plate channel is of considerable practical importance. Noting that $K_c = Re_c\lambda^{1/2}$, the numerical values for the critical Reynolds number $Re_c$ may be computed readily from the neutral stability results for a given curvature ratio $\lambda$. The neutral stability results for the Reynolds number are plotted in Fig. 96 with curvature ratio $\lambda$ as parameter. The critical value of the Reynolds number based on Tollmien-Schlichting type instability for the fully developed laminar flow in a straight parallel-plate channel is also indicated by a dashed line in Fig. 96 for comparison. The critical values given by Kin [138] and Chen [139] are also noted there. It is noted that the Reynolds number is based on the channel width and mean velocity i.e. $Re = W_m(2a)/\nu$.

From an inspection of the figure, it is seen that the Taylor-Görtler longitudinal vortices have a priority of occurence over that of Tollmien-Schlichting travelling waves even in a slightly curved parallel-plate channel such as $\lambda = 10^{-4}$ with fully developed laminar flow. The implication here is that even with a very small curvature ratio $\lambda$, the possibility for the occurence of Taylor-Görtler vortices should be examined. The above conclusion is based on the assumption that the Tollmien-Schlichting type instability is not influenced by the curvature effect. Apparently, the extension

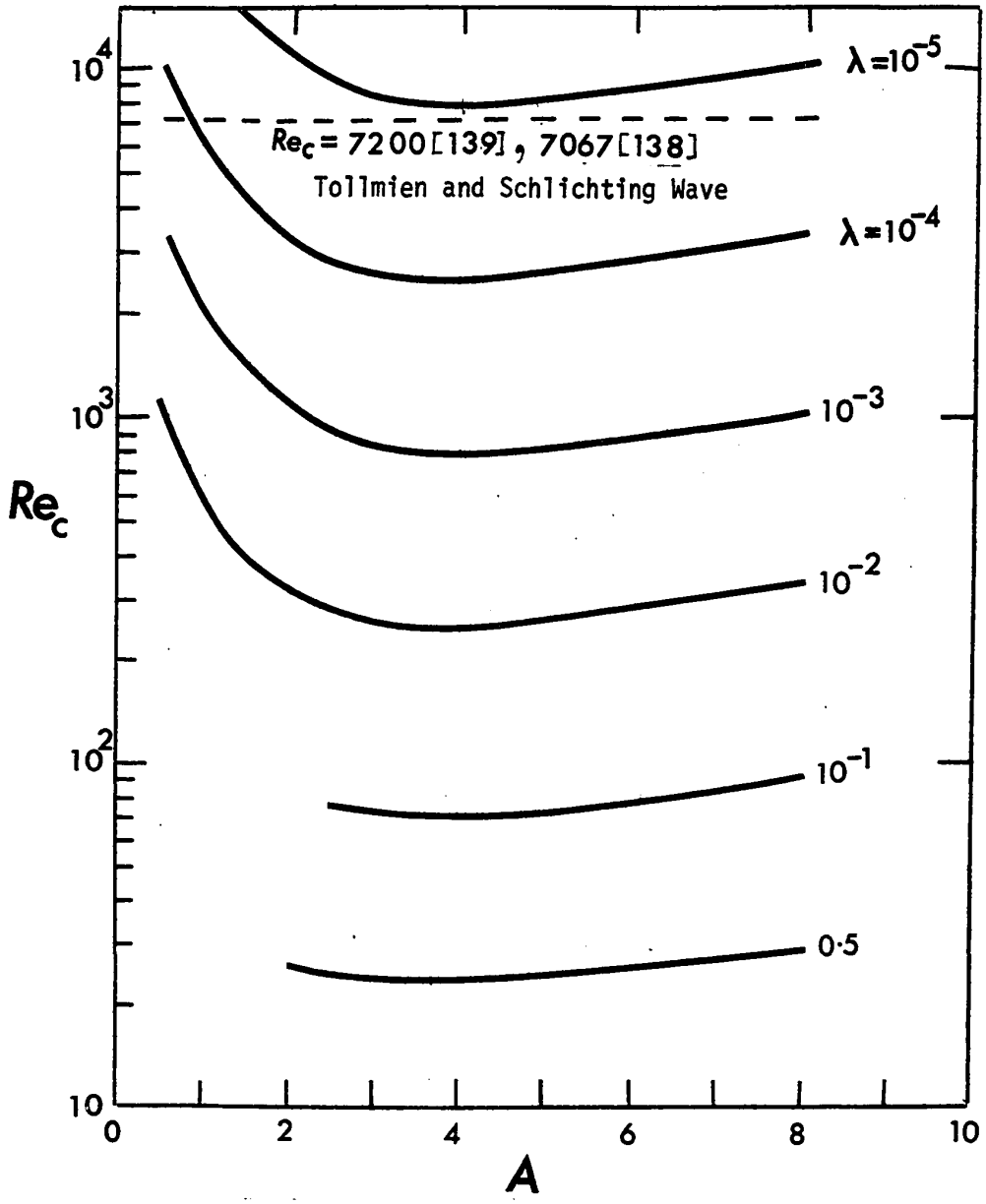


Fig. 96 Critical Reynolds Number Results for Various Curvature Ratios $\lambda$

of the stability theory of transverse wave disturbances to the fully developed laminar flow in a curved parallel-plate channel is highly desirable. The difficulty for a theoretical investigation of the stability of laminar flow in a curved pipe was pointed out by Dean [126] in 1928. In this respect, the possibility for the curved parallel-plate should be explored as a starting point.

Since the centrifugal instability is somewhat analogous to thermal instability, some inference from the results of thermal instability may be useful in speculating the possibilities for the Tollmien-Schlichting waves in a curved parallel-plate channel. Experimental investigations on thermal instability of laminar natural convection flow in inclined isothermal plates were carried out by Lloyd and Sparrow [140]. They established clearly that when the inclination angle exceeds $17^{o}$ from the vertical, the instability is characterized by longitudinal vortices, whereas, the mode of instability is Tollmien-Schlichting waves for inclination angles of less than $14^{o}$ relative to the vertical. The range between $14^{o}$ and $17^{o}$ was identified as a zone of continuous transition with the two modes of instability co-existing. It is noted here that the effect of inclination angle on the thermal instability is qualitatively similar to the effect of curvature ratio on centrifugal instability in a curved channel. For a straight parallel-plate channel $\lambda = 0$, Tollmien-Schlichting waves have priority and one may speculate that for some range of curvature ratios, the two modes of instability may co-exist. This possibility is also suggested

by the results shown in Fig. 96. Future investigations along this line should prove to be very interesting.

The effect of curvature ratio on minimum critical Dean number and Reynolds number is shown in Fig. 97.

## 7.5 CONCLUDING REMARKS

1. A formulation is presented for the hydrodynamic instability in the entrance region of a parallel-plate channel by taking curvature ratio effect into consideration. The numerical stability results are presented for the fully developed laminar flow with curvature ratios $\lambda = 10^{-10}$, $10^{-2}$, $10^{-1}$ and 0.5.

2. The neutral stability results for $\lambda = 10^{-10}$ agree very well with Reid's results [128] and it is found that the curvature ratio effect can be neglected practically up to $\lambda = 10^{-2}$.

3. The curvature effect is clearly seen to be a de-stabilizing effect and the curvature ratio effect is already appreciable at $\lambda = 10^{-1}$. As shown in Fig. 95, the minimum critical Dean number decreases with the increase of the curvature ratio $\lambda$ and the corresponding wavenumber decreases rather slowly with $\lambda$.

4. It appears that a Taylor-Görtler type instability has priority of occurrence over a Tollmien-Schlichting type instability at $\lambda = 10^{-4}$. However, the Tollmien-Schlichting instability in a slightly curved parallel-plate channel should be investigated in future.

5. The present analysis and the computer program can be applied to obtain neutral stability results for entry flow in a

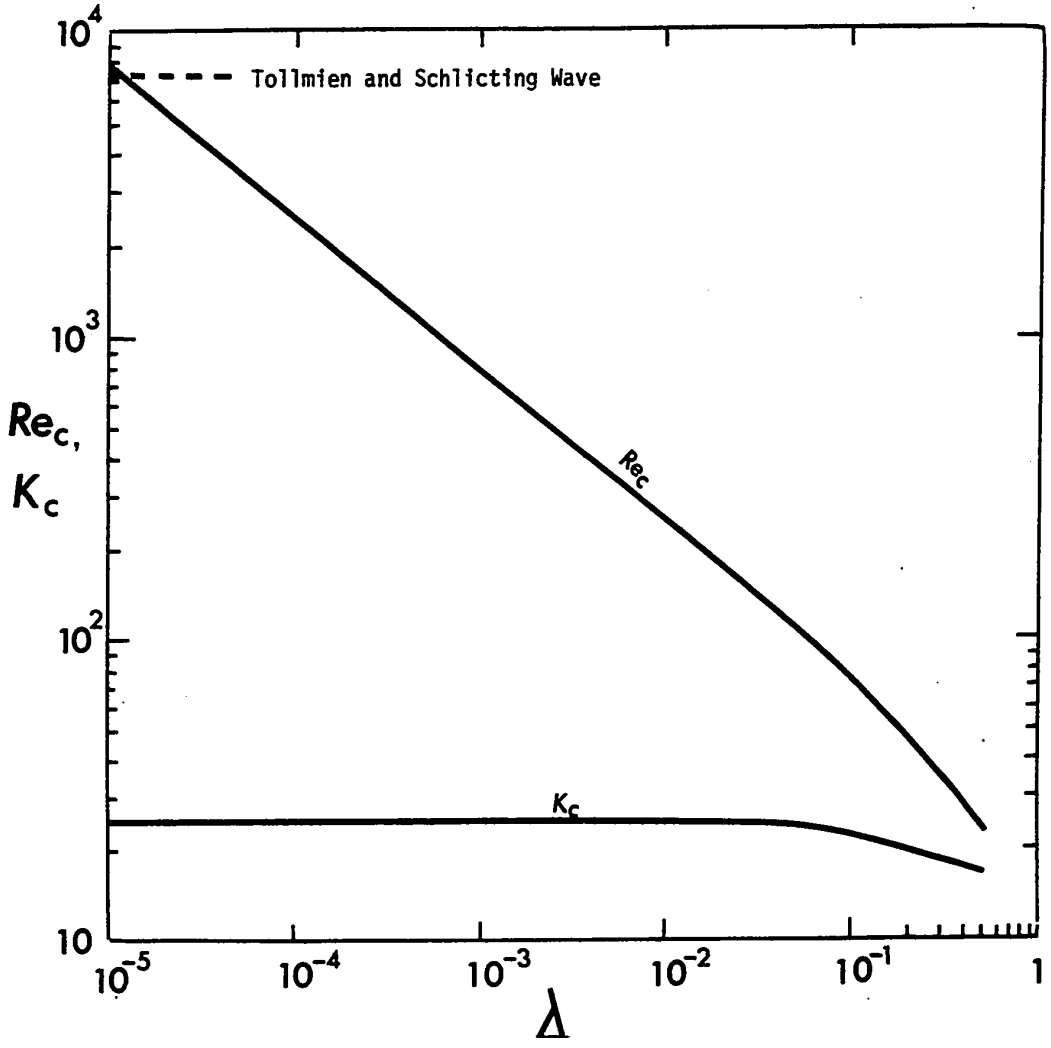


Fig. 97 Critical Dean Number $K_c$ and Reynolds Number $Re_c$ vs. Curvature Ratio $\lambda$

curved parallel-plate channel. However, the possibility of using higher order finite-difference approximation [139,141] should also be considered to increase the numerical accuracy and reduce computing time.

# CHAPTER VIII

## SCOPE OF RESULTS, CONCLUSIONS, AND SIGNIFICANCE

With the appearance of secondary flow caused by such body forces as buoyancy, centrifugal and Coriolis forces in ducts or channels, the analytical solution of such basic flow and convective heat transfer problems as hydrodynamic entrance flow, thermal entrance heat transfer and simultaneous hydrodynamic and thermal entry flow becomes extremely difficult. Considering only flow and heat transfer in curved ducts or channels, it becomes clear that certain thermal entrance region problems (Graetz problem) can be approached by a numerical method when one notes that unsteady two-dimensional heat conduction problem can be solved by a numerical technique.

For the solution of complex physical problems, the deductive analysis [95] is a useful tool in identifying the mathematical models which are tractable and clarifying the physical parameters involved. For this reason, the basic general equations governing the steady incompressible laminar flow and heat transfer in curved circular pipes and rectangular channels are studied using deductive analysis considering both the buoyancy and centrifugal forces effects. As a result of the order of magnitude analysis, the tractable sets of equations and the related physical parameters are obtained in a somewhat mathematically formal manner. The new characteristic parameters appearing in the general entrance region problem in curved pipes or channels are centrifugal Froude number $W_c^2/R_c g$, centrifugal Rayleigh

number $Ra_c = K^2Pr$ and the parameter denoting the importance of buoyancy effect in the centrifugal force field $GrK^{-2}$.

As a first step toward the numerical soltuion of Graetz problem (thermal entrance region problem), the fully developed laminar flow in curved pipes is solved numerically using boundary vorticity method. The numerical solution is found to be applicable up to Dean number of approximately 300. Some numerical experiments regarding the relative merits of boundary vorticity method as compared with the conventional stream function vorticity method are also made. It is noted here that at very low Dean numbers analytical solution using perturbation method can be used. On the other hand, an approximate analytical method based on boundary-layer and potential-core model is known to be applicable at high Dean numbers. It is seen that the numerical technique can bridge the gap between the two approximate analytical methods for the fully developed laminar flow in curved pipes. In this respect, it is noteworthy that recently (1973) Austin and Seader [140] presented numerical solution up to Dean number of 1000.

Heat transfer results for fully developed laminar forced convection in curved pipes under the thermal boundary condition of axially uniform wall heat flux with peripherally uniform wall temperature are also abtained for Prandtl number ranging from 0 to 500. A correlation equation for Nusselt number is proposed using the parameter $K^2Pr$ and the result is compared against the available results. The correlation equation is believed to be valid for

$Pr \geq 1$ but additional future confirmation is desirable. It is noted that numerical difficulty arises when the parameter becomes large. Recently Kalb and Seader [87] also presented numerical results for Dean numbers from 1 to 1,200 and Prandtl numbers from 0.005 to 1,600.

The numerical solution of Graetz problem in curved pipes is one of the primary goals of this investigation. By using ADI method for the energy equation, the numerical solution is obtained for the two basic thermal boundary conditions of uniform wall temperature and uniform wall heat flux. The Prandtl number effect is studied in detail. At higher values of the parameter $K^2Pr$, say $10^4$, the local Nusselt number exhibits fluctuating phenomenon before reaching an asymptotic value. The same phenomenon was also observed by Dravid, Smith, Merrill and Brian [82] in their numerical solution of the energy equation using velocity field obtained from approximate analytical solution for the case of Dean number 225 only. In this investigation, the fluctuating phenomenon for local Nusselt number is interpreted as a manifestation of numerical instability whereas Dravid et al [82] regard the phenomenon as a true physical solution. Some numerical experiments concerning a possible numerical instability are reported using different finite-difference approximations for the convective terms due to secondary flow in energy equations. Some physical reasonings are also presented to support the present numerical instability assertion.

The numerical solution for hydrodynamic entrance region problem in curved parallel-plate channels is obtained using a newly

developed direct vorticity method for the uniform, parabolic and triangular entrance velocities. It is found that the curvature effect on pressure drop in the entrance region can be practically neglected up to the curvature ratio $\lambda = 0.1$.

The Dean's hydrodynamic instability for the onset of Taylor-Görtler longitudinal vortices is extended to the hydrodynamic entrance flow in curved parallel-plate channels and the neutral stability results are obtained for the fully developed condition. It is found that the neutral stability results for curvature ratios $\lambda = 10^{-10} \sim 10^{-2}$ are practically identical with those of Dean's instability problem based on parabolic basic velocity profile ($\lambda = 0$) and the simplified perturbation equations. The curvature effect on neutral stability result is found to be appreciable at $\lambda = 0.1$. In other words, the curvature effect on pressure drop in hydrodynamic entrance region can be neglected up to $\lambda = 0.1$ but the curvature effect on neutral stability result is important for curvature ratios $\lambda = 0.01 \sim 0.1$

After summarizing the main result and indicating the scope of the investigation, the following specific further remarks may be in order.

1. The result of the deductive analysis for flow and heat transfer in horizontal curved pipes or channels reveals that the importance of the free convection effect in the centrifugal force field is represented by the parameter $K^{-2}Gr$. Specifically, when the magnitude of the parameter $K^{-2}Gr/2$ is much less than one, the free convection effects may

be negligible. The inclusion of the free convection effect in the analysis for the laminar forced convection in curved pipes or channels will no doubt increase the complexity of the problem. In this respect, the coupled effects of buoyancy and centrifugal forces may be studied by a numerical method for thermally fully developed condition in curved pipes or channels as a starting point. For Graetz problem the large Prandtl number case may offer some possibility for numerical solution.

2. When Prandtl number is large, some simplifications result and will be noted here. Under the conditions that $Pr >> O[1]$ and $Re^2 >> O[1]$, one may neglect the lateral inertia terms involving u, v in the momentum equation and the continuity equation can be decomposed into the one involving main flow w alone and the other one involving secondary flow for u and v only. The above simplifications may be useful for hydrodynamic and thermal entrance region problems. Furthermore, under the conditions that $Pr >> O[1]$ and $Pr^2Re^2 = Pe^2 >> O[1]$, the lateral and axial inertia terms in the momentum equations can be neglected. However, the continuity equation remains three-dimensional.

With $Pr >> O[1]$ and additionally $Re^2 >> O[1]$ or $Pr^2Re^2 >> O[1]$, the lateral inertia terms may be neglected for Graetz problem (thermal entrance region problem) with fully developed laminar flow. However, the centrifugal force term must be retained. The above observations may be useful in dealing with the problem where the centrifugal and buoyancy forces effects co-exist. For example, for large Prandtl number fluids, the main flow will be distorted only by the centrifugal

force effect and the secondary flow caused by buoyancy forces will not affect the main flow. It is also noteworthy that when Prandtl number is large and curvature ratio $\lambda$ is small, the parameter $K^2Pr$ becomes the sole parameter in the governing equations and the heat transfer results may be correlated using this parameter.

3. It is well understood that when Dean number is large, the flow resistance and heat transfer rate increase. However, when the magnitude of the centrifugal Froude number is large, then the term involving Froude number acts to intensify the centrifugal force effect on heat transfer for heating case but tends to suppress the centrifugal force effect on heat transfer for cooling case.

4. Apparently the thermal entrance region problem in curved pipes or channels needs further investigations both theoretically and experimentally. In this respect, the simulation of experimental thermal boundary conditions should be studied carefully before theoretical and experimental results may be compared meaningfully. Noting the peripheral heat conduction effect for uniformly heated wall in experimental investigations, one may have the problem of heat conduction in pipe wall and convection inside the pipe. With the appearance of the fluctuating local Nusselt number before reaching an asymptotic value for numerical solution at high parameter region for $K^2Pr$, some uncertainty regarding the asymptotic behavior of Nusselt number also exists. This is another reason more works are required for Graetz problem in curved pipes or channels.

5. In solving the hydrodynamic entry flow problem in curved

parallel-plate channels, the axial viscous terms are neglected. It is also noted that the range of curvature ratios $1 \geq \lambda \gtrsim 0.5$ may be quite limited in practical configurations for curved channels. However, it is possible that the curved parallel-plate channels may be preceded and also followed by a straight parallel-plate channel. This leads to a variety of flat channel bend problems involving various degrees of bends such as $45^{o}$, $90^{o}$ and $180^{o}$. Of course, for these channel bend problems, the axial viscous terms must be included in the analysis. In view of the difficulty with the theoretical analysis of the various pipe bends problem, the flat channel bends problems may offer some possibility for future theoretical work.

6. The limitation of the Dean's hydrodynamic instability formulation for the onset of Taylor-Görtler vortices in curved parallel-plate channels with respect to curvature effect is clarified by the present investigation. For the hydrodynamic instability problem, the curvature effect cannot be neglected in the perturbation equations for curvature ratio greater than $\lambda = 0.01$. The experimental facilities for the present centrifugal instability problem are already available and it is expected that some experimental results may be obtained shortly. It is useful to note that the present centrifugal instability problem may arise in a curved rectangular channel with large aspect ratio (height/width) say greater than 10.

7. A question may arise as to whether the Taylor-Görtler type instability or the Tollmien-Schlichting type instability will have priority for fully developed laminar flow in a slightly curved parallel-plate channel. To answer this question, one may consider an example

with curvature ratio $\lambda = a/R_c = 10^{-4}$. Assuming that the channel width 2a is 2 inches, the radius of curvature becomes $R_c = 833.3$ feet. In such an almost straight channel, the critical Reynolds number for the Taylor-Görtler vortices is $Re_c \simeq 2500$. On the other hand, the critical Reynolds number for the Tollmien-Schlichting waves is known to be $Re_c \simeq 7500$ if one neglects the curvature effect. The above example illustrates clearly the importance of Taylor-Görtler type instability in even a slightly curved and almost straight parallel- plate channel.

8. In view of the practical importance of Dean's instability problem in a slightly curved parallel-plate channel up to $\lambda = 0.01$ and the fact that the curvature effect for main flow may be neglected up to $\lambda = 0.01$, one may use the basic flow results in the entrance region of straight parallel-plate channel for the neutral stability analysis in the entrance flow of a curved parallel-plate channel. Futhermore, in the perturbation equations, some terms may be neglected using the assumption of small curvature ratio $\lambda$. In this formulation, the entrance velocity profile can be arbitrary and the numerical method of solution developed in this investigation can be adapted readily.

9. All the computer programs for this study are listed in Appendix 10.

## REFERENCES


1. Akiyama, M., Hwang, G.J., and Cheng,K.C., "Experiments on the Onset of Longitudinal Vortices in Laminar Forced Convection Between Horizontal Plates", Journal of Heat Transfer, Trans. ASME, Series C, Vol. 93, No. 4, Nov. 1971, pp. 335-341.
2. Nakayama, W., Hwang, G.J., and Cheng, K.C., "Thermal Instability in Plane Poiseuille Flow", Journal of Heat Transfer, Trans. ASME, Series C, Vol. 92, No. 1, Feb. 1970, pp. 61-68.
3. Thomson, J., "On the Origin of Windings of Rivers in Alluvial Plains, with Remarks on the Flow of Water Round Bends in Pipes", Proceedings of Royal Society, Series A, Vol. 25, 1876, pp. 5-8.
4. Thomson, J., "Experimental Demonstration in Respect to the Origin of Windings of Rivers in Alluvial Plains, and the Mode of Flow of Water around Bends of Pipes", Proceedings of Royal Society, Series A, Vol. 26, 356ff, 1877.
5. Goldstein, S., "Modern Developments in Fluid Mechanics", Edited, Vol. 1, Dover Publications, Inc., N.Y., 1965, pp. 84-87.
6. Ito, H., "Secondary Flow Problems in Hydrodynamics", Journal of Japan Society of Mechanical Engineers, Vol. 66, No. 537, 1963, pp. 1368-1375.
7. Ito, H., "Recent Trends on Secondary Flow Studies", Science of Machine, Yhokendo, Japan, Vol. 17, No. 10, 1965, pp. 1230-1236.
8. Grindley, J.H., and Gibson, A.H., "On the Frictional Resistance to the Flow of Air through a Pipe", Proceedings of Royal Society, Series A, Vol. 80, 1908.

9. Eustice, J., "Flow of Water in Curved Pipes", Proceedings of Royal Society, Series A, Vol. 84, 1910, pp. 107-118.

10. Eustice, J., "Experiments on Stream-Line Motion in Curved Pipes", Proceedings of Royal Society, Series A, Vol. 85, 1911, pp. 119-131.

11. Eustice, J., "Flow of Fluids in Curved Passages", Engineering, Vol. 13, 1925, pp. 604-605.

12. Dean, W.R., "Note on the Motion of Fluid in a Curved Pipe", Philosophical Magazine and Journal of Science, Series 7, Vol. 4, 1927, pp. 208-223.

13. Dean, W.R., "The Stream-Line Motion of Fluid in a Curved Pipe", Philosophical Magazine and Journal of Science, Series 7, Vol. 5, No. 30, 1928, pp. 673-695.

14. Morton, B.R., "Laminar Convection in Uniformly Heated Horizontal Pipes at Low Rayleigh Numbers", Quarterly Journal of Mechanics and Applied Mathematics, Vol. 12, Pt. 4, 1959, pp. 410-420.

15. Trefethen, L., "Fluid Flow in Radial Rotating Tubes", IX$^{e}$ Congrés International de Méchanique Appliqueé, Université de Bruxelles, Vol. 2, 1957, pp. 341-351.

16. Taylor, G.I., "The Criterion for Turbulence in Curved Pipes", Proceedings of Royal Society, Series A, Vol. 124, 1929, pp. 243-249.

17. White, C.M., "Streamline Flow Through Curved Pipes", Proceedings of Royal Society, Series A, Vol. 123, 1929, pp. 645-663.

18. White, C.M., "Modern Developments in Fluid Mechanics", Goldstein, S., Editor, Vol. 1, Dover Publications, Inc., N.Y., 1965, pp. 313-314.

19. Adler, M., "Strömung in gekrümmten Rohren", Zeitsahrift für angewandte Mathematik und Mechanik, Vol. 14, No. 4, 1934, pp. 257-275.

20. Hawes, W.B., "Some Sidelights on the Heat Transfer Problem", Transactions of Institution of Chemical Engineers, London, Vol. 10, 1932, pp. 161-167.

21. Yarnell, D.L. and Nagler, F.A., "Flow of Water Around Bends in Pipes", Proceedings of the American Society of Civil Engineers, Vol. 60, 1934, pp. 783-797.

22. Wattendorf, F.L., "A Study of the Effect of Curvature on Fully Developed Turbulent Flow", Proceedings of Royal Society, Vol. 148, 1935, pp. 565-598.

23. Keulegan, G.H., and Beij, K.H., "Pressure Losses for Fluid Flow in Curved Pipes", Journal of Research of the National Bureau of Standards, Vol. 18, 1937, pp. 89-114.

24. Weske, J.R., "Investigations of the Flow in Curved Ducts at Large Reynolds Numbers", Journal of Applied Mechanics, Trans. of ASME, Vol. 15, 1948, pp. 344-348.

25. Itō, H., "Theory on Laminar Flows Through Curved Pipes of Elliptic and Rectangular Cross-Sections", The Reports of the Institute of High Speed Mechanics, Tōhoku University, Sendai, Japan, Vol. 1, 1951, pp. 1-16.

26. Ludwieg, H., "Die ausgebildete Kanalströmung in einem rotierenden System", Ingenieur-Archiv, Vol. 19, 1951, pp. 296-308.

27. Hawthorne, W.R., "Secondary Circulation in Fluid Flow", Proceedings of Royal Society, Series A, Vol. 206, 1951, pp. 374-387.

28. Cuming, H.G., "The Secondary Flow in Curved Pipes", Aeronautical Research Council, Reports and Memoranda, No. 2880, Feb., 1952.

29. Eichenberger, H.P., "Secondary Flow Within a Bend", Journal of Mathematics and Physics, Vol. 32, 1953, pp. 34-42.

30. Detra, R.W., "The Secondary Flow in Curved Pipes", Mitteilungen aus dem Institut für Aerodynamik, An der eidgenössischen technischen Hochschule in Zürich, Nr. 20, 1953.

31. Eskinazi, S., and Yeh, H., "An Investigation on Fully Developed Turbulent Flows in a Curved Channel", Journal of the Aeronautical Sciences, Vol. 23, 1956, pp. 23-34 and p. 75.

32. Dean, W.R., and Hurst, J.M., "Note on the Motion of Fluid in a Curved Pipe", Mathematika, Vol. 6, 1959, pp. 77-85.

33. Itō, H., "Friction Factors for Turbulent Flow in Curved Pipes", Journal of Basic Engineering, Trans. of ASME, Series D, Vol. 81, 1959, pp. 123-134.

34. Barua, S.N., "On Secondary Flow in Stationary Curved Pipes", Quarterly Journal of Mechanics and Applied Mathematics, Vol. 16, pt. 1, 1963, pp. 61-77.

35. Truesdell, L.C., Jr., "Numerical Treatment of Laminar Flow Through Helical Conduits", Ph.D. Thesis, Case Institute of Technology, 1963; available from University Microfilms, Ann Arbor, Mich.

36. Truesdell, L.C., Jr., and Adler, R.J., "Numerical Treatment of Fully Developed Laminar Flow in Helically Coiled Tubes", A.I.Ch.E. Journal, Vol. 16, 1970, pp. 1010-1015.

37. Kapur, J.N., Tyagi, V.P. and Srivastava, R.C., "Streamline Flow Through a Curved Annulus", Applied Scientific Research, Section A, Vol. 14, 1964, pp. 253-267.

38. Kubair, V., and Kuloor, N.R., "Heat Transfer to Newtonian Fluids in Coiled Pipes in Laminar Flow", International Journal of Heat and Mass Transfer, Vol. 9, 1966, pp. 63-75.

39. Topakoglu, H.C., "Steady Laminar Flows of an Incompressible Viscous Fluid in Curved Pipes", Journal of Mathematics and Mechanics, Vol. 16, No. 12, 1967, pp. 1321-1337.

40. McConalogue, D.J., and Srivastava, R.S., "Motion of a Fluid in a Curved Tube", Proceedings of Royal Society, Series A, Vol. 307, 1968, pp. 37-53.

41. Itō, H., "Laminar Flow in Curved Pipes", Zeitsahrift für angewandte Mathematik und Mechanik, Vol. 49, 1969, pp. 653-663.

42. Larrain, J., and Bonilla, C.F., "Theoretical Analysis of Pressure Drop in the Laminar Flow of Fluid in a Coiled Pipe", Transactions of the Society of Rheology, Vol. 14, No. 2, 1970, pp. 135-147.

43. Baylis, J.A., "Experiments on Laminar Flow in Curved Channels of Square Section", Journal of Fluid Mechanics, Vol. 48, 1971, pp. 417-422.

44. Jones, J.R., "Flow of a Non-Newtonian Liquid in a Curved Pipe", Quarterly Journal of Mechanics and Applied Mathematics, Vol. 13, 1960, pp. 428-443.

45. Clegg, D.B., and Power, G., "Flow of a Bingham Fluid in a Slightly Curved Tube", Applied Scientific Research, Section A, Vol. 12, 1963, pp. 199-212.

46. Thomas, R.H., and Walters, K., Journal of Fluid Mechanics, Vol. 16, 1963, 228ff.

47. Thomas, R.H., and Walters, K., Journal of Fluid Mechanics, Vol. 21, 1965, 173ff.

48. Jones, D.T., Ph.D. Thesis, University of Wales, 1967.

49. Jones, D.T., and Walters, K., A.I.Ch.E. Journal, Vol. 14, 1968, 658ff.

50. Barnes, H.A., and Walters, K., "On the Flow of Viscous and Elastico-Viscous Liquids through Straight and Curved Pipes", Proceedings of Royal Society of London, Series A, Vol. 314, 1969, pp. 85-109.

51. Jeschke, D., "Wärmeübergang und Druckverlust in Rohrshlagen", Z. Ver. deut. Ing., Band 69, 1925, 1526ff.

52. Jeschke, D., Z. Ver. deut. Ing., Erganzungsheft, Band 24, 1925, 1ff.

53. Merkel, F., "Die Grundlagen der Wärmeübertragung", Steinkopf, Leipzig, 1927, 51ff.

54. McAdams, W.H., "Heat Transmission", 3rd Edition, McGraw-Hill Book Co., Inc., N.Y., 1954, p. 228.

55. Pratt, N.H., "The Heat Transfer in a Reaction Tank Cooled by Means of a Coil", Transactions of Institution of Chemical Engineers, Vol. 25, 1947, pp. 163-180.

56. Berg, R.R., and Bonilla, C.F., "Heating of Fluids in Coils", Transactions of New York Acad. Sci., Vol. 13, 1950, pp. 12-18.

57. Kreith, F., "The Influence of Curvature on Heat Transfer to Incompressible Fluids", Transactions of the American Society of Mechanical Engineers, Vol. 77, 1955, pp. 1247-1256.

58. Eckert, E.R.G., and Irvine, T.F., Jr., "Rearrangement of the Temperature Field in Flow Around a Bend", Transactions of ASME, Nov. 1958, pp. 1765-1772.

59. Ede, A.J., "The Effect of a Right-Angled Bend on Heat Transfer in a Pipe", International Developments in Heat Transfer, 1961, pp. 634-642.

60. Tangri, N.N., and Jayaraman, R., "Heat Transfer Studies on a Spiral Plate Heat Exchanger", Transaction of Inst. Chem. Engrs., Vol. 40, 1962, pp. 161-168.

61. Seban, R.A. and McLaughlin, E.F., "Heat Transfer in Tube Coils with Laminar and Turbulent Flow", International Journal of Heat and Mass Transfer, Vol. 6, 1963, pp. 387-395.

62. Kubair, V., and Kuloor, N.R., "Secondary Flow in Helical Coils", Indian Journal of Technology, Vol. 1, 1963, pp. 333-335.

63. Rogers, G.F.C., and Mayhew, Y.R., "Heat Transfer and Pressure Loss in Helically Coiled Tubes With Turbulent Flow", International Journal of Heat and Mass Transfer, Vol. 7, 1964, pp. 1207-1216.

64. Maekawa, H., "Fully Developed Laminar Forced Convective Heat Transfer in Slightly Curved Pipes", Proceedings of 1st Japan Heat Transfer Symposium, 1964, pp. 13-16.

65. Mori, Y., and Nakayama, W., "Study on Forced Convective Heat Transfer in Curved Pipes (1st Report, Laminar Region)", International Journal of Heat and Mass Transfer, Vol. 8, 1965, pp. 67-82.

66. Mori, Y., and Nakayama, W., "Study on Forced Convective Heat Transfer in Curved Pipes (2nd Report, Turbulent Region)", International Journal of Heat and Mass Transfer, Vol. 10, 1967, pp. 37-59.

67. Mori, Y., and Nakayama, W., "Study on Forced Convective Heat Transfer in Curved Pipes (3rd Report, Theoretical Analysis under the Condition of Uniform Wall Temperature and Practical Formulae)", International Journal of Heat and Mass Transfer, Vol. 10, 1967, pp. 681-695.

68. Kubair, V., and Kuloor, N.R., "Heat Transfer to Newtonian Fluids in Coiled Pipes in Laminar Flow", International Journal of Heat and Mass Transfer, Vol. 9, 1966, pp. 63-75.

69. Kubair, V., and Kuloor, N.R., "Comparison of Performance of Helical and Spiral Coil Heat Exchangers", Indian Journal of Technology, Vol. 4, 1966, pp. 1-3.

70. Mori, Y., and Uchida, Y., "Study on Forced Convective Heat Transfer in Curved Square Channel (1st Report, Theory of Laminar Region)", Transactions of The Japan Society of Mechanical Engineers, Vol. 33, 1967, pp. 1836-1846.

71. Mori, Y., Nakayama, W., and Uchida, Y., "Convective Heat Transfer in Ducts with Secondary Flow", Journal of The Japan Society of Mechanical Engineers, Vol. 70, No. 583, 1967, pp. 1188-1196.

72. Schmidt, E.F., "Wärmeübergang und Druckverlust in Rohrschlangen", Chemie Ingenieur Technik, Vol. 13, 1967, pp. 781-832.

73. Shchukin, V.K., and Filin, V.A., "Convective Heat Transfer in Short Curved Channels", Journal of Engineering Physics, Vol. 12, 1971, pp. 78-82.

74. Özisik, M.N., and Topakoglu, A.C., "Heat Transfer for Laminar Flow in a Curved Pipe", Journal of Heat Transfer, Trans. ASME, Series C, Vol. 90, 1968, pp. 313-318.

75. Srinivasan, P.S., Nandapukar, S.S., and Holland, F.A., "Pressure Drop and Heat Transfer in Coils", Chemical Engineering, 1968, pp. 113-119.

76. Shchukin, V.K., "Correlation of Experimental Data on Heat Transfer in Curved Pipes", Thermal Engineering, Vo. , 19 , pp. 72-76, also in Teploenergetika, Vol. 16, 1969, pp. 50-52.

77. Miropol'skii, Z.L., Annadurdyev, Kh., and Kakabaev, A., Heat Transfer and Pressure Drop in the Heating and Cooling of Liquids in Curvilinear Channels", International Chemical Engineering, Vol. 9, No. 3, 1969, pp. 410-414.

78. Cheng, K.C., and Akiyama, M., "Laminar Forced Convection Heat Transfer in Curved Rectangular Channels", International Journal of Heat and Mass Transfer, Vol. 13, 1970, pp. 471-490.

79. Akiyama, M., "Laminar Forced Convection Heat Transfer in Curved Rectangular Channels", University of Alberta, Edmonton 7, Alberta, Canada, M.Sc. Thesis, 1969.

80. Akiyama, M., and Cheng, K.C., "Boundary Vorticity Method for Laminar Forced Convection Heat Transfer in Curved Pipes", International Journal of Heat and Mass Transfer, Vol. 14, 1971, pp. 1659-1675.

81. Cheng, K.C., Hwang, G.J., and Akiyama, M., "On a Simple Correlation for Prandtl Number Effect on Forced Convective Heat Transfer With Secondary Flow", International Journal of Heat and Mass Transfer, Vol. 15, 1972, pp. 172-175.

82. Dravid, A.N., Smith, K.A., Merrill, E.W., and Brian, P.L.T., "Effect of Secondary Fluid Motion on Laminar Flow Heat Transfer in Helically Coiled Tubes", A.I.Ch.E. Journal, Vol. 17, 1971, pp. 1114-1122.

83. Dravid, A.N., "The Effect of Secondary Fluid Motion on Laminar Flow Heat Transfer in Helically Coiled Tubes", Sc.D. Thesis, Massachusetts Institute of Technology, 1969.

84. Akiyama, M., and Cheng, K.C., "Laminar Forced Convection in the Thermal Entrance Region of Curved Pipes With Uniform Wall Temperature - The Graetz Problem", 4th Western Canadian Heat Transfer Conference, University of Manitoba, Winnipeg, Manitoba, Canada, May 24-31, 1972.

85. Miyazaki, H., "Combined Free and Forced Convective Heat Transfer and Fluid Flow in a Rotating Curved Circular Tube", International Journal of Heat and Mass Transfer, Vol. 14, 1971, pp. 1295-1309.

86. Akiyama, M., and Cheng, K.C., "Laminar Forced Convective Heat Transfer in Curved Pipes With Uniform Wall Temperature", International Journal of Heat and Mass Transfer, Vol. 15, 1972, pp. 1426-1431.

87. Kalb, C.E., and Seader, J.D., "Heat and Mass Transfer Phenomena for Viscous Flow in Curved Circular Tubes", International Journal of Heat and Mass Transfer, Vol. 15, 1972, pp. 801-817.

88. Erdogan, M.E., and Chatwin, P.C., "The Effects of Curvature and Buoyancy on the Laminar Dispersion of Solute in a Horizontal Tube", Journal of Fluid Mechanics, Vol. 29, 1967, pp. 465-484.

89. Weissman, M.H., and Mockros, L.F., "Gas Transfer to Blood Flowing in Coiled Circular Tubes", Proceedings of the American Society of Civil Engineers, EM3, June 1968, pp. 857-872.

90. McConalogue, D.J., "The Effects of Secondary Flow on the Laminar Dispersion of an Injected Substance in a Curved Tube", Proceedings of Royal Society, London, Series A, 1970, pp. 99-113.

91. Chang, H.K., and Mockros, L.F., "Convective Dispersion of Blood Gases in Curved Channel Exchangers", A.I.Ch.E. Journal, Vol. 17, 1971, pp. 541-549.

92. Ruthven, D.M., "The Residence Time Distribution for Ideal Laminar Flow in a Helical Tube", Chemical Engineering Science, Vol. 26, 1971, pp. 1113-1121.

93. Nunge, R.J., Lin, T.-S., and Gill, W.N., "Laminar Dispersion in Curved Tubes and Channels", Journal of Fluid Mechanics, Vol. 51, 1972, pp. 363-383.

94. Rosenhead, L., "Laminar Boundary Layers", Editor, Oxford University Press, 1966, pp. 129-134.

95. Ostrach, S., "Role of Analysis in the Solution of Complex Physical Problem", Proceedings of the Third International Heat Transfer Conference, Vol. 6, 1966, pp. 31-43.

96. Hwang, G.J., and Cheng, K.C., "Boundary Vorticity Method for Convective Heat Transfer With Secondary Flow - Application to the Combined Free and Forced Laminar Convection in Horizontal Tubes", Proceedings, Fourth International Heat Transfer Conference, Vol. 4, Paris-Versailles, 1970, NC3.5.

97. Cheng, K.C., and Hong, S.W., "Combined Free and Forced Laminar Convection in Inclined Tubes", Applied Scientific Research, Vol. 27, 1972, pp. 19-38.

98. Varga, R.S., "Matrix Iterative Analysis", Prentice-Hall, Inc., Englewood Cliffs, New Jersey, 1962, p. 177.

99. Young, D., "The Numerical Solution of Elliptic and Parabolic Partial Differential Equations", Survey of Numerical Analysis, Edited by Todd, J., Chapter 11, 1963.

100. Forsythe, G.E., and Wasow, W.R., "Finite-Difference Methods for Partial Differential Equations", John Wiley and Sons, Inc., New York, 1967, p. 136.

101. Lax, P.D., and Richtmyer, R.D., "Survey of the Stability of Linear Finite Difference Equations", Comm. Pure Appl. Math., Vol. 9, 1956, pp. 267-293.

102. Barakat, H.Z., and Clark, J.A., "Analytical and Experimental Study of The Transient Laminar Natural Convection Flows in Partially Filled Liquid Containers", Proceedings of the Third International Heat Transfer Conference, Vol. II, Chicago, Illinois, August 1966, pp. 152-162.

103. Runchal, A.K., Spalding, D.B., and Wolfshtein, M., "Numerical Solution of the Elliptic Equations for Transport of Vorticity, Heat, and Matter in Two-Dimensional Flow", High-Speed Computing in Fluid Dynamics, The Physics of Fluids Supplement II, 1969, pp. II-21-28.

104. Douglas, J., Jr., "On the Numerical Integration of $\frac{\partial^2 u}{\partial x^2} + \frac{\partial^2 u}{\partial y^2} = \frac{\partial u}{\partial t}$ by Implicit Methods", Journal Soc. Indust. Appl. Math., Vol. 3, 1955, pp. 42-65.

105. Conte, S.D., "Elementaty Numerical Analysis", McGraw-Hill, Inc., New York, 1965, p. 164.

106. Leveque, M.A., "Les lois de la transmission de chaleur par convection", Annls Mines, Paris-Mém, Ser. 12, 13. 1929, pp. 283-290.

107. Hausen, H., "Darstellung des Wärmeüberganges in Rohren durch verallgemeinerte Potenzbeziehungen", Z. Ver. Deut. Ing., Beihefte Verfahrenstechnik, No. 4, 1943, pp. 91-98.

108. Kay, W.M., "Numerical Solutions for Laminar-Flow Heat Transfer in Circular Tubes", Transaction of ASME, Vol. 58, 1955, pp. 1265-1274.

109. Hsu, C-J., " An Exact Analysis of Low Peclet Number Thermal Entry Region Heat Transfer in Transversely Nonuniform Velocity Fields", AIChE Journal, Vol. 17, No. 3, 1971, pp. 732-740.

110. Hsu, C-J., "Low Peclet Number Mass Transfer in Laminar Flow Through Circular Tubes", International Journal of Heat and Mass Transfer", Vol. 15, 1972, pp. 2187-2201.

111. Sparrow, E.M., Lin, S.H., and Lundgren, T.S., "Flow Development in the Hydrodynamic Entrance Region of Tubes and Ducts", Physics of Fluids, Vol. 7, 1964, pp. 338-347.

112. Lundgren, T.S., Sparrow, E.M., and Starr, J.B., "Pressure Drop Due to the Entrance Region in Ducts of Rectangular Cross Section", Journal of Basic Engineering, Transaction of ASME, Series D, Vol. 86, 1964, pp. 620-626.

113. Kawaguti , M., "Numerical Study of the Flow of a Viscous Fluid in a Curved Channel", High-Speed Computing in Fluid Dynamics The Physics of Fluids, Supplement II, 1969, pp. 101 104.

114. Hurd, A.C. and Peters, A.R., "Analysis of Flow Seperation in a Confined Two - Dimensional Channel", Transactions of ASME, Journal of Basic Engineering, Vol. 92, Series D, No. 4, 1970, pp. 909-914.

115. Wang, Y.L. and Longwell, P.A., "Laminar Flow in the Inlet Section of Parallel Plates", AIChE Journal, Vol. 10, No. 3, 1964, pp. 323-329.

116. Ames, W.F.,"Numerical Methods for Partial Differential Equations", Thomas Nelson and Sons Ltd., 36 Park Street London W1, 1969, ff. 50

117. Schlichting, H., "Laminare Kanaleinlaufstroemung", Ztschr. f. angew. Math. und Mec., Band 14, Heft 6, 1934, pp. 368-373.

118. Bodoia, J.R. and Osterle J.F., "Finite Difference Analysis of Plane Poiseuille and Couette Flow Developments", Appl. Sci. Res., Section A, Vol. 10, 1961, pp. 265-276.

119. Collins, M. and Schowalter, W.R., "Behavior of Non-Newtonian Fluids in the Inlet Region of a Channel", AIChE Journal, Vol. 9, No. 1, 1963, pp. 98-102.

120. Beavers, G.S., Sparrow, E.M. and Magnuson, R.A., "Experiments on Hydrodynamically Developing Flow in Rectangular Ducts of Arbitrary Aspect Ratio", International Journal of Heat and Mass Transfer, Vol. 13, 1970, pp. 689-702.

121. Han, L.S., "Hydrodynamic Entrance Lengths for Laminar Incompressible Laminar Flow in Rectangular Ducts", J. Appl. Mech., Vol. 27, 1960, pp. 403-409.

122. Goldstein, S., ibid., 1965, pp. 315-316.

123. Taylor, G.I., "Stability of a Viscous Liquid Contained Between Two Rotating Cylinders", Phil. Trans., Series A, Vol. 223, 1923, pp. 289-293.

124. Görtler, H., "Über eine dreidimensionale Instabilität Laminarer Grenzschichten an Konkaven Wänden", Nachr. Wiss. Ges. Göttingen, Math. Phys. Klasse, Neue Folge 2, No. 1, 1940.

125. Stuart, J.T., "Hydrodynamic Stability", edited by L. Rosenhead, 1963, pp. 492-579.

126. Dean, W.R., "Fluid Motion in a Curved Channel", Prc. Ray. Soc. London, Series A, Vol. 121, 1928, pp. 402-420.

127. Yih, C-S., and Sangster, W.M., "Stability of Laminar Flow in Curved Channels", Phil. Mag., Ser. 8, Vol. 2, No. 15, 1957, pp. 305-310.

128. Reid, W.H., " On the Stability of Viscous Flow in a Curved Channel", Proc. Roy. Soc., Series A, Vol. 244, 1958, pp. 186-198.

129. Hämmerlin, G., "Die Stabilität der Strömung in einem gekrümmten Kanal", Arch. rat. Mech. Anal., Heidelberg, Vol. 1, 1958, pp. 212-224.

130. Mori, Y., and Uchida Y., "Forced Convective Heat Transfer in a Curved Channel", JSME 1967 Semi-International Symposium, Tokyo, Japan, 1967, pp. 222-190.

131. Smith, A.M.O., "On the Growth of Taylor-Görtler Vortices Along Highly Concave Walls", Quart. Appl. Math., Vol. 13, 1955, pp. 233-262.

132. Conte, S.D., "Elementary Numerical Analysis", McGraw-Hill Book Company, New York, 1965, ff. 169.

133. Ralston, A., "A First Course in Numerical Analysis", McGraw-Hill Book Company, New York, 1965, pp. 323-328.

134. National Physical Laboratory, "Modern Computing Methods", Notes on Applied Science No. 16, Second Edition, Her Majesty's Stationery Office, London, 1961.

135. Wilkinson, J.H., "Error Analysis of Direct Method of Matrix Inversion", Association of Computing Machinery Journal, Vol. 8, 1961, pp. 281-330.

136. Forsythe, G.E., and Moler, C.B., "Computer Solution of Linear Algebraic System", Prentice Hall Inc., 1967.

137. Young, D., "The Numerical Solution of Elliptic and Parabolic Partial Differential Equations", ibid.

138. Lin, C.C., "The Theory of Hydrodynamic Stability", Cambridge University Press., 1955, p. 48.

139. Chen, T-S., "Hydrodynamic Stability of Developing Flow in a Parallel-Plate Channel", Ph.D. Thesis, Univeristy of Minnesota, 1966.

140. Lloyd, J.E. and Sparrow, E.M., " On the instability of Natural Convection Flow on Inclined Plates", J. Fluid Mech., Vol. 42, 1970, pp. 465-470.

141. Thomas, L.H., " The Stability of Plane Poiseuille Flow", Phys. Rev., Vol. 91, No. 4, 1953, pp. 780, 783.

142. Ames, W.F., ibid., 1969, p. 276.

143. Jenson, V.G., "Viscous Flow Round a Sphere at Low Reynolds Numbers (<40)", Proc. Roy. Soc. London, Series A, Vol. 249, 1959, pp. 346-366.

144. Austin, L.R., and Seader, J.D., "Fully Developed Viscous Flow in Coiled Circular Pipes", AIhCE Journal, Vol. 19, No. 1, 1973, pp. 85-94.

APPENDIX 1

GOVERNING EQUATIONS IN

GENERAL ORTHOGONAL COORDINATES

Denoting $x_1$, $x_2$ and $x_3$ as the general orthogonal coordinates and letting $h_1$, $h_2$ and $h_3$ be the corresponding three metric coefficients, the governing equations in general orthogonal coordinates can be written as:

Continuity equation

$$\frac{\partial \rho}{\partial t} + \frac{1}{h_1 h_2 h_3} \frac{\partial}{\partial x_1} (h_2 h_3 \rho u_1) + \frac{\partial}{\partial x_2} (h_3 h_1 \rho u_2) + \frac{\partial}{\partial x_3} (h_1 h_2 \rho u_3) = 0 \qquad \text{(A-1)}$$

Navier-Stokes equations of motion

$x_1$ - component

$$\rho\{\frac{\partial u_1}{\partial t} + \frac{u_1}{h_1}\frac{\partial u_1}{\partial x_1} + \frac{u_2}{h_2}\frac{\partial u_1}{\partial x_2} + \frac{u_3}{h_3}\frac{\partial u_1}{\partial x_3}$$

$$- u_2(\frac{u_2}{h_2 h_1}\frac{\partial h_2}{\partial x_1} - \frac{u_2}{h_1 h_2}\frac{\partial h_1}{\partial x_2}) - u_3(\frac{u_3}{h_3 h_1}\frac{\partial h_3}{\partial x_1} - \frac{u_1}{h_1 h_3}\frac{\partial h_1}{\partial x_3})\}$$

$$= -\frac{1}{h_1}\frac{\partial p}{\partial x_1}$$

$$+ \frac{1}{h_1 h_2 h_3}[\frac{\partial}{\partial x_1}\{\mu h_2 h_3(\frac{1}{h_1}\frac{\partial u_1}{\partial x_1} + \frac{u_2}{h_1 h_2}\frac{\partial h_1}{\partial x_2} + \frac{u_3}{h_3 h_1}\frac{\partial h_1}{\partial x_3})\}$$

$$+ \frac{\partial}{\partial x_2}\{\mu h_3 h_1[\frac{h_2}{h_1}\frac{\partial}{\partial x_1}(\frac{u_2}{h_2}) + \frac{h_1}{h_2}\frac{\partial}{\partial x_2}(\frac{u_1}{h_1})]\}$$

$$+ \frac{\partial}{\partial x_3} \{\mu h_1 h_2 [\frac{h_1}{h_3} \frac{\partial}{\partial x_3} (\frac{u_1}{h_1}) + \frac{h_3}{h_1} \frac{\partial}{\partial x_1} (\frac{u_3}{h_3})]\}]$$

$$+ \frac{\mu}{h_1 h_2} \{\frac{h_2}{h_1} \frac{\partial}{\partial x_1} (\frac{u_2}{h_2}) + \frac{h_1}{h_2} \frac{\partial}{\partial x_2} (\frac{u_1}{h_1})\} \frac{\partial h_1}{\partial x_2}$$

$$+ \frac{\mu}{h_1 h_3} \{\frac{h_1}{h_3} \frac{\partial}{\partial x_3} (\frac{u_1}{h_1}) + \frac{h_3}{h_1} \frac{\partial}{\partial x_1} (\frac{u_3}{h_3})\} \frac{\partial h_1}{\partial x_3}$$

$$- \frac{2\mu}{h_1 h_2} \{\frac{1}{h_2} \frac{\partial u_2}{\partial x_2} + \frac{u_3}{h_2 h_3} \frac{\partial h_2}{\partial x_3} - \frac{u_1}{h_1 h_2} \frac{\partial h_2}{\partial x_1}\} \frac{\partial h_2}{\partial x_1}$$

$$- \frac{2\mu}{h_1 h_3} \{\frac{1}{h_3} \frac{\partial u_3}{\partial x_3} + \frac{u_1}{h_3 h_1} \frac{\partial h_3}{\partial x_1} + \frac{u_1}{h_2 h_3} \frac{\partial h_3}{\partial x_2}\} \frac{\partial h_3}{\partial x_1}$$

$$+ F_1 \qquad \text{(A-2)}$$

$x_2$-component

$$\rho[\frac{\partial u_2}{\partial t} + \frac{u_1}{h_1} \frac{\partial u_2}{\partial x_1} + \frac{u_2}{h_2} \frac{\partial u_2}{\partial x_2} + \frac{u_3}{h_3} \frac{\partial u_2}{\partial x_3}$$

$$- u_3 (\frac{u_3}{h_3 h_2} \frac{\partial h_3}{\partial x_2} - \frac{u_2}{h_2 h_3} \frac{\partial h_2}{\partial x_3})$$

$$- u_1 (\frac{u_1}{h_1 h_2} \frac{\partial h_1}{\partial x_2} - \frac{u_2}{h_2 h_1} \frac{\partial h_2}{\partial x_1})$$

$$= - \frac{1}{h_2} \frac{\partial p}{\partial x_2}$$

$$+ \frac{1}{h_1 h_2 h_3} [\frac{\partial}{\partial x_1} \{\mu h_2 h_3 [\frac{h_2}{h_1} \frac{\partial}{\partial x_1} (\frac{u_2}{h_2}) + \frac{h_1}{h_2} \frac{\partial}{\partial x_2} (\frac{u_1}{h_1})]\}$$

$$+ \frac{\partial}{\partial x_2}\{ 2\mu h_3 h_1 (\frac{1}{h_2} \frac{u_2}{\partial x_2} + \frac{u_3}{h_2 h_3} \frac{\partial h_2}{\partial x_3} + \frac{u_1}{h_1 h_2} \frac{\partial h_2}{\partial x_1})$$

$$+ \frac{\partial}{\partial x_3}\{ \mu h_1 h_2 [\frac{h_3}{h_1} \frac{\partial}{\partial x_2} (\frac{u_3}{h_3}) + \frac{h_2}{h_3} \frac{\partial}{\partial x_3} (\frac{u_1}{h_2})]\}]$$

$$+ \frac{\mu}{h_2 h_3}\{ \frac{h_3}{h_2} \frac{\partial}{\partial x_2} (\frac{u_3}{h_3}) + \frac{h_2}{h_3} \frac{\partial}{\partial x_3} (\frac{u_2}{h_2})\} \frac{\partial h_2}{\partial x_3}$$

$$+ \frac{\mu}{h_2 h_1}\{ \frac{h_2}{h_1} \frac{\partial}{\partial x_1} (\frac{u_2}{h_2}) + \frac{h_1}{h_2} \frac{\partial}{\partial x_2} (\frac{u_1}{h_1})\} \frac{\partial h_2}{\partial x_1}$$

$$- \frac{2\mu}{h_2 h_3}\{ \frac{1}{h_3} \frac{\partial u_3}{x_3} + \frac{u_1}{h_3 h_1} \frac{\partial h_3}{x_1} + \frac{u_2}{h_2 h_3} \frac{\partial h_3}{x_2}\} \frac{\partial h_3}{x_2}$$

$$- \frac{2\mu}{h_2 h_1}\{ \frac{1}{h_1} \frac{\partial u_1}{\partial x_1} + \frac{u_2}{h_1 h_2} \frac{\partial h_1}{\partial x_2} + \frac{u_3}{h_3 h_1} \frac{\partial h_1}{\partial x_3}\} \frac{\partial h_1}{\partial x_2}$$

$$+ F_2 \qquad \text{(A-3)}$$

$x_3$-component

$$\rho[\frac{\partial u_3}{t} + \frac{u_1}{h_1} \frac{\partial u_3}{\partial x_1} + \frac{u_2}{h_2} \frac{\partial u_3}{\partial x_2} + \frac{u_3}{h_3} \frac{\partial u_3}{\partial x_3}$$

$$- u_1 (\frac{u_1}{h_1 h_3} \frac{\partial h_1}{\partial x_3} - \frac{u_3}{h_3 h_1} \frac{\partial h_3}{\partial x_1})$$

$$- u_2 (\frac{u_2}{h_2 h_3} \frac{\partial h_2}{\partial x_3} - \frac{u_3}{h_3 h_2} \frac{\partial h_3}{\partial x_2})]$$

$$= - \frac{1}{h_3} \frac{\partial p}{\partial x_3}$$

$$+\frac{1}{h_1h_2h_3}\left[\frac{\partial}{\partial x_1}\left\{\mu h_2h_3\left[\frac{h_1}{h_3}\frac{\partial}{\partial x_3}\left(\frac{u_1}{h_1}\right)+\frac{h_3}{h_1}\frac{\partial}{\partial x_1}\left(\frac{u_3}{h_3}\right)\right]\right\}\right.$$

$$+\frac{\partial}{\partial x_2}\left\{\mu h_3h_1\left[\frac{h_3}{h_2}\frac{\partial}{\partial x_2}\left(\frac{u_3}{h_3}\right)+\frac{h_2}{h_3}\frac{\partial}{\partial x_3}\left(\frac{u_2}{h_2}\right)\right]\right.$$

$$\left.\left.+\frac{\partial}{\partial x_3}\left\{2\mu h_1h_2\left(\frac{1}{h_3}\frac{\partial u_3}{\partial x_3}+\frac{u_1}{h_3h_1}\frac{\partial h_3}{\partial x_1}+\frac{u_2}{h_2h_3}\frac{\partial h_3}{\partial x_2}\right)\right\}\right]\right.$$

$$+\frac{\mu}{h_1h_3}\left\{\frac{h_1}{h_3}\frac{\partial}{\partial x_3}\left(\frac{u_1}{h_1}\right)+\frac{h_3}{h_1}\frac{\partial}{\partial x_1}\left(\frac{u_3}{h_3}\right)\right\}\cdot\frac{\partial h_3}{\partial x_1}$$

$$+\frac{\mu}{h_3h_2}\left\{\frac{h_3}{h_2}\frac{\partial}{x_2}\left(\frac{u_3}{h_3}\right)+\frac{h_2}{h_3}\frac{\partial}{x_3}\left(\frac{u_3}{h_2}\right)\right\}\cdot\frac{\partial h_3}{\partial x_2}$$

$$-\frac{2\mu}{h_3h_1}\left\{\frac{1}{h_1}\frac{\partial u_1}{\partial x_1}+\frac{u_2}{h_1h_2}\frac{\partial h_1}{\partial x_2}+\frac{u_3}{h_3h_1}\frac{\partial h_1}{\partial x_3}\right\}\frac{\partial h_1}{\partial x_3}$$

$$-\frac{2\mu}{h_3h_2}\left\{\frac{1}{h_2}\frac{\partial u_2}{\partial x_2}+\frac{u_3}{h_2h_3}\frac{\partial h_2}{\partial x_3}+\frac{u_1}{h_1h_2}\frac{\partial h_2}{\partial x_1}\right\}\frac{\partial h_2}{\partial x_3}$$

$$+F_3 \qquad \text{(A-4)}$$

Energy equation

$$\rho C_p\left(\frac{\partial T}{\partial t}+\frac{u_1}{h_1}\frac{\partial T}{\partial x_1}+\frac{u_2}{h_2}\frac{\partial T}{\partial x_2}+\frac{u_3}{h_3}\frac{\partial T}{\partial x_3}\right)$$

$$=k\left\{\frac{1}{h_1h_2h_3}\left[\frac{\partial}{x_1}\left(\frac{h_2h_3}{h_1}\frac{\partial T}{\partial x_1}\right)+\frac{\partial}{\partial x_2}\left(\frac{h_3h_1}{h_2}\frac{\partial T}{\partial x_2}\right)\right.\right.$$

$$\left.\left.+\frac{\partial}{\partial x_3}\left(\frac{h_1h_2}{h_3}\frac{\partial T}{\partial x_3}\right)\right]\right\} \qquad \text{(A-5)}$$

The metric coefficients $h_1$, $h_2$ and $h_3$ are

$$h_1 \equiv \left[\left(\frac{\partial X_1}{\partial x_1}\right)^2 + \left(\frac{\partial X_2}{\partial x_1}\right)^2 + \left(\frac{\partial X_3}{\partial x_1}\right)^2\right]^{1/2}$$

$$h_2 \equiv \left[\left(\frac{\partial X_1}{\partial x_2}\right)^2 + \left(\frac{\partial X_2}{\partial x_2}\right)^2 + \left(\frac{\partial X_3}{\partial x_2}\right)^2\right]^{1/2}$$

$$h_3 \equiv \left[\left(\frac{\partial X_1}{\partial x_3}\right)^2 + \left(\frac{\partial X_2}{\partial x_3}\right)^2 + \left(\frac{\partial X_3}{\partial x_3}\right)^2\right]^{1/2} \qquad \text{(A-6)}$$

and $X_1$, $X_2$ and $X_3$ are the orthogonal cartesian coordinates. $(F_1, F_2, F_3)$ represents the components of the extraneous force $\overline{F}$ per unit volume.

The derivation of individual terms of the invariant vector forms can be found, for example , in [94].

## APPENDIX 2

## DERIVATION OF THE GOVERNING EQUATIONS IN TOROIDAL COORDINATES FOR FLOW IN CURVED PIPES

The toroidal geometry shown in Fig. A-1 is characterized by the radius of curvature of the toroid axis $R_c$ and the radius of the toroid a. The relationships among the Cartesian coordinates $(X_1, X_2, X_3)$ and the toroidal coordinates $(R, \Phi, \Omega)$ shown in Fig. A-1 are:

$$X_1 = (R_c + R \cos \Phi) \cos \Omega - R_c$$

$$X_2 = R \sin \Phi$$

$$X_3 = (R_c + R \cos \Phi) \sin \Omega \qquad \text{(A-7)}$$

If $R$, $\Phi$, $\Omega$ are taken as $X_1$, $X_2$, $X_3$, respectively, in equation (A-6), then

$$h_1 \equiv \left[\left(\frac{\partial X_1}{\partial R}\right)^2 + \left(\frac{\partial X_2}{\partial R}\right)^2 + \left(\frac{\partial X_3}{\partial R}\right)^2\right]^{1/2} = 1$$

$$h_2 \equiv \left[\left(\frac{\partial X_1}{\partial \Phi}\right)^2 + \left(\frac{\partial X_2}{\partial \Phi}\right)^2 + \left(\frac{\partial X_3}{\partial \Phi}\right)^2\right]^{1/2} = R$$

$$h_3 \equiv \left[\left(\frac{\partial X_1}{\partial \Omega}\right)^2 + \left(\frac{\partial X_2}{\partial \Omega}\right)^2 + \left(\frac{\partial X_3}{\partial \Omega}\right)^2\right]^{1/2} = R_c + R \cos \Phi \qquad \text{(A-8)}$$

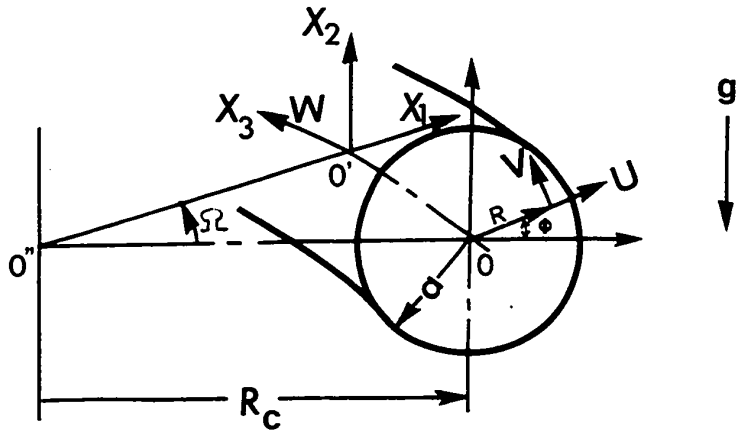


Fig. A-1 Toroidal Coordinate System

One notes that the toroidal coordinate system reduces to the two limiting cases of cylindrical and spherical coordinate systems as $R_c \to \infty$ and $R_c \to 0$, respectively. Using equations (A-8), the governing equations (A-1) - (A-5) become:

Continuity equation

$$\frac{1}{R(R_c + R\cos\Phi)} \frac{\partial}{\partial R}[R(R_c + R\cos\Phi)U]$$

$$+ \frac{1}{R_c + R\cos\Phi} \frac{\partial}{R\partial\Phi}[(R_c + R\cos\Phi)V]$$

$$+ \frac{1}{R_c + R\cos\Phi}\frac{\partial W}{\partial \Omega} = 0 \qquad \text{(A-9)}$$

R-momentum equation

$$U\frac{\partial U}{\partial R} + \frac{V}{R}\frac{\partial U}{\partial \Phi} + \frac{W}{R_c + R\cos\Phi}\frac{\partial U}{\partial \Omega} - \frac{V^2}{R} - \frac{\cos\Phi}{R_c + R\cos\Phi}W^2$$

$$= -\frac{1}{\rho}\frac{\partial P}{\partial R} + \beta g(T - T_W)\sin\Phi + \beta\frac{\cos\Phi}{R_c + R\cos\Phi}W^2(T - T_W)$$

$$- \nu\left[\frac{1}{R}\frac{\partial^2 V}{\partial\Phi\partial R} + \frac{1}{R^2}\frac{\partial V}{\partial\Phi} - \frac{1}{R^2}\frac{\partial^2 U}{\partial\Phi^2} - \frac{\sin\Phi}{R_c + R\cos\Phi}\left(\frac{\partial V}{\partial R} + \frac{V}{R} - \frac{1}{R}\frac{\partial U}{\partial\Phi}\right)\right.$$

$$\left. - \frac{1}{R_c + R\cos\Phi}\left(\frac{1}{R_c + R\cos\Phi}\frac{\partial^2 U}{\partial\Omega^2} - \frac{\partial^2 W}{\partial R\partial\Omega} - \frac{\cos\Phi}{R_c + R\cos\Phi}\frac{\partial W}{\partial\Omega}\right)\right] \qquad \text{(A-10)}$$

$\phi$-momentum equation

$$U\frac{\partial V}{\partial R} + \frac{V}{R}\frac{\partial V}{\partial\Phi} + \frac{W}{R_c + R\cos\Phi}\frac{\partial V}{\partial\Omega} + \frac{UV}{R} + \frac{\sin\Phi}{R_c + R\cos\Phi}W^2$$

$$= -\frac{1}{\rho}\frac{1}{R}\frac{\partial P}{\partial\Phi} + \beta g(T - T_W)\cos\Phi + \beta\frac{\sin\Phi}{R_c + R\cos\Phi}W^2(T - T_W)$$

$$+ \nu\left[\frac{\partial^2 V}{\partial R^2} + \frac{1}{R}\frac{\partial V}{\partial R} - \frac{V}{R^2} - \frac{1}{R}\frac{\partial^2 U}{\partial\Phi\partial R} + \frac{1}{R^2}\frac{\partial U}{\partial\Phi}\right.$$

$$+ \frac{\cos\Phi}{R_c + R\cos\Phi}\left(\frac{\partial V}{\partial R} + \frac{V}{R} - \frac{1}{R}\frac{\partial U}{\partial\Phi}\right)$$

$$\left. - \frac{1}{R_c + R\cos\Phi}\left(\frac{1\partial^2}{R\partial\Phi\partial\Omega} - \frac{\sin\Phi}{R_c + R\cos\Phi}\frac{\partial}{\partial\Omega} - \frac{1}{R_c + R\cos\Phi}\frac{\partial^2}{\partial\Omega^2}\right)\right] \qquad \text{(A-11)}$$

Ω-momentum equation

$$U\frac{\partial W}{\partial R}+\frac{V}{R}\frac{\partial W}{\partial \Phi}+\frac{W}{R_c+R\cos\Phi}\frac{\partial W}{\partial \Omega}+\frac{\cos\Phi}{R_c+R\cos\Phi}UW-\frac{\sin\Phi}{R_c+R\cos\Phi}VW$$

$$=-\frac{1}{\rho}\frac{1}{R_c+R\cos\Phi}\frac{\partial P}{\partial \Omega}+$$

$$+\nu\Big[\frac{\partial^2 W}{\partial R^2}+\frac{\cos\Phi}{R_c+R\cos\Phi}\frac{\partial W}{\partial R}-\frac{1}{(R_c+R\cos\Phi)^2}W$$

$$+\frac{1}{R}\frac{\partial W}{\partial R}+\frac{1}{R^2}\frac{\partial^2 W}{\partial \Phi^2}-\frac{\sin\Phi}{R_c+R\cos\Phi}\frac{1}{R}\frac{\partial W}{\partial \Phi}$$

$$+\frac{1}{(R_c+R\cos\Phi)^2}\Big(\frac{\partial^2 W}{\partial \Omega^2}+2\cos\Phi\frac{\partial U}{\partial \Omega}$$

$$-2\sin\Phi\frac{\partial V}{\partial \Omega}\Big)\Big] \qquad \text{(A-12)}$$

Energy equation

$$U\frac{\partial T}{\partial R}+\frac{V}{R}\frac{\partial T}{\partial \Phi}+\frac{W}{R_c+R\cos\Phi}\frac{\partial T}{\partial \Omega}$$

$$=\Big[\frac{\partial^2 T}{\partial R^2}+\frac{1}{R}\frac{\partial T}{\partial R}+\frac{\cos\Phi}{R_c+R\cos\Phi}\frac{\partial T}{\partial R}+\frac{1}{R^2}\frac{\partial^2 T}{\partial \Phi^2}$$

$$-\frac{\sin\Phi}{R_c+R\cos\Phi}\frac{1}{R}\frac{\partial T}{\partial \Phi}+\frac{1}{(R_c+R\cos\Phi)^2}\frac{\partial^2 T}{\partial \Omega^2}\Big] \qquad \text{(A-13)}$$

It is seen that the governing equations shown above do not

accommodate all the effects of the buoyancy forces. In this respect, it should be pointed out that any acceleration field associated with density variation will give rise to buoyancy forces. For example, in equation (A-10) the buoyancy force term in the centrifugal force field using the Boussinesq approximation is included. On the other hand, the following terms, representing the buoyancy forces in the Coriolis acceleration field, are not included in the $\Omega$-momentum equation.

$$\beta \left\{ - \frac{\cos \Phi}{R_c + R \cos \Phi} UW + \frac{\sin \Phi}{(R_c + R \cos \Phi)} VW \right\} (T - T_W)$$

Apparently, the buoyancy forces due to density variation in the convective acceleration field are usually neglected. The importance of the particular buoyancy force depends on the magnitude of its acceleration relative to the gravitational acceleration g.

# APPENDIX 3

## DERIVATION OF THE GOVERNING EQUATIONS IN RECTANGULAR TOROIDAL COORDINATES FOR FLOW IN CURVED RECTANGULAR CHANNELS

Referring to the Cartesian Coordinates $(X_1, X_2, X_3)$ and the rectangular toroidal coordinates $(X, Y, \Omega)$ shown in Fig. A-Z, one obtains

$$X_1 = (R_c + X) \cos \Omega - R_c$$

$$X_2 = Y$$

$$X_3 = (R_c + X) \sin \Omega \qquad \text{(A-14)}$$

Then the three metric coefficients $h_1$, $h_2$, $h_3$ in the general orthogonal coordinates become

$$h_1 \equiv \left[\left(\frac{\partial X_1}{\partial X}\right)^2 + \left(\frac{\partial X_2}{\partial X}\right)^2 + \left(\frac{\partial X_3}{\partial X}\right)^2\right]^{1/2} = 1$$

$$h_2 \equiv \left[\left(\frac{\partial X_1}{\partial Y}\right)^2 + \left(\frac{\partial X_2}{\partial Y}\right)^2 + \left(\frac{\partial X_3}{\partial Y}\right)^2\right]^{1/2} = 1$$

$$h_3 \equiv \left[\left(\frac{\partial X_1}{\partial \Omega}\right)^2 + \left(\frac{\partial X_2}{\partial \Omega}\right)^2 + \left(\frac{\partial X_3}{\partial \Omega}\right)^2\right]^{1/2} = R_c + X \qquad \text{(A-15)}$$

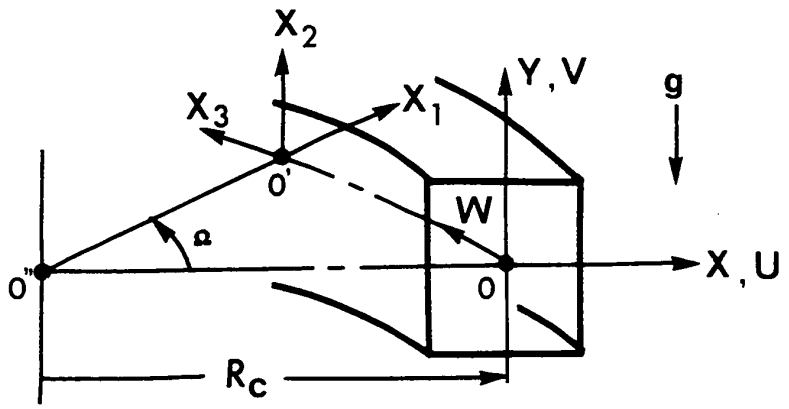


Fig. A-2 Rectangular Toroidal Coordinate System

It is seen that the rectangular toroidal coordinate system reduces to the common rectangular and cylindrical coordinate systems as $R_c \to \infty$ and $R_c \to 0$, respectively. With equation (A-15), the governing equations can be written as:

Continuity equation

$$\frac{\partial}{\partial X}\left[(R_c + X)\, U\right] + \frac{\partial}{\partial Y}\left[(R_c + X)\, V\right] + \frac{\partial W}{\partial \Omega} = 0 \qquad \text{(A-16)}$$

X-momentum equation

$$U \frac{\partial U}{\partial X} + V \frac{\partial U}{\partial Y} + \frac{W}{R_c + X} \frac{\partial U}{\partial \Omega} - \frac{W^2}{R_c + X}$$

$$= - \frac{1}{\rho} \frac{\partial P}{\partial X} - \beta \frac{W^2}{(R_c + X)} (T - T_W) + \nu \left[ \frac{\partial^2 U}{\partial Y^2} + \frac{1}{(R_c + X)^2} \frac{\partial^2 U}{\partial \Omega^2} - \frac{\partial^2 V}{\partial X \partial Y} \right.$$

$$\left. - \frac{1}{R_c + X} \frac{\partial^2 W}{\partial X \partial \Omega} - \frac{1}{(R_c + X)^2} \frac{\partial W}{\partial \Omega} \right] \qquad \text{(A-17)}$$

Y-momentum equation

$$U \frac{\partial V}{\partial X} + \frac{\partial V}{\partial Y} + \frac{W}{R_c + X} \frac{\partial V}{\partial \Omega}$$

$$= - \frac{1}{\rho} \frac{\partial P}{\partial Y} + \beta g (T - T_W)$$

$$+ \nu \left[ - \frac{\partial^2 U}{\partial X \partial Y} - \frac{1}{(R_c + X)} \frac{\partial U}{\partial Y} + \frac{\partial^2 V}{\partial X^2} + \frac{1}{R_c + X} \frac{\partial V}{\partial X} \right.$$

$$\left. + \frac{1}{(R_c + X)^2} \frac{\partial^2 V}{\partial \Omega^2} - \frac{1}{(R_c + X)} \frac{\partial^2 W}{\partial Y \partial \Omega} \right] \qquad \text{(A-18)}$$

Ω-momentum equation

$$U \frac{\partial W}{\partial X} + V \frac{\partial W}{\partial Y} + \frac{W}{R_c + X} \frac{\partial W}{\partial \Omega} + \frac{UW}{R_c + X}$$

$$= - \frac{1}{\rho} \frac{1}{R_c + X} \frac{\partial P}{\partial \Omega}$$

$$+ \nu\left[\frac{1}{(R_c + X)^2}\frac{\partial^2 W}{\partial \Omega^2} + \frac{2}{(R_c + X)^2}\frac{\partial U}{\partial \Omega} + \frac{\partial^2 W}{\partial X^2} + \frac{1}{R_c + X}\frac{\partial W}{\partial X}\right.$$

$$\left. - \frac{W}{(R_c + X)^2} + \frac{\partial^2 W}{\partial Y^2}\right] \qquad \text{(A-19)}$$

Energy equation

$$U\frac{\partial T}{\partial X} + V\frac{\partial T}{\partial Y} + \frac{W}{R_c + X}\frac{\partial T}{\partial \Omega}$$

$$= \alpha\left[\frac{\partial^2 T}{\partial X^2} + \frac{1}{R_c + X}\frac{\partial T}{\partial X} + \frac{\partial^2 T}{\partial Y^2} + \frac{1}{(R_c + X)^2}\frac{\partial^2 T}{\partial \Omega^2}\right] \qquad \text{(A-20)}$$

## APPENDIX 4

## A DEDUCTIVE ANALYSIS OF THE GOVERNING EQUATIONS FOR CURVED RECTANGULAR CHANNELS

Referring to the coordinate system shown in Fig. A-2, one may introduce suitable reference quantities and define the following normalized variables:

$$u = U/U_c, \quad v = V/V_c, \quad w = W/W_c,$$

$$x = X/a, \quad y = Y/b, \quad \omega = \Omega/\Omega_c,$$

$$p = P/P_c \text{ and } \theta = (T - T_w)/\Theta_c$$

where subscript c indicates a reference quantity. In terms of the dimensionless variables defined above, the continuity equation (A-16) becomes

$$[\frac{U_c}{V_c}][\frac{b}{a}] \left(\frac{\partial u}{\partial x} + [\lambda] \frac{u}{(1 + \lambda x)} + [\lambda][\frac{W_c}{\Omega_c U_c}] \frac{1}{(1 + \lambda x)} \frac{\partial w}{\partial \omega}\right)$$

$$+ \frac{\partial v}{\partial y} = 0 \qquad \text{(A-21)}$$

where $\lambda = a/R_c$

By considering secondary flow, one may regard $\partial u/\partial x$ and $\partial v/\partial y$ be of equal order of magnitude.

This observation leads to

$$[\frac{U_c}{V_c}][\frac{b}{a}] = [\frac{U_c}{V_c}][\gamma] = O[1] \qquad \text{(A-22)}$$

The continuity equation now becomes

$$\frac{\partial u}{\partial x} + [\lambda]\frac{u}{(1+\lambda x)} + \frac{\partial v}{\partial y} + [\lambda]\left[\frac{W_c}{\Omega_c U_c}\right]\frac{1}{(1+\lambda x)}\frac{\partial w}{\partial \omega} = 0$$

or

$$\frac{\partial u}{\partial x} + [\lambda]\frac{u}{(1+\lambda x)} + \frac{\partial v}{\partial y} + \left[\frac{W_c}{U_c}\right]\sigma\frac{1}{(1+\lambda x)}\frac{\partial w}{\partial \omega} = 0 \qquad \text{(A-24)}$$

where

$$\sigma = \lambda/\Omega_c = a/(R_c\Omega_c) \qquad \text{(A-25)}$$

A Deductive Analysis Based on the Assumption that the Centrifugal Force Term is of Order Unity

The following relation results from the X-momentum equation by considering the centrifugal force term and the viscous terms to be of equal importance.

$$\frac{U_c}{W_c} = \frac{1}{2}(Re\lambda^{1/2}) \cdot \lambda^{1/2} \cdot \gamma^2 \qquad \text{(A-26)}$$

where $\lambda = a/R_c$, $\gamma = b/a$

Using the above relationship, the governing equations become:

Continuity equation

$$\frac{\partial u}{\partial x} + \lambda\frac{u}{(1+x)} + \frac{\partial v}{\partial y} + K^{-1}\gamma^2\lambda^{-1/2}\frac{2}{(1+\lambda x)}\frac{\partial w}{\partial \omega} = 0 \qquad \text{(A-27)}$$

X-momentum equation

$$K^2\gamma^4 \frac{1}{4}\left(u\frac{\partial u}{\partial x} + v\frac{\partial u}{\partial y}\right) + K\gamma^2\sigma\lambda^{-1/2}\frac{1}{2(1+\lambda x)} w\frac{\partial u}{\partial \omega}$$

$$= -\frac{P_c}{\rho W_c^2}\lambda^{-1}\frac{\partial p}{\partial x} + \frac{\partial^2 u}{\partial y^2} - \gamma^2\frac{\partial^2 v}{\partial x \partial y} - K^{-1}\sigma\lambda^{-1/2}\frac{2}{(1+\lambda x)}\frac{\partial^2 w}{\partial x \partial \omega}$$

$$- K^{-1}\sigma\lambda^{1/2}\frac{2}{(1+\lambda x)}\frac{\partial w}{\partial \omega}$$

$$+ \frac{w^2}{(1+\lambda x)} - \frac{1}{4}\mathrm{Gr}K^{-2}\mathrm{Fr}\theta\frac{w^2}{(1+\lambda x)} \qquad \text{(A-28)}$$

Y-momentum equation

$$K^2\gamma^4 \frac{1}{4}\left(u\frac{\partial v}{\partial x} + v\frac{\partial v}{\partial y}\right) + K\gamma^2\sigma\lambda^{-1/2}\frac{1}{2(1+\lambda x)} w\frac{\partial v}{\partial \omega}$$

$$= -\frac{P_2}{\rho W_c^2}\lambda^{-1}\gamma^{-2}\frac{\partial p}{\partial y} - \frac{\partial^2 u}{\partial x \partial y} - \lambda\frac{1}{(1+\lambda x)}\frac{\partial u}{\partial y} + \gamma^2\frac{\partial^2 v}{\partial x^2}$$

$$+ \lambda\gamma^2\frac{1}{(1+\lambda x)}\frac{\partial v}{\partial x} + \gamma^2\sigma^2\frac{1}{(1+\lambda x)}\frac{\partial^2 v}{\partial \omega^2}$$

$$+ 2K^{-1}\gamma^{-2}\sigma\lambda^{-1/2}\frac{1}{(1+\lambda x)}\frac{\partial^2 w}{\partial y \partial \omega}$$

$$+ \mathrm{Gr}\frac{1}{4}K^{-2}\gamma^{-1}\theta \qquad \text{(A-29)}$$

Ω-momentum equation

$$K^2\gamma^4 \frac{1}{4}\left(u\frac{\partial w}{\partial x} + v\frac{\partial w}{\partial y}\right) + K\gamma^2\sigma\lambda^{-1/2}\frac{1}{2(1+\lambda x)} w\frac{\partial w}{\partial \omega}$$

$$= -\frac{P_c}{\rho w_c^2}\gamma^2\frac{\partial D}{\partial \omega}$$

$$+ \sigma^2\lambda\gamma^2\left(\lambda\frac{2}{(1+\lambda x)^2}\frac{\partial u}{\partial \omega} + \frac{1}{(1+\lambda x)^2}\frac{\partial^2 w}{\partial \omega^2}\right)$$

$$+ \gamma^2\left(\frac{\partial^2 w}{\partial x^2} + \frac{1}{(1+\lambda x)}\frac{\partial w}{\partial x} - \lambda^2\frac{w}{(1+\lambda x)^2} + \frac{\partial^2 w}{\partial y^2}\right)$$

$$- K\gamma^4\lambda\frac{uw}{4(1+\lambda x)} \qquad \text{(A-30)}$$

Energy equation

$$K^2 Pr\gamma^4\frac{1}{4}\left(u\frac{\partial \theta}{\partial x} + v\frac{\partial \theta}{\partial y}\right) + K\gamma^2\sigma_\theta\lambda^{-1/2}Pr\frac{w}{2(1+\lambda_a x)}\frac{\partial \theta}{\partial \omega}$$

$$= \gamma^2\left(\frac{\partial^2\theta}{\partial x^2} + \lambda\frac{1}{(1+\lambda x)}\frac{\partial \theta}{\partial x} + \gamma^{-2}\frac{\partial^2\theta}{\partial y^2}\right) + \sigma_\theta^2\lambda\gamma^2\frac{1}{(1+\lambda x)^2}\frac{\partial^2\theta}{\partial \omega^2} \qquad \text{(A-31)}$$

One notes that the characteristic parameters appearing in the governing equations are similar to those given in equations (6) to (10) for curved circular pipes. Because of the geometrical configuration, the aspect ratio $\gamma = b/a$ appears additionally as a geometrical parameter for the present problem. Another set of governing equations can be

obtained by considering the lateral convective terms to be of the same order of magnitude as the lateral conduction terms in the energy equation.

A Deductive Analysis Based on the Assumption that the Lateral Convective Terms in the Energy Equation are of Order Unity

The results of the analysis are as follows:

$$\frac{\partial u}{\partial x} + \lambda\frac{u}{(1+\lambda x)} + \frac{\partial v}{\partial y} + \frac{1}{2}\,KPr\sigma\lambda^{-1/2}\gamma^2\,\frac{1}{(1+\lambda x)}\,\frac{\partial w}{\partial \omega} = 0 \qquad \text{(A-32)}$$

X-momentum equation

$$\gamma^4 Pr^{-1}\left(u\,\frac{\partial u}{\partial x} + v\,\frac{\partial u}{\partial y}\right) + \frac{1}{2}\,K\gamma^2\sigma\lambda^{-1/2}\,\frac{1}{(1+\lambda x)}\,w\,\frac{\partial u}{\partial \omega}$$

$$= -\frac{1}{2}\,Pr\sigma^{-1}K\lambda^{-1/2}\,\frac{\partial p}{\partial x} + \frac{\partial^2 u}{\partial y^2} - \gamma^2\,\frac{\partial^2 v}{\partial x \partial y} + \frac{1}{2}\,KPr\sigma\lambda^{-1/2}\,\frac{1}{(1+\lambda x)}\,\frac{\partial^2 w}{\partial x \partial \omega}$$

$$-\frac{1}{2}\,KPr\sigma\lambda^{1/2}\,\frac{1}{(1+\lambda x)}\,\frac{\partial w}{\partial \omega} + \frac{w^2}{(1+\lambda x)} \qquad \text{(A-33)}$$

Y-momentum equation

$$\gamma^4 Pr^{-1}\left(u\,\frac{\partial v}{\partial x} + v\,\frac{\partial v}{\partial y}\right) + \frac{1}{2}\,K\gamma^2\sigma\lambda^{-1/2}\,\frac{1}{(1+\lambda x)}\,w\,\frac{\partial v}{\partial \omega}$$

$$= -\frac{1}{2}\,Pr\sigma^{-1}K\lambda^{-1/2}\,\frac{\partial p}{\partial y} - \frac{\partial^2 u}{\partial x \partial y} - \lambda\frac{1}{(1+\lambda x)}\,\frac{\partial u}{\partial y} + \gamma^2\,\frac{\partial^2 v}{\partial x^2}$$

$$+ \lambda\gamma^2 \frac{1}{(1+\lambda x)} \frac{\partial v}{\partial x} + \gamma^2\sigma^2 \frac{1}{(1+\lambda x)} \frac{\partial^2 v}{\partial \omega^2}$$

$$+ \frac{1}{2} KPr\sigma\lambda^{-1/2}\gamma^{-2} \frac{1}{(1+\lambda x)} \frac{\partial^2 w}{\partial y \partial \omega}$$

$$+ \frac{1}{8} GrPr\theta \qquad \text{(A-34)}$$

Ω-momentum equation

$$\gamma^4 Pr^{-1}(u \frac{\partial w}{\partial x} + v \frac{\partial w}{\partial y}) + \frac{1}{2} K\sigma\gamma^2\lambda^{-1/2} \frac{1}{(1+\lambda x)} w \frac{\partial w}{\partial \omega}$$

$$= \frac{1}{(1+\lambda x)} \frac{\partial p}{\partial \omega} + \gamma^2(\frac{\partial^2 w}{\partial x^2} + \lambda \frac{1}{(1+\lambda x)} \frac{\partial w}{\partial x} - \lambda^2 \frac{w}{(1+\lambda x)^2} + \frac{\partial^2 w}{\partial y^2})$$

$$+ \sigma^2 Pr^{-1}\gamma^2\lambda(\lambda \frac{2}{(1+\lambda x)^2} \frac{\partial u}{\partial \omega} + \frac{1}{(1+\lambda x)^2} \frac{\partial^2 w}{\partial \omega^2})$$

$$- Pr^{-1}\lambda\gamma^4 \frac{uw}{(1+x)} \qquad \text{(A-35)}$$

Energy equation

$$u \frac{\partial \theta}{\partial x} + v \frac{\partial \theta}{\partial y} + \frac{1}{2} KPr\sigma_\theta\gamma^2\lambda^{-1/2} w \frac{\partial \theta}{\partial \omega_\theta}$$

$$= \gamma^2(\frac{\partial^2 \theta}{\partial x^2} + \lambda \frac{1}{(1+\lambda x)} \frac{\partial \theta}{\partial x} + \gamma^{-2} \frac{\partial^2 \theta}{\partial y^2}) + \sigma_\theta^2\lambda\gamma^2 \frac{1}{(1+\lambda x)^2} \frac{\partial^2 \theta}{\partial \omega^2} \qquad \text{(A-36)}$$

The foregoing two sets of governing equations are equally applicable to hydro ynamically and thermally developing flow fields.

However, it is clear that the first set of equations (A-27) to (A-31) is preferable when the hydrodynamic entrance region is of primary interest whereas the latter set of equations (A-32) to (A-36) may be more suitable if the emphasis is on developing thermal fields such as the classical Graetz problem. As shown in Sections 2.3 to 2.5, a simplification of the governing equations is possible by such assumptions as large Reynolds numbers, large Peclet numbers, large Prandtl number fluids and small curvature ratios $\lambda$ . However, these possibilities will not be discussed further since they are analogous to those of curved circular pipes.

# APPENDIX 5

## A NOTE ON VORTICITY METHODS IN NUMERICAL SOLUTIONS

### 5.1 INTRODUCTION

In dealing with the steady two dimensional flow problem, the introduction of a stream function leads to a fourth order quasi-linear elliptic partial differential equation representing the vorticity transport equation. When one introduces the vorticity, the fourth order differential equation can be decomposed into two second order differential equations. This use of vorticity is gaining its popularity in treating many two dimensional flow problems numerically.

For the purpose of discussing the numerical solution, one may consider the following set of equations without loss of generality.

$$\frac{\partial^2 \psi}{\partial x^2} + \frac{\partial^2 \psi}{\partial y^2} = \zeta \qquad \text{(A-37)}$$

$$\frac{\partial^2 \zeta}{\partial x^2} + \frac{\partial^2 \zeta}{\partial y^2} = f \qquad \text{(A-38)}$$

where f is a known function. It is noted that the function f may include the nonlinear terms in the vorticity transport equation.

For convenience, one may consider the solutions of equations (A-37) and (A-38) for a square region with the following boundary conditions:

$$\psi = \zeta = 0 \quad \text{on} \quad AB \quad \text{and} \quad OC$$

$$\psi = \frac{\partial \psi}{\partial y} = 0 \quad \text{on} \quad OA \quad \text{and} \quad BC$$

The coordinate system, boundary conditions and nodal points are shown in Fig. A-3. Note that, physically the lines OA and BC represent walls of the channel and the conditions on AB and OC signify the line of symmetry. This rather special arrangement of the boundary conditions is somewhat similar to that applied to the problem written in cylindrical coordinates seen in Chapter III.

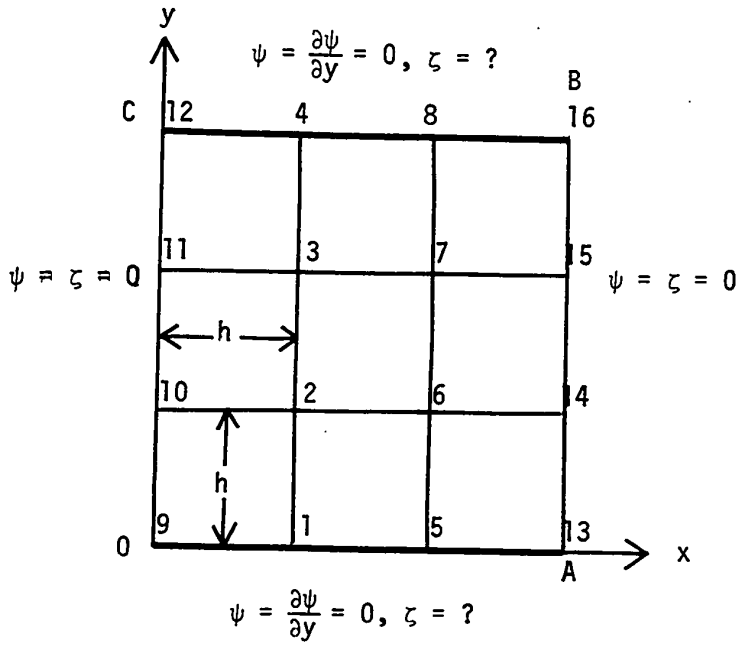


Fig. A-3 Coordinate System and Numerical Grid

Using a five-point finite-difference approximation and considering the boundary conditions indicated in Fig. A-3 the systems of linear algebraic equations representing equations (A-37) and (A-38) become

$$\begin{bmatrix} -4 & 2 & 0 & 0 & 1 & 0 & 0 & 0 \\ 1 & -4 & 1 & 0 & 0 & 1 & 0 & 0 \\ 0 & 1 & -4 & 1 & 0 & 0 & 1 & 0 \\ 0 & 0 & 2 & -4 & 0 & 0 & 0 & 1 \\ 1 & 0 & 0 & 0 & -4 & 2 & 0 & 0 \\ 0 & 1 & 0 & 0 & 1 & -4 & 1 & 0 \\ 0 & 0 & 1 & 0 & 0 & 1 & -4 & 1 \\ 0 & 0 & 0 & 1 & 0 & 0 & 2 & -4 \end{bmatrix} \begin{bmatrix} \psi_1 \\ \psi_2 \\ \psi_3 \\ \psi_4 \\ \psi_5 \\ \psi_6 \\ \psi_7 \\ \psi_8 \end{bmatrix} = h^2 \begin{bmatrix} \zeta_1 \\ \zeta_2 \\ \zeta_3 \\ \zeta_4 \\ \zeta_5 \\ \zeta_6 \\ \zeta_7 \\ \zeta_8 \end{bmatrix} \tag{A-39}$$

$$\begin{bmatrix} -4 & 1 & 1 & 0 \\ 1 & -4 & 0 & 1 \\ 1 & 0 & -4 & 1 \\ 0 & 1 & 1 & -4 \end{bmatrix} \begin{bmatrix} \zeta_2 \\ \zeta_3 \\ \zeta_6 \\ \zeta_7 \end{bmatrix} = h^2 \begin{bmatrix} f_2 \\ f_3 \\ f_6 \\ f_7 \end{bmatrix} - \begin{bmatrix} \zeta_1 \\ \zeta_4 \\ \zeta_5 \\ \zeta_8 \end{bmatrix} \tag{A-40}$$

In the above set of equations, the boundary conditions, $\psi_1 = \psi_4 = \psi_5$ $\psi_8 = 0$, have not been applied yet. A total of 12 algebraic equations for 16 unknowns are obtained at this stage, and the unknown boundary vorticities $\zeta_1$, $\zeta_4$, $\zeta_5$ and $\zeta_8$ have to be determined. The methods of solving the problem expressed by equations (A-39) and (A-40) with vorticity may be categorized into two types depending on the usage of the re-

lationship between vorticity and stream function.

The first type may be called the "stream function-vorticity" method [142] which consists, usually, of an iterative use of the following procedure:

(1) evaluation of the stream function with equation (A-39) using assigned vorticity values,

(2) calculation of the values of vorticity at the boundary with the equation for the relationship between stream function and vorticity at the boundary using the new values for stream function obtained in step (1),

(3) calculation of interior vorticities with equation (A-40) using the stream functions and the boundary vorticity obtained in step (1) and (2), respectively.

The second type may be called the vorticity method where a linear relationship between vorticity and stream function will directly be applied thereby avoiding an iteration process in determining the values for vorticity as well as for the stream function. Particularly, a method of this type called the "boundary vorticity" method is used in the combined forced and free convection problem in a horizontal tube by Hwang and Cheng [96]. A natural extension of the above method which will be referred to as the "direct vorticity method" is also presented here.

Generally, all three methods mentioned above can be applied together with the line successive relaxation method in solving the system of equations (A-39) and (A-40). For example, consider points 1, 2, 3, and 4 along a fixed column in Fig. A-3. The algebraic equations for this column can be expressed as follows after rearranging equations

(A-37) and (A-38)

$$\begin{bmatrix} -4 & 2 & 0 & 0 \\ 1 & -4 & 1 & 0 \\ 0 & 1 & -4 & 1 \\ 0 & 0 & 2 & -4 \end{bmatrix} \begin{bmatrix} \psi_1 \\ \psi_2 \\ \psi_3 \\ \psi_4 \end{bmatrix} = \begin{bmatrix} h_2\zeta_1 - \psi_5 \\ h^2\zeta_2 - \psi_6 \\ h^2\zeta_3 - \psi_7 \\ h^2\zeta_4 - \psi_8 \end{bmatrix} \tag{A-41}$$

$$\begin{bmatrix} -4 & 1 \\ 1 & -4 \end{bmatrix} \begin{bmatrix} \zeta_2 \\ \zeta_3 \end{bmatrix} = \begin{bmatrix} h^2f_2 - \zeta_1 - \zeta_6 \\ h^2f_3 - \zeta_4 - \zeta_7 \end{bmatrix} \tag{A-42}$$

As noted earlier, in deriving equation (A-37) and (A-38), the boundary conditions, $\psi_1 = \psi_5 = \psi_4 = \psi_8 = 0$, have not been used yet in the above equations. The values for $\zeta_6$, $\zeta_7$, $\psi_6$ and $\psi_7$ are known and taken from the latest iteration step. Thus, along the line, one has a total of six equations (A-41) and (A-42) for eight unknowns, $\psi_i$ and $\zeta_i$($i$ = 1,2, 3, and 4). Now the problem is to determine the unknown vortices $\zeta_1$ and $\zeta_4$. Since each method has its different features, some explanation and illustration of the individual methods will be given next.

## 5.2 STREAM FUNCTION-VORTICITY METHOD

In the stream function-vorticity method, two more algebraic equations will be directly established by using the boundary conditions of $\psi_1 = \psi_5 = \psi_4 = \psi_8 = 0$. When one substitutes these boundary conditions into the first and last equations of equation number (A-41), one has

$$\zeta_1 = 2\psi_2/h^2 \text{ and } \zeta_4 = 2\psi_3/h^2 \tag{A-43}$$

Thus, all the unknowns in equation (A-41) and (A-42) can be determined by applying the above relationships. One notes that the truncation error in equation (A-43) is of order h.

Instead of equation (A-41) for the relationships between the vorticities and the stream functions at the boundary points 1 and 4, higher order approximation equations may be desirable. For example, Jenson [143] gives the following expressions.

$$\zeta_1 = (8\psi_2 - \psi_3)/(2h^2) \tag{A-44}$$

and

$$\zeta_4 = (8\psi_3 - \psi_2)/(2h^2)$$

The above equations will now be used in place of the first and second equations in equation number (A-41). The truncation error in the above equation is now of order $h^2$, but these require two interior point values for the stream functions $\psi_2$ and $\psi_3$.

Using the vorticities adjacent to the boundary point $\zeta_2$ and $\zeta_3$, one can have another type of approximation [103] as follows:

$$\zeta_1 = -\zeta_2/2 - 3\psi_2/h^2 \tag{A-45}$$

$$\zeta_4 = -\zeta_3/2 + 3\psi_3/h^4$$

The order of truncation error of the above equation is also $h^2$.

The usual computational procedure is as follows: First calculate $\psi_2$ and $\psi_3$ using equation (A-41) by assigning suitable values

for $\zeta_1$, $\zeta_2$, $\zeta_3$ and $\zeta_4$ and using the boundary conditions $\psi_1 = \psi_4 = \psi_5 = \psi_8 = 0$. Use equation (A-43), (A-44) or (A-45) to get $\zeta_1$ and $\zeta_4$. Then by using equation (A-42), new values for $\zeta_2$ and $\zeta_3$ can be found. The process will now move to the next line containing points 5, 6, 7 and 8. The whole procedure will be repeated until the following condition is satisfied:

$$\max\left\{ \left| \frac{\psi_i^{n+1} - \psi_i^n}{\psi_i} \right| \left| \frac{\zeta_i^{n+1} - \zeta_i^n}{\zeta_i^n} \right| \right\} \leq \varepsilon \qquad \text{(A-46)}$$

where $\varepsilon$ is a small prescribed quantity.

Some remarks on the choice of stream function-vorticity relationship at the boundary are in order. The first approximation using equation (A-43) has a large truncation error of O[h], but is a stable approximation in many cases and most often used. Equation (A-44) is an approximation having a truncation error of $O[h^2]$, but some numerical experiments [103] showed greater instability with this equation. The slightly less accurate approximation of equation (A-45) is recommended in order to avoid a rather unrealistic discontinuity [103] in vorticity at the boundary points encountered using equation (A-43).

## 5.3 THE VORTICITY METHODS

### The Boundary Vorticity Method

After eliminating the unknowns at nodal points 2 and 3, one obtains the following linear relationship between $\psi_1$, $\psi_4$ and $\zeta_1$, $\zeta_4$ from equation (A-41) and (A-42) [96];

$$\begin{bmatrix} \psi_1 \\ \psi_4 \end{bmatrix} = \begin{bmatrix} a_{11} & a_{12} \\ a_{21} & a_{22} \end{bmatrix} \begin{bmatrix} \zeta_1 \\ \zeta_4 \end{bmatrix} + \begin{bmatrix} k_1 \\ k_2 \end{bmatrix} \qquad \text{(A-47)}$$

The procedure of finding the coefficient elements $a_{11}$, $a_{12}$, $a_{21}$, $k_1$ and $k_2$ follows next. At the beginning one assumes that $\zeta_1 = \zeta_1^{(1)}$ and $\zeta_4 = \zeta_4^{(1)}$ in equations (A-42). Then equation (A-42) can be solved simultaneously for $\zeta_2$ and $\zeta_3$ by using the Thomas method [137]. Using the obtained vorticities $\zeta_2$ and $\zeta_3$ and assumed vorticities $\zeta_1 = \zeta_1^{(1)}$ and $\zeta_4 = \zeta_4^{(1)}$, the right hand column vector of the matrix equation (A-41) can be evaluated. Applying the Thomas method to equation (A-41), the values for the stream function $\psi_1$, $\psi_2$, $\psi_3$ and $\psi_4$ can be found and the boundary values $\psi_1 = \psi_1^{(1)}$ and $\psi_4 = \psi_4^{(1)}$ and $\psi_4 = \psi_4^{(1)}$ will be stored. By assuming again $\zeta_1 = \zeta_1^{(2)}$, $\zeta_4 = \zeta_4^{(2)}$ and $\zeta_1 = \zeta_1^{(3)}$, $\zeta_3 = \zeta_4^{(3)}$ and following exactly the same procedure, the second and third boundary values $\psi_1 = \psi_1^{(2)}$, $\psi_4 = \psi_4^{(2)}$ and $\psi_1 = \psi_1^{(3)}$, $\psi_5 = \psi_5^{(3)}$ can be obtained, respectively. Upon substituting the values $\zeta_1^{(i)}$, $\zeta_4^{(i)}$ and $\psi_1^{(i)}$, $\psi_4^{(i)}$ $(i = 1,2,3)$ into equation (A-47), one has the following six linear algebraic equations for the six unknowns $a_{i,j}$ and $k_i$ $(i, j = 1,2)$.

$$\begin{bmatrix} \zeta_1^{(1)} & \zeta_4^{(1)} & 0 & 0 & 1 & 0 \\ 0 & 0 & \zeta_1^{(1)} & \zeta_4^{(1)} & 0 & 1 \\ \zeta_1^{(2)} & \zeta_4^{(2)} & 0 & 0 & 1 & 0 \\ 0 & 0 & \zeta_1^{(2)} & \zeta_4^{(2)} & 0 & 1 \\ \zeta_1^{(3)} & \zeta_4^{(3)} & 0 & 0 & 1 & 0 \\ 0 & 0 & \zeta_1^{(3)} & \zeta_4^{(3)} & 0 & 1 \end{bmatrix} \begin{bmatrix} a_{11} \\ a_{12} \\ a_{21} \\ a_{22} \\ k_1 \\ k_2 \end{bmatrix} = \begin{bmatrix} \psi_1^{(1)} \\ \psi_4^{(1)} \\ \psi_1^{(2)} \\ \psi_4^{(2)} \\ \psi_1^{(3)} \\ \psi_4^{(3)} \end{bmatrix} \qquad \text{(A-48)}$$

Provided the matrix is not singular, the values for $a_{i,j}$ and $k_i$ can be determined. Thus using the newly obtained values for $a_{i,j}$ and $k_i$ and with equation (A-47) and the boundary conditions $\psi_1 = \psi_4 = \psi_5$ $\psi_8 = 0$, the boundary vorticities $\zeta_1$ and $\zeta_4$, which represent the final solutions on the boundary points can be found. Substituting these boundary vorticities into equation (A-41) and (A-42) and solving for $\zeta_i$ and $\psi_i$($i$ = 1,2,3, and 4), one obtains the numerical solutions along this particular line. The same computational procedure will be repeated for succeeding lines. This line iteration procedure will be terminated when the criteria given by equation (A-46) is satisfied.

In Chapter III, an application of the above boundary vorticity method is shown together with a numerical experiment of the stream function-vorticity method. Some observations regarding the efficiency and convergence of both methods are also presented there.

In the above boundary vorticity method, the boundary conditions $(\partial\psi/\partial y)_1 = (\partial\psi/\partial y)_4 = 0$ are used in formulating equation (A-41), and later the boundary conditions, $\psi_1 = \psi_4 = 0$ are applied in equation

(A-47). Alternatively, one can formulate a equation analogous to equation (A-45) with $\psi_1 = \psi_4 = 0$ [96]. In other words the following equation can be used instead of equation (A-41) [96].

$$\begin{bmatrix} -1 & 2 & 0 & 0 \\ 1 & -4 & 1 & 0 \\ 0 & 1 & -4 & 1 \\ 0 & 0 & 2 & -1 \end{bmatrix} \begin{bmatrix} \Delta\psi_1 \\ \psi_1 \\ \psi_3 \\ \Delta\psi_4 \end{bmatrix} = \begin{bmatrix} h^2\zeta_1 \\ h^2\zeta_2 - \psi_6 \\ h^2\zeta_3 - \psi_7 \\ h^2\zeta_4 \end{bmatrix} \tag{A-49}$$

where $\Delta\psi_i = h\,(\partial\psi/\partial y)_i$, $(i = 1,4)$.

The boundary conditions $\Delta\psi_1 = \Delta\psi_4 = 0$ now must be used to determine the boundary vorticities $\zeta_1$ and $\zeta_4$. After eliminating the values for the interior points in equations (A-42) and (A-49), one has

$$\begin{bmatrix} \Delta\psi_1 \\ \Delta\psi_4 \end{bmatrix} = \begin{bmatrix} a_{11} & a_{12} \\ a_{21} & a_{22} \end{bmatrix} \begin{bmatrix} \zeta_1 \\ \zeta_4 \end{bmatrix} + \begin{bmatrix} k_1 \\ k_2 \end{bmatrix} \tag{A-50}$$

This equation corresponds to equation (A-47) for the first type of the boundary vorticity method. The procedure of determining $\zeta_1$ and $\zeta_4$ using equation (A-50) is similar to the previous case.

Direct Vorticity Method

In the boundary vorticity method, the linear relationship between the vorticity and the stream function is obtained for the boundary points as one has seen in equation (A-47) or (A-50). It is pointed out here that a similar linear relationship exists for the interior points of the domain.

Combining equations (A-41) and (A-49), one has;

$$\begin{bmatrix} -1 & 0 & 2 & 0 & 0 & 0 \\ 0 & -4 & 2 & 0 & 0 & 0 \\ 0 & 1 & -4 & 1 & 0 & 0 \\ 0 & 0 & 1 & -4 & 1 & 0 \\ 0 & 0 & 0 & 2 & -4 & 0 \\ 0 & 0 & 0 & 2 & 0 & -1 \end{bmatrix} \begin{bmatrix} \Delta\psi_1 \\ \psi_1 \\ \psi_2 \\ \psi_3 \\ \psi_4 \\ \Delta\psi_4 \end{bmatrix} = \begin{bmatrix} h^2\zeta_1 \\ h^2\zeta_1 - \psi_5 \\ h^2\zeta_2 - \psi_6 \\ h^2\zeta_3 - \psi_7 \\ h^2\zeta_4 - \psi_8 \\ h^2\zeta_4 \end{bmatrix} \qquad \text{(A-51)}$$

Now it is possible to eliminate the unknowns from equations (A-42) and (A-51) and the following relationship between vorticity and stream function may be obtained:

$$\begin{bmatrix} \psi_4 \\ \Delta\psi_4 \end{bmatrix} = \begin{bmatrix} a_{11} & a_{12} \\ a_{21} & a_{22} \end{bmatrix} \begin{bmatrix} \zeta_1 \\ \zeta_2 \end{bmatrix} + \begin{bmatrix} k_1 \\ k_2 \end{bmatrix} \qquad \text{(A-52)}$$

where $\Delta\psi_4 = h(\partial\psi/\partial y)_4$.

By using the above relationship, one does not require a simultaneous elimination procedure such as that required in the Thomas method to solve equations (A-41) and (A-42). Finding $\zeta_1$ and $\zeta_2$, with the aid of equation (A-52) one can directly calculate values for $\zeta_3$, $\zeta_4$ and $\psi_2$, $\psi_3$, $\psi_4$ successively using equations (A-42) and (A-51). By this direct calculation, one can save the computer time required for the arrangement of the coefficient matrix with Thomas' method. The present method may be called the "direct vorticity method".

The general procedure for determining the unknown coefficients $a_{i,j}$ and $k_i$ ($i = 1,2$) in equation (A-52) is similar to the one for the "boundary vorticity" method and need not be repeated here. The resulting equation is simply,

$$\begin{bmatrix} \zeta_1^{(1)} & \zeta_2^{(1)} & 0 & 0 & 1 & 0 \\ 0 & 0 & \zeta_1^{(1)} & \zeta_2^{(1)} & 0 & 1 \\ \zeta_1^{(2)} & \zeta_2^{(2)} & 0 & 0 & 1 & 0 \\ 0 & 0 & \zeta_1^{(2)} & \zeta_2^{(2)} & 0 & 1 \\ \zeta_1^{(3)} & \zeta_2^{(3)} & 0 & 0 & 1 & 0 \\ 0 & 0 & \zeta_1^{(3)} & \zeta_2^{(3)} & 0 & 1 \end{bmatrix} \begin{bmatrix} a_{11} \\ a_{12} \\ a_{21} \\ a_{22} \\ k_1 \\ k_2 \end{bmatrix} = \begin{bmatrix} \psi_4^{(1)} \\ \Delta\psi_4^{(1)} \\ \psi_4^{(2)} \\ \Delta\psi_4^{(2)} \\ \psi_4^{(3)} \\ \Delta\psi_4^{(3)} \end{bmatrix} \qquad \text{(A-53)}$$

For illustration and simplicity, here one may assume some special values for $\zeta_1^{(i)}$ and $\zeta_2^{(i)}$ ($i = 1,2,3$) and the procedure of obtaining a final numerical solution will be explained next.

(1) At first, in equation (A-52), one sets

$$\zeta_1^{(1)} = \zeta_2^{(1)} = 0$$

where the superscript (1) indicates the first step. Then using the first equation of equation (A-42), one can determine $\zeta_3^{(1)}$ and successively using the second equation, $\zeta_4^{(1)}$ can be obtained. By the use of all the obtained vorticities $\zeta_1^{(1)}$ to $\zeta_4^{(1)}$ and the boundary condition $\Delta\psi_1 = 0$,

the left hand column vector of the algebraic equation (A-51) can be calculated. The boundary values $\psi_4^{(1)}$ and $\Delta\psi_4^{(1)}$ will be stored since the values correspond to the values of $k_1$ and $k_2$, respectively, in equation (A-52). That is

$$k_1 = \psi_4^{(1)} \quad \text{and} \quad k_2 = \Delta\psi_4^{(1)}$$

(2) Similarly, one may further assume

$$\zeta_1^{(2)} = 0 \quad \text{and} \quad \zeta_2^{(2)} = 1$$

and following exactly the same procedure, one can determine the coefficients as

$$a_{12} = \psi_4^{(2)} - k_1$$

and

$$a_{22} = \Delta\psi_4^{(2)} - k_2$$

(3) Thirdly, by assuming the vorticities as,

$$\zeta_1^{(3)} = 1 \quad \text{and} \quad \zeta_2^{(3)} = 0$$

One obtains

$$a_{11} = \psi_4^{(3)} - k_1$$

and $$a_{21} = (\Delta\psi_4)^{(3)} - k_2 \ .$$

By carrying out the same three steps, one obtains all the values for the coefficients $a_{i,j}$ and $K_i$(i and j = 1,2) in equation (A-52).

(4) Finally, by assigning the given appropriate boundary conditions for $\psi_4$ and $\Delta\psi_4$ and using the values obtained for $a_{i,j}$ and $K_i$, one can now evaluate the values for $\zeta_1$ and $\zeta_2$. After solving equation (A-53) for $\zeta_1$ and $\zeta_2$, one has

$$\zeta_1 = \frac{a_{22}(\psi_4-k_1) - a_{12}(\Delta\psi_4-k_2)}{(a_{11}a_{22}-a_{12}a_{21})}$$

$$\zeta_2 = \frac{a_{21}(\psi_4-k_1) - a_{11}(\Delta\psi_4-k_2)}{(a_{12}a_{21}-a_{22}a_{11})} \qquad \text{(A-54)}$$

These newly obtained values of $\zeta_1$ and $\zeta_2$, represent the final solution for the boundary point 1 and the point 2 adjacent to the boundary. Substituting these vorticity values into equations (A-42) and (A-51) successively, one can determine all values for $\zeta_i$ and $\psi_i$(i = 1,2, 3 and 4) which represent the numerical solution along this particular line.

Since some of the boundary conditions for $\psi_1$, $\Delta\psi_1$, $\Delta\zeta_1$, and $\psi_4$, $\Delta\psi_4$, $\Delta\zeta_4$ may not be given prior to the determination of $\zeta_1$ and $\zeta_4$ explicitly, the choice of the relationships represented by equation (A-47), (A-50) and (A-52) and other possible relationships are largely dictated by the given specific boundary conditions. However, one must note that a significant difference exists between the "boundary vorticity" method and the present "direct vorticity" method. It is

noted that either equation (A-47) or (A-50), for the boundary vorticity method, expresses the relationship between the vorticity and stream function or its gradient using the values at the two boundary points 1 and 4. On the other hand, in equation (A-52), one uses the value for the interior vorticity $\zeta_2$ to establish the vorticity-stream function relationship thereby eliminating any use of simultaneous elimination procedure to solve equations (A-42) and (A-47) or (A-50).

In Chapter 6, the above "direct vorticity" method is applied for solving the hydrodynamic entrance region problem in curved parallel-plate channels where the boundary conditions are $\psi_4 = 1$ and $\Delta\psi_4 = 0$.

## APPENDIX 6

## NUMERICAL RESULTS FOR CHAPTER III

Friction Coefficient Ratio, $fRe/(fRe)_0$

| K | $fRe/(fRe)_0$ | K | $fRe/(fRe)_0$ |
|---|---|---|---|
| 3.1438 | 1.0032 | 37.394 | 1.1888 |
| 5.4435 | 1.0040 | 49.613 | 1.2673 |
| 6.2583 | 1.0077 | 58.510 | 1.3164 |
| 8.8406 | 1.0090 | 62.582 | 1.3327 |
| 9.8563 | 1.0104 | 66.133 | 1.3494 |
| 13.867 | 1.0178 | 69.346 | 1.3651 |
| 16.857 | 1.0369 | 72.334 | 1.3794 |
| 19.714 | 1.0639 | 94.702 | 1.4863 |
| 23.917 | 1.0953 | 111.13 | 1.5541 |
| 25.157 | 1.1030 | 123.24 | 1.6130 |
| 27.111 | 1.1221 | 196.33 | 1.8620 |

Note: $fRe/(fRe)_0 = [(fRe)_1 + (fRe)_2]/2(fRe)_0$,

$(fRe)_0 = 16.000$

Nusselt Number Ratio, $Nu/(Nu)_0$

Pr = 0

| K | $Nu/(Nu)_0$ | K | $Nu/(Nu)_0$ |
|---|---|---|---|
| 16.030 | 1.0050 | 26.999 | 1.0255 |
| 18.936 | 1.0110 | 28.301 | 1.0289 |
| 21.071 | 1.0144 | 37.392 | 1.0524 |
| 22.850 | 1.0152 | 44.138 | 1.0785 |
| 24.510 | 1.0186 | 123.24 | 1.2000 |
| 25.566 | 1.0220 | | |

Pr = 0

| K | $Nu/(Nu)_0$ | K | $Nu/(Nu)_0$ |
|---|---|---|---|
| 9.7826 | 1.0094 | 72.092 | 1.1608 |
| 13.790 | 1.0108 | 94.704 | 1.2039 |
| 19.378 | 1.0165 | 111.131 | 1.2335 |
| 22.604 | 1.0221 | 123.24 | 1.2558 |
| 68.900 | 1.1510 | | |

Pr = 0.7

| K | $Nu/(Nu)_0$ | K | $Nu/(Nu)_0$ |
|---|---|---|---|
| 13.789 | 1.0130 | 62.582 | 1.4578 |
| 18.724 | 1.0343 | 66.133 | 1.4883 |
| 22.476 | 1.0584 | 69.346 | 1.5151 |
| 25.431 | 1.0896 | 72.334 | 1.5391 |
| 27.948 | 1.1180 | 94.702 | 1.7001 |
| 37.394 | 1.2068 | 111.13 | 1.8162 |
| 49.613 | 1.3378 | 123.24 | 1.9254 |
| 58.510 | 1.4200 | | |

Pr = 1.0

| K | $Nu/(Nu)_0$ | K | $Nu/(Nu)_0$ |
|---|---|---|---|
| 9.7829 | 1.0144 | 49.635 | 1.4907 |
| 16.788 | 1.0268 | 54.365 | 1.5429 |
| 18.807 | 1.0518 | 58.865 | 1.5913 |
| 20.977 | 1.0789 | 62.303 | 1.6243 |
| 22.864 | 1.0988 | 65.999 | 1.6606 |
| 24.518 | 1.1352 | 69.304 | 1.6918 |
| 25.565 | 1.1517 | 71.545 | 1.7167 |
| 26.994 | 1.1745 | 72.314 | 1.7197 |
| 28.298 | 1.1960 | 94.721 | 1.9420 |
| 37.392 | 1.3340 | 123.24 | 2.1757 |
| 44.635 | 1.4246 | 196.33 | 2.7214 |

Pr = 4

| K | $Nu/(Nu)_0$ | K | $Nu/(Nu)_0$ |
|---|---|---|---|
| 6.9769 | 1.0164 | 25.708 | 1.5384 |
| 9.8563 | 1.0657 | 27.111 | 1.5713 |
| 13.867 | 1.2022 | 28.363 | 1.5999 |
| 16.857 | 1.2768 | 37.134 | 1.7924 |
| 19.314 | 1.3593 | 44.635 | 1.8952 |
| 20.887 | 1.4050 | 54.365 | 2.0729 |
| 22.775 | 1.4625 | | |
| 24.157 | 1.4988 | | |

Pr = 25

| K | $Nu/(Nu)_0$ | K | $Nu/(Nu)_0$ |
|---|---|---|---|
| 3.1256 | 1.0345 | 8.8406 | 1.4665 |
| 4.4229 | 1.0764 | 9.8698 | 1.5319 |
| 6.2593 | 1.2495 | 13.367 | 1.7119 |
| 7.6647 | 1.3774 | 16.857 | 1.8514 |

Pr = 100

| K | $Nu/(Nu)_0$ | K | $Nu/(Nu)_0$ |
|---|---|---|---|
| 1.4039 | 1.0181 | 4.4463 | 1.4707 |
| 1.9866 | 1.0677 | 5.4435 | 1.5874 |
| 2.4333 | 1.1391 | 6.2859 | 1.6639 |
| 2.8110 | 1.19873 | 7.6647 | 1.8073 |
| 3.1438 | 1.2529 | | |

Pr = 500

| K | $Nu/(Nu)_0$ | K | $Nu/(Nu)_0$ |
|---|---|---|---|
| 0.62692 | 1.0035 | 1.4046 | 1.2522 |
| 0.76820 | 1.0291 | 2.8109 | 1.6624 |
| 0.99255 | 1.0903 | 4.4440 | 2.0074 |

Note: $Nu = [(Nu)_1 + (Nu)_2]/2(Nu)_0$,

$(Nu)_0 = 48/11$

## APPENDIX 7

## NUMERICAL RESULTS FOR CHAPTER IV

Pr = 0.1, K = 123.2

| 1/Gz | Nu | 1/Gz | Nu |
|---|---|---|---|
| | | $0.19318 \times 10^{-1}$ | 5.137 |
| $0.68228 \times 10^{-3}$ | 13.44 | 0.20682 | 5.078 |
| $0.13333 \times 10^{-2}$ | 10.80 | 0.25494 | 4.929 |
| 0.19856 | 9.505 | 0.30364 | 4.837 |
| 0.26384 | 8.685 | 0.35292 | 4.782 |
| 0.32928 | 8.106 | 0.40281 | 4.751 |
| 0.39481 | 7.670 | 0.45332 | 4.735 |
| 0.46043 | 7.325 | 0.50447 | 4.727 |
| 0.59203 | 6.809 | 0.60121 | 4.730 |
| 0.65792 | 6.610 | 0.70030 | 4.741 |
| 0.72401 | 6.438 | 0.80187 | 4.752 |
| 0.79020 | 6.288 | 0.90606 | 4.763 |
| 0.85647 | 6.155 | $0.10046 \times 10^{0}$ | 4.771 |
| 0.92285 | 6.037 | 0.11057 | 4.778 |
| 0.98932 | 5.932 | 0.12006 | 4.783 |
| $0.10559 \times 10^{-1}$ | 5.837 | 0.13067 | 4.787 |
| 0.11226 | 5.751 | 0.14065 | 4.789 |
| 0.11894 | 5.673 | 0.15088 | 4.790 |
| 0.12564 | 5.602 | 0.16040 | 4.790 |
| 0.13234 | 5.537 | 0.17016 | 4.790 |
| 0.13905 | 5.477 | 0.18016 | 4.789 |
| 0.14578 | 5.422 | 0.19041 | 4.789 |
| 0.15927 | 5.324 | 0.20092 | 4.789 |
| 0.17958 | 5.203 | 0.21063 | 4.790 |
| | | 0.21834 | 4.790 |

Pr = 0.7, K = 123.2

| 1/Gz | Nu | 1/Gz | Nu |
|---|---|---|---|
| $0.10070 \times 10^{-3}$ | 27.35 | $0.20682 \times 10^{-1}$ | 7.381 |
| 0.12199 | 25.26 | 0.22363 | 7.561 |
| 0.14096 | 23.99 | 0.24094 | 7.752 |
| 0.16000 | 23.04 | 0.25878 | 7.947 |
| 0.20068 | 21.52 | 0.27532 | 8.123 |
| 0.49920 | 15.32 | 0.29620 | 8.333 |
| 0.60016 | 13.98 | 0.31586 | 8.514 |
| 0.75237 | 13.01 | 0.33621 | 8.680 |
| 0.90584 | 12.26 | 0.35730 | 8.829 |
| $0.10606 \times 10^{-2}$ | 11.66 | 0.37918 | 8.958 |
| 0.12899 | 10.99 | 0.40193 | 9.063 |
| 0.23671 | 9.109 | 0.42560 | 9.146 |
| 0.24880 | 8.974 | 0.45027 | 9.206 |
| 0.3589 | 8.100 | 0.50027 | 9.262 |
| 0.48350 | 7.522 | 0.54898 | 9.259 |
| 0.61094 | 7.170 | 0.60755 | 9.259 |
| 0.74126 | 6.951 | 0.70033 | 9.259 |
| 0.87456 | 6.822 | 0.80470 | 9.259 |
| $0.10110 \times 10^{-1}$ | 6.760 | 0.90907 | 9.259 |
| 0.11507 | 6.750 | $0.10018 \times 10^{0}$ | 9.259 |
| 0.12939 | 6.781 | 0.15005 | 9.260 |
| 0.14407 | 6.848 | 0.20108 | 9.260 |
| 0.15913 | 6.945 | 0.30081 | 9.260 |
| 0.17460 | 7.069 | 0.40055 | 9.260 |
| 0.19048 | 7.216 | 0.44462 | 9.260 |

Pr = 10, K = 7.655

| 1/Gz | Nu | 1/Gz | Nu |
|---|---|---|---|
| $0.12533 \times 10^{-2}$ | 9.445 | $0.26910 \times 10^{-1}$ | 4.245 |
| 0.24991 | 7.510 | 0.30004 | 4.236 |
| 0.38004 | 6.569 | 0.33465 | 4.244 |
| 0.51623 | 5.981 | 0.37391 | 4.269 |
| 0.65910 | 5.569 | 0.41929 | 4.311 |
| 0.80931 | 5.262 | 0.47303 | 4.370 |
| 0.96766 | 5.023 | 0.53894 | 4.444 |
| $0.11351 \times 10^{-1}$ | 4.833 | 0.62420 | 4.529 |
| 0.13127 | 4.679 | 0.74511 | 4.623 |
| 0.15018 | 4.554 | 0.95512 | 4.717 |
| 0.17040 | 4.454 | $0.10532 \times 10^{0}$ | 4.714 |
| 0.19213 | 4.375 | 0.11721 | 4.710 |
| 0.21560 | 4.314 | 0.14236 | 4.710 |
| 0.24113 | 4.271 | | |

Pr = 500, K = 4.444

| 1/Gz | Nu | 1/Gz | Nu |
|---|---|---|---|
| $0.10031 \times 10^{-3}$ | 22.53 | 0.60047 | 9.136 |
| 0.30528 | 15.13 | 0.65117 | 9.292 |
| 0.50106 | 12.90 | 0.71521 | 9.490 |
| 0.60874 | 12.12 | 0.75789 | 9.604 |
| 0.70236 | 11.59 | 0.80058 | 9.687 |
| 0.81216 | 11.08 | 0.84327 | 9.722 |
| 0.90953 | 10.72 | 0.90731 | 9.656 |
| $0.10072 \times 10^{-2}$ | 10.42 | 0.95000 | 9.528 |
| 0.12574 | 9.813 | $0.10140 \times 10^{-1}$ | 9.230 |
| 0.14992 | 9.411 | 0.12488 | 7.958 |
| 0.18677 | 9.098 | 0.15049 | 7.610 |
| 0.20090 | 8.901 | 0.17611 | 7.920 |
| 0.23372 | 8.725 | 0.20172 | 7.973 |
| 0.26607 | 8.624 | 0.22520 | 7.658 |
| 0.29999 | 8.574 | 0.25081 | 7.519 |
| 0.33326 | 8.566 | 0.27429 | 7.623 |
| 0.36820 | 8.590 | 0.30204 | 7.674 |
| 0.40244 | 8.637 | 0.32552 | 7.573 |
| 0.45171 | 8.733 | 0.35114 | 7.520 |
| 0.50175 | 8.854 | 0.37461 | 7.566 |
| 0.55249 | 8.993 | 0.40023 | 7.591 |
| | | 0.42584 | 7.555 |
| | | 0.45146 | 7.536 |
| | | 0.47494 | 7.554 |
| | | 0.50055 | 7.564 |
| | | 0.52616 | 7.551 |
| | | 0.55178 | 7.554 |
| | | 0.57526 | 7.551 |
| | | 0.60087 | 7.555 |
| | | 0.70119 | 7.552 |
| | | 0.80151 | 7.551 |
| | | 0.90183 | 7.551 |

where $Nu = [(Nu)_1 + (Nu)_2]/2$

Note: The first local maximum value of the local Nusselt number is taken to be the asymptotic value whenever the fluctuating phenomenon appears in the numerical solution.

## APPENDIX 8

## NUMERICAL RESULTS FOR CHAPTER V

$Nu = [(Nu)_1 + (Nu)]/2$

$Pr = 0.1, \quad K = 123.2$

| 1/Gz | Nu | 1/Gz | Nu |
|---|---|---|---|
| | | $0.20008 \times 10^{-1}$ | 6.113 |
| $0.85305 \times 10^{-3}$ | 15.002 | 0.25158 | 5.886 |
| $0.16673 \times 10^{-2}$ | 12.061 | 0.30372 | 5.737 |
| 0.24834 | 10.630 | 0.35653 | 5.637 |
| 0.33009 | 9.734 | 0.40107 | 5.579 |
| 0.41202 | 9.102 | 0.45518 | 5.530 |
| 0.49410 | 8.626 | 0.50082 | 5.503 |
| 0.57639 | 8.250 | 0.55628 | 5.481 |
| 0.65878 | 7.945 | 0.60308 | 5.470 |
| 0.74138 | 7.690 | 0.70799 | 5.460 |
| 0.82416 | 7.474 | 0.80576 | 5.460 |
| 0.90707 | 7.289 | 0.90596 | 5.465 |
| 0.99019 | 7.127 | $0.10086 \times 10^{0}$ | 5.472 |
| $0.10734 \times 10^{-1}$ | 6.985 | 0.11034 | 5.479 |
| 0.11569 | 6.860 | 0.12004 | 5.486 |
| 0.12405 | 6.748 | 0.12997 | 5.486 |
| 0.13242 | 6.648 | 0.14016 | 5.485 |
| 0.14082 | 6.558 | 0.15061 | 5.485 |
| 0.14923 | 6.476 | 0.16013 | 5.485 |
| 0.15767 | 6.401 | 0.16988 | 5.485 |
| 0.16611 | 6.333 | 0.17986 | 5.485 |
| 0.17458 | 6.271 | 0.19010 | 5.485 |
| 0.18306 | 6.214 | 0.20061 | 5.485 |

Pr = 0.7, K = 123.2

| 1/Gz | Nu | 1/Gz | Nu |
|---|---|---|---|
| $0.12306 \times 10^{-2}$ | 15.35 | $0.33725 \times 10^{-1}$ | 9.225 |
| 0.24275 | 11.77 | 0.35837 | 9.404 |
| 0.36496 | 9.579 | 0.38030 | 9.563 |
| 0.48980 | 8.832 | 0.40309 | 9.695 |
| 0.61739 | 8.392 | 0.42681 | 9.794 |
| 0.74785 | 8.053 | 0.45154 | 9.856 |
| 0.88131 | 7.855 | 0.47737 | 9.861 |
| $0.10179 \times 10^{-1}$ | 7.736 | 0.50441 | 9.862 |
| 0.11578 | 7.675 | 0.53277 | 9.853 |
| 0.13011 | 7.657 | 0.56259 | 9.852 |
| 0.14481 | 7.673 | 0.59402 | 9.856 |
| 0.15989 | 7.717 | 0.62726 | 9.854 |
| 0.17538 | 7.787 | 0.66252 | 9.857 |
| 0.19129 | 7.880 | 0.70006 | 9.856 |
| 0.20769 | 7.995 | 0.88061 | 9.852 |
| 0.22448 | 8.131 | $0.10662 \times 10^{0}$ | 9.849 |
| 0.24182 | 8.286 | 0.11442 | 9.851 |
| 0.25969 | 8.458 | 0.12342 | 9.852 |
| 0.27813 | 8.643 | 0.13409 | 9.852 |
| 0.29717 | 8.837 | | |
| 0.31686 | 9.033 | | |

Pr = 10, K = 7.655

| 1/Gz | Nu | 1/Gz | Nu |
|---|---|---|---|
| $0.30830 \times 10^{-3}$ | 18.42 | $0.15435 \times 10^{-1}$ | 5.599 |
| 0.60500 | 14.72 | 0.17488 | 5.471 |
| 0.90474 | 12.89 | 0.20244 | 5.342 |
| $0.12076 \times 10^{-2}$ | 11.72 | 0.22711 | 5.260 |
| 0.15136 | 10.89 | 0.26076 | 5.183 |
| 0.18228 | 10.26 | 0.30703 | 5.122 |
| 0.21354 | 9.750 | 0.3324 | 5.105 |
| 0.24513 | 9.331 | 0.36203 | 5.097 |
| 0.27707 | 8.978 | 0.40546 | 5.101 |
| 0.30936 | 8.674 | 0.42986 | 5.111 |
| 0.34202 | 8.408 | 0.47076 | 5.135 |
| 0.37504 | 8.173 | 0.50161 | 5.159 |
| 0.40844 | 7.963 | 0.53610 | 5.189 |
| 0.44222 | 7.774 | 0.57522 | 5.226 |
| 0.47640 | 7.603 | 0.62039 | 5.271 |
| 0.51099 | 7.446 | 0.64591 | 5.297 |
| 0.54599 | 7.302 | 0.67386 | 5.325 |
| 0.58141 | 7.170 | 0.70478 | 5.355 |
| 0.61727 | 7.048 | 0.73936 | 5.387 |
| 0.65358 | 6.933 | 0.82392 | 5.458 |
| 0.72757 | 6.728 | 0.87760 | 5.496 |
| 0.80349 | 6.547 | 0.94341 | 5.535 |
| 0.92120 | 6.313 | $0.10285 \times 10^{0}$ | 5.573 |
| $0.10023 \times 10^{-1}$ | 6.177 | 0.11490 | 5.606 |
| 0.12604 | 5.845 | 0.12521 | 5.592 |
| | | 0.14097 | 5.593 |

Pr = 500, K = 4.444

| 1/Gz | Nu | 1/Gz | Nu |
|---|---|---|---|
| $0.11620 \times 10^{-3}$ | 25.12 | $0.75118 \times 10^{-3}$ | 13.76 |
| 0.14518 | 23.29 | 0.78287 | 13.59 |
| 0.17429 | 21.98 | 0.81471 | 13.42 |
| 0.20352 | 20.92 | 0.84669 | 13.26 |
| 0.23287 | 20.03 | 0.87882 | 13.11 |
| 0.26234 | 19.28 | 0.91109 | 12.97 |
| 0.29193 | 18.62 | 0.94350 | 12.83 |
| 0.32164 | 18.05 | 0.97607 | 12.70 |
| 0.35148 | 17.54 | $0.10087 \times 10^{-2}$ | 12.58 |
| 0.38144 | 17.08 | 0.10416 | 12.46 |
| 0.41153 | 16.67 | 0.10746 | 12.34 |
| 0.44175 | 16.29 | 0.12421 | 11.83 |
| 0.47210 | 15.95 | 0.15184 | 11.19 |
| 0.50257 | 15.63 | 0.20295 | 10.42 |
| 0.53317 | 15.34 | 0.25394 | 9.972 |
| 0.56391 | 15.07 | 0.30014 | 9.760 |
| 0.59478 | 14.81 | 0.31328 | 9.733 |
| 0.62579 | 14.58 | 0.32217 | 9.723 |
| 0.65693 | 14.35 | 0.33118 | 9.721 |
| 0.68821 | 14.15 | 0.34030 | 9.726 |
| 0.71963 | 13.95 | 0.34491 | 9.731 |
| | | $0.31975 \times 10^{-2}$ | 9.731 |
| | | 0.36582 | 9.779 |
| | | 0.41508 | 10.00 |
| | | 0.46800 | 10.30 |
| | | 0.52518 | 10.57 |
| | | 0.58736 | 10.76 |
| | | 0.65549 | 10.85 |
| | | 0.73085 | 10.91 |
| | | 0.81515 | 11.28 |
| | | 0.91079 | 10.94 |
| | | $0.10213 \times 10^{-1}$ | 10.70 |
| | | 0.11522 | 10.11 |
| | | 0.13127 | 9.357 |
| | | 0.15204 | 8.943 |
| | | 0.18149 | 9.176 |
| | | 0.23265 | 9.097 |

## APPENDIX 9

## NUMERICAL RESULTS FOR CHAPTER VI

| $\lambda$ | $(f)_{C,\infty}/(f)_{S,\infty}$ | $\lambda$ | $(f)_{C,\infty}/(f)_{S,\infty}$ |
|---|---|---|---|
| 1.00000 | 4/5 | .70000 | 1.0875937 |
| .99999 | 1.3333067 | .60000 | 1.0587817 |
| | | .50000 | 1.0381266 |
| .99995 | 1.3332004 | .40000 | 1.0231805 |
| .99990 | 1.3330680 | .30000 | 1.0125590 |
| .99950 | 1.3320233 | .20000 | 1.0054405 |
| .99900 | 1.3307449 | .10000 | 1.0013399 |
| .99500 | 1.3212240 | .05000 | 1.0003337 |
| .99000 | 1.3105091 | .01000 | 1.0000133 |
| .95000 | 1.2474215 | .00000 | 1 |
| .90000 | 1.1954808 | | |
| .80000 | 1.1293560 | | |

Note: $(f)_{C,\infty}/(f)_{S,\infty}$ is computed from equation (161).

Uniform Inlet Velocity Profile

| $\omega$ \ $\lambda$ | $\Delta p$ | | | $f/(f)_{s,\infty}$ | | |
|---|---|---|---|---|---|---|
| | 0.0 | 0.1 | 0.5 | 0.0 | 0.1 | 0.5 |
| 0.00 | 0.000 | 0.000 | 0.000 | | | |
| 0.01 | 0.189 | 0.189 | 0.192 | 6.300 | 6.301 | 6.400 |
| 0.02 | 0.270 | 0.270 | 0.282 | 4.500 | 4.500 | 4.700 |
| 0.03 | 0.330 | 0.330 | 0.365 | 3.666 | 3.667 | 4.055 |
| 0.04 | 0.380 | 0.380 | 0.413 | 3.166 | 3.167 | 3.441 |
| 0.05 | 0.423 | 0.423 | 0.465 | 2.820 | 2.820 | 3.106 |
| 0.06 | 0.464 | 0.465 | 0.513 | 2.577 | 2.583 | 2.850 |
| 0.07 | 0.503 | 0.504 | 0.558 | 2.395 | 2.400 | 2.657 |
| 0.08 | 0.539 | 0.540 | 0.601 | 2.246 | 2.250 | 2.504 |
| 0.09 | 0.575 | 0.576 | 0.644 | 2.129 | 2.133 | 2.385 |
| 0.10 | 0.610 | 0.611 | 0.686 | 2.033 | 2.036 | 2.286 |
| 0.11 | 0.645 | 0.656 | 0.725 | 1.954 | 1.957 | 2.196 |
| 0.12 | 0.680 | 0.681 | 0.764 | 1.888 | 1.891 | 2.122 |
| 0.13 | 0.715 | 0.717 | 0.802 | 1.833 | 1.838 | 2.056 |
| 0.14 | 0.744 | 0.747 | 0.839 | 1.771 | 1.778 | 1.997 |
| 0.15 | 0.782 | 0.785 | 0.876 | 1.737 | 1.744 | 1.946 |
| 0.16 | 0.815 | 0.818 | 0.912 | 1.697 | 1.704 | 1.900 |
| 0.17 | 0.847 | 0.850 | 0.948 | 1.660 | 1.666 | 1.858 |
| 0.18 | 0.879 | 0.882 | 0.984 | 1.627 | 1.633 | 1.822 |
| 0.19 | 0.912 | 0.915 | 1.019 | 1.600 | 1.605 | 1.787 |
| 0.20 | 0.944 | 0.947 | 1.053 | 1.573 | 1.578 | 1.755 |
| 0.30 | 1.250 | 1.253 | 1.478 | 1.388 | 1.392 | 1.602 |
| 0.40 | 1.552 | 1.557 | 1.688 | 1.2933 | 1.297 | 1.406 |
| 0.50 | 1.852 | 1.858 | 2.000 | 1.234 | 1.238 | 1.334 |

Parabolic Inlet Velocity Profile

| $\omega$ \ $\lambda$ | $\Delta p$ | | | $f/(f)_{s,\infty}$ | | |
|---|---|---|---|---|---|---|
| | 0.0 | 0.1 | 0.5 | 0.0 | 0.1 | 0.5 |
| 0.0 | 0.000 | 0.000 | 0.000 | | | |
| 0.01 | 0.030 | 0.030 | 0.030 | 1.00 | 1.00 | 1.000 |
| 0.02 | 0.060 | 0.060 | 0.060 | 1.00 | 1.00 | 1.0000 |
| 0.03 | | 0.090 | 0.091 | | 1.00 | 1.0110 |
| 0.04 | | 0.120 | 0.121 | | 1.00 | 1.0080 |
| 0.05 | | 0.150 | 0.151 | | 1.00 | 1.0067 |
| 0.06 | | 0.180 | 0.182 | | 1.00 | 1.0100 |
| 0.07 | | 0.210 | 0.213 | | 1.00 | 1.0142 |
| 0.08 | | 0.240 | 0.243 | | 1.00 | 1.0125 |
| 0.09 | | 0.270 | 0.274 | | 1.00 | 1.0148 |
| 0.10 | | 0.300 | 0.305 | | 1.00 | 1.0166 |
| 0.15 | | 0.451 | 0.460 | | 1.00 | 1.0222 |
| 0.20 | | 0.601 | 0.616 | | 1.00 | 1.0266 |
| 0.30 | | 0.901 | 0.931 | | 1.00 | 1.0344 |
| 0.40 | | 1.202 | 1.239 | | 1.00 | 1.0325 |

Triangular Inlet Velocity Profile

| $\omega$ \ $\lambda$ | $\Delta p$ | | | $f/(f)_{s,\infty}$ | | |
|---|---|---|---|---|---|---|
| | 0.0 | 0.1 | 0.5 | 0.0 | 0.1 | 0.5 |
| 0.00 | 0.000 | 0.000 | 0.000 | — | — | — |
| 0.01 | 0.025 | 0.027 | 0.056 | 0.833 | 0.900 | 1.866 |
| 0.02 | 0.052 | 0.055 | 0.106 | 0.866 | 0.916 | 1.766 |
| 0.03 | 0.081 | 0.083 | 0.153 | 0.900 | 0.922 | 1.700 |
| 0.04 | 0.110 | 0.112 | 0.195 | 0.916 | 0.933 | 1.625 |
| 0.05 | 0.138 | 0.141 | 0.234 | 0.920 | 0.940 | 1.560 |
| 0.06 | 0.168 | 0.171 | 0.261 | 0.933 | 0.951 | 1.450 |
| 0.07 | 0.197 | 0.200 | 0.304 | 0.938 | 0.952 | 1.447 |
| 0.08 | 0.226 | 0.229 | 0.342 | 0.941 | 0.954 | 1.425 |
| 0.09 | 0.256 | 0.259 | 0.376 | 0.948 | 0.959 | 1.392 |
| 0.10 | 0.285 | 0.289 | 0.410 | 0.950 | 0.963 | 1.366 |
| 0.11 | 0.315 | 0.318 | 0.443 | 0.954 | 0.963 | 1.342 |
| 0.12 | 0.344 | 0.348 | 0.475 | 0.955 | 0.966 | 1.319 |
| 0.13 | 0.374 | 0.378 | 0.507 | 0.958 | 0.969 | 1.300 |
| 0.14 | 0.404 | 0.408 | 0.539 | 0.961 | 0.971 | 1.283 |
| 0.15 | 0.438 | 0.438 | 0.571 | 0.973 | 0.973 | 1.268 |
| 0.20 | 0.583 | 0.588 | 0.727 | 0.972 | 0.980 | 1.211 |
| 0.30 | 0.893 | 0.888 | 1.132 | 0.992 | 0.986 | 1.157 |
| 0.40 | 1.193 | 1.188 | 1.350 | 0.003 | 0.990 | 1.125 |

# APPENDIX 10

## COMPUTER PROGRAMS

```
      **********************************

      * IN THE SIXTH COLUMN INDICATES
      CONTINUATION FROM PREVIOUS LINE

      **********************************
```

```
C     ***** LAMINAR FORCED CONVENTION HEAT TRANSFER *****
C     ***** IN CURVED CIRCULER CHANNELS             *****
C     ***** (RC IS LARGE)                          *****
C
      DIMENSION W(16,16),T(16,16),U(16,16),V(16,16),BWVTS(16
     *  ,16),
     1AW(16,16),CW(16,16),PW(16,16),S(16,16),SS(16,16),VW(16
     *  ,16),
     2VO(16,16),TT(16,16),AT(16,16),CT(16,16),PT(16,16),AS(1
     *  6,16),
     3PHI(16),R(16),ZA(16),ZB(16),ZC(16),CS(16,16),PS(16,16)
      COMMON HR,HR2,HP,HP2,CK,CON,PR,STD,TOLE,ZA,ZB,ZC,R,PHI
     *  ,BWVTS,W,T,
     1V,OMEGM,OMEGS,OMEGT,U
      COMMON M,N,MI,M1,NI,N1,MSTD,NO
      REAL NU1,NU2
      READ(5,100)M,N,STD,TOLE
      PI=3.141593
   33 MI=M-1
      M1=M+1
      NI=N-1
      N1=N+1
      NOO=10
      DO 12 J=1,N1
      DO 10 I=1,M1
      W(I,J)=0.0
      VW(I,J)=0.0
      T(I,J)=0.0
      TT(I,J)=0.0
      SS(I,J)=0.0
      S(I,J)=0.0
      VO(I,J)=0.0
      U(I,J)=0.0
      V(I,J)=0.0
   10 CONTINUE
```



F585

```
   12 CONTINUE
      READ (5,72)(( W(I,J),I=1,M1),J=1,N1)
      READ (5,72)((VW(I,J),I=1,M1),J=1,N1)
      READ (5,72)(( S(I,J),I=1,M1),J=1,N1)
      READ (5,72)((SS(I,J),I=1,M1),J=1,N1)
      READ (5,72)((VO(I,J),I=1,M1),J=1,N1)
      READ (5,72)(( U(I,J),I=1,M1),J=1,N1)
      READ (5,72)(( V(I,J),I=1,M1),J=1,N1)
      READ (5,72)(( T(I,J),I=1,M1),J=1,N1)
      READ (5,72)((TT(I,J),I=1,M1),J=1,N1)
   72 FORMAT(20A4)
   99 READ(5,100) M,N,STD,TOLE
      NO=0
  100 FORMAT(2I4,2E10.5)
      WRITE(6,2000) M,N,STD,TOLE
 2000 FORMAT(1X,2I4,2E15.5)
      IF(M.EQ.0) GO TO 150
      READ(5,201) CCN,PR
  201 FORMAT(2E10.5)
      WRITE(6,2001) CCN,PR
 2001 FORMAT(1X,2E15.5)
      READ(5,250) CMEGM,OMEGS,OMEGT,MSTD,MTIM
  250 FORMAT(3F5.2,2I5)
      HR=1.0/M
      HR2=HR**2
      HP=PI/N
      HP2=HP**2
      PHI(1)=0.0
      DO 9 J=2,N1
    9 PHI(J)=PHI(J-1)+HP
      R(1)=0.0
      DO 8 I=2,M1
      R(I)=R(I-1)+HR
      ZA(I)=HR/(2*R(I))
      ZB(I)=(HR/(HP*R(I)))**2
      ZC(I)=HR**2/(2*R(I)*HP)
    8 CONTINUE
      WRITE(6,2002) CMEGM,OMEGS,OMEGT,MSTD,MTIM
 2002 FORMAT(1X,3E15.5,2I5)
      DO 11 J=1,N1
      DO 7 I=2,M1
      BWVTS(I,J)=(1+ZB(I))*(-2)
      AS(I,J)=1-ZA(I)
      CS(I,J)=1+ZA(I)
    7 CONTINUE
   11 CONTINUE
    1 CONTINUE
      DO 26 J=1,N1
```

```
      AS(M1,J)=2.0
      AW(2,J)=1-ZA(2)+0.5*HR*U(2,J)
      CW(2,J)=1+ZA(2)-0.5*HR*U(2,J)
      PW(2,J)=CW(2,J)/BWVTS(2,J)
      AT(2,J)=1-ZA(2)+0.5*PR*HR*U(2,J)
      CT(2,J)=1+ZA(2)-0.5*PR*HR*U(2,J)
      PT(2,J)=CT(2,J)/BWVTS(2,J)
      PS(2,J)=CS(2,J)/BWVTS(2,J)
      DO 25 I=3,M
      AW(I,J)=1-ZA(I)+0.5*HR*U(I,J)
      CW(I,J)=1+ZA(I)-0.5*HR*U(I,J)
      PW(I,J)=CW(I,J)/(BWVTS(I,J)-AW(I,J)*PW(I-1,J))
      AT(I,J)=1-ZA(I)+0.5*PR*HR*U(I,J)
      CT(I,J)=1+ZA(I)-0.5*PR*HR*U(I,J)
      PT(I,J)=CT(I,J)/(BWVTS(I,J)-AT(I,J)*PT(I-1,J))
      PS(I,J)=CS(I,J)/(BWVTS(I,J)-AS(I,J)*PS(I-1,J))
   25 CONTINUE
   26 CONTINUE
      WRITE(6,2101)
 2101 FORMAT(' ','ENTER TO SUVW')
      CALL SUBW(VW,AW,CW,PW,ERRW,MTIM)
      WRITE(6,2102)
 2102 FORMAT(' ','ENTER TO SUBVS')
      CALL SUBVS(S,VO,SS,AS,CS,PS,AW,CW,PW,MTIM,ERRS)
      WRITE(6,2103)
 2103 FORMAT(' ','ENTER TO SUBUV')
      CALL SUBUV(S,ERRUV)
      IF(ERRUV.LT.TOLE.OR.NC.GT.MSTD) GO TO 60
      NO=NO+1
      IF(NO/10*10.NE.NC) GO TO 1
      WRITE(6,151) NO,ERRUV
      GO TO 1
   60 CONTINUE
      WRITE(6,151) NO,ERRUV
  151 FORMAT(' ',10X,'NO ',I5,5X,'ERRUV',E14.6)
      NOT=0
      NOOT=10
   61 CONTINUE
      CALL SUBT(TT,AT,CT,PT,ERRT)
      IF(ERRT.LT.TOLE.OR.NOT.GT.MSTD) GO TO 62
      NOT=NOT+1
      IF(NOT/10*10.NE.NOT) GO TO 61
      WRITE(6,621) NOT,ERRT
  621 FORMAT(' ',10X,'NOT',I4,5X,'ERRT',E14.6)
      GO TO 61
   62 WRITE(6,620) NOT,ERRT
  620 FORMAT(11X,'NOT',I5,5X,'ERRT ',E14.6)
      CALL FHR(SWP,SWT,SGT,SGW,BLKT,FRE1,FRE2,NU1,NU2,RFE1,R
     *  FE2,RNU1,
```

```
     1RNU2,ARNU,STP,AVEN,AVEF,RFE12)
      WRITE(6,105)
  105 FORMAT('1','AXIAL VELCCITY',3X,'I FROM 1 TO M, J FROM
     *  1 TO N')
      WRITE(6,113) ((W(I,J),I=1,M),J=1,N1)
  113 FORMAT(' ',7E18.6)
      WRITE(6,107)
  107 FORMAT('1','VORTICITY')
      WRITE(6,113) ((VC(I,J),I=2,M1),J=1,N1)
      WRITE(6,108)
  108 FORMAT('1','STREAM FUNCTION')
      WRITE(6,113) ((S(I,J),I=2,M1),J=1,N1)
      WRITE(6,109)
  109 FORMAT('1','SECONDARY VELOCITY IN R-DIRECTION U')
      WRITE(6,113) ((U(I,J),I=1,M),J=1,N1)
      WRITE(6,110)
  110 FORMAT('1','SECONDARY VELOCITY IN PHI-DIRECTION V')
      WRITE(6,113) ((V(I,J),I=1,M),J=1,N1)
      WRITE(6,106)
  106 FORMAT('1','TEMPERATURE')
      WRITE(6,113)  ((T(I,J),I=1,M),J=1,N1)
      WRITE(6,202)M,N
  202 FORMAT('1',30X,'MESH SIZE',I5,2X,'BY',I5)
      WRITE(6,203) STD,TOLE
  203 FORMAT('C',30X,'ERROR LIMIT',2E20.6)
      WRITE(6,204) CON,DK,PR
  204 FORMAT('0',30X,'CON',E10.5,10X,'DK',E10.5,10X,'PR',E10
     *  .5)
      WRITE(6,400) ERRW
  400 FORMAT('0',50X,'ERRW ',15X,E14.6)
      WRITE(6,401) ERRS
  401 FORMAT('C',50X,'ERRS ',15X,E14.6)
      WRITE(6,116) NO
      WRITE(6,101) ERRUV
  101 FORMAT('C',50X,'ERRUV',15X,E14.6)
      WRITE(6,116) NOT
  116 FORMAT('0',45X,'NUMBER OF ITERATIONS',10X,I10)
      WRITE(6,102) ERRT
  102 FORMAT('C',50X,'ERRT',15X,E14.6)
      WRITE(6,205) CMEGM,CMEGS,OMEGT
  205 FORMAT('0',30X,'RELAXATION PARAMETER FOR W',5X,F5.2,5X
     *  ,'FOR S',5X,
     1F5.2,5X,'FOR T',5X,F5.2)
      WRITE(6,210)
  210 FORMAT('1',' ***** HEAT TRANSFER RESULTS*****',///)
      WRITE(6,111) BLKT
  111 FORMAT('C',10X,'BULK TEMPERATURE IN PHI-DIRECTION',F15
     *  .6)
```

```
      WRITE(6,212) STP
  212 FORMAT('0',10X,'MEAN TEMPERATURE       ',F15.6)
      WRITE(6,112) SWP
  112 FORMAT('0',10X,'AVERAGE VELOCITY IN AXIAL DIRECTION ',
     *  F15.6)
      WRITE(6,114) FRE1,FRE2,AVEF
  114 FORMAT('0',10X,'FRE1',E15.5,'FRE2',E15.5,'AVEF',E15.5)
      WRITE(6,121) RFE1,RFE2,RFE12
  121 FORMAT('0',10X,'FRE1/FRE0',E15.5,'FRE2/FRE0',E15.5,
     1'AVERAGE',E15.5)
      WRITE(6,115) NU1,NU2,AVEN
  115 FORMAT('C',10X,'NU1',E15.5,'NU2',E15.5,'AVEN',E15.5)
      WRITE(6,122) RNU1,RNU2,ARNU
  122 FORMAT('C',10X,'NU1/NU0',E15.5,'NU2/NU0',E15.5,'ARNU',
     *  E15.5)
      WRITE(6,120) SWT,SGT,SGW
  120 FORMAT('0',10X,'SWT',E15.5,'SGT',E15.5,'SGW',E15.5)
      WRITE(6,211)
  211 FORMAT('0',///'***** END *****',///)
      SGT2=2.0*SGT
      ST0=STP/0.1875
      SGW2=SGW/2.0
      PRK=DK**0.5*PR**0.25
      WRITE(6,301)
  301 FORMAT('1',6X,'CON',1CX,'DK',9X,'SWP',9X,'2*SGT',8X,'F
     *  RE1',9X,
     1'FRE2',9X,'AVEF',9X,'RFE1',9X,'RFE2',9X,'RFE12')
      WRITE(6,302) CON,DK,SWP,SGT2,FRE1,FRE2,AVEF,RFE1,RFE2,
     *  RFE12
  302 FORMAT(1X,10E13.6)
      WRITE(6,303)
  303 FORMAT('0',4X,'PRK',1CX,'STP',7X,'STP/STP0',7X,'SGW/2'
     *  ,9X,'NU1',
     110X,'NU2',9X,'AVEN',8X,'NU1/NU0',6X,'NU2/NU0',7X,'ARNU
     *  ')
      WRITE(6,302)PRK,STP,ST0,SGW2,NU1,NU2,AVEN,RNU1,RNU2,AR
     *  NU
      WRITE(6,721)M,N
  721 FORMAT('1',10X,2I5)
      WRITE(7,71)(( W(I,J),I=1,M1),J=1,N1)
      WRITE(7,71)((VW(I,J),I=1,M1),J=1,N1)
      WRITE(7,71)(( S(I,J),I=1,M1),J=1,N1)
      WRITE(7,71)((SS(I,J),I=1,M1),J=1,N1)
      WRITE(7,71)((VC(I,J),I=1,M1),J=1,N1)
      WRITE(7,71)(( U(I,J),I=1,M1),J=1,N1)
      WRITE(7,71)(( V(I,J),I=1,M1),J=1,N1)
      WRITE(7,71)(( T(I,J),I=1,M1),J=1,N1)
      WRITE(7,71)((TT(I,J),I=1,M1),J=1,N1)
```

```
 71 FORMAT(20A4)
    GO TO 99
150 STOP
    END
    SUBROUTINE SUBW(VW,AW,CW,PW,ERRW,MTIM)
    DIMENSION W(16,16),U(16,16),V(16,16),BWVTS(16,16),AW(1
   *  6,16),
   1CW(16,16),PW(16,16),QW(16,16),PHI(16),R(16),ZA(16),DW(
   *  16,16),
   2ZB(16),ZC(16),VW(16,16),T(16,16)
    COMMON HR,HR2,HP,HP2,DK,CON,PR,STD,TOLE,ZA,ZB,ZC,R,PHI
   *  ,BWVTS,W,T,
   1V,OMEGM,CMEGS,CMEGT,U
    COMMON M,N,MI,M1,NI,N1,MSTD,NO
    NOW=1
  5 CONTINUE
    VW(1,1)=0.25*((1-HR*U(1,1)/2)*W(2,1)+(1+HR*U(1,1)/2)*W
   *  (2,N1)
   1          +2*W(2,N/2+1)+4*HR2)
    DO 9 J=2,N
    VW(1,J)=VW(1,1)
  9 CONTINUE
    VW(1,N1)=VW(1,1)
    DW(2, 1)=-4*HR2-2*ZB(2)*VW(2, 2)-AW(2,1)*VW(1,1)
    DO 10 J=2,N
    DW(2,J)=-4.0*HR2-(ZB(2)+ZC(2)*V(2,J))*VW(2,J-1)-(ZB(2)
   *  -ZC(2)*
   1          V(2,J))*VW(2,J+1)-AW(2,J)*VW(1,J)
 10 CONTINUE
    DW(2,N1)=-4*HR2-2*ZB(2)*VW(2, N)-AW(2,N1)*VW(1,N1)
    QW(2,1)=DW(2,1)/BWVTS(2,1)
    DO 11 J=2,N
    QW(2,J)=CW(2,J)/BWVTS(2,J)
 11 CONTINUE
    QW(2,N1)=DW(2,N1)/BWVTS(2,N1)
    DO 12 I=3,M
    DW(I,1)=-4*HR2-2*ZB(I)*VW(I,1)
 12 CONTINUE
    DO 14 J=2,N
    DO 13 I=3,M
    DW(I,J)=-4*HR2-(ZB(I)+ZC(I)*V(I,J))*VW(I,J-1)-(ZB(I)-Z
   *  C(I)*V(I,J))
   1          *VW(I,J+1)
 13 CONTINUE
 14 CONTINUE
    DO 15 I=3,M
    DW(I,N1)=-4*HR2-2*ZB(I)*VW(I,N)
 15 CONTINUE
```

```
      DO 16 I=3,M
      QW(I,1)=(DW(I,1)-AW(I,1)*QW(I-1,1))/
     1(BWVTS(I,1)-AW(I,1)*PW(I-1,1))
   16 CONTINUE
      DO 18 J=2,N
      DO 17 I=3,M
      QW(I,J)=(DW(I,J)-AW(I,J)*QW(I-1,J))/(BWVTS(I,J)-AW(I,J
     *   )*PW(I-1,J))
   17 CONTINUE
   18 CONTINUE
      DO 19 I=3,M
      QW(I,N1)=(DW(I,N1)-AW(I,N1)*QW(I-1,N1))/
     1(BWVTS(I,N1)-AW(I,N1)*PW(I-1,N1))
   19 CONTINUE
      DO 20 J=1,N1
      VW(M,J)=QW(M,J)
   20 CONTINUE
      DO 21 J=1,N1
      DO 4 II=2,MI
      I=M1-II
      VW(I,J)=QW(I,J)-PW(I,J)*VW(I+1,J)
    4 CONTINUE
   21 CONTINUE
      WD=0.0
      WSUM=0.0
      DO 31 J=1,N1
      DO 8 I=1,M
      DI=OMEGM*(VW(I,J)-W(I,J))
      W(I,J)=W(I,J)+DI
      WD=WD+ABS(DI)
      WSUM=WSUM+ABS(W(I,J))
    8 CONTINUE
   31 CONTINUE
      ERRW=WD/WSUM
      IF(ERRW.LT.TOLE.OR.NOW.GT.MTIM) GO TO 41
      NOW=NOW+1
      GO TO 5
   41 CONTINUE
      RETURN
      END
      SUBROUTINE SUBVS(S,VC,SS,AS,CS,PS,AW,CW,PW,MTIM,ERRS)
      DIMENSION W(16,16),U(16,16),V(16,16),BWVTS(16,16),AS(1
     *   6,16),
     1CS(16,16),PS(16,16),QS(16,16),AW(16,16),CW(16,16),PW(1
     *   6,16),
     2VO(16,16),VO(16,16),DS(16,16),SM1(3),VM1(3),PHI(16),R
     *   (16),ZA(16),
     3ZB(16),DVO(16,16),TCON(16,16),SS(16,16),S(16,16),ZC(16
     *   ),T(16,16)
```

```
      COMMON HR,HR2,HP,HP2,DK,CON,PR,STD,TOLE,ZA,ZB,ZC,R,PHI
     *   ,BWVTS,W,T,
     1V,CMEGM,CMEGS,CMEGT,U
      COMMON M,N,MI,M1,NI,N1,MSTD,NO
      NOS=1
    5 CONTINUE
      DO 17 J=2,N
      DO 10 I=2,M
      TCON(I,J)=CON*W(I,J)*(COS(PHI(J))*(W(I,J+1)-W(I,J-1))*
     *   ZC(I)*2.0
     1           +SIN(PHI(J))*(W(I+1,J)-W(I-1,J))*HR)
   10 CONTINUE
      K=0
      VM1(1)=0.0
   20 K=K+1
      VO(M1,J)=VM1(K)
      DO 9 I=2,M
      DVO(I,J)=TCON(I,J)-(ZE(I)+ZC(I)*V(I,J))*VO(I,J-1)-(ZB(
     *   I)-ZC(I)*
     1          V(I,J))*VO(I,J+1)
      IF(I.EQ.M) DVO(I,J)=TCON(I,J)-(ZB(I)+ZC(I)*V(I,J))*VO(
     *   I,J-1)
     1                          -(ZE(I)-ZC(I)*V(I,J))*VO(I,J+1)
     2                          -CW(I,J)*VO(M1,J)
    9 CONTINUE
      QVO(2,J)=DVO(2,J)/BWVTS(2,J)
      DO 8 I=3,M
    8 QVO(I,J)=(DVO(I,J)-AW(I,J)*QVO(I-1,J))/(BWVTS(I,J)-AW(
     *   I,J)
     1          *PW(I-1,J))
      VO(M,J)=QVO(M,J)
      DO 4 II=2,MI
      I=M1-II
    4 VO(I,J)=QVO(I,J)-PW(I,J)*VO(I+1,J)
      DO 3 I=2,M
      DS(I,J)=-(ZB(I)*(SS(I,J-1)+SS(I,J+1)))+HR2*VO(I,J)
      IF(I.EQ.2) GO TO 2
      QS(I,J)=(DS(I,J)-AS(I,J)*QS(I-1,J))/(BWVTS(I,J)-AS(I,J
     *   )*PS(I-1,J))
    2 QS(2,J)=DS(2,J)/BWVTS(2,J)
    3 CONTINUE
      DS(M1,J)=-(ZB(M1)*(SS(M1,J-1)+SS(M1,J+1)))+HR2*VO(M1,J
     *   )
      QS(M1,J)=(DS(M1,J)-AS(M1,J)*QS(M,J))/
     1          (BWVTS(M1,J)-AS(M1,J)*PS(M,J))
      SM1(K)=QS(M1,J)
      IF(K-2) 50,51,52
   50 VM1(2)=-100.0
```

```
      GO TO 20
   51 VM1(3)=100.0*SM1(1)/(SM1(2)-SM1(1))
      GO TO 20
   52 SS(M1,J)=SM1(K)
      DO 18 II=1,M1
      I=M1-II
   18 SS(I,J)=QS(I,J)-PS(I,J)*SS(I+1,J)
   17 CONTINUE
      SD=0.0
      SSUM=0.0
      DO 79 J=2,N
      DO 78 I=2,M1
      DI=OMEGS*(SS(I,J)-S(I,J))
      S(I,J)=S(I,J)+DI
      SD=SD+ABS(DI)
      SSUM=SSUM+ABS(S(I,J))
   78 CONTINUE
   79 CONTINUE
      IF(SSUM.NE.0.0) GO TO 80
      ERRS=0.0
      GO TO 81
   80 ERRS=SD/SSUM
   81 CONTINUE
      IF(ERRS.LT.TOLE.OR.NOS.GT.MTIM) GO TO 83
      NOS=NOS+1
      GO TO 5
   83 CONTINUE
      RETURN
      END
      SUBROUTINE SUBUV(S,ERRUV)
      DIMENSION W(16,16),U(16,16),V(16,16),BWVTS(16,16),PHI(
     *  16),R(16),
     1ZA(16),ZB(16),ZC(16),VU(16,16),VV(16,16),S(16,16),TT(1
     *  6,16),
     2T(16,16)
      COMMON HR,HR2,HP,HP2,DK,CON,PR,STD,TOLE,ZA,ZB,ZC,R,PHI
     *  ,BWVTS,W,T,
     1V,OMEGM,OMEGS,OMEGT,U
      COMMON M,N,MI,M1,NI,N1,MSTD,NO
      WRITE(6,21)M,N,MI,M1,NI,N1
   21 FORMAT(' ',6I5)
      DO 12 I=2,M
      RH6=R(I)*HP*6
      RH12=R(I)*HP*12
      VU(I,1)=(8*S(I,2)-S(I,3))/RH6
      VU(I,2)=(-S(I,2)+8*S(I,3)-S(I,4))/RH12
      VU(I,N1)=(S(I,NI)-8*S(I,N))/RH6
      VU(I,N)=(S(I,N-2)-8*S(I,NI)+S(I,N))/RH12
```

```
      DO 10 J=3,NI
      VU(I,J)=(S(I,J-2)-8*S(I,J-1)+8*S(I,J+1)-S(I,J+2))/RH12
   10 CONTINUE
   12 CONTINUE
      WRITE(6,22)
   22 FORMAT(' ','KOD1')
      HR12=HR*12
      DO 9 J=2,N
      VV(2,J)=(10*S(2,J)-18*S(3,J)+6*S(4,J)-S(5,J))/HR12
      DO 14 I=3,MI
      VV(I,J)=(S(I+2,J)-8*S(I+1,J)+8*S(I-1,J)-S(I-2,J))/HR12
   14 CONTINUE
      VV(M,J)=(S(M-3,J)-6*S(M-2,J)+18*S(M-1,J)-10*S(M,J)-3*S
     *  (M+1,J))/
     1HR12
    9 CONTINUE
      WRITE(6,23)
   23 FORMAT(' ','KOD2')
      VU(1,1)=(8*S(2,N/2+1)-S(3,N/2+1))/(6*HR)
      DO 8 J=1,N1
      VU(1,J)=VU(1,1)
    8 VV(1,J)=0.0
      DO 7 I=2,M
      VV(I,1)=0.0
    7 VV(I,N1)=0.0
      SD=0.0
      SUM=0.0
      DO 13 I=1,M
      DO 6 J=I,N1
      DU=VU(I,J)-U(I,J)
      DV=VV(I,J)-V(I,J)
      SD=SD+ABS(DU)+ABS(DV)
      SUM=SUM+ABS(VV(I,J))+ABS(VU(I,J))
      U(I,J)=VU(I,J)
      V(I,J)=VV(I,J)
    6 CONTINUE
   13 CONTINUE
      IF(SUM.NE.0.0) GO TO 11
      ERRUV=0.0
      RETURN
   11 ERRUV=SD/SUM
      RETURN
      END
      SUBROUTINE SUBT(TT,AT,CT,PT,ERRT)
      DIMENSION W(16,16),T(16,16),U(16,16),V(16,16),BWVTS(16
     *  ,16),
     1AT(16,16),CT(16,16),DT(16,16),PT(16,16),QT(16,16),TT(1
     *  6,16),
```

```
     2PHI(16),R(16),ZA(16),ZC(16),ZB(16)
      COMMON HR,HR2,HP,HP2,DK,CON,PR,STD,TOLE,ZA,ZB,ZC,R,PHI
     *   ,BWVTS,W,T,
     1V,CMEGM,CMEGS,CMEGT,U
      COMMON M,N,M1,M1,N1,N1,MSTD,NO
      TT(1,1)=0.25*(TT(2,1)*(1-HR*PR*U(1,1)/2)+2*TT(2,N/2+1)
     *   +TT(2,N1)
     1          *(1.0+HR*PR*U(1,1)/2.0)+HR2*W(1,1))
      DO 1 J=2,N1
      TT(1,J)=TT(1,1)
    1 CONTINUE
      DT(2, 1)=-2*ZB(2)*TT(2,2)-HR2*W(2, 1)-AT(2, 1)*TT(1,1)
      DO 2 J=2,N
      DT(2,J)=-(ZB(2)+ZC(2)*PR*V(2,J))*TT(2,J-1)-(ZB(2)-ZC(2
     *   )*PR*V(2,J))
     1          *TT(2,J+1)-HR2*W(2,J)-AT(2,J)*TT(1,J)
    2 CONTINUE
      DT(2,N1)=-2*ZB(2)*TT(2,N)-HR2*W(2,N1)-AT(2,N1)*TT(1,1)
      DO 3 J=1,N1
      DT(2, J)=DT(2, J)/BWVTS(2, J)
    3 CONTINUE
      DO 4 I=3,M
      DT(I, 1)=-2*ZB(I)*TT(I, 2)-HR2*W(I, 1)
    4 CONTINUE
      DO 6 J=2,N
      DO 5 I=3,M
      DT(I,J)=(ZC(I)*PR*V(I,J)-ZB(I))*TT(I,J+1)
     1          -(ZB(I)+ZC(I)*PR*V(I,J))*TT(I,J-1)-HR2*W(I,J)
    5 CONTINUE
    6 CONTINUE
      DO 7 I=3,M
      DT(I,N1)=-2*ZB(I)*TT(I, N)-HR2*W(I,N1)
    7 CONTINUE
      DO 8 I=3,M
      QT(I, 1)=(DT(I,1)-AT(I,1)*QT(I-1,1))/
     1        (BWVTS(I,1)-AT(I,1)*PT(I-1,1))
    8 CONTINUE
      DO 10 J=2,N
      DO 9 I=3,M
      QT(I,J)=(DT(I,J)-AT(I,J)*QT(I-1,J))/(BWVTS(I,J)-AT(I,J
     *   )*PT(I-1,J))
    9 CONTINUE
   10 CONTINUE
      DO 11 I=3,M
      QT(I,N1)=(DT(I,N1)-AT(I,N1)*QT(I-1,N1))/
     1       (BWVTS(I,N1)-AT(I,N1)*PT(I-1,N1))
   11 CONTINUE
      DO 12 J=1,N1
```

```
      TT(M,J)=QT(M,J)
   12 CONTINUE
      DO 14 J=1,N1
      DO 13 II=2,MI
      I=MI-II
      TT(I,J)=QT(I,J)-PT(I,J)*TT(I+1,J)
   13 CONTINUE
   14 CONTINUE
      TD=0.0
      TSUM=0.0
      DO 78 J=1,N1
      DO 77 I=1,M
      DTT=CMEGT*(TT(I,J)-T(I,J))
      T(I,J)=T(I,J)+DTT
      TD=TD+ABS(DTT)
      TSUM=TSUM+ABS(T(I,J))
   77 CONTINUE
   78 CONTINUE
      ERRT=TD/TSUM
      RETURN
      END
      SUBROUTINE FHR(SWP,SWT,SGT,SGW,BLKT,FRE1,FRE2,NU1,NU2,
     *  RFE1,RFE2,
     1RNU1,RNU2,ARNU,STP,AVEN,AVEF,RFE12)
      DIMENSION W(16,16),T(16,16),U(16,16),V(16,16),BWVTS(16
     *  ,16),TS(16),
     1WT(16),WP(16),GT(16),GW(16),PHI(16),R(16),ZA(16),ZB(16
     *  ),ZC(16)
     2,FRE1(16),UN1(16)
      COMMON HR,HR2,HP,HP2,DK,CON,PR,STD,TOLE,ZA,ZB,ZC,R,PHI
     *  ,BWVTS,W,T,
     1V,OMEGM,OMEGS,OMEGT,U
      COMMON M,N,MI,M1,NI,N1,MSTD,NO
      REAL NU1,NU2
      PI=3.141593
      DO 10 J=1,N1
      GT(J)=-(T(M-3,J)/4-4*T(M-2,J)/3+3*T(MI,J)-4*T(M,J))/HR
      GW(J)=-(W(M-3,J)/4-4*W(M-2,J)/3+3*W(MI,J)-4*W(M,J))/HR
   10 CONTINUE
      SGT=GT(1)+GT(N1)
      SGW=GW(1)+GW(N1)
      DO 9 J=2,N,2
      SGT=SGT+GT(J)*4
      SGW=SGW+GW(J)*4
    9 CONTINUE
      DO 8 J=3,NI,2
      SGT=SGT+GT(J)*2
    8 SGW=SGW+GW(J)*2
```

```
      SGT=HP*SGT/(3*PI)
      SGW=HP*SGW/(3*PI)
      DO 7 I=2,M
      WT(I)=W(I,1)*T(I,1)+W(I,N1)*T(I,N1)
      TS(I)=T(I,1)+T(I,N1)
      WP(I)=W(I,1)+W(I,N1)
      DO 6 J=2,N,2
      WT(I)=WT(I)+W(I,J)*T(I,J)*4
      TS(I)=TS(I)+T(I,J)*4
    6 WP(I)=WP(I)+W(I,J)*4
      DO 5 J=3,N1,2
      WT(I)=WT(I)+W(I,J)*T(I,J)*2
      TS(I)=TS(I)+T(I,J)*2
    5 WP(I)=WP(I)+W(I,J)*2
      WT(I)=HP*WT(I)/3
      TS(I)=HP*TS(I)/3
      WP(I)=HP*WP(I)/3
    7 CONTINUE
      SWT=0.0
      STP=0.0
      SWP=0.0
      DO 4 I=2,M,2
      SWT=SWT+WT(I)*R(I)*4
      STP=STP+TS(I)*R(I)*4
      SWP=SWP+WP(I)*R(I)*4
    4 CONTINUE
      DO 3 I=3,MI,2
      SWT=SWT+WT(I)*R(I)*2
      STP=STP+TS(I)*R(I)*2
      SWP=SWP+WP(I)*R(I)*2
    3 CONTINUE
      SWT=HR*SWT*2/(3*PI)
      SWP=HR*SWP*2/(3*PI)
      STP=HR*STP*2/(3*HP)
      BLKT=SWT/SWP
      DK=CON**0.5*SWP*2.0
      FRE1=4*SGW/SWP
      FRE2=8/SWP
      NU1=2*SWP*SGT/SWT
      NU2=SWP**2/SWT
      RFE1=FRE1/16
      RFE2=FRE2/16
      RNU1=NU1*11/48
      RNU2=NU2*11/48
      ARNU=(RNU1+RNU2)/2
      AVEN=(NU1+NU2)/2
      AVEF=(FRE1+FRE2)/2
      RFE12=(RFE1+RFE2)/2
```

```
      WRITE(6,21)
   21 FORMAT('1',5X,'J',4X,'GW(J)',15X,'GT(J)',15X,'FREI(J)'
     *   ,13X
     1,'NUI(J)')
      DO 23 J=1,N1
      FREI(J)=4*GW(J)/SWP
      UNI(J)=2*SWP*GT(J)/SWT
      WRITE(6,22) J,GW(J),GT(J),FREI(J),UNI(J)
   22 FORMAT(4X,I2,4X,4(E13.5,7X))
   23 CONTINUE
      RETURN
      END
```

```
                    **********
                    * IN THE SIXTH COLUMN INDICATES
                    CONTINUATION FROM PREVIOUS LINE
                    **********
C
C
C     ***************************************************
C     *****  LAMINAR FORCED CONVECTION HEAT TRANSFER  *****
C     *****  IN CURVED CIRCULER CHANNELS              *****
C     *****  ( A/RC IS SMALL, GRAETZE FLOW PROBLEM    *****
C     *****   WITH NEUMANN   CONDITION )              *****
C     *****  (  LOG SCALE STEP )                      *****
C     ***************************************************
C
C
C
      DIMENSION T(29,29),W(29,29),U(29,29),V(29,29),R(29),
     1Z1(29),Z2(29),Z3(29),Z4(29),A(29,29),B(29,29),C(29,29)
     2,D(29,29),E(29,29),F(29,29),TPC(29,29),TPF(29,29),
     3TG(29,29),TH(29,29),TQG(29,29),TQH(29,29),NUI(29),
     4GI(29),WI(29),TS(29),WP(29),GOTW(29),TT(29,29)
      REAL NUI,NU1,NU2,NU1M,NU2M
      READ(5,1) M,N
    1 FORMAT(2I5)
      PI=3.141593
      MI=M-1
      M1=M+1
      NI=N-1
      N1=N+1
      ETA=0.0
      OME=0.0
      OMEG=0.0
      R(1)=0.0
      ONU1=0.0
      ONU2=0.0
      NU1M=0.0
      NU2M=0.0
      OMEO=0.0
      DO 3 J=1,NI
```

```
      DO 3 I=1,M1
      W(I,J)=0.0
      U(I,J)=0.0
      V(I,J)=0.0
      T(I,J)=0.0
      TT(I,J)=0.0
    3 CONTINUE
      READ(5,5)((W(I,J),I=1,M1),J=1,N1)
      READ(5,5)((U(I,J),I=1,M1),J=1,N1)
      READ(5,5)((V(I,J),I=1,M1),J=1,N1)
    5 FORMAT(20A4)
      WRITE(6,6) M,N
    6 FORMAT('1','***** MAIN FLOW DISTRIBUTION,W WITH MESH'
     1,' SIZE',I5,2X,'BY',I5,'  *****')
      WRITE(6,9) W(1,1)
      WRITE(6,49)(( W(I,J),I=2,M1),J=1,N1)
      WRITE(6,7) M,N
    7 FORMAT('1','*****  R-DIRECTION FLOW DISTRIBUTION,U',
     1' WITH MESH SIZE',I5,2X,'BY',I5,'  *****')
      WRITE(6,9) U(1,1)
      WRITE(6,49)(( U(I,J),I=2,M1),J=1,N1)
      WRITE(6,8) M,N
    8 FORMAT('1','*****  PHI-DIRECTION FLOW DISTRIBUTION,V',
     1' WITH MESH SIZE',I5,2X,'BY',I5,'  *****')
      WRITE(6,9) V(1,1)
      WRITE(6,49)(( V(I,J),I=2,M1),J=1,N1)
    9 FORMAT('0',E18.6)
      READ(5,10) PR,RARC
      READ(5,10) CON,DK
      READ(5,10) DETA,ETALIM
   10 FORMAT(2E10.5)
      WRITE(6,11)
   11 FORMAT('1')
C
C
C     SETTING OF CONSTANTS
C
      HR=1.0/M
      HR2=HR**2.0
      HR3=HR/2.0
      HP=PI/N
      HP2=HP**2.0
C
      H1=PR*HR3
      H2=PR*CON**.5*RARC**.5*2.0*HR2
      H3=PR*HR2/2.0/HP
      H4=HR2/HP2
      H5=2.0*H4
```

```
C
      DO 14 I=2,M1
      R(I)=R(I-1)+HR
      Z1(I)=HR3/R(I)
      Z2(I)=H4/R(I)**2
      Z3(I)=H5/R(I)**2
      Z4(I)=H3/R(I)
   14 CONTINUE
C
C
C     SETTING OF COEFFICIENTS
C     CONSTANT COEFFICENTS
C
      DO 16 I=2,M1
      A(I,1)=-H1*U(I,1)-1.0+Z1(I)
      C(I,1)= H1*U(I,1)-1.0-Z1(I)
      F(I,1)=Z3(I)
      DO 15 J=2,N
      A(I,J)=-H1*U(I,J)-1.0+Z1(I)
      C(I,J)= H1*U(I,J)-1.0-Z1(I)
      D(I,J)=Z4(I)*V(I,J)+Z2(I)
      F(I,J)=-Z4(I)*V(I,J)+Z2(I)
   15 CONTINUE
      A(I,N1)=-H1*U(I,N1)-1.0+Z1(I)
      C(I,N1)= H1*U(I,N1)-1.0-Z1(I)
      D(I,N1)=Z3(I)
   16 CONTINUE
      DO 17 J=1,N1
      A(M1,J)=A(M1,J)+C(M1,J)
   17 CONTINUE
      KOUNT=0
      KOUNN=0
      KTT=0
      KOUTT=0
   20 CONTINUE
C
C
C     INCREMENT OF DISTANCE IN MAIN FLOW DIRECTION
C
      ETA=ETA+DETA
      ETA1=1.0-ETA
      ETA2=1./ETA1
      OMEG=ALOG(ETA2)
C     MODIFIED PECLET NUMBER,PECMOD=RED*PR*2A/(RC*OMEG)
      PEMOD=2.0*DK*PR*RARC**.5/OMEG
      RPEMD=1./PEMOD
      PO=2.0*RARC/OMEG
      DOMG=OMEG-OMEO
```

```
      RED=DK/RARC**.5
C
C
C
C     ALTERNATIVE DIRECTIONAL METHOD
C
C
C
C     CALCULATION OF PHI_DIRECTION USING
C     GAUSSIAN ELIMINATION
C
C
C     ELIMINATION OF T(I,J-1) IN COLUMN
C
      DO 34 I=2,M1
      B(I,1)=-H2*W(I,1)/DOMG+2.0
      E(I,1)=-H2*W(I,1)/DOMG-Z3(I)
      TPF(I,1)=F(I,1)/E(I,1)
      DO 33 J=2,N1
      B(I,J)=-H2*W(I,J)/DOMG+2.0
      E(I,J)=-H2*W(I,J)/DOMG-Z3(I)
      TPF(I,J)=F(I,J)/(E(I,J)-D(I,J)*TPF(I,J-1))
   33 CONTINUE
   34 CONTINUE
      DO 36 I=2,M
      DO 36 J=1,N1
      TH(I,J)=A(I,J)*TT(I-1,J)+B(I,J)*TT(I,J)+C(I,J)*TT(I+1,
     *  J)
   36 CONTINUE
      DO 40 I=2,M
      TQH(I,1)=TH(I,1)/E(I,1)
      DO 38 J=2,N1
      TQH(I,J)=(TH(I,J)-D(I,J)*TQH(I,J-1))
     1          /(E(I,J)-D(I,J)*TPF(I,J-1))
   38 CONTINUE
   40 CONTINUE
C
C     BACK SUBSTITUTION
C
      DO 45 I=2,M
      T(I,N1)=TQH(I,N1)
      DO 43 K=1,N
      J=N1-K
      T(I,J)=TQH(I,J)-TPF(I,J)*T(I,J+1)
   43 CONTINUE
   45 CONTINUE
      T(M1,1)=(                    A(M1,1)*T (M,1)
     1       +2.0*C(M1,1)*HR-F(M1,1)*T (M1,2))
```

```
     2       /(E(M1,1)-B(M1,1))
             DO 451 J=2,N
             T(M1,J)=(                    A(M1,J)*T (M,J)
     1       +2.0*C(M1,J)*HR-D(M1,J)*T (M1,J-1)-F(M1,J)*T (M1
     *  ,J+1))
     2       /(E(M1,J)-B(M1,J))
   451 CONTINUE
             T(M1,N1)=(                      A(M1,N1)*T (M,N1)
     1       +2.0*C(M1,N1)*HR-D(M1,N1)*T (M1,N))
     2        /(E(M1,N1)-B(M1,N1))
C
C      CENTRE PCINT BY PRESENT POINTS AND
C     1  THE PREVIOUS CENTRE POINT ,T(1,1)
C
       T(1,1)=(TT(1,1)*(-H2*W(1,1)/DOMG+2.0)
     1         + T(2,1)*(H1*U(1,1)-1.0)
     2         -T(2,N1)*(H1*U(1,1)+1.0)
     3          -T(2,N/2+1)*2.0)/(-H2*W(1,1)/DOMG-2.0)
             DO 46 J=2,N1
             T(1,J)=T(1,1)
    46 CONTINUE
C
C
C      CALCULATION CF R_DIRECTION USING
C      GAUSSIAN ELIMINATION
C
C      ELIMINATION OF T(I-1,J) IN COLUMN
C
             DO 22 I=2,M1
             DO 22 J=1,N1
             B(I,J)=H2*W(I,J)/DOMG+2.0
             E(I,J)=H2*W(I,J)/DOMG-Z3(I)
    22 CONTINUE
             DO 24 J=1,N1
             TPC(2,J)=C(2,J)/B(2,J)
             DO 23 I=3,M1
             TPC(I,J)=C(I,J)/(B(I,J)-A(I,J)*TPC(I-1,J))
    23 CONTINUE
    24 CONTINUE
C       CENTRE POINT BY PREVICUS POINTS
             T(1,1)=(T (1,1)*(H2*W(1,1)/DOMG-2.0)
       1         +T (2,N/2+1)*2.0-T (2,1)*(H1*U(1,1)-1.0)
       2         +T (2,N1)*(H1*U(1,1)+1.0))/(H2*W(1,1)/DOMG+2.0)
             DO 25 J=2,N1
             T(1,J)=T(1,1)
    25 CONTINUE
             TG(2,1)=F(2,1)*T (2,2)+E(2,1)*T (2,1)-A(2,1)*T (1,1)
             TG(M1,1)=F(M1,1)*T (M1,2)+E(M1,1)*T (M1,1)
```

```
     1       -2.0*C(M1,1)*HR
             DO 26 J=2,N
             TG(2,J)=D(2,J)*T (2,J-1)+E(2,J)*T (2,J)+F(2,J)*T (2,J+
            *  1)
     1       -A(2,J)*T (1,J)
             TG(M1,J)=D(M1,J)*T (M1,J-1)+E(M1,J)*T (M1,J)
     1       +F(M1,J)*T (M1,J+1)-2.0*C(M1,J)*HR
          26 CONTINUE
             TG(2,N1)=D(2,N1)*T (2,N)+E(2,N1)*T (2,N1)
     1       -A(2,N1)*T (1,N1)
             TG(M1,N1)=D(M1,N1)*T (M1,N)+E(M1,N1)*T (M1,N1)
     1       -2.0*C(M1,N1)*HR
             DO 28 I=3,M
             TG(I,1)=F(I,1)*T (I,2)+E(I,1)*T (I,1)
             DO 27 J=2,N
             TG(I,J)=D(I,J)*T (I,J-1)+E(I,J)*T (I,J)+F(I,J)*T (I,J+
            *  1)
          27 CONTINUE
             TG(I,N1)=D(I,N1)*T (I,N)+E(I,N1)*T (I,N1)
          28 CONTINUE
             DO 30 J=1,N1
             TQG(2,J)=TG(2,J)/B(2,J)
             DO 29 I=3,M1
             TQG(I,J)=(TG(I,J)-A(I,J)*TQG(I-1,J))
     1          /(B(I,J)-A(I,J)*TPC(I-1,J))
          29 CONTINUE
          30 CONTINUE
C
C       BACK SUBSTITUTION
C
             DO 32 J=1,N1
             T (M1,J)=TQG(M1,J)
             DO 31 K=1,MI
             I=M1-K
             T(I,J)=TQG(I,J)-TPC(I,J)*T(I+1,J)
          31 CONTINUE
          32 CONTINUE
             IF(KOUNT/20*20.NE.KOUNT) GO TO  4901
             WRITE(6,47) M,N
          47 FORMAT('1','*****  TEMPERATURE DISTRIBUTION WITH',
            1' MESH SIZE',I5,2X,'BY',I5,'  *****')
             WRITE(6,48) T(1,1)
          48 FORMAT('0',1E18.6)
             DO 492 J=1,N1
             WRITE(6,491)
         491 FORMAT(' ')
             WRITE(6,49) (T(I,J),I=2,M1)
          49 FORMAT(' ',7E18.6)
```

```
  492 CONTINUE
 4901 CONTINUE
      KOUNT=KOUNT+1
C
C
C
C     CALCULATION OF  HEAT TRANSFER RELATIONSHIPS
C
C
      DO 50 I=1,M1
      WT(I)=0.0
      TS(I)=0.0
   50 CONTINUE
      DO 51 J=1,N1
      GT(J)=1.0
   51 CONTINUE
      SGT=1.0
      TSS=0.0
      TSS=TSS+T(M1,1)+T(M1,N1)
      SGT=GT(1)+GT(N1)
      DO 52 J=2,N,2
      TSS=TSS+T(M1,J)*4.
   52 CONTINUE
      DO 53 J=3,NI,2
      TSS=TSS+T(M1,J)*2.
   53 CONTINUE
      TSS=HP*TSS/(3.*PI)
      DO 56 I=2,M
      GOTW(I)=(TT(I,1)-TT(I,1))/DOMG*W(I,1)
     1       +(T(I,N1)-TT(I,N1))/DOMG*W(I,N1)
      WT(I)=W(I,1)*(T(I,1)-TSS)+W(I,N1)*(T(I,N1)-TSS)
      TS(I)=T(I,1)+T(I,N1)
      WP(I)=W(I,1)+W(I,N1)
      DO 54 J=2,N,2
      GOTW(I)=GOTW(I)+(TT(I,J)-TT(I,J))/DOMG*W(I,J)*4.
      WT(I)=WT(I)+W(I,J)*(T(I,J)-TSS)*4.
      TS(I)=TS(I)+T(I,J)*4.
      WP(I)=WP(I)+W(I,J)*4.
   54 CONTINUE
      DO 55 J=3,NI,2
      GOTW(I)=GOTW(I)+(TT(I,J)-TT(I,J))/DOMG*W(I,J)*2.
      WT(I)=WT(I)+W(I,J)*(T(I,J)-TSS)*2.
      TS(I)=TS(I)+T(I,J)*2.
      WP(I)=WP(I)+W(I,J)*2.
   55 CONTINUE
      GOTW(I)=HP*GOTW(I)/(3.*PI)
      WT(I)=HP*WT(I)/(3.*PI)
      TS(I)=HP*TS(I)/(3.*PI)
```

```
      WP(I)=HP*WP(I)/(3.*PI)
   56 CONTINUE
      SGTW=0.0
      SWT=0.0
      STP=0.0
      SWP=0.0
      GOTW(1)=(T(1,1)-TT(1,1))/DOMG*W(1,1)
C     GOTW(M1)=0.0,SINCE W(M1,J)=0.0
      GOTW(M1)=0.0
      SGTW=SGTW+GOTW(M1)+GOTW(1)
      DO 57 I=2,M,2
      SGTW=SGTW+GOTW(I)*R(I)*4.
      SWT=SWT+WT(I)*R(I)*4.
      STP=STP+TS(I)*R(I)*4.
      SWP=SWP+WP(I)*R(I)*4.
   57 CONTINUE
      DO 58 I=3,M1,2
      SGTW=SGTW+GOTW(I)*R(I)*2.
      SWT=SWT+WT(I)*R(I)*2.
      STP=STP+TS(I)*R(I)*2.
      SWP=SWP+WP(I)*R(I)*2.
   58 CONTINUE
      SGTW=HR*SGTW*2/3.
      SWT=HR*SWT*2/3.
      SWP=HR*SWP*2/3.
      STP=HR*STP*2./3.
C     BULK TEMPARETURE ,BLKT
      BLKT=SWT/SWP
      NU1=   SWP*SGT/SWT
      NU2= PR*CON**.5*RARC**.5*SGTW*SWP/SWT
C     AVERAGE NUSSELT NUMBER,AVEN
      AVEN=( NU1+NU2)/2.
C     NUSSELT NUMBER RATICS TO THEFULLY DEVELOPED FLOW
C     IN STRAIGHT PIPE ,
      RNU1=NU1/4.360
      RNU2=NU2/4.360
      ARNU=(RNU1+RNU2)/2.
      DO 59 J=1,N1
      NUI(J)=2.*SWP*GT(J)/SWT
   59 CONTINUE
      IF(KOUNN/20*20.NE.KOUNN) GO TO 5902
      WRITE(6,5901) N1
 5901 FORMAT('0',' *****  NUSSELT NUMBER DISTRIBUTION FROM',
     1' J= 1 TO',I3,'  *****')
      WRITE(6,48) NUI(1)
      WRITE(6,49) (NUI(J),J=2,N1)
 5902 KOUNN=KOUNN+1
C
```

```
      SGT2=2.*SGT
      ST0=STP/.1875
      PRK=DK**.5*PR**.25
      NU1M=(NU1M*OMEG+(ONU1+NU1)/2.*DOMG)/OMEG
      NU2M=(NU2M*OMEG+(ONU2+NU2)/2.*DOMG)/OMEG
      AVENM=(NU1M+NU2M)/2.
      RNU1M=NU1M/4.360
      RNU2M=NU2M/4.360
      ARNUM=(RNU1M+RNU2M)/2.
      IF(KTT/20*20.NE.KTT) GO TO 5909
      WRITE(6,60)
   60 FORMAT('0'/6X,'CON',10X,'DK',9X,'SWP',9X,'2*SGT',8X,
     1         'ETA',8X,'POSITION',6X,'OMEGA    ',8X,'A/RC',7X,
     2         'PEMODIF',6X,'DOMG')
      WRITE(6,61) CON,DK,SWP,SGT2,ETA,PO,OMEG,RARC,PEMOD
     1,DOMG
   61 FORMAT(1X,10E13.6)
      WRITE(6,62)
   62 FORMAT(' ',4X,'PRK',10X,'STP',7X,'  TSS    ',8X,'RED',
     1          10X,'NU1',10X,'NU2',9X,'AVEN',8X,'NU1/NU0',6X,
     2          'NU2/NU0',7X,'ARNU')
      WRITE(6,61) PRK,STP,TSS,RED,NU1,NU2,AVEN,RNU1,RNU2,ARN
     *  U
      WRITE(6,6201)
 6201 FORMAT(' ',5X,'PR',10X,'NU1M',11X,'NU2M',9X,'AVENM',
     17X,'NU1M/NU0',5X,'NU2M/NU0',5X,'ARNUM',6X,'RPEMD',
     C6X,'BLKT',6X,'RMPRK')
      WRITE(6,61) PR,NU1M,NU2M,AVENM,RNU1M,RNU2M,ARNUM
     1,RPEMD,BLKT,RMPRK
 5909 KTT=KTT+1
      OMEO=OMEG
      ONU1=NU1
      ONU2=NU2
      DO 63 I=1,M1
      DO 63 J=1,N1
      TT(I,J)=T(I,J)
   63 CONTINUE
      IF(PEMOD.LT.200.) GO TO 65
   64 CONTINUE
      IF(ETA.LT.ETALIM) GO TO 20
      STOP
   65 CONTINUE
      IF(KOUTT.NE.0) GO TO 64
      WRITE(7,66)((TT(I,J),I=1,M1),J=1,N1)
   66 FORMAT(20A4)
      WRITE(7,67) OMEO
      WRITE(7,67) NU1M
      WRITE(7,67) NU2M
```

```
 67 FORMAT(E13.6)
    KOUTT=KOUTT+1
    GO TO 64
    END
```

```
                    **********************************

                    * IN THE SIXTH COLUMN INDICATES
                    CONTINUATION FROM PREVIOUS LINE

                    **********************************


C
C
C     ************************************************************
C     *****  LAMINAR FORCED CONVECTION HEAT TRANSFER  *************
C     *****  IN CURVED CIRCULER CHANNELS              *************
C     *****  ( A/RC IS SMALL, GRAETZE FLOW PROBLEM    *************
C     *****   WITH DIRICHLET CONDITION )              *************
C     *****  (  LOG SCALE STEP )                      *************
C     ************************************************************
C
C
C
      DIMENSION T(29,29),W(29,29),U(29,29),V(29,29),R(29),
     1Z1(29),Z2(29),Z3(29),Z4(29),A(29,29),B(29,29),C(29,29)
     2,D(29,29),E(29,29),F(29,29),TPC(29,29),TPF(29,29),
     3TG(29,29),TH(29,29),TQG(29,29),TQH(29,29),NUI(29),
     4GT(29),WT(29),TS(29),WP(29),GOTW(29),TT(29,29)
      REAL NUI,NU1,NU2,NU1M,NU2M
      READ(5,1) M,N
    1 FORMAT(2I5)
      PI=3.141593
      MI=M-1
      M1=M+1
      NI=N-1
      N1=N+1
      ETA=0.0
      OME=0.0
      OMEG=0.0
      R(1)=0.0
      ONU1=0.0
      ONU2=0.0
      NU1M=0.0
      NU2M=0.0
      OMEO=0.0
      DO 3 J=1,N1
```

```
      DO 3 I=1,M1
      W(I,J)=0.0
      U(I,J)=C.C
      V(I,J)=0.0
      T(I,J)=1.0
      TT(I,J)=1.0
    3 CONTINUE
      DO 4 J=1,N1
      T(M1,J)=0.0
      TT(M1,J)=0.0
    4 CONTINUE
      READ(5,5) ((W(I,J),I=1,M1),J=1,N1)
      READ(5,5) ((U(I,J),I=1,M1),J=1,N1)
      READ(5,5) ((V(I,J),I=1,M1),J=1,N1)
    5 FORMAT(20A4)
      WRITE(6,6) M,N
    6 FORMAT('1','*****  MAIN FLOW DISTRIBUTICN,W WITH MESH'
     1,' SIZE',I5,2X,'BY',I5,'  *****')
      WRITE(6,9) W(1,1)
      WRITE(6,49)(( W(I,J),I=2,M1),J=1,N1)
      WRITE(6,7) M,N
    7 FORMAT('1','*****  R-DIRECTION FLOW DISTRIBUTION,U',
     1' WITH MESH SIZE',I5,2X,'BY',I5,'  *****')
      WRITE(6,9) U(1,1)
      WRITE(6,49)(( U(I,J),I=2,M1),J=1,N1)
      WRITE(6,8) M,N
    8 FORMAT('1','*****  PHI-DIRECTION FLOW DISTRIBUTION,V',
     1' WITH MESH SIZE',I5,2X,'BY',I5,'  *****')
      WRITE(6,9) V(1,1)
      WRITE(6,49)(( V(I,J),I=2,M1),J=1,N1)
    9 FORMAT('0',E18.6)
      READ(5,10) PR,RARC
      READ(5,10) CON,DK
      READ(5,10) DETA,ETALIM
   10 FORMAT(2E10.5)
      WRITE(6,11)
   11 FORMAT('1')
C
C
C     SETTING OF CONSTANTS
C
      HR=1.C/M
      HR2=HR**2.0
      HR3=HR/2.C
      HP=PI/N
      HP2=HP**2.0
C
      H1=PR*HR3
```

```
      H2=PR*CON**.5*RARC**.5*2.0*HR2
      H3=PR*HR2/2.0/HP
      H4=HR2/HP2
      H5=2.C*H4
C
      DO 14 I=2,M1
      R(I)=R(I-1)+HR
      Z1(I)=HR3/R(I)
      Z2(I)=H4/R(I)**2
      Z3(I)=H5/R(I)**2
      Z4(I)=H3/R(I)
   14 CONTINUE
C
C
C     SETTING OF COEFFICIENTS
C     CONSTANT COEFFICENTS
C
      DO 16 I=2,M1
      A(I,1)=-H1*U(I,1)-1.0+Z1(I)
      C(I,1)= H1*U(I,1)-1.0-Z1(I)
      F(I,1)=Z3(I)
      DO 15 J=2,N
      A(I,J)=-H1*U(I,J)-1.0+Z1(I)
      C(I,J)= H1*U(I,J)-1.0-Z1(I)
      D(I,J)=Z4(I)*V(I,J)+Z2(I)
      F(I,J)=-Z4(I)*V(I,J)+Z2(I)
   15 CONTINUE
      A(I,N1)=-H1*U(I,N1)-1.0+Z1(I)
      C(I,N1)= H1*U(I,N1)-1.0-Z1(I)
      D(I,N1)=Z3(I)
   16 CONTINUE
      KOUNT=0
      KOUTT=0
      KTT=0
   20 CONTINUE
C
C
C     INCREMENT OF DISTANCE IN MAIN FLOW DIRECTION
C
      ETA=ETA+DETA
      ETA1=1.0-ETA
      ETA2=1./ETA1
      OMEG=ALOG(ETA2)
C     MODIFIED PECLET NUMBER,PECMOD=RED*PR*2A/(RC*OMEG)
      PEMOD=2.0*DK*PR*RARC**.5/OMEG
      RPEMD=1./PEMOD
      PO=2.0*RARC/OMEG
      DOMG=OMEG-OMEO
```

```
      RED=DK/RARC**.5
C
C
C
C     ALTERNATIVE DIRECTIONAL METHOD
C
C
C     CALCULATION OF R_DIRECTION USING
C     GAUSSIAN ELIMINATION
C
C     ELIMINATION OF T(I-1,J)  IN COLUMN
C
      DO 22 I=2,M
      DO 22 J=1,N1
      B(I,J)=H2*W(I,J)/DOMG+2.0
      E(I,J)=H2*W(I,J)/DOMG-Z3(I)
   22 CONTINUE
      DO 24 J=1,N1
      TPC(2,J)=C(2,J)/B(2,J)
      DO 23 I=3,M
      TPC(I,J)=C(I,J)/(B(I,J)-A(I,J)*TPC(I-1,J))
   23 CONTINUE
   24 CONTINUE
C     CENTRE POINT BY PREVIOUS POINTS
      T(1,1)=(TT(1,1)*(H2*W(1,1)/DOMG-2.0)
     1       +TT(2,N/2+1)*2.0-TT(2,1)*(H1*U(1,1)-1.0)
     2       +TT(2,N1)*(H1*U(1,1)+1.0))/(H2*W(1,1)/DOMG+2.0)
      DO 25 J=2,N1
      T(1,J)=T(1,1)
   25 CONTINUE
      TG(2,1)=F(2,1)*TT(2,2)+E(2,1)*TT(2,1)-A(2,1)*TT(1,1)
      DO 26 J=2,N
      TG(2,J)=D(2,J)*TT(2,J-1)+E(2,J)*TT(2,J)+F(2,J)*TT(2,J+
     *  1)
     1      -A(2,J)*TT(1,J)
   26 CONTINUE
      TG(2,N1)=D(2,N1)*TT(2,N)+E(2,N1)*TT(2,N1)
     1       -A(2,N1)*TT(1,N1)
      DO 28 I=3,M
      TG(I,1)=F(I,1)*TT(I,2)+E(I,1)*TT(I,1)
      DO 27 J=2,N
      TG(I,J)=D(I,J)*TT(I,J-1)+E(I,J)*TT(I,J)+F(I,J)*TT(I,J+
     *  1)
   27 CONTINUE
      TG(I,N1)=D(I,N1)*TT(I,N)+E(I,N1)*TT(I,N1)
   28 CONTINUE
      DO 30 J=1,N1
      TQG(2,J)=TG(2,J)/B(2,J)
```

```
      DO 29 I=3,M
      TQG(I,J)=(TG(I,J)-A(I,J)*TQG(I-1,J))
     1        /(B(I,J)-A(I,J)*TPC(I-1,J))
   29 CONTINUE
   30 CONTINUE
C
C     BACK SUBSTITUTION
C
      DO 32 J=1,N1
      T(M1,J)=0.0
      T (M,J)=TQG(M,J)
      DO 31 K=2,MI
      I=M1-K
      T(I,J)=TQG(I,J)-TPC(I,J)*T(I+1,J)
   31 CONTINUE
   32 CONTINUE
C
C
C
C     CALCULATION OF PHI_DIRECTION USING
C     GAUSSIAN ELIMINATION
C
C
C     ELIMINATION OF T(I,J-1) IN COLUMN
C
      DO 34 I=2,M
      B(I,1)=-H2*W(I,1)/DOMG+2.0
      E(I,1)=-H2*W(I,1)/DOMG-Z3(I)
      TPF(I,1)=F(I,1)/E(I,1)
      DO 33 J=2,N1
      B(I,J)=-H2*W(I,J)/DOMG+2.0
      E(I,J)=-H2*W(I,J)/DOMG-Z3(I)
      TPF(I,J)=F(I,J)/(E(I,J)-D(I,J)*TPF(I,J-1))
   33 CONTINUE
   34 CONTINUE
      DO 36 I=2,M
      DO 36 J=1,N1
      TH(I,J)=A(I,J)*T(I-1,J)+B(I,J)*T(I,J)+C(I,J)*T(I+1,J)
   36 CONTINUE
      DO 40 I=2,M
      TQH(I,1)=TH(I,1)/E(I,1)
      DO 38 J=2,N1
      TQH(I,J)=(TH(I,J)-D(I,J)*TQH(I,J-1))
     1        /(E(I,J)-D(I,J)*TPF(I,J-1))
   38 CONTINUE
   40 CONTINUE
C
C     BACK SUBSTITUTION
```

```
C
      DO 45 I=2,M
      T(I,N1)=TQH(I,N1)
      DO 43 K=1,N
      J=N1-K
      T(I,J)=TQH(I,J)-TPF(I,J)*T(I,J+1)
   43 CONTINUE
   45 CONTINUE
C
C     CENTRE POINT BY PRESENT POINTS AND
C    1  THE PREVIOUS CENTRE PCINT ,T(1,1)
C
      T(1,1)=(T(1,1)*(-H2*W(1,1)/DOMG+2.0)
     1       + T(2,1)*(H1*U(1,1)-1.0)
     2       -T(2,N1)*(H1*U(1,1)+1.0)
     3        -T(2,N/2+1)*2.0)/(-H2*W(1,1)/DOMG-2.0)
      DO 46 J=2,N1
      T(1,J)=T(1,1)
   46 CONTINUE
      IF(KOUNT/20*20.NE.KOUNT) GO TO  4901
      WRITE(6,47) M,N
   47 FORMAT('1','*****  TEMPERATURE DISTRIBUTION WITH',
     1' MESH SIZE',I5,2X,'BY',I5,'  *****')
      WRITE(6,48) T(1,1)
   48 FORMAT('0',1E18.6)
      DO 492 J=1,N1
      WRITE(6,491)
  491 FORMAT(' ')
      WRITE(6,49) (T(I,J),I=2,M1)
   49 FORMAT(' ',7E18.6)
  492 CONTINUE
 4901 CONTINUE
      KOUNT=KOUNT+1
C
C
C
C     CALCULATION OF  HEAT TRANSFER RELATIONSHIPS
C
C
      DO 50 I=1,M1
      WT(I)=0.0
      TS(I)=0.0
   50 CONTINUE
      DO 51 J=1,N1
      GT(J)=-(T(M-3,J)/4-4*T(M-2,J)/3.+3.*T(MI,J)
     1       -4.*T(M,J))/HR
   51 CONTINUE
      SGT=GT(1)+GT(N1)
```

```
      DO 52 J=2,N,2
      SGT=SGT+GT(J)*4.
   52 CONTINUE
      DO 53 J=3,NI,2
      SGT=SGT+GT(J)*2.
   53 CONTINUE
      SGT=HP*SGT/(3.*PI)
      DO 56 I=2,M
      GOTW(I)=(T(I,1)-TT(I,1))/DOMG*W(I,1)
     1       +(T(I,N1)-TT(I,N1))/DOMG*W(I,N1)
      WT(I)=W(I,1)*T(I,1)+W(I,N1)*T(I,N1)
      TS(I)=T(I,1)+T(I,N1)
      WP(I)=W(I,1)+W(I,N1)
      DO 54 J=2,N,2
      GOTW(I)=GOTW(I)+(T(I,J)-TT(I,J))/DOMG*W(I,J)*4.
      WT(I)=WT(I)+W(I,J)*T(I,J)*4.
      TS(I)=TS(I)+T(I,J)*4.
      WP(I)=WP(I)+W(I,J)*4.
   54 CONTINUE
      DO 55 J=3,NI,2
      GOTW(I)=GOTW(I)+(T(I,J)-TT(I,J))/DOMG*W(I,J)*2.
      WT(I)=WT(I)+W(I,J)*T(I,J)*2.
      TS(I)=TS(I)+T(I,J)*2.
      WP(I)=WP(I)+W(I,J)*2.
   55 CONTINUE
      GOTW(I)=HP*GOTW(I)/3.
      WT(I)=HP*WT(I)/3.
      TS(I)=HP*TS(I)/3.
      WP(I)=HP*WP(I)/3.
   56 CONTINUE
      SGTW=0.0
      SWT=0.0
      STP=0.0
      SWP=0.0
      DO 57 I=2,M,2
      SGTW=SGTW+GOTW(I)*R(I)*4.
      SWT=SWT+WT(I)*R(I)*4.
      STP=STP+TS(I)*R(I)*4.
      SWP=SWP+WP(I)*R(I)*4.
   57 CONTINUE
      DO 58 I=3,MI,2
      SGTW=SGTW+GOTW(I)*R(I)*2.
      SWT=SWT+WT(I)*R(I)*2.
      STP=STP+TS(I)*R(I)*2.
      SWP=SWP+WP(I)*R(I)*2.
   58 CONTINUE
      SGTW=HR*SGTW*2/(3*PI)
      SWT=HR*SWT*2/(3*PI)
```

```
      SWP=HR*SWP*2/(3*PI)
      STP=HR*STP*2./(3.*HP)
C     BULK TEMPARETURE ,BLKT
      BLKT=SWT/SWP
      NU1=2.*SWP*SGT/SWT
      NU2=-PR*CON**.5*RARC**.5*SGTW*SWP/SWT
C     AVERAGE NUSSELT NUMBER,AVEN
      AVEN=( NU1+NU2)/2.
C     NUSSELT NUMBER RATIOS TC THEFULLY DEVELCPED FLOW
C     IN STRAIGHT PIPE ,
      RNU1=NU1/3.657
      RNU2=NU2/3.657
      ARNU=(RNU1+RNU2)/2.
      DO 59 J=1,N1
      NUI(J)=2.*SWP*GT(J)/SWT
   59 CONTINUE
      IF(KOUNT/10*10.NE.KOUNT) GO TO 5902
      WRITE(6,5901) N1
 5901 FORMAT('0','*****  NUSSELT NUMBER DISTRIBUTION FRCM',
     1' J= 1 TO',I3,'  *****')
      WRITE(6,48) NUI(1)
      WRITE(6,49) (NUI(J),J=2,N1)
 5902 CONTINUE
C
      SGT2=2.*SGT
      ST0=STP/.1875
      PRK=DK**.5*PR**.25
      NU1M=(NU1M*OMEO+(ONU1+NU1)/2.*DCMG)/CMEG
      NU2M=(NU2M*OMEO+(ONU2+NU2)/2.*DOMG)/OMEG
      AVENM=(NU1M+NU2M)/2.
      RNU1M=NU1M/3.657
      RNU2M=NU2M/3.657
      ARNUM=(RNU1M+RNU2M)/2.
      IF(KTT/20*20.NE.KTT) GO TC 5909
      WRITE(6,60)
   60 FORMAT('0'/6X,'CON',10X,'DK',9X,'SWP',9X,'2*SGT',8X,
     1       'ETA',8X,'POSITICN',6X,'CMEGA   ',8X,'A/RC',7X,
     2       'PEMODIF',6X,'DCMG')
      WRITE(6,61) CON,DK,SWP,SGT2,ETA,PO,OMEG,RARC,PEMOD
     1,DOMG
   61 FORMAT(1X,10E13.6)
      WRITE(6,62)
   62 FORMAT(' ',4X,'PRK',10X,'STP',7X,'STP/STPO',8X,'RED',
     1        10X,'NU1',10X,'NU2',9X,'AVEN',8X,'NU1/NU0',6X,
     2        'NU2/NU0',7X,'ARNU')
      WRITE(6,61) PRK,STP,ST0,RED,NU1,NU2,AVEN,RNU1,RNU2,ARN
     *  U
      WRITE(6,6201)
```

```
 6201 FORMAT(' ',5X,'PR',10X,'NU1M',11X,'NU2M',9X,'AVENM',
     17X,'NU1M/NU0',5X,'NU2M/NU0',5X,'ARNUM',6X,'RPEMD',
     C6X,'BLKT',6X,'RMPRK')
      WRITE(6,61) PR,NU1M,NU2M,AVENM,RNU1M,RNU2M,ARNUM
     1,RPEMD,BLKT,RMPRK
 5909 KTT=KTT+1
      OMEO=CMEG
      ONU1=NU1
      ONU2=NU2
      DO 63 I=1,M1
      DO 63 J=1,N1
      TT(I,J)=T(I,J)
   63 CONTINUE
      IF(RPEMD.GT.0.8E-2) GO TO 65
   64 CONTINUE
      IF(ETA.LT.ETALIM) GO TO 20
      STOP
   65 CONTINUE
      IF(KOUTT.NE.0) GO TO 64
      WRITE(7,66)((TT(I,J),I=1,M1),J=1,N1)
   66 FORMAT(20A4)
      WRITE(7,67) OMEO
      WRITE(7,67) NU1M
      WRITE(7,67) NU2M
   67 FORMAT(E13.6)
      KOUTT=KOUTT+1
      GO TO 64
      END
```

```
                ********************************

                * IN THE SIXTH CCLUMN INDICATES
                CONTINUATION FROM PREVIOUS LINE

                ********************************


C       ***** LAMINAR FLOW IN CURVED PARALLEL *****
C       ***** CHANNELS                        *****
C       ***** ( DEAN NUMBER IS LARGE, MAIN    *****
C       ***** FLOW ,  ENTRANCE )
C       ***** TRIANGLE VELOCITY AT ENTRANCE   *****
        DOUBLE PRECISION W(41,61),U(41,61),S(41,61),SS(41,61),
       1VO(41,61),X(41),XR(41),XRL(41),SG(41,61),
       2HH,HX,HX4,HX2,HX22,LAM,OMEG,
       3B1,B2,A11,A12,A21,A22,UA,WA,
       4DI,SD,SSUM,ERRS,TOLE
       5,POSI(61),PO,T
       6,Q
        COMMON HH,HX,HX4,HX2,HX22,XR,XRL,LAM,X,OMEG
        COMMON M,M1,M2,M3,MI,MJ,MK,N,NI,NJ,NK,N1,NOST,NO,J
        READ(5,5) M,N,T,NOST,TOLE,OMEG
      5 FORMAT(2I10,D10.5,I10,2D10.5)
        READ(5,6) LAM
      6 FORMAT(D10.5)
        READ(5,6) Q
C        SETTING OF CONSTANTS
        M1=M+1
        M2=M+2
        M3=M+3
        MI=M-1
        MJ=M-2
        MK=M-3
        N1=N+1
        NI=N-1
        NJ=N-2
        NK=N-3
        HH=1.D00/(N*T)
        HH=1.0/HH
        HX=2.0/M
        HX2=HX/2.0
        HX4=HX/4.0
```

```
      HX22=HX**2.0
      DO 8 I=1,M1
      X(I)=HX*(I-1)-1.0D00
      XR(I)=1.0/(1.0+LAM*X(I))
      XRL(I)=LAM*XR(I)
    8 CONTINUE
C
C
      DO 1 J=1,N1
      DO 1 I=1,M1
      VO(I,J)=XR(I)*(LAM+Q+2.0D+0*LAM*Q*X(I))
      W(I,J)=1.0D+0+Q*X(I)
      S(I,J)=X(I)+0.5D+0*X(I)*X(I)*Q-0.5D+0*Q
      U (I,J)=0.0
    1 CONTINUE
      WRITE(6,461) LAM,M,N,T,TOLE,OMEG
  461 FORMAT(/5X,'LAM=',D10.3,2X,'M,N,L=',
     12I4,D10.3,2X,'TOLE=',
     1      D10.3,2X,'OMEG=',D10.3)
      DO 2 J=1,N1
      S(1,J)=-1.0
      SS(1,J)=-1.0
      S(M1,J)=+1.0
    2 CONTINUE
      DO 45 J=2,N1
      NO=0
   10 CONTINUE
      CALL SUBVOS(W,U,S,SS,VO,ERRS)
      IF(ERRS.LT.TOLE.OR.NO.GT.NOST) GO TO 15
      NO=NO+1
      GO TO 10
   15 CONTINUE
   45 CONTINUE
      DO 451 J=2,N1
C
C     CALCULATION OF VELOCITIES,W AND U
      W(1,J)=0.0
      W(2,J)=(S(2,J)-8.0*S(1,J)+8.0*S(3,J)-S(4,J))/(12.0*HX)
      DO 30 I=3,MI
      W(I,J)=(S(I-2,J)-8.0*S(I-1,J)+8.0*S(I+1,J)
     1      -S(I+2,J))/(12.0*HX)
   30 CONTINUE
      W(M,J)=(S(MJ,J)-8.0*S(MI,J)+8.0*S(M1,J)
     1      -S(M,J))/(12.0*HX)
      W(M1,J)=0.0
      U(1,J)=0.0
      IF(J.EQ.2) GO TO 35
      IF(J.EQ.N ) GO TO 37
```

```
      IF(J.EQ.N1) GO TO 39
      DO 31 I=2,M
      U(I,J)=-(S(I,J-2)-8.0*S(I,J-1)+8.0*S(I,J+1)
     1        -S(I,J+2))/12.0*HH*XR(I)
   31 CONTINUE
      GO TO 41
   35 CONTINUE
      DO 36 I=2,M
      U(I,2)=-(-7.0*S(I,1)+8.0*S(I,3)-S(I,4))/12.0*HH*XR(I)
   36 CONTINUE
      GO TO 41
   37 CONTINUE
      DO 38 I=2,M
      U(I,N)=-(S(I,NJ)-8.0*S(I,NI)+7.0*S(I,N1))/12.0*HH*XR(I
     *  )
   38 CONTINUE
      GO TO 41
   39 CONTINUE
      DO 40 I=2,M
      U(I,N1)=-(3.0*S(I,N1)-3.0*S(I,N)-2.0*S(I,NI)
     1       +3.0*S(I,NJ)-S(I,NK))/2.0*HH
   40 CONTINUE
   41 CONTINUE
      U(M1,J)=0.0
  451 CONTINUE
      WRITE(6,47)
   47 FORMAT(/5X,'VORTICITY VO')
      DO 471 J=1,N1
      WRITE(6,48) (VO(I,J),I=1,M1)
  471 CONTINUE
   48 FORMAT(' ',10D13.5)
      WRITE(6,49)
   49 FORMAT(/5X,'STREAM FUNCTION,S')
      DO 491 J=1,N1
      WRITE(6,48) (S(I,J),I=1,M1)
  491 CONTINUE
      WRITE(6,50)
   50 FORMAT(/5X,'VELOCITY,W')
      DO 501 J=1,N1
      WRITE(6,48) (W(I,J),I=1,M1)
  501 CONTINUE
      WRITE(6,51)
   51 FORMAT(/5X,'VELOCITY,U')
      DO 511 J=1,N1
      WRITE(6,48) (U(I,J),I=1,M1)
  511 CONTINUE
      CALL FLOW(W,U)
      DO 512 J=1,N1
```

```
      POSI(J)=0.D00
  512 CONTINUE
      PO=0.D00
      DO 513 J=2,N1
      PO=PO+1.D00/HH
      POSI(J)=PC
  513 CONTINUE
      WRITE(6,514)
  514 FORMAT(/5X,'POSITION IN CMEGER-DIRECTION,POSI(J)')
      WRITE(6,48)(POSI(J),J=1,N1)
      STOP
      END
      SUBROUTINE SUBVOS(W,U,S,SS,VO,ERRS)
      DOUBLE PRECISION W(41,61),U(41,61),S(41,61),SS(41,61),
     1VO(41,61),X(41),XR(41),XRL(41),SG(41,61),
     2HH,HX,HX4,HX2,HX22,LAM,OMEG,
     3B1,B2,A11,A12,A21,A22,UA,WA,
     4DI,SD,SSUM,ERRS,TOLE
      COMMON HH,HX,HX4,HX2,HX22,XR,XRL,LAM,X,OMEG
      COMMON M,M1,M2,M3,MI,MJ,MK,N,NI,NJ,NK,N1,NOST,NO,J
      K=0
      B1=0.0
      B2=0.0
      A11=0.0
      A12=0.0
      A21=0.0
      A22=0.0
      UA=0.C
      WA=0.0
C     SETTING OF VORTICITY,VO,BY DIRECT_VORTICITY METHOD
    5 CONTINUE
      K=K+1
      VO(1,J)=0.0
      VO(2,J)=0.0
      GO TO 9
    6 CONTINUE
      K=K+1
      VO(1,J)=1.0
      VO(2,J)=0.0
      GO TO 9
    7 CONTINUE
      K=K+1
      VO(1,J)=0.0
      VO(2,J)=1.0
      GO TO 9
    8 CONTINUE
      K=K+1
      VO(1,J)=(A12*B2-A22*(1.0+B1))/(A12*A21-A22*A11)
```

```
      VO(2,J)=(A11*B2-A21*(1.0+B1))/(A11*A22-A21*A12)
    9 CONTINUE
      DO 10 I=3,M1
      UA=(S(I-1,J)-S(I-1,J-1))*HH
      WA=.25/HX*(S(I,J-1)-S(I-2,J-1)+S(I,J)-S(I-2,J))
      VO(I,J)=((-0.5+XRL(I-1)*HX4-UA*HX4)*VO(I-2,J-1)
     1       +(1.0-XR(I-1)*WA*HX22*HH)*VO(I-1,J-1)
     2       +(-0.5-XRL(I-1)*HX4+UA*HX4)*VO(I,J-1)
     3       +(-0.5+XRL(I-1)*HX4-UA*HX4)*VO(I-2,J)
     4       +(1.0+XR(I-1)*WA*HX22*HH)*VO(I-1,J))/
     5       (0.5+XRL(I-1)*HX4-UA*HX4)
   10 CONTINUE
C     CALCULATION OF STREAM FUNCTION
      SS(2,J)=-1.0+0.5*HX22*VO(1,J)
      DO 11 I=3,M2
      SS(I,J)=(    HX22*VO(I-1,J)+2.0*SS(I-1,J)
     1     +(-1.0+HX2*XRL(I-1))*SS(I-2,J))/
     2       (1.0+HX2*XRL(I-1))
   11 CONTINUE
      IF(K.EQ.4) GO TO 20
      SG(M1,J)=(SS(M2,J)-SS(M,J))/(2.0*HX)
      IF(K-2) 15,16,17
   15 CONTINUE
      B1=-SS(M1,J)
      B2=-SG(M1,J)
      GO TO 6
   16 CONTINUE
      A11=SS(M1,J)+B1
      A21=SG(M1,J)+B2
      GO TO 7
   17 CONTINUE
      A12=SS(M1,J)+B1
      A22=SG(M1,J)+B2
      GO TO 8
   20 CONTINUE
      K=0
      SD=0.0
      SSUM=0.0
      DO 25 I=1,M1
      DI=OMEG*(SS(I,J)-S(I,J))
      S(I,J)=S(I,J)+DI
      SD=SD+DABS(DI)
      SSUM=SSUM+DABS(S(I,J))
   25 CONTINUE
      ERRS=SD/SSUM
      WRITE(6,46) NO,ERRS
   46 FORMAT(' ',5X,'NO=',I5,5X,'ERRS=',E15.6)
      S(2,J) =SS(2,J)
```

```
      DO 47 I=3,M1
      S(I,J)=SS(I,J)
   47 CONTINUE
      RETURN
      END
      SUBROUTINE FLOW(W,U)
      DOUBLE PRECISION W(41,61),U(41,61),S(41,61),SS(41,61),
     1VO(41,61),X(41),XR(41),XRL(41),SG(41,61),
     CPHI(61),DPHI(61),DPX(41,61),DPPH(41,61),
     CAVDPH(61),P(41,61),AVP(61),FRICC(61),RFRIC(61),
     2HH,HX,HX4,HX2,HX22,LAM,OMEG,PHIO,ETA,ETA2,
     3B1,B2,A11,A12,A21,A22,UA,WA,
     4DI,SD,SSUM,ERRS,TOLE
      COMMON HH,HX,HX4,HX2,HX22,XR,XRL,LAM,X,OMEG
      COMMON M,M1,M2,M3,MI,MJ,MK,N,NI,NJ,NK,N1,NOST,NO
      HH=HH*2.0
      DO 4J=1,N1
      DO 4 I=1,M1
      DPX(I,J)=XRL(I)*W(I,J)*W(I,J)
    4 CONTINUE
      DPPH(1,1)=(11.0*W(5,1)-56.0*W(4,1)+114.0*W(3,1)
     C      -104.0*W(2,1))/(12.0*HX**2.0)
     C      +XRL(1)*(-6.0*W(5,1)+32.0*W(4,1)
     C      -72.0*W(3,1)+96.0*W(2,1))/(24.0*HX)
      DPPH(2,1)=(-W(5,1)+4.0*W(4,1)+6.0*W(3,1)
     C      -20.0*W(2,1))/(12.0*HX**2.0)
     C      +XRL(2)*(W(5,1)-6.0*W(4,1)+18.0*W(3,1)
     C      -10.0*W(2,1))/(12.0*HX)
     C      -XRL(2)**2.0*W(2,1)-XR(2)*W(2,1)*(W(2,2)-W(2,1))
     C      *HH
      DO 5 I=3,MI
      DPPH(I,1)=(-W(I+2,1)+16.0*W(I+1,1)-30.0*W(I,1)
     C       +16.0*W(I-1,1)-W(I-2,1))/(12.0*HX**2.0)
     C      +XRL(I)*(-W(I+2,1)+8.0*W(I+1,1)-8.0*W(I-1,1)
     C      +W(I-2,1))/(12.0*HX)
     C      -XRL(I)**2.0*W(I,1)-XR(I)*W(I,1)*(W(I,2)-W(I,1))
     C      *HH
    5 CONTINUE
      DPPH(M,1)=(-20.0*W(M,1)+6.0*W(MI,1)+4.0*W(MJ,1)
     C      -W(MK,1))/(12.0*HX**2.0)
     C      +XRL(M)*(-10.0*W(M,1)+18.0*W(MI,1)
     C      -6.0*W(MJ,1)+W(MK,1))/(-12.0*HX)
     C      -XRL(M)**2.0*W(M,1)-XR(M)*W(M,1)*(W(M,2)-W(M,1))
     C      *HH
      DPPH(M1,1)=(-104.0*W(M,1)+114.0*W(MI,1)-56.0*W(MJ,1)
     C      +11.0*W(MK,1))/(12.0*HX**2.0)
     C      +XRL(M1)*(96.0*W(M,1)-72.0*W(MI,1)
     C      +32.0*W(MJ,1)-6.0*W(MK,1))/(-24.0*HX)
```

```
      DO 10 J=2,N
      DPPH(1,J)=(11.0*W(5,J)-56.0*W(4,J)+114.0*W(3,J)
     C       -104.0*W(2,J))/(12.0*HX**2.0)
     C       +XRL(1)*(-6.0*W(5,J)+32.0*W(4,J)-72.0*W(3,J)
     C       +96.0*W(2,J))/(24.0*HX)
      DPPH(2,J)=(-W(5,J)+4.0*W(4,J)+6.0*W(3,J)-20.0*W(2,J))
     C        /(12.0*HX**2.0)
     C       +(-U(2,J)+XRL(2))*(W(5,J)-6.0*W(4,J)
     C       +18.0*W(3,J)-10.0*W(2,J))/(12.0*HX)
     C       -XRL(2)**2.0*W(2,J)-XRL(2)*U(2,J)*W(2,J)
     C       -XRL(2)**2.0*W(2,J)-XRL(2)*U(2,J)*W(2,J)
     C       -XR(2)*W(2,J)*0.5*HH*(W(2,J+1)-W(2,J-1))
      DO 8 I=3,MI
      DPPH(I,J)=(-W(I+2,J)+16.0*W(I+1,J)-30.0*W(I,J)
     C       +16.0*W(I-1,J)-W(I-2,J))/(12.0*HX**2.0)
     C       +(-U(I,J)+XRL(I))*(-W(I+2,J)+8.0*W(I+1,J)
     C       -8.0*W(I-1,J)+W(I-2,J))/(12.0*HX)
     C       -XRL(I)**2.0*W(I,J)
     C       -XRL(I)*U(I,J)*W(I,J)
     C       -XR(I)*W(I,J)*0.5*HH*(W(I,J+1)-W(I,J-1))
    8 CONTINUE
      DPPH(M,J)=(-20.0*W(M,J)+6.0*W(MI,J)
     C       +4.0*W(MJ,J)-W(MK,J))/(12.0*HX**2.0)
     C       +(-U(M,J)+XRL(M))*(-10.0*W(M,J)+18.0*W(MI,J)
     C       -6.0*W(MJ,J)+W(MK,J))/(-12.0*HX)
     C       -XRL(M)**2.0*W(M,J)-XRL(M)*U(M,J)*W(M,J)
     C       -XR(M)*W(M,J)*0.5*HH*(W(M,J+1)-W(M,J-1))
      DPPH(M1,J)=(-104.0*W(M,J)+114.0*W(MI,J)
     C       -56.0*W(MJ,J)+11.0*W(MK,J))/(12.0*HX**2.0)
     C       +XRL(M1)*(96.0*W(M,J)
     C       -72.0*W(MI,J)+32.0*W(MJ,J)-6.0*W(MK,J))/
     C       (-24.0*HX)
   10 CONTINUE
      DPPH(1,N1)=(11.0*W(5,N1)-56.0*W(4,N1)
     C       +114.0*W(3,N1))/(12.0*HX**2.0)
     C       +XRL(1)*(-6.0*W(5,N1)+32.0*W(4,N1)
     C       -72.0*W(3,N1)+96.0*W(2,N1))/(24.0*HX)
      DPPH(2,N1)=(-W(5,N1)+4.0*W(4,N1)+6.0*W(3,N1)
     C       -20.0*W(2,N1))/(12.0*HX**2.0)
     C       +XRL(2)*(W(5,N1)-6.0*W(4,N1)
     C       +18.0*W(3,N1)-10.0*W(2,N1))/(12.0*HX)
     C       -XRL(2)**2.0*W(2,N1)
      DO 12 I=3,MI
      DPPH(I,N1)=(-W(2+2,N1)+16.0*W(I+1,N1)
     C       -30.0*W(I,N1)+16.0*W(I-1,N1)
     C       -W(I-2,N1))/(12.0*HX**2.0)
     C       +XRL(I)*(-W(I+2,N1)+8.0*W(I+1,N1)
     C       -8.0*W(I-1,N1)+W(I-2,N1))/(12.0*HX)
```

```
C       -XRL(I)**2.0*W(I,N1)
 12 CONTINUE
    DPPH(M,N1)=(-20.0*W(M,N1)+6.0*W(MI,N1)
C       +4.0*W(MJ,N1)-W(MK,N1))/(12.0*HX**2.0)
C       +XRL(M)*(-10.0*W(M,N1)+18.0*W(MI,N1)
C       -6.0*W(MJ,N1)+W(MK,N1))/(-12.0*HX)
C       -XRL(M)**2.0*W(M,N1)
    DPPH(M1,N1)=(-104.0*W(M,N1)+114.0*W(MI,N1)
C       -56.0*W(MJ,N1)+11.0*W(MK,N1))/(12.0*HX**2.0)
C       +XRL(M1)*(96.0*W(M,N1)-72.0*W(MI,N1)
C       +32.0*W(MJ,N1)-6.0*W(MK,N1))/(-24.0*HX)
    DO 20 J=1,N1
    RFRIC(J)=0.0D0
    FRICC(J)=C.0D0
    DO 20 I=1,M1
    P(I,J)=0.0
 20 CONTINUE
    DO 30 J=1,N1
    AVDPH(J)=DPPH(1,J)+DPPH(M1,J)
    DO 26 I=2,M,2
    AVDPH(J)=AVDPH(J)+DPPH(I,J)*4.0
 26 CONTINUE
    DO 27 I=3,MI,2
    AVDPH(J)=AVDPH(J)+DPPH(I,J)*2.0
 27 CONTINUE
    AVDPH(J)=(HX/2.0)*AVDPH(J)/3.0
    FRICC(J)=2.0*AVDPH(J)*4.0
    RFRIC(J)=FRICC(J)/24.0
 30 CONTINUE
    DO 31 J=2,N
    DO31 I=1,M1
    P(I,J)=P(I,J-1)+.5*(DPPH(I,J)+DPPH(I,J-1))/HH
    AVP(J)=AVP(J-1)+.5*(AVDPH(J)+AVDPH(J-1))/HH
 31 CONTINUE
    WRITE(6,32)
 32 FORMAT(/5X,'PRESSUR GRADIENT IN X_DIRECTICN,DPX(I,J)')
    DO 36 J=1,N1
    WRITE(6,35) (DPX(I,J),I=1,M1)
 35 FORMAT(' ',10D13.5)
 36 CONTINUE
    WRITE(6,37)
 37 FORMAT(/5X,'PRESSURE GRADIANT IN
   1      PHI-DIRECTICN,DPPH(I,J)')
    DO 38 J=1,N1
    WRITE(6,35) (DPPH(I,J),I=1,M1)
 38 CONTINUE
    WRITE(6,39)
 39 FORMAT(/5X,'AVERAGE PRESSURE GRADIENT IN
```

```
     1      PHI-DIRECTION,AVDPH(J)')
            WRITE(6,35)  (AVDPH(J),J=1,N1)
            WRITE(6,40)
       40   FORMAT(/5X,'PRESSURE DEVELOPMENT,P(I,J)')
            DO 41 J=1,N1
            WRITE(6,35)  (P(I,J),I=1,M1)
       41   CONTINUE
            WRITE(6,42)
       42   FORMAT(/5X,'AVERAGE PRESSRE DEVELOPMENT,AVP(J)')
            WRITE(6,35)  (AVP(J),J=1,N1)
            WRITE(6,43)
       43   FORMAT(/5X,'FRICTION,F*RE=FRICC(J)=2.*AVDPH(J)')
            WRITE(6,35)  (FRICC(J),J=1,N1)
            WRITE(6,44)
       44   FORMAT(/5X,'RATIO OF FRICTIONCOEFF.,RFRIC(J)=FRICC(J)/
           *  24.')
            WRITE(6,35)  (RFRIC(J),J=1,N1)
            RETURN
            END
```

```
                    **********
                    * IN THE SIXTH COLUMN INDICATES
                    CONTINUATION FROM PREVIOUS LINE
                    **********
C     ************************************************************
C     ***** STABILITY PROBLEM IN  CURVED PARALLEL        *****
C     ***** CHANNELS                                     *****
C     ************************************************************
C     ***** REDUCED SINGLE MATRIX METHOD                 *****
C     ***** FOR ARBITRARY LAMDER                         *****
C     ************************************************************
C
C
C
      DOUBLE PRECISION X(81),RCX(81),RAX(81),DRAX(81),
     1TRAX(81),TETRAX(81),W(81),U(81),DU(81),DUP(81),DW(81),
     2C1(81),C2(81),C3(81),C4(81),CC1(81),CC2(81),
     3CA(81),CB(81),CC(81),CD(81),CE(81),
     4CCA(81),CCB(81),CCC(81),CCD(81),CCE(81),CCF(81),
     5AA(81,81),BB(81,81),C(81,81),
     6DK(3),F(3),      COEF(81),CCOEF(81),A,A2,DLAM,
     7H,H2,H3,H4,HH,HH2,HH3,HH4,AMAX,TMPA
     8,RE(3)
     9,Q
      COMMON DK,A2,DLAM,W,DW,DUP,RAX,COEF,CCOEF,
     1CA,CB,CC,CD,CE,CCA,CCB,CCC,CCD,CCE,CCF
      COMMON N,N1,NI,NJ,NK,M
      READ(5,1) N
    1 FORMAT(I5)
      N1=N+1
      NI=N-1
      NJ=N-2
      NK=N-3
C
C     SETTING OF CONSTANTS
C
      H=2D00/N
      H2=H**2D00
      H3=H*H2
```

```
      H4=H2*H2
      HH=1D00/H
      HH2=1D00/H2
      HH3=1D00/H3
      HH4=1D00/H4
C
      READ(5,2) DLAM
    2 FORMAT(D10.5)
      READ(5,2)A
      A2=A**2D00
      DO 3 I=1,N1
      X(I)=-1D00+H*(I-1)
      RCX(I)=1D00+DLAM*X(I)
      RAX(I)=DLAM/RCX(I)
      DRAX(I)=RAX(I)**2D00
      TRAX(I)=RAX(I)*DRAX(I)
      TETRAX(I)=DRAX(I)**2D00
    3 CONTINUE
C
C
C     CALCULATION FO CONSTANT COEFFICIENTS FOR MATRIX
C
      DO 15 I=1,N1
      C1(I)=-U(I)+2D00*RAX(I)
      C2(I)=+A2*2D00+DU(I)-U(I)*RAX(I)-3D00*DRAX(I)
      C3(I)=-DU(I)*RAX(I)+A2*2D00*RAX(I)+2D00*DRAX(I)*U(I)
     1      +3D00*TRAX(I)-A2*U(I)/4D00
      C4(I)=-3D00*TETRAX(I)-2D00*U(I)*TRAX(I)
     1      -A2*2D00*DRAX(I)+DU(I)*DRAX(I)-A2*DU(I)/4D00
     2      +A2*A2/16D00
      CC1(I)=RAX(I)-U(I)
      CC2(I)=-DRAX(I)-A2      +DU(I)
   15 CONTINUE
      DO 16 I=2,N
      CA(I)=HH4-HH3/2D00*C1(I)-HH2/12D00*C2(I)+HH/12D00*C3(I
     *  )
      CB(I)=-4D00*HH4+HH3*C1(I)+16D00*HH2*C2(I)/12D00
     1      -8D00*HH/12D00*C3(I)
      CC(I)=6D00*HH4-30D00/12D00*HH2*C2(I)+C4(I)
      CD(I)=-4D00*HH4-HH3*C1(I)+16D00/12D00*HH2*C2(I)
     1      +8D00*HH/12D00*C3(I)
      CE(I)=HH4+HH3/2D00*C1(I)-HH2/12D00*C2(I)
     1      -HH/12D00*C3(I)
   16 CONTINUE
      DO 17 I=3,NI
      CCA(I)=-HH2/12D00+HH/12D00*CC1(I)
      CCB(I)=16D00/12D00*HH2-8D00/12D00*HH*CC1(I)
      CCC(I)=-30D00/12D00*HH2+CC2(I)
```

```
      CCD(I)=16D00/12D00*HH2+8D00/12D00*HH*CC1(I)
      CCE(I)=-HH2/12D00-HH/12D00*CC1(I)
   17 CONTINUE
      CC(2)=CC(2)+6D00*CA(2)
      CD(2)=CD(2)-2D00*CA(2)
      CE(2)=CE(2)+1D00/3D00*CA(2)
      CA(N)=CA(N)+1D00/3D00*CE(N)
      CB(N)=CB(N)-2D00*CE(N)
      CC(N)=CC(N)+6D00*CE(N)
      CCC(2)=-20D00/12D00*HH2-10D00/12D00*CC1(2)*HH+CC2(2)
      CCD(2)=5D-1*HH2+18D00/12D00*HH*CC1(2)
      CCE(2)=4D00/12D00*HH2-5D-1*HH*CC1(2)
      CCF(2)=-HH2/12D00+HH/12D00*CC1(2)
      CCF(N)=-HH2/12D00-HH/12D00*CC1(N)
      CCA(N)=4D00/12D00*HH2+5D-1*HH*CC1(N)
      CCB(N)=5D-1*HH2-18D00/12D00*HH*CC1(N)
      CCC(N)=-20D00/12D00*HH2+10D00/12D00*HH*CC1(N)+CC2(N)
C
C
C     CALCULATION OF THE VELOCITY GRADIENTS, DW=DW/DX.
C
      READ(5,20)  (W(I),I=1,N1)
   20 FORMAT(10A8)
      WRITE(6,21)  (W(I),I=1,N1)
   21 FORMAT(10D13.4)
      DW(1)=(-6D00*W(5)+32D00*W(4)-72D00*W(3)
     1       +96D00*W(2))/24D00*HH
      DW(2)=(W(5)-6D00*W(4)+18D00*W(3)-10D00*W(2))
     1       /12D00*HH
      DO 22 I=3,NI
      DW(I)=(-W(I+2)+8D00*W(I+1)-8D00*W(I-1)+W(I-2))
     1       /12D00*HH
   22 CONTINUE
      DW(N)=(10D00*W(N)-18D00*W(N-1)+6D00*W(N-2)
     1       -W(N-3))/12D00*HH
      DW(N1)=(-96D00*W(N)+72D00*W(N-1)-32D00*W(N-2)
     1       +6D00*W(N-3))/24D00*HH
      DO 23 I=1,N1
      DU(I)=0D00
      DUP(I)=0D00
      U(I)=CD00
   23 CONTINUE
      READ(5,25)  (DK(M),M=1,2)
   25 FORMAT(2D20.10)
      RE(1)=DK(1)/(DLAM**0.5D+0)
      RE(2)=DK(2)/(DLAM**0.5D+0)
C
C
```

```
C
C
      M=1
      NO=0
      CALL  COEFCT(C)
      CALL  DETMT(C,F)
      M=M+1
      CALL  COEFCT(C)
      CALL  DETMT(C,F)
      WRITE(6,29) A,DLAM,N
   29 FORMAT('1',5X,'CRITICAL DEAN NUMBER , DK'//
     15X,'A=',F8.5,3X,'LAMDER=',F7.4,3X,'N=',I2)
      WRITE(6,30) DK(1),RE(1),F(1),NO,DK(2),RE(2),F(2)
   30 FORMAT('0',7X,'NO.',3X,'DEAN NUMBER ',5X,'RE.NO.',10X,
     1      'DETERMINANT'//11X,D15.8,2X,D15.8,2X,D15.8//7X,
     2      I3,1X,D15.8,2X,D15.8,2X,D15.8)
      F(2)=F(2)/DABS(F(2))
      NOO=1
   31 CONTINUE
      NNO=1
  311 CONTINUE
      DK(3)=2.D00*DK(2)-DK(1)
      RE(3)=DK(3)/(DLAM**0.5D+0)
      M=M+1
      CALL  COEFCT(C)
      CALL  DETMT(C,F)
      NO=NO+1
      WRITE(6,32) NO,DK(3),RE(3),F(3)
   32 FORMAT(/7X,I3,1X,D15.8,2X,D15.8,2X,D15.8)
      DK(1)=DK(2)
      DK(2)=DK(3)
      M=2
      F(3)=F(3)/DABS(F(3))
      Q=F(3)*F(2)
      F(2)=F(3)
      IF(Q.GT.0.D00) GO TO 3111
      GO TO 31
 3111 CONTINUE
      NNO=NNO+1
      IF(NNO.NE.25) GO TO 311
      NOO=NOO+1
      IF(NOO.NE.2) GO TO 40
      GO TO 31
   40 STOP
      END
      SUBROUTINE COEFCT(C)
      DOUBLE PRECISION X(81),RCX(81),RAX(81),DRAX(81),
     1TRAX(81),TETRAX(81),W(81),U(81),DU(81),DUP(81),DW(81),
```

```
     2C1(81),C2(81),C3(81),C4(81),CC1(81),CC2(81),
     3CA(81),CB(81),CC(81),CD(81),CE(81),
     4CCA(81),CCB(81),CCC(81),CCD(81),CCE(81),CCF(81),
     5AA(81,81),BB(81,81),C(81,81),
     6DK(3),F(3),      COEF(81),CCOEF(81),A,A2,DLAM,
     7H,H2,H3,H4,HH,HH2,HH3,HH4,AMAX,TMPA
      COMMON DK,A2,DLAM,W,DW,DUP,RAX,COEF,CCOEF,
     1CA,CB,CC,CD,CE,CCA,CCB,CCC,CCD,CCE,CCF
      COMMON N,N1,NI,NJ,NK,M
C
C
C     CALCULATION OF VARIABLE COEFFICIENTS AND
C     THE FINAL MATRIX FORM ,C(I,J)
C
      DO 2 J=2,N
      DO 1 I=2,N
      AA(I,J)=0D00
      BB(I,J)=0.D00
      C (I,J)=0D00
    1 CONTINUE
    2 CONTINUE
      DO 3 I=2,N
      COEF(I)=A2*RAX(I)*2D00*DLAM**(-5D-1)
     1       *(+DUP(I)/DK(M)-W(I)*DK(M)/2D00)
      CCOEF(I)=DK(M)*DLAM**(-5D-1)/2D00
     1       *(DW(I)+W(I)*RAX(I))
    3 CONTINUE
      DO 4 J=4,N
      AA(J,J-2)=CA(J)/COEF(J)
    4 CONTINUE
      DO 5 J=3,N
      AA(J,J-1)=CB(J)/COEF(J)
    5 CONTINUE
      DO 6 J=2,N
      AA(J,J)=CC(J)/COEF(J)
    6 CONTINUE
      DO 7 J=2,NI
      AA(J,J+1)=CD(J)/COEF(J)
    7 CONTINUE
      DO 8 J=2,NJ
      AA(J,J+2)=CE(J)/COEF(J)
    8 CONTINUE
      DO 9 J=4,N
      BB(J,J-2)=CCA(J)/CCOEF(J)
    9 CONTINUE
      DO 10 J=3,N
      BB(J,J-1)=CCB(J)/CCOEF(J)
   10 CONTINUE
```

```
      DO 11 J=2,N
      BB(J,J)=CCC(J)/CCOEF(J)
   11 CONTINUE
      DO 12 J=2,NI
      BB(J,J+1)=CCD(J)/CCOEF(J)
   12 CONTINUE
      DO 13 J=2,NJ
      BB(J,J+2)=CCE(J)/CCOEF(J)
   13 CONTINUE
      BB(2,5)=CCF(2)/CCOEF(2)
      BB(N,N-1)=CCF(N)/CCOEF(N)
C
C
      DO 16 J=2,N
      DO 15 I=2,N
      DO 14 K=2,N
      C(I,J)=AA(I,K)*BB(K,J)+C(I,J)
   14 CONTINUE
   15 CONTINUE
   16 CONTINUE
      DO 17 J=2,N
      C(J,J)=C(J,J)-1D00
   17 CONTINUE
      DO 21 J=2,N
      DO 20 I=2,N
      C(I,J)=C(I,J)/5.0D+6
   20 CONTINUE
   21 CONTINUE
      RETURN
      END
      SUBROUTINE DETMT(C,F)
      DOUBLE PRECISION X(81),RCX(81),RAX(81),DRAX(81),
     1TRAX(81),TETRAX(81),W(81),U(81),DU(81),DUP(81),DW(81),
     2C1(81),C2(81),C3(81),C4(81),CC1(81),CC2(81),
     3CA(81),CB(81),CC(81),CD(81),CE(81),
     4CCA(81),CCB(81),CCC(81),CCD(81),CCE(81),CCF(81),
     5AA(81,81),BB(81,81),C(81,81),
     6DK(3),F(3),      COEF(81),CCOEF(81),A,A2,DLAM,
     7H,H2,H3,H4,HH,HH2,HH3,HH4,AMAX,TMPA
      COMMON DK,A2,DLAM,W,DW,DUP,RAX,COEF,CCOEF,
     1CA,CB,CC,CD,CE,CCA,CCB,CCC,CCD,CCE,CCF
      COMMON N,N1,NI,NJ,NK,M
C
C     DETAMINANT SOLVER
C
C
C
C
```

```
      NN=1
C     FINDING OF THE PIVOTING ROW
C
      DO 15 K=2,N
      AMAX=0D00
      DO 5 L=K,N
      IF(AMAX.GE.DABS(C(L,K))) GO TO 5
      AMAX=DABS(C(L,K))
      MAX=L
    5 CONTINUE
C
C
C     CHECKING OF SINGULARITY
C
      IF(AMAX.GE.0.1D-60) GO TO 7
      WRITE(6,6)
    6 FORMAT(/'0',2X,'THE MATRIX IS A SINGULAR ONE',
     1      ' OR NEARY SINGULER')
      GO TO 20
    7 CONTINUE
C
C
C     INTERCHANGING OF ROWS
C
      DO 8 J=K,N
      TMPA=C(MAX,J)
      C(MAX,J)=C(K,J)
      C(K,J)=TMPA
    8 CONTINUE
      NN=NN+MAX-K
C
C
C     ELIMINATION PROCEDURE
C
      IF(K.EQ.N) GO TO 17
      K1=K+1
      DO 12 I=K1,N
      C(I,K)=C(I,K)/C(K,K)
      DO 10 J=K1,N
      C(I,J)=C(I,J)-C(I,K)*C(K,J)
   10 CONTINUE
   12 CONTINUE
   15 CONTINUE
   17 CONTINUE
C
C
C     DETAMINANT
C
```

```
      TMPA=1D00
      DO 18 I=2,N
      TMPA=C(I,I)*TMPA
   18 CONTINUE
      IF(NN/10*10.NE.NN) GO TO 19
      F(M)=-TMPA
   19 CONTINUE
      F(M)=TMPA
      RETURN
   20 STOP
      END
```

# END OF REEL

ARC-30